

19th World Congress of Soil Science

Symposium 2.2.1

Biogeochemical interfaces in soils

Soil Solutions for a Changing World,

Brisbane, Australia

1 – 6 August 2010

Table of Contents

	Page
Table of Contents	ii
1 A study of adsorption of simple organic molecules onto inorganic soil components using DRIFTS	1
2 Admixture of <i>Alnus subcordata</i> with <i>Populus euramericana</i> improved soil nitrogen	5
3 Biochar addition to soil changed microbial community structure and decreased microbial biomass carbon and net inorganic nitrogen mineralized	9
4 Biomolecular complexation affects microbial adhesion to iron (oxyhydr)oxides	13
5 Cadmium and Zinc Concentrations in the Soils of the Oil Palm Plantations from Long Term Application of Phosphate Rock	17
6 The thermodynamics stability of soil humic and fulvic acids	20
7 Contribution of the carboxyl group of acetate to the ¹⁴ C-containing gas production in agricultural soils	24
8 Depth profiling of soil clay-xanthan complexes using step-scan mid-infrared photoacoustic spectroscopy	27
9 Development of a method for sequential extraction of Si-pools from soils	31
10 Development of an analytical methodology for ultra-trace selenium speciation determination in soils	35
11 Distribution of a nonylphenol isomer and the herbicide MCPA in soil derived organo-clay complexes	39
12 Distribution of silicon in soils and sediments of a small catchment area: similarities and differences	42
13 Distributions of soil phosphorus in China's densely populated village landscapes	46
14 Diurnal and seasonal greenhouse gases exchange in a salt marsh in central Japan	50
15 Effect of different cation saturations on the sorption and mineralization of the hydrophobic organic compounds nonylphenol and phenanthrene in soils	54
16 Effect of nutrient cycle by different thinning practice in temperate forest	58

Table of Contents (Cont.)

	Page
17 Effect of tillage systems on soil aggregation and hydraulic properties in SW Spain	62
18 Experiments and modeling of electron-transfer of DIRB	66
19 Ferrihydrite enhances phenanthrene sorption to artificial soils	70
20 Formation of biogeochemical interfaces in soils as controlled by mineral and organic components	74
21 Formation of clay pans in south-west Queensland, Australia	78
22 Formation of iron plaque and vivianite on the roots of paddy rice	82
23 Formation of soil geochemical anomalies by plant uptake of trace elements	86
24 Forms and characteristics of insoluble Fe-humic substances used for Fe nutrition of cucumber (<i>Cucumis sativus</i> L.)	90
25 From atom to pedon: Linking processes to phenomena and function	94
26 From Gene to Model – Linking Microorganisms to Microhabitat Functions	98
27 Geochemistry and mineralogy of volcanic soils from Ocean Fogo island (Cape Verde)	102
28 Geochemistry, mineralogy and micropaleontology of a pedogenic calcrete profile (Slimene, NE Tunisia)	106
29 Influence of temperature on solute release from organic horizons in Siberian permafrost terrain	110
30 Influences of applying biosolids on the characteristics of five alkaline soil series and biomass of switchgrass	114
31 Interactions of organic pollutants with soil components investigated by means of molecular modelling	117
32 Investigating phosphate sorption reactions in acid soils through solution, NMR, and L- and K-edge XANES analyses	121
33 Iodine sorption and its chemical form in the soil–soil solution system in Japanese agricultural fields	125
34 Isotopic exchange kinetics of soil P under <i>Pinus radiata</i> and Lucerne Understorey	129
35 Liming and acidification kinetics of some acid, neutral and alkaline soils	133

Table of Contents (Cont.)

	Page
36 Linkage and structure elucidation of non-extractable NP and MCPA residues in organo-clay complexes	137
37 Litter effects on N dynamics and potential leaching in acid grassland soils	141
38 Mechanisms controlling dynamics at the soil-water interface	145
39 Method for water extractable phosphorous in saline-sodic soils	149
40 Microbial dynamics in soils under long-term glyphosate tolerant cropping systems	153
41 Multivariate evaluation by microbiological indicators of winter-summer crop rotation and no-tillage system in Oxisol (Brazil)	157
42 Nickel Speciation in Serpentine Soils using Synchrotron Radiation Techniques	160
43 Nitrate reduction in the interactive reaction system of L17 and soil minerals	163
44 Phenolic compounds in NaOH extracts of UK soils and their contribution to antioxidant capacity	167
45 Phosphate Dissolution Caused by Bioreduction of Poorly Crystalline Al(III)/Fe(III) Hydroxide Coprecipitated Minerals	171
46 Restructuring of biogeochemical interfaces: Role of cations and heat treatment	175
47 Retention of Na ⁺ Cations in Nanopores and Its Implications to Sodic Soils	179
48 Sensitive analysis of poly-carboxylic acids in soil solution by capillary electrophoresis after excimer-forming fluorescence derivatization	183
49 Soil microbial ecology of laurel-leaved and <i>Cryptomeria japonica</i> forests assessed by dilution plate count and direct microscopic count methods	187
50 Spectroscopic studies of ternary interactions in an öocyst-surfactant-hematite system	191
51 The biogeochemistry of Sphagnum mosses - the effects of substrate source on their phenolic composition	195
52 The Isolation and Characterization of Humic Substances and Humin from Grey Brown Podzolic and Gley Grassland Soils	198
53 The mobility and persistence of the insecticidal Cry1Aa toxin, Bt (<i>Bacillus thuringiensis</i>) in soils	202

Table of Contents (Cont.)

	Page
54 Topography and surface properties of clay minerals analyzed by atomic force microscopy	206
55 Tracing impact of pedogenic processes on soil solutions with Si and Mg isotopes	210
56 Use of elemental and isotopic ratios to distinguish between lithogenic and biogenic sources of soil mineral nutrients	214
57 Spatial Variability of Soil Nutrients and Microbial Biomass of Moso Bamboo Forest under Different Management Types	218

A study of adsorption of simple organic molecules onto inorganic soil components using DRIFTS

Joan Thomas^A and Michael Kelley^B

^{A,B}FEL Division, Jefferson Laboratory and Department of Applied Science; The College of William and Mary, Williamsburg VA 23187-8795, USA, Email thomasj@jlab.org; mkelley@jlab.org

Abstract

Diffuse Reflectance Infrared Spectroscopy (DRIFTS) was used to investigate the adsorption of simple carboxylic acids to the surface of kaolinite clay and to alumina. Dry powder samples were examined without evacuation or blending with KBr. Difference spectra were generated by subtraction of spectra of sample with and without treatment with organic. Resolution of organic peaks was achieved for coverage at 0.02 molecules per nm². Monolayer coverage of the organics on the minerals was determined from spectral analysis. The competitive adsorption of different organics was also investigated. Studies included adsorption from aqueous solution and or solution in hexane. Under ambient conditions, minerals have a surface layer of water approximately 3 molecules thick. The importance of this layer was shown by spectral features of salicylic acid deposited on γ -alumina (at sub monolayer coverage) from hexane being not distinguishable from those deposited from water. Spectral features associated with the carboxyl moiety were altered, in all cases, indicating a significant role in the adsorption mechanism. The results using hexane as solvent suggest surface adsorbed hydroxyl and molecular water, present on mineral oxides under ambient conditions, are a key determinant of interaction of an organic with the inorganic surface and of molecular adsorbate architecture.

Key Words

DRIFTS; oxide minerals; adsorption; carboxylic acids; surface water

Introduction

The adsorption of organic molecules onto mineral oxides is of fundamental importance for the understanding of environmental processes. The finely divided power form of these minerals (and of soils in general) is particularly suited to examination by DRIFTS but this technique has had limited use in obtaining quantitative information. DRIFTS has been used in the study of soils and soil components. Spark and Swift (2001), investigated humic materials isolated from a variety soils and analyzed for the relative distribution of component organics. Techniques, using DRIFTS, have been developed for soils to determine moisture content and total organic carbon (Janik *et al.*, 1998). An important approach of study is a carefully-constructed model system comprised of pure-phase organic compounds with polar functional groups, interacting with well characterized mineral forms. The spectral analysis of montmorillonite clay exposed to neat liquid organics onto montmorillonite has been reported (Parker and Frost, 1996, 1998), information regarding bonding was obtained as was multi-component analysis of mixtures of montmorillonite with different adsorbed organics.

In our studies mineral oxides including kaolinite, alumina and quartz, were selected. Kaolinite was chosen since this class of clay is a simpler starting model than the 'swelling' montmorillonite type clays which have interstitial layers of water; γ -alumina was used because of its structural similarities with kaolinite. The organics selected were simple molecules with different shapes, with or without polar functional groups. The solubility of salicylic acid (HO.C₆H₄.COOH) in both water and in hexane enabled an important focus of the study. Adsorption of myristic acid (C₁₃H₂₇.COOH) was also studied, including competitive adsorption with salicylic acid. Under atmospheric conditions, mineral oxide surfaces have hydroxyls and a layer of water ~3 molecules thick. This layer was sufficient to give DRIFT spectra consistent with data available from in situ ATR. In addition, results from our studies using hexane as solvent suggest that this water was a key determinant of the interaction of polar functional groups with the inorganic surface. The existence of a layer of water within the force field of the surface of clays (including kaolinite) was shown to exist by J.J. Fripiat *et al.*(1984); thermodynamic and NMR studies of clay in a gel showed two populations of water, free water in the pores, but also a second phase (a layer 3 molecules thick) directly influenced by the surface. More recent studies have been made of water on mica, including experimental studies (Cheng *et al.*, 2001) and modeling methods (Park and Sposito, 2002). The results again showed water interacting with the mica surface, the closest layers having strong lateral ordering, but overall the nature of the layer being liquid like. The special properties of the innermost layers extended to about 0.4 nm. The DRIFT technique used in our studies [Thomas and Kelley, 2008, 2009] gave spectra which were analyzed to provide quantitative information in addition to qualitative

information as to structure and bonding. DRIFT spectra were taken using samples neat (without mixing with KBr). For each sample, the spectrum of the adsorbed organic was highlighted by computing a difference spectrum of the mineral treated with organic and that of a mineral sample treated as in the same manner but without the organic (mineral “blank”). The use of samples without dilution with KBr allowed greater sensitivity as to the presence of adsorbed organic and eliminated the problem of a consistent distribution of sample in the KBr mix in achieving quantitative analysis.

Method

Sample preparation: Full details can be found in Thomas and Kelley (2008; 2009). To achieve approximately equal surface areas for each, 1.0 g of γ -alumina and 2.0 g of kaolinite were used giving an area of $53 \pm 1 \text{ m}^2$. For adsorption from aqueous solution, weighed samples of organic were dissolved in 0.1 M sodium perchlorate solution (prepared using purified water) to provide a consistent high ionic background. The pH was left at that generated by the solute. The pH of the corresponding ‘blank’ was adjusted to match the sample. Samples were also prepared using hexane as the solvent. The hexane blanks were checked for residual solvent after a 24 h drying period, by examining the $3000 - 2700 \text{ cm}^{-1}$ region for aliphatic carbon peaks. The samples were prepared and stored in glass vials or flasks and covered with foil to exclude light. Selected samples with excess organic remaining in solution were set aside and the solvent was permitted to evaporate (‘dried-down’). Samples for the study of competitive adsorption of salicylic and myristic acid were prepared such that each treating solution contained the same molar quantity of each organic.

Spectroscopy: In preparation for DRIFTS, samples were added to the cup with no dilution with KBr. Spectra were collected using a Nicolet NEXUS 670 spectrometer fitted with a SPECTRA-TECH “COLLECTOR II”, DRIFTS unit purged with air passed through a “BALSTON” air drier. The number of scans was set at 100 with a resolution of 4 cm^{-1} , over the range $4000 - 600 \text{ cm}^{-1}$. The aperture setting was 100 and the scan velocity 0.158 minutes per scan. These settings maximize the collection of the IR radiation but allow for a spectral resolution of 4 cm^{-1} . There was no use of automatic corrections. Quantitative analysis of DRIFT spectra required the use of Kubelka-Munk (KM) units in the graphical format calculated by instrument software from the recorded % transmission (Smith, 1996). Spectra of the materials treated with organic and the prepared blank were both collected against a KBr background spectrum. Changes to the surface due to the organic were highlighted by a “difference spectrum”, the spectrum of the organic treated mineral minus the spectrum of the mineral blank, computed by simple subtraction. When displaying multiple spectra baseline correction may have been performed and this is noted in the caption. Selected peaks were baseline corrected for determination of the peak height.

Results

Qualitative information as to bonding

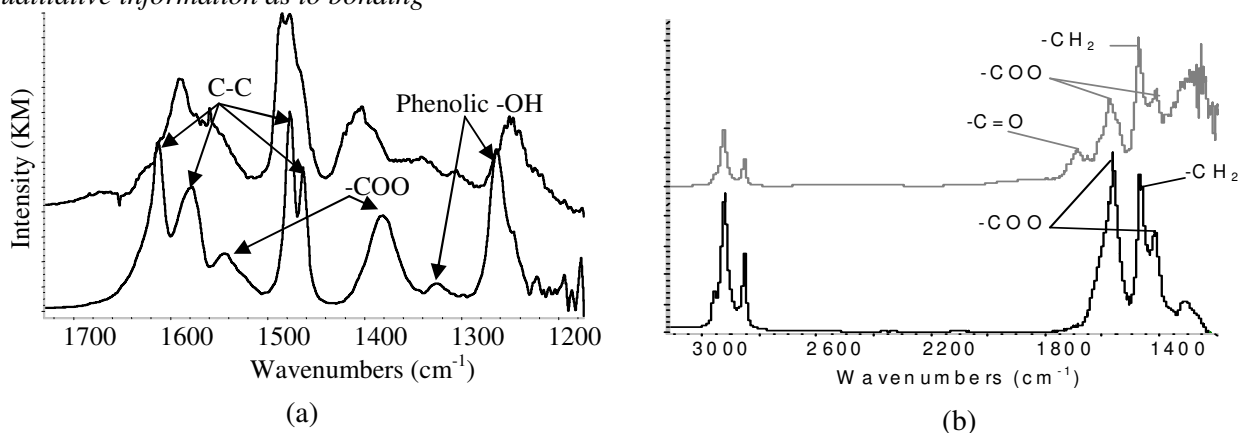


Figure 1. (a): Difference spectra for γ -alumina treated with salicylic acid (spectra both shown full scale and with displacement). UPPER (displaced, scale -1.0-2.2 KM) sample treated with excess salicylic acid and unwashed. LOWER- (scale 0-6 KM) washed sample. (b) DRIFT subtraction spectra of myristic acid adsorbed onto: kaolinite (grey, displaced, scale 0 – 1.0 KM); γ -alumina (black, scale 0-12 KM).

Quantitative information

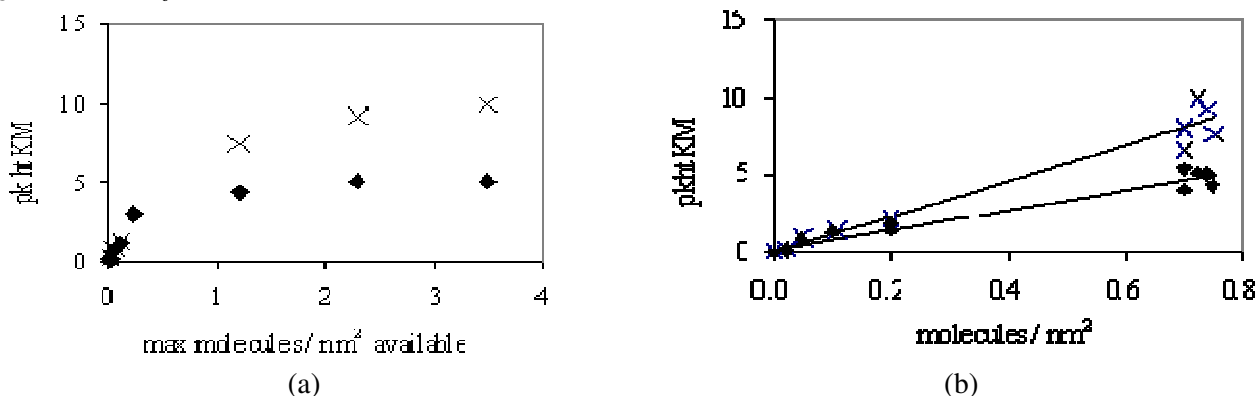


Figure 2. Correlation of carboxylate ('X' peak at 1382 cm⁻¹) and phenol group ('♦' peak at 1263 cm⁻¹) peak height with available molecules of salicylic acid in solution (a) and adsorbed (b) as determined by changes in solution concentration.

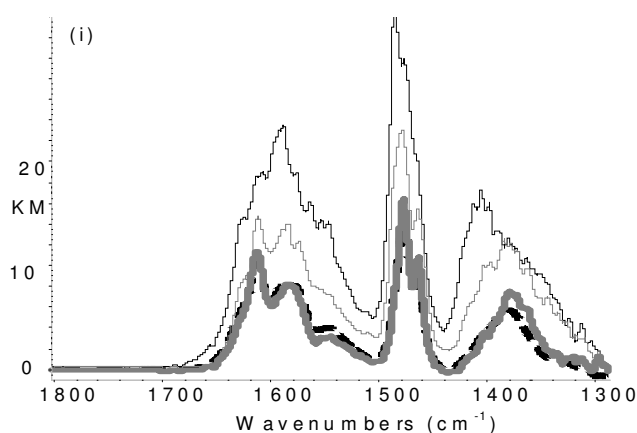


Figure 3. Spectra of γ -alumina with adsorbed salicylic acid from hexane solution. (Black) maximum loading for adsorption from hexane (~3.0 molecules/nm²); (grey) same sample with an additional short water rinse; (bold grey) same sample with 36 h water wash; (bold black dashed) sample prepared with an aqueous solution with analysis showing 0.7 molecules/nm² adsorbed.

Competitive adsorption

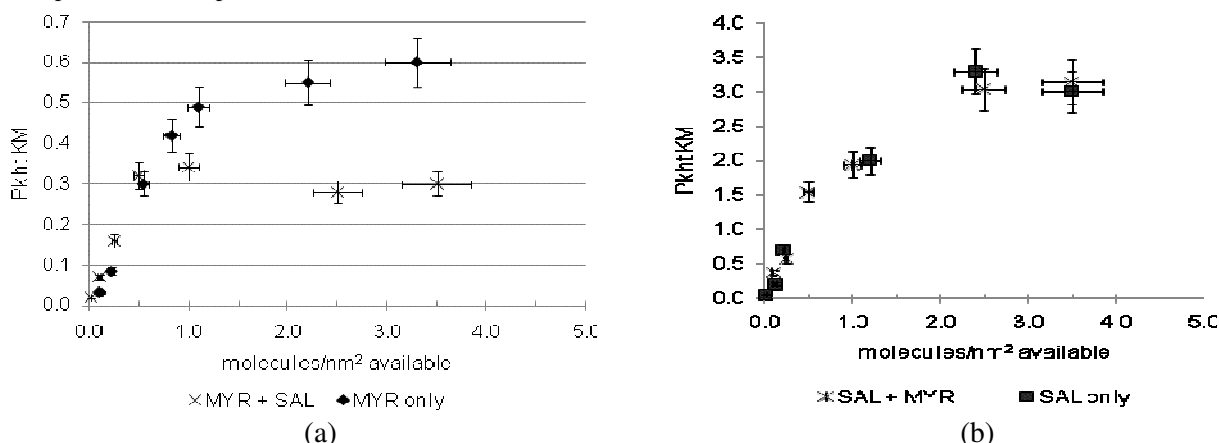


Figure 4(a): Variation in the height of the peak at 2926 cm⁻¹, arising from the alkyl chain, with the exposure of kaolinite samples to myristic acid in hexane either as the sole component or in combination with an equal quantity of salicylic acid. **4(b):** Variation in the height of the peak at 1476 cm⁻¹, arising from the aromatic ring, with the exposure of kaolinite samples to salicylic acid in hexane either as the sole component or in combination with an equal quantity of myristic acid (corrected was made for the contribution of myristic acid at this wavenumber).

Conclusions

The DRIFT technique used in our studies (Thomas and Kelley, 2008; 2009) gave spectra providing quantitative information (Figure 2) in addition to qualitative information (Figure 1) as to structure and bonding. The use of samples without dilution with KBr allowed greater sensitivity in detecting adsorbed organic and eliminated the problem of a consistent distribution of sample in the KBr mix in achieving quantitative analysis. The density of monolayer coverage of molecules adsorbed onto the mineral oxides was determined and detection limits of the order of 1-10 molecules per 100 nm² for γ -alumina were achieved.

Adsorption of salicylic acid from aqueous solution onto γ - alumina was as carboxylate, together with evidence of interaction of the phenol group with the surface. Of particular note was that when using hexane as the solvent, adsorption of salicylic and myristic acid as the carboxylate again occurs, indicating that the surface hydroxyl groups and adsorbed water strongly influence the interaction of the polar groups with the surface. There was no clear evidence of the carbonyl group on the surface of either mineral for the hexane washed samples. The maximum loading of salicylic acid adsorbed onto γ - alumina and kaolinite, was in the range of 2 - 4 molecules /nm² when hexane was used as the solvent compared with 0.1 – 0.7 molecules /nm² for aqueous solution. Water washing the samples prepared with hexane decreased the coverage to the maximum level observed with adsorption from aqueous solution. In the case of γ - alumina, adsorption of the organic above the maximum level observed with aqueous solution was accompanied by new peaks for the ring and each of the functional groups. These were the peaks removed by water washing. The position of the phenol group for organic adsorbed to these sites indicated less hydrogen bonding with the surface. The ready removal of this extra material with water also indicated a weaker interaction of the carboxylate group with the surface. These observations support hexane allowing adsorption onto the same set of sites accessible from aqueous solution and, when these are all occupied, allowing interaction with other less favourable sites. The results of quantitative studies using hexane as the solvent, were used as calibration in the study of the competitive adsorption of salicylic and myristic acids onto γ -alumina and kaolinite. Peaks unique to the ring or the chain were selected for analysis. The surface loading of salicylic acid was not influenced by the presence of myristic acid on either mineral but the maximum loading of myristic acid was decreased (46 - 50 %) by salicylic acid. A 25 % increase in the maximum loading was observed for kaolinite, but not for γ -alumina. Displacement of myristic acid from γ -alumina, but not kaolinite, was observed when excess salicylic acid remained in solution. On γ -alumina, after a loading of 1 molecule per nm², increased exposure resulted in salicylic acid adsorption only, this value being approximately the same as for salicylic acid adsorption from aqueous solution or for water washed hexane treated samples. Thus a set of sites for adsorption of either acid is indicated together with other energetically less favourable sites, which can be occupied by salicylic, but not by myristic, acid.

References

- Cheng L, Fenter P, Nagy KL, Schlegel ML, Sturchio NC (2001) Molecular-scale density oscillations in water adjacent to a mica surface. *Phys. Rev. Lett.* **87-15**, 156103.
- Fripiat JJ, Letellier M, Levitz P (1984) Interaction of water with clay surfaces. *Phil. Trans. R. Soc. Lond. A.* **311**, 287-299.
- Janik LJ, Merry RH, Skjemstad JO (1998) Can mid infrared diffuse reflectance analysis replace soil extractions, *Australian Journal of Experimental Agriculture*, **38**, 681.
- Park S-Ho, Sposito G (2002) Structure of water adsorbed on a mica surface. *Phys. Rev Lett.* **89-8**, 085501
- Smith BC (1996) Fundamentals of Fourier Transform Infrared Spectroscopy, CRC Press, Boca Raton FL.
- Parker RW, Frost RL (1996) The application of DRIFT spectroscopy to the multicomponent analysis of organic chemicals adsorbed on montmorillonite, *Clays and Clay Minerals*, **44-1**, 32-40.
- Parker RW, Frost RL (1998) Monitoring the sorption of propanoic acid by montmorillonite using diffuse reflectance Fourier transform infrared spectroscopy, *Fourier Transform Spectroscopy: 11th International Conference*, J.A.de Haseth (Ed), The American Institute of Physics 1-56396-746-4/98.
- Spark KM, Swift RS (2001) Analysis of the molecular weight fractions of a soil humic acid using DRIFT spectroscopy. In, *Understanding and Managing Organic Matter in Soils, Sediments and Waters*, R.S. Swift and K.M. Spark (Eds) IHSS.
- Thomas JE, Kelley MJ (2008) Interaction of mineral surfaces with simple organic molecules by diffuse reflectance IR spectroscopy (DRIFT). *J. Colloid Interface Sci.* **322-2**, 516.
- Thomas JE, Kelley MJ (2009) The adsorption of salicylic acid onto γ -alumina and kaolinite from solution in hexane studied using diffuse reflectance IR spectroscopy (DRIFT). *J. Colloid Interface Sci.* **338-2**, 389.
- Thomas JE, Kelley MJ (2009 submitted) A study of competitive adsorption of organic molecules onto mineral oxides using DRIFTS. *J. Colloid Interface Sci.*

Admixture of *Alnus subcordata* with *Populus euramericana* improved soil nitrogen

Ehsan Sayad

Forestry Department, Higher Education Complex of Behbahan, Iran, Email ehsansaiad@yahoo.com

Abstract

Concerns about the decline in soil fertility and long-term productivity of fast-growing plantations have promoted interest in using nitrogen-fixing trees in mixed species plantations. Plantations of monoculture *Populus euramericana* and mixed with *Alnus subcordata* were planted in 1987 in Noor, Iran. After 16 years, the effects of species interactions on soil properties were assessed. The results indicated that soil nitrogen, C: N ratio and organic matter at 0-15 cm and 15-30 cm depth of mixed plantation were higher. It can be conclude that admixture of *Alnus subcordata* with *Populus euramericana* improved soil fertility.

Key Words

Nitrogen fixing trees (NFT), mixed plantation, soil fertility, *Populus euramericana*, *Alnus subcordata*

Introduction

Poplars (*Populus* L. spp.) are preferred plantation species, because their fast growth is expected to meet the extensive demands of wood for poles, pulp and fuel (Kiadaliri 2003; Ghasemi 2000; Ziabari 1993). Productivity of plantations depends strongly on soil nutrient supply and may be malleable under the influence of management practices and species (Binkley 1997). Almost all the industrial plantations are monocultures, and questions are being raised about the sustainability of their growth and their effects on the site (Khanna 1997). Repeated harvesting of fast-growing trees such as poplar plantations on short rotations may deplete site nutrients. Nitrogen losses are likely to be very important for future growth. It is therefore appropriate to explore new systems of plantation management in which N may be added via fixation (Khanna 1997). Mixed plantation systems seem to be the most appropriate for providing a broader range of options, such as production, protection, biodiversity conservation, and restoration (Montagnini *et al.* 1995; Keenan *et al.* 1995; Guariguata *et al.* 1995; Parrotta and Knowles 1999).

A mixture of species, each with different nutrient requirements and different nutrient cycling properties, may be overall less demanding on site nutrients than monoculture stands (Montagnini 2000). Concerns about the decline in soil fertility and long-term productivity of fast-growing plantations have promoted interest in using nitrogen-fixing trees in mixed species plantations (Rhoades and Binkley 1996). Nitrogen-fixing trees, mainly leguminous species, have been widely extolled for their soil-improving characteristics related to their production of nitrogen-rich, often rapidly decomposing leaf litter (Parrotta 1999). Experiments in some parts of world such as North America have shown enhanced growth of *Populus* spp. when grown as an intercrop with *Alnus* L. spp. (FAO 1992, Coté and Camiré 1987, Hansen and Dawson 1982, Radwan and DeBell 1988). The present study was undertaken to assess the influence of *Alnus subcordata* C.A.Mey and *Populus Euramericana* (Dode) Guinier plantations on soil fertility parameters.

Methods

Site characteristics

The study area is located at the Chamestan experiment station, in Mazandaran province, on the northern parts of Iran (36°29' N, 51°59' E). Experimental plots were located at an altitude of 100 m above sea level and with low slope (0–3%). Annual rainfall averages 803 mm, with wetter months occurring between September and February, and a dry season from April to August monthly rainfall usually averages < 40 mm for 4 months. Average daily temperatures ranges from 11.7 °C in February to 29.5 °C in August. The soils are well-drained, and have a silty loam texture with a pH 7.6–8.1. Previously (approximately 50 years ago) this area was dominated by natural forests containing native tree species such as *Quercus castaneifolia* C.A.Meyer., *Gleditschia caspica* Desp., *Carpinus betulus* L., etc. The surrounding area is dominated by agricultural fields and commercial building.

Experimental Design

Plantations of monoculture *Populus euramericana* and mixed with *Alnus subcordata* (50% *P. Euramericana* + 50% *A. subcordata* (50P:50A)), were established in 1987 in Noor, Iran. Tree spacing within plantations was 2 m × 2 m and two species were systematically mixed between rows. Containerized seedlings, 50–100 cm in height, were used for planting in April 1996. Seedlings of both species were planted simultaneously in monocultures and mixed plantations. Two plantations are beside each other and each of them is about 2 hectare. The control area was in near unmanaged land.

Soils

Soils were randomly sampled from four points in both plantations and control area. Samples were taken to a depth of 60 cm in both plantations in August using a 7.6 cm diameter core sampler (n = 3 cores/plot). Soil samples were taken at two 15 cm and a 30 cm interval. After air drying, soils were passed through a 2.0 mm (20 mesh) sieve to remove roots prior to chemical analyses. Soil organic matter was determined using the Walkley-Black method. Total N was determined using the Kjeldhal method.

Statistical analyses

One-way analyses of variance (ANOVA) were used to compare soil properties among experimental treatments. The Duncan test was used to separate the means of dependent variables which were significantly affected by treatment.

Results

Organic matter was different between 0–15 cm depth for monoculture and mixed plantations, whereas no significant differences were found in deeper soil layer ($p < .08$, Duncan) (Figure 1,a). Total nitrogen had a significant difference between the treatments in 0–15 cm and 15–30 cm soil layers, whereas no significant difference was found in 30–60 cm depth. Total nitrogen in 0–15 cm depth was significantly higher in the mixed plantation ($p < .05$, Duncan) (Figure 1,b). C:N ratio show significant differences between the treatments in 0–15 cm and 15–30 cm depth of soil but not in 30–60 cm depth (Figure 1,c).

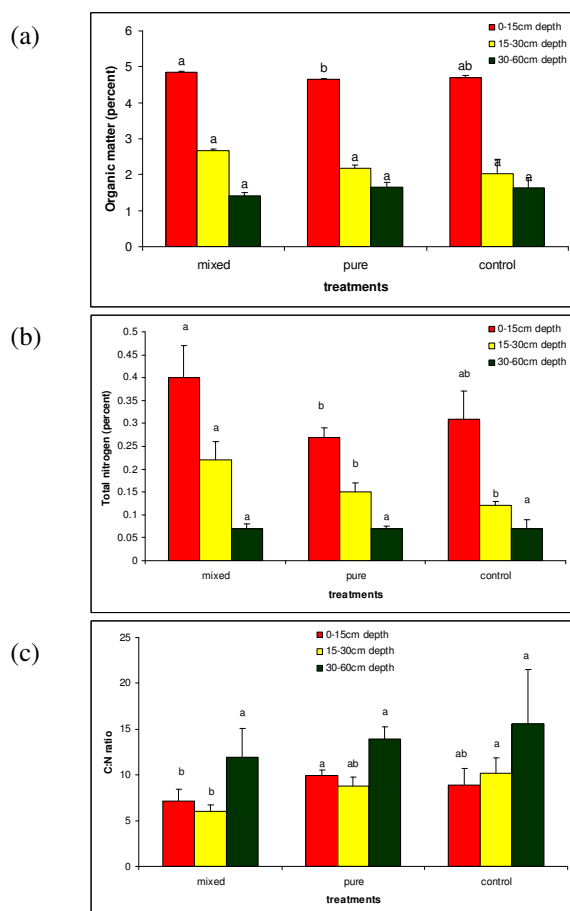


Figure 1. a) organic matter(percent), b) total nitrogen, c) C:N ratio The letters on different column indicate a significant difference. Mean values with the same letter within a tree species do not differ significantly from each other.

Conclusion

Higher Organic matter was observed in the 0-15 cm soil layer for the mixed plantation. This could be due to *Alnus* increasing soil nitrogen in 0-15cm, which is a positive influence of mixed plantations with *Alnus* as an N-fixing tree on nutrition (Fisher and Binkley 1999). The main reason that there was not any significant differences in the deeper soil layer might be the result of higher biological activity in the top soil. Parrotta (1999) came to the same conclusion. Total nitrogen was significantly higher in mixed plantations in comparison with monoculture plantations of *Populus euramericana*. The increase in soil nitrogen of mixed plantations might be the result of nitrogen fixation by nodules of *Alnus* roots and higher litter decomposition rate. Binkley (1997) and Garcia-Montiel and Binkley (1998) found that *Albizia* increased soil nitrogen more than *Eucalyptus*. Parrotta (1999) and to some extent Montagnini (2000) did not observe any significant differences in soil nitrogen between monocultures and mixed plantations. Hansen and Dawson (1982) observed that mixed plantations of *Populus* and *Alnus glutinosa* resulted in increasing soil nitrogen in comparison with their monoculture plantations (FAO 1992). Significant differences were observed in the C:N ratio. The main reason might be N-fixation by *Alnus* in mixed plantations that resulted in increasing nitrogen. Parrotta (1999) obtained the same result for monocultures and mixed plantations of *Eucalyptus* and two NFTs. Finally we can conclude that mixed plantations of these two species improved soil fertility.

References

- Binkley D (1997) Bioassays of the influence of *Eucalyptus saligna* and *Albizia falcataria* on soil nutrient supply and limitation. *Forest Ecology and Management* **91**, 229–234.
- Coté B, Camiré CC (1987) Tree growth and nutrient cycling in dense plantings hybrid poplar and black alder. *Canadian Journal of Forest Research* **17**, 516–523.
- FAO (1992) 'Mixed and pure forest plantation in the tropics and subtropics'. FAO Forestry Paper 103. (FAO: Rome)
- Fisher R, Binkley D (1999) 'Ecology and management of forest soil'. 3rd edition. (JohnWiley and Sons, Inc.).
- Garcia-Montiel DC, Binkley D (1998) Effect of *Eucalyptus saligna* and *Albizia falcataria* on soil processes and nitrogen supply in Hawaii. *Oecologia* **113**, 547–556.
- Ghasemi R (2000) Study of phenology of different *Populus* in Karaj and Safrabasteh Gilan. M.Sc. thesis, Tarbiat Modarres University.
- Guariguata MR, Rheingans R, Montagnini F (1995) Early woody invasion under tree plantations in Costa Rica: implications for forest restoration. *Restoration Ecology* **3**, 252–260.
- Hansen EA, Dawson JO (1982) Effect of *Alnus glutinosa* on hybrid poplar height growth in a shortrotation intensively cultured plantations. *Forest Science* **28**, 49–59.
- Keenan RJ, Lamb D, Sexton G (1995) Experience with mixed species rainforest plantations in North Queensland. *Commonwealth Forestry Review* **74**, 315–321.
- Khanna PK (1997) Comparison of growth and nutrition of young monocultures and mixed stands of *Eucalyptus globules* and *Acacia mearnsii*. *Forest Ecology and Management* **94**, 105–113.
- Kiadaliri Sh (2003) Study of populus plantations on different soils in western parts of Mazandaran. M.Sc. thesis, Tarbiat Modarres University.
- Montagnini F (2000) Accumulation in above-ground biomass and soil storage of mineral nutrients in pure and mixed plantations in a humid tropical lowland. *Forest Ecology and Management* **134**, 257–270.
- Montagnini F, Gonzalez E, Rheingans R, Porras C (1995) Mixed and pure forest plantations in the humid neotropics: a comparison of early growth, pest damage and establishment costs. *Commonwealth Forestry Review* **74**, 306–314.
- Parrotta JA (1999) Productivity, nutrient cycling, and succession in single- and mixed-species plantations of *Casuarina equisetifolia*, *Eucalyptus robusta*, and *Leucaena leucocephala* in Puerto Rico. *Forest Ecology and Management* **124**, 45–77.
- Parrotta JA, Knowles OH (1999) Restoration of tropical moist forests on bauxite-mined lands in the Brazilian Amazon. *Restoration Ecology* **7**, 103–116.
- Radwan MA, DeBell DP (1988) Nutrient relations in coppiced black cottonwood and red alder. *Plant and Soil* **106**, 171–177.

Rhoades C, Binkley D (1996) Factors influencing decline in soil pH in Hawaiian Eucalyptus and Albizia plantations. *Forest Ecology and Management* **80**, 47–56.

Ziabari ZF (1993) The importance of Populus in forestry. In 'Proceedings of forest restoration and forestry'. (Research Institute of Forests and Range Lands publication: Iran).

Mechanisms controlling dynamics at the soil-water interface

Dörte Diehl, Gabriele E. Schaumann

Department of Environmental and Soil Chemistry, Institute for Environmental Sciences, University Koblenz-Landau, Landau, Germany.
Email diehl@uni-landau.de

Abstract

Since the characteristics of the soil-water interface are not static but continuously changing, the relevant processes and mechanisms have a high impact on habitat, filter, buffer, storage and transformation functions. Linking the individual results and conclusions of recent studies regarding the dynamics of wetting characteristics under changing environmental conditions as water content (WC), pH and drying and wetting temperature of two contrasting anthropogenic sites in Berlin (Germany), lead to two hypothetical models explaining differences in the nature of repellency between the sites and between wettable and repellent samples within each site. The chemical nature of repellency found at the one site can be best explained by hydrolysis-condensation reactions. The physicochemical nature of repellency on the other site seems to be controlled by the arrangement of amphiphilic molecules as micelles or reverse micelles during the drying process. The surface characteristics of the so formed layers on the soil particle surfaces depend on number and size of amphiphilic molecules, pH and ionic strength in the soil solution.

Probably, specific local soil characteristics determine which mechanism dominates and controls the nature of repellency. Thus, critical conditions which may favour SWR may be identified.

A challenge for the further research is the development of methods which may verify the suggested mechanisms with model substances as well as with complex natural soil samples and to verify the relevance of the suggested mechanisms for soils of differing soil-type, climate, and land-use.

Key Words

Soil water repellency, pH, wetting, drying, activation energy, amphiphile

Introduction

Surface characteristics of soils are one of the main factors controlling processes at the soil-water interface like wetting, sorption or dissolution processes and, thereby, have a high impact on natural soil functions like habitat, filter, buffer, storage and transformation functions. Since surface characteristics are not static soil properties but continuously changing, the relevant processes and mechanisms are in the focus of the presented study. These mechanisms help to gain further insight into the behaviour of soil and its dynamics under changing environmental conditions.

In recent studies, the wetting and surface characteristics of soils from two contrasting anthropogenic sites, the former sewage disposal field Berlin-Buch and the inner-city park Berlin-Tiergarten were investigated with regard to their dependence on environmental parameters such as water content (WC), pH and drying and wetting temperature of wettable and repellent soils (Hurraß & Schaumann, 2006; Bayer & Schaumann, 2007; Diehl & Schaumann, 2007; Diehl *et al.*, 2009; Diehl *et al.*, submitted).

The aim of the present discussion is to link the individual results and conclusions of these studies with each other and to find a more general explanation for dynamics at the soil-water interface.

Results

The overview of main results obtained at the two sites Buch and Tiergarten (Table 1) not only shows a correlation of repellency with environmental conditions but also highlights principal differences in responses of repellency to changes in environmental conditions between the respective sites:

In Buch samples, drying resulted in an approach of SWR of initially wettable and repellent samples. Higher drying temperatures lead to an increased degree of surface hydrophobicity. Since wetting, the reverse process, requires high activation energy, the surface hydrophobization is probably controlled by chemical processes which are strongly linked with changes in water content. The effect of pH on repellency is only observable when moisture status of samples remained unchanged during artificial pH alteration.

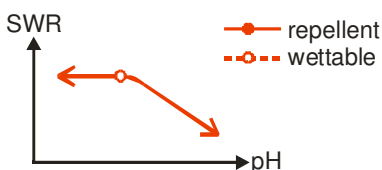
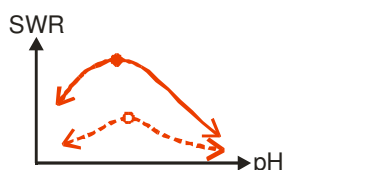
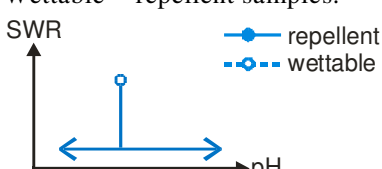
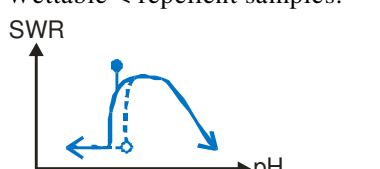
In Tiergarten samples, repellency differences between initially wettable and repellent samples remain following drying under various conditions as well as following artificially induced pH changes via gas phase. These differences disappear only after addition of liquid NaOH. In contrast to Buch samples, repellent Tiergarten samples have a lower pH and a higher EC in its aqueous extracts than wettable samples and the wetting process requires activation energy in the range of physicochemical processes.

Discussion

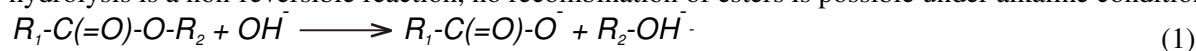
Chemical nature of repellency in Buch samples

To our current knowledge, hydrolysis-condensation reactions can be best explaining the nature of repellency of Buch samples (Table 1). Ester hydrolysis has already been suggested as a possible chemical reaction in the course of wetting of water repellent samples (Todoruk *et al.*, 2003). Bound by ester groups, aliphatic dicarboxylic acids may act as bridges between alkyl chains and fatty acids, alcohols and aromatic acids and may be disrupted by base catalysed hydrolysis (Grasset & Amblès, 1998) leading to an increasing number of carboxylate groups, i.e., an increasing number of charged sites at the SOM surface and thus an increased wettability.

Table 1 Overview of the main observations of differences in soil characteristics and in responses on changes in environmental conditions between wettable and repellent samples from Buch and Tiergarten

	Buch	Tiergarten
Drying (Diehl <i>et al.</i> , 2009)	Increases repellency; differences between wettable and repellent samples decrease.	Increases repellency; differences between wettable and repellent samples remain.
High drying temperature (Diehl <i>et al.</i> , 2009)	Increases surface hydrophobicity (DRIFT-CH _N).	Does not significantly affect surface hydrophobicity (DRIFT-CH _N).
Activation energy of wetting (Diehl & Schaumann, 2007)	65-94 kJ mol ⁻¹ Chemical reactions.	8-42 kJ mol ⁻¹ Physicochemical processes.
pH alteration via gas phase: - exposition to NH ₃ or gaseous HCl enriched atmosphere (Diehl <i>et al.</i> , submitted)	 <p>Wettable = repellent samples.</p>	 <p>Wettable < repellent samples.</p>
pH alteration via liquid phase: - addition of liquid NaOH or HNO ₃ solution (Bayer & Schaumann, 2007)	 <p>Wettable = repellent samples.</p>	 <p>Wettable = repellent samples.</p>
Field pH (Hurraß & Schaumann, 2006)	No significant relation with SWR.	Repellency only with pH < 4.6.
Electrical conductivity (Hurraß & Schaumann, 2006)	No significant relation with SWR.	Higher conductivity for repellent samples.
Surface tension of aqueous extracts (Hurraß & Schaumann, 2006)	Lower surface tension for repellent samples.	Lower surface tension for repellent samples.

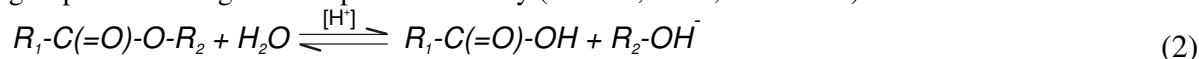
The base catalysed hydrolysis (Equation 1) is an irreversible process (Schmeer *et al.*, 1990) and follows two competing reaction pathways in its second step. The one is characterised by a direct proton transfer, and the other by a water-assisted proton transfer through which the energy barrier for the decomposition is significantly lower than through the direct proton transfer (Zhan *et al.*, 2000). Thus, under dry conditions, these reactions are slow and accelerated only by increasing OH⁻ concentration, i.e. with increasing pH. This may explain why the dry Buch samples develop increasing wettability with increasing pH after treatment with gaseous NH₃ (Table 1, Buch, red curve). The presence of water accelerates alkaline hydrolysis reactions (Zhan *et al.*, 2000). This could explain why Buch samples are completely wettable after addition of liquid NaOH and subsequent incubation for 1 week at 20°C in closed containers (Bayer & Schaumann, 2007); (Table 1, Buch, blue curve). Since alkaline hydrolysis is a non-reversible reaction, no recombination of esters is possible under alkaline conditions:



In contrast, long-term drying and drying at elevated temperatures under the original acidic pH conditions led to enhanced esterification and to an establishment of cross-linking, e.g. between carboxylic and hydroxyl functional groups. This has been observed in solid state reactions between carboxylic acids and hydroxyl-groups of cellulosic material (Pantze *et al.*, 2008) and could explain why samples from Buch which reveal significant differences in wettability in field moist state reached a comparable degree of repellency after long-term drying

or after drying at elevated temperatures.

A reduction in pH favours acidic catalysed hydrolysis (Equation 2) which is a reversible process driven by excess or deficiency of water. The ester concentration at the equilibrium point is independent from the pH but highly depends on the amount of available water. The pH solely determines the rate at which the equilibrium is reached. This can explain why the repellency of dry Buch samples remains constant with decreasing pH (Table 1, Buch, red curve). Only the addition of liquid acid solution (Bayer & Schaumann, 2007) provides the excess of water necessary for shifting the equilibrium towards a significantly higher number of hydroxyl and carboxyl groups and leading to a complete wettability (Table 1, Buch, blue curve).



The suggested mechanism is not restricted to esterification but generally includes hydrolysis-condensation reactions which in SOM can occur between a variety of substances, e.g., carbohydrates, proteins, lipids etc.

Physicochemical nature of repellency in Tiergarten

The physicochemical nature of repellency in Tiergarten linked with differences in pH, electrical conductivity (EC) and surface tension in aqueous extracts between wettable and repellent samples may be best explained by changes in the spatial orientation of amphiphilic molecules on the soil particle surface during wetting and subsequent drying:

At high ionic strength, repulsion forces between charged functional groups are effectively shielded by the counter ions (Fleer *et al.*, 1993). This allows charged groups to stay closer to each other and leads to more compact structures at the water-air interface. Upon drying, water evaporates slowly from the outside to the inside of the hydrated SOM surface layer. Hydrophilic groups orientate towards the inwards receding water front whereas hydrophobic chains orientate towards the air (Swift, 1999; Horne & McIntosh, 2000). Smaller, water-soluble amphiphilic molecules may form a hydrophobic layer by micelle-like intermolecular aggregations at the surface (Terashima *et al.*, 2004); (Figure 1, top).

At low ionic strength, a smaller amount of amphiphilic molecules may enrich at the water-air interface resulting in a higher concentration in the solution. This leads to the formation of micelles when critical micelle concentration is reached. Upon drying, hydrophilic groups tend to stay as long as possible in contact with water avoiding approaching each other, and form an outward directed hydrophilic layer (Figure 1, bottom).

These mechanisms may also explain how the addition of liquid NaOH solution may transform wettable into repellent samples. Thereby not only pH but also ionic strength increases and may therefore induce a change in conformational arrangement of amphiphilic molecules at the SOM surface. Despite increasing pH and an increasing number of negatively charged groups, repellency persists within a certain pH range because the ionic strength also increases. At a higher pH, deprotonation overbalances the effects of ionic strength. Thus, in a pH range above 7, repulsion forces cannot be effectively weakened leading to an aggregation of hydrophobic groups and surface exposition of hydrophilic groups (Table 1, Tiergarten, blue curve).

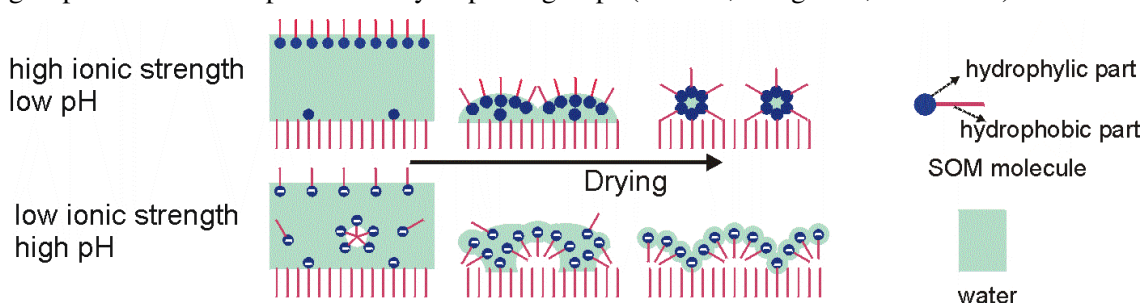


Figure 1 Suggested model of orientation of amphiphilic organic molecules at the SOM surface during drying in dependence of pH and ionic strength of the soil solution

Conclusion

The differences in the nature of repellency between the sites and between wettable and repellent samples within each site help to draw some conclusions on the appearance of SWR and on the factors which determine the degree and nature of SWR.

The two suggested mechanisms of chemical and physicochemical control of repellency are probably not restricted to one of the two sites but occur in some degree on both sites. Furthermore, it cannot be excluded that additional mechanisms play an important role for repellency at other sites. Specific local soil characteristics determine which mechanism dominates and controls the nature of repellency. However, the two suggested mechanisms together with the previous history of the sites allow identifying critical conditions which may favour SWR: Long hot and dry periods may enhance soil water repellency especially in soils with low pH and

high organic accumulation. In these soils chemically bonded water can be released from organic matter by condensation reactions. Rewetting requires high activation energy, i.e. it is slow at ambient temperatures but can be accelerated by elevated temperature as long as the water does not evaporate. Special care is also needed in soils with a relatively high salt concentration, a low pH, and a SOM containing a relatively high amount of water soluble amphiphilic molecules. The combination of high ionic strength and low pH in the soil solution can favour the appearance of SWR after drying.

In order to verify the suggested mechanisms, further investigations are needed. On the one hand, smaller-scaled methods are required to investigate the respective processes in molecular range, starting with model substances and extending these methods to complex natural soil samples. On the other hand, the relevance of the identified processes for a wide ranges of climates, soil types and land-use has to be tested and, eventually, additional relevant processes to be identified.

References

- Bayer, J.V. & G.E. Schaumann. 2007. Development of soil water repellency in the course of isothermal drying and upon pH changes in two urban soils. *Hydrological Processes*, 21, 2266 - 2275. DOI:10.1002/hyp.6759.
- Diehl, D., J.V. Bayer, S.K. Woche, R. Bryant, S.H. Doerr & G.E. Schaumann. submitted. Reaction of soil water repellency on artificially induced changes in soil pH. *Geoderma*.
- Diehl, D., R.H. Ellerbrock & G.E. Schaumann. 2009. DRIFT-Spectroscopy of untreated and dried soil samples of different wettability. *European Journal of Soil Science*, 60, 557-566. DOI:10.1111/j.1365-2389.2009.01150.x.
- Diehl, D. & G.E. Schaumann. 2007. Wetting mechanism assessed from time dependent sessile drop shape. *Hydrological Processes*, 21, 2255 - 2265. DOI:10.1002/hyp.6745.
- Fleer, G.J., M.A.C. Stuart, M.H.M. Scheutjens, T. Cosgrove & B. Vincent. 1993. *Polymers at interfaces*. Chapman & Hall, London.
- Grasset, L. & A. Amblès. 1998. Structure of humin and humic acid from an acid soil as revealed by phase transfer catalyzed hydrolysis. *ORGANIC GEOCHEMISTRY*, 29, 881-891. DOI:10.1016/S0146-6380(98)00193-4
- Horne, D.J. & J.C. McIntosh. 2000. Hydrophobic compounds in sands in New Zealand—extraction, characterisation and proposed mechanisms for repellency expression. *Journal of Hydrology*, 231-232, 35-46. DOI:10.1016/S0022-1694(00)00181-5
- Hurraß, J. & G.E. Schaumann. 2006. Properties of soil organic matter and aqueous extracts of actually water repellent and wettable soil samples. *Geoderma*, 132, 222-239. DOI:10.1016/j.geoderma.2005.05.012
- Pantze, A., O. Karlsson & U. Westermark. 2008. Esterification of carboxylic acids on cellulosic material: Solidstate reactions. *Holzforschung*, 62, 136–141. DOI:10.1515/HF.2008.027.
- Schmeer, G., S. Riembauer & J. Barthel. 1990. The influence of hydrophobic solvation on the alkaline hydrolysis of ethyl esters of polar substituted 2-methylpropionic acids in water. *Journal of Solution Chemistry*, 19, 1175-1189. DOI:10.1007/BF00652543.
- Swift, R.S. 1999. Macromolecular properties of soil humic substances: fact, fiction, and opinion. *Soil Science*, 164, 790-802.
- Terashima, M., M. Fukushima & S. Tanaka. 2004. Influence of pH on the surface activity of humic acid. Micelle-like aggregate formation and interfacial adsorption. *Colloids and Surfaces, A: Physicochemical and Engineering Aspects*, 247, 77-83. DOI:10.1016/j.colsurfa.2004.08.028
- Todoruk, T.R., M. Litvina, A. Kantzas & C.H. Langford. 2003. Low-Field NMR Relaxometry: A Study of Interactions of Water with Water-Repellant Soils. *Environmental Science and Technology*, 37, 2878-2882.
- Zhan, C.-G., D.W. Landry & R.L. Ornstein. 2000. Reaction Pathways and Energy Barriers for Alkaline Hydrolysis of Carboxylic Acid Esters in Water Studied by a Hybrid Supermolecule-Polarizable Continuum Approach. *Journal of American Chemical Society*, 122, 2621-2627. DOI:10.1021/ja9937932.

Biomolecular complexation affects microbial adhesion to iron (oxyhydr)oxides

Jon Chorover and Xiaodong Gao^A

^ADepartment of Soil, Water and Environmental Science, University of Arizona, Tucson, USA Email chorover@cals.arizona.edu

Abstract

Interfacial reactions in soil biogeochemical systems are often mediated by microorganisms that become directly attached or closely associated with mineral and organic surfaces. Elucidation of mechanisms of microbe-mineral interactions at the molecular-scale requires the use of *in situ* molecular spectroscopy. We have employed attenuated total reflectance Fourier transform infrared (ATR-FTIR) spectroscopy to identify the types of molecules and the nature of bonds that mediate interaction between surficial biomolecules and mineral surface functional groups for a variety of systems of interest. This paper reviews our recent research on biomolecule-iron oxide interactions, with a particular emphasis on adhesion of extracellular polymeric substances (EPS), bacterial cells (*Pseudomonas aeruginosa*, *Bacillus subtilis*), and pathogenic protozoa (*Cryptosporidium parvum*). Evidence for direct, inner-sphere complexation of biomolecular functional groups is discussed, and linkages are made to macro-scale transport phenomena.

Key Words

Biogeochemical interfaces, mineral-microbe interaction, ATR-FTIR spectroscopy, biomolecule adsorption

Introduction

Microbial cells, especially bacteria and protozoa, can be transported over relatively long distances in porous media prior to attaching to mineral or organic surfaces (Hornberger *et al.* 1992; Schafer *et al.* 1998; Redman *et al.* 2004). Bacterial adhesion often involves the coating of substrata and eventually of growing cells with extracellular polymeric substances (EPS), i.e., an incipient biofilm that evolves into a complex micro-environment at the solid-water interface. Because of the diversity of biomolecular and mineral surface structures and functionalities, their mutual interactions have the potential to involve a multitude of biomolecule-surface interactions that can contribute to or diminish cell-surface adhesion. Steric and dispersion forces similar to those that act on bare and polymer-coated surfaces, are superimposed on wide range of localized molecular bonding possibilities (hydrophobic, van der Waals, ion bridging, covalent).

As a result of the predominance of weakly acidic carboxyl, phosphoryl, and hydroxyl functional groups, microbial surfaces tend to exhibit net negative charge over a wide pH range representative of natural waters. Thus, individual microbial cells may be transported over long distances in porous media. This can be beneficial when contaminant remediation requires microbiological augmentation (Scow and Hicks, 2005). Or, it can be detrimental when it involves the transport of pathogenic microbes (e.g., *Cryptosporidium sp.*, *Giardia sp.*, or *Escherichia coli*). Recent history contains several cases where pathogens have been transported in aqueous suspension through porous geomeedia and into community water supplies (Curriero *et al.* 2001). Hence, an understanding of adhesion processes is essential. Mean field models, based on Derjaguin-Landau-Verwey-Overbeek (DLVO) theory of reactive particle transport and adhesion to surfaces, do not closely match experimental adhesion measurements because key interaction mechanisms of bio-particles and mineral surfaces are not included among the classical DLVO (van der Waals and electrostatic) forces (Ginn *et al.* 2002). More effective data fits for *E. coli* adhesion to silica, for example, were made when models included a steric term to account for the “polymer brush” surface of microbial cells (Camesano and Logan, 2000). Toward the goal of better predicting adhesion processes, our work has focused on developing an understanding of molecular-scale bonding interactions using *in situ* spectroscopy of these biogeochemical interfaces.

Biomolecular Bonding to Mineral Surfaces

In addition to providing the potential for steric effects and/mixing entropy of the polymer brush, surface biomolecules also can enter into direct (e.g., covalent) bonding interactions with hydroxylated mineral surfaces (Parikh and Chorover, 2006). Laboratory and field experiments with microorganisms have shown that ferric oxyhydroxide coatings are important in the removal of microorganisms in saturated porous media, even in the presence of organic matter and phosphate, which can block microorganism attachment (Harvey and Ryan, 2004). As a sorbent for biomolecules, the hydroxylated surfaces of Fe and Al (oxyhydr)oxides differ significantly from the siloxane surfaces of primary silicates and clay minerals. Whereas the basal surfaces of clay minerals tend to effectively sequester aliphatic molecules such as lipids, the hydroxylated surfaces of

hydrous oxides exhibit affinity for phosphorylated and carboxylated compounds.

Early adhesion processes likely involve some degree of mineral-surface conditioning film formation by free or cell-bound EPS. Microbial exudates and lysates comprise a mixture of polysaccharides, proteins, nucleic acids and lipids whose relative affinities for mineral surfaces depend on the structure and functional group chemistry of the substrate surface, as well as solution chemistry conditions. Data on the adsorption of EPS from the bacterial strains *Bacillus subtilis* and *Pseudomonas aeruginosa* to the goethite (α -FeOOH) surface are shown in Figure 1. Macroscopic sorption data (depicted as K_d values in left side of Figure 1) indicate that reaction of EPS with goethite favors preferential uptake of P-containing biomolecules relative to bulk C or N (Omoike and Chorover, 2006). One explanation for this organic P-selectivity comes from infrared spectroscopic data (right side of Figure 1) of goethite-EPS complexes indicating the ligand exchange of biomolecular phosphoryl groups at goethite surface hydroxyls (i.e., $\equiv\text{Fe-OP-R}$ bonding). These infrared spectroscopic results are consistent with ab initio quantum chemical calculations of complexation of phosphodiester groups, such as those associated with nucleic acids, bonded to Fe metal centers (Omoike *et al.* 2004). ATR-FTIR spectroscopic studies of live bacterial-Fe oxide systems also show the formation of $\equiv\text{Fe-OP-R(s)}$ bonds, suggesting that cell-bound phosphorylated molecules also play an important role in whole cell adhesion to unconditioned oxide surfaces (Parikh and Chorover, 2006).

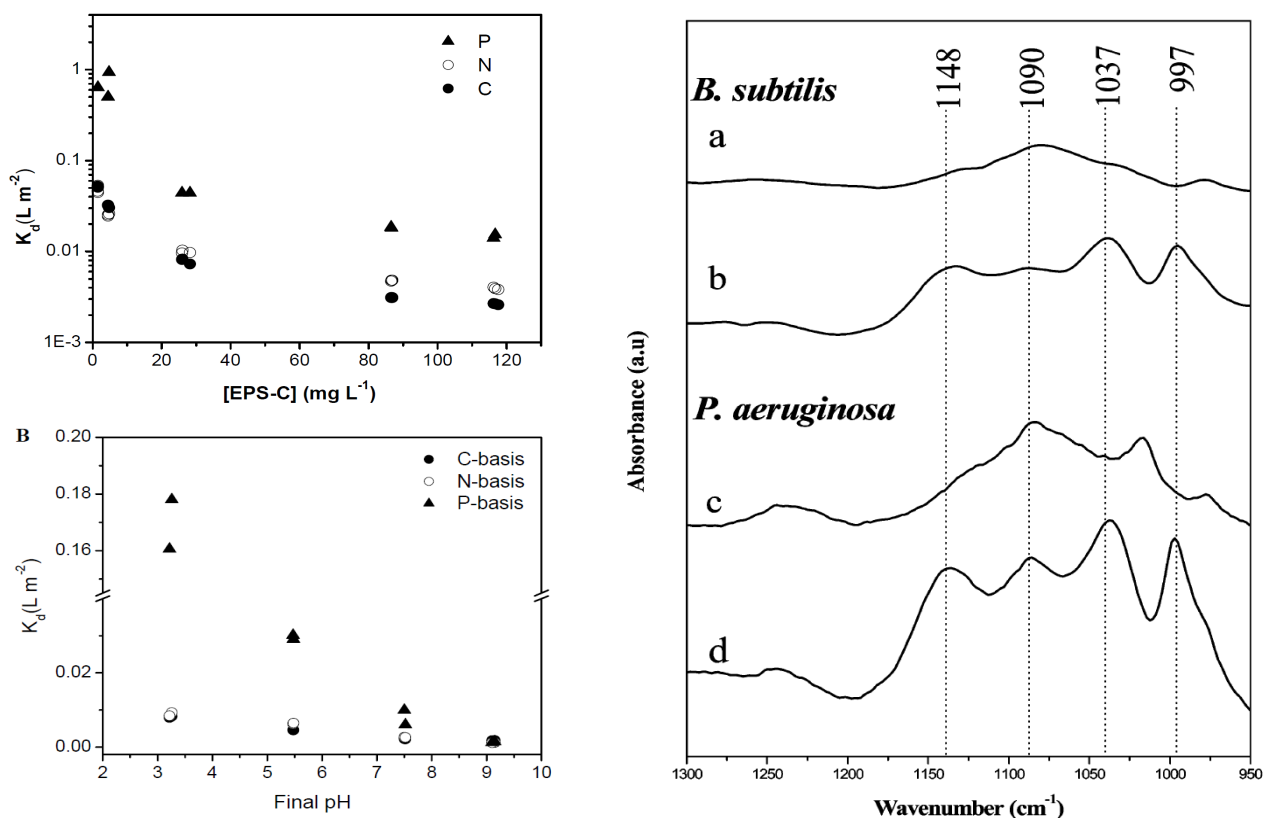


Figure 1. Left side shows macroscopic data on adsorption of EPS from *Bacillus subtilis* to the surface of α -FeOOH as a function of EPS concentration (carbon basis, top left) and pH (bottom left). Data indicate preferential adsorption of P-containing moieties (Omoike and Chorover, 2006). Right side shows attenuated total reflectance Fourier transform infrared (ATR-FTIR) spectra of EPS from *B. subtilis* and *Pseudomonas aeruginosa* either free in solution (a, c) or adsorbed to the surface of goethite (b, d). Emergence of new peaks for adsorbed EPS is indicative of formation of inner-sphere PO-Fe bonds as a result of ligand exchange (Omoike *et al.*, 2004).

The transport of pathogenic microbial contaminants is likewise affected by mineral-microbe bonding interaction. As shown in the left side of Figure 2, the progressive coating of quartz sand surfaces with iron oxyhydroxide results in a significant decrease in *Cryptosporidium parvum* oocyst breakthrough from porous media columns, and an increase in adhesion, as reflected in the collision efficiency parameter, α (Abudalo *et al.* 2005). The right side of Figure 2 shows ATR-FTIR studies of oocyst surface functional group chemistry upon adhesion to uncoated (top) and iron-oxide-coated (bottom) surfaces. The data show that at the pH of the

transport experiments, oocysts are adhered to Fe oxide surfaces through inner-sphere complexation of carboxylate groups at Fe(III) metal centers (Gao *et al.* 2009). Hence, in addition to the influence of electrostatic attraction for microbial adhesion to Fe oxide at this pH, direct bonding effects likely also play a role in retarding pathogen transport.

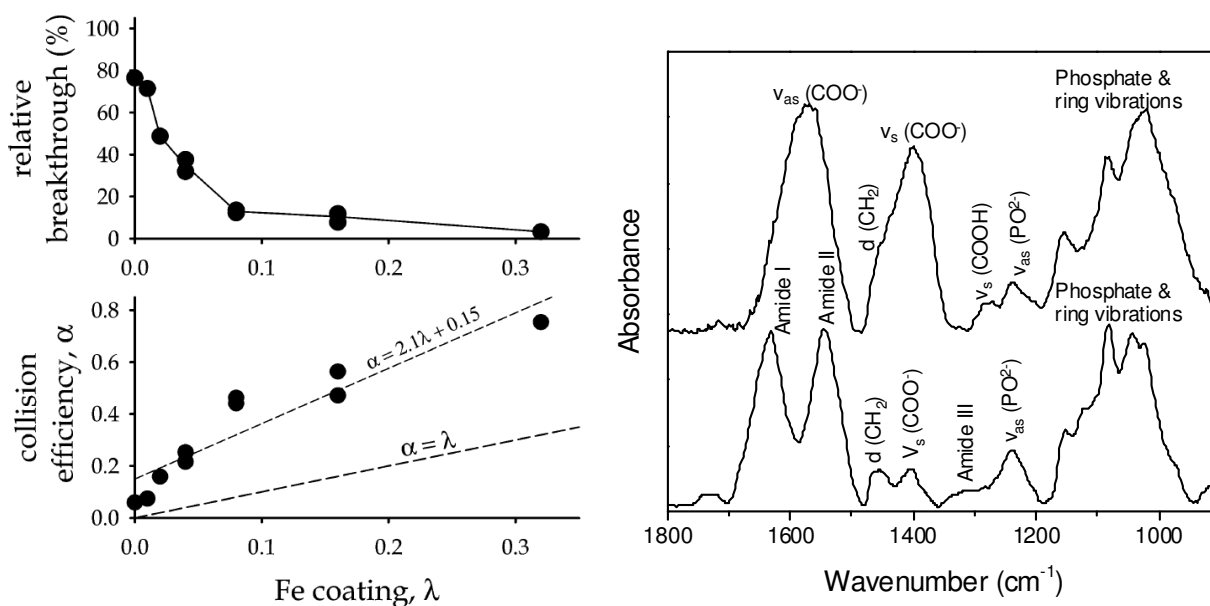


Figure 2. Macroscopic transport data left side shows that relative breakthrough decreases and collision efficiency increases for *Cryptosporidium parvum* oocysts as a function of the fraction of the Fe(III) oxide surface coating of a quartz sand at pH 5.6-5.8 and 0.1 mM NaCl (Abudalo *et al.* 2005). (Zeta potential of oocysts under these conditions was -10 mV.) Right side uses molecular spectroscopy to depict the mechanism. ATR-FTIR spectra of oocysts adhering to an uncoated (bottom spectrum) and α -Fe₂O₃-coated (top spectrum) internal reflection element surface indicates the inner-sphere complexation of oocyst carboxylate groups at hematite Fe(III) metal centers (Gao *et al.* 2009).

Following initial adhesion to mineral surfaces, further accumulation of cells and EPS can result in the formation of incipient biofilm, where the nature of biopolymeric exudates are driven partly by cell physiological response to the local interfacial environment. Indeed, Geoghegan *et al.* (2008) proposed that “cell attachment and related cell growth behaviour is mediated by macromolecular physics and chemistry in the interfacial environment. Ecological success depends on the genetic potential to favourably influence the interface through adaptation of the macromolecular structure.”

Conclusions

In-situ ATR-FTIR spectroscopy studies indicate that adhesion of microbial cells to iron (oxyhydr)oxide surfaces involves not only mean field interactions, such as electrostatic and van der Waals associations that are incorporated into traditional DLVO theory, but also biomolecule-surface metal bonding interactions. We have observed inner-sphere complexation of phosphoryl and carboxyl groups during adhesion of bacterial cells and *C. parvum* oocysts, respectively, and contend that such interactions play an important role in the formation of the microbe-mineral interface.

References

- Abudalo RA, Bogatsu YG, Ryan JN, Harvey RW, Metge DW, Elimelech M (2005) Effect of ferric oxyhydroxide grain coatings on the transport of bacteriophage PRD1 and *Cryptosporidium parvum* oocysts in saturated porous media. *Environmental Science & Technology* **39**, 6412-6419.
- Camesano TA, Logan BE (2000) Probing bacterial electrosteric interactions using atomic force microscopy. *Environmental Science & Technology* **34**, 3354-3362.
- Curriero FC, Patz JA, Rose JB, Lele S (2001) The association between extreme precipitation and waterborne disease outbreaks in the United States, 1948-1994. *American Journal of Public Health* **91**, 1194-1199.

- Gao X, Mettge DW, Ray C, Harvey RW, Chorover J (2009) Surface complexation of carboxylate adheres *Cryptosporidium parvum* oocysts to the hematite/water interface. *Environmental Science & Technology* **43**, 7423-7429.
- Geoghegan M, Andrews JS, Biggs CA, Eboigbodin KE, Elliott DR, Rolfe S, Scholes J, Ojeda JJ, Romero-Gonzalez ME, Edyvean RGJ, Swanson L, Rutkaite R, Fernando R, Pen Y, Zhang ZY, Banwart SA (2008). The polymer physics and chemistry of microbial cell attachment and adhesion. *Faraday Discussions* **139**, 85-103.
- Ginn TR, Wood BD, Nelson KE, Scheibe TD, Murphy EM, Clement TP (2002) Processes in microbial transport in the natural subsurface. *Advances in Water Resources* **25**, 1017-1042.
- Harvey RW, Ryan JN (2004). Use of PRDI bacteriophage in groundwater viral transport, inactivation, and attachment studies. *FEMS Microbiology Ecology* **49**, 3-16.
- Hornberger GM, Mills AL, Herman JS (1992) Bacterial Transport in Porous-Media - Evaluation of a Model Using Laboratory Observations. *Water Resources Research* **28**, 915-923.
- Omoike A, Chorover J (2006) Adsorption to goethite of extracellular polymeric substances from *Bacillus subtilis*. *Geochimica et Cosmochimica Acta* **70**, 827-838.
- Omoike A, Chorover J, Kwon KD, Kubicki JD (2004) Adhesion of bacterial exopolymers to alpha-FeOOH: Inner-sphere complexation of phosphodiester groups. *Langmuir* **20**, 11108-11114.
- Parikh SJ, Chorover J (2006) ATR-FTIR spectroscopy reveals bond formation during bacterial adhesion to iron oxide. *Langmuir* **22**, 8492-8500.
- Redman JA, Walker SL, Elimelech M (2004) Bacterial adhesion and transport in porous media: Role of the secondary energy minimum. *Environmental Science & Technology* **38**, 1777-1785.
- Schafer A, Ustohal P, Harms H, Stauffer F, Dracos T, Zehnder AJB (1998) Transport of bacteria in unsaturated porous media. *Journal of Contaminant Hydrology* **33**, 149-169.
- Scow KM, Hicks KA (2005) Natural attenuation and enhanced bioremediation of organic contaminants in groundwater. *Current Opinion in Biotechnology* **16**, 246-253.

Cadmium and Zinc Concentrations in the Soils of the Oil Palm Plantations from Long Term Application of Phosphate Rock

Aini Azura Ali, Fauziah Che Ishak and Samsuri Abdul Wahid

Department of Land Management, Faculty of Agriculture, University Putra Malaysia, 43400 Serdang, Selangor, Malaysia, Email fauziah@agri.upm.edu.my

Abstract

Nowadays, there is an increasing concern about Cd and Zn accumulation in the soil caused by the continuous application of phosphate rock (PR) fertilizer. To investigate on this issue in Malaysia's oil palm plantation, two well maintained oil palm plantations were selected. Six soils series with three different ages of oil palm (<10, >15, >20 years) that undergo scheduled fertilizer program was collected. Jawa, Selangor and Sedu series were selected from coastal areas. Munchong, Rengam and Segamat series were collected to represent inland areas. To support the findings of the field study, Zn and Cd adsorption isotherms were investigated using the same soil series. Also, studies on pH effect on Zn adsorption and competitive adsorption between Zn and Cd were conducted. Soil heavy metals mean concentrations were compared between three different ages of oil palm for each soil series. Results indicated no accumulation of Cd in all soil series but there are accumulations of Zn for Selangor and Segamat series. Of all the soil series studied, the Segamat series exhibited the highest amount of Cd and Zn adsorption. For Selangor and Segamat series, Cd adsorption was severely depressed by the presence of Zn. The increasing soil pH of the Selangor series as the age of the oil palm trees increased, led to the accumulation of Zn.

Key Words

Cadmium and Zn accumulation; adsorption isotherm; competitive adsorption; adsorption envelope

Introduction

Many studies from temperate regions show that long term application of phosphate rock (PR) fertilizer leads to the accumulation of Cd in agricultural soils due to the presence of this metal as an impurity in all phosphate rocks (Nziguheba and Smolders 2008). Phosphate rock (PR) is the main phosphorus fertilizer (PF) which is effectively and extensively used in the oil palm plantation. The amount added in a single fertilizer application may be insignificant compared with the volume of receiving soil but repeated application may lead to an increase in availability of these elements in agricultural soils over time (Camelo *et al.* 1997). Zinc is also found in PR as an impurity. In nature, there is high Zn to Cd ratio in PR. Two plantations, one located in the coastal area and the other in inland area were selected to represent oil palm plantations in Peninsular Malaysia that undergo scheduled fertilizer program. Different phosphorus fertilizer (PF) programs were practiced by these two plantations. Oil palm in the coastal area was annually applied with 0.34 kg-0.51 kg P₂O₅/tree using Christmas Island phosphate rock (CIRP) which ended when the age of the oil palm was 20 years. For inland soil, 0.23-0.58 kg P₂O₅/tree was applied using PR fertilizer until the oil palm trees were cut down. Generally, an oil palm tree will be cut down when the age exceeded 25 years because of the poor productivity. During the productive period, the PF program was carried out annually and there is a speculation that continuous application of PRs may lead to a gradual buildup of Cd in the oil palm soil system over time. However, there is lack of study on Cd accumulation in acid tropical soil due to PRs application. Adsorption is the process that may actively bind Cd and Zn to the solid phases of soils. Competitive adsorption between Cd and Zn to occupy adsorption sites in soil. Adsorption envelope measurement is necessary since pH is one of the most important parameters that affect metal adsorption in soil. Hence, this study was conducted to determine Cd and Zn in soil of different ages of oil palm grown on the same soil series and also to determine Cd and Zn adsorptive capacity potential and competitive adsorption between Cd and Zn soil grown used to grown oil palm. An Adsorption envelope was determined may occur to study Zn adsorption as a function of equilibrium solution pH.

Methods

To conduct this study, three dominant soil series each were selected from the two oil palm plantations. Soils of the coastal area consist of Jawa, Selangor and Sedu series. Munchong, Rengam and Segamat seires were collected as the inland soil series. For each soil series, three categories of oil palm age (<10, >15 and >20 years) were selected. For each categories, six soil points were randomly collected whereby for every sample soil was collected at fronds heap and planting circle of oil palm at two depths (0-15 cm and 15-30 cm). Then the soils

were composited together by depth. Total Cd and Zn were determined by the aqua-regia extractant. Cadmium and Zn adsorption capacity potential and competitive adsorption were determined by batch experiment on the same soil series grown with oil palm but the soils were collected from an undisturbed, unfertilized area. Initial concentration for adsorption isotherm: 0, 10, 20, 30, 40, 50, 60, 70, 80, 90 and 100 mg/L of Cd/Zn. The adsorption isotherm was fitted to both Freundlich and Langmuir equation. Selangor and Segamat series were selected for competitive adsorption and adsorption envelope measurement. For competitive adsorption, 100 mg/L of Zn was selected and Cd concentrations were varied (1, 5, 10, 20, 40, 50, 100 mg/L) to give Zn:Cd ratio 1:100, 1:20, 1:10, 1:5, 1:2.5, 1:2 and 1:1. The adsorption envelope study was carried out at 50 mg/L of Zn. The mixture was adjusted to pH 3, 4, 5, 6, 7, 8, 9 and 10 with 0.001 M NaOH or HCl. After 24 hours of shaking, pH equilibrium of the mixture was recorded. Cadmium and Zn were analyzed using the flame atomic absorption spectrophotometry (Perkin Elmer 5100).

Results and discussion

For total Cd, Sedu, Rengam and Segamat series show significant differences ($p < 0.05$) between three different ages of oil palm. However, for Segamat series, soil total Cd for oil palm age >20 years was less than soil total Cd for oil palm age >15 years. Meanwhile for Rengam series, soil total Cd for oil palm age >20 years shows a lower mean value than soil total Cd for oil palm age < 10 years. Soil total Cd for Sedu series decreased with the increase in oil palm age (Figure 1). For total Zn, only Selangor and Segamat series show significant differences ($p < 0.05$) and an increment of soil total Zn with the increase in oil palm age (Figure 1).

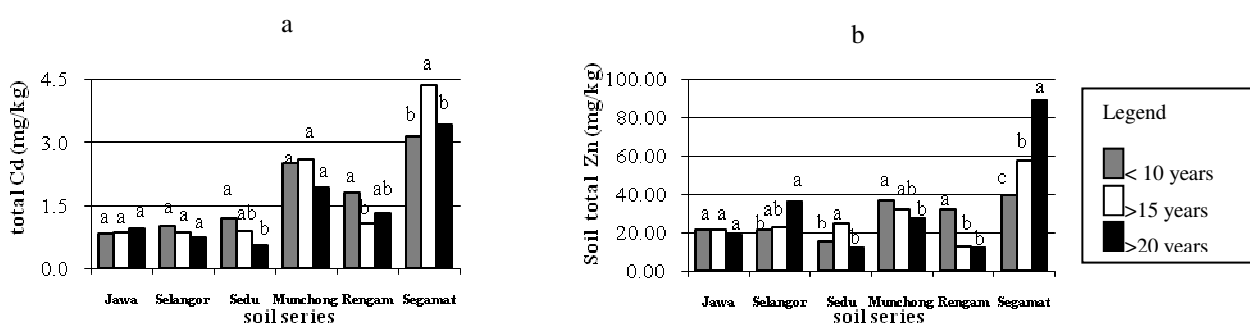


Figure 1. Total Cd (a) and total Zn (b) in soils for all soil series at three different categories of oil palm age.

From the adsorption isotherm studied, Cd and Zn adsorption data was better described by Freundlich equation. Values of Freundlich and Langmuir equation parameters as shown in Table 1. Segamat series gives the highest value of maximum adsorption (b) and can retain the largest amounts of Zn and Cd based on Kf values. Furthermore, Zn was adsorbed (range 250 to 1000 mg/kg) about one double the amount of Cd (range 143 to 500 mg/kg) for most of the soils series. This may possibly be the reason for the higher total Zn in oil palm plantations compared to the total Cd aside from naturally higher Zn than Cd in soils. The b and k values for Munchong series are not stated in the table because of the negative slope given by the linear form of the equation.

For both soil series, Zn adsorption is low at low equilibrium pH but, increased with increasing pH (Figure. 2). Increasing pH led to the increased number of negatively charged surface sites that consequently increased the number of sites available for Zn sorption. This might be the reason for the increase in soil total Zn for the Selangor series (field study) as the age of the oil palm trees increased. For the Segamat series, maximum

Table 1. Value of K_f (capacity adsorption), $1/n$ (rate of adsorption) of Freundlich equation and b (maximum adsorption), k (energy bonding) of Langmuir equation.

Soil series	Freundlich				Langmuir			
	K_f (m^3/kg)		$1/n$		b (mg/kg)		k	
	Cd	Zn	Cd	Zn	Cd	Zn	Cd	Zn
Jawa	4.05	8.83	0.791	0.783	250	500	0.012	0.013
Selangor	4.90	1.10	0.658	0.962	143	500	0.018	0.002
Sedu	2.74	8.17	0.917	0.723	333	333	0.010	0.016
Munchong	17.18	1.43	1.543	1.191	-	-	-	-
Rengam	1.62	1.15	0.847	0.892	167	250	0.008	0.003
Segamat	55.98	56.36	0.451	0.513	500	1000	0.051	0.028

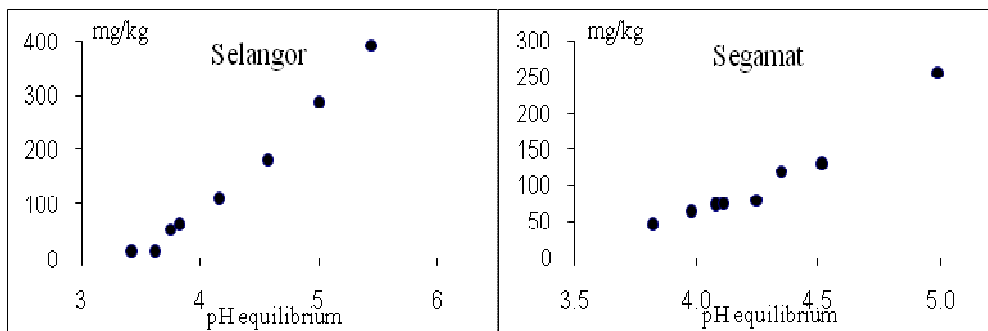


Figure 2. Adsorption envelope of Zn for Selangor series (coastal) and Segamat series (inland).

adsorption occurs at pH 5. This may be due to the deprotonation of the most active surface of goethite as a result of surface hydrolysis with an increase in pH from 5 to 6 (Mustafa *et al.* 2004). This explains the increased accumulation of soil total Zn for the Segamat series with increasing age of the oil palm trees.

The trend of competitive adsorption for Segamat series is the same as when the Cd was added individually but the amount adsorbed was much lower than the single adsorption. For Selangor series, increasing the initial concentration of Cd from 1, 5, 10, 20, 40, 50 and 100 mg/L while maintaining the initial Zn concentration at a constant 100 mg/L resulted in no Cd adsorption except for Zn:Cd ratio 1:1, though the amount adsorbed was much less than single adsorption. Figure 3 shows clearly that the presence of Zn significantly reduced Cd adsorption due to the competition for adsorption sites. Also, Zn exhibits a higher affinity for soil surface, thus more Zn was adsorbed compared to Cd. This could be the reason for the low retention of Cd for all soil series in oil palm plantation.

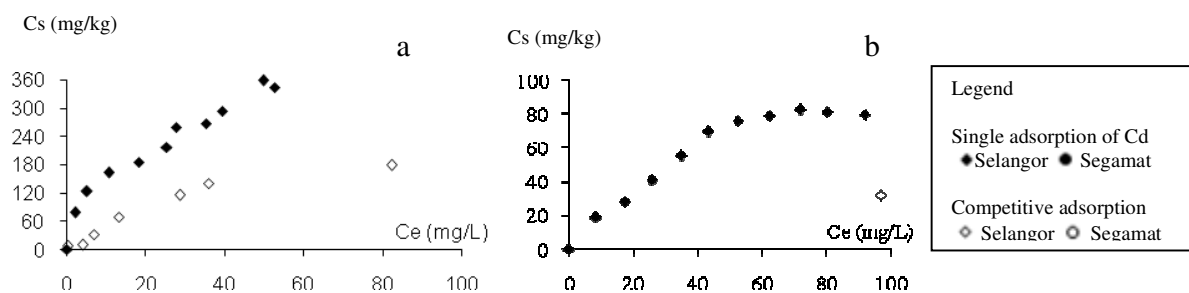


Figure 3. Single adsorption (adsorption isotherm) of Cd and competitive adsorption between Cd and Zn in the a) Segamat series b) Selangor series.

Data in Table 1 and Fig 3 shows that Segamat series has the highest capacity to adsorb cations. This might be the reason that Segamat series can adsorb Cd for all Zn:Cd ratios. For other soil series, Zn competes strongly in soils with a lower capacity to hold metal cations (Fontes and Gomes 2003; Lu and Xu 2009) where Cd site was occupied by Zn and may possibly result in the zero adsorption of Cd for all Cd concentrations except for Zn:Cd ratio 1:1.

Conclusion

There was no clear trend of accumulation of Cd in the soil between different ages of oil palm grown on the same soil series, but there were accumulations of Zn in Selangor and Segamat series. Zinc accumulation in Segamat and Selangor series is consistent with results of the adsorption study. Cadmium adsorption was significantly reduced by the presence of Zn.

References

- Camelo LGL, Miguez SR, Marbán L (1997) Heavy metal input with phosphate fertilizers used in Argentina. Fontes MPF, Gomes PC (2003) Simultaneous competitive adsorption of heavy metals by the mineral matrix of tropical soils. *Applied Geochemistry* **18**, 795-804.
- Lu SG, Xu QF (2009) Competitive adsorption of Cd, Cu, Pb and Zn by different soils of Eastern China. *Environment Geology* **57**, 685-693.
- Nziguheba G, Smolders E (2008) Inputs of trace elements in agricultural soils via phosphate fertilizers in European countries. *Science of the Total Environment* **390**, 53-57.

The thermodynamics stability of soil humic and fulvic acids

Sen Dou^A, Yves Tardy^B, Jinjing Zhang^A, Kai Li^{A,C}

^AFaculty of Natural Resource and Environment, Jilin Agricultural University, Changchun, Jilin province, China 130118; Email dousen@tom.com

^BENSAT, Montgeard, 31560 Nailloux, Toulouse, France

^CDepartment of art and science of Jilin Agricultural Science and Technology College, Jilin, Jilin province, China 132101

Abstract

The formation and transformation of humus is mainly a process of soil biochemical changes. However, it belongs to a thermodynamics stability field if we pay attention to the energy changes for initial and terminal states in humus. There are many factors that affect humus stability in soil. However, to calculate the reaction equilibrium constant ($\log K_R$) and the changes of standard Gibbs formation free energy (ΔG_f°), only the following three factors, capillary water activity ($[H_2O]$), oxygen partial pressure (pO_2) and carbon dioxide partial pressure (pCO_2), are taken into consideration supposing the temperature is 25°C. By utilizing the $\log k_R$ and $1/n\Delta G_R^\circ$, we can calculate the thermodynamics stability range of FA and HA. The sequence of stability to $[H_2O]$ and pCO_2 is FA > HA, and the stability to pO_2 is HA > FA. Under the controlled incubation experiments, more moisture, relatively low temperature, low oxygen concentration and high carbon dioxide concentration generally lead to the formation of FA.

Key Words

Thermodynamics stability, humic acid, fulvic acid, elemental composition formula, soil condition parameter

Introduction

Compared with live organic components (e.g. micro-organisms and plants), soil humus is more inert. In the sense, the soil humus and clay have similar properties and behaviors, such as the space-time continuity in composition, polymerization or degradation, being assembled and scattered, hydration or dehydration. Like clay, soil humus can adapt to themselves, constantly change into each other, be destroyed and newly formed in response to soil water, gas, heat and soil solution composition. Thus, it is possible to handle more complex soil humus the same as mineral elements from the perspective of thermodynamic stability (Tardy *et al.*, 1997). In soils, there are a number of factors, such as type and content of clays, vegetation, microorganisms, moisture, temperature, air composition, chemical composition and concentration of solution, acidity, status of redox, can affect the formation and transformation of soil humus. But from the aspect of thermodynamics, the above soil conditions can be simplified into three parameters, i.e. water activity ($[H_2O]$), oxygen partial pressure (pO_2) and carbon dioxide partial pressure (pCO_2), in order to calculate the reaction equilibrium constant ($\log K_R$) and Gibbs formation energies (ΔG_f°) at a given temperature of 25°C. As what we know, all organic substances are composed of the three elements and would eventually be decomposed into H_2O and CO_2 that contain the three elements. Owing to different conditions, various organic components are in different stages of the equilibrium system, and have different energy level (Dou, 2001).

Methods

Black soil (Typic Hapludoll) collected from the cultivated topsoil (0-20 cm) on the eastern side of Chang-Yi Road, Jilin Agricultural University Farm Changchun, Jilin, China (E125°23'45", N43°48'44"), in April, 2000, was used to prepare HA and FA. Aeolian soil (Quartzipsamments) collected from the cultivated topsoil (0-20 cm) on Yaojingzi Grassland Research Station, Northeast Normal University, Changling, Jilin, China (E123°45', N44°45'), in April, 2001, was used in the incubation experiment. The soil samples were air-dried and passed through 2 mm mesh sieve. The soil moisture was adjusted to 70%-80% of the field capacity. Then they were incubated preliminarily for 7 days before adding corn stalk. The corn stalk was dried at 50-70°C, ground and passed through 0.25 mm mesh sieve. The OC content, total nitrogen and C/N of the corn stalk was 442.3 g kg⁻¹, 5.6 g kg⁻¹ and 79, respectively. The C/N ratio was adjusted to 25:1 by mixing 6 g corn straw and 0.53 g (NH₄)₂SO₄ with 175 g aeolian soil. Eleven treatments with 3 repetitions were carried out in this experiment. The temperature treatments included 4 treatments: 10°C, 25°C, 40°C and 55°C. The moisture treatments included 4 treatments: 20 % (20W), 70 % (70W), 90 % (90W) of the field capacity, respectively, and waterlogged (Y). The oxygen (O₂) treatments included 3 treatments: 5 % O₂ (O1), 21 % O₂, 50 % O₂ (O3) treatments. The carbon dioxide (CO₂) treatments included 3 treatments: normal CO₂ concentration (C0), 3 % CO₂ (C1), 30 % CO₂ (C2). At the same time, control experiments for these 11 treatments mentioned above were done without corn straw

(CK). Sampling times were on days 1, 3, 7, 15, 30, 60, 90, 120 and 180d, respectively.

The method for preparing HA and FA was the same as previously reported (Dou *et al.* 1991). The elemental composition of HA and FA was measured with a Vario EL.CHN analyzer. The reaction equilibrium constant ($\log K_R$) and Gibbs formation free energy (ΔG°_f) of HA and FA were measured by “the elemental composition-soil condition parameter method”. The method of humus composition modification was used in HA and FA quantitative analysis (Dou *et al.*, 2007). Organic carbon was measured by $K_2Cr_2O_7-H_2SO_4$ method, $CO_3^{2-} HCO_3^-$ was measured by double-indicator method, and NO_3^- and NH_4^+ were measured by the electrode method. Other analyses were measured by conventional methods (Lao, 1998).

Results

Thermodynamic stability range of HA and FA

The Proportions of C, H, O, N in HA or FA of soil generally accounted for more than 97% of their elemental composition. This can be written to a simplified formula, that is $nC_xH_yO_zN$. The tested element composition of HA and FA from black soil is shown in Table 1.

Table 1. The elemental composition of humic acid and fulvic acid in black soil (on an ash- and water-free basis).

Humus	C g/kg	H g/kg	N g/kg	O+S g/kg	C/H mol	C/N mol	O/C mol	simplified formula
HA	581.1	47.4	32.8	338.7	1.022	20.67	0.437	$nC_{21}H_{21}O_9N$
FA	473.8	54.8	23.2	448.2	0.720	23.83	0.709	$nC_{24}H_{33}O_{17}N$

According to the data in Table 1 and the simplified formula $nC_xH_yO_zN$, the HA and FA of black soil can be expressed as $nC_{21}H_{21}O_9N$ ($1/n=431$ g/mol) and $nC_{24}H_{33}O_{17}N$ ($1/n=607$ g/mol). It must be noted that the simplified formula does not represent the true size of molecules, as it is hard to determine the n. From the simplified formula, if the condensation degree of HA (C/H) is high, the oxidation degree of FA (O/C) is also high.

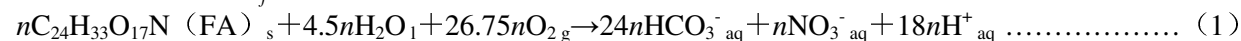
In addition, the soil conditional parameters and related thermodynamic data are also essential for the calculation of thermodynamic stability (see table 2).

Table 2. The soil conditional parameters and related thermodynamic data in the experimental black soil.

Item	P_{CO_2} (g)	P_{O_2} (g)	$[H_2O]$ (l)	e^-	H^+ (aq)	HCO_3^- (aq)	NO_3^- (aq)	NH_4^+ (aq)
$\log[mol L^{-1}]$ or $\log P$ (0.1MPa)	-1.50	-31.54	-0.155	-2)	-7.0	-2.3	-3.46	-1.37
G_f° (kJ mol ⁻¹)	-394.4	0	-237.2	0	0	-587.1	-110.5	-79.5

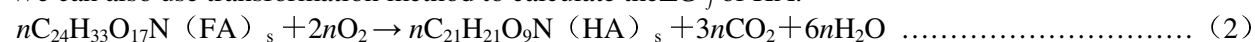
1) $\log PCO_2 = \log[HCO_3^-]$ (mol L⁻¹) - pH + 7.8; $\log PO_2 = \log([NO_3^-]/2$ (mol L⁻¹) - log $[NH_4^+]/2$ (mol L⁻¹) - pH - 23.5; $[H_2O]$ is calculated by 70% of soil relative humidity. 2) not measured

Using the data listed in Table 2, we can calculate the ΔG_f° of HA and FA. The decomposition method can be used to calculate ΔG_f° of FA.



$$\log K_R = 660; 1/n\Delta G_R^\circ = -5.707 \log K_R = -3765 \text{ kJ mol}^{-1}; 1/n\Delta G_f^\circ (FA)_s = 24\Delta G_f^\circ (HCO_3^-)_{aq} + \Delta G_f^\circ (NO_3^-)_{aq} + 18\Delta G_f^\circ (H^+)_{aq} - 4.5\Delta G_f^\circ (H_2O)_1 - 26.75\Delta G_f^\circ (O_2)_g - \Delta G_R^\circ = -10983 \text{ kJ mol}^{-1}$$

We can also use transformation method to calculate the ΔG_f° of HA.

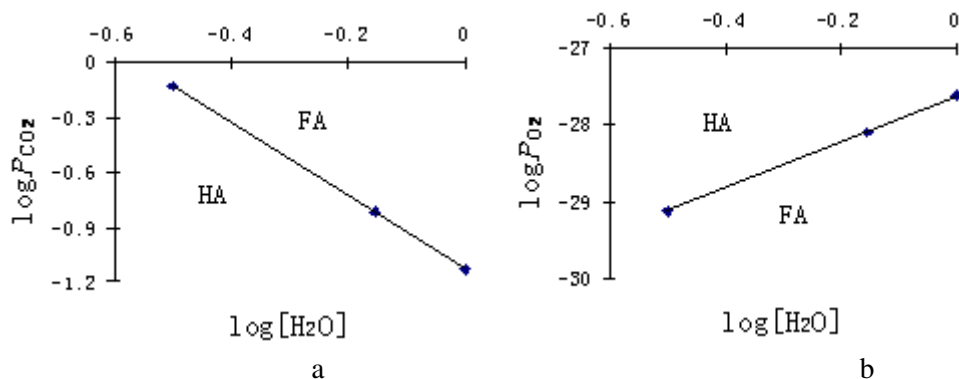


$$\log K_R = 57.7; 1/n\Delta G_R^\circ = -5.707 \log K_R = -329 \text{ kJ mol}^{-1}; 1/n\Delta G_f^\circ (HA)_s = 3\Delta G_f^\circ (CO_2)_g - 6\Delta G_f^\circ (H_2O)_1 + \Delta G_f^\circ (FA)_s - 2\Delta G_f^\circ (O_2)_g + \Delta G_R^\circ = -8268 \text{ kJ mol}^{-1}$$

The equation (2) demonstrate that the transformation, from HA to FA, is a process of condensation, oxidation decarboxylation and dehydration, accompanied by decreased of C/N ratio. On the contrary, from HA to FA, it is a depolymerization, reduction and hydration process with an increased of C/N ratio.

In $1/n\Delta G_f^\circ$, n depends on the size of the molecular weight. If the molecular weight hardly determined, then we can just compare $1/n\Delta G_f^\circ$. If the average molecular weights for HA and FA are 6,000 and 1,500 respectively, the n value for HA and FA would be 14 and 2.5 respectively. Thus $1/n\Delta G_f^\circ$ of HA and FA are -115752 kJ mol⁻¹ and -27458 kJ mol⁻¹, respectively. If the given monomer model of HA is $C_{308}H_{335}O_{90}N_5$ and its molecular

weight is 5541 g mol^{-1} , the n value is 13, and thus $1/n\Delta G_f^\circ$ is $-107484 \text{ kJ mol}^{-1}$. With the $\log K_R$ values in reaction(2), the thermodynamic stability range of FA and HA can be calculated(Figure 1).As is shown,for $[\text{H}_2\text{O}]$ and $p\text{CO}_2$, the stability order is $\text{FA} > \text{HA}$ (Figure 1a); but for $p\text{O}_2$, the stability order is $\text{HA} > \text{FA}$ (Figure 1b).



(a: $\log P_{\text{CO}_2}$ - $\log[\text{H}_2\text{O}]$, $\log P_{\text{O}_2}$ =-31.54; b: $\log P_{\text{O}_2}$ - $\log[\text{H}_2\text{O}]$, $\log P_{\text{CO}_2}$ =-1.5)
Figure 1. Thermodynamics stability range of FA and HA in black soil (25°C).

It should be noted that although FA has high oxidation degree, it is more stable under the conditions of lacking of O₂, much moisture and high CO₂ concentration. HA is the opposite. In fact, under the conditions of bad ventilation, high moisture and acidity, such as cold podzols, tropical podzols and red soil, FA has more advantage than HA. On the contrary, in the environment of good ventilation, good drainage, much saline groups and lack of acidity, such as black soil, chernozem, it is beneficial to polymerization and thus HA is more stable. Of course, the opposite situation may exist. For example, the HA/FA in paddy soil is much higher than that in the corresponding upland soil. From hill to basin, the HA/FA in perennial cold soak field is higher than that in red soil, yellow-mud field and alluvial land.

Effect of temperature, moisture, O₂ and CO₂ on humus composition

To verify the method of thermodynamic stability offered above and to study on the effect of mono-environmental factors on the formation and transformation of HA and FA, PQ (the proportion of HA in extracted HS) of incubated soil under different temperature, H₂O, pO₂ and pCO₂ conditions was analyzed. Considering the entire incubation period (Figure 2a), the effect of temperature on the values of PQ was not significant. But the values of PQ in the treatments of 40°C and 55°C were slightly but not significant higher than those in the treatments of 10°C and 25°C. This indicated that high temperature was beneficial to the formation of HA or the transformation from FA into HA.

Figure 2b shows that the change regularity of PQ under different moisture treatments had poor logical order during the entire incubation period. But on the average (A), the value of PQ of water-logged treatment (Y) was much lower. Thus, waterlogged condition is beneficial to transform HA into FA, which coincides with the result that high moisture is beneficial to the formation of FA (Tardy *et al.*, 1997; Dou, 2007).

Fig.3 shows the effect of O₂ and CO₂ concentration on HS, the values of PQ of various treatments became much lower with addition of corn straw. This indicated that the initial speed for FA formation was higher than that of HA formation in the decomposition period of corn straw. On different time points, most of PQ values were in the sequence of O3 > O2 > O1 among different O₂ concentration treatments (Figure 3a). This showed that high O₂ concentration favored the formation of HA or FA further transformation into HA. This is coincided with the result that soil with low moisture, good ventilation was beneficial to the formation of HA, but was unfavorable to the formation of FA (Tardy *et al.*, 1997; Dou, 2007), although this issue needs further study.

From Figure 3b, it could be seen that the values of PQ of C2 treatments were almost the lowest in the entire process of incubation, but the PQ values of C1 and C0 were much higher than C2. Thus, the accumulation of HA under high CO₂ concentration treatment (C2) was lower than under low CO₂ concentration treatments (C1 and C0). Another possibility might be that FA was more stable under the condition of high CO₂ concentration, which coincided with the thermodynamic stability results mentioned above.

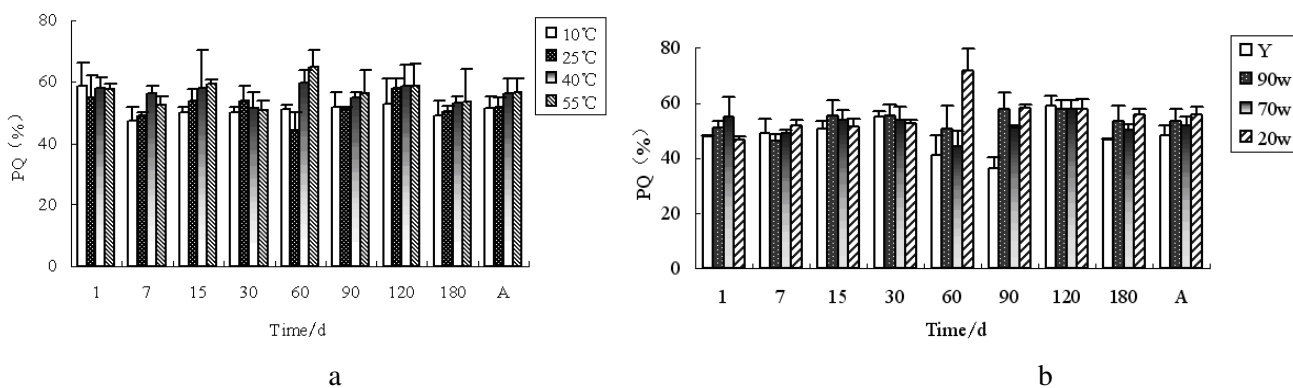


Figure 2. PQ values of soil humic substances under different temperatures and moistures (“A” is the average of PQ)
a : different temperatures ; b : moistures, 20W, 70W and 90W mean the 20%, 70% and 90% of field moisture capacity, respectively, and Y means waterlogged.

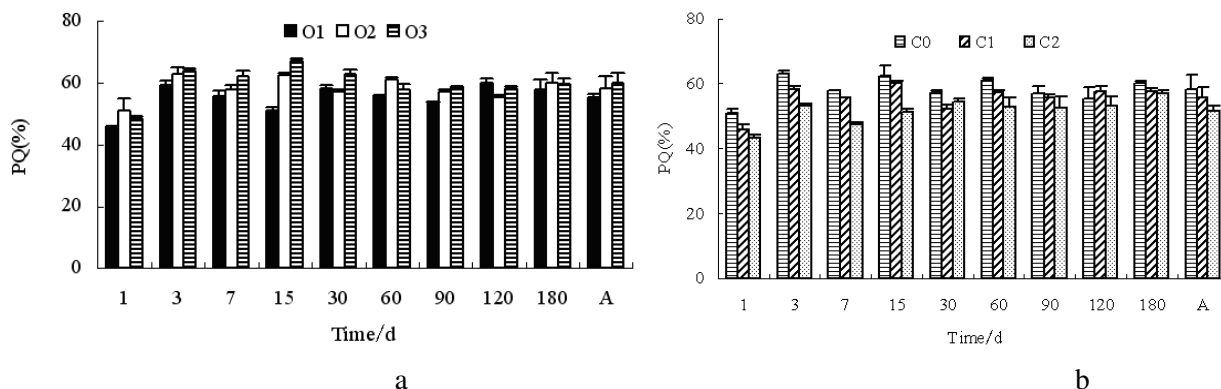


Figure 3. PQ values of soil humic substances under different O₂ and CO₂ concentrations (“A” is the average of PQ)
a: different O₂ (O1:5%, O2: 21%, O3: 50%); b: different CO₂ (C0: normal CO₂ concentration, C1: 3% CO₂, C2: 30% CO₂)

Conclusion

The stability order of two HS fractions analyzed by this method was FA > HA for [H₂O] and pCO₂, but was HA > FA for pO₂. This indicates that high moisture and high CO₂ concentration were beneficial to the formation and stability of FA. Incubation experiments showed that low temperature, high moisture and high CO₂ concentration were more beneficial to the formation of FA, while low moisture and high O₂ concentration were more beneficial to the formation of HA.

Acknowledgements

This research was supported by the Natural Science Foundation of China (NSFC) (40271069; 40471076; 40871107).

Reference

- Dou S (2001) Soil organic matter. In Li X Y. Soil Chemistry. Beijing: Higher Education Press, 33-46
- Dou S, Tan S W, Xu X C, *et al.* (1991) Effect of pig manure application on structural characteristics of humic acid in brown earth. *Pedosphere* **1**(4), 345-354.
- Dou S, Yu S Q, Zhang J J, *et al.* (2007) Effect of carbon dioxide concentration on humus formation in corn stalk decomposition. *Acta Pedologica Sinica* **44**(3), 458-466.
- Lao J S (1988) Analytical Handbook for Soil and Agricultural Chemistry. Beijing: Agricultural Press, 237-239.
- Tardy Y, Schaul R, Duplay J, *et al.* (1997) Domaines de stabilité thermodynamiques des humus, de la microflore et des plantes. *C. R. Acad. Sci. Paris* **324**(2), 969-976.

Contribution of the carboxyl group of acetate to the ^{14}C -containing gas production in agricultural soils

Nobuyoshi Ishii^A, Hiroyuki Koiso^B and Shigeo Uchida^A

^A Office of Biospheric Assessment for Waste Disposal, National Institute of Radiological Sciences, 4-9-1, Anagawa, Inage-ku, Chiba, Japan, Email nobu@nirs.go.jp

^B Tokyo Nuclear Services Co., Ltd., Ueno, Daitou-ku, Tokyo, Japan.

Abstract

The ^{14}C -containing gas production ratios were determined by batch tests using 142 agricultural (upland and paddy) soil samples. Each of the soil samples was suspended in deionized water containing either $[1-^{14}\text{C}]$ sodium acetate or $[1,2-^{14}\text{C}]$ sodium acetate and shake-incubated for 7 days. Production ratios, on average, were 68.6% for $[1-^{14}\text{C}]$ sodium acetate and 59.1% for $[1,2-^{14}\text{C}]$ sodium acetate. From the results, the ^{14}C -containing gas production ratio for $[2-^{14}\text{C}]$ sodium acetate was calculated to be 49.6%. The carboxyl group of sodium acetate, therefore, is easily released as gas in Japanese agricultural soils. Land use also affected the ^{14}C -containing gas production. The production ratios of upland soil samples were significantly lower than those of paddy soil samples.

Key Words

Radioactive waste, radiocarbon, carboxyl group, acetic acid, gasification, agricultural soil

Introduction

The demand for nuclear power plants is growing to achieve a low-carbon society. On the other hand, there is increasing concern about potential radioactive contamination of agricultural soils by the promotion of nuclear policies. Thus, understanding of behaviors of radioactive contaminants in agricultural soils is a considerable issue.

Transuranic (TRU) waste containing radionuclides is generated during the operation of reprocessing facilities and mixed oxide (MOX) fuel fabrication facilities. One of the dominant nuclides contributing to the dose from TRU waste is ^{14}C . Recently, it was found that organic ^{14}C -containing compounds such as low molecular weight carboxylic acids are released from metallic TRU waste (Kaneko *et al.* 2003). In a previous study using paddy soils containing $[1, 2-^{14}\text{C}]$ sodium acetate, a relatively large amount of the ^{14}C in acetate was released into the air from the soil samples (Ishii *et al.* in press). Although acetate has two carbon atom-containing moieties (methyl and carboxyl groups) in a molecule, there are no data for the gas production ratio of each under the previous experimental conditions. Obtaining the gas production ratios of the ^{14}C bearing methyl and carboxyl groups will provide a better understanding of underlying mechanisms of the ^{14}C behavior. In the present study, the gas production ratios of the ^{14}C -bearing carboxyl group in sodium acetate were determined. In addition, the relationship between gas production ratios and land use such as paddy and upland uses were determined.

Methods

Soil samples

A total of 142 Japanese agricultural soil samples (63 paddy soil and 72 upland soil samples) were collected throughout Japan (Ishikawa *et al.* 2008). The soil samples were dried at room temperature, and then passed through a 2-mm-mesh-sieve to obtain homogeneity. The air-dried soil samples were stored in polypropylene bottles at room temperature.

Radioactive tracer experiments

The carrier-free $[1-^{14}\text{C}]$ sodium acetate (specific activity: 2035 MBq/mmol; American Radiolabeled Chemicals, Inc., St. Louis, MO) was diluted to a concentration of 0.9 kBq/mL, and the radioactive solution was filter-sterilized before being added to a 50 mL polypropylene tube with a screw cap closing. In addition, the carrier-free $[1, 2-^{14}\text{C}]$ sodium acetate (specific activity: 4070 MBq/mmol; American Radiolabeled Chemicals, Inc., St. Louis, MO) was also used and had a concentration of 1.8 kBq/mL. Each air-dried soil sample was placed in contact with the radioactive solution at a solid-liquid ratio of 0.5 g to 5 mL. This soil suspension was shake-incubated at 25°C for 7 days in the dark. At the end of incubation, a subsample of the soil suspension was collected to measure the activity of ^{14}C . The ^{14}C activities of the subsample were counted in an Aquasol-2 scintillator (PerkinElmer Japan Co., Ltd., Yokohama, Japan) using a Tri-Carb-25WTR Liquid Scintillation

Analyzer (Packard Instrument Co., Inc., Tokyo, Japan). For the soil suspension subsamples, ^{14}C was counted in the gel phase scintillation cocktail. The gas production ratios were determined by the difference between initial and final ^{14}C concentrations. All experiments were triplicated.

pH measurement

Soil solution pH was measured using a pH meter (B-211; Horiba, Kyoto, Japan). To obtain a soil solution, each soil suspension sample was centrifuged at $3,780 \times g$ for 10 min at the end of the incubation. The obtained supernatant was filtered through a $0.2\text{-}\mu\text{m}$ -pore-size cellulose acetate filter.

Results

The production ratios of ^{14}C -containing gas for $[1\text{-}^{14}\text{C}]$ sodium acetate were determined using 142 agricultural soil samples on day 7 of incubation (Table 1). The mean value of the production ratios was 68.6%. The narrow range between quantile-25% and quantile-75% suggests a small variation for the gas production ratios among agricultural soils although the difference between minimum (F5 sample) and maximum (F61 sample) values was big. Both of these samples were upland soils. Soil characteristics such as particle size, particle density, water content, and carbon content were compared among soil samples but were not special for F5 and F61 samples.

Table 1. Descriptive statistics of ^{14}C -containing gas production ratios (% of total added).

Statistic	Category of sample		
	All	Upland	Paddy
Mean	68.6	66.3	71.4
Median	70.9	69.5	71.7
Minimum	4.6	4.6	61.0
Maximum	81.5	81.5	81.0
Quantile-25%	66.1	64.6	68.6
Quantile-75%	74.5	74.8	74.3
Number of samples	142	79	63

The effect of land use on the production ratios of ^{14}C -containing gas was determined (Table 1). The production ratios of upland soil samples were significantly lower than those of paddy soil samples (*t*-test, $P < 0.01$). Because a previous study indicated that the production of ^{14}C -containing gas was negatively correlated with soil pH (Ishii *et al.* in press), the pH values of soil solutions were compared between the upland soil and the paddy soil samples (Figure 1). For the upland soil samples, the range of pH values was wide, and the median pH value was high compared with that for the paddy samples. The mean values of pH were 6.6 for upland and 6.2 for paddy soil samples, and the difference was significant (*t*-test, $P < 0.01$). The pH values for 20 of 79 upland soil samples were more than 7.0, and the mean value of the gas production ratios for these samples was 58.5%. The ^{14}C -containing gas production will be controlled by soil pH. This control may be explained by the solubility of CO_2 . It is well known that the maximum total amount of CO_2 that may dissolve in water is a function of pH. If the released ^{14}C -containing gas is CO_2 , more $^{14}\text{CO}_2$ gas will be dissolved in the liquid phase with increasing pH.

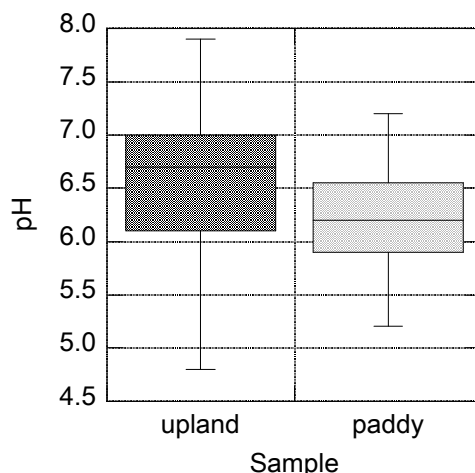


Figure 1. Box and whisker plots illustrating the range of the pH of upland and paddy soil samples.

In the present study, the production ratios of the ^{14}C -containing gas were also determined by using $[1,2-^{14}\text{C}]$ sodium acetate, which has ^{14}C in both carboxyl and methyl groups in the molecule. The slope of the regression line (Figure 2, dashed line) was similar to that of the solid line. This means that the behavior of ^{14}C in acetate is similar for $[1-^{14}\text{C}]$ sodium acetate and $[1,2-^{14}\text{C}]$ sodium acetate.

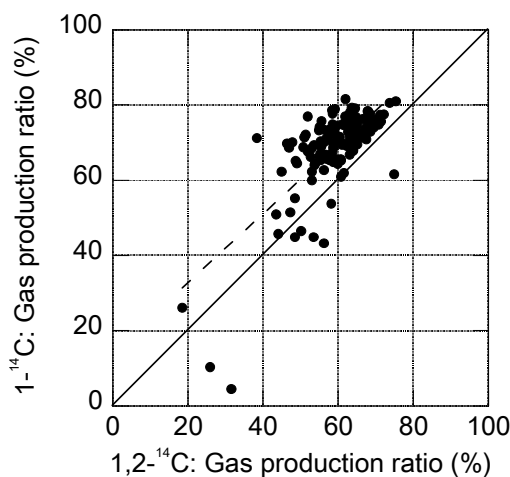


Figure 2. Correlation of ^{14}C -containing gas production ratios between $[1,2-^{14}\text{C}]$ sodium acetate and $[1-^{14}\text{C}]$ sodium acetate. The solid and the dashed lines show “ $y = x$ ” and the regression line, respectively. The regression equation for the scattered points was given by $y = 0.92x + 14.4$, and the correlation coefficient (r) was 0.72 ($n = 142$).

Most of the points were above the solid line (Figure 2), suggesting that the gas production ratios for $[1-^{14}\text{C}]$ sodium acetate are higher than those for $[1,2-^{14}\text{C}]$ sodium acetate. The ^{14}C in carboxyl group will be easily released as gas. The mean values of the ^{14}C -containing gas production ratios were 68.6% for $[1-^{14}\text{C}]$ sodium acetate (Table 1) and 59.1% for $[1,2-^{14}\text{C}]$ sodium acetate, and the difference in the ratio was significant (t -test, $P < 0.01$). From those values, the ^{14}C -containing gas production ratio for $[2-^{14}\text{C}]$ sodium acetate was calculated to be 49.6%. In a future study, it must be experimentally confirmed whether the ^{14}C -containing gas production ratios are really low for $[2-^{14}\text{C}]$ sodium acetate.

Conclusion

The production ratios of ^{14}C -containing gas from $[1-^{14}\text{C}]$ sodium acetate were determined. Of the two types of carbon moieties in sodium acetate, the ^{14}C of the carboxyl group was released as gas at high production ratios. The gas production ratios were negatively correlated with the pH values of soil solutions. In the comparison between paddy and upland soil samples, the gas production ratios of the paddy samples were higher than those of upland soil samples. The high values of gas production ratios of the paddy soil samples can be explained by the low pH of the paddy samples. The position of ^{14}C in the acetate and the pH of soil solutions are important parameters for the behavior of ^{14}C of acetate in agricultural soils. The production ratios of the ^{14}C -containing gas from $[2-^{14}\text{C}]$ sodium acetate will next be determined to assure the relationship between the position of the C in the acetate and the gas production ratio in a planned future study.

Acknowledgment

This work has been partially supported by the Agency for Natural Resources and Energy, the Ministry of Economy, Trade and Industry (METI), Japan.

References

- Ishii N, Koiso H, Takeda H, Uchida S. Partitioning of ^{14}C into solid, liquid and gas phases for various paddy soils in Japan. *J Nucl Sci Technol.* (in press).
- Ishikawa N, Uchida S, Tagami K (2008) Soil–soil solution distribution coefficients for Se, Sr, Sn, Sb, and Cs in Japanese agricultural soils. *Proceedings of Waste Management '08*, Phoenix, AZ, 34-8093, 1–7.
- Kaneko S, Tanabe H, Sasoh M, Takahashi R, Shibano T, Tateyama S (2003) A study on the chemical forms and migration behavior of Carbon-14 leached from the simulated hull waste in the underground condition, *Res. Soc. Symp. Proc.* **757**, 621-626.

Depth profiling of soil clay-xanthan complexes using step-scan mid-infrared photoacoustic spectroscopy

Du Changwen, Zhou Guiqin, Wang Huoyan, Chen Xiaoqin, Zhou Jianmin

Institute of Soil Science Chinese Academy of Sciences, East Beijing Road 71, Nanjing 210008, China, Email chwdu@issas.ac.cn

Abstract

Many soil micro-organisms produce extracellular polysaccharides (EPS); former studies demonstrate that EPS are produced in soil and are closely associated with the surrounding clay particles, and the formed clay-EPS complexes play an important role in soil biogeochemistry. In the present study, experimental clay-xanthan complexes were prepared as models for the soil/biota interface, and the step-scan function of FTIR-PAS technique was initially applied to *in situ* explore the characteristics of surface layers. The variances of depth profiling spectra of montmorillonite are higher than that of kaolin, and more xanthan information was observed in the depth profiling spectra of montmorillonite, which was specifically verified by absorption in the region of 600-1200 cm^{-1} . The xanthan structure changed significantly due to the interaction between xanthan functional group and clay surface. The surface of montmorillonite is more hydrophilic than that of kaolin as indicated by absorption at 1640 cm^{-1} ; montmorillonite seems to interact more easily with hydrophilic xanthan and a much broader surface layer was observed through depth profiling PAS spectra (9.8 μm vs 3.8 μm). The thicker surface layer resulted in stronger water retention capability, and may provide a basis for interpreting the variance of soil quality.

Key Words

Kaolin; Montmorillonite; Polysaccharides; Xanthan; Infrared photoacoustic spectroscopy

Introduction

Xanthan is a high molecular weight natural extracellular polysaccharides (EPS) produced by bacteria (Sereno *et al.* 2007), Many soil micro-organisms produce EPS, and former studies demonstrate that EPS are produced in soil and are closely associated with the surrounding clay particles as an amorphous sheath, and this sheath is in turn coated with clay minerals that are impregnated by EPS. The clay-EPS complexes play an important role in soil biogeochemistry (Chenu, 1993). Complexes of polysaccharides and minerals particles can be directly visualised using electron microscopy (Curry *et al.* 2007); the interaction mechanism of mineral particles is explained by the adsorption of EPS onto the mineral surfaces, creating attachment points and, by the formation of bridges, connecting different mineral particles altogether (Koegel-Knabner *et al.* 2008). NMR measurements (Simpson *et al.* 2006), and FTIR allow the understanding of the general mechanisms that govern the interaction of organic moieties with mineral particles. In spite of this accumulation of knowledge on these complexes (Huang *et al.* 2005), understanding at the spatial characteristics of interface layer occurring in these clay-polysaccharides complexes remains unclear due to the limit of *in situ* monitoring techniques.

Fourier transform infrared spectroscopy (FTIR) is a widely used analytical technique that is routinely applied for the characterization of soils (McCarty and Reeves, 2006) however, conventional infrared spectroscopic techniques, such as transmittance spectroscopy and reflectance spectroscopy, are usually used for homogeneous materials, and need sample pretreatments; thus, real time monitoring, especially for heterogeneous samples, can not be achieved using the conventional infrared techniques. Recently, a novel infrared technique, i. e. Fourier transform infrared photoacoustic spectroscopy (FTIR-PAS), has been used in the soil analysis, and a good performance was obtained (Du *et al.* 2008). A photoacoustic (PAS) signal is generated when infrared radiation absorbed by samples is converted into heat within the sample. This heat diffuses to the sample's surface and into the adjacent atmosphere (usually, helium). Thermal expansion of this gas produces the PAS signal (Figure.2) (Irudayaraj and Yang, 2002). The signal generation process isolates a layer extending beneath the sample's surface, which has a unique function of *in situ* depth profiling, and this function will be useful in the study of heterogeneous or layered materials. Several depth profile studies of biological substances have been reported (Irudayaraj and Yang, 2002); however, to our knowledge, there is no study applying FTIR-PAS to depth profiling of soil organo-mineral complexes. The objective of the present study was to explore the characteristics of interface in soil organo-mineral complexes using the novel technique of FTIR-PAS; it is quite possible to roughly estimate the probing depth and to investigate the interface of organo-mineral complexes in the depth direction through FTIR-PAS measurements.

Methods

Soil clay

Source clays kaolin (KGa-1b) and montmorillonite (STx-1b) were used without purification (American Mineral Clay Society), the properties of the source clays were published in Patricia (2001). Xanthan was from *Xanthomonas campestris* (Sigma Chemicals).

Preparation of soil clay-xanthan complexes

Clay-xanthan complexes were prepared by mixing 2 g kg⁻¹ aqueous solution of xanthan with 100 g kg⁻¹ clay suspensions. The clay-xanthan mixtures were incubated in 25°C for 24 h, and centrifuged at 10000 g, then removed the supernatant; the residues were washed with deionized water twice, and then air dried in room temperature for use.

Recording of mid-infrared photoacoustic spectra

The photoacoustic spectra were recorded for all samples (clay, xanthan and clay-xanthan complexes) using a Nicolet 380 spectrophotometer (Thomalelemental, USA) equipped with a photoacoustic cell (Model 300, MTEC, USA). Briefly, the samples (about 200 mg) were placed in the cell holding cup (diameter 5 mm, height 3 mm), after which the cell was purged with dry helium (10 mL min⁻¹) for 30 s to minimize the interference due to water vapor and impurities. The samples were then scanned at wavelengths of 600-4000 cm⁻¹ with a resolution of 4 cm⁻¹ and a mirror velocity of 0.16 cm s⁻¹, 0.32 cm s⁻¹, 0.64 cm s⁻¹, and 1.89 cm s⁻¹. The PAS spectra were ratioed against a carbon black background, and 32 successive scans were recorded and the average value was reported.

Spectral data treatments

Photoacoustic spectra were pre-processed using a smoothing filter (Savitzky & Golay, 1964). Min-Max normalization was used during preprocessing of the filtered spectral data; Matlab 7.0 was used to do the above data analysis.

Results

Figure 1 depicts the FTIR-PAS spectra of kaolin measured at the various moving-mirror velocities. The spectral outline and band positions show no significant change with moving mirror velocities except the band densities. However, the intensities of bands at lower wavenumbers significantly increase relative to those at higher wavenumbers. A likely explanation for this tendency is saturation of the photoacoustic signal caused by an increase in the probing depth, which equates to an increase of sample thickness. Although the results described here provide no conclusive evidence to account for these changes of relative intensity with moving-mirror velocity, such changes can be, if the photoacoustic saturation occurs, regarded as proof that the FTIR-PAS spectra include a depth profile on the region closest to the surface of kaolin-xanthan complex.

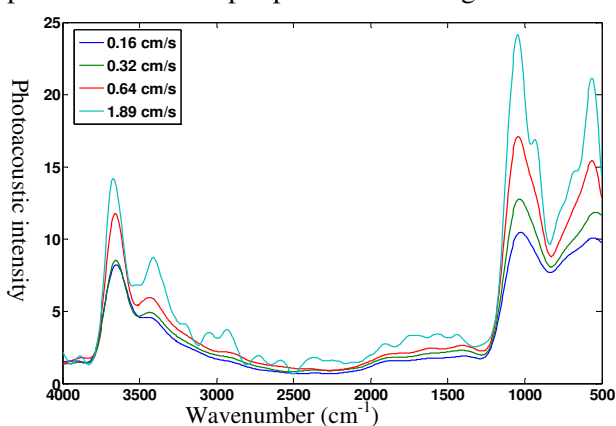


Figure 1. Depth profiling FTIR-PAS spectra of kaolin-xanthan complex

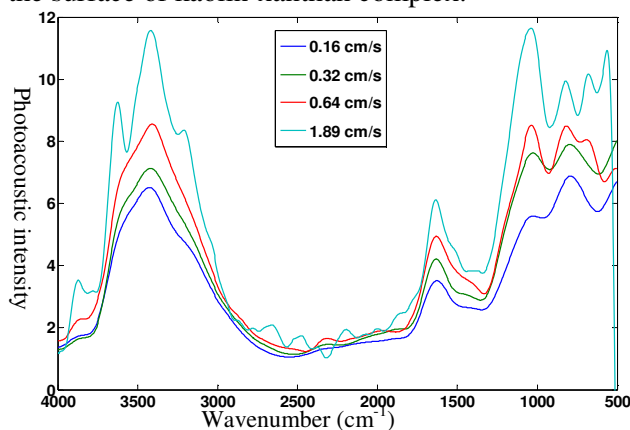


Figure 2. Depth profiling FTIR-PAS spectra of montmorillonite-xanthan complex

FTIR-PAS spectra of montmorillonite-xanthan complex under different moving mirror velocities are demonstrated in Figure 2. The band intensities significantly increase with increasing moving mirror velocity and the relative band intensities have significantly changed in the region of 600-1200 cm⁻¹. In other words, the intensities of the bands assigned to Si-O, Al-O decrease as the thermal sensing length becomes shorter. The spectral changes around 1640 cm⁻¹ indicate that the moisture content (both absorbed in montmorillonite surface

and combined with xantahn) increases. Xantahn is likely to significantly contribute to the water retention capability of montmorillonite-xantahn complex, but the contrition is less for kaolin-xantahn complex.

The photoacoustic probing depth should be determined from the shorter of the thermal diffusive length (μ_s) and the optical wave decay length (μ_β). The thermal diffusive length can be controlled by the moving-mirror velocity, because μ_s is given by

$$\mu_s = \sqrt{\frac{D}{\pi V \nu}}$$

for an opaque sample such as soil clay, where D is the thermal diffusivity of sample, V the moving-mirror velocity, and ν is the frequency of infrared radiation. Therefore, depth profiling is possible for the soil clay-polysaccharide complexes provided that μ_s is shorter than μ_β . μ_s of complex samples were roughly calculated with the typical thermal diffusivity of soil clay ($1.0 \times 10^{-3} \text{ cm}^2 \text{ s}^{-1}$) under different moving mirror velocities and radiation frequencies (Table 1).

Table 1. thermal diffusion distance of soil clay-xantahn complexes calculated from the typical thermal diffusivity of soil clay ($1 \times 10^{-3} \text{ cm}^2 \text{ s}^{-1}$) against the specific infrared frequencies in wavenumber at various moving-mirror velocities

Mirror velocity, V (cm s^{-1})	Thermal diffusion distance, μ_s (μm)		
	1040 cm^{-1}	1640 cm^{-1}	3400 cm^{-1}
0.15	14.3	11.4	7.9
0.32	9.8	7.8	5.4
0.64	6.9	5.5	3.8
1.89	4	3.2	2.2

The band of kaolin-xantahn complex spectra at 3400 cm^{-1} is influenced xantahn in the mineral surface (Figure 1). The change of band intensity is very small with the first two moving mirror velocities (0.16 cm s^{-1} and 0.32 cm s^{-1}). Hence, most of the probing depth is in mineral section. The intensity increases significantly with the moving mirror velocity of 0.64 cm s^{-1} , which means that the organic layer in the kaolin-xantahn complex accounts for some of the probing depth (3.8 μm). The intensity is stronger with mirror velocity of 1.89 cm s^{-1} , and the organic layer may contribute to most of the probing depth (2.2 μm). The kaolin surface layer can be roughly divided in to two layers: interface layer and xantahn layer, and the thicknesses are roughly evaluated as 1.6 μm and 2.2 μm , respectively. Water content is higher in the interface layer, while it is less in xantahn layer.

The main band changes are observed in the region of 600-1200 cm^{-1} in the depth profiling spectra of the montmorillonite-xantahn complex (Figure 2). The bands in this region with moving mirror velocity of 0.32 cm s^{-1} is significantly different from that with moving mirror velocity of 0.16 cm s^{-1} , but is similar with band under moving mirror velocity of 0.64 cm s^{-1} . Therefore, probing depth under moving mirror velocity of 0.32 cm s^{-1} can be regarded as montmorillonite surface layer, and probing depth under moving mirror velocity of 0.64 cm s^{-1} is likely as xantahn layer since the similarity with the absorption band under moving mirror velocity of 1.89 cm s^{-1} . Thus the montmorillonite surface layer can also be roughly divided in to two layers, and the thicknesses are roughly evaluated as 2.9 μm and 6.9 μm , respectively. Obviously, the thickness of the surface layer is much higher than that in kaolin surface. The great difference in surface layer may deprive from mineral surface properties as well as the xantahn conformations (helix or random coil) (Horton *et al.* 1985).

The thickness of the mineral surface layer will directly impact on soil quality, such as nutrient bioavailability, water retention, micro-organism diversity etc. Thicker surface layer has higher water retention capability, and more nutrients can be absorbed, which can be indicated by the fact that montmorillonite based soils are usually fertile than kaolin based soils. In real soil situations, organo-mineral complexes are complicated but clay-xantahn complexes can be the precursor of the complicated organo-mineral complexes (Lii *et al.* 2002), and a thicker surface layer may approximate real complicated organo-mineral complexes (Wattel-koekkoek *et al.* 2001). This initial study is based on relatively simple model clay-polysaccharide complexes, and it may provide some basic knowledge on the spatial configuration of real surface layers, however, the results need more exploration using various methods and involving more minerals and polysaccharides.

Conclusion

Soil clay and xantahn were successfully characterized using FTIR-PAS technique, and valuable information of the interface layer in the clay-xantahn complexes was obtained using the depth profiling analysis through FTIR-PAS. The profiling indicated that montmorillonite was more hydrophilic compared with kaolin, and thus more easily interacted with xantahn. The Montmorillonite-xantahn complex had a much thicker surface layer (both

interface layer and xanthan layer), which resulted in a stronger water retention capability and favored the formation of more complicated soil organo-mineral complexes. The thicker surface layer may provide an inner mechanism for interpreting the variance of soil fertility.

References

- Brown DJ, Shepherd KD, Walsh MG, Mays MD, Reinsch TG (2006) Global soil characterization with VNIR diffuse reflectance spectroscopy. *Geoderma* **132**, 273-290.
- Chenu C (1993) Clay-or sand-polysaccharide associations as models for the interface between micro-organisms and soil: water related properties and microstructure. *Geoderma* **56**, 143-156.
- Chenu C, Guerif J (1991) Mechanical strength of clay-minerals as influenced by an adsorbed polysaccharide. *Soil Science Society of America Journal* **55**, 1076-1080.
- Curry KJ, Bennett RH, Mayer LM, Curry A, Abril M, Biesiot PM, Hulbert MH (2007) Direct visualization of clay microfabric signatures driving organic matter preservation in fine-grained sediment. *Geochimica Et Cosmochimica Acta* **71**, 1709-1720.
- Du CW, Linker R, Shaviv A, Zhou JM (2008) Soil identification with Fourier transform infrared photoacoustic spectroscopy. *Geoderma* **143**, 85-90.
- Garcia-Ochoa F, Santos VE, Casas JA, Gomez E (2000) Xanthan gum: production, recovery, and properties. *Biotechnology Advances* **18**, 549-579.
- Horton D, Hols O, Walaszak Z, Wernau WC (1985) Structural and biosynthetic studies on xanthan by ¹³C-NMR spectroscopy. *Carbohydr Res* **141**, 340-346.
- Huang PM, Wang MK., Chiu CY (2005) Soil mineral-organic matter-microbe interactions: impact on biogeochemical processes and biodiversity in soils. *Pedobiologia* **49**, 609-635.
- Irudayaraj J, Yang H (2002) Depth profiling of a heterogeneous food-packaging model using step-scan Fourier transform infrared photoacoustic spectroscopy. *Journal of Food Engineering* **55**, 25-33.
- Koegel-Knabner L, Guggenberger G, Kleber M, Kandeler E, Kalbitz K, Scheu S, Eusterhues K, Leinweber P (2008) Organo-mineral associations in temperate soils: Integrating biology, mineralogy, and organic matter chemistry. *Journal of Plant Nutrition and Soil Science* **171**, 61-82.
- Lii CY, Liaw SC, Lai VMF, Tomasik P (2002) Xanthan gum-gelatin complexes. *European Polymer Journal* **38**, 1377-1381.
- McCarty GW, Reeves JB (2006) Comparison of near infrared and mid infrared diffuse reflectance spectroscopy for field-scale measurement of soil fertility parameters. *Soil Sci* **171**, 94-102.
- Patricial MC (2001) Baseline studies of the clay minerals society source clay: introduction. *Clay Clay Min* **49**, 372-373.
- Savitzky A, Golay MJE (1964) Smoothing and differentiation of data by simplified least-squares procedures. *Anal Chem* **36**, 1627-1639.
- Sereno NM, Hill SE, Mitchell JR (2007) Impact of the extrusion process on xanthan gum behavior. *Carbohydrate Research* **342**, 1333-1342.
- Simpson AJ, Simpson MJ, Kingery WL, Lefebvre BA, Moser A, Williams AJ, Kvasha M, Kelleher BP (2006) The application of ¹H high-resolution magic-angle spinning NMR for the study of clay-organic associations in natural and synthetic complexes. *Langmuir* **22**, 4498-4503.
- Wattel-Koekkoek EJW, van Genuchten PPL, Buurman P, van Lagen B (2001) Amount and composition of clay-associate soil organic matter in a range of kaolinitic and smectitic soils. *Geoderma* **99**, 27-49.
- Yang H, Irudayaraj J (2001) Characterization of beef and pork using Fourier-Transform infrared photoacoustic spectroscopy. *Lebensm Wiss. u. Technol* **34**, 402-409.
- Zhang WR, Lowe C, Smith R (2009) Depth profiling of coil coating using step-scan photoacoustic FTIR. *Progress in Organic Coatings* **65**, 469-476.

Development of a method for sequential extraction of Si-pools from soils

Anna Danilova^A, Daniela Sauer^A, Jörn Breuer^B, Ludger Herrmann^A, Mehdi Zarei^A, Karl Stahr^A

^AInstitute of Soil Science and Land Evaluation, Hohenheim University, Emil-Wolff-Str. 27, D-70599 Stuttgart, Germany, Email danilova@uni-hohenheim.de

^BState Institute for Agricultural Chemistry, University Hohenheim, Emil-Wolff-Str. 14, D-70599 Stuttgart, Germany

Abstract

For the first time, a method for sequential extraction of silicon (Si) from soils has been developed. This new method enables investigating different Si pools in soils and thus represents an important contribution to improve our understanding of biogeochemical Si-processes and global Si-cycling. The method fractionates and analyses various Si-pools, from the most mobile to immobile phases in soils. The sequential extraction allows differentiation of soluble and biogenic as well as pedogenic amorphous and crystalline silicon, so that the different Si-pools can be analysed. Firstly, the most mobile phase is separated by extraction with CaCl₂, followed by extraction of the adsorbed Si-fraction with acetic acid. Thereafter, the fraction of silicon occluded in sesquioxides is isolated by treatment with ammonium oxalate in the light. Oxidation with hydrogen peroxide releases silicon bound in organic matter. Bio-opals (mainly phytoliths) are separated with sodium polytungstate, while minerogenic (chemically precipitated) amorphous silica is extracted with sodium hydroxide. The total silica content is determined by fusion with lithium borate and subsequent dissolving in nitric acid. Si contents in the extracts are measured by ICP-OES. The share of crystalline silicates is calculated.

The new method was applied to a soil catena in the Black Forest in SW-Germany. The results of the sequential extraction indicate that most of the Si (98- 99%) is bound in primary and secondary silicates. Up to 1% of Si originates from the abiotic amorphous phase or from organic matter.

Key Words

Sequential extraction, amorphous silica, bio-opal

Introduction

Silicon (Si) is the second most abundant element in the earth's crust after oxygen. More than 1/4 (26.3%) of the earth's crust's mass is silicon (Holleman and Wiberg, 2007). This element has central functions for biogeochemical processes, as a nutrient for marine and terrestrial biota, in buffering soil acidification and in the regulation of atmospheric carbon dioxide (Derry *et al.*, 2005). Silicon plays multiple roles in plant life and crop performance (Epstein, 2001). Nevertheless, the silicon turnover in soils – an important compartment within the global silicon cycle – has received little attention so far. There is no specific information about the silicon pools and dynamics, in the following sequence: **rock weathering** → **soil** → **hydrosphere and biosphere**. However, without such information the modelling of global Si-cycles is impossible. The lack of knowledge to the basic magnitudes of the Si-release is partly due to the fact, that no technique for quantitative extraction is available for the Si-Pools in soils in the sense of a chemical fractionating extraction method (Sauer *et al.*, 2006).

A large variety of silicon fractions may occur in soils. Soil particles can adsorb dissolved silicic acid from the soil solution. Silica can also be included in sesquioxides or bound to organic matter. Amorphous silica exists in the form of biogenic (e.g. phytoliths) and minerogenic opal (e.g. silica cutans). Moreover, Si in the form of dissolved silicic acid is retained in the soil solution. Finally, many primary and secondary crystalline silicates (e.g. quartz, feldspar, micas, clay minerals) are generally found in soils. While the knowledge about crystalline minerals is advanced, the quantification of other Si fractions such as Si in amorphous silica is not thoroughly discussed in the literature.

The existing methods for extracting amorphous silica are in general extractions at high temperature with e.g. sodium carbonate (DeMaster, 1981), sodium hydroxide (e.g. Foster, 1953; Koning *et al.*, 2002), Tiron (Biermans and Baert, 1997). The results obtained by these methods depend on the efficiency of the extracting agent. The problem thereby is that clay minerals are extremely sensitive and easily attacked by the chemical agents. Hence, the contribution of mineral-Si to the amounts of Si measured in amorphous silica extraction needs to be considered, and the extraction results need to be corrected for this portion of Si. Such correction is common in marine sedimentology but not in soil science. The extrapolation method from DeMaster, (1981) (Figure 1) used in marine sedimentology is a better approach than the simple extractions that are commonly used in soil science. The technique is based on the observation that under these extraction conditions (high pH, 80-85°C) most biogenic silica dissolves completely within the first 2 h of the extraction, while alumino-silicates release Si at constant rate over the whole extraction time, which allows for the determination of biogenic silica by extrapolation the Si release through time back to the intercept to correct mineral dissolution (Sauer *et al.*,

2006). In this work, quantitative chemical extractions that are commonly used in soil and aquatic sciences for extracting silicon from different soil fractions have been tested and improved.

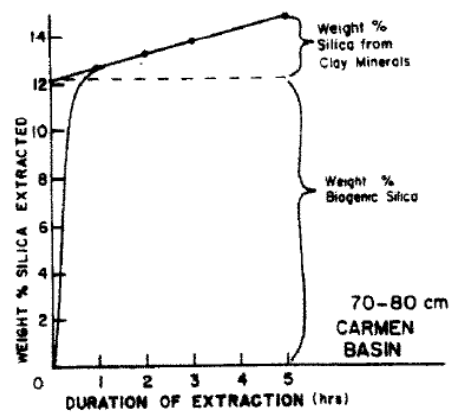


Figure 1. Weight percent silica extracted from a sediment sample versus time (from DeMaster 1981).

Methods

Soils

Samples were taken in the northern part of the Black Forest in SW Germany (8°E and 48°N). The vegetation in this area is dominated by fir and spruce, and the underlying parent rock is Lower Triassic sandstone. The humid-temperate climate is characterised by a mean annual precipitation of 1935 mm and a mean air temperature of 6.5°C (Sommer *et al.*, 2002). The soils along the catena (Figure 2) include a Podzol with abundant eluvial horizon (pedon 1), a Podzol with abundant illuvial horizon (pedon 2) and a Cambisol (pedon 3).

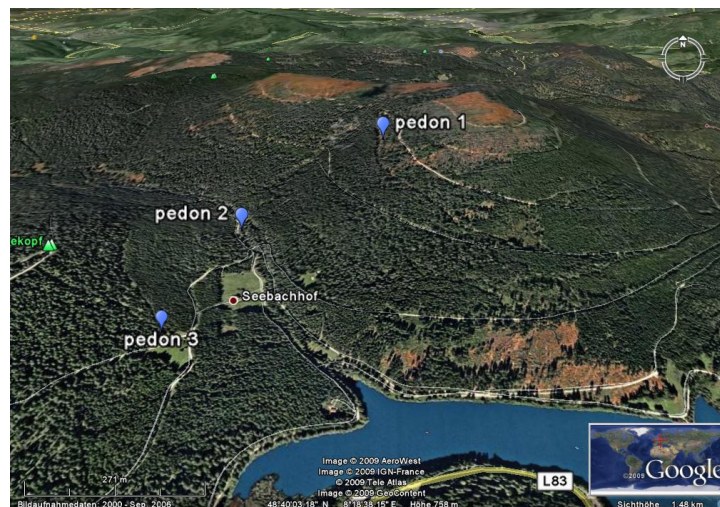


Figure 2. Location of the pedons in the northern part of the Black Forest in SW Germany. From Google Earth (2009).

The pedons were described in the field and sampled horizon-wise. The soil samples were air-dried and passed through a 2-mm sieve. The mineralogical composition of the clay fraction ($< 2\mu\text{m}$) was determined by X-ray diffraction analysis with Cu-K α radiation (Siemens D 500-Diffractometer). Percentages of clay minerals were calculated by use of the software Diffrac AT 3.3. Particle size distribution of the soil samples was determined by wet sieving (sand fractions) and pipette method (silt and clay) (Schlichting *et al.* 1995).

Sequential extraction

The most mobile phase was separated by extraction with 0.01M CaCl₂ 1:5 soil suspensions were put on a horizontal shaker for 24h. They were shaken only for 1 minute per hour in order to accelerate the extraction but at the same time to avoid Si abrasion from mineral grains. The next extraction step was modified from Snyder (2001) for determination of the adsorbed Si-fraction: 1:10 soil suspensions with 0.01M acetic acid were horizontally shaken for 24h (1 minute per hour). The Si-fraction, occluded in sesquioxides, was extracted by a method described by Schwertmann (1964), using oxalate solution (17.56 g (COOH)₂ 2H₂O + 28.4 g (COONH₄)₂ H₂O) in the light. Subsequently, the samples were treated with H₂O₂ in a water bath at 85°C, until

the soil colour had turned to grey. Afterwards the samples were divided in two aliquots.

One aliquot was used for bio opal separation according to the method of Madella et al. (1997). The samples were dispersed overnight with NH_3 and wet-sieved through a 63- μm sieve to exclude the sand fraction. The bio opals (in the fine fractions) were separated with sodium polytungstate ($\text{Na}_6(\text{H}_2\text{W}_{12}\text{O}_{40})\text{H}_2\text{O}$), $\rho = 2.3 \text{ g cm}^{-3}$. The silicon from bio opal was extracted with 0.2M sodium hydroxide, shaking the samples permanently horizontally for 24 h.

The second aliquot of each sample was analysed for minerogenic amorphous silica. The samples were extracted with 0.2M sodium hydroxide (soil to solution ratio 1:400) at room temperature in three time steps (5h, 24h and 48h), thus modifying the method of DeMaster (1981). To calculate the amounts of Si from amorphous silica, Si-concentrations were plotted against extraction time. The obtained extraction curves were extrapolated to the y-axis (Fig.1), yielding the amounts of Si from total amorphous silica (biogenic + minerogenic). The amounts of Si from minerogenic amorphous silica were obtained by subtracting Si from biogenic silica.

The total Si in the soil samples was determined by fusion of soil samples 200 mg di-lithium-tetraborate and 800 mg lithium-metaborate and subsequent dissolving in 0.5 M nitric acid (DIN ISO 14869-2, 2003).

All extracts were centrifuged at 3000 rpm, filtered with paper filter and analysed for Si with ICP-OES at the wavelengths 250.690, 251.611 and 288.158 nm. The samples were washed with distilled water after each step of the extraction procedure.

After analysing all fractions, the balance of silicon in the samples could be established:

$$\text{Si}_i = \text{Si}_{\text{mo}} + \text{Si}_{\text{ad}} + \text{Si}_{\text{occ}} + \text{Si}_{\text{org}} + \text{Si}_{\text{ba}} + \text{Si}_{\text{ma}} + \text{Si}_{\text{min}}$$

where Si_i is total silicon in the sample, Si_{mo} is silicon from the mobile phase, Si_{ad} is silicon from adsorbed silica, Si_{occ} is silicon occluded in sesquioxides, Si_{org} is silicon bound to organic substances, Si_{ba} is silicon from biogenic amorphous silica, Si_{ma} is silicon from minerogenic amorphous silica, Si_{min} is silicon from primary and secondary silicates.

Results

The clay fractions of the soils are characterised by a mixture of kaolinite, illite, vermiculite, secondary chlorite and illite-vermiculite mixed layer clay minerals. Large quantities of secondary chlorites are found in the eluvial horizons of all pedons and in the illuvial horizon of pedon 2. The clay fraction increases downslope within the catena.

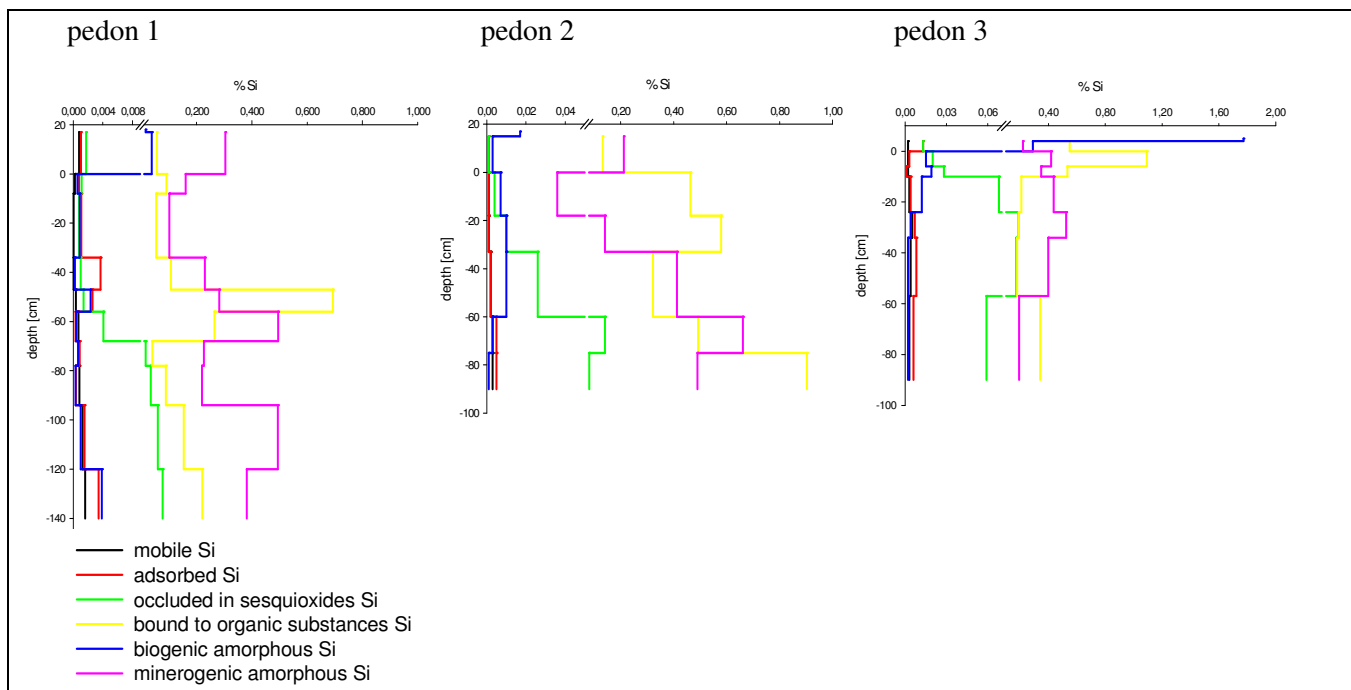


Figure 3. Depth functions of Si (wt. %) in different fractions after sequential extraction.

As shown in Figure 3, silicon extracted by the sequential extraction method makes up maximal 1-2% of the total silicon content, whereas 98-99% of silicon in the soils is in primary and secondary silicates. The amounts of Si in the mobile and adsorbed fractions are very small in all three soil profiles (always < 0.01%). The amounts of Si occluded in sesquioxides are very small in the upper horizons of all pedons and increase with depth. The

highest amounts of this fraction are found in the Cambisol.

High amounts of biogenic amorphous Si occur in the upper horizons, especially in the Cambisol. Si extracted by H₂O₂ and NaOH (silicon bound to organic matter and silicon from minerogenic amorphous silica, respectively) constitute the largest fraction of extractable Si in almost all samples, with the only exception being the O-horizon of the Cambisol (in which Si from bio opal is the predominant extractable Si fraction).

Conclusion

A sequential extraction method for determination of different Si fractions in soils was developed and tested on soils on sandstone in the Black Forest, SW-Germany. Using the extraction solutions and conditions (temperatures, extraction times, soil:solution ratios) described above, silicon can be sequentially extracted from different Si-pools in soils. Silicon from minerogenic amorphous silica and organically bound silicon make up the highest proportion of extractable silicon in the soils analysed in this study. However it comprises only up to 1-2% of total Si. The majority of silicon in the investigated soils is in secondary and primary silicates. The method needs to be applied to more soils with different parent materials in order to obtain an overview about typical ranges in the proportions of the different Si fractions in soils.

Acknowledgment

The authors thank the German Research Foundation DFG for funding the project “Development of a method for fractionating analysis of Si in soils”, which is part of the project package “Multiscale Analysis of the Si-dynamics of terrestrial biogeosystems”.

References

- Biermans V, Baert L (1997) Selective extraction of amorphous Al, Fe and Si oxides using an alkaline Tiron solution. *Clay Minerals* **12**, 127-135.
- DeMaster DJ (1981) The supply and accumulation of silica in the marine environment. *Geochimica et Cosmochimica Acta* **45**, 1715-1732.
- Derry LA, Kurtz AC, Ziegler K, Chadwick OA (2005) Biological control of terrestrial silica cycling and export fluxes to watersheds. *Nature* **433**, 728-731.
- DIN ISO 14869-2 (2003) Soil quality- Dissolution for the determination of total element content- Part 2: Dissolution by alkaline fusion.
- Epstein E (2001) Silicon in plants: facts vs. Concepts. In: Silicon in Agriculture (eds Datnoff LE, Snyder GH, Korndörger GH), pp. 1-15. Elsevier Science B.V.: Amsterdam.
- Foster MD (1953) Geochemical studies of clay minerals 3. The determination of free silica and free alumina in montmorillonites. *Geochimica et Cosmochimica Acta* **3**, 143-154.
- Holleman AF, Wiberg N (2007) Lehrbuch der anorganische chemie - 102. de Gruyter, Berlin pp. 918.
- Koning E, Epping E, Van Raaphorst W (2002) Determining biogenic silica in marine samples by tracking silicate and aluminium concentrations in alkaline leaching solutions. *Aquatic Geochemistry* **8**, 37-67.
- Madella M, Powers-Jones AH, Jones MK (1997) A simple method of extraction of opal phytoliths from sediments using a non-toxic heavy liquid. *Journal of Archaeological Science* **25** (8), 801-803.
- Sauer D, Saccone L, Conley DJ, Herrmann L, Sommer M (2006) Review of methodologies for extracting plant-available and amorphous Si from soils and aquatic sediments. *Biogeochemistry* **80** (1), 89-108
- Schlichting E, Blume HP, Stahr K (1995) Soil Practical. Blackwell, Hamburg pp. 295.
- Schwertmann U (1964) Differenzierung der Eisenoxide des Bodens durch Extraktion mit Ammoniumoxalat-Lösung. *Zeitschrift für Pflanzenernährung und Bodenkunde* **105**, 844-850.
- Sommer M, Halm D, Geisinger C; Andruschkewitsch I, Zarei M, Stahr K (2001) Lateral podzolization in a sandstone catchment. *Geoderma* **103**, 231-247.

Development of an analytical methodology for ultra-trace selenium speciation determination in soils

Julie Tolu^{A, B}, Isabelle Le Hécho^A, Maïté Bueno^A, Yves Thiry^B and Martine Potin-Gautier^A

^ALaboratory of Environment and Bio-Inorganic Analytical Chemistry (LCABIE), Pau, France, Email julie.tolu@etud.univ-pau.fr

^BNational Radioactive Waste Management Agency (ANDRA), Châtenay-Malabry, France, Email yvesthiry@andra.fr

Abstract

This study aimed to develop a methodology to determine selenium speciation in soils at ultra-trace level. This methodology was optimised with a soil containing 431 ± 44 $\mu\text{g}/\text{kg}$ of native selenium. Analytical procedure was based on liquid chromatography-inductively coupled plasma mass spectrometry (HPLC-ICP-MS). A special attention was paid on selenium species extraction optimisation. Extractants were chosen on the basis of reagents used in Se sequential extraction schemes. Conservation of the original Se speciation in soil during extraction was checked for each extractant. After extraction, total Se was quantified in dissolved (extracts) and solid phases. Extraction efficiencies were in order waters \ll citric acid \approx phosphate buffers $<$ nitric acid \ll sodium hydroxide. Speciation analyses indicate the occurrence of selenite (SeIV) in all extracts whereas selenate (SeVI) and a Se containing compound, with retention time close to the one of selenocystine specie (SeCys₂), were detected only in water extracts.

Key Words

Metalloid, environment, solid matrix, hyphenated technique, separation, biogeochemistry

Introduction

Selenium is a very important trace element because of the small difference between its essential and toxic levels (Barceloux 1999). Its long-lived radioisotope ⁷⁹Se is found in high- and intermediate level and long-lived nuclear wastes for which a geological disposal in deep clay formations is considered to be a safe and feasible option (ANDRA 2005). The safety assessment of nuclear waste disposal involves the determination of potential radiological consequences. That implies the understanding of Se transfers in biosphere. In that context, Se speciation data in the different soil components (solid phase, soil solution and associated colloids) are important because the various Se species have different toxicity and different behaviours in the environment (Séby *et al.* 1998). The speciation determination can be obtained by solid analysis techniques for samples with high Se concentrations (mg/kg). Such results are not transposable to samples containing low selenium concentrations ($\mu\text{g}/\text{kg}$), in particular in a radiological context or biosphere monitoring. In this case, inductively coupled plasma mass spectrometry (ICP-MS) is one of the most often used detection systems for total and speciation analyses due to its high sensitivity and its easy coupling to HPLC (Darrouzès *et al.* 2005; Montes-Bayon *et al.* 2003; Ponce De León *et al.* 2002). However, studies on Se speciation in soils using these hyphenated techniques are scarce in literature. An extraction step is necessary before analysis of dissolved species (Séby *et al.* 1997). In this study the extraction step was optimised to ensure sample integrity, i.e. original distribution of the Se species. Different reagents were selected on the basis of sequential extractions schemes and tested (Coppin *et al.* 2006; Ponce de León *et al.* 2003). Extractant efficiencies were calculated from total Se determinations in supernatant and residual solid phase. HPLC-ICP-MS analyses were performed allowing determination of selenite (SeIV), selenate (SeVI), selenomethionine (SeMet) and selenocystine (SeCys₂) depending on extraction solution (Darrouzès *et al.* 2005).

Material and method

Reagents and samples

All reagents used were analytical grade. Ultrapure water was obtained from Milli-Q System (18,2 $\Omega\cdot\text{cm}$). An English meadow clay loam soil (Rothamsted) was used for method optimisation. It was air dried, sieved (<2 mm) and grinded in zirconium bowl during 7 minutes at 30 Hz before mineralization and extraction.

Soil mineralization and extractions procedures

The soil was mineralized by microwave-assisted acid digestion (Milestone). To validate the mineralization, 3 reference soil materials (ZC73001, BCR-143R and GBW 07405) were digested in the same manner. According to the literature, seven selective chemical solutions were tested: nitric acid (1 mol/L), citric acid (0.1 mol/L), ultra-pure water, calcium chloride ($5 \cdot 10^{-4}$ mol/L), phosphate buffer ($\text{KH}_2\text{PO}_4/\text{K}_2\text{HPO}_4$; 0.1 mol/L) with pH 7 and 8, and sodium hydroxide (0.1 mol/L). Each extraction was realized in triplicate with following operating

conditions: 150 mg of soil was placed in polypropylene tubes with 5 mL of the extractant, the mixture was shaken at 250 rpm during 24h. Then, suspension was centrifuged at 15000 g for 30 min at 4°C. The supernatant was taken up and stored in polypropylene tubes at 4°C until analysis. Residual solid phase was mineralized.

Total and speciation selenium determination

Total selenium was determined with an Agilent 7500ce ICP-MS instrument equipped with an octopole collision/reaction cell. The sample introduction system was constituted of a Micromist nebuliser and a Scott spray chamber. Operating conditions were optimised daily and m/z monitored with ⁷⁸Se. Selenium speciation was determined by a High Performance Liquid Chromatography (Agilent Series 1100) hyphenated to ICP-MS. Chromatographic separation of SeCys₂, SeIV, SeMet and SeVI, was carried on anionic exchange column (Hamilton PRP-X100, 25cm x 4.1 mm i.d) using a 5 mmol/L ammonium citrate buffer at pH 5.2 (Darrouzès *et al.* 2005). The mobile phase was delivered at 1 mL/min isocratically. The HPLC-ICP-MS interface consisted simply in a polyetheretherketone (PEEK) capillary.

Results

Analytical performances and matrix effects studies

Analytical performances were determined for mineralization and extractions procedures according to IUPAC recommendations (IUPAC 1987):

$$\begin{aligned} \text{D.L.} &= (3\sigma)/p & \text{with } \sigma &= \text{standard deviation of 10 blanks (i.e. recreated matrix)} & 1 \\ \text{Q.L.} &= (10\sigma)/p & p &= \text{matrix calibration slope} & 2 \end{aligned}$$

Detection and quantification limits are, respectively from 0.2 to 23 and 0.7 to 77 µg/kg depending on the extraction matrix. For speciation, they are from 0.002 to 0.2 and 0.01 to 0.7 µg/kg in function of matrix and Se species. Moreover, external calibration realized in a recreated matrix (extraction or mineralization) and standards additions were performed the same day in order to control matrix effect during Se quantifications.

Selenium speciation stability during extractions

Individual Se species standards were prepared in the matrix extraction. They were analysed by HPLC-ICP-MS just after preparation and after 7 days of storage at 4°C. Speciation conservation was evaluated using the ratio R_s , which is the mean value ($[\text{Se species}]_{\text{at 7 days}}$) of 3 determinations made after 7 days storage divided by the mean value for 3 initial measurements ($[\text{Se species}]_{\text{at 0 days}}$) (Equation 3). The uncertainty measurement (U) was obtained from the variation coefficient (CV) calculated for 3 measurements (Equation 4). No instability can be concluded when the value 1 is comprised between the range $R_s \pm U$ (Kramer *et al.* 2001).

$$R_s = [\text{Se species}]_{\text{at 7 days}} / [\text{Se species}]_{\text{at 0 days}} \quad 3$$

$$U = R_s \cdot (\text{CV}^2_{\text{at 7 days}} + \text{CV}^2_{\text{at 0 days}})^{1/2} / 100 \quad 4$$

Only results obtained for Se species observed in soil extracts (i.e. SeIV, SeVI and SeCys₂) are presented in this paper (Table 1). Results indicate that selenium species are stable in extractant solutions during 7 days.

Table 1. Selenium speciation stability during extractions (n.d. = No Determined)

	SeIV: $R_s \pm U$	SeVI: $R_s \pm U$	SeCys ₂ : $R_s \pm U$
Nitric acid and citric acid	n.d. – strong matrix effect on chromatographic separation		
Ultrapure water	0.99 ± 0.05	1.00 ± 0.03	0.97 ± 0.04
Phosphate buffer pH 7	0.98 ± 0.02	0.99 ± 0.04	1.00 ± 0.02
Phosphate buffer pH 8	0.98 ± 0.06	1.00 ± 0.05	0.99 ± 0.02
Sodium hydroxide	1.00 ± 0.04	0.99 ± 0.04	0.98 ± 0.03

Validation of the selenium total determination protocol and Se_{total} concentration in the Rothamsted soil

Total selenium concentrations of soil reference materials obtained after mineralization and ICP-MS analyses were in complete agreement with theoretical values (Table 2). Thus, the protocol of total Se determination in soil was validated.

Table 2. Selenium total concentrations in the studied soil and reference soil materials (in µg(Se)/kg, mean values on 12 replicates, s.d. = standard deviation)

	Rothamsted soil	NCS ZC73001	BCR-143R	GBW-07405
Theoretical values	423 (no s.d.)*	210 ± 20	600 (no s.d.)	1560 (no s.d.)
Obtained values	431 ± 44	225 ± 30	532 ± 54	1536 ± 123

* value obtained by Arras Laboratory (INRA, France)

Calculated mass balances (Extracted Se + residual Se) resulting from tested extractions indicate that no contamination or losses occurred during extraction (Figure 1) allowing validation of the extraction protocol.

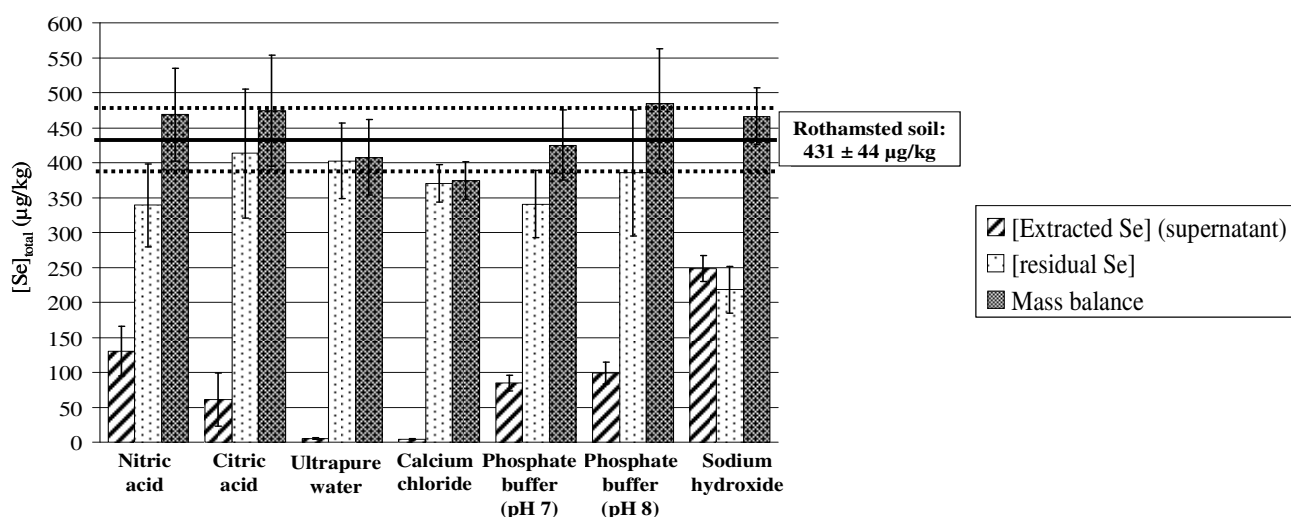


Figure 1. Mass balances for each extraction (— : $[\text{Se}]_{\text{total}}$ in Rothamsted soil; - - : standard deviation of $[\text{Se}]_{\text{total}}$)

Extraction efficiencies and selenium speciation

The efficiencies of tested extractants increase following: ultrapure water \approx calcium chloride \ll citric acid \approx phosphate buffer pH 7 \approx phosphate buffer pH 8 < nitric acid \ll sodium hydroxide (Table 3), which is consistent with their successive use in sequential extraction scheme for selenium (Coppin *et al.* 2006; Martens and Suarez 1997; Ponce de León *et al.* 2003; Wright *et al.* 2003; Zhang and Moore 1996).

Table 3. Efficiencies of extractions and Se speciation in extracts (n.d. = No Determined)

Extractant	Efficiency (%)	Se speciation (% of $[\text{extracted Se}]_{\text{total}}$)
Ultrapure water	1.1 ± 0.3	SeIV = 30 ± 1 ; SeVI = 15 ± 1 ; SeCys ₂ = 19 ± 1 ; Unknown species ≈ 36
Calcium chloride	1.9 ± 0.4	SeIV = 28 ± 2 ; SeVI = 9 ± 1 ; SeCys ₂ = 34 ± 3 ; Unknown species ≈ 29
Citric acid	18 ± 3	n.d. (strong matrix effect on chromatographic separation)
Phosphate buffer pH 7	20 ± 1	SeIV = 94 ± 9
Phosphate buffer pH 8	22 ± 3	SeIV = 94 ± 3
Nitric acid	30 ± 7	n.d. (strong matrix effect on chromatographic separation)
Sodium hydroxide	58 ± 3	SeIV = 78 ± 9 ; Unknown species ≈ 22

Obtained extraction efficiencies are in the order of magnitude of those reported in the literature (Coppin *et al.* 2006; Kang *et al.* 1991; Martens and Suarez 1997; Séby *et al.* 1997; Zhang and Moore 1996). In the case of Se spiked soils, extraction efficiencies may be higher (Darcheville *et al.* 2008) because spiked Se is usually easier to extract than native Se. For phosphate buffer extractant, pH adjustment to 8 does not increase extraction efficiency contrary to Wright *et al.* (2003) study. But these authors have worked on synthetic model sediments spiked with Se. Selenium speciation was not determined in acidic extractions due to their strong matrix effect on chromatographic separation. Selenite was detected in all extracts (i.e. other than acidic ones), as single Se species in phosphate buffers ($94 \pm 9\%$ of total Se) and sodium hydroxide ($78 \pm 9\%$) extracts. Selenate was quantified only in ultrapure water and calcium chloride extracts. A Se-containing compound with retention time close to the one of selenocystine (SeCys₂) specie was also detected in these samples. The sum of species concentrations is in the range 64 - 78% of total Se, excepted for phosphate buffer extractants. These results could indicate i) the presence of dissolved selenium species that are not eluted by the chromatographic separation chosen. This can be checked by the use of complementary chromatographic mechanisms (e.g., reverse phase); ii) the presence of colloidal selenium species (inorganic or organic SeIV and/or SeVI or colloidal Se(0)). To confirm this last hypothesis, extract analyses with Flux Force Fractionation (FFF) hyphenated to Multi-Angle Laser Light Scattering and UV would allow identification and characterisation of the different colloid families. Corresponding total selenium concentrations can be obtained by FFF - ICP-MS coupling.

Conclusion

For each extractant, ultra-trace total and speciation selenium quantification was carefully controlled by matrix effect studies. Repeatability and reproducibility of developed analytical methodology are below 10%. In this study, relevance of the different extractants was evaluated on the basis of three key factors: i) sample integrity preservation (i.e. original distribution of Se species in soil sample); ii) quantitative Se extraction; iii) Se binding phase assessment (i.e. mobility data). Selenium species stability was controlled for all extractants excepted for

acidic ones due to their strong matrix effect on chromatographic separation. Three extractants showed to be of particular interest: sodium hydroxide, phosphate buffer at pH 7 and ultrapure water. Indeed, highest extraction efficiencies (about 60%) were obtained with sodium hydroxide, a reagent usually used to dissolve organic solid phase. Both phosphate buffers (pH 7 and 8) showed similar results with an extraction efficiency of about 21%; a pH 7 buffer is generally used in literature to access Se fraction bounded to Fe, Al and Mn (oxy)hydroxides and clays. The amount of Se extracted with ultrapure water was low (about 1%) but such determination is very important since water soluble selenium is considered as mobile and available fraction for living organisms (Gissel-Nielsen and Bisbjerg 1970), especially with regards to native Se. For the Rothamsted soil, three Se species (SeIV, SeVI and a Se containing compound, probably SeCys₂) were observed in the water extracts whereas SeIV was the single extracted Se species in phosphate buffers and sodium hydroxide.

References

- ANDRA (2005) Dossier Argile : Synthèse. Evaluation de la faisabilité du stockage géologique en formation argileuse
- Barceloux DG (1999) Selenium. *Journal of Toxicology - Clinical Toxicology* **37**, 145-172.
- Coppin F, Chabrouillet C, Martin-Garin A, Balesdent J, Gaudet JP (2006) Methodological approach to assess the effect of soil ageing on selenium behavior: first results concerning mobility and solid fractionation of selenium. *Biology and Fertility of Soils* **42**, 379-386.
- Darcheville O, Février L, Haichar FZ, Berge O, Martin-Garin A, Renault P (2008) Aqueous, solid and gaseous partitioning of selenium in an oxic sandy soil under different microbiological states. *Journal of Environmental Radioactivity* **99**, 981-992.
- Darrouzès J, Bueno M, Lespès G, Potin-Gautier M (2005) Operational optimisation of ICP-octopole collision/reaction cell-MS for applications to ultratrace selenium total and speciation determination. *Journal of Analytical Atomic Spectrometry* **20**, 88-94.
- Gissel-Nielsen G, Bisbjerg B (1970) The uptake of applied selenium by agricultural plants - 2. The utilization of various selenium compounds *Plant and Soil* **32**, 382-396.
- IUPAC (1987) Recommendations for the definition, estimation and use of the detection limit *The Analyst* **112**, 199-204
- Kang Y, Yamada H, Kyuma K, Hattori T, Kigasawa S (1991) Selenium in soil humic acid. *Soil Science and Plant Nutrition* **37**, 241-248.
- Kramer KJM, Kramer GN, Muntau H (2001) Practical Manual for the Production of Laboratory Reference Materials. *Project "Training on Production and Use of Laboratory Reference Materials for Use in Routine Quality Control" (TRAP-LRM) MERMAYDE, Bergen, Netherland.*
- Martens DA, Suarez DL (1997) Selenium Speciation of Soil/Sediment Determined with Sequential Extractions and Hydride Generation Atomic Absorption Spectrophotometry. *Environment Science and Technology* **31**, 133-139.
- Montes-Bayon M, DeNicola K, Caruso JA (2003) Liquid chromatography-inductively coupled plasma mass spectrometry. *Journal of Chromatography A* **1000**, 457-476.
- Ponce de León CA, DeNicola K, Montes-Bayon M, Caruso JA (2003) Sequential extractions of selenium soils from Stewart Lake: total selenium and speciation measurements with ICP-MS detection. *Journal of Environmental Monitoring* **5**, 435-444.
- Ponce De León CA, Montes-Bayón M, Caruso JA (2002) Elemental speciation by chromatographic separation with inductively coupled plasma mass spectrometry detection. *Journal of Chromatography A* **974**, 1-21
- Séby F, Potin-Gautier M, Giffaut E, Donard OFX (1998) Assessing the speciation and the biogeochemical processes affecting the mobility of selenium from a geological repository of radioactive wastes to the biosphere. *Analisis* **26**, 193-198.
- Séby F, Potin-Gautier M, Lespes G, Astruc M (1997) Selenium speciation in soils after alkaline extraction. *The Science of the Total Environment* **207**, 81-90.
- Wright MT, Parker DR, Amrhein C (2003) Critical Evaluation of the Ability of Sequential Extraction Procedures To Quantify Discrete Forms of Selenium in Sediments and Soils. *Environment Science and Technology* **37**, 4709-4716.
- Zhang Y, Moore JN (1996) Selenium Fractionation and Speciation in a Wetland System. *Environment Science and Technology* **30**, 2613-2619.

Distribution of a nonylphenol isomer and the herbicide MCPA in soil derived organo-clay complexes

Timm Klausmeyer^A, Patrick Riefer^B, Andreas Schäffer^A, Jan Schwarzbauer^B and Burkhard Schmidt^A

^AInst. for Environmental Biology and Chemodynamics (UBC), RWTH Aachen University, Germany, Timm.Klausmeyer@bio5.rwth-aachen.de

^BInst. for Geology and Geochemistry of Petroleum and Coal (LEK), RWTH Aachen University, Germany, riefer@lek.rwth-aachen.de

Abstract

Organo-clay complexes in soil play an important role in the immobilization and persistence of xenobiotics. In this study, the fate of ¹⁴C-labeled 4-(3,5-dimethylhept-3-yl)phenol (NP) and 4-chloro-2-methylphenoxyacetic acid (MCPA) in soil was examined using incubation periods from 1d to 180d (NP) and 1d to 120d (MCPA). Special emphasis was on the distributions of the compounds and its degradation products among the soil sub-fractions sand, silt and clay, which were obtained by particle size fractionation. Additionally the soil organic matter complexed to the clay fraction was fractionated by a conventional procedure into an humic acids (HA), fulvic acids (FA) and humin (HU) in order to localize the site of binding of the xenobiotics within this important soil fraction.

During the experiments, which were performed with two concentrations of the xenobiotics, the microbial activity in the assays was examined by determination of the DMSO reductase activity. A considerable reduction of the microbial activity was observed with the high concentrations of MCPA and NP (1 mg /g) as compared to the low concentrations (MCPA 559 µg per 100 g, NP: 121 µg per 100 g of soil).

A different incorporation behavior was observed for NP and MCPA which resulted in distinctly different distributions of radioactivity within soil sub-fractions. MCPA exhibited a lower tendency to interact with soil particles, although the portions associated with soil particles were non-extractable with organic solvents. In contrast, the high affinity of NP to particles was accompanied by a lower formation of non-extractable residues. The total distribution of ¹⁴C seemed to be influenced significantly by the physico-chemical properties of the contaminants and the microbial activity in soil.

Key Words

4-(3,5-dimethylhept-3-yl)phenol (NP), 4-chloro-2-methylphenoxyacetic acid (MCPA), organo-clay complexes, xenobiotics, microbial activity

Introduction

Xenobiotics in agricultural soils originate predominantly from the application of pesticides and fertilizers including sewage sludge. Organic contaminants released into soils exhibit a complex environmental behavior. Besides extractable and therefore, available portions, chemicals can form so-called non-extractable or bound residues. The processes leading to these kind of residues including aging have been investigated for decades, especially regarding pesticides (Dec *et al.* 1997; Barriuso *et al.* 2008; Mac Rae 1986). So far, however, the knowledge on soil bound residues of xenobiotics is prevalingly restricted to the determination and of amounts of free and bound fractions. In contrast, detailed information on the behavior of chemicals in particular regarding their distribution in sub-fractions of soils is limited (e.g. Nieman *et al.* 1999).

Therefore, the aim of the present study was to follow the behavior of the anthropogenic contaminants MCPA, 4-chloro-2-methylphenoxyacetic acid, and a defined nonylphenol isomer, 4-(3,5-dimethylhept-3-yl)phenol (NP), in soils with time concerning different soil sub-fractions. The herbicide MCPA was regarded as representative for pesticides, the nonylphenol isomer as representative for sewage sludge derived xenobiotics. Besides different pathways of pollution, MCPA and NP also exhibit different physico-chemical properties which might result in a different behavior in soils (Xie *et al.* 1997). Special focus was laid on organo-clay complexes since these are known to play an important role for the formation of bound residues (Wang and Xing 2005).

Methods

Chemicals - ¹⁴C-labeled 4-(3,5-dimethylhept-3-yl)phenol (NP, 304.14 MBq/mmol) was synthesized via Friedel-Crafts alkylation using 3,5-dimethylheptan-3-ol and a mixture of unlabeled and [ring-U-¹⁴C] phenol (2.220 MBq/mmol) according to (Russ *et al.* 2005). [Ring-U-¹⁴C] 4-chloro-2-methylphenoxyacetic acid (MCPA, 59.94 MBq/mmol) was provided by Prof. M. H. Gerzabek (University of Vienna) as a mixture of 92 % MCPA methylester and 8 % of the free acid.

Spiking experiments - Aliquots of 559 µg (0.167 MBq) of MCPA dissolved in 0.5 mL methanol were applied to 100 g of air-dried, homogenized and sieved (≤ 2 mm) soil samples from Fuhrberg, Germany. In a second experiment, 121 µg (0.167 MBq) of NP dissolved in 0.5 mL petrolether was similarly applied to a soil sample from the same location. Directly after application, the solvent was evaporated and the flasks were shaken for 15 min in an overhead shaker. Thereafter, the water content of the samples was adjusted to 60% of maximum water holding capacity. The flasks were closed with an absorption device for $^{14}\text{CO}_2$ containing soda lime (approx. 15 g). After incubation periods of 1 d to 180 d (NP) and 1 d to 120 d (MCPA) at 20 °C in the dark, 20g of the soil samples (based on dry weight) were suspended in 100 mL of water and subjected to ultrasonic assisted disaggregation (total energy 22 kJ) as described by Morra *et al.* (1991). The soda lime was dissolved in conc. HCl and the liberated $^{14}\text{CO}_2$ was captured in scintillation cocktail Lumasafe™ plus (Lumac), and was examined by a 2250CA TRI-CarB® scintillation counter (Canberra-Packard). A similar approach was applied in an experiment using 1 mg per g soil of non-labeled NP and MCPA, while the assays contained 50 g of soil.

Particle size separation and fractionation of humic substances - Sand, silt and clay fractions were obtained by manual wet sieving for separation of sand from silt and clay. Silt and clay were then separated by centrifugation according to (Stemmer *et al.* 1998). Subsequently, the clay fraction containing predominantly organo-clay complexes was extracted using a Soxhlet apparatus and methanol and dichloromethane consecutively. The remaining extracted clay was then suspended in 0.5 M NaOH for 24 h with shaking. The mixture was subsequently subjected to centrifugation in order to separate the insoluble humin fraction (HU) from the solubilized humic acids (HA) and fulvic acids (FA). The latter fraction was finally acidified with HCl (pH 1). Pricipitated HA were separated from the FA, which remained in solution, by centrifugation.

Radioanalysis – Radioactivity contained in solid samples (aliquots of sand, silt and clay fractions) were combusted using a Biological Oxidizer OX500 (R. J. Harvey Instrument Corp.) and emerging $^{14}\text{CO}_2$ was trapped in Oxyvolve C-400 scintillation cocktail (Zinnser Analytic). Radioactivity contained in liquid samples was determined by dissolving aliquots in Lumasafe™ plus (Lumac) scintillation cocktail.

Microbial activity – The reduction of dimethylsulfoxide to dimethylsulfide was utilized for the determination of microbial activity in soil samples (Alef and Kleiner 1989). For this purpose, 1 g soil was transferred to a 20 ml flask. After application of 200 µl of 5% DMSO in water (v/v) the flasks were closed tightly. After incubation for 24 h, 100 µl of the headspace of the flasks was analyzed for developed DMS using an Agilent 6890N gas chromatograph equipped with a flame ionization detector.

Results

Mineralization – Concerning mineralization in the samples with low concentration (MCPA: 559 µg per 100 g of soil; NP: 121 µg per 100 g of soil), both substances exhibited an initial lag phase for 7 days, which was followed by a linear increase of mineralization for subsequent 7 days in case of MCPA and subsequent 24 days in case of NP. The mineralization rate decreased with both substances after 14 days and 30 days of incubation, respectively. After 14 days incubation times we detected 3% and on day 90 14% mineralization for NP, and for MCPA (at days 30, 60 and 120) 34%, 46%, and 48%, respectively. Samples with 1 mg xenobiotic per g of soil produced 0,6% and 2,3 % ^{14}C -CO₂ for NP after 14 and 90 days and for MCPA 1,2%, 3,8% and 57% mineralization respectively at days 30, 60 and 120. At the higher concentrations of the xenobitoics the microbial (DMSO reductase) activity was reduced by 50% as compared to the samples with low concentrations.

Percentages of ^{14}C in soil particle fractions – In the assays incubated with low concentration of MCPA for up to 14 days, most of the radioactivity contained in the samples was extracted with the water used for particle separation. About 20% of applied radioactivity was localized in the clay and silt fractions. In the assays with 1 mg /g of MCPA, however, about 60% of applied ^{14}C were detected in the water used for particle separation, and only 8% to 12% were associated with the clay and silt fractions. In case of NP, on average 32% of the applied radioactivity was found each in the clay and silt fractions, whereas only 6-11% of applied ^{14}C were extracted with the water used for particle separation.

Percentages of ^{14}C in organic matter associated with clay fractions – A significant increase of the portions of non-extractable residues in all organic matter fractions examined were observed during the first 14 days of incubation in the assays with low concentrations of both MCPA and NP. Generally, smaller amounts of radioactivity were extracted (methanol and dichloromethane) in case of MCPA as compared to NP. With both compounds, the fulvic acids fractions contained the lowest amounts of ^{14}C -residues. 5% of applied ^{14}C -MCPA were bound to the FA, 6% to HU, and 8% to the HA after 120 days of incubation. A similar result was obtained

for NP: after 180 days, 4% were associated with the FA, 9% with HU, and 14% with the HA fraction. In case of high MCPA concentrations in soil (1 mg /g), portions of ¹⁴C in these organic matter fractions were 40% to 60% lower than those obtained in soils incubated with low concentrations .

Conclusions

Organo-clay complexes as biogeochemical interfaces as well as the characteristics of the applied substances were of great importance for their immobilization and persistence in soil. Additionally the microbial activity in the soil influenced the mineralization rate as well as the immobilization and persistence of xenobiotics in soil. The present findings suggest that the lowered microbial activity detected during the first 60 days of incubation with 1 mg /g of MCPA had a considerable effect on the formation of non-extractable residues of the compounds.

References

- Alef K, Kleiner D (1989) Rapid and Sensitive Determination of Microbial Activity in Soils and in Soil Aggregates by Dimethylsulfoxide Reduction. *Biology and Fertility of Soils* **8**, 349-355.
- Barriuso E, Benoit P, Dubus IG (2008) Formation of pesticide nonextractable (bound) residues in soil: Magnitude, controlling factors and reversibility. *Environmental Science and Technology* **42**, 1845-1854.
- Dec J, Haider K, Rangaswamy V, Schaffer A, Fernandes E, Bollag JM (1997) Formation of soil-bound residues of cyprodinil and their plant uptake. *Journal of Agricultural and Food Chemistry* **45**, 514-520.
- Mac Rae IC (1986) Formation and degradation of soil-bound [¹⁴C] fenitrothion residues in two agricultural soils. *Soil Biology and Biochemistry* **18**, 221-225.
- Morra MJ, Blank RR, Freeborn LL, Shafii B (1991) Size Fractionation of Soil Organo-Mineral Complexes Using Ultrasonic Dispersion. *Soil Science* **152**, 294-303.
- Nieman JKC, Sims RC, Sims JL, Sorensen DL, McLean JE, Rice JA (1999) [¹⁴C]Pyrene Bound Residue Evaluation Using MIBK Fractionation Method for Creosote-Contaminated Soil. *Environmental Science and Technology* **33**, 776-781.
- Russ AS, Vinken R, Schuphan I, Schmidt B (2005) Synthesis of branched para-nonylphenol isomers: Occurrence and quantification in two commercial mixtures. *Chemosphere* **60**, 1624-1635.
- Stemmer M, Gerzabek MH, Kandeler E (1998) Organic matter and enzyme activity in particle-size fractions of soils obtained after low-energy sonication. *Soil Biology & Biochemistry* **30**, 9-17.
- Wang KJ, Xing BS (2005) Structural and sorption characteristics of adsorbed humic acid on clay minerals. *Journal of Environmental Quality* **34**, 342-349.
- Xie H, Guetzloff TF, Rice JA (1997) Fractionation of pesticide residues bound to humin. *Soil Science* **162**, 421-429.

Distribution of silicon in soils and sediments of a small catchment area: similarities and differences

Petra Tallberg, Maria Lehtimäki and Virpi Siipola

Department of Food and Environmental Sciences, Section of Soil Science, PO Box 27. FIN-00014 University of Helsinki, Finland, Email petra.tallberg@helsinki.fi

Abstract

The uptake and transformation of silicon (Si) by terrestrial plants is of importance for both the plants themselves and for the transport of Si from the watershed. The occurrence and transport of potentially bio-available Si pools from soil in the drainage area to rivers, lakes and the sea may significantly influence the phytoplankton composition and ecological state of the receiving water body due to complicated ecological interactions. The distribution of biogenic Si in soil, seston (suspended particles), and sediment in samples from a small watershed in Southern Finland was studied and the different compartments compared to each other and to environmental variables. The biogenic Si content in the different parts of the watershed varied, and biogenic Si produced by diatom algae in the aquatic part of the watershed appeared to be more important than the transformation of dissolved Si into phytoliths by terrestrial plants in the soil. More information on the variability of the biogenic Si (phytolith) content in different types of soil and on the differentiation between diatom and phytolith Si in waters are needed.

Key Words

Silicon, Soil, sediment, seston, catchment, watershed

Introduction

Although silicon (Si) is one of the most abundant elements on earth in general (Wollast and McKenzie, 1983) and in soil in particular (see Sommer *et al.*, 2006), most of this Si is inert on the time-scales relevant when short-term chemical and biological processes involving the element are concerned. Such processes of ecological relevance are, for example, Si uptake by plants and the transport of Si from soil to adjacent water bodies (leaching). Although Si is not considered an essential element for plant growth, its role as an important ameliorative factor has recently been more and more widely recognized (e.g. Ma and Yamaji, 2006; Vaculik *et al.*, 2009). The Si taken up by terrestrial plants is transformed into silica bodies known as phytoliths or plant opal (bio-opal), which are relatively resistant to dissolution and remain in the soil upon the decay of the plant (see e.g. Alexandre *et al.*, 1997).

Leaching of Si from soil in the watershed to the receiving water bodies is, also, a major qualitative factor which affects the constitution of the food web in the water body concerned (Smayda, 1990; Humborg *et al.*, 2000). Some algae, mainly the diatoms, have a high and absolute requirement for Si, and the supply of Si from the watershed thus affects the composition of the phytoplanktonic community responsible for the primary production in lakes and oceans drastically (e.g. Reynolds, 1980). A decrease in the supply of Si may e.g. cause a shift in the planktonic community from the often relatively benign diatoms to e.g. toxic cyanobacteria or dinoflagellates (which do not require Si at a macronutrient level). Silicon may be transported into the waters in dissolved, biogenic or particulate form, with phytoliths playing a so-far relatively little known role (e.g. Alexandre *et al.*, 1997). In order to understand the processes that affect the transport of Si from the watershed to lakes, rivers and oceans, a better understanding of the distribution of potentially mobile forms of Si in soil and the processes affecting them is needed. In this study, the distribution of one of the main potentially mobile forms of Si (biogenic Si) in soil, seston and sediment samples from a small watershed in Southern Finland was studied. Two different methodologies developed for biogenic Si analysis were used and their comparability estimated.

Methods

Study area

Samples were taken from the Vikträsk sub-catchment (a sub-area of the Siuntionjoki River catchment) situated in Southern Finland in the boreal vegetation zone (Figure 1). The soil in the study area consists predominantly of glacial clay and silt deposits, with some sand eskers and moraine deposits. The bedrock in the area consists of granite. Most of the catchment is covered by forest (ca 60%, coniferous and mixed deciduous/coniferous, mostly pine, spruce and birch), with 30% cultivated fields (wheat, cultivated lawn) and the rest mainly urban areas.



Figure 1. The study area (Vikträsk sub-catchment) in Southern Finland (1: 115 000). Samples were taken from each lake, river and from the catchment soil (see text for details).

Sampling

Topsoil samples (0-10 cm) were taken with a hand-held corer from representative sampling sites covering the main soil types and forms of land use (Figure 1). Sediment samples (0-1 cm) were taken from the rivers (including small ditches) and lakes in the study area. Samples for suspended particulate material (seston) were taken from the same water bodies using a Limnos tube sampler. Soil and sediment samples were oven-dried (+60°C) and carefully homogenized with a mortar and pestle before analysis. Seston was collected by filtering the water samples through 0.2 µm polycarbonate membrane filters, which were then also oven-dried at +60°C. Flow velocity in the brooks was measured with a

Background data (soil type, vegetation and land use, physical and chemical water quality data from the studied water bodies) were obtained from the data bases at the Finnish Environment Institute.

Analyses

Dissolved Si was analysed from 0.2 µm (polycarbonate filters, Nuclepore) filtered water samples using ICP-OES (inductively coupled plasma optical emission spectrometry). From the soil and sediment samples biogenic Si was analysed using a modification of the procedure by DeMaster (1981). Thirty (+/-5) mg of dry material was weighed into polyethylene 100 ml bottles (Plastex Ltd) and extracted with 40 ml 1% sodium carbonate (Na₂CO₃) in a +85°C water bath for 5 hours.. At 3, 4 and 5 h 1 ml- samples for Si analysis (ICP-OES) were taken from each bottle and diluted with 9 ml of 0.021N HCl. The biogenic Si concentration of the sediment samples was then calculated as the intercept of the linear regression line through the 3, 4 and 5 h time points.

The analysis (mineral correction) is based on the assumption that all biogenic Si in the sediment samples has dissolved during the first three hours of the extraction, while mineral-derived Si is dissolved from the sample in smaller amounts at a constant rate throughout the extraction (see e.g. Conley 1998 for a closer description).

From the seston (suspended particulate material) samples, biogenic Si was analysed according to Ragueneau *et al.* (2005). 40-100 ml water subsamples were filtered through 0.2 µm polycarbonate filters (Nuclepore), and the filters were dried in open test-tubes at +60°C. The dried filters were extracted with 4 ml 0.2 M NaOH in a water bath at 100°C for 40 min. After this, they were acidified with 1.0 ml 1.0 M HCl, centrifuged (2500 rpm, 10 min), and a subsample for Si and Al analysis (by ICP-OES) was taken. The filter was thereafter washed three times with deionised water and dried at +60°C, whereafter the extraction and sampling was repeated. The concentration of biogenic Si in the sample was thereafter calculated as biogenic Si = $Si_1 - Al_1(Si_2/Al_2)$, where Si_1 and Al_1 are the concentration of Si and Al measured after the first extraction and Si_2 and Al_2 the concentrations after the second extraction. The analysis is based on the assumption that all the biogenic Si and some of the minerogenic Si and Al is extracted in the first digestion, while the Si:Al ratio of the second digestion is characteristic of the silicate minerals in the sample.

Diatom and other phytoplankton concentrations were enumerated from all water samples using the inverted microscope technique described by Utermöhl (1958). From the seston, soil and sediment samples the organic material was removed using acid microwave digestion and samples for diatom and phytolith analysis were prepared using standard techniques (see e.g. Battarbee, 1986).

Results

Both the methods used for biogenic Si analysis worked well for the analysed samples, although in samples with high amounts of organic material the removal of the excess organic matter (by acid digestion) was needed (data not shown).

Table 1. The concentration of diatoms (mg/l water) and their percentual share of the phytoplankton biomass in the studied water bodies. Average flow velocity (Q, m³/s) and concentration of dissolved Si (DSi, mg/l), total phosphorus (P_{tot}, µg/l) and total nitrogen (N_{tot}, µg/l) is also shown when available.

	Diatoms, %	Diatoms, mg/l	Q, m ³ /s	DSi, mg/l	P _{tot} , µg/l	N _{tot} , µg/l
River Sjunby	65	0.24	5.21	2.01	88.6	1550
Lake Rudträsk	24	0.09	-	9.30	14.0	1700
Rudbäck Brook	17	0.03	0.02	9.33	17.5	788
Billskogbäcken Brook	0.0	0.00	0.02	18.9		
Bölebäcken Brook	57	0.11	0.05			
Lake Lilla Bladträsk	35	4.33	-			
Lake Stora Bladträsk	0.3	0.03	-			
Stora Bladträsk-Långträsk Brook	0.0	0.00	0.00			
Lake Långträsk	7.3	0.04	-	3.14	15.0	570
Långträsk-Lapträsk Brook	3.9	0.01	0.00			
Mörtviken Brook	22	0.02	0.00	7.35		
Lake Lapträsk	39	0.07	-	1.03	15.0	408
Lapträskbäcken Brook	35	0.08	0.01			
Lake Vikträsk	98	11.5	-		77.7	1400
River Pikkalalanjoki	53	0.17	5.21	6.89	69.2	1370
Pikkalanlahti Bay	24	0.02	-			

Diatoms generally dominated the phytoplankton in the studied lakes, brooks and rivers, although the biomass (mg/l) was often low (Table 1). The concentration of biogenic Si was different in soils from the different parts of the watershed (Figure 2). Soil type influenced the concentration of biogenic Si both in the water and the soil, mainly through the availability of dissolved Si (Table 1 and Figure 2). In the water bodies, the BSi or diatom content was also related to the trophic state of the water body (i.e. to the availability of other main nutrients, N and P) and to the flow velocity of the water (Table 1).

Conclusion

The BSi content in the different parts of the watershed varied significantly. The transformation of dissolved Si into biogenic Si by diatom algae in the aquatic part of the watershed appeared to be more important in the studied area than the transformation of dissolved Si into phytoliths by terrestrial plants in the soil. More studies on, especially, the variability of the biogenic Si (phytolith) content in different types of soil are urgently needed.

References

- Alexandre A, Meunier J-D, Colin F, Koud J-M (1997) Plant impact on the biogeochemical cycle of silicon and related weathering processes. *Geochim. Cosmochim. Acta* **61**, 677-82.
- Battarbee RW (1986) Diatom analysis. In "Handbook of Holocene palaeoecology and palaeohydrology" (Ed. B.E. Berglund), pp 527-570. (Wiley, Chichester).
- Conley D (1998) An interlaboratory comparison for the measurement of biogenic silica in sediments. *Mar Chem* **63**, 39-48.
- DeMaster D (1981) The supply and accumulation of silica in the marine environment. *Geochim Cosmochim Acta* **45**, 1715-1732.
- Humborg C, Conley D, Rahm L, Wulff F, Cociasu A, Ittekkot V (2000) Silicon retention in river basins: Far-reaching effects on biogeochemistry and aquatic food webs in coastal marine environments. *Ambio* **29**, 45-50.
- Ma JF, Yamaji N (2006) Silicon uptake and accumulation in higher plants. *Trends Plant Sci* **11**, 392-397.
- Ragueneau O, Savoye N, Del Amo Y, Cotton J, Tardiveau B, Leynaert A (2005) A new method for the measurement of biogenic silica in suspended matter of coastal waters: using Si: Al ratios to correct for the mineral interference. *Cont. Shelf. Res.* **25**, 697-710.
- Reynolds C (1980) The ecology of freshwater phytoplankton. Cambridge U.Press, Cambridge. 384 p.
- Smayda T (1990) Novel and nuisance phytoplankton blooms in the sea: Evidence for a global epidemic. *Toxic marine phytoplankton* 29-40.
- Sommer M, Kaczorek D, Kuzyakov Y, Breuer J (2006) Silicon pools and fluxes in soils and landscapes: a review. *Journal of Plant Nutrition and Soil Science* **169**, 294-314.
- Utermöhl H (1958) Zur Vervollkommnung der quantitativen Phytoplankton-Metodik. *Mitt. int. Ver. Limnol.* **9**, 1-38.
- Vaculik M, Lux A, Luxova M, Tanimoto E, Lichtscheidl I (2009) Silicon mitigates cadmium inhibitory effects in young maize plants. *Environmental and Experimental Botany* **67**, 52-58.
- Wollast R, McKenzie FT (1983) The global cycle of silica. In "Silicon geochemistry and biochemistry." (Ed. Aston SR), pp. 39-76. (Academic Press: San Diego).

Distributions of soil phosphorus in China's densely populated village landscapes

Linzhang Yang

Institute of Soil Science, Chinese Academy of Sciences, Nanjing, 210008, China

Abstract

Village landscapes, which integrate small-scale agriculture with housing, forestry and other land use practices, cover more than 2×10^6 km² across China. And accumulation of excess phosphorus in soils has become an important contributor to eutrophication across China. The aim of this study was to investigate relationships between fine-scale patterns of agricultural management and soil total phosphorus (STP) within China's village landscapes. The results showed that STP stock across five village regions (0.9×10^6 km²) was approximately 0.14 Pg (1 Pg=10¹⁵ g), with village landscape STP density varying significantly with precipitation and temperature. Outside the Tropical Hilly Region, STP densities also varied significantly with land use, and cover. As expected, the highest STP densities were found in agricultural lands and in areas near buildings, while the lowest were in nonproductive lands and forestry lands. A surprisingly large portion of village STP stock was associated with built structures and disturbed lands surrounding them, which had a significant relationship with population density. Our results demonstrated that local patterns of land management and human residence were associated with substantial differences in STP both within and across China's village landscapes.

Key Words

Phosphorus density, village landscape, China.

Introduction

Phosphorus (P) is highly heterogeneous in spatial distribution, and P inputs are critical in determining whether eutrophication occurs (Vadas *et al.* 2007). It is therefore critical to understand how P varies in response to climate, land use, and other factors when evaluating the role of terrestrial ecosystem processes in altering the global P cycle. Landscape change is an important part of environmental earth dynamics (Vitousek 1994). Densely populated villages cover approximately 8×10^6 km² globally, and in China alone, village landscapes was about 25% of the global village area (Ellis 2004). Changes in land use and land cover within China's intensively populated village landscapes are dominated by fine-scale landscape changes, preventing the precise measurement of these changes using conventional, coarse-resolution (≥ 30 m), land-use mapping systems (Ellis *et al.* 2006). For this reason, fine-scale (<1 m) feature-based mapping is an especially useful system for these small changes (Ellis *et al.* 2000; Ellis *et al.* 2006).

Methods

Study area and landscape classification

China's village landscapes (>150 persons per square kilometer) were first stratified into five biophysically distinct initial regions using a K-means cluster analysis of data for terrain, climate, and soil fertility as illustrated in Table 1 (Verburg *et al.* 1999). Within each region, a single 100 km² rural landscape site was then selected for detailed field research. Within each site, 12 500×500 m square landscape sample cells (25 ha) were then selected for fine-scale mapping, soil sampling, and other field measurements using a regional cluster analysis of land cover patterns (Ellis 2004).

Ecologically-distinct anthropogenic landscape features were mapped across each sample cell based on 1 m resolution IKONOS imagery and orthorectified across each site in 2002 (Ellis *et al.*, 2006). Landscape features were classified into ecotopes using the four level classification hierarchy:

FORM→USE→COVER→GROUP+TYPE, combining simple land use and cover classes (FORM, USE, COVER) with a set of more detailed feature management and vegetation classes (GROUPs) stratified into TYPEs (Ellis *et al.* 2006; <http://ecotope.org/aem/classification>).

Sampling and Analysis

Soil samples were selected using a multi-stage stratified sampling procedure designed to allocate a maximum of about 150 soil sample points within each site among the ecotope classes. First, a maximum of 10 and a minimum of 3 samples were allocated to each ecotope class in direct proportion to their regional areas. A spatially random point location was then chosen within each feature using GIS. Soil core was extracted using an

AMS Split Core sampler (AMS, American Falls, Idaho), and the submerged sediments in Yangtze Plain Region were sampled using a coring tube system (Uwitec, Austria). All statistical tests were conducted using SPSS 11.5 (SPSS, Chicago, Illinois, USA). P values < 0.05 were used to test statistical significance in all analyses. One-way analysis of variance (ANOVA) was used to examine the effect of land use, and land cover classes on STP densities.

Table 1. Sampled regions and sites (modified from Ellis 2004)

Region	Site (County, Province)	Main soil types (US Soil Taxonomy, suborder level)	Agricultural Population density (pers km ²)	Area (10 ³ km ²)	Arable Land (%)	Flat land (%)	Poor soils (%)	Annual Precipitation (mm)	Annual Mean Temperature (°C)
North China Plain	Gaoyi, Hebei	Ochrepts, Umbrepts	321	486	51	61	6	645	9
Yangtze Plain	Yixing, Jiangsu	Fluvents	464	75	44	70	17	1312	16
Sichuan Hilly	Jintang, Sichuan	Orthents, Psammments	248	198	30	4	5	950	11
Subtropical Hilly	Yiyang, Hunan	Aqualfs	188	172	18	5	85	1426	14
Tropical Hilly	Dianbai, Guangdong	Aqualts	233	71	20	16	78	1651	20

Results

STP densities and stocks

Total STP stock (0–30 cm) across the 0.908×106 km² area of the five regions was approximately 0.144 Pg, and the average STP density was 0.16 kg m⁻² (30 cm) (Table 2). The regionally STP density ranged from 0.08±0.04 kg/m² in Tropical Hilly to 0.22 kg m⁻² both in North China Plain (0.22±0.04 kg/m²) and in Yangtze Floodplain (0.22±0.19 kg/m²), which was almost a four fold difference (Table 2).

The Tropical Hilly Regions had the lowest STP density because the hydrothermal conditions of high precipitation and temperature can enhance the degree of soil weathering and P loss through surface soil erosion (Neufeldt *et al.* 2000). In contrast, the higher STP densities of the North China Plain and the Yangtze Plain may be attributed to the large area of arable land with high P fertilizer inputs (Tang *et al.* 2003). In our study, the annual precipitation (R=0.99, P=0.02) and mean annual temperature (R=0.95, P=0.05) were highly related to STP densities. In the natural land ecosystem, the STP density was highest in the North China Plain, and lowest in the Tropical Hilly, and the distribution and cycle of STP at the regional scale related to climatic, geography (China Agriculture University, 1998), the same rule in our study (except the Yangtze Plain).

Table 2. STP density and stock across five regions

Region (site)	Area (10 ⁶ km ²)	Samples	Sampled ecotope area [‡] (%)	STP (kg /m ²)	STP stock (Pg)
North China Plain (Gaoyi)	0.276	134	94.4	0.22±0.04	0.062±0.011
Yangtze Floodplain (Yixing)	0.086	153	91.8	0.22±0.19	0.019±0.016
Sichuan Hilly (Jintang)	0.084	147	91.0	0.19±0.04	0.016±0.003
Subtropical Hilly (Yiyang)	0.284	152	92.0	0.11±0.03	0.032±0.009
Tropical Hilly (Dianbai)	0.178	149	93.3	0.08±0.04	0.014±0.007
All regions	0.908	735	92.5	0.16	0.144

[‡] Total sampled ecotope area was less than 100%, because ecotope classes with areas ≤ 0.25% of each site were omitted from the sample.

Hierarchical scale-effects on STP densities and stocks

STP densities varied strongly with land use in every region except Tropical Hilly (Table 3), demonstrating that land use was likely a significant factor controlling STP densities in village landscapes. In all regions, the Constructed (Artificial surfaces and structures) had the highest STP density, because of runoff carrying high levels of P from human and animal waste origin; and decomposing of plant and animal bones releasing high levels of P (China Agricultural University 1998). While, the Forestry USE (0.10 kg m⁻²) had the lowest average STP density, confirming Grerup *et al.*'s (2006) results that total P tended to be higher in the formerly cultivated fields than in the continuously forested land. Variations in STP distribution results could be affected by differences in parent material, soil weathering, human effects, and the relative importance of these factors among regions.

STP stock was calculated using STP density and its area. It was therefore not surprising that the largest STP for a given region was related to the extent of the land USE. Each region had a unique dominant land Use and STP stock: North China plain (Irrigated, 78.4%), Yangtze Plain (Paddy, 51.2%), Sichuan Hilly (Rainfed, 49.9%), Subtropical Hilly (Paddy, 37.5%), Tropical Hilly (Forestry, 42.4%) (Table 3).

In each region, the distribution of STP density under the level of land COVER was presented in Table 4. Across the five regions, the highest average STP density presented was Sealed COVER (0.23 kg m⁻²), followed by

perennial (0.19 kg m⁻²) and annual COVER (0.17 kg /m²), and the lowest STP density was found in Barren COVER (0.07 kg /m²) (Table 4). But in our results, the Sealed COVER with low vegetation cover had the highest STP density. This is because the sealed COVER (roads, housings) had high soil bulk densities due to human and vehicle's traffic along with considerable human disturbance and P pollution which coupled contributed to high STP densities.

The Annual COVER had the highest STP stock percentage in each region except Tropical Hilly (Perennial COVER had the highest STP stock percentage). There was an obvious STP stock gradient from north to south due to climate and geography: the STP stock in Annual decreased from 76.2% in North China Plain to 16.6% in Tropical Hilly, however, the STP stock in Perennial COVER increased from 1.0% in North China Plain to 46.8% in Tropical Hilly (Table 4).

Table 3. Relative STP stocks and densities among land USE classes within each region.

Land USE	North China Plain		Yangtze Plain		Sichuan Hilly		Subtropical Hilly		Tropical Hilly		All Regions
	stock (%)	density (kg /m ²)	stock (%)	density (kg /m ²)	stock (%)	Mean density (kg /m ²)	stock (%)	density (kg /m ²)	stock (%)	density (kg /m ²)	Mean density (kg /m ²)
Aquaculture	—	—	8.9	0.11±0.10 bc	—	—	—	—	—	—	0.11
Constructed	12.3	0.22±0.06 bc	9.4	0.35±0.31 a	6.4	0.19±0.05 ab	5.8	0.12±0.06 abc	0.7	0.11±0.06	0.20
Disturbed	1.0	0.20±0.05 bc	3.7	0.32±0.37 abc	3.8	0.16±0.04 b	4.3	0.12±0.03 ab	6.5	0.11±0.07	0.18
Fallow	0.3	0.13±0.01 d	5.1	0.10±0.02 c	—	—	0.3	0.07±0.04 abc	—	—	0.10
Forestry	—	—	0.6	0.11±0.01 bc	14.7	0.15±0.04 b	33.2	0.08±0.03 c	42.2	0.07±0.03	0.10
Horticulture	0.3	0.30±0.06 a	—	—	—	—	—	—	—	—	0.30
Irrigated	78.4	0.23±0.06 b	5.7	0.20±0.07 ab	—	—	—	—	—	—	0.22
Mine & Fill	—	—	—	—	—	—	0.3	0.08±0.01 bc	0.1	0.07±0.03	0.08
Ornamental	0.8	0.17±0.03 bcd	0.1	0.09±0.03 bc	—	—	—	—	—	—	0.13
Paddy	—	—	51.2	0.20±0.23 abc	16.1	0.20±0.04 a	37.5	0.15±0.03 a	17.5	0.07±0.02	0.16
Rainfed	1.0	0.19±0.03 bcd	7.8	0.32±0.30 a	49.9	0.21±0.08 a	8.5	0.14±0.07 a	26.1	0.09±0.10	0.19
Variable	0.3	0.15±0.03 cd	—	—	—	—	—	—	—	—	0.15

Table 4. Relative STP stocks and densities among land COVER classes within each region.

Land COVER	North China Plain		Yangtze Plain		Sichuan Hilly		Subtropical Hilly		Tropical Hilly		All Regions
	stock (%)	density (kg /m ²)	stock (%)	density (kg /m ²)	stock (%)	Mean density (kg /m ²)	stock (%)	density (kg /m ²)	stock (%)	density (kg /m ²)	Mean density (kg /m ²)
Annual	76.2	0.23±0.06 ab	56.5	0.22±0.19 c	61.0	0.20±0.07	44.0	0.14±0.05 bc	16.6	0.07±0.03	0.17
Bare soil	2.9	0.27±0.05 a	0.3	0.12±0.03 bc	1.4	0.23±0.06	1.9	0.09±0.02 bc	—	—	0.16
Mixed	1.5	0.15±0.03 c	2.5	0.25±0.19 ab	2.6	0.17±0.07	3.5	0.20±0.13 abc	28.4	0.08±0.09	0.17
Perennial	1.0	0.18±0.04 bc	6.2	0.38±0.41 abc	21.5	0.18±0.06	36.2	0.09±0.03 a	46.8	0.08±0.05	0.19
Sealed	11.0	0.22±0.06 ab	16.6	0.38±0.32 a	4.4	0.17±0.04	6.3	0.13±0.07 abc	1.3	0.11±0.06	0.23
Variable	1.8	0.14±0.02 c	—	—	—	—	—	—	—	—	0.14
Water	—	—	9.7	0.11±0.08 ab	—	—	—	—	—	—	0.11
Barren	—	—	—	—	—	—	—	—	0.3	0.07±0.03	0.07

Ecotope-level analysis further revealed fine-scale heterogeneity of STP density within five regions. The types and numbers of ecotope were much more than that of the land USE/COVER in each regions (the data was too large, so it was not presented), and there were high values of coefficient of variation (CV) of STP density at the ecotope level (Table 5). Consequently, The STP density and stock of each ecotope within regions were much more complex than that of the coarser land USE/COVER. The CV of STP density ranged from 81% of ecotope in Yangtze Plain to 13% of land COVER in Sichuan Hilly with an average of 40% across the five regions. The CV of STP densities of the land USE, COVER and ecotope levels were highest in Yangtze Plain and lowest in Sichuan Hilly (Table 5). From the results above, we can conclude that at the regional scale, the spatial variation of STP between densely populated village landscapes was related to the climatic factors (precipitation and temperature) and geography; while within village landscape, the spatial variation of STP was mainly attributable to human activities, such as soil nutrient management, fertilizer application, and so on.

Since STP density between land USE, COVER, and ecotope was highly heterogeneous, estimations and comparisons of STP density at local or regional scales may contain errors if fine variations were ignored. In regional and especially in global analyses, most of the landscapes we sampled were characterized as consisting entirely of croplands- this was undoubtedly a source of substantial error in regional STP estimates. However, many researches usually neglect the small variations because of their limited resources (Lardy *et al.* 2002). Meanwhile, the large variation in the STP density across regions suggested that further study was needed to determine the macroscopical climate and geography. Generally, the variations of STP density within and across

regions both need to be considered.

Table 5. Variation in STP densities in land use, cover and ecotope classes within and among regions.

Region	With regions									Among regions [†]		
	Land use			Land cover			Ecotope			Mean	SD	CV
	Mean	SD	CV	Mean	SD	CV	Mean	SD	CV			
North China Plain	0.20	0.05	27%	0.20	0.05	25%	0.20	0.05	29%			
Yangtze Plain	0.20	0.11	53%	0.24	0.12	49%	0.22	0.18	81%			
Sichuan Hilly	0.18	0.03	14%	0.19	0.03	13%	0.19	0.04	22%	0.16	0.07	40%
Subtropical Hilly	0.11	0.03	29%	0.13	0.05	35%	0.11	0.04	34%			
Tropical Hilly	0.09	0.02	23%	0.08	0.02	20%	0.08	0.03	40%			

Conclusions

This study integrated high spatial resolution mapping with soil sampling to demonstrate that local patterns of land management and human residence were associated with substantial differences in STP both within and across China's village landscapes. The high STP density around the housings demonstrated soil P must be considered to be a significant global pool of P and also a potential contribution to P pollution. With the rapidly change in land use/land cover in Chinese densely populated landscapes, such information is essential for rational planning of future management to make agricultural development sustainable.

References

- China Agricultural University (1998) Agricultural chemistry. Beijing: Agricultural press, pp 115–123
- Ellis EC (2004) Long-term ecological changes in the densely populated rural landscapes of China. In 'Ecosystems and Land Use Change. American Geophysical' (Eds RS DeFries, GP Asner, RA Houghton) pp 303–320. (Union, Washington, DC.).
- Ellis EC, Li RG, Yang LZ, Cheng X (2000) Long-term change in village-scale ecosystems in China using landscape and statistical methods. *Ecol. Appl.* **10**, 1057–1073.
- Ellis EC, Wang H, Xiao HS, Peng K, Liu XP, Li SC, Ouyang H, Cheng X, Yang LZ (2006) Measuring long-term ecological changes in densely populated landscapes using current and historical high resolution imagery. *Remote Sens. Environ.* **100**, 457–473.
- Grerup UF, Brink DJT, Brunet J (2006) Land use effects on soil N, P, C and pH persist over 40–80 years of forest growth on agricultural soils. *Forest Ecol. Manag.* **225**, 74–81.
- Lardy LC, Brossard M, Assad MLL, Laurent JY (2002) Carbon and phosphorus stocks of clayey Ferralsols in Cerrado native and agroecosystems, Brazil. *Agr. Ecosyst. Environ.* **92**, 147–158.
- Neufeldt H, Silva JED, Ayarza MA, Zech W (2000) Land-use effects on phosphorus fractions in Cerrado oxisols. *Biol Fertil Soils* **31**, 30–37.
- Tang JD, Ye XY, Rao GL, Lin BS (2003) Effect of human activities on quality of cultivated land in Guangdong province. *Soil* **1**, 8–12. (in Chinese)
- Vadas PA, Gburek WJ, Sharpley AN, Kleinman PJA, Moore PA, Cabrera ML, Harmel RD (2007) A model for phosphorus transformation and runoff loss for surface-applied manures. *J. Environ. Qual.* **36**(1), 324–332.
- Verburg PH, Veldkamp A, Fresco LO (1999) Simulation of changes in the spatial pattern of land use in China. *Applied Geography* **19**(3), 211–233.
- Vitousek PM (1994) Beyond global warming: Ecology and global change. *Ecology* **75**, 1861–1876.

Diurnal and seasonal greenhouse gases exchange in a salt marsh in central Japan

Kosuke Noborio^A, and Ken-ichi Inagaki^B

^ASchool of Agriculture, Meiji University, Kawasaki, Kanagawa, Japan, Email noboriok@isc.meiji.ac.jp

^BFormerly School of Agriculture, Meiji University, Kawasaki, Kanagawa, Japan

Abstract

Diurnal and seasonal fluctuations of greenhouse gas (GHG) exchange in a salt marsh were measured using the closed chamber method. The salt marsh sediment seemed to act as the source for CO₂ and N₂O and as a sink for CH₄ during winter but as a source during summer. With diurnal fluctuation of water level at the salt marsh, methane and nitrous oxide were emitted all day long whereas carbon dioxide was absorbed.

Key Words

Carbon dioxide, nitrous oxide, methane, redox potential, electrical conductivity, closed chamber method.

Introduction

Salt marshes may exist in any estuaries where a big river flows into sea. River water transports large amounts of nutrients from upper streams and deposits them in salt marshes in estuaries. Nutrients involving nitrate nitrogen (NO₃⁻-N), plant residues, and organic matters may result in greenhouse gas (GHG) emissions in salt marshes. Soil in salt marshes located in a tidal effect area may become alternately aerobic and anaerobic conditions. Under such conditions, nitrous oxide (N₂O) and methane (CH₄) gases tend to be emitted (Hou *et al.* 2000). These gases are considered as very strong GHGs relative to carbon dioxide (CO₂) gas. Salinity and sulfate ion in sea water are reported to suppress the emission of N₂O and CH₄ gases (Supparattanapan *et al.* 2009; Martens and Berner 1974). In contrarily, Oremland *et al.* (1982) reported that CH₄ production and sulphate reduction simultaneously occurred in salt marsh sediments.

Methods

GHG sampling

Four samples of GHG were collected with 10 min intervals using a syringe with a closed chamber (144 mm in dia., 235 mm high) for seasonal measurement inserted about 50 mm into sediment. For diurnal measurement, larger chambers (600 mm long, 300 mm wide, 1,060 mm high) were used. The gas chambers were quadruplet. Gas sampling was duplicated or triplicated. Gas samples collected were stored in vials that were kept in a cooler box during transporting to the laboratory. The gas samples were analysed for CO₂, N₂O, and CH₄ using a gas chromatography with FID and ECD (model 6890N, Agilent Technologies, CA).

GHG flux estimation

Gas flux, J_g (mg/m²/h), was estimated as (De Mello and Hines 1994):

$$J_g = 1000 \frac{V}{A} \frac{dC(t)}{dt} \Big|_{t=0} \quad (1)$$

where V is the flux chamber volume (m³), A the flux chamber basal area (m²), and $[dC(t)/dt]_{t=0}$ is the slope of a gas concentration change curve at time $t=0$ (g/m³/h) as expressed in Eq. (2). Temporal changes in gas concentration in the flux chamber covering on the soil surface may be expressed (de Mello and Hines, 1994) as:

$$C(t) = C_{\max} - (C_{\max} - C_0) \exp(-kt) \quad (2)$$

where $C(t)$ is the gas concentration (g/m³) in a closed chamber at time t after deployment, C_{\max} the maximal concentration (g/m³) reached when the gas concentration in the closed chamber equilibrates to the gas concentration of soil pores, C_0 the gas concentration (g/m³) at $t=0$ in the closed chamber, and k a rate constant. Differentiating Eq. (2) with respect to t and providing $t=0$ to the resultant are:

$$\frac{dC(t)}{dt} \Big|_{t=0} = k(C_{\max} - C_0) \quad (3)$$

in which the values of k , C_{\max} , and C_0 are estimated by fitting Eq. (2) to gas concentrations measured with time. A curve fitting procedure was performed using the solver function of Excel spreadsheet software in a similar manner that reported by Wraith and Or (1998).

Results

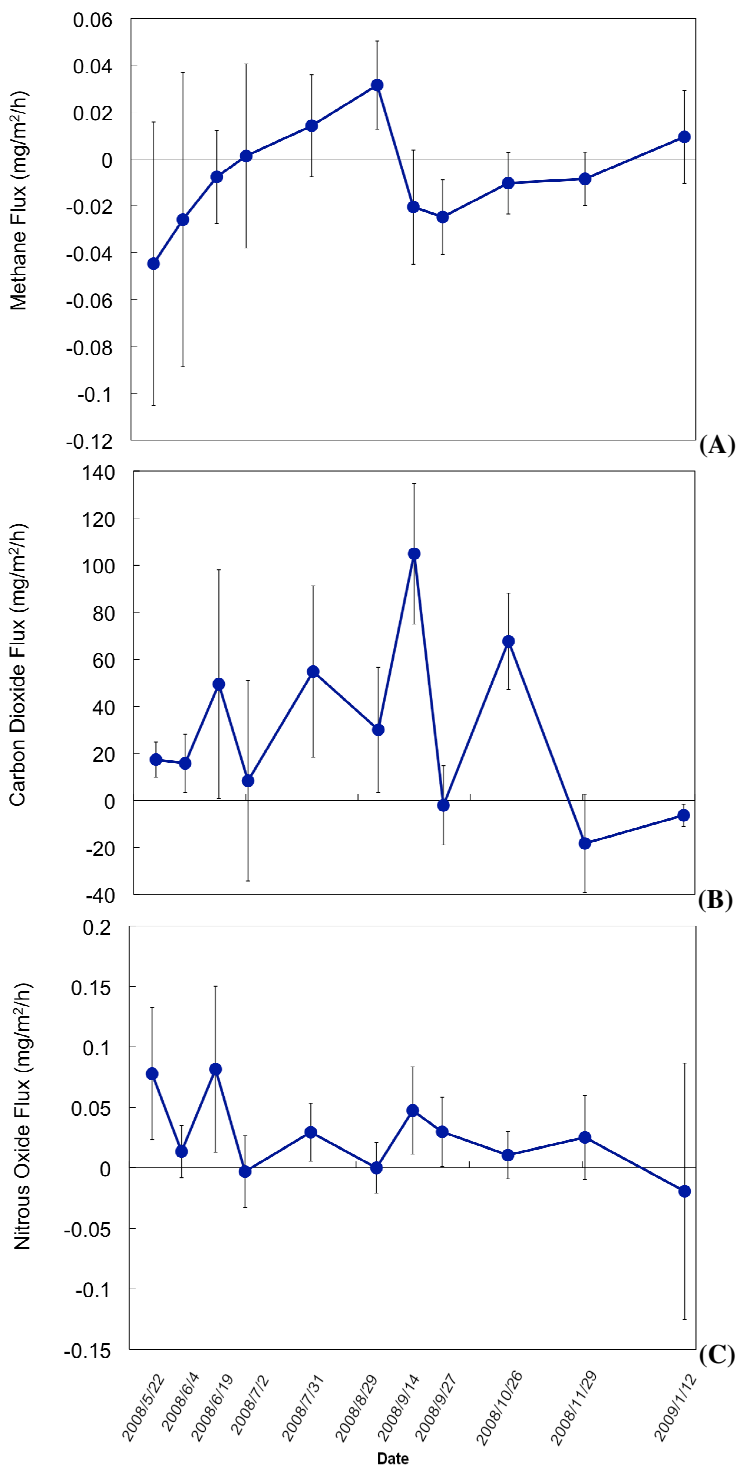


Figure 1. Seasonal changes in methane (A), carbon dioxide (B), and nitrous oxide (C) exchange between the atmosphere and the salt marsh sediment.

Methane emission was tended to increase during summer whereas its absorption increased during fall (Figure 1A). Carbon dioxide, on the other hand, was emitted mostly all year around with some fluctuations (Figure 1B). The degree of emission was tended to increase in summer and to decrease in winter. Nitrous oxide was emitted all year around with some fluctuations as well (Figure 1C). The salt marsh sediment seemed to act as the source for CO₂ and N₂O while as the sink for CH₄ during winter but as the source during summer.

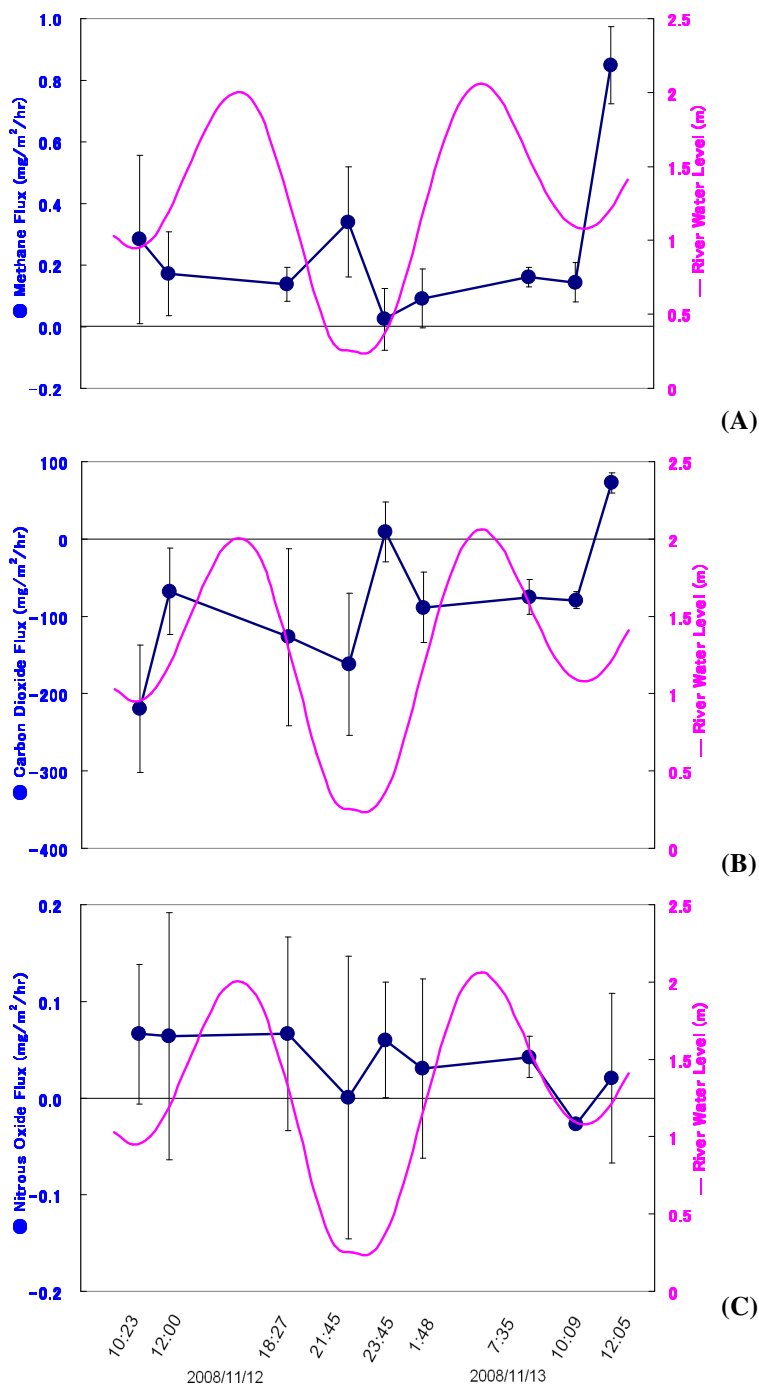


Figure 2. Diurnal changes on November 12th and 13th in water level at the salt marsh along with methane (A), carbon dioxide (B), and nitrous oxide (C) exchange between the atmosphere and the salt marsh.

Diurnal fluctuation of water level was apparent as shown in Figure 2. Methane and nitrous oxide were emitted (Figures 2A, 2C) all day long whereas carbon dioxide was absorbed (Figure 2B). Emissions and absorptions were larger as water level was lower. High tide seems to suppress the emission and absorption.

Conclusion

Salt marsh had dynamic exchange of GHG between the atmosphere and the sediment. It acted mostly as sources for CO₂ and N₂O whereas as a sink for CH₄ during winter. More comprehensive research is needed for further knowledge.

References

- Hou AX, Chen GX, Wang ZP, Van Cleemput O, Patrick WH (2000) Methane and nitrous oxide emissions from a rice field in relation to soil redox and microbiological processes. *Soil Science Society of America Journal* **64**, 2180–2186.
- Oremland RS, Marsh LM Polcin P (1982) Methane production and simultaneous sulphate reduction in anoxic, salt marsh sediments. *Nature* **296**, 143-145.
- Martens CS, Berner RA (1974) Methane production in the interstitial waters of sulfate-depleted marine sediments. *Nature* **185**, 1167-1169.
- Supparattanapan S, Saenjan P, Quantin C, Meaght JL, Grunberger O (2009) Salinity and organic amendment effects on methane emission from a rain-fed saline paddy field. *Soil Science and Plant Nutrition* **55**, 142-149.
- De Mello WZ, Hines ME (1994) Application of static and dynamic enclosure for determining dimethyl sulfide and carbonyl sulfide exchange in Sphagnum peatlands: Implications for the magnitude and direction of flux. *Journal of Geophysical Research* **99**, 14601-14607.
- Wraith JM, Or D (1998) Nonlinear parameter estimation using spreadsheet software. *Journal of Natural Resources and Life Sciences Education* **27**, 13-19.

Effect of different cation saturations on the sorption and mineralization of the hydrophobic organic compounds nonylphenol and phenanthrene in soils

Bernd Marschner and Anastasia Shchegolikhina

Dept. Soil Science and Soil Ecology, Geographical Institute, Ruhr-University Bochum, Germany.

Abstract

Based on the assumption that the relative density and flexibility of SOM is affected by cations at the exchange sites, nonylphenol (NP) and phenanthrene (PHE) sorption and mineralization experiments were conducted with a sandy soil that had been treated with solutions of NaCl, CaCl₂ or AlCl₃. Sorption and desorption of the ¹⁴C-labelled compounds was determined in batch equilibrium assays. Mineralization was determined by monitoring ¹⁴CO₂ efflux from samples that were additionally supplemented with organic substrates. For NP, organic carbon normalized sorption and desorption coefficients were increased in Na- and Al-treatments, for PHE in the Na-treatment and a water-washed control soil. Mineralization of NP was enhanced by addition of glucose and wood flour, indicating that it is substrate limited and most likely co-metabolic. At high mineralization rates, bioavailability of NP is limited in the Ca- and Al-treatments.

Key Words

Xenobiotics, SOM conformation, cations, sorption, mineralization

Introduction

Bound residues of hydrophobic organic compounds develop mainly through interactions with soil organic matter (SOM), either through sorption to specific sites (i.e. hydrophobic cavities) or through slow diffusion into less accessible domains. The relative density and flexibility of SOM is affected by cations at the exchange sites (Schaumann *et al.* 2006). Strongly hydrated monovalent cations (i.e. Na⁺) cause SOM to expand and thus make it more accessible to xenobiotics. Polyvalent cations (i.e. Ca²⁺ or Al³⁺) reduce the volume and flexibility of SOM through cation bridging, which can thus limit diffusion of xenobiotics into the matrix and back out again. The higher rigidity of Ca²⁺ or Al³⁺-saturated humic acids has been shown to reduce atrazine sorption, while it increased with Na⁺ relative to the H-saturated humic acid (Clapp *et al.* 2001). Yuan and Xing (2001) showed that an Al-saturated humic acid strongly increased the non-linearity and irreversibility (hysteresis) of PAH sorption. Lu and Pignatello (2004) made similar observations for naphthalene and trichlorobenzene and explain this by the restricted access of sorption sites in the more rigid Al-saturated humic acid. In our study, we test two hypotheses: (1) the structural conformation of SOM affects sorption and desorption kinetics of xenobiotics and thus influences the formation of "bound residues". (2) The addition of substrates can enhance the biodegradation of bound residues, either through co-metabolism or through enhanced degradation of the sorbent (priming effects).

Methods

Soil sampling and treatment

Soil was sampled from a permanent pasture near Hannover, Germany. The sandy gleyic podzol with a pH of 5.7 had an SOC content of 3.2% and a clay content of 2.3%. After sieving to 2 mm and air drying, subsamples of the soil were percolated under saturated conditions with solutions containing 0.1 M NaCl, CaCl₂ or AlCl₃ until a final soil:solution ratio 1:50. After the cation treatment, samples were washed with deionized water at 1:15.

Chemicals

Ring ¹⁴C-labelled nonylphenol [4-(3,5-Dimethyl-3-heptyl)phenol] (NP) was obtained at 98% radiochemical purity from A. Schaeffer (RWTH Aachen) in petrolether. Uniformly-¹⁴C-labelled phenanthrene (PHE) with radiochemical purity 99.7% was purchased from Campo Scientific GmbH, Germany in methanol.

Sorption and desorption

Two g soil samples were placed into one half of a 10 ml double-cell Teflon chamber separated by a dialysis membrane with MWCO 1000 Da. After filling both halves with deionized water, the ¹⁴C-labelled NP and Phe were injected into the soil-free half of the chamber at concentrations 5.5 µg/g and 1.2 µg/g respectively, which is below the water solubility of the compounds. To prevent the microbial activity, NaN₃ at 5 mg/l was added to the system. The acidity of all soil solutions was reduced to pH of 5 by addition of 0.01 M HCl. Ratio between

solid and liquid parts in system was 1:5. Sorption kinetics were determined by removing 200 μ l samples from the soil free half-cell and analysing ^{14}C -activity by liquid scintillation counting (LSC). Desorption experiments were carried out after sorption equilibrium was reached (generally after 72-110 hr) by replacing the complete aqueous solution of the soil-free half-cell with deionized water repeatedly.

Mineralization assays

The cation-treated and control soil samples of 40 g were re-wetted to 40% water holding capacity and preincubated for 2 weeks at 20°C in the dark prior to spiking them with the ^{14}C -labelled NP. For spiking, NP dissolved in petrolether was added to 1 g acid washed quartz sand, left to dry and then mixed into the soil sample. Contaminated soils with concentration of NP of 1.2 $\mu\text{g/g}$ were then wetted to 60% WHC and incubated in an automated respirometer Respicond-apparatus (Nordgren Innovations) that monitors CO_2 production and collects respired CO_2 in 0.6 m KOH solution. Periodically, ^{14}C -activity was determined in the KOH solutions via LSC. To determine the effects of different substrate additions on the mineralization of NP, after 3 weeks of preincubation some samples were supplied with glucose, catechol or beech wood flour at concentrations of around 500, 300 and 10000 mg/kg respectively and incubated 3 weeks more.

Results

The sorption of NP to the soil as determined in the batch equilibrium experiments was slightly enhanced in the Al-treatment, but differences to the control were not significant (Figure 1). For desorption, the organic carbon normalized partitioning coefficient K_{oc} was much higher than for sorption in all soils, reflecting a strong hysteresis. Here, the Na- and Al-treated soils showed significantly higher K_{oc} -values than the control and Ca-treatments.

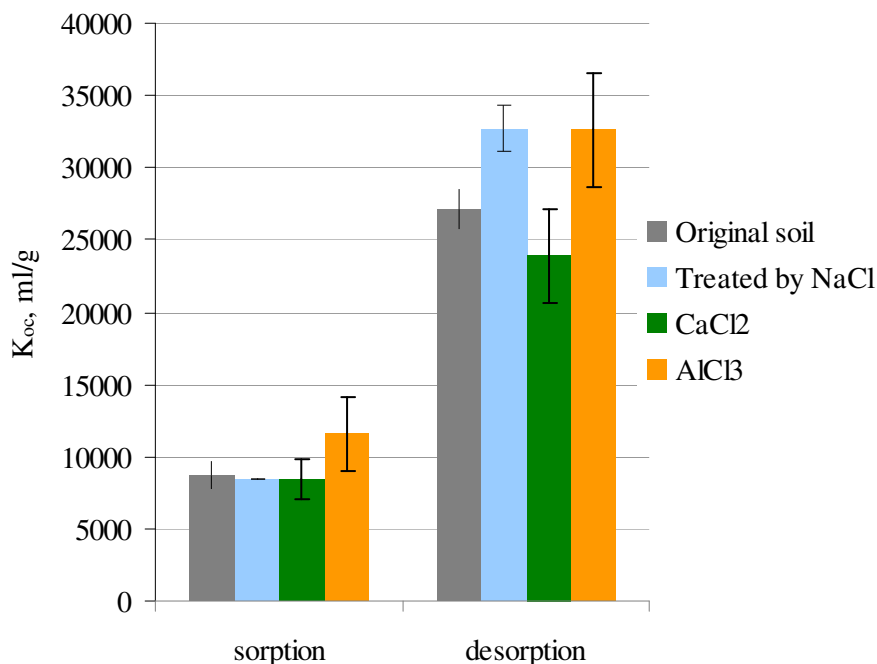


Figure 1. Organic carbon normalized coefficient of sorption and desorption of nonylphenol at the equilibrium time in soils treated with different salt solutions

Mineralisation rates of NP were very low, reaching only 0.4 to 0.5% within the first two weeks before substrate additions (Figure 2). After this period, the addition of water stimulated mineralization in all treatments but most markedly in the untreated control soil. Glucose additions stimulated NP mineralization to an even greater degree, reaching up to 1.5% in the original soil, which again showed the highest values. The strongest stimulation of NP mineralization occurred after the addition of wood flour. This treatment also increased soil respiration to the highest degree, showing that this organic substrate was readily utilized by the soil microorganisms. Here, the mineralization of NP was significantly higher in the original soil and in the Na-treatment than in the Ca- and Al-treatments. Since total CO_2 release was not markedly affected by the

treatments, this indicates that at high degradation rates, NP bioavailability may be limited in the treatments with the higher charged cations.

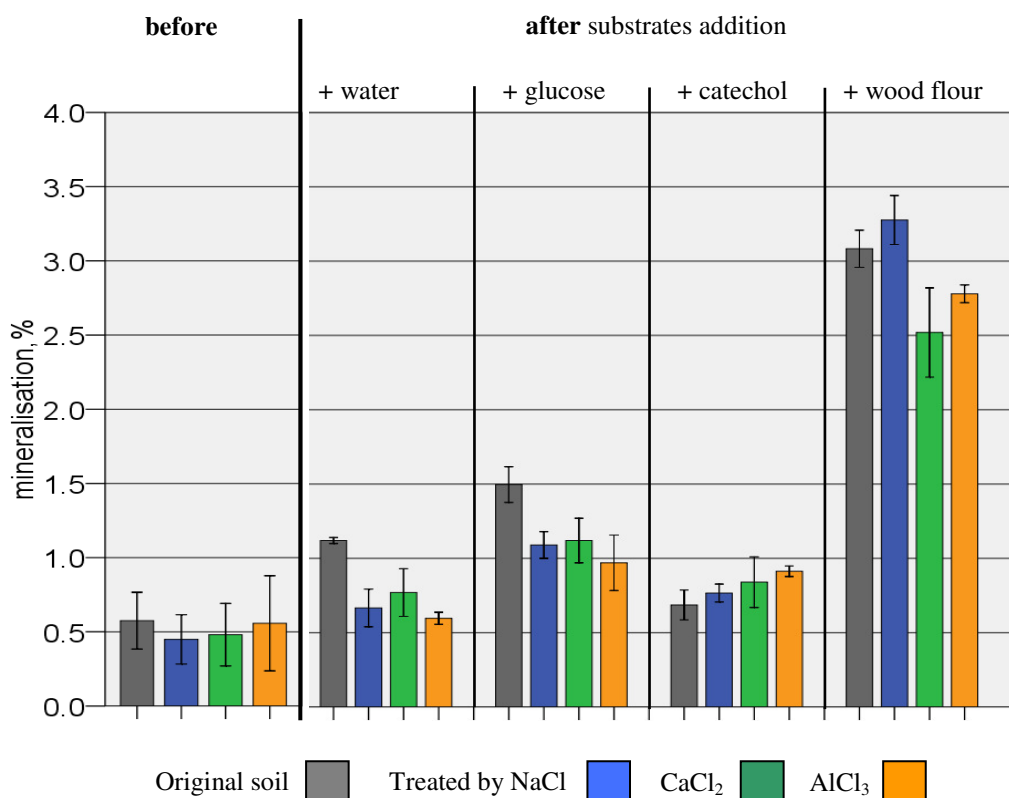


Figure 2. Total mineralisation of nonylphenol with and without substrate additions in soils treated with different salt solutions

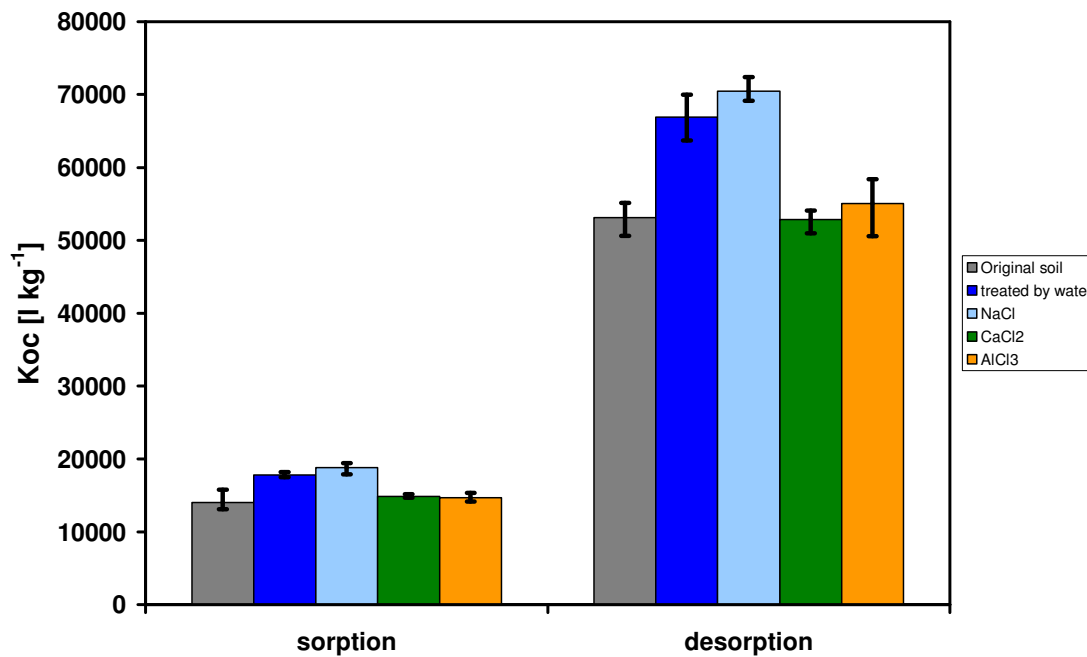


Figure 3. Organic carbon normalized coefficient of sorption and desorption of phenanthrene at the equilibrium time in the soils treated with different salt solutions

For the sorption experiments with PHE, an additional control treatment was included where the same amount of deionized water was percolated through the samples as in the cation treatments. As shown in Figure 3, the water and Na-treatments increased the carbon-normalized partition coefficients for sorption and desorption of PHE compared to the original soil and the Ca- and Al-treatments. If this is due to the leaching of hydrophilic low molecular organic compounds, leaving more hydrophobic sorption domains accessible for PHE or due to better accessibility of sorption sites due to swelling and expansion of the SOM matrix is unclear at the moment.

Conclusion

Our results show that the saturation of exchange sites with different cations affects the sorption/desorption and mineralization of the hydrophobic test compounds. However, there is no general trend for higher sorption or lower bioavailability in soils treated with multivalent cations as we had expected. We are currently conducting longer-term aging experiments to investigate, if the observed effects persist or even are amplified if the compounds have more time to interact with the sorbent matrix.

References

- Clapp CE, Hayes MHB, Mingelgrin U (2001). Measurements of sorption –desorption and isotherm analyses. In 'Humic Substances and Chemical Contaminants'. (Eds CE Clapp, MHB Hayes, N Senesi, P Bloom, PM Jardine) pp. 205-240. (Soil Science Society of America, Madison).
- Pignatello JJ, Xing B (1996). Mechanism of slow sorption of organic chemicals to natural particles. *Environmental Science and Technology* **30**, 1-11.
- Schaumann GE, Lang F, Frank J (2006). Do multivalent cations induce cross-links in dissolved organic matter precipitates? In 'Humic Substances - Linking Structure to Functions' (Eds FH Frimmel, G Abbt-Braun) pp. 941-944. Proceeding 13th Meeting IHSS, (Karlsruhe, Germany).
- Yuan GS, Xing BS (2001). Effects of metal cations on sorption and desorption of organic compounds in humic acids. *Soil Science* **166**, 107-115.

Effect of nutrient cycle by different thinning practice in temperate forest

Po Neng Chiang^A, Jui Chu Yu^B, Ya Nan Wang^{CD} and Yu Min Tzou^E

^AAssistant Researcher of Experimental Forest, National Taiwan University, Nantou, Taiwan, Email: pnchiang@ntu.edu.tw

^BResearch Assistant of Experimental Forest, National Taiwan University, Nantou, Taiwan, Email: 1329@exfo.ntu.edu.tw

^CDirector of Experimental Forest, National Taiwan University, Nantou, Taiwan

^DProfessor of School of Forest Environment and Resource, National Taiwan University, Taipei, Taiwan, Email: m627@ntu.edu.tw

^EProfessor of Soil Environmental Science, National Taiwan University, Taichung, Taiwan, E-mail: ymtzou@dragon.nchu.edu.tw

Abstract

The plantation thinning and associated managements can influence the functions and structure of forest ecosystems as well as the status and dynamics of soil nutrients and organic matter that affect the forest ecosystem and related environment reciprocally. The objective of this study was to investigate the influences of thinning treatments to soil nutrient cycles and dissolved organic matter. This study was carried out in a 40-year-old *Cryptomeria japonica* plantation located at central Taiwan. Thinning intensity divided to control, 40% and 60%. Before and after thinning, soil was sampled and analysed for soil properties and dissolved nutrients such as dissolved organic carbon (DOC), cations and anions. The dissolved K^+ of control treatments was significantly higher than that of thinning treatments suggesting that K^+ was leaching down by rainfall after thinning treatment. The nitrate concentration extracted from fresh soil increased with thinning intensity indicating that fresh litter accumulated in the soil, the litter was decomposed by microbes and protein was released from plant tissue. Organic matter decomposed from litter was also transformed to NO_3^- , and therefore increased NO_3^- concentration. Thinning treatments affected concentrations of K^+ , $Fe^{3+} + Al^{3+}$, and anions. Although the DOC concentrations showed no significantly difference, it might be complexed with induced with cations such Fe^{3+} and Al^{3+} . Nutrients are released from fresh litter decomposition after thinning treatment. Therefore, DOC plays an important role after plantation thinning. The results also can be a reference for nutrient management of plantation.

Key Words

Dissolved organic carbon, nutrient cycle, thinning practice

Introduction

Reasonable management of plantations is one of the most important strategies to improve timber production and stabilize forest ecosystems. Plantation thinning and associated managements can influence the functions and structure of forest ecosystems as well as the status and dynamics of soil nutrients and organic matter that affect the forest ecosystem and related environment. Litter accumulation and decomposition rate are affected by different thinning treatments. When litter decomposes, it also releases dissolved organic matter (DOM), such as dissolved organic carbon (DOC). The DOM can be stored in soil mineral layers and also affect the nutrient sorption capacity by soil (McDowell and Linkens 1988; Qualls and Haines 1991a; Currie *et al.* 1996). However, the transformation and dynamic of DOM is still obscure. Thus, the objective of this study was to investigate the influences of thinning treatments on soil nutrient cycles and dissolved organic matter.

Methods

Site Descriptions and Thinning Treatments

This study was carried out in a 40-year-old *Cryptomeria japonica* plantation located at Experimental Forest of National Taiwan University, Sitou, central Taiwan (Figure 1). The study site is a montane area with elevations ranging from 1800 to 1900 m. The annual precipitation is 2500 mm, occurring mainly between May and September, characteristically as thunderstorms associated with typhoons. The mean annual temperature of the site is 17.9°C. The parent materials are sandstones and clay sediments interbedded with Tertiary shale and slate (Ho, 1988). These three thinning treatments were setup at late 2008 as control (i.e., 0%), 40% and 60% thinning treatments according to the thinning intensities. Before the thinning treatment, we set four plots in each thinning treatment. Study zones are separated by 50 m and plot size was 5 x 5 m. Plots were randomly located within each zone. Four soil samples in each plot were collected from the O horizon (0-15cm) and A horizon (15-30 cm) at randomly as background for soil physical and chemical analyses. Soil samples were air-dried, sieved and passed through 2 mm sieve. The soils can be classified as sandy loam or silty loam, mixed, mesic, Typic Dystrudepts (Soil Survey Staff, 2006). The pH of soil samples was measured in distilled water (soil to solution = 1:2 w/w). Total C and N contents of the soils were determined by a CHN analyzer. Cation-exchange

capacity (CEC) of the soils was determined by ammonium acetate (NH₄OAc) exchange method (Rhoades, 1982). The exchangeable cations were determined by conductivity coupled plasma atomic emission spectroscopy (ICP-AES) (Perkin Elmer Optima 2000DV).

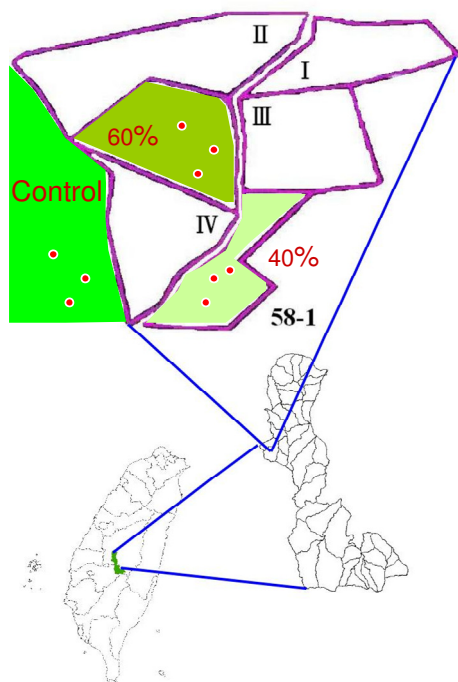


Figure 1. Location of sampling site.

Dissolved nutrient analysis

Before and after thinning, fresh soils (0-15 cm) were collected 1 kg from each plot and immediately sieved and passed through 4 mm sieve. The sub-samples were then stored in 4 °C freezer for analysis. Fresh soil samples (100 g) were extracted with 1000 mL distilled water on a mechanical shaker for 4 hr. Soil extracts were filtered with a 0.22µm filter. The extracted solution was analysed for anions by ion chromatography (Metrohm IC 792), cations by ICP-AES, and dissolved organic carbon by TOC analyser (Shimadzu TOC-VCS).

Results

1. Soil properties before thinning treatment

The texture and soil pH of O and A horizons were sandy loam and loam and 4.9 and 5.1, respectively. The organic carbon and total nitrogen of O and A horizons were 38.8 and 55.2 and 3.6 and 4.9 g/kg, respectively (Table 1). Soil dissolved organic carbon of O and A horizons were 205 and 321 mg C/kg, respectively (Table 2). The results of extracted solutions showed that Cl⁻, SO₄²⁻, and PO₄³⁻ were the main anions in the soils.

Table 1. Soil properties for the plantation before thinning treatment.

Horizon	Depth cm	pH	O.C. g/kg	T.N. g/kg	C/N	Exchangeable				CEC
						Na	K	Mg	Ca	
O	0-15	4.9	38.8	3.6	10.7	0.7	0.2	0.5	0.4	23.1
		(0.02)	(0.20)	(0.10)		(0.00)	(0.00)	(0.00)	(0.00)	(0.78)
A	15-30	5.1	55.2	4.9	11.3	0.2	0.3	0.8	0.4	28.5
		(0.03)	(0.22)	(0.10)		(0.00)	(0.00)	(0.00)	(0.00)	(0.01)

Mean (SD); CEC: cation exchangeable capacity

Table 2. Amounts of exchangeable phosphate, dissolved organic carbon and anions in air-dried soil before the thinning treatment.

Horizon	Depth cm	Exchangeable P	DOC	Cl ⁻	NO ₃ ⁻	PO ₄ ³⁻	SO ₄ ²⁻
		mg/kg	mgC/kg	-----mg/kg-----			
O	0-15	85	205	29.4	140.6	nd	26.3
		(3.5)	(9.9)	(1.6)	(7.2)	nd	(0.8)
A	15-30	117	321	28.6	193.2	nd	25.5
		(6.8)	(12.5)	(3.5)	(4.9)	nd	(1.9)

DOC: dissolved organic carbon; nd: not detected

2. Soil cations, anions, and dissolved organic carbon after thinning treatment

Soil dissolved organic carbon concentration of A horizon with control, 40% and 60% thinning treatments were 134, 133 and 139 mg C/kg, respectively (Table 3). The DOC concentrations did not show a difference among treatments. The dissolved K⁺ of control treatments is significantly higher than that of thinning treatments. It suggests that K⁺ were leaching down by rainfall after thinning treatment. Liang *et al.* (2009) reported that K⁺ loss from soil was affected by acid rainfall. The concentration of soil dissolved Fe³⁺ significantly increased to 3.8 mg/kg after 60% thinning treatment. On the other hand, the concentration of soil dissolved Al³⁺ also increased with thinning intensity. It suggested that litter accumulation immediately was increased by thinning treatments. Organic acids can be released after litter decomposition and leached down to soil. The fixed aluminium and iron were dissolved at low pH and complex with organic acids. Therefore, more litter accumulation, more concentrations of dissolved organic Fe³⁺ and Al³⁺ in the soil after thinning treatment.

Table 3. Concentrations of dissolved organic carbon and cations in fresh soil (0-15 cm) after the thinning treatment.

Treatment	DOC mgC/kg	Dissolved					
		Na ⁺	K ⁺	Mg ²⁺	Ca ²⁺	Fe ³⁺	Al ³⁺
		-----mg/kg-----					
Control	134	13.9	26.2	4.9	119	nd	3.6
	(9.5)	(3.6)	(5.6)	(0.2)	(6.4)	nd	(0.7)
40 %	133	14.3	14.8	nd	79.4	nd	5.1
	(6.9)	(2.8)	(0.4)	nd	(10.1)	nd	(1.4)
60%	139	12.7	17	4.3	106.1	3.8	6.0
	(2.0)	(4.0)	(0.9)	(0.7)	(7.5)	(2.4)	(1.3)

The nitrate concentration extracted from fresh soil increased with thinning intensity (Table 4). It indicated that fresh litter accumulated in the soil, the litter was decomposed by microbe and protein was released from plant tissue. These organic matters decomposed from litter were also transformed to NO₃⁻, and therefore increased NO₃⁻ concentration. The sulfate concentrations also significantly increased with thinning intensity (Table 4). It indicated that sulfate extracted from fresh soil was from atmospheric deposition. The sulfate can be retained by cations such as Ca²⁺, Fe³⁺ and Al³⁺. The plantation was created gaps after thinning treatments, therefore, these gaps received more sulfate from atmospheric deposition.

Table 4. Concentrations of anions in fresh soil (0-15 cm) after the thinning treatment.

Treatment	Dissolved			
	Cl ⁻	NO ₃ ⁻	PO ₄ ³⁻	SO ₄ ²⁻
	-----mg/kg-----			
Control	15.0	270	nd	19.6
	(3.3)	(6.6)	nd	(1.9)
40 %	19.6	389	nd	25.9
	(0.7)	(4.9)	nd	(1.1)
60%	15.9	510	nd	21.4
	(4.9)	(19.4)	nd	(2.1)

Conclusion

Thinning treatments affected concentrations of K⁺, Fe³⁺ + Al³⁺, and anions. Although the DOC concentrations were not significant difference, it might be complex and induced with cations such Fe²⁺ and Al³⁺. The nutrient released from fresh litter decomposition after thinning treatment. Therefore, DOC plays an important role after plantation thinning practice. The results also can be a reference for nutrient management of plantation.

Acknowledgement

We thank the National Science Council, Taiwan for financial support under the projects (NSC 97-2313-B-002-046, 98-2313-B-002-005-MY3). We also thank the Experimental Forest of National Taiwan University for financial support.

References

- Qualls RG, Haines BL (1991) Fluxes of dissolved organic nutrients and humic substances in a deciduous forest. *Ecology* **72**, 254-266.
- Liang YL, Lin TC, Hwong JL, Lin NH, Wang CP (2009) Fog and Precipitation Chemistry at a Mid-land Forest in Central Taiwan. *Journal of Environmental Quality* **38**, 627-636.
- Currie WS, Aber JD, McDowell WH, Boone RD, Magill AH (1996) Vertical transport of dissolved organic C and N under long-term N amendments in pine and hardwood forests. *Biogeochemistry* **35**, 471-505.
- McDowell WH, Likens GE (1988) Origin, composition and flux of dissolved organic carbon in the Hubbard Brook valley. *Ecological Monographs* **58**, 177-195.
- Soil Survey Staff: Key Soil Taxonomy (2006) In 'United States Department of Agriculture and Soil Conservation Service'. Washington DC.

Effect of tillage systems on soil aggregation and hydraulic properties in SW Spain

Rosa López-Garrido^A, María V. López^B, Sebastiana Melero^A, José M. Murillo^A, Ignacio Girón^A, Engracia Madejón^A, **Félix Moreno^A**

^AInstituto de Recursos Naturales y Agrobiología de Sevilla (IRNAS-CSIC). P.O. Box 1052, 41080 Sevilla, Spain.

fmoreno@irnase.csic.es

^BEstación Experimental de Aula Dei, CSIC, Zaragoza, Spain.

Abstract

Conservation tillage is particularly important in arid and semi-arid zones, where water is the limiting factor for crop development under rainfed conditions. Conservation tillage improves physical properties and increases organic matter of soils under Mediterranean conditions. This work studies the influence of two tillage systems (traditional tillage, TT, and conservation (reduced) tillage, RT) on soil hydraulic properties and on soil aggregation after 15 years of experimentation. The effect of no-tillage (NT) in a short-term experimentation (4 years) was also considered. In the long-term experiment, the aggregate size distribution (ASD), mean weight diameter (MWD) and aggregation index (AI) values were greater in RT than in TT, although differences were not significant. Water stability (WAS) values for 1-2 mm size aggregates were greater in TT, despite the organic carbon (OC) and CaCO₃ contents in these aggregates were greater in RT. However, under our conditions NT seems to have a greater effect on WAS. The increase of this variable in NT respect to TT, was observed after only three years of experimentation. In the long-term experiment, the hydraulic conductivity was higher in TT than in RT for $h > -20$ mm in agreement with a greater characteristic mean pore radius for $h > -20$ mm. In the short-term experiment, the lower hydraulic conductivity in NT than in TT suggests a lack of interconnected pores in NT treatment.

Key Words

Soil aggregate stability, conservation tillage, no tillage, traditional tillage, physical properties, soil quality

Introduction

The efficiency of conservation tillage for reducing soil erosion and improving water storage is universally recognised. This is particularly important in arid and semi-arid zones, where water is the limiting factor for crop development under rainfed conditions. In these areas, the management of crop residues is also of prime importance for obtaining sustainable crop productions (Du Preez et al., 2001). The improvement of the soil water profile and hydraulic properties, under conservation tillage, has been reported by Pelegrín et al. (1990) and Moreno et al. (1997) for the conditions of southern Spain. On the other hand, an increase in soil organic matter is a desirable aim as it is associated with better plant nutrition, cultivation and seed performance, and better soil physical properties (greater aggregate stability, reduced bulk density, improved water holding capacity at low suctions, enhanced porosity and earlier warming in spring).

Soil aggregates and their stability have a strong influence on physical properties such as infiltration, hydraulic characteristics, aeration, soil strength, erosion, and the soil's ability to transmit liquids, solutes, gases, and heat. Thus, aggregate stability can provide key information about the capacity of soil to function, which defines soil quality. The aim of this study was to determine the influence of two tillage systems (traditional tillage, TT, and conservation (reduced) tillage, RT) on soil hydraulic properties, dry soil aggregate size distribution and wet aggregate soil stability after 15 years of experimentation. The effect of no-tillage in a short-term experimentation (4 years) is also considered.

Materials and methods

The experiment was established in 1992 at the experimental farm of the Instituto de Recursos Naturales y Agrobiología (CSIC) in the Sevilla province (SW Spain). Soil was classified as Xerofluvent. Climate of the zone is typically Mediterranean, with mild rainy winters (500 mm mean rainfall, average of 1971-2004) and very hot, dry summers. An area of about 2,500 m² was selected to establish the experimental plots in 1991. Two tillage treatments were established: TT used in the area for rainfed agriculture (consisted of mouldboard ploughing 30 cm depth, after burning the straw of the preceding crop; straw burning was suppressed since 2003) and a RT characterized by not using mouldboard ploughing, by reduction of the number of tillage operations and leaving the crop residues on the surface (for more details see Moreno et al., 1997). A wheat (*Triticum aestivum*, L.)-sunflower (*Helianthus annuus*, L.) crop rotation was established for both treatments. In 2005 a fodder pea crop (*Pisum arvense*, L.) was included in the rotation. In 2003 a short experiment was established

with a TT and a no tillage (NT, direct drilling) treatments with the same crop rotation as in the long-term experiment. Soil samplings were conducted on October 2007 (0-5, 5-10 and 10-20 cm depths) in the long-term experiment, and in March and October in the short term experiment. Size distribution of dry aggregates was determined using an electromagnetic sieving machine with consecutive sieves of 4, 2, 1, 0.5, 0.25 and 0.05 mm mesh. Aggregate water stability was determined on dry aggregates of 1-2 mm in diameter following the method of Kemper and Rosenau (1986). A tension disc infiltrometer (Perroux and White, 1988) was used to determine in situ the hydraulic conductivity and sorptivity, in the range near saturation ($-120 < h < 0$ mm), using the approach of Ankeny et al. (1991).

Results and discussion

In the long-term experiment the aggregate size distribution (ASD), mean weight diameter (MWD) and aggregation index (AI) values were slightly greater in RT than in TT, although differences were not significant (Figure 1). On the contrary, water stability (WAS) values for field-moist 1-2 mm size aggregates were greater in TT, despite the organic carbon (OC) and CaCO_3 contents in these aggregates were greater in RT (OC, 12.4 g kg^{-1} in TT, and 14.0 g kg^{-1} in RT; CaCO_3 , 136 g kg^{-1} in TT and 190 g kg^{-1} in RT, values at 0-5 cm depth). Aggregation is a temporal variable property, product of interactions of the soil biota, mineral and organic components, that is affected by soil use and management. For example, increasing loads, and soil density, can enhance the relative water stability. Earthworm activity, greater under RT, can also alter the structural stability by either a stabilizing or a disrupting effect on soil aggregates, depending on the soil texture and mineralogy, an aspect to be studied under our conditions. Other possible cause could have been the effect of the straw burning carried out in previous years in the TT treatment.

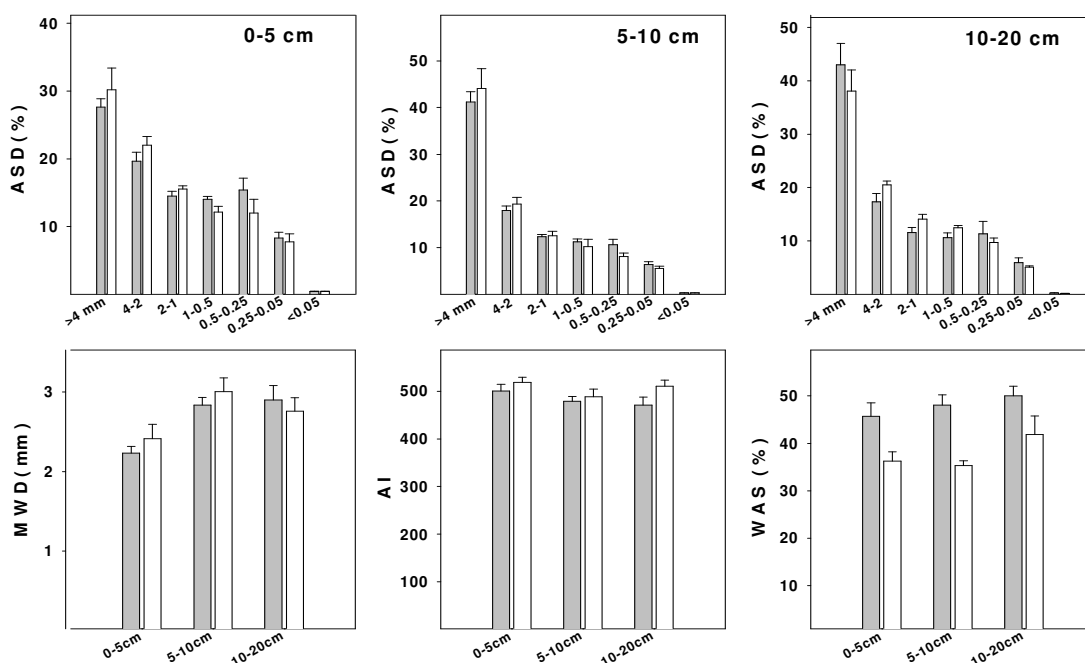


Figure 1. Dry aggregate size distribution (ASD), mean weight diameter (MWD), aggregation index (AI) and water stability of air-dry 1-2 mm size aggregates (WAS) of TT (grey bars) and RT (white bars) treatments in the long-term experiment. (mean values \pm standard error).

In the short-term experiment the aggregate size distribution (ASD), mean weight diameter (MWD) and aggregation index (AI) values were similar in both treatments (traditional tillage, TT and no-tillage, NT), data not shown.

Figure 2 shows the results of the water stability of air-dry aggregates in two sampling date. Under our conditions NT seems to have a greater effect on water stability of aggregates than RT, both in comparison with the respective TT treatment. We have observed an increase of this variable, in NT respect to TT, after only four years of experimentation.

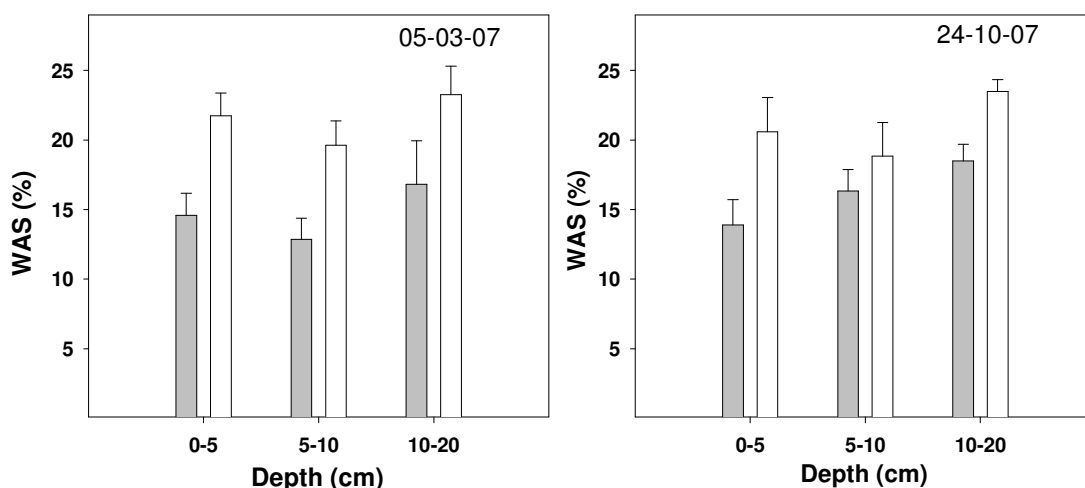


Figure 2. Water stability of air-dry 1-2 mm size aggregates in two dates in the short-term experiment. TT (grey bars) and NT (white bars). (mean values \pm standard error).

In Figure 3 are shown the results of hydraulic conductivity (K), sorptivity (S) and characteristic mean pore radius (λ_m) measured in situ at the soil surface in the long- and short-term experiment. The hydraulic conductivity (Figure 3a) was significantly higher ($p < 0.05$) in TT than RT for $h > -20$ mm in the long-term experiment.

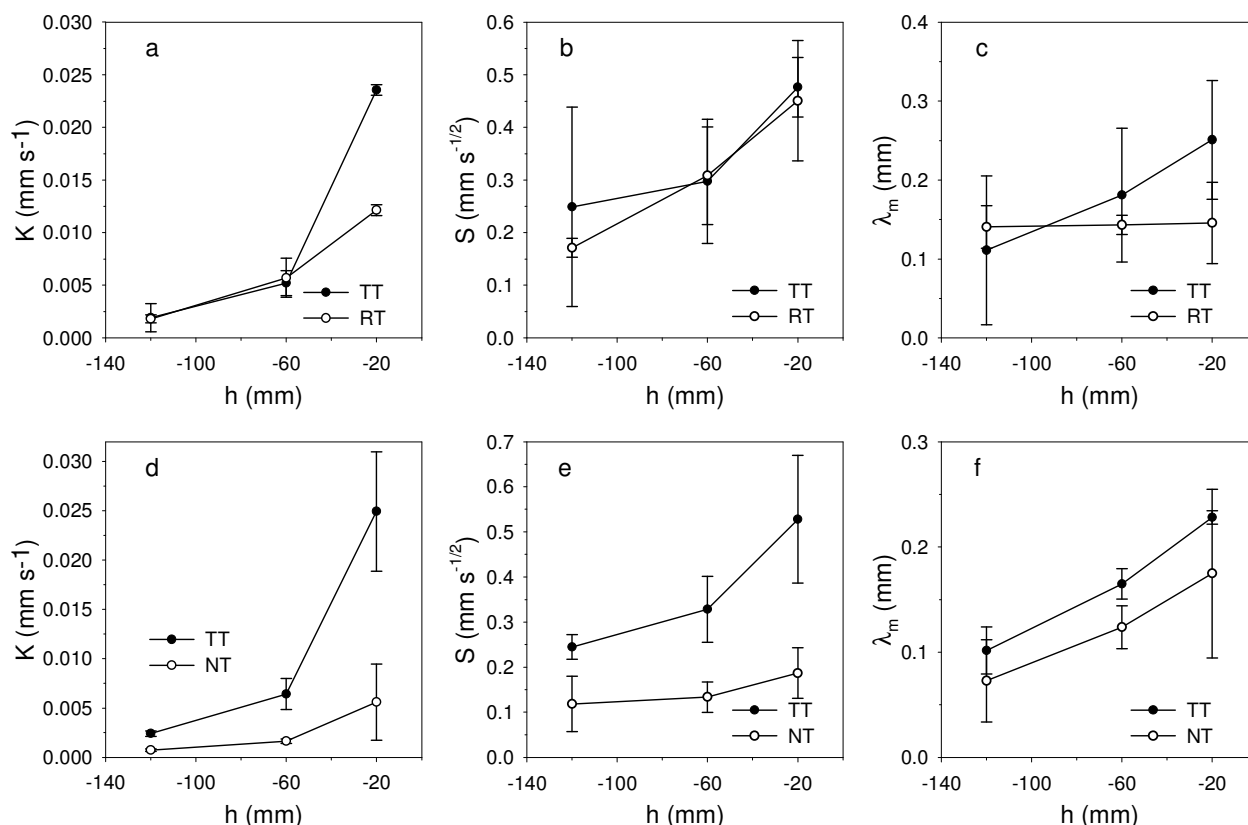


Figure 3. Variation with the imposed water suction (h) of the hydraulic conductivity (K), sorptivity (S) and characteristic mean pore radius (λ_m): a, b and c for the TT and RT treatments in the long-term experiment, and d, e and f for TT and NT treatments in the short-term experiment. Vertical bars are standard deviations.

Sorptivity was similar under both treatments (Figure 3b). Differences in hydraulic conductivity between the two treatments can be attributed to a different soil consolidation, and in agreement with a characteristic mean pore radius greater in TT than in RT for $h > -60$ mm (Figure 3c). These results are similar to those found by Moreno et al. (1997) three years after this long-term experiment was established.

In the short-term experiment K, S and λ_m values (Figures 3d, 3e and 3f, respectively) were higher (significantly

different at $p < 0.05$ for K and S) in the TT treatment than in the NT treatment in the range $-120 < h < 0$ mm. The lower hydraulic conductivity in NT than in TT is in apparent contradiction with the fact that λ_m was not significantly different between treatments, and suggests a lack of interconnected pores in NT treatment as reported by Angulo-Jaramillo et al. (1997).

Conclusions

In the long-term experiment, the aggregate size distribution (ASD), mean weight diameter (MWD) and aggregation index (AI) values were slightly greater in RT than in TT, although differences were not significant. Water stability (WAS) values for 1-2 mm size aggregates were greater in TT, despite the organic carbon (OC) and CaCO_3 contents in these aggregates were greater in RT.

On the contrary, under our conditions NT seems to have a greater effect on water stability of aggregates. We have observed an increase of this variable, respect to TT, after only four years of experimentation.

In the long-term experiment, the hydraulic conductivity was higher in TT than in RT for $h > -20$ mm in agreement with a greater characteristic mean pore radius for $h > -20$ mm. In the short-term experiment, the lower hydraulic conductivity in NT than in TT suggests a lack of interconnected pores in NT treatment.

References

- Ankeny MD, Ahmed M, Kaspar TC, Horton R (1991) Simple field method determining unsaturated hydraulic conductivity. *Soil Science Society of America Journal* **55**, 467-470.
- Angulo-Jaramillo R, Moreno F, Clothier BE, Thony JL, Vachaud G, Fernández-Boy E, Cayuela JA (1997). Seasonal variation of hydraulic properties of soils measured using a tension disk infiltrometer. *Soil Science Society of America Journal* **61**, 27-32.
- Du Preez CC, Steyn JT, Kotze E (2001) Long-term effects of wheat residue management on some fertility indicators of a semi-arid plinthosol. *Soil & Tillage Research* **63**, 25-33.
- Kemper WD, Rosenau RC (1986) Aggregate stability and size distribution. In: Klute A, editor. *Methods of Soil Analysis, Part 2*. Agronomy-Madison: Soil Science Society of America; p. 425-442.
- Moreno F, Pelegrín F, Fernández JE, Murillo JM (1997) Soil physical properties, water depletion and crop development under traditional and conservation tillage in southern Spain. *Soil & Tillage Research* **41**, 25-42.
- Pelegrín F, Moreno F, Martín-Aranda J, Camps M (1990) The influence of tillage methods on soil physical properties and water balance for a typical crop rotation of SW Spain. *Soil & Tillage Research* **16**, 345-358.
- Perroux KM, White I (1988) Designs for disc permeameters. *Soil Science Society of America Journal* **52**, 1205-1215.

Experiments and modeling of electron-transfer of DIRB

James Kubicki^A, Brendan Puls^A, Yufeng Qian^B and Ming Tien^B

^ADepartment of Geosciences, The Pennsylvania State University, University Park, PA, USA, Email jdk7@psu.edu

^BDepartment of Biochemistry & Molecular Biology, The Pennsylvania State University, University Park, PA, USA, Email mxt3@psu.edu

Abstract

We use quantum chemical calculations and experimental data to describe the structures and functions of mediator molecules used in the terminal electron transfer step of dissimilatory iron-reducing bacteria (DIRB). Mediator molecules increase the rate of electron transfer by either chelating reducible iron (Fe^{3+}) or shuttling electrons between outer-membrane cytochromes and iron-oxide minerals. Examples of mediator molecules examined in recent literature include ethylenediaminetetraacetic acid (EDTA) (Wang *et al.* 2008), citric acid (Wang *et al.* 2008), riboflavin (Canstein *et al.* 2008), flavin mononucleotide (FMN) (Canstein *et al.* 2008), menaquinone (Newman and Kolter 2000), and anthraquinone disulfonate (AQDS) (Lovley *et al.* 1998). Focusing on several of these mediator molecules, our goals are to 1) determine the potential for each mediator to chelate reducible iron and 2) determine the potential for each mediator to shuttle electrons. We use UV/Vis spectroscopy to measure the electronic spectra and quantum chemistry to calculate the minimum energies of each mediator in four states: 1) oxidized, 2) reduced, 3) bound to reducible iron (Fe^{3+}), and 4) bound to reduced iron (Fe^{2+}). We determine the potential for each mediator to chelate reducible iron or shuttle electrons by comparing the measured spectra and calculated minimum energies. As a future part of this study, we plan to explore the function of the mediator molecules as iron chelators by measuring binding constants for each mediator with reducible iron (Fe^{3+}) and reduced iron (Fe^{2+}) using isothermal titration calorimetry (ITC). This study is conceived as the first step towards characterizing the role of microbial iron reduction mediators on a molecular level. The next step will be to characterize the interactions of the mediator molecules with the electron donor (outer-membrane cytochromes) and the electron acceptor (iron-oxide minerals) of the terminal electron transfer step of microbial iron reduction.

Key Words

Quantum- mechanical, electron-transfer, flavin, iron-oxide.

Introduction

Recent research on the reduction of iron by DIRB has focused on determining how its rate and long-term extent are controlled in natural environments. In a study of the reduction of Fe-oxyhydroxide minerals with a wide range of specific surface areas, crystallographic structures, and thermodynamic properties by DIRB, Roden (2006) found that the rate and long-term extent of reduction are strictly limited by access to the substrate. The interfacial rate-limiting reaction, however, has not yet been characterized on a molecular level (Frederickson *et al.* 2008). Research has revealed three methods of substrate access by DIRB: 1) direct adhesion to insoluble substrates (Caccavo and Das 2002), 2) reduction of soluble electron shuttles (Newman and Kolter 2000), and 3) reduction of soluble metal chelates (Nevin *et al.* 2002). In most natural systems where direct access to Fe-oxyhydroxide minerals is limited or where DIRB cells grow in biofilms, the presence of soluble electron shuttles or metal chelates increases the bioavailability of reducible iron and consequently the rate of microbial iron reduction (Nevin *et al.* 2002). Bioremediation systems based on the stimulation of DIRB growth and activity can therefore use the addition of soluble substrates to promote microbial iron reduction.

Methods

Experimental

UV/Vis spectra were measured for 1) flavin mononucleotide (FMN), 2) riboflavin (RBF), 3) FeCl_3 , 4) FMN mixed with FeCl_3 , and 5) RBF mixed with FeCl_3 . All species were dissolved at 100 μM and adjusted to pH 7 with NaOH or HCl. No buffer was added to avoid unwanted interactions. Peaks were selected at the local maxima of the spectra with no other curve fitting. UV/Vis spectra were measured over the range of 200 to 800 nm at a resolution of 0.1 nm. The background was measured prior to solution measurement and subtracted from each of the solution spectra. All solutions were measured with a dual beam relative to a blank which contained distilled water. Difference spectra were calculated by subtracting the mixed FMN/ FeCl_3 and RBF/ FeCl_3 solutions from the sums of the the FMN and FeCl_3 solutions and RBF and FeCl_3 solutions, respectively.

Computational

Gas-phase structures were optimized using Gaussian 03. The calculations were performed using the Becke 3-parameter exchange functional and the Lee-Yang-Parr correlation functional (B3LYP) using the 6-311G(d,p) basis set. Vibrational frequency calculations were performed for each of the optimized structures to verify that these were true minima and to estimate Gibbs free energies. Using the optimized structures, UV/Vis peaks were calculated using time-dependent density functional theory (TD-DFT). Peaks were calculated separately for singlet and triplet electronic transitions over the UV/Vis range to compare to experimental measurements. Free energies were calculated using the gas-phase optimized and frequency-corrected energies for the individual species and adjusting for stoichiometry. Changes in free energy upon binding were calculated by subtracting the energies of the FMN, RBF, and Fe^{3+} monomers from the energies of the FMN/ Fe^{3+} and RBF/ Fe^{3+} complexes. Several configurations for FMN/ Fe^{3+} and RBF/ Fe^{3+} complexes were used to achieve theoretical binding structures. The comparison of the calculated peaks for the theoretical binding structures to the measured UV/Vis peaks is a test of the validity of the theoretical structures.

Results

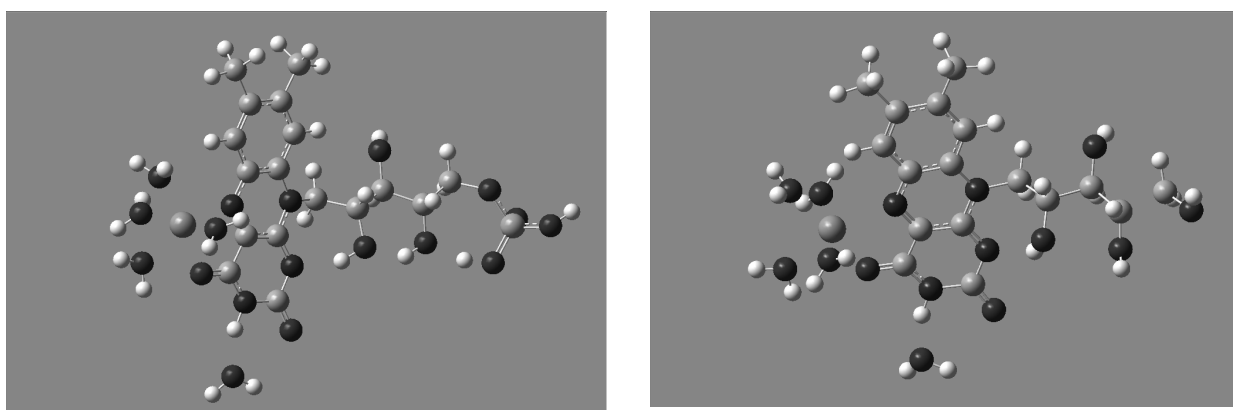


Figure 2. Gas-phase optimized structures for example configurations of FMN/ Fe^{3+} (left) and RBF/ Fe^{3+} (right). All calculations done using the Gaussian 03 (B3LYP 6-311G(d,p)).

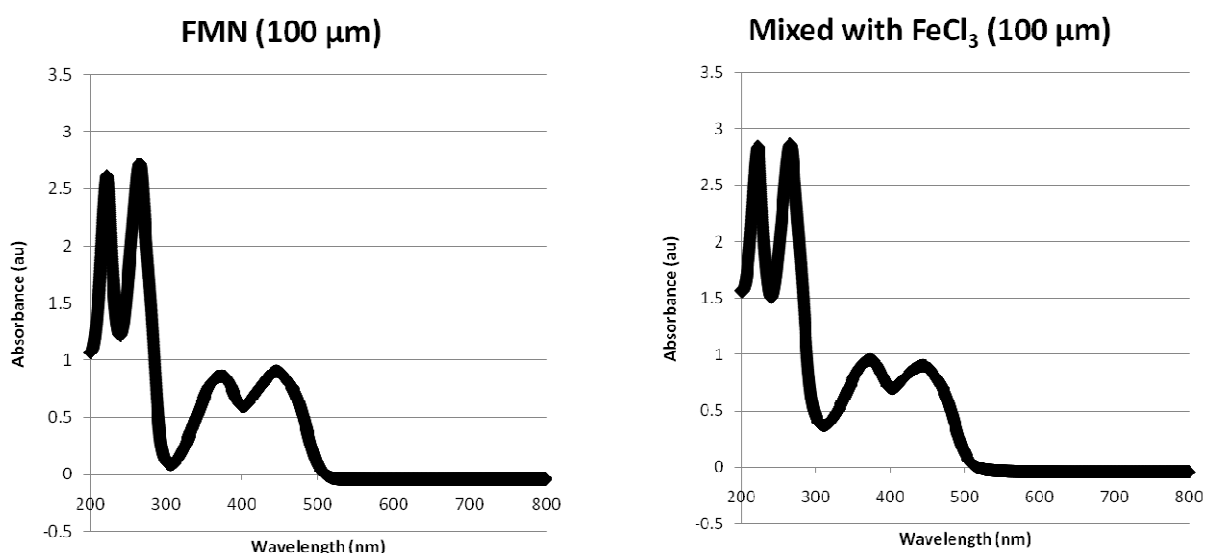


Figure 3. UV/Vis spectra for FMN (left) and FMN/ Fe^{3+} (right). All dissolved species at 100 μM and pH 7.

Table 2. Wavelengths (nm) and intensities (au) of measured UV/Vis peaks for FMN, FMN/Fe³⁺, RBF, and RBF/Fe³⁺. All dissolved species at 100 μM and pH 7.

Spectrum	Peak #1	Peak #2	Peak #3	Peak #4
FMN	222.3 nm	265.2 nm	373.1 nm	445.1 nm
(100 μL)	2.616 au	2.717 au	0.865 au	0.905 au
Mixed with FeCl ₃	221.1 nm	265.7 nm	373.0 nm	443.1 nm
(100 μL)	2.844 au	2.863 au	0.954 au	0.907 au
RBF	219.8 nm	261.6 nm	371.1 nm	(none)
(100 μL)	2.703 au	2.673 au	0.810 au	
Mixed with FeCl ₃	219.5 nm	261.8 nm	356.3 nm	(none)
(100 μL)	2.994 au	2.865 au	0.942 au	

Table 3. Wavelengths (nm) and intensities (au/f-values) of measured and calculated UV/Vis peaks for FMN and RBF. All species at 100 μM and pH 7. Calculations done using the Gaussian 03 (TD-DFT B3LYP 6-311G(d,p)).

Spectrum	Peak #1	Peak #2	Peak #3	Peak #4
Measured FMN	222.3 nm	265.2 nm	373.1 nm	445.1 nm
(100 μL)	2.616 au	2.717 au	0.865 au	0.905 au
Calculated FMN	217.1 nm	252.8 nm	333.0 nm	405.0 nm
(N/A)	(0.3740)	(0.3015)	(0.1854)	(0.1300)
Measured RBF	219.8 nm	261.6 nm	371.1 nm	(none)
(100 μL)	2.703 au	2.673 au	0.810 au	
Calculated RBF	216.1 nm	253.6 nm	332.8 nm	(none)
(N/A)	(0.1702)	(0.3762)	(0.1668)	

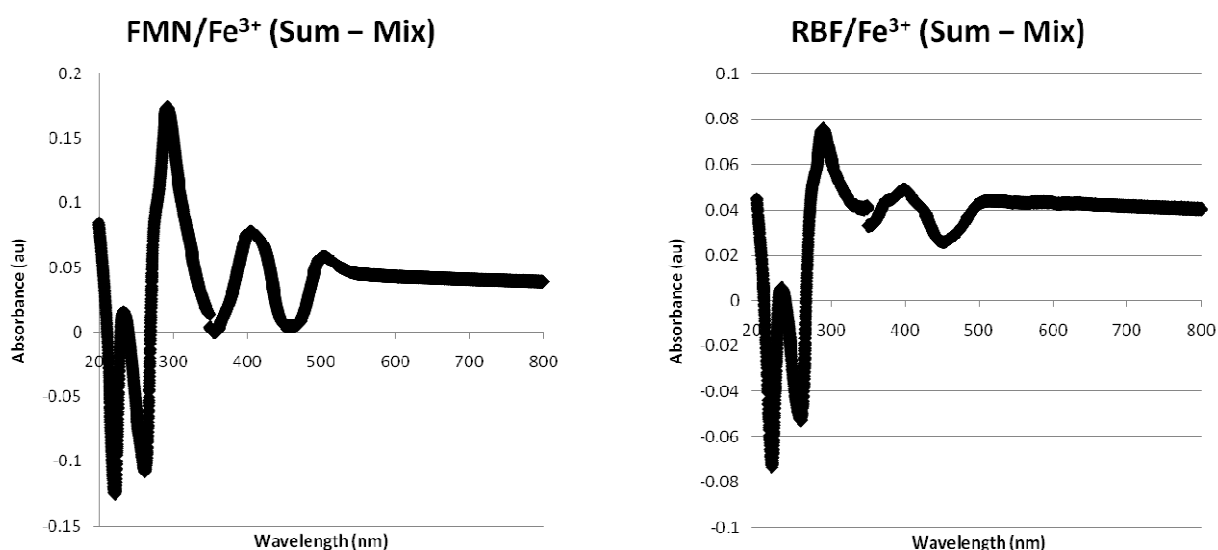


Figure 4. Difference spectra for FMN/Fe³⁺ (left) and RBF/Fe³⁺ (right). All dissolved species at 100 μM and pH 7.

Conclusions

UV/Vis spectra were measured for 1) FMN, 2) RBF, 3) FMN mixed with FeCl₃, and 4) RBF mixed with FeCl₃. Based on the measured spectra, peak shifts upon mixing with FeCl₃ are within 2 nm. This may be interpreted as a sign of weak or absent binding. However, the spectra do exhibit significant changes in the absorbance. Absorbance changes may indicate a binding event. Absorbance changes measured during a UV/Vis titration can indicate the strength of the binding. Peaks were calculated for FMN and RBF. Calculated peaks appear to be shifted down from measured peaks. However, the calculated peaks were based on gas-phase optimized structures that do not account for solvent. Calculated absorbance values appear to scale roughly with the measured absorbance values. Reoptimization of the gas-phase structures with a continuum solvent model may correct the down-shifted peaks. In addition, energy calculations for the solvent-optimized structures will show differences in stability among the several configurations tested. Repeating the calculations with Fe²⁺ will allow comparison of energy changes upon binding among the theoretical configurations. Based on the gas-phase optimizations, changes in free energy are expected to be negative upon binding. This indicates that binding is thermodynamically favored. For FMN, the change in free energy for the binding is lower for the configuration with Fe³⁺ bound to the phosphate group than for the configuration with Fe³⁺ bound to the isoalloxazine unit.

This may indicate that binding to the phosphate group is the favored configuration.

References

- Caccavo F Jr, Das A (2002) Adhesion of dissimilatory Fe(III)-reducing bacteria to Fe(III) minerals. *Geomicrobiol. J.* **19**, 161–177
- Canstein H Von, Ogawa J, Shimizu S, Lloyd JR (2008) Secretion of flavins by *Shewanella* species and their role in extracellular electron transfer. *Appl. Environ. Microbiol.* **74**, 615-623.
- Fredrickson JK, Zachara JM (2008) Electron transfer at the microbe-mineral interface: A grand challenge in biogeochemistry. *Geobiol.* **6**, 245-253.
- Lovley DR, Fraga JL, Blunt-Harris EL, Hayes LA, Phillips EJP, Coates JD (1998) Humic substances as a mediator for microbially catalyzed iron reduction. *Acta Hydrochim. Hydrobiol.* **26**, 152-157.
- Newman DK, Kolter R (2000) A role for excreted quinones in extracellular electron transfer. *Nature* **405**, 94-97.
- Roden E (2006) Geochemical and microbiological controls on dissimilatory iron reduction. *C.R. Geosci.* **338**, 456-467.
- Wang Z, Liu C, Wang X, Marshall MJ, Zachara JM, Rosso KM, Dupuis M, Fredrickson JK, Heald S, Shi L (2008) Kinetics of Reduction of Fe(III) Complexes by Outer Membrane Cytochromes MtrC and OmcA of *Shewanella oneidensis* MR-1. *Appl. Environ. Microbiol.* **74**, 6746-6755.

Ferrihydrite enhances phenanthrene sorption to artificial soils

Geertje Pronk, Katja Heister, Ingrid Kögel-Knabner

Lehrstuhl für Bodenkunde, Technische Universität München, 85350 Freising-Weihenstephan, Germany, pronk@wzw.tum.de

Abstract

In order to investigate the effect of mineral composition on the sorption of hydrophobic organic chemicals in soil, phenanthrene sorption experiments were carried out to the <20 μ m fraction of artificial soils containing illite, ferrihydrite and both minerals. The sorption isotherms of the ferrihydrite containing samples show a significant increase in linearity and K'_f with respect to the sample containing only illite. This difference could not be explained by carbon content or BET-N₂ specific surface area as these parameters were very similar for the sample containing only illite and that containing illite and ferrihydrite. These results indicate that the presence of ferrihydrite increased the sorption capacity of the artificial soils. This could be due to sorption of phenanthrene to the ferrihydrite itself, but it is more probable that the presence of ferrihydrite changes the properties of the biogeochemical interfaces in the soil, thereby increasing the sorption capacity.

Keywords

Biogeochemical interfaces, sorption isotherm, K_{oc} , specific surface area, PAH

Introduction

The structure and properties of biogeochemical interfaces are an important factor controlling the fate and behaviour of organic chemicals in soil (Totsche *et al.* 2010). Recent studies show that next to organic matter composition, minerals in soil also have an important effect on the sorption of hydrophobic organic chemicals. However, how different minerals affect sorption capacity is not yet clear. At low organic carbon contents, chemicals may sorb directly onto mineral surfaces (Müller *et al.* 2007), but it is also possible that the association of organic matter with minerals changes its affinity for organic chemicals (Ahangar *et al.* 2008). One of the main groups of organic chemicals that are important to investigate are the polycyclic aromatic hydrocarbons (PAH) as they have a low solubility and therefore a high potential to be retained in soil. Phenanthrene is used as a model compound to represent this group of chemicals.

In order to gain more insight into the contribution of specific minerals to sorption of phenanthrene to soil, we carried out phenanthrene sorption experiments to artificial soils with different mineral compositions (quartz, illite and ferrihydrite). The artificial soils were composed in the laboratory from the main components that are present in most natural soils. They have a clearly defined composition and texture and the only difference between the different samples is mineral composition. Therefore these artificial soils give us the possibility to investigate the specific effect of mineral composition on phenanthrene sorption.

Methods

Materials

Artificial soils (Kögel-Knabner *et al.*, 2010) were produced from model materials, the minerals quartz, illite and ferrihydrite. Sterilized manure was added as an organic matter component. The soils were inoculated with the water extractable microbial community of a Eutric Cambisol. Soil texture was provided by adding sand and silt-sized quartz and was composed of 42% sand, 52 % silt and 6% clay. The soils were incubated for 3 months at 60% of the water holding capacity. Soil solution was composed of 0.01 M CaCl₂ in order to provide an ionic strength similar to that of natural soils.

For this study, soils with 3 different mineral compositions were used; illite (B), ferrihydrite (C) and illite + ferrihydrite (F). Quartz was present in all soils and in the soil without illite, clay-sized quartz was added to maintain the same texture. Illite and ferrihydrite were present at 8 and 1% mass respectively. The particle size fractions <20 μ m were obtained by sieving and consecutive freeze-drying of the soils. These fractions were used for the sorption experiments in order to concentrate the minerals of interest and to reduce the effect of the quartz sand and particulate organic matter present in the coarser fractions. Carbon and nitrogen content, C/N ratio and BET-N₂ specific surface area (SSA) of the samples were determined.

Sorption experiment

Phenanthrene sorption experiments were carried out in batch incubation experiments according to the guideline of the (OECD, 2000) in a concentration range from 10 to 50% of the water solubility of phenanthrene. One gram of sample was added to 75 ml of 0.01 M CaCl₂ solution, spiked with phenanthrene and incubated for 24 hours. The batches were centrifuged and phenanthrene was extracted from the supernatant using Bakerbond C18 material. Phenanthrene concentration was measured using GC-MS and quantified with deuterated phenanthrene as an internal standard.

Sorption isotherms were calculated using the solubility-normalized Freundlich isotherm (Carmo *et al.* 2000) according to equation 1:

$$\log C_{(a)s} = \log K'_f + n^{-1} \log(C_{(a)aq}/S) \quad (1)$$

Where $C_{(a)s}$ is the concentration of phenanthrene adsorbed to the sample, $C_{(a)aq}$ is the concentration of phenanthrene in solution at equilibrium, S is the super cooled liquid solubility of phenanthrene, n^{-1} is a measure of sorption linearity and K'_f is the Freundlich isotherm coefficient. The K'_{oc} was calculated by normalizing the K'_f to organic matter concentration and K'_{SSA} was calculated by dividing the K'_f by the specific surface area of the sample.

Results and discussion

The 3 month incubation has allowed for limited development of the soils (Kögel-Knabner *et al.*, 2010). Carbon concentrations (table 1) in all samples are relatively low although that of soil C is slightly higher than the others. The small difference in C/N ratio of the samples suggests that organic matter composition is relatively similar. The specific surface area of the two samples containing illite are similar while that of the sample containing only ferrihydrite is lower suggesting the presence of illite is an important factor determining SSA.

Table 4. Sample characterisation

name	major mineral	C content mg g ⁻¹	C/N	SSA m ² g ⁻¹
B	illite	8.8 ± 0.8	6.7	9.0 ± 0.4
C	ferrihydrite	12.8 ± 0.1	6.7	6.8 ± 0.4
F	illite+ferrihydrite	7.8 ± 0.2	6.4	9.6 ± 0.4

The phenanthrene sorption isotherms are presented in figure 1. The isotherms for the two samples containing ferrihydrite have the same slope with slightly higher sorption in sample C than sample F.

The isotherm for sample B has a lower slope and although sorption at the two lowest concentrations is higher than in samples C and F, it is lower at the other concentrations.

These differences are reflected in the calculated Freundlich isotherm coefficients and nonlinearity constants (table 2). R^2 of all three isotherms is 0.99 which shows that the Freundlich isotherm model can be used to explain the data. The calculated distribution coefficients K'_f (table 2) for samples C and F are rather similar while that for soil B is much lower. Furthermore it can be seen clearly that the phenanthrene sorption to samples C and F was linear with a nonlinearity constant close to 1 while that of sample B was nonlinear with an n of 0.64.

The K'_{oc} values (table 2) show no clear pattern and cannot be used to explain the difference in sorption behaviour between sample B and samples C and F. This can also be concluded from the carbon concentrations (table 1). The carbon concentration for sample B and F is very similar while phenanthrene sorption is significantly different. It is possible that the slightly higher sorption to sample C relative to F is due to its higher carbon content. However, there is a significant difference in the K'_{oc} of these two samples. This may be due to the calculation method because differences in carbon content could have a disproportionately large effect on the K'_{oc} at these low concentrations. It may also indicate that other differences between the samples are also important for phenanthrene sorption. It is possible that during the 3 months of incubation, the artificial soils developed differently leading to a difference in organic matter composition between the 3 soils. Several studies have shown that organic matter composition has an effect on phenanthrene sorption and this might explain the differences in K'_{oc} values.

Table 5. Freundlich isotherm parameters; the solubility normalized distribution coefficient K'_f , the isotherm linearity constant n , correlation coefficient R^2 , the distribution constant normalized to organic carbon content in g g^{-1} K'_{oc} and the distribution constant normalized to specific surface area in g m^{-2} K'_{SSA}

sample	K'_f	n	R^2	K'_{oc}	K'_{SSA}
B	174	0.64	0.99	$2.0 \cdot 10^4$	19
C	589	0.97	0.99	$4.6 \cdot 10^4$	87
F	646	1.03	0.99	$8.3 \cdot 10^4$	67

The K'_{SSA} values (table 2) also show no clear relation between the samples. Again, specific surface area was very similar for sample B and F indicating that their difference in sorption behaviour cannot be explained by differences in SSA.

As organic matter content and specific surface area cannot be used to explain the significant difference in sorption behaviour between samples C and F which contain ferrihydrite and sample B which does not, we must conclude that the presence of ferrihydrite itself affects sorption behaviour. The presence of illite is of low importance in this experiment. It might be that some sorption of phenanthrene to ferrihydrite itself takes place. However, it is also possible that the ferrihydrite affected the development of biogeochemical interfaces in the soil during the 3 months of incubation. The association of organic matter with ferrihydrite could have given it a different structure, providing an interface with a higher affinity towards phenanthrene.

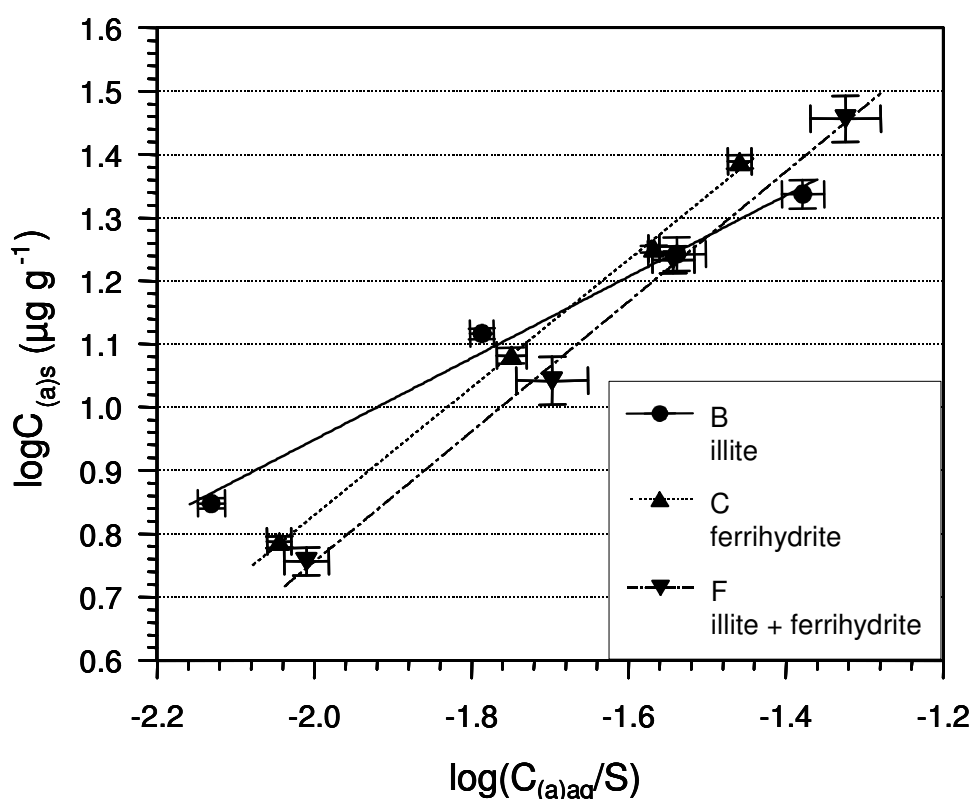


Figure 1. Phenanthrene sorption isotherm, $C_{(a)s}$ is the equilibrium concentration of adsorbed phenanthrene in the solid phase in $\mu\text{g g}^{-1}$, $C_{(a)aq}$ is the equilibrium concentration of phenanthrene in the aqueous phase in $\mu\text{g ml}^{-1}$ and S is the supercooled liquid solubility of phenanthrene in $\mu\text{g ml}^{-1}$. The error bars represent the standard deviation of the three replicates for each sample.

Conclusions

1. The presence of ferrihydrite lead to an increase in sorption capacity and sorption linearity compared to the soil containing only illite.
2. This difference cannot be explained by carbon content or specific surface area.
3. Overall, either significant sorption of phenanthrene to ferrihydrite itself occurs or, most probably, ferrihydrite has affected the properties and structure of the biogeochemical interfaces in the soil formed during the 3 month incubation, increasing its affinity to phenanthrene.

References

- Ahangar AG, Smernik RJ, Kookana RS, Chittleborough DJ (2008) Separating the effects of organic matter-mineral interactions and organic matter chemistry on the sorption of diuron and phenanthrene. *Chemosphere* **72**, 886-890.
- Carmo AM, Hundal LS, Thompson ML (2000) Sorption of Hydrophobic Organic Compounds by Soil Materials: Application of Unit Equivalent Freundlich Coefficients, doi:10.1021/es000968v. *Environmental Science & Technology* **34**, 4363-4369.
- Kögel-Knabner I, Ding GC, Heister K, Pronk GJ, Schaumann GE, Schloter M, Schulz S, Schwarz J, Smalla K (2010) Formation of biogeochemical interfaces in soils as controlled by mineral and organic components. *World Congress of Soil Science, Soil Solutions for a Changing World*, 1-6 August 2010, **accepted**
- Müller S, Totsche KU, Kögel-Knabner I (2007) Sorption of polycyclic aromatic hydrocarbons to mineral surfaces, doi:10.1111/j.1365-2389.2007.00930.x. *European Journal of Soil Science* **58**, 918-931.
- OECD (2000) Adsorption/desorption using a batch equilibrium method, test guideline 106. *OECD guidelines for testing chemicals, OECD publications, Paris*.
- Totsche KU, Rennert T, Gerzabek MH, Kögel-Knabner I, Smalla K, Spiteller M, Vogel HJ (2010) Biogeochemical interfaces in soil: The interdisciplinary challenge for soil science. *Journal of Plant Nutrition and Soil Science* **173**, 88-99.

Formation of biogeochemical interfaces in soils as controlled by mineral and organic components

Ingrid Kögel-Knabner^A, Guo-Chun Ding^B, Katja Heister^A, Geertje J. Pronk^A, Gabriele E. Schaumann^C, Michael Schlöter^D, Stephan Schulz^D, Jette Schwarz^C, Kornelia Smalla^B

^ALehrstuhl für Bodenkunde, Technische Universität München, D-85350, Freising-Weihenstephan, Germany

^BJulius Kühn-Institut - Federal Research Centre for Cultivated Plants (JKI), Institute for Epidemiology and Pathogen Diagnostics, Messeweg 11-12, D-38104 Braunschweig, Germany

^CSoil and Environmental Chemistry, Institute of Environmental Sciences, Universität Koblenz-Landau, Fortstr. 7, D-76829 Landau, Germany

^DHelmholtz Zentrum München, Abteilung für terrestrische Ökogenetik, Ingolstädter Landstr. 1, D-85758 Oberschleißheim, Germany

Abstract

The formation of soil interfaces is controlled by the type of particle surfaces present and the assemblage of organic matter and mineral particles. The formation of interfaces was studied with artificial soils which were produced in a long-term biogeochemical laboratory incubation experiment (3 and 6 months). The experiment used clay minerals, iron oxides and charcoal as major model components controlling the formation of interfaces because they exhibit high surface area and microporosity. Soil interface characteristics are analyzed in relation to microbial community structure and function that developed after 6 months of incubation. Already after 6 months of incubation the artificial soils exhibited different properties in relation to their composition. Major effects are observed for artificial soils formed in the presence of montmorillonite, ferrihydrite and charcoal.

Key Words

Biogeochemical interface, soil formation, clay, iron oxides, char, microbial community structure and function, DSC

Introduction

The biogeochemical interfaces of soils are a dynamic and hierarchically organized system of various organic and inorganic constituents and organisms, the spatial structure of which defines a large, complex and heterogeneous interface (Totsche *et al.* 2010). Major solid phase constituents of soils are rock fragments, minerals like quartz, carbonates, clay minerals and the (hydr)oxides of iron, manganese, and aluminium. Carbonaceous materials including charred organic carbon of biogenic origin (Biochar) and, of course, the soil organic matter (SOM) are a second major ingredient of soils. These components are of different provenience, complexity and molecular size. Their arrangement during pedogenesis results in the spatial and temporal development of complex biogeochemical interfaces in soils. The natural diversity in soil structural components leads to isolated areas of enhanced biogeochemical activity, popularly known as hot spots, and at the same time zones of lower biogeochemical activity in soils. The existence and importance of such a differentiation of active and inactive spots in soils, i.e. a patchy distribution of soil properties, are recognized in the ecological community, but a solid understanding of the underlying mechanisms that produce this differentiation is still lacking. We hypothesize that the formation of soil interfaces is controlled by the type of particle surface(s) present and the assemblage of organic matter and mineral particles. We consider clay minerals, iron oxides and charcoal as major components controlling the formation of interfaces because they exhibit high surface area and microporosity. The objective of our work is to characterize the heterogeneous architecture of soil interfaces as it develops depending on the type of particle surface present and to link it with the structure and function of the microbial communities. The formation of interfaces is studied in batch incubation experiments with inoculated artificial soils consisting of model compounds, thus artificial soil materials comprised of model compounds with increasing complexity of interfaces were created.

Methods

Artificial soil

The components used for the artificial soil incubation experiment were quartz sand, clay minerals (illite and montmorillonite), iron oxide (ferrihydrite), aluminium hydroxide (boehmite) and charcoal (Table 1). A microbial inoculum for this experiment was obtained from the water extractable community of a Eutric Cambisol from Ultuna, Sweden. Organic matter obtained from sterilized manure was used as C and nutrient source during incubation. The soils were incubated at a water content of 60% of the water holding capacity. Soil

solution consisted of 0.01 M CaCl₂. Samples were obtained after 3 days (t=0), 3 months (t=1) and 6 months (t=2) of incubation.

C and N content

Carbon and nitrogen content were determined after 3 and 6 months of incubation.

Table 1. Composition of the artificial soils

	A	B	C	D	E	F	G	H	<i>Differential scanning calorimetry</i>
Manure	X	X	X	X	X	X	X	X	
Quartz	X	X	X	X	X	X	X	X	
Montmorillonite	X			X	X				
Illite		X		X		X	X	X	
Ferrihydrite			X			X		X	
Boehmite							X		
Charcoal					X			X	Six month

s incubated artificial soil samples were analyzed in a ramp of -50°C to 550 °C with 10 K min⁻¹ heating and synthetic air as purge gas (50 mL min⁻¹). DSC measured the energy transformation in the samples occurring during heating. In this experiment, the combustion process was monitored. This analysis gives insight into the development of organic matter quality from the manure in the soils under the influence of various minerals and charcoal with respect to thermal stability.

Microbial community and function

Microbial communities were followed by DGGE of 16S rRNA gene fragments amplified from directly extracted DNA. Samples were taken at Day 1, 9, 31 and 90. Microbial community structure was analyzed by fingerprinting of PCR products of the 16S rRNA genes from DNA extracted from soil. As an example for microbial community function, degradation of wheat litter was investigated in a batch incubation experiment using the different artificial soils that had been incubated for 3 months. As an indicator abundance pattern of the alkane monooxygenase, gene (*alkB*) which catalyzes the degradation of plant waxes and other alkane containing substances was chosen.

Results and Discussion

C and N stabilization

C contents in soils (figure 1 left) E and H are higher, due to the presence of charcoal. Already after 6 months of incubation, the different artificial soil materials show a large difference in C stabilization, although the amount of C substrate added as manure was similar for all soils (figure 1 right). C losses are specifically low in the presence of oxides ferrihydrite (soil F) or boehmite (soil G). Losses are high from both soils containing charcoal (E and H), indicating that the charcoal has a stimulating effect on C mineralization or is itself mineralized already in the beginning of the incubation. Nitrogen was lost from the soil at a relatively constant ratio to carbon loss with a ratio of C loss/N loss between 8 and 12.

Differential scanning calorimetry

The DSC thermograms show –besides a weak endotherm below 100°C indicating water evaporation– pronounced exotherms in the temperature region I (200°C-400°C) and region II (400-550°C) (figure 2). This may in a first attempt be interpreted as combustion of two types of organic matter differing in thermal stability. The two most striking observations are: (i) In the exotherms of region II distinctly structured peaks occur only for the samples A and D containing montmorillonite, (ii) the exotherm in region II differs significantly between the samples containing charcoal and the samples without charcoal.

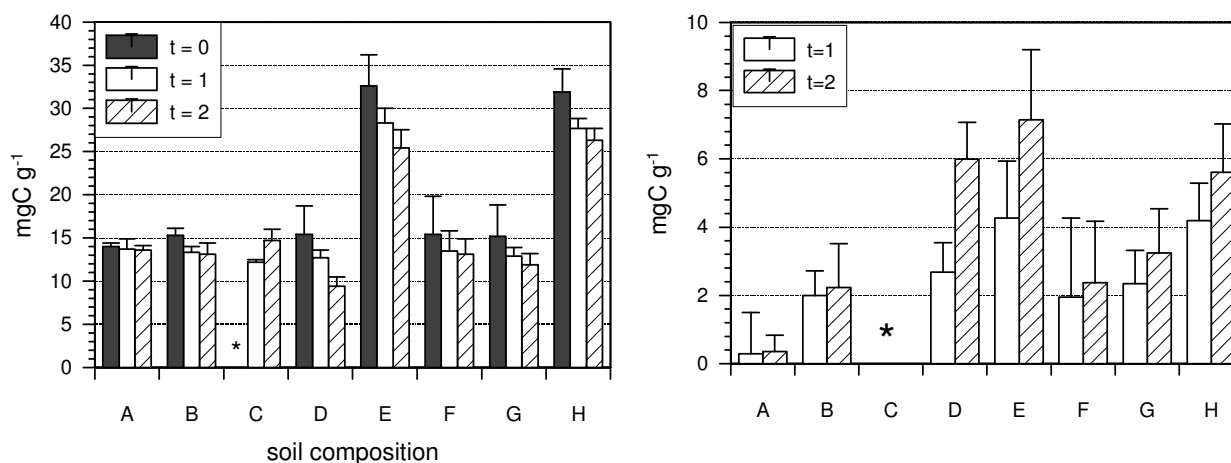


Figure 1. Carbon concentration of the artificial soils (left) after 3 days ($t=0$), 3 ($t=1$) and 6 ($t=2$) months of incubation, and amount of carbon lost from the soils calculated from the carbon concentration at $t=0$ minus the carbon concentration at $t=1$ and $t=2$ respectively (right). Results and standard deviations were calculated from the three replicates for each soil. * not determined.

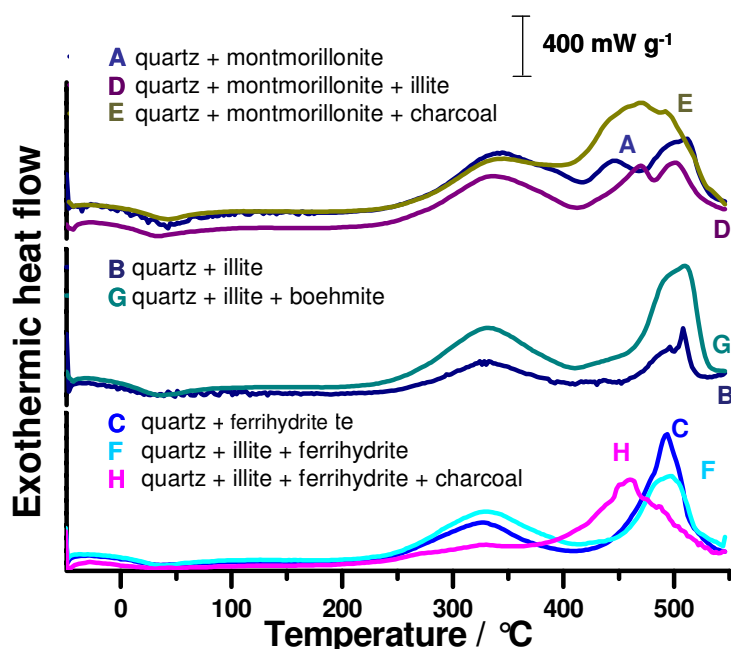


Figure 2. Exothermic heat flow from selected artificial soils measured by differential scanning calorimetry.

Microbial community

Soil-like bacterial communities' patterns could already be observed 9 days after inoculation. Charcoal was found to strongly influence the reassembly of bacterial communities. UPGMA clusters analysis of communities' profiles showed that separate clusters were always formed for those samples with charcoal. Effects of montmorillonite, illite and iron oxides on microbial communities could clearly be observed until day 90. Bacterial communities of samples with montmorillonite differed from those of the corresponding samples with illite. Separated clusters for samples with iron oxides were also formed in betaproteobacterial and actinobacterial communities, but no clear difference was observed between ferrihydrite and boehmite.

Alkane monooxygenase

Already three months after the incubation of the different soil mixtures clear differences in the abundance of the *alkB* gene during litter degradation are visible in the different artificial soil mixtures at different interfaces (figure 3). Mainly those artificial soils that contain montmorillonite have a tendency to lower *alkB* numbers at the soil-litter interface. The obtained numbers are already comparable to values that can be found in fully developed soils.

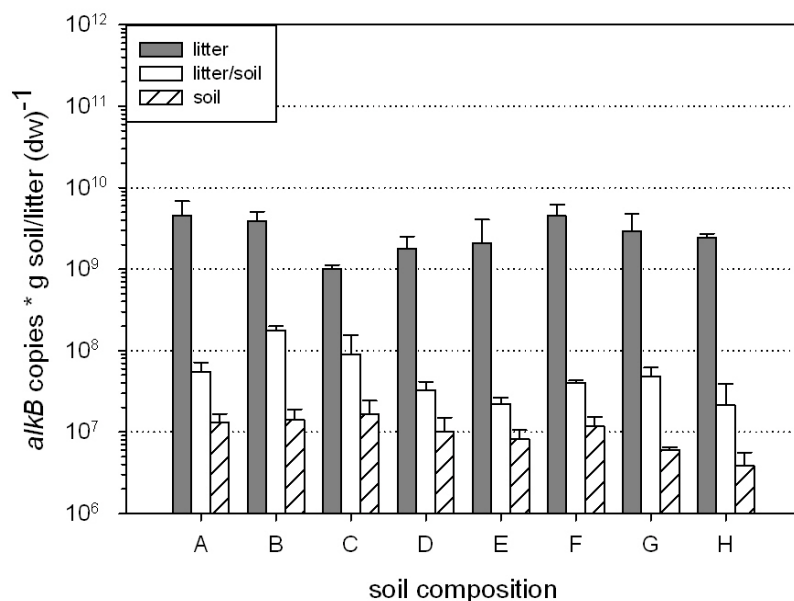


Figure 3. Abundance of the alkane monooxygenase gene (*alkB*) during degradation of wheat litter at different interfaces (litter, litter/soil, soil) after two weeks of incubation in the different artificial soils at t=1. The bars indicate standard errors (n=3).

Conclusions

Already after 6 months of incubation, the different artificial soil materials show a large difference in C stabilization, although the amount of C substrate added as manure was similar for all soils. At the current stage of research, a contribution of charcoal to OM stability cannot be excluded but has to be shown in further analyses. The preliminary results suggest, however, that the minerals present during formation of biogeochemical interfaces, determine stabilization and quality of organic matter.

The presence of charcoal and mineral composition had a clear effect on the development of the microbial community after only 3 months of incubation. Furthermore, clear differences in the microbial community function, expressed in the abundance of the *alkB* gene, which is involved in the degradation of plant waxes during litter degradation are visible in the different artificial soils at different interfaces. The presence of an expandable clay mineral (montmorillonite) and of ferrihydrite had clear effects on the formation and properties of the biogeochemical interface in the artificial soils, as well as the presence of charcoal. These differences in the biogeochemical interface formation also lead to different sorptive properties of the interface for phenanthrene (Pronk *et al.* 2010).

References

- Pronk GJ, Heister K, Kögel-Knabner I (2010) Ferrihydrite enhances phenanthrene sorption to artificial soils. *World Congress of Soil Science, Soil Solutions for a Changing World*, 1-6 August 2010, **submitted**
- Totsche KU, Rennert T, Gerzabek M, Kögel-Knabner I, Smalla K, Spiteller M (2010) Biogeochemical interfaces in soil: The new challenge for soil science. *Journal of Plant Nutrition and Soil Science*, **in press**.

Formation of clay pans in south-west Queensland, Australia

Kristie Williams^A and Andrew Biggs^B

^ADepartment of Environment and Resource Management, Toowoomba, QLD, Australia, Email kristie.williams@derm.qld.gov.au

^BDepartment of Environment and Resource Management, Toowoomba, QLD, Australia, Email andrew.biggs@derm.qld.gov.au

Abstract

Clay pans are hard, bare, unproductive areas found throughout south-west Queensland. While anecdotal evidence suggested various mechanisms for how clay pans form, no detailed investigations had been done to identify the causal processes leading to the formation of clay pans. This study assessed 11 clay pans in an area west of Roma, examining the morphological, physical and chemical properties of the soils in the clay pans and in nearby grassed areas. The driving factor causing clay pans to form was a loss of cover which exposed the soil surface to raindrop impact and erosion, leading to surface sealing/crusting. The particle size distribution of the soil surface is a key contributing factor, with clay pans being dominated by fine sand.

Key Words

Vegetative cover, surface seal, particle size distribution, scalded area

Introduction

The area west of Roma, in south-west Queensland, is known to have many bare, “scalded” areas (Figure 1), which are locally referred to as clay pans. They are found in footslopes and in depressions, particularly on alluvial plains. The clay pans have been in the region for many years—local landholders remember seeing them at least since the 1940s. It is likely that clay pans have increased in area over time, due to continuous grazing and/or drought, but they are currently relatively stable in size.



Figure 1. Typical clay pans in the area west of Roma.

In early 2007, a project assessing salinity risk was being carried out in the region by the Department of Environment and Resource Management on behalf of the Queensland Murray-Darling Committee (QMDC). QMDC identified several areas where additional information was needed to guide decisions about where their salinity management efforts should be focused—the clay pans in the Roma region were included in the list.

Historically, salinity had been considered as a causal factor leading to the development of the clay pans. Sodicity had also been identified as a major contributor. However, the causal processes have never been thoroughly investigated, though some management trials have been conducted over the past 15 years at one clay pan in the area. These include saltbush plantings, constructing shallow banks to pond water, tree plantings, installing bores to monitor groundwater levels and fencing off the area to exclude stock. Unfortunately the trials have not been regularly maintained or monitored over time and detailed records have been lost. Some of these trials were more aimed at managing salinity, rather than reclaiming the clay pan itself, as it was thought that salinity was the main reason the area was scalded. Koch *et al.* (1994) conducted a study tour of scalded sites in far-west Queensland, assessing the success of management options such as shallow ponding.

In August and November 2007, soil investigations were undertaken to better understand the nature of the clay pans, and their possible causal processes—how were these clay pans forming? Was salinity the main contributing factor? Understanding how clay pans form, together with information about their physical and chemical properties could then be used to inform management activities for the clay pans. In July 2008, a field day was held to communicate the results to local landholders and community groups. A series of information sheets about clay pan formation and management were produced and distributed in August 2008.

Methods

A combination of aerial photography, satellite imagery, historical information and local expert knowledge were used to identify a number of clay pans to be investigated in the region. Eleven sites, across six properties, were assessed (Figure 2, Table 1). Soil profiles were taken with 50 mm hydraulic driven soil cores (~1.8 m length) to depths ranging from 0.9 to 1.7 m. Profiles were described using methods outlined in McDonald *et al.* (1990), field pH and electrical conductivity tests were carried out down the profile, and 57 soil samples were collected (from the soil surface, and then generally from 10 cm sections at 30 cm intervals) and analysed at the Department of Environment and Resource Management laboratories for pH, electrical conductivity, chloride, cations and exchange capacity, moisture content and particle size analysis, using standard methods outlined in Rayment and Higginson (1992).

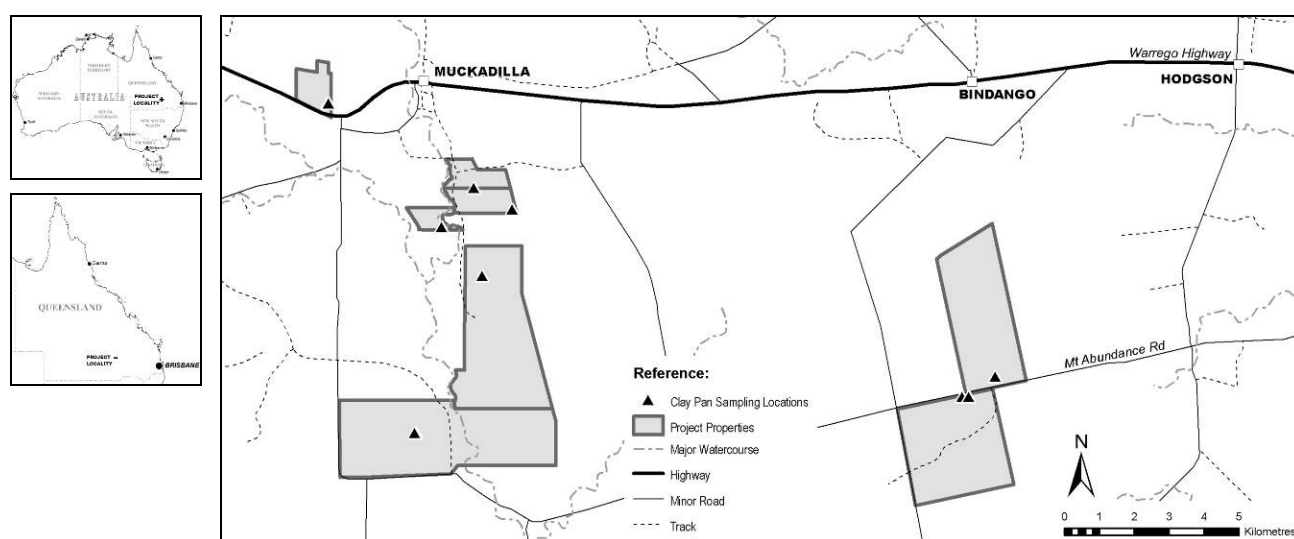


Figure 2. Location of clay pan sampling sites and properties.

Table 1. Summary of clay pan sites.

Date sampled	Site number	Property number	Comments
2/08/07	136	1	Site located in clay pan; 0–1.7 m; 11 samples analysed; previous management trials conducted at this clay pan
8/11/07	136	1	Re-visited clay pan; collected 0–0.02 m surface sample for analysis
8/11/07	143	2	Paired site 1; site located in clay pan; 0–0.9 m, five samples analysed
8/11/07	144	2	Paired site 1; site located in Mitchell grass area, about five metres from site 143; 0–1.2 m; six samples analysed
8/11/07	145	3	Site located in clay pan, about 10 metres away from an area of the clay pan that had previously been ripped; 0–1.3 m; field pH and EC tests only
8/11/07	146	4	Paired site 2; site located in clay pan; 0–1.1 m; five samples analysed
8/11/07	147	4	Paired site 2; site located in vegetated area within the same clay pan, about 20 m from site 146; 0–1.5 m; six samples analysed
9/11/07	148	5	Site located in a bare patch within a partially remediated clay pan; 0–1.2 m; six samples analysed
9/11/07	149	5	Site located in clay pan, adjacent to creek; 0–0.9 m; five samples analysed
9/11/07	150	5	Paired site 3; site located in a wheat crop which had been a bare clay pan prior to ploughing and planting; 0–1.2 m; five samples analysed
9/11/07	150b	5	Paired site 3; site located in a wheat crop (not a prior clay pan area), about 300 m from site 150; field pH and EC tests only to 1.4 m
9/11/07	151	6	Site located in clay pan; 0–1.2 m; six samples analysed

Results and Discussion

This study found that the formation of clay pans is driven by a lack of ground cover and that the particle size distribution of the soil surface is a key contributing factor. Most clay pan sites are non-saline at the surface (0–0.05 m), but are usually saline at depth (site 136 had the highest EC of 5.4 dS/m at 0.5 m).

Vegetative cover is lost mainly through overgrazing and/or drought. Grass and herb growth is usually better in parts of the landscape which receive more water, i.e. in footslope areas, depressions etc. This can lead to preferential grazing (or patch grazing) by stock in these areas. Even though the overall paddock stocking rate may be suitable, stock will overgraze these areas as they stay greener for longer and have sweeter feed, especially during dry times. Overgrazing and loss of cover is the start of the clay pan formation process. Many areas in the region may have been overgrazed by sheep and rabbits in the early 1900s during the Great Drought, leading to a loss of cover.

Once ground cover is lost, two key factors come into play—raindrop impact and erosion. Without cover, the soil surface becomes more susceptible to raindrop impact—the physical action of raindrops hitting the soil surface is enough to ‘sort’ the soil so that the fine sand, silt and clay particles are re-arranged until they eventually pack together, filling the pore spaces at the surface, causing a surface seal and setting hard like concrete which limits infiltration of water. All of the clay pans investigated in the study area had a visible layer of silt/fine sand on the soil surface which set quite hard and appeared to be limiting infiltration of water. A number of the clay pans also had a vesicular layer (Figure 3). Particle size analysis showed that the clay pan surface is dominated by fine sand, while vegetated sites were dominated by clay in the surface (Table 2).



Figure 3. Surface clod from site 148 (a bare patch of soil within a fenced off clay pan). A firmly packed layer of fine sand/silt, approximately 10 mm thick is evident, with an underlying vesicular layer.

Table 2. Comparison of particle size analysis results between clay pans and grassed areas, at the soil surface and at 0.5–0.6 m. Clay pans were dominated by fine sand at the surface (>50%), though by 0.5 m, their particle size distribution was dominated by clay, more like the ‘normal’ grassed sites.

Clay pan sites	Depth (cm)		Grassed area sites	Depth (cm)	
	0–5	50–60		0–5	50–60
146			Vegetated area within a clay pan (147)		
143			Mitchell grass area (144)		
149					

Coarse sand

Silt

Fine sand

Clay

In some clay pans, it is also possible that the surface seal made up of fine sand, silt and clay particles has been deposited by surface wash over time. A key factor influencing this is slope and the management of the surrounding upslope areas. If there has been a loss of cover in the upslope areas (e.g. they have been cleared, grazed, cropped etc), then this is more likely to occur. The soil particles tend to be deposited in footslope areas and depressions, building up the surface crust.

As with the other clay pans in the study area, results from site 149 (clay pan located near a creek) showed that a surface seal was present. Sampling at this site also revealed that the soil underneath the seal had no obvious serious chemical limitations to vegetation growth. It therefore seems very likely that this area is bare simply due to the physical action of raindrop impact sealing the surface, leading to reduced infiltration and seedling emergence.

The creek clay pan area was re-visited in March 2008 and again in July 2008. At both times, sections of the former bare area had recovered quite well and had reasonable cover. The property received about 500 mm of rain in December 07/January 08. Given that the landholder had not touched the area since November 2007, this highlights that some clay pans (especially the ones with no serious underlying chemical limitations e.g. salinity or sodicity) can regenerate somewhat without human interference. It also highlights how clay pans can change from season to season, and the importance of good rain and a suitable seed source (in this case the Mitchell grass area upslope) for clay pan remediation.

Many soils in the region are naturally saline and sodic at depth (Macnish, 1987). With reduced infiltration and leaching under crusted/sealed soils, evaporative accumulation of salts at the surface can occur. Once cover is lost and a surface seal is in place, even light rainfalls will usually be lost as runoff. This means that over time, soil salt, chloride and sodium levels are all likely to increase in a clay pan, compared to vegetated areas. This can give the impression that salinity is causing the clay pan as testing will show elevated salts at the surface, but in effect, it is usually a symptom of the clay pan formation process, rather than a contributing factor.

A number of factors combine to restrict plant growth on clay pans:

- The soil is too hard for roots to penetrate or water to infiltrate;
- High levels of salts close to the surface inhibit plant growth;
- Surface temperatures on a dry bare area can exceed the shade air temperature by up to 11°C in winter and by up to 25°C in summer (since summer surface temperatures will regularly reach 65°C, this means bare areas can reach 90°C);
- Light falls of rain are ineffective (due to low infiltration, high runoff and high evaporation rates) while heavy rainfalls are lost as runoff;
- Loose wind-blown sand particles can develop sufficient velocity on bare areas to cut plant tissue, exposing the affected plant to desiccation; and
- In bigger clay pans there are usually low levels of seed supplies in the immediate surrounding area.

Conclusion

This study found that the majority of clay pans are likely to have formed from the following sequence of events:

1. Vegetative cover is lost through overgrazing and/or drought.
2. The soil surface becomes exposed and susceptible to raindrop impact.
3. This leads to 'sorting' of the soil surface, resulting in a surface seal or crust which limits infiltration and seedling emergence.
4. Evaporation brings any salts that may be present naturally at depth in the soil profile closer to the surface.
5. Eventually the salts accumulate due to evaporative concentration.
6. Any vegetation that tries to grow can't get established due to limited water and/or a hostile soil environment, so the area remains bare.

References

- Koch AJ, Bryant WJ, Herbert JG, Muller AD and Gray HJ (1994). *Guidelines for the Rehabilitation of Degraded Native Pastures Using Shallow Ponds and Water Spreading Techniques*. 6–9 June 1994. Queensland Department of Primary Industries, Brisbane.
- Macnish SE (Ed) (1987) *Land Management Field Manual Roma District*. Queensland Department of Primary Industries, Brisbane.
- McDonald RC, Isbell RF, Speight JG, Walker J and Hopkins MS (1990) *Australian Soil and Land Survey Field Handbook*, 2nd Edition. CSIRO Publishing, Canberra.
- Rayment GE and Higginson FR (1992) *Australian Laboratory Handbook of Soil and Water Chemical Methods*. Inkata Press, Melbourne.

Formation of iron plaque and vivianite on the roots of paddy rice

Masami Nanzyo^A, Hidenori Yaginuma^A, Hitoshi Kanno^A and Tadashi Takahashi^A

^AGraduate School of Agricultural Science, Tohoku University, Sendai, 981-8555, Japan, Email: nanzyo@bios.tohoku.ac.jp

Abstract

A redox interface is one of the important sites of chemical reactions in soil science and soil morphological properties. One such interface appears on the root surface of paddy rice. We examined paddy rice roots at different growth stages using optical and electron microscopy. The paddy rice plants were grown under continuous flooding in pots. Although the new rice roots develop one after another and the root system is always a mixture of young and aged roots, thick iron plaque was relatively more common in the earlier growth stage. The thin iron plaque prevailed in the middle growth stage. The major elements in the iron plaque were Fe, Ca and P. Blue vivianite crystal aggregates were found on the rice roots during the ripening growth stage. As vivianite requires ferrous iron, it was probably found on the aged roots after dissolution of the iron plaque. Further study is needed regarding vivianite formation on the aged roots in the earlier growth stage and soil-plant environmental factors affecting the vivianite nucleation.

Key Words

Iron plaque, vivianite, paddy rice, rice root, redox, phosphate

Introduction

The root surface of paddy rice is an interface where redox conditions vigorously change. The Ap horizon soil of paddy fields is reduced under flooding. Hydrous iron oxides are reduced to form ferrous iron in the bulk soil. In contrast, oxidizing conditions are caused by aeration through the inside of the active rice roots. Iron plaques are formed on the active rice roots moving ferrous iron from the bulk soil to the rice roots. However, with aging of the roots, the plaques fade due to prevailing anoxic conditions (Kimura *et al.*, 1984). As new rice roots develop one after another and the redox conditions near the roots change with the position of the roots and age of the roots, formation and fading of the plaques take place at different sites during the early middle to maturity stage of rice growth in the Ap horizon of paddy fields. In this paper, we describe the changes in the iron minerals on the rice roots grown in limed paddy soil using a scanning electron microscope (SEM) and energy dispersive X-ray (EDX) analysis. The present rice cultivation was conducted in pots. The differences in the present pot cultivation from the rice cultivation in a field as a community are a small rhizosphere volume, no downward percolation of water, large amounts of fertilizers, continuous flooding, and abundant sunlight.

Methods

Properties of the soil

The soil was taken from the Ap horizon of a paddy rice field in the northern part of Miyagi Prefecture, Japan. The paddy rice field is weakly contaminated with Cd and was previously limed to reduce the Cd uptake by the rice. The pH(H₂O) of the air-dried fine earth fraction was 7.9 and the texture was clay loam. The total C and N contents were 19.1 and 1.69 g kg⁻¹, respectively. The oxalate-extractable Al, Fe and Si contents were 1.4, 13.2 and 1.1 g kg⁻¹, respectively. The labile P₂O₅ content (Truog) was 145 mg kg⁻¹ and the Ca(H₂PO₄)₂-extractable SO₄ was 204 mg kg⁻¹. The oxalate-extractable Fe content was excessive compared to the amount of the Ca(H₂PO₄)₂-extractable SO₄ plus that of SO₄ contained in the superphosphate.

Rice cultivation in pots

To a/5000 pot, 3 kg each of air-dried soil (ground to pass through 5 mm sieve) was placed, 1 g N (poly-olefin coated urea), 1 g P₂O₅ (powdered superphosphate) and 1 g K₂O (poly-olefin coated potassium sulfate) were applied to the soil, and then the soil was flooded with tap water. Three rice seedlings at the 3.5 leaved stage (*Oryza sativa* L, var. Japonica) were transplanted on June 5th, 2008. The rice-growing pot was submerged in water using a/2000 pot at the middle growth stage to keep it easily flooding. On July 7th, August 2nd, and September 2nd, the above-ground part was cut-off and the rice roots were separated from the soil by washing with tap water, and dried at 75 degrees C. The rice roots sampled on October 7th were air-dried to avoid heat alteration of the materials on the roots.

Analytical methods

Rice roots having thick and thin iron plaques were collected from the oven-dried roots (August 2nd) and the

blue crystals were collected from the air-dried rice roots (October 7th) using an optical microscope. The materials formed on the rice roots were observed using an optical microscope and SEM (Hitachi S4200 operated at 15 kV). The elemental composition of the materials on the roots was examined by EDX attached to the SEM. The RINT RAPID II-CMF (Rigaku Corporation) generating a micro-beam (0.05 mm diameter) of CoK α (40kV and 15 mA) was used to obtain an X-ray diffraction (XRD) pattern of the crystalline material.

Results

Growth of rice plants after transplanting was normal until ripening and harvest in this limed soil. On July 7th, the plant height (the maximum length of the above-ground part) was about 40 cm and the number of tillers was 14 per plant. The soil color started to turn partly black, showing the formation of noncrystalline ferrous sulfate because the superphosphate contained gypsum. The plant height was greater than 70 cm and the number of the tillers was 20 on August 2nd. On September 2nd, the plant height was about 100 cm and the number of tillers was 18-19 per plant. The color of the leaves and ears turned yellow and the rice plants were at the ordinary ripening stage on October 7th. The soil color turned completely black at this stage because flooding was maintained throughout the rice-growing season.

Thick and thin brown-colored iron plaque was easily found on the washed roots using an optical microscope on July 7th. The thick brown cylindrical iron plaque was relatively common at this stage compared to the later growth stages. On October 7th, although the root color was black, especially in the middle or deeper part just after washing, the black color of the roots almost completely faded with air-drying within one day at room temperature.

Thick iron plaque

The thick iron plaque was partly broken into many short cylindrical parts possibly during the washing and drying (Figure 1-(1)). According to the SEM observations and EDX analysis of the selected area (Figures 1-(1)-a and (5)), the major elements of the iron plaques were, Fe, Ca and P. These elements were almost evenly distributed in the plaque as shown in the element maps (Figures 1-(2, 3 and 4)). Hydrous iron oxide in the bulk soil was reduced and ferrous iron was solubilized, and then it moved to the rice roots, re-oxidized, and hydrous iron oxide precipitated on the rice roots. Phosphorus was also partly solubilized in the bulk soil under reducing conditions and was moved to the roots and sorbed on the iron plaque.

Thin iron plaque

Thin iron plaque (Figure 2-(1)) was also found on many roots and was more common than on the thick ones. The thin iron plaque was also partly broken during washing, drying or sample preparation for the SEM observations. The iron plaque in Figure 2-(1) appears so thin that it has a shape similar to the outer part of the root cells. Although the peak intensities are weak, the thin iron plaque has Fe, Ca and P as the major elements (Figure 2-(5)) and this set of elements is similar to that of the thick iron plaque (Figure 1-(5)). The thin iron plaque may be found on a relatively aged roots with a declining amount of the thick iron plaque (Figure 1) or formed on the roots with a lower air supply.

Vivianite

Vivianite is ferrous phosphate [Fe₃(PO₄)₂·8H₂O] formed under reducing conditions. Although vivianite was postulated when discussing the P concentration in soil water under reducing conditions, it was not found in the Ap horizon of the paddy rice field. However, we found small blue crystals on the air-dried rice roots collected on October 7th, 2008 using the optical microscope (Figure 3 (1, 2)). The abundance of the vivianite particles tends to be found slightly more on the tertiary rice roots (Figure 3-(1)). The vivianite crystals on the rice roots are aggregates of platy crystals (Figure 4-(1, 2)). The chemical composition of the crystals is close to that for vivianite having an atomic Fe:P ratio of 3:2 according to the EDX spectra (Figure 4-(5)) although they were not obtained using a thin section. Very small amounts of Ca and Mn were also detected in the crystals weakly suggesting the nature of paravivianite. The X-ray micro-diffraction pattern of the crystal aggregates was close to that for vivianite and has been reported elsewhere (Nanzyo *et al.*, 2010). The vivianite crystals remained on the rice roots even after a thorough washing with water to remove the soil. The formation of vivianite needs ferrous iron thus indicating that it must probably be nucleated on the aged rice roots after dissolution of the iron plaque. As new rice roots develop one after another, the rice rhizosphere is a mixture of aged and young roots. Thus, vivianite can also be found on the aged roots in the earlier growth stage than that presently studied. Further studies are needed on the function of vivianite in the paddy rice fields, and natural and artificial wetlands.

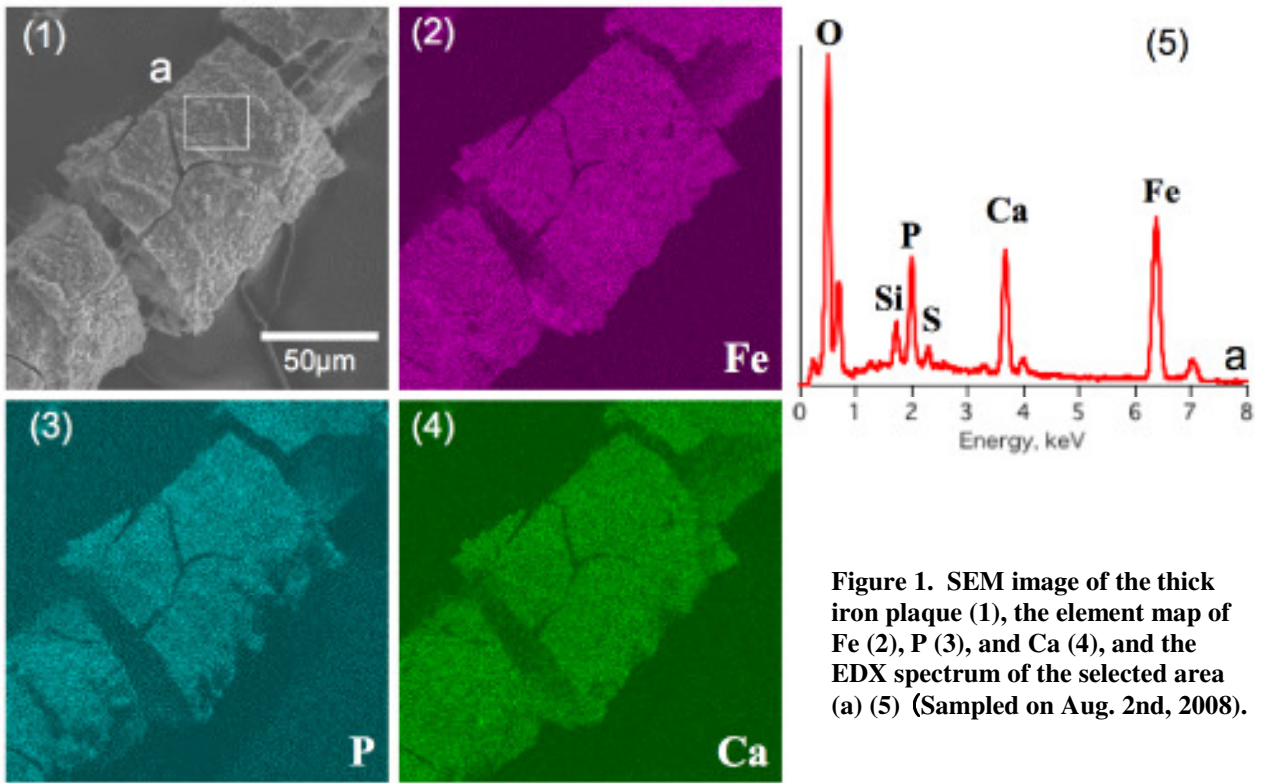


Figure 1. SEM image of the thick iron plaque (1), the element map of Fe (2), P (3), and Ca (4), and the EDX spectrum of the selected area (a) (5) (Sampled on Aug. 2nd, 2008).

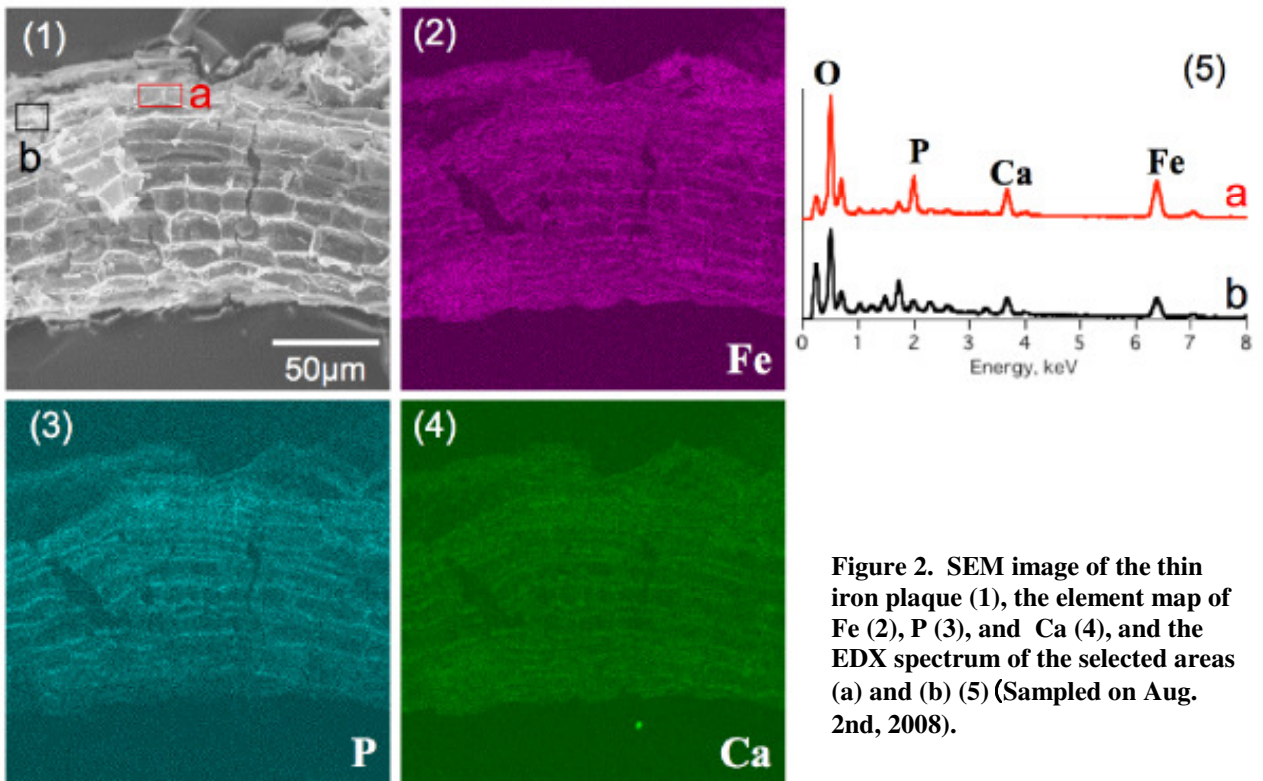


Figure 2. SEM image of the thin iron plaque (1), the element map of Fe (2), P (3), and Ca (4), and the EDX spectrum of the selected areas (a) and (b) (5) (Sampled on Aug. 2nd, 2008).

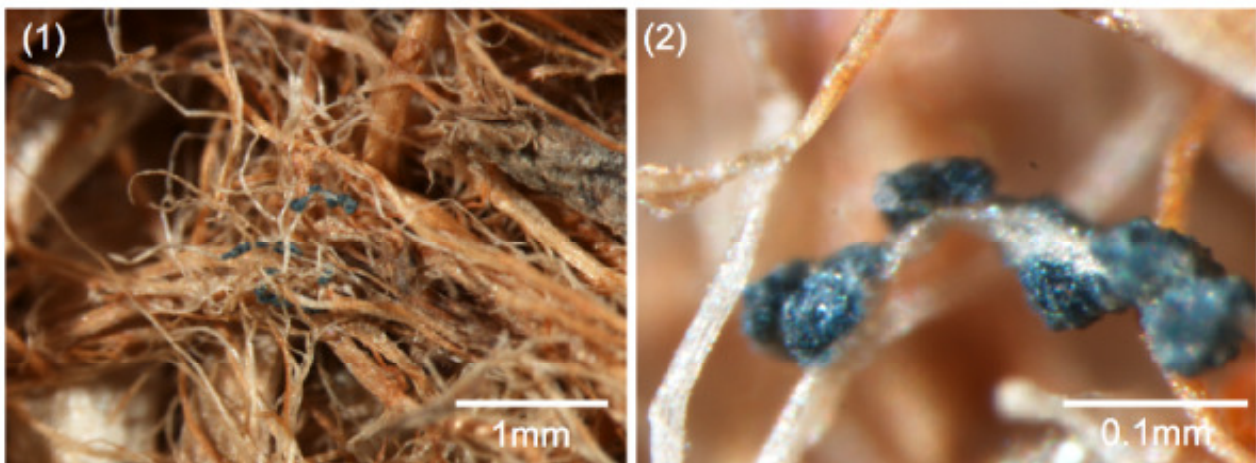


Figure 3. Optical microscope images of rice roots (1) and blue crystals (2) formed on the rice root sampled on Oct. 7th, 2008.

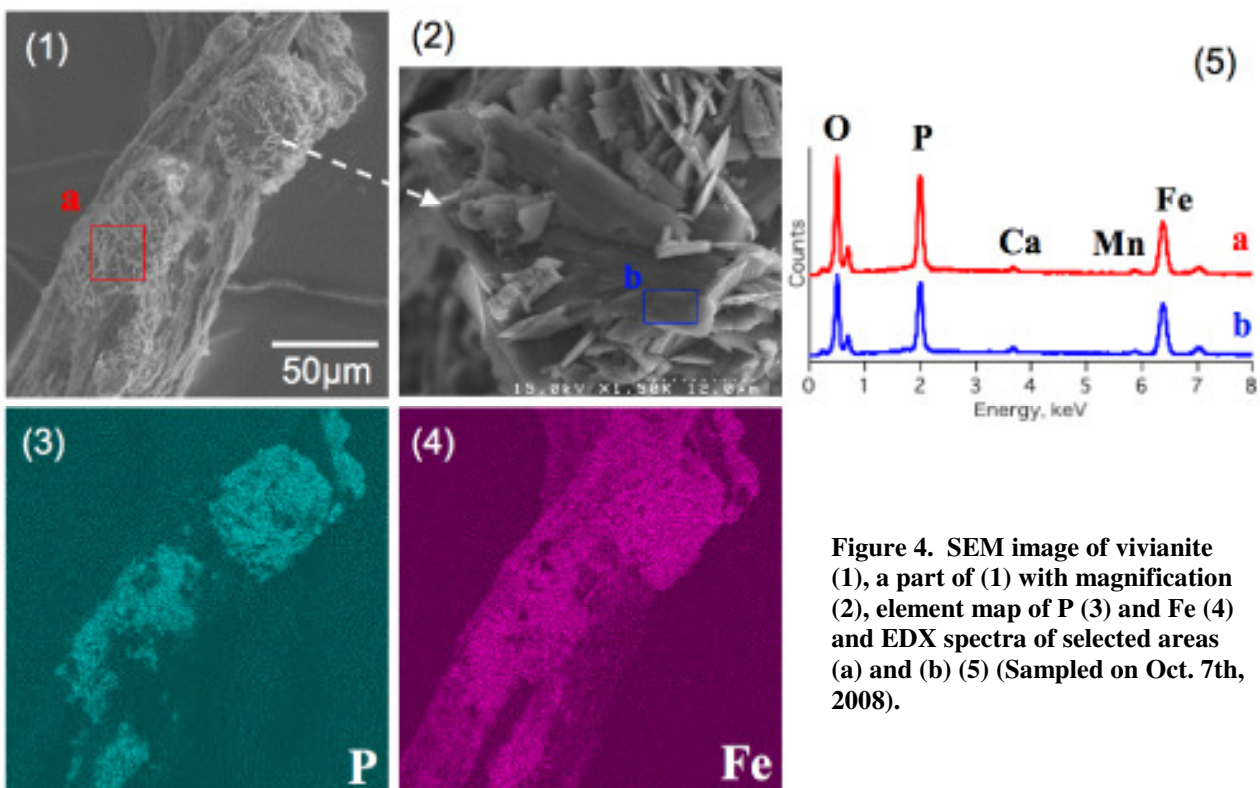


Figure 4. SEM image of vivianite (1), a part of (1) with magnification (2), element map of P (3) and Fe (4) and EDX spectra of selected areas (a) and (b) (5) (Sampled on Oct. 7th, 2008).

Acknowledgement

The authors thank Ms. Mari Saigo of the X-ray Diffraction Group Application Laboratory, Rigaku Corporation, Japan, for obtaining the XRD data of iron phosphate crystals formed on the rice root surface. The coated urea and the coated potassium sulfate were provided by Chisso Asahi Co., Ltd.

References

- Kimura M, Wada H Takai Y (1984) Studies on the rhizosphere of paddy rice. VIII. Precipitation of ferric hydroxide, manganese oxide, and ferrous sulfide around rice roots. *Japanese Journal of Soil Science and Plant Nutrition* **55**, 332-337.
- Nanzyo M, Kanno H, Obara S (2004) Effect of reducing conditions on P sorption of soils. *Soil Science and Plant Nutrition* **50**, 1028-1028.
- Nanzyo M, Yaginuma H, Sasaki K, Ito K, Aikawa Y, Kanno H, Takahashi T (2010) Identification of vivianite formed on the root of paddy rice grown in pots. *Soil Sci. Plant Nutr.* (in print)
- Nanzyo M, Yaginuma H, Takahashi T, Kanno H (2009) Iron materials on rice roots grown in pot. *Abstracts of the Annual Meeting, Japanese Society of Clay Science* **53**, 192-193.

Formation of soil geochemical anomalies by plant uptake of trace elements

Andrew W Rate^A and Yamin Ma^B

^ASchool of Earth and Environment, The University of Western Australia, Crawley, WA, Australia, Email Andrew.Rate@uwa.edu.au

^BContaminated Land Management, Parsons Brinckerhoff, West Perth, WA, Australia, Email YMa@pb.com.au

Abstract

Geochemical anomalies in surface soils may aid in exploration for buried mineral deposits. Most mechanisms proposed for the formation of surface soil geochemical anomalies are based on abiotic processes, but trace elements could also become locally enriched in soils above ore bodies as a result of uptake by plants and surface recycling. In this paper, we present a conceptual model of trace element biogeochemical cycling and use a simplified mass-balance calculation and calculations based in coupled first-order differential equations, both based on the conceptual model, to evaluate the possibility that soil anomalies form via plant uptake. The existence of soil geochemical anomalies depends on the balance between ecosystem net primary productivity and trace element losses through soil erosion and leaching. Mass-balance calculations predict that accumulation in soils should be favoured for more bioavailable elements. We suggest that soil geochemical anomalies are transient geological features, forming and dispersing as a result of the relative sizes of the accumulative and loss fluxes, and this is supported by our numerical model.

Key Words

Exploration; trace elements; geochemical anomalies; modelling; vegetation

Introduction

In landscapes where basement rocks are covered by deep chemically weathered and/or transported regolith, soils present a key sampling medium for geochemical exploration (Rose *et al.*, 1979). The mechanisms by which anomalous concentrations of trace elements accumulate in transported regolith have been discussed in some detail from an abiotic perspective (Hamilton, 1998; Kelley *et al.*, 2006). Biological mechanisms for enrichment of surface soils with trace elements have been proposed (Butt, 1992), but these processes have not been considered in detail despite the historical and current use of plants as geochemical sampling media for exploration (e.g., Dunn, 1986).

The distribution of elements with depth in soils can be controlled by plant uptake and surface recycling, and characteristic biogenic depth distributions involving surface enrichment relative to depletion at depth are well-known for major elements such as potassium (Brantley *et al.*, 2007; Jobbagy and Jackson, 2001). In semiarid to arid climate zones, in particular, plants root to considerable depth (Canadell *et al.*, 1996) meaning that uptake of trace element ions from buried mineralisation is feasible (Rate, 2002).

The addition of trace elements to surface soils by vegetation must be considered together with losses of the same elements by other mechanisms. A detailed analysis of the biogeochemical fluxes of trace elements in terrestrial environments (Ma and Rate, 2009) suggests that the controlling processes are net primary productivity, soil erosion and soil solute transport; the fluxes relevant to these processes depend on the concentrations of trace elements in the vegetation, surface soil and soil pore-water reservoirs. An additional issue is that although the reservoir of trace elements in an ore body may be very large, the fraction of this reservoir (or its weathered dispersion halo) which is physically accessible and bioavailable to vegetation may be much smaller, and potentially subject to depletion by plant uptake and redistribution. The net accumulation of any trace element in surface soils via vegetation therefore will depend on the relative sizes of addition and depletion processes (Ma and Rate, 2009). Dilution, as a result of mixing with barren material (bioturbation and sediment deposition), will also affect measurable soil accumulation of trace elements but these processes will not be considered in this paper. The relative sizes of trace element fluxes will not be constant with time; for example, the plant uptake flux is expected to be a first-order process dependent on the concentration in the bioavailable reservoir, and therefore will decrease relative to other fluxes should the bioavailable reservoir be depleted. Surface soil anomalies may therefore be transient features as shown in **Figure 5**.

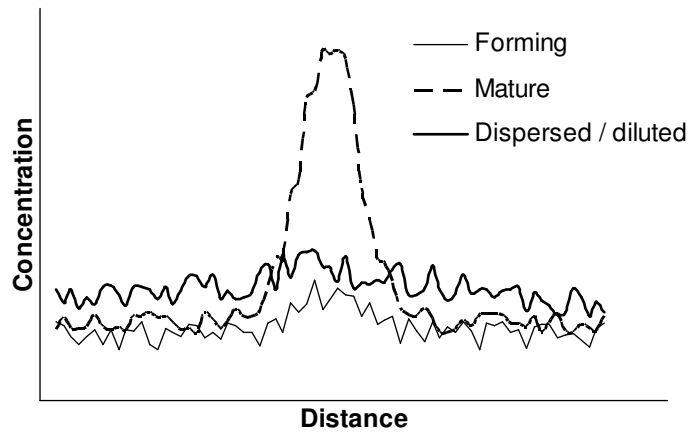


Figure 5. Hypothetical forms of transient soil anomalies showing forming, mature and dispersed phases (re-drawn from Ma and Rate, 2009).

Methods

Mass balance calculations

Estimation of net fluxes from buried mineralisation into surface soils were evaluated using a simple mass balance expression (Equation (1)):

$$A = c_p \cdot \text{NPP} - (c_s \cdot f_s + c_w \cdot f_w) \quad (1)$$

where A = net accumulation in the soil, c_p = trace element content of plants, NPP = net primary productivity, c_s = trace element content of soil, f_s = soil erosion flux, c_w = trace element content of soil solution, and f_w = vertical water flux; all concentrations (mass/mass), all fluxes (mass/area/time)

Differential equation calculations

All calculations were based on the assumption of first- or zero-order differential equations.

The vegetation reservoir dynamics were described by Equation (2):

$$\frac{dc_p}{dt} = ((k_1 \cdot c_R + k_2 \cdot c_s - k_3 \cdot c_p) \cdot c_p) - \frac{(k_1 \cdot c_R + k_2 \cdot c_s - k_3 \cdot c_p) \cdot (c_p)^2}{c_{p(\max)}} \quad (2)$$

where c_p is the concentration of the target element measured in vegetation, c_R is the concentration in the (deep) regolith source, c_s is the initial concentration of the soil reservoir, k_1 is the rate constant for deep element uptake, k_2 is the rate constant for shallow element uptake, and k_3 is the rate constant for return of the target element to the soil reservoir. For simplicity, we assumed that the net plant return, k_3 , reflects the sum of the total element uptake, such that whatever is gained by the plant reservoir is returned to the soil. The concentration in the vegetation reservoir was constrained to a maximum value ($c_{p(\max)}$), and so the equation therefore takes on a logistic form shown by the fractional term at the right hand side of Equation (2).

The surface soil reservoir dynamics were described by Equation (3):

$$\frac{dc_s}{dt} = k_3 \cdot c_p - k_2 \cdot c_s - k_4 \cdot c_s - k_5 \cdot c_s \quad (3)$$

where k_3 is the rate constant for plant return to soil (y^{-1}); k_4 is the rate constant for erosional loss from soil (y^{-1}), and k_5 is the rate constant for leaching (deep drainage) loss from soil (y^{-1}).

Rate constants for deep (regolith source) and shallow (surface recycling) plant uptake were defined by Equations (4) and:

$$k_1 = a \cdot (\text{NPP} \cdot c_R) \cdot \mathcal{E} \quad (4)$$

$$k_2 = (\text{NPP} \cdot c_s) \cdot \mathcal{E} \quad (5)$$

where a is the ratio between the rate constants for deep (k_1) and the shallow (k_2) element uptake flux (based on

work on phreatic/soil water use ratios and deep/shallow root biomass ratios, and taking values between 0.02-0.05) and \mathcal{E} is the vegetation standing biomass. Rate constants for other processes were selected to represent realistic rates based on literature values for litter fall, soil erosion, and leaching.

Results

Results of mass balances for a range of elements are summarised in **Figure 6**, which shows values of NPP/erosion for different elements which reduce net surface soil accumulation to zero, plotted at set values of erosion or NPP. In this instance, critical values of erosion rates are plotted in the bottom two curves at set NPP values of 5000 kg/ha/y (square symbols) and at 500 kg/ha/y (circular symbols). Values of NPP at which net element accumulation is zero are plotted in the top curve (triangular symbols), at a fixed erosion rate of 500 kg/ha/y. The plant: soil concentration ratio in **Figure 6** represents an index of bioavailability. For example, for the readily bioavailable trace element, Zn, for a large NPP value of 5000 kg/ha/yr, the critical erosion rate at which net loss will occur from the soil pool (1000 kg/ha/yr) is high relative to other less bioavailable elements. For net surface soil accumulation of less bioavailable Cr to occur, soil erosion must be negligible. The likelihood of forming a surface soil anomaly via vegetation uptake decreases in the order $Zn > Cu > Au > Ni > Cr > As > Co$ for Ni/Cr-poor (felsic) soil environments and in the order $Zn > Cu > Au > As > Co \approx Ni > Cr$ for Ni/Cr-rich (mafic-ultramafic) soil environments.

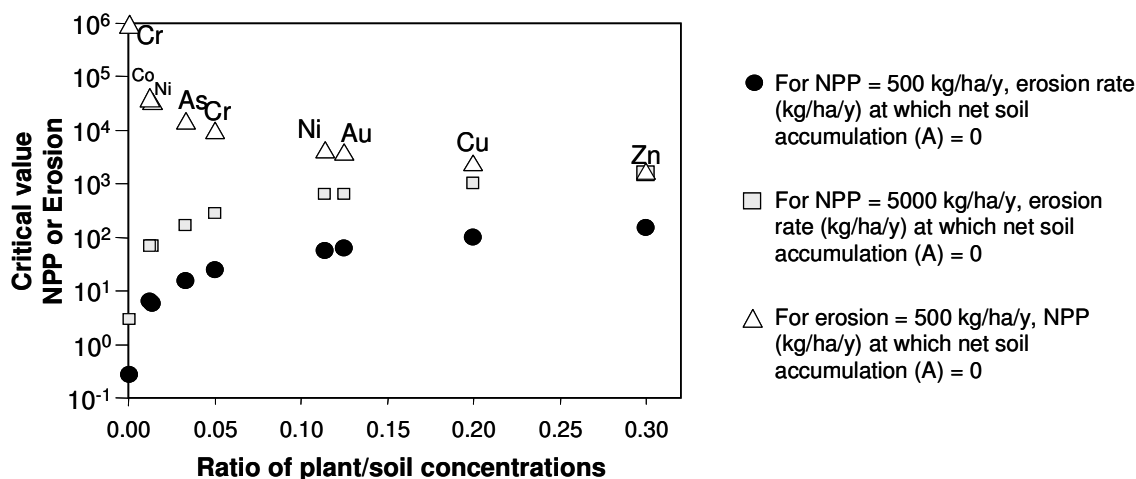


Figure 6. Critical values for soil anomaly formation plotted against realistic plant/soil concentration ratios for the elements considered (re-drawn from Ma and Rate, 2009).

The dynamics of surface soil accumulation described by differential equation calculations were highly dependent on the input parameters. For example, for gold, with NPP = 2000 kg/ha/y, the regolith concentration of Au needs to be at least 20 ppm for significant anomalism (soil response >5 times background) to occur, even in the absence of erosional losses. Such results do not always match field observations in landscapes with transported regolith, and do not agree with the mass balance presented above or with published studies (e.g., Lintern *et al.*, 1997), where sometimes significant accumulation in the soil and vegetation reservoirs occurs over <1 ppm of source Au.

In a simulation parameterised for copper (**Figure 7**), at a low erosion rate of 10 kg/ha/y, the loss from the soil produces a peak in accumulation and eventual decline in the soil reservoir. The vegetation concentration also shows a gradual decline from a maximum concentration (the constrained concentration) due to the feedback loop into the vegetation reservoir as the shallow uptake flux from the soil reduces (Figure 6 2 (a)). Increasing the erosion rate to 25 kg/ha/y produces a sharper peak in both the soil and vegetation reservoirs (Figure 6 2 (b)). Thus, the higher the erosional loss from soil, the more rapidly the biogeochemical anomaly declines. Anomalism measured by the soil response ratio for Cu is low, as Cu is an abundant element in the surface environment, and therefore the background is relatively high compared to the peak input from the deep source.

For some elements (e.g., Cu, As and Au; see **Figure 7** for Cu), some depletion in the surface soil occurs initially (through erosion and shallow uptake by the vegetation), since there is a lag time ($\sim 10^5$ y) for elements taken up from depth to accumulate in the surface soil (small deep uptake rates).

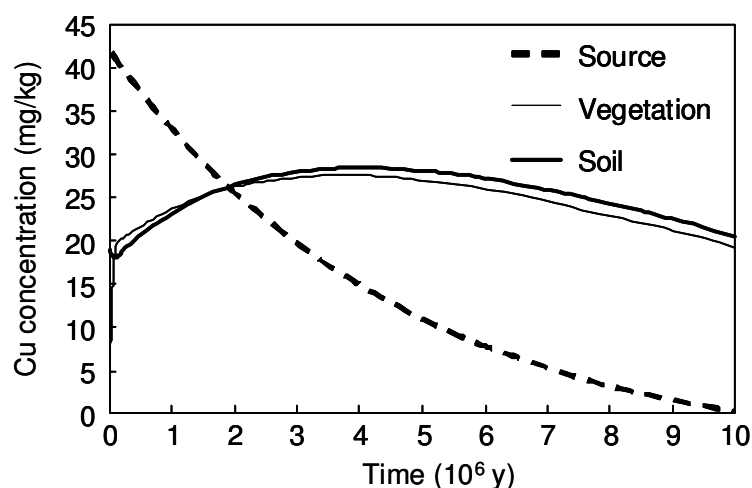


Figure 7. Calculated Cu concentrations in the source, vegetation and soil reservoirs. (Input parameters: biomass=15 t/ha; NPP=2000 kg/ha/y; erosion =10 kg/ha/y; initial soil concentration= 2.2 mg/kg; initial source Concentration[2] 42 (mg/kg); initial vegetation concentration 10 mg/kg. Rate constants: deep uptake (k_1) $3.0 \times 10^{-7} \text{ y}^{-1}$; shallow uptake (k_2) $2.9 \times 10^{-6} \text{ y}^{-1}$; plant return (k_3) $3.6 \times 10^{-7} \text{ y}^{-1}$; soil erosion (k_4) $1.3 \times 10^{-7} \text{ y}^{-1}$. Leaching was not considered in this calculation.)

Conclusion

Our analysis of the potential for vegetation uptake to generate surface soil geochemical anomalies for trace elements has shown that this mechanism is feasible and should be considered in exploration models. The extent of surface soil accumulation by plant uptake is strongly dependent on the balance between deep uptake and recycling, net primary productivity and soil erosion with a minor contribution from leaching. Our modelling also suggests that biogenic surface soil anomalies will be transient geological features.

References

- Brantley SL, Goldhaber MB, Ragnarsdottir KV (2007) Crossing disciplines and scales to understand the critical zone. *Elements* **3**, 307-314.
- Butt CRM (1992) Semiarid and arid terrains. In 'Regolith Exploration Geochemistry in Tropical and Subtropical Terrains'. (Eds CRM Butt, H Zeegers) pp. 295-391. (Elsevier: Amsterdam).
- Canadell J, Jackson RB, Ehleringer JR, Mooney HA, Sala OE, Schulze ED (1996) Maximum rooting depth of vegetation types at the global scale. *Oecologia* **108**, 583-595.
- Dunn CE (1986) Biogeochemistry as an aid to exploration for gold, platinum and palladium in the northern forests of Saskatchewan, Canada. *Journal of Geochemical Exploration* **25**, 21-40.
- Hamilton SM (1998) Electrochemical mass-transport in overburden: a new model to account for the formation of selective leach geochemical anomalies in glacial terrain. *Journal of Geochemical Exploration* **63**, 155-172.
- Jobbagy EG, Jackson RB (2001) The distribution of soil nutrients with depth: Global patterns and the imprint of plants. *Biogeochemistry* **53**, 51-77.
- Kelley DL, Kelley KD, Coker WB, Caughlin B, Doherty ME (2006) Beyond the obvious limits of ore deposits: The use of mineralogical, geochemical, and biological features for the remote detection of mineralization. *Economic Geology* **101**, 729-752.
- Lintern MJ, Butt CRM, Scott KM (1997) Gold in vegetation and soil - three case studies from the goldfields of southern Western Australia. *Journal of Geochemical Exploration* **58**, 1-14.
- Ma Y, Rate AW (2009) Formation of trace element biogeochemical anomalies in surface soils: the role of biota. *Geochemistry - Exploration, Environment, Analysis*, **9**, 353-367.
- Rate AW (2002) Formation of soil geochemical anomalies by biological processes. In 'FutureSoils: Managing Soil Resources to Ensure Access to Markets for Future Generations', Proceedings of the Australian Society of Soil Science National Conference, Perth, Western Australia, 2-6 December 2002, pp. 146-147. (ASSSI: Mornington, VIC, Australia).
- Rose A, Hawkes HE, Webb JS (1979) 'Geochemistry in Mineral Exploration.' (Academic Press: London).

Forms and characteristics of insoluble Fe-humic substances used for Fe nutrition of cucumber (*Cucumis sativus* L.)

C Colombo^A, G Palumbo^A, VM Sellitto^A, C Rizzardo^B, N Tomasi^B, R Pinton^B and S Cesco^B

^ADip. di Scienze Animali, Vegetali e dell'Ambiente, Università del Molise. Via De Sanctis, 86100 Campobasso (CB) Italy, Email colombo@unimol.it

^BDip. di Scienze Agrarie e Ambientali, Università di Udine, via delle Scienze 208, 33100 Udine (UD) Italy.

Abstract

In the present research, different forms and reactions of insoluble Fe-humic substance complexes (Fe-HS) and a soluble Fe-EDDHA complex, were compared. Five Fe-HS complexes were synthesized by neutralizing Fe(II) ions and humic substances using different synthesis conditions. Analysis was centred on chemical extraction developed to study iron distribution associated with humic substance (HS). Insoluble Fe-HS showed characteristics that differ from those of poorly ordered Fe oxides, indicating the presence of Fe hydrolytic products that were co-precipitated with HS in large molecules. Fe-HS and Fe-EDDHA were tested for their ability to cure chlorosis in Fe-deficient cucumber plants; the sources were used applying 0.03, 0.3 or 3 μmol of Fe in a nutrient solution (300 mL) buffered to pH 7.5. Results indicate that both Fe sources allowed plants to recover from chlorosis, with the effectiveness depending on the Fe source applied. Data here presented suggest that insoluble Fe-HS complexes could represent an environment and friendly tool for preventing Fe deficiency in crops and for correcting Fe availability in soils.

Key Words

Insoluble Fe-Humic complexes, poorly ordered iron oxides, Fe deficiency, chlorosis

Introduction

Iron deficiency is an important nutritional problem affecting many cultivated plant species, particularly in calcareous soils (Lucena 2003), causing relevant loss in quantity and quality of agricultural yields (Rombolà and Tagliavini 2006). This nutritional disorder, which triggers the yellowing of young leaves (chlorosis), is due to a low availability of iron, which depends on the low solubility of Fe crystalline oxides, particularly in alkaline conditions (Mengel 1994). On the other hand, it is well accepted that humified substance (HS) of soil organic matter plays an important role in the processes which control the levels of Fe in the soil solution via formation of Fe complexes (Stevenson 1994). For this reason, natural Fe-humates are of great interest in soil science and in surface chemistry. Humic substances are acidic, negatively charged polyelectrolytes of variable molecular weight. It has been largely demonstrated that HS of low and high molecular weight can strongly react with the surfaces of Fe oxides, reducing their crystallization process and the mineralogy of the iron phase (Schnitzer 1986). In addition, HS can enhance Fe availability for plants by formation of soluble complexes and by increasing Fe diffusion to roots (Cesco *et al.* 2000). It has been demonstrated that iron complexed to water soluble humic substances can be used as an Fe source by Fe-deficient plants grown in hydroponics; in dicots, this process occurs via reduction-based mechanism at the plasma-membrane level of Fe(III)-HS (Pinton *et al.* 1999), while *gramineae* use complexed Fe via ligand exchange between HS and phytosiderophores (Cesco *et al.* 2002). The objective of this research was to study the forms and the characteristics of insoluble Fe-HS complexes and to evaluate their efficacy as an Fe source for a cultivated plant species for preventing Fe deficiency in crops and for correcting Fe availability in soils.

Methods

Preparation and characterization of Fe complexes

In this research we used two different Fe sources: 1) five Fe-insoluble humic substance complexes (Fe-HS); 2) one soluble Fe-EDDHA complex (Fe-EDDHA). Fe-EDDHA was prepared following the setting of Cesco *et al.* 2000. Fe-HS samples were prepared mixing FeSO_4 with humic substances using a commercial liquid mixture of humic and fulvic acids (Leonardite extracted CIFOUMIC, CIFO). Five types of complexes were synthesized, modifying the order and the amount of Fe added to the humic substances (3-6 mmol Fe g /HS) and the OH/Fe molar ratios. A, B and E were prepared by adding 3 mmol of FeSO_4 acid solution, C and D with 3 mmol of FeSO_4 , respectively, to the alkaline solutions of humic substances; for sample A and C. The pH was previously adjusted to 5.0, after 2 hours the suspensions were stabilized and 0.5 M NaOH solution was gradually added to reach pH 7.0; the pH of sample B and D was directly neutralized with NaOH up to pH 7.0. Sample E was

obtained as for sample A but inverting the sequential order of adding Fe and HS. Part of the Fe-HS complexes were freeze dried for chemical analysis, the rest was stored as a concentrated stock solution (1.6 g/L TOC), dialyzed and then purified for plant experiments. Dynamic light scattering (DLS) experiments were conducted with diluted sample suspensions to determine their relative size as a function of reflective properties. The light scattering setup consisted of a Zetasizer nano ZS laser delivering (www.malvern.com/zetasizernano, USA).

Selective chemical extraction

Four selective dissolutions were carried out on the Fe-HS complexes depending on the different forms of Fe: 1) Fe total content (Fe_t) in the Fe-HS complexes was determined following acid digestion with HCl and HNO_3 ; 2) DTPA-extractable (Diethylene-Triamine-Penta-Acetate) Fe (Fe_{DTPA}) was determined extracting with DTPA + 0.01 mol/L $CaCl_2$ + 0.01 mol/L TEA, pH 7.3 for 2 h; 3) the Fe short-range ordered phase (Fe_o) was extracted with ammonium oxalate ($(NH_4)_2C_2O_4$) 0.2 M, pH 3 for 4 h in the dark; 4) Fe exchangeable and complexed to organic matter (Fe_p) was extracted with Na-pyrophosphate 0.1 M, pH 10.0 for 16 h. The extractions were carried out at room temperature in 100 ml polypropylene bottles, using 1 g of air-dried sample. After each chemical treatment, the extracts were separated by centrifugation and the Fe in the supernatant was determined by ICP-AES. Although the extractions used are not specific for a given Fe pool and for Fe availability, some of them are reasonably specific as nutrition tests for most soils. Following commonly used interpretations, Fe pools were grouped as follows, ordered by decreasing stability and affinity with humic substances: Fe_o/Fe_t = total Fe in poorly ordered Fe oxides; Fe_p/Fe_t = Fe exchangeable and complexed to organic matter; Fe_{DTPA}/Fe_t = Fe bonded to organic matter.

Plant material and growth conditions

To evaluate the contribution of these Fe sources in the micronutrient acquisition by plants, the Fe-HS sample A was used according the suitable chemical properties of the complexes (i.e. better solubility, high Fe coprecipitated). For this propose, cucumber (*Cucumis sativus* L.) plants had been grown for 15 days in hydroponics with pH buffered at 7.5 and without any supplies of exogenous Fe sources. The plants had then been grown for a further 11 days, divided into the following treatments: 1) not supply with any exogenous Fe sources (-Fe control); 2) supplied with sample A that was characterized by Fe complexed to poorly soluble, high molecular-weight-humic substances (Fe-HS); 3) supplied with a soluble synthetic Fe chelate (Fe-EDDHA), widely used in agriculture to cure and prevent Fe chlorosis. In a 300 mL nutrient solution, 0.03, 0.3 or 3 μ mol of each Fe sources was supplied; the soluble Fe fraction had been measured via ICP-AES after 0.2- μ m filtration of the solutions. SPAD-index values of leaves had been measured along the treatments. At the end of the experiment, pictures of root and leaf tissues were taken.

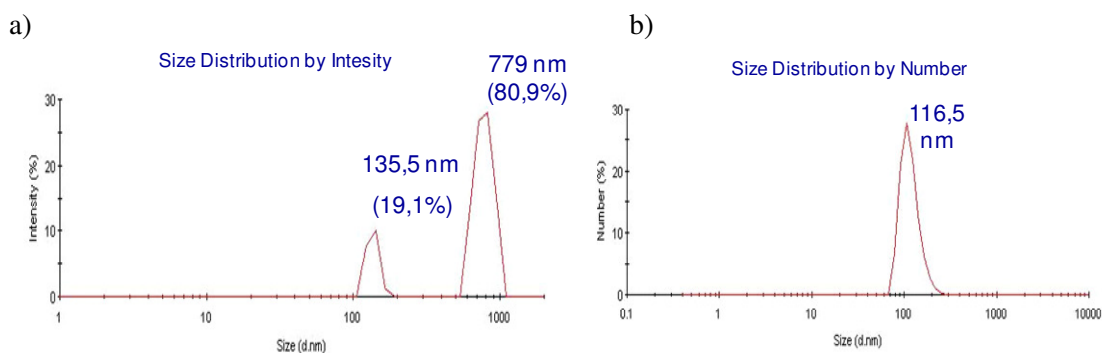
Results

The relationships between the Fe pools released with different chemical extractions can provide information about the sources from which Fe is extracted. The chemical extractions of the insoluble Fe-HS complexes are summarized in Table 1. Acid oxalate is commonly used to estimate short-range-order Fe hydroxides and oxihydroxides and Fe bonded to organic matter. The ratio Fe_o/Fe_t and Fe_p/Fe_t so is a measure of the relative distribution of Fe between the mineral and the organic phases of the organic complexes. Chemical extractions show that Fe_o and Fe_p values were very high in all samples, the Fe pool is dominated by short-range order Fe phases strongly associated with organic complexes. All samples showed $Fe_o/Fe_t > 0.9$ while the ratio was reduced ($Fe_p/Fe_t = 0.57$ and 0.77) in the samples obtained with 6 mmol Fe g /HS. In spite of the dominance of the mineral Fe reactive pool in most of the studied complexes, the pool of reactive Fe is large in all samples, as indicated by the fact that pyrophosphate extracts an amount of Fe_p very similar to Fe_o in particular in the samples A, B and E. The amounts extracted by DTPA were smaller than those obtained by using the oxalate and pyrophosphate methods and with very comparable values in the five samples. In particular the chemical data show that A, B and E samples contained similar Fe forms (poorly ordered, organic complexes, exchangeable and soluble), while sample C and D, obtained with 6 mmol Fe g /HS, have an excess of insoluble iron that could indicate a low degree of iron availability. The low amount of DTPA extractable Fe may be ascribed to Fe exchange between HS and DTPA. In soil available Fe was normally high correlate with Fe extracted by oxalate and citrate-ascorbate-extractable (De Santiago and Delgado 2006).

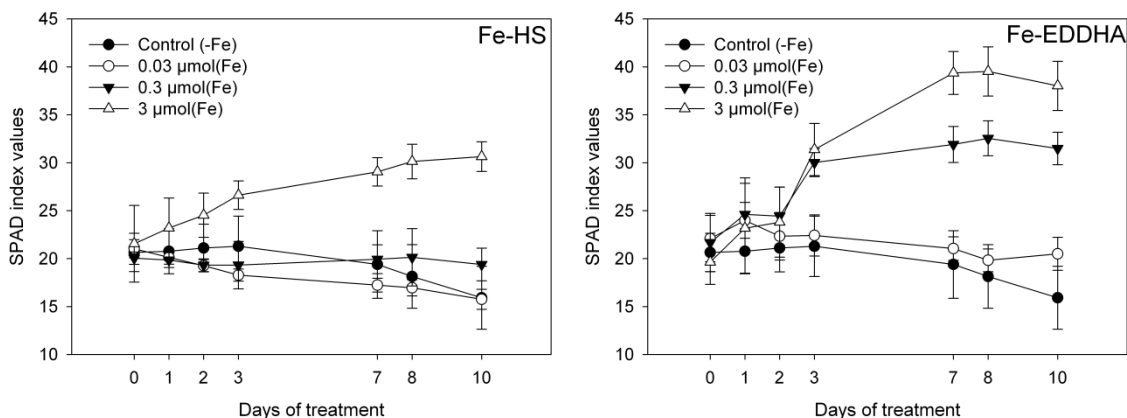
Table 1. Fe forms according to the chemical extractions of Fe-HS samples.

	Fe _t	Fe _o	Fe _p	FeDTPA	Fe _o /Fe _t	Fe _p /Fe _t	FeDTPA/Fe _t	FeDTPA/Fe _p
	(-----g/kg-----)							
A	84.3	84.0	85.5	6.3	1.00	1.01	0.07	0.07
B	90.3	83.6	84.0	7.2	0.93	0.93	0.08	0.09
C	135.4	131.6	77.2	7.6	0.97	0.57	0.06	0.10
D	155.8	143.8	119.3	6.3	0.92	0.77	0.04	0.05
E	97.5	89.1	92.6	8.6	0.91	0.95	0.09	0.09

The Fe-HS complexes observed with the Dynamic light scattering (DLS) contain particles with a higher molecular mass than the ones used by Pinton *et al.* (1999), but in the range of that used by de Santiago and Delgado (2007). Figure 1a shows the size distribution obtained in sample A. The size distribution of Fe-HS complex A showed the dominant presence of large particles (81%) in the micron size range of 779 nm, with an additional 19% of 135 nm particles. Ferrihydrite showed instead a monomodal size distribution with small particles of 116 nm (Figure 1b).

**Figure 1. Intensity size distribution obtained with DLS of Fe-HS sample a) and Ferrihydrite b).**

As expected, the Fe-HS complex sample A exhibited a poor solubility in the conditions used in this work (pH 7.5); in the 0.03- μmol Fe treatments, the amount of soluble-Fe fraction in the nutrient solution from Fe-HS complex was about 3 times lower than that measured when equal amount of Fe-EDDHA was applied, while in the case of the 3- μmol -Fe treatments, the difference increased to 20 times (data not shown). On the other hand, when used for curing Fe chlorosis on cucumber plants, both Fe sources were able to alleviate Fe-deficiency symptoms (SPAD-index values; Figure 2) and to allow a shoot root and higher biomass accumulation (Figure 3) in cucumber plants; however the effectiveness, particularly at a low concentration, was dependent on the Fe source used (FeEDDHA>Fe-HS). Results of the present work show that Fe coprecipitated with insoluble humic substances can be absorbed by roots and translocated to the shoot of cucumber plants.

**Figure 2. SPAD-index values of Fe-deficient cucumber plants treated for 11 days with 0.03, 0.3 or 3 μmol Fe of Fe-HS sample A or Fe-EDDHA.**

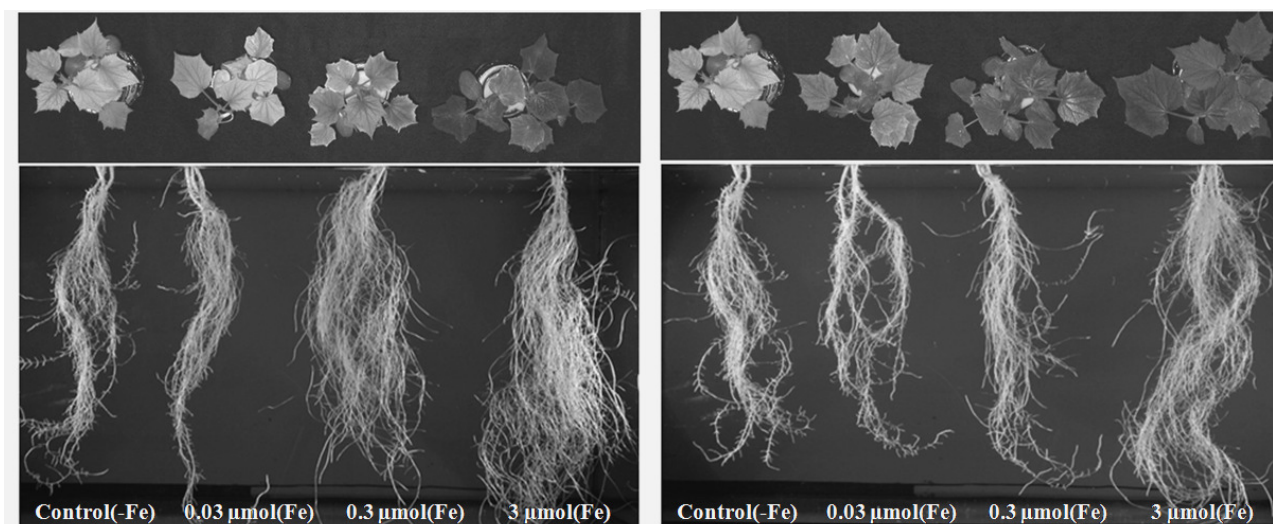


Figure 3. Fe-deficient-cucumber plants treated for 11 days with 0 (Control, -Fe), 0.03, 0.3 or 3 μmol Fe of Fe-HS sample A (left) or Fe-EDDHA (right).

Conclusions

In this preliminary study, analysis centred on chemical extraction procedures was applied to study iron distribution associated with humic substance (HS). The content in poorly crystalline Fe oxides (ferrihydrite), estimated by extraction with oxalate (Fe_o) showed similar values compared with Fe exchangeable and complexed to organic matter (Fe_p) in the sample with 3 mmol Fe g /HS. Dynamic light scattering (DLS) observation indicated that the Fe-HS showed characteristics that differed from those of poorly ordered Fe oxides (ferrihydrite), indicating the presence of large molecules formed by hydrolytic products of Fe co-precipitated with humic substances. Fe-HS seemed to contain multiple forms of Fe, with different behavior when treated with various chemical extractants. Selected Fe-HS were also used by cucumber plants as a Fe source, although the effectiveness of Fe-HS in curing Fe chlorosis at low concentration was lower than that of a synthetic Fe source, which is widely used in agriculture and were particularly expensive and not eco-compatible. Insoluble Fe-HS seems to play a significant role in the Fe nutrition and is consistent with the observation that it can be a good source of Fe for plants. In conclusion, all the data here presented indicate that these organo-mineral complexes could represent an environmentally friendly tool for preventing Fe deficiency in crops and for correcting Fe availability in soils.

Acknowledgments

Research was supported by grants from the Italian M.U.R.S.T, P.R.I.N. programs.

References

- Cesco S, Römheld V, Varanini Z, Pinton R (2000) Solubilization of iron by water-extractable humic substances. *J Plant Nutr Soil Sci* **163**, 285–290
- Lucena JJ (2003) Fe chelates for remediation of Fe chlorosis in Strategy I plants. *J Plant Nutr* **26**, 1969–1984
- Mengel K (1994) Iron availability in plants tissues-iron chlorosis on calcareous soils. *Plant Soil* **165**, 275–283
- Pinton R, Cesco S, Santi S, Agnolon F, Varanini Z (1999) Water extractable humic substances enhance iron deficiency responses by Fe-deficient cucumber plants. *Plant Soil* **210**, 145–157
- Rombolà AD, Tagliavini M (2006) Iron nutrition of fruit tree crops. In 'Iron Nutrition in Plants and Rhizospheric Microorganisms'. (Eds L Barton and J Abadia) pp. 61-83. (Springer Verlag: Berlin, Germany).
- de Santiago A, Delgado A (2007) Effects of humic substances on iron nutrition of lupin. *Biol Fertil Soils* **43**, 829–836
- Schnitzer M (1986) Binding of Humic Substances by Soil Mineral Colloids. In 'Interactions of Soil Minerals with Natural Organics and Microbes' (Eds PM Huang, M Schnitzer). pp. 77-101. (Soil Science Society of America, Special Publication No. 17, Madison).
- Stevenson FJ (1994) 'Humus Chemistry: Genesis, Composition, Reaction'. (John Wiley & Sons: New York).

From atom to pedon: linking processes to phenomena and function

Kai U. Totsche^A

^ALS Hydrogeologie, Institut für Geowissenschaften, Friedrich-Schiller Universität Jena, Germany, Email kai.totsche@uni-jena.de

Abstract

The fundamental fact that the processes in soil cannot be observed directly demands inverse methods which explain the phenomena on the continuum scale with processes at the local scale in a mechanistic way. In this paper, an approach will be presented which links retardation, a continuum scale phenomena related to reactive transport, to the governing sorption processes. This approach builds upon effective models considering both the role of soil structure and the physicochemical properties of the interface. A multi-domain sorption model has been developed accordingly and will be used to predict sorption and retardation of polycyclic aromatic hydrocarbons at the local and the pedon scale, respectively. The parameters and coefficient functions can be directly parameterized from local scale spectroscopic and spectromicroscopic information. An important additional back-up on the “atom scale” is provided by molecular modelling techniques which can be used to confirm the validity of the measured properties and interaction mechanisms.

Key Words

Biogeochemical interfaces, sorption, effective model, spectro-microscopy, molecular modelling

Introduction

Soils are basis to key ecosystem functions including plant productivity, biodiversity and water quality. The processes in soils control fate and transport of contaminants and nutrients in the critical zone. The three-dimensional structure of soil, its “architecture”, is a dynamic, frequently hierarchically organized system of aggregates formed out of the biogenic and lithogenic parent materials by diverse biotic and abiotic structuring processes. This architecture defines a three-dimensional system of interconnected voids and pores ranging from the (nano)pores of the primary particles to the macropores and fractures of aggregated soils. As such, it provides a large, complex structured and physicochemically heterogeneous biogeochemical interface (BGI). The properties and processes at BGI control interactions, bioavailability, the stability of the pore structure as well as the spatial distribution and movement of liquid and gaseous phases (Totsche *et al.* 2010). Organic compounds of different origin may enter soil as dissolved species or may be attached to colloidal or suspended particles (Totsche *et al.* 2007). Once in soil, they might be transported to deeper soil horizons, to the vadose zone or even to the aquifer. The major fraction, however, is dispersed and retained by interactions with BGI. Due to the opaque nature of soil, direct observation of the processes and properties which control the fate of organic compounds is impossible. We are thus constrained to obtain the information on the governing mechanisms by the rigorous analysis of the related phenomena employing inverse techniques. Organic compound sorption to BGI, e.g., results in retardation, a phenomenon that can be observed on the continuum scale. Retardation can be quantified by the comparison of the mean transport velocity of a solute to the mean pore water velocity using an adequate continuum pedon scale mathematical formulation of reactive transport. Exemplified by the process of sorption and the phenomena of retardation, this paper presents an approach which links phenomena at the continuum or pedon scale to information on the local or atomic scale obtained by spectromicroscopic techniques.

Methods

Sorbates

As model solutes, we selected polycyclic aromatic hydrocarbons (PAHs) of different polarity: Phenanthrene, anthracene, pyrene and benzo(a)pyrene. For standard solutions, crystalline PAHs (Promochem, Germany) were weighed and dissolved in methanol (Suprapur; Merck, Germany). Stock solutions for the batch sorption experiments were diluted from the standard solutions.

Sorbents

For the sorption studies, different soil minerals and subsurface soil materials were used. Pure Ca-exchanged montmorillonite (Ca-MM) from Wyoming (Source Clay Minerals Repository, University of Missouri) with particle sizes < 2 µm and specific surface area of 33.6 m² g⁻¹ was used. The total concentration of iron including that which is in the lattice and on particle surfaces was determined by means of Mössbauer spectroscopy and

comprised 29 mg g⁻¹. Approximately 1 mg g⁻¹ of iron was found to be on the particle surfaces. Goethite-coated quartz samples with Fe concentrations of 0.6 and 1.3 mg g⁻¹ were prepared via mixing of goethite dissolved in a NaNO₃ solution with the quartz sand.

Batch sorption and column transport experiments

The sorption of PAH to the individual sorbents was studied at different time steps of increasing contact time 4, 8, 16, 24, 48, 72, 96, and 120 hours, respectively, using batch sorption experiments. The batch experiments were conducted with a sorbent:solution ratio of 1:5, under dark conditions at a temperature of 20 °C and by horizontally shaking of the samples 15 min per hour to reduce abrasion. After equilibration, the liquid and solid phases were immediately separated by centrifugation and decantation of the supernatant. Residues of the liquid phase in the solid phase were determined by weighing. Both the PAH concentrations in the separated liquid and in the separated solid phase were analyzed by GC-MS. Transport experiments were run with a soil column system using the same soil materials as for the batch sorption experiments

Numerical analysis and identification of the parameters

To inversely identify the parameter values of the effective sorption model, a constrained nonlinear minimization algorithm, implemented within Mathcad 14.0 (Mathsoft inc., USA), was applied to the batch sorption data. The objective function subject to minimization is based on the sum of the squared Euclidian distances of the observed and the predicted values (SSQ). Beside maximum error and root mean square error (RMSE) the precision of the particular fits was estimated by the coefficient of determination (CD) and the modeling efficiency (MEF). In addition, the performance of the model was evaluated by comparison to the linear partitioning model, the nonlinear Freundlich-model and the Pore-filling-partitioning model (Allen-King *et al.* 2002.) within a model discrimination exercise. Model performance was based on a newly developed general reference criteria which is based on the weighted differences of the sum of the squared Euclidian distances of the paired modeled and observed data points. Forward simulations of the breakthrough behavior using such parameterized effective model were done with the GNU C++ computer code CARRY (Totsche *et al.* 1997; Totsche & Kögel-Knabner 2004).

Results

The effective sorption model

For the derivation, it is presumed that the soil is composed of three domains, i.e. the Langmuir domain (I), the Polanyi domain (II) and the partitioning domain (III). In the Langmuir domain, the solutes interact with surface sorption sites. Within the Polanyi-domain, sorption is controlled by interactions of the solutes with the micropores of the sorbent. In the partitioning domain, the interactions are controlled by equilibration in between two bulk phases. The sorption sites of domain I are located on the surface of the aggregates and on the walls of the pores distinctly larger than 20 Å. Solute interactions with the surface in terms of a sorption process holds for pore surfaces with apertures larger than 20Å. At the surface, the adsorbates may form two-dimensional layers or a two-dimensional interfacial solution phase. Such a sorption process can be formulated in terms of a mass-action law and results therefore in Langmuir-type/Lattice Gas sorption processes. The interactions of solutes with surfaces within pores and voids smaller than 20Å (domain II) is assumed to be controlled by a different mechanism. At this small dimensions (only a few adsorbate diameters), the adsorbate molecule is affected by the overlapping potential fields of the walls of the voids and micropores. Thus, the attractive or repulsive interactions between the adsorbate and the sorbent wall will be much larger than the interactions between the adsorbent and plane or weakly curved sorbent surfaces. The sorption is thus like filling process powered by the overlapping potential fields of the sorbent walls. For microporous solids, e.g. zeolithes, solid gels and coals, Polanyi's potential is used and adapted for liquid-solid systems. The overall mass adsorbed is then calculated by integrating the three domains.

Batch sorption isotherms

Figure 1 shows the sorption of pyrene to the different sorbents (data of the sorption to the minerals from Müller *et al.* 2007). The sorption kinetics of PAHs to the mineral sorbents was fast and obviously completed within 4 hours of contact time. This fairly rapid sorption was found for the soil material (Spodosol B-horizon), also.

In the absence of organic matter the mineral surfaces sorbed considerable amounts of PAHs, except for phenanthrene and anthracene sorption to quartz at low liquid phase concentrations (data not shown). Under these conditions sorption to quartz is limited to HOCs with a log K_{OW} value larger than 4.6.

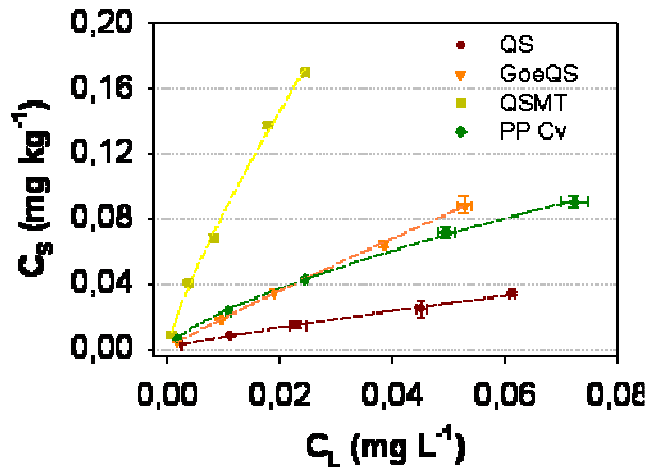


Figure 1. Sorption of pyrene to quartz (QS), goethite-coated quartz-(GoeMS), a mixture of quartz with montmorillonite (QS/MT) and a Spodol B horizon. Symbols: measured data. Broken lines: results of the parameterization using the effective model.

The sorption isotherms of pyrene to all three minerals are convex-shaped, indicating a saturation of the solid phase at increasing aqueous phase concentrations. Nonlinear convex-shaped isotherms are well known in literature for the sorption of HOCs to soil or sediment material (Weber *et al.* 1983; Huang *et al.* 1998). The curvatures increase in the order goethite-coated quartz < quartz < quartz–montmorillonite. The pyrene isotherms contrast with the sorption results of phenanthrene (data not shown), indicating a sorbent saturation already attained at lower liquid phase concentrations for the more hydrophobic PAH.

The sorption of pyrene to the spodosol B-horizons compares quite well with the sorption to the goethite-coated quartz material. This indeed indicates that the dominant sorbents in this soil material are the pedogenic iron-oxides. This points to the important role of iron-oxides as sorbents for hydrophobic organic substances in natural soil, also

Inverse modeling of the sorption data

Figure 2 shows the results of the inverse modelling of the batch sorption data exemplified for the sorption of pyrene to the spodosol B-material.

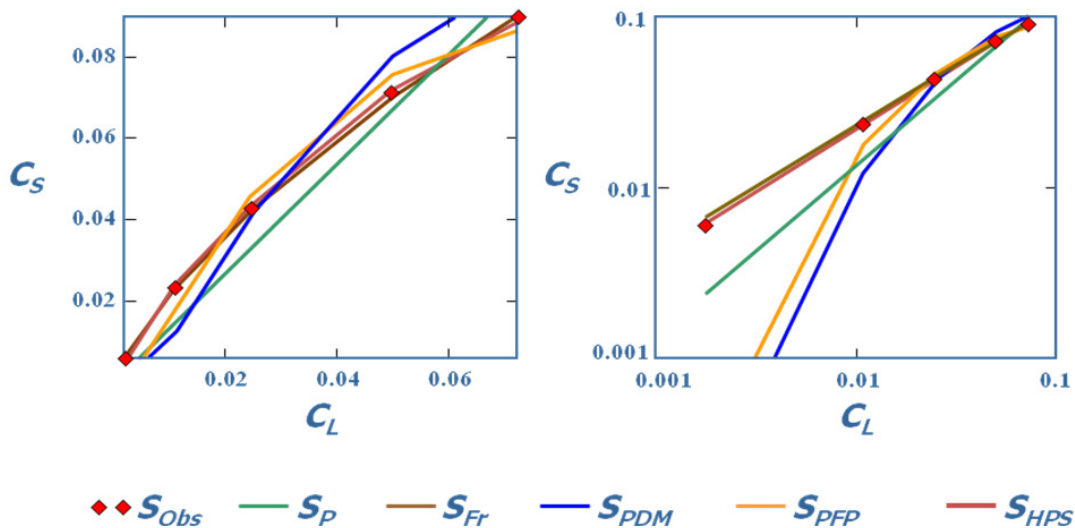


Figure 2. Results of the discrimination of the different sorption models. Symbols: Measured data of pyrene sorption to the spodosol B material. S_P : Partitioning-Model; S_{Fr} : Freundlich-Model; S_{PDM} : Pore-filling model; S_{PFP} : Pore-filling partitioning; S_{HPS} : effective sorption model.

Among the different isotherm models the sorption isotherms of pyrene were best described by the effective continuum or pedon scale model and, equally good, by the Freundlich isotherm model except for phenanthrene sorption to quartz sand (linear sorption isotherm, data not shown). High fit qualities were also obtained for the

multi-site dual-mode isotherm. The discrimination within the isotherm models highlighted the advantages of the model efficacy approach. Unfortunately, the sorption experiments including microporous sorbents were not finished at time of preparation of this paper. Thus, the superiority of the developed effective sorption model still awaits proof.

Back-up information on the local scale can be obtained from spectroscopic and spectromicroscopic observations and/or from theoretical considerations. Results employing computational chemistry (Tunega *et al.* 2009) corroborate our experimental findings that iron-oxides indeed can serve as specific sorbents for HOC. At present, we apply atomic force microscopy (AFM) to characterize sorbent properties and interactions. AFM is an emerging yet powerful tool to study surfaces and their properties such as morphology, roughness, and specific basal and edge areas (see also presentation of Macht *et al.*). Using more advanced modes of operation of the AFM, surface properties such as surface potential, elasticity and mass as well as interaction forces and energies can be measured. Such information is used to back up theoretical studies (e.g. molecular modeling), but also to link such information to continuum or pedon scale phenomena in a mechanistic way.

Conclusion

It is meanwhile accepted that the phenomena at the pedon scale are controlled by processes and structural properties operative at much smaller spatial scales (atomic, molecular). Yet, we still lack a conceptual framework which allows linking processes at the local scale to the phenomena at the pedon scale in a mechanistic way, thereby considering the interplay and interdependencies of physical, chemical and biological processes at biogeochemical interfaces (Totsche *et al.* 2010). A successful approach can build on the development of process models on the continuum scale to replace the widely used empirical approaches. These “physically” based models must acknowledge the governing role of soil structure, the properties of which are parameterized in effective ways: The parameters and coefficient functions used with the model must be either physically based or derived by a rigorous scaling approach from “first principles”. Additional back-up information on the “atom scale” is provided by molecular modelling techniques which can be used to confirm the validity of the measured properties and interaction mechanisms.

References

- Allen-King RM, Grathwohl P, Ball WP (2002) New modeling paradigms for the sorption of hydrophobic organic chemicals to heterogeneous carbonaceous matter in soils, sediments, and rocks. *Advances in Water Research* **25**, 985-1016.
- Huang W, Yu H, Weber WJ Jr (1998) Hysteresis in the sorption and desorption of hydrophobic organic contaminants by soils and sediments. 1. A comparative analysis of experimental protocols. *Journal of Contaminant Hydrology* **31**, 129-148.
- Muller S, Totsche KU, Kogel-Knabner I (2007) Sorption of polycyclic aromatic hydrocarbons to mineral surfaces. *European Journal of Soil Science* **58**, 918-931.
- Totsche KU, Kogel-Knabner I (2004) Mobile organic sorbent affected contaminant transport in soil: Numerical case studies for enhanced and reduced mobility. *Vadose Zone Journal* **3**, 352-367.
- Totsche KU, Rennert T, Gerzabek MH, Kogel-Knabner I, Smalla K, Spiteller M, Vogel HJ (2010) Biogeochemical interfaces in soil: The interdisciplinary challenge for soil science. *J. Plant Nutr. Soil Sci.* **173**, 88-90.
- Tunega D, Gerzabek MH, Haberhauer G, Totsche KU, Lischka H (2009) Model study on sorption of polycyclic aromatic hydrocarbons to goethite. *Journal of Colloid and Interface Science* **330**, 244-249.

From Gene to Model – Linking Microorganisms to Microhabitat Functions

Ellen Kandeler^{A*}, Christian Poll^A, Holger Pagel^B, Fabrice Martin-Laurent^C, Marion Devers^C, Joachim Ingwersen^B, Thilo Streck^B

^A Institute of Soil Science and Land Evaluation, Soil Biology Section, University of Hohenheim, D 70593 Stuttgart, Germany, Email kandeler@uni-hohenheim.de

^B Institute of Soil Science and Land Evaluation, Biogeophysic Section, University of Hohenheim, D 70593 Stuttgart, Germany, Email tstreck@uni-hohenheim.de

^C Laboratory of Soil and Environmental Microbiology, INRA-University of Burgundy, France, Email Fabrice.Martin@dijon.inra.fr

Abstract

A microcosm approach was designed to link the abundances of bacteria and fungi to microhabitat functions of soil microbiota. In microcosms, we used MCPA (2-methyl-4-chlorophenoxyacetic acid) as a model organic substance due to its well-known degradation pathways (*tfdA* genes) and due to the availability of primers targeting the *tfdA* gene encoding the enzyme responsible for the first step in degradation of this compound. We used maize litter to create a well-defined soil-litter interface (detritosphere). We studied microbial degradation, microbial abundance of degraders, adsorption, desorption and transport of MCPA along a gradient of decreasing availability of dissolved organic matter. Isotopic data (¹⁴CO₂, ¹⁴C_{mic}, ¹⁴C-DOC, ¹⁴C_{org}, ¹⁴C-MCPA, ¹⁴C in the leachate) and molecular data (*tfdA*, 16S rDNA and 18S rDNA sequence copy numbers) were used as input variables for a mechanistic model. We showed that the quantification of the abundance of genes encoding specific functions of soil microbial communities helps to clarify the regulation of degradation of complex organic compounds at a biogeochemical interface.

Key Words

MCPA, functional genes, *tfdA*, microhabitat, detritosphere, biogeochemical interface

Introduction

The importance of close interdisciplinary approaches in soil science was recognized by the German Funding Agency (DFG). DFG is currently funding a special research programme SPP 1315 "Biogeochemical Interfaces in Soil" stimulating studies on biogeochemical interfaces in soils (http://www.spp1315.uni-jena.de/General_Information.html). In the frame of this programme, several organic compounds (e.g. MCPA, phenanthrene and hexadecan) are used as model substances to gain a mechanistic understanding of the interplay and interdependencies of the physical, chemical and biological processes operative at biogeochemical interfaces. K.U. Totsche, the coordinator of the programme, stated that "The grand challenges are to identify the factors controlling the architecture of biogeochemical interfaces, to link the processes operative at the molecular and organism scale to the phenomena active at the aggregate scale in a mechanistic way, and to explain the medium- to long-term behaviour of organic chemicals in soil within a general mechanistic framework."

We have chosen the widely-used phenoxy acid herbicide MCPA as well as the polycyclic aromatic hydrocarbon (PAH) phenanthrene for our project because these compounds show similar degradation rates, but different sorption properties. Our project aims to quantify the relative abundances of bacterial and fungal communities involved in the degradation of MCPA and phenanthrene in the detritosphere and to link these quantities to biogeophysical processes ruling the dynamics of degradation. During the first phase of our project we focused on degradation of MCPA. Therefore, metabolism and co-metabolism of MCPA by a diverse microbial community were studied in the detritosphere along decreasing availability of low molecular weight organic substances within a distance of 10 mm to the litter. We hypothesized that dissolved organic carbon (DOC) from the litter, which may be considered a natural analog of MCPA, might enhance MCPA biodegradation by serving either as substrate for catabolic enzymes and/or as cooxidized substrate during co-metabolism.

Material and Methods

The experimental design includes the following treatments: (1) MCPA, no litter, (2) MCPA, litter, (3) control, no litter, (4) control, litter. Each treatment was replicated nine times (three cores were pooled to yield nine gram of sample per layer, an amount which is needed to cover all analyses). The soil was homogenized after thawing, amended with MCPA solution (50 mg kg⁻¹ soil) to a volumetric water content of 35.2% corresponding to a matric potential of -63 hPa (pF 1.8), filled into cylinders (PVC, diameter 5.6 cm, height 3 cm) and compacted to a bulk density of 1.2 g cm⁻³. The soil cores were subsequently placed on ceramic plates and a matric potential of -63 hPa was applied to ensure approximately homogeneous conditions (Figure 1). The day before the start of

the incubation, 0.75 g of maize litter were weighed for each cylinder and rewetted with 2 ml of 0.01 M CaCl₂ solution. The litter was placed on top of each soil core. The cylinders were irrigated once with 4 ml and four times with 3ml of 0.01 M CaCl₂ solution. At the first irrigation event, 4 ml CaCl₂ solution was applied to account for differences in soil moisture originating from the preparation of soil cores. Leachate was collected and analysed for MCPA and dissolved organic carbon. CO₂ production was monitored on a daily basis. The microcosms were incubated for 20 days at 20°C.

The litter was removed at the end of the incubation. The cores were frozen and subsequently cut into slices using a cryostat microtome. These slices were taken at the following distances to the soil-litter interface: 0-1, 1-2, 2-3, 3-4, 4-5, 5-7 and 7-10 mm. Bacterial and fungal abundances were estimated by qPCR targeted on 16S rRNA and 18S rRNA sequences, respectively (Martin-Laurent *et al.*, 2003). The MCPA degrading genetic potential of bacteria was estimated by qPCR targeted on *tfdA* and *tfdAα* sequences coding isoenzymes specifically involved in the first step of MCPA degradation (Ledger *et al.*, 2006, Vieublè Gonod *et al.*, 2006). Information on further chemical and physical analyses will be given by Poll *et al.* (2009, in prep.).

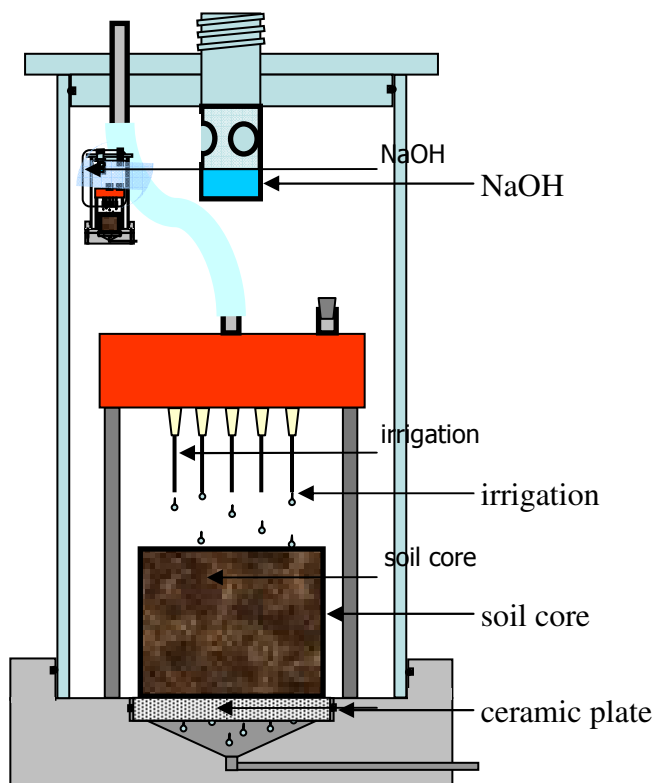


Figure 1. Microcosm prepared to estimate ¹⁴C MCPA degradation within the detritusphere. ¹⁴CO₂ evolved from ¹⁴C-MCPA and column leachate were collected on a regular basis. A set up of 36 microcosms was settled with the following treatments: (1) MCPA, no litter, (2) MCPA, litter, (3) control, no litter, (4) control, litter.

Results and Discussion

Phenoxy acid degrading bacterial strains belonging to various species have been isolated from disparate regions of the world (Vallaey and Soulas, 1992; Baelum *et al.*, 2006), degradative pathways have been studied (Bell, 1957; Beadle and Smith, 1982; Evans *et al.*, 1971), and genetic tools including probes and primers are available (Vallaey *et al.*, 1996; Leander *et al.*, 1998). The *tfdA* gene encodes 2,4-dichlorophenoxyacetic (2,4)/α-ketoglutarate dioxygenase that catalyses the initial step in the degradation of phenoxy acid herbicides such as 2,4-D. The *tfdA* enzyme cleaves the ether bonds of MCPA to produce 4-chloro-2-methylphenol (MCP). This intermediate may then be transformed to chlorophenol by a chlorophenol hydroxylases encoded by the *tfdB* (Ledger *et al.*, 2006).

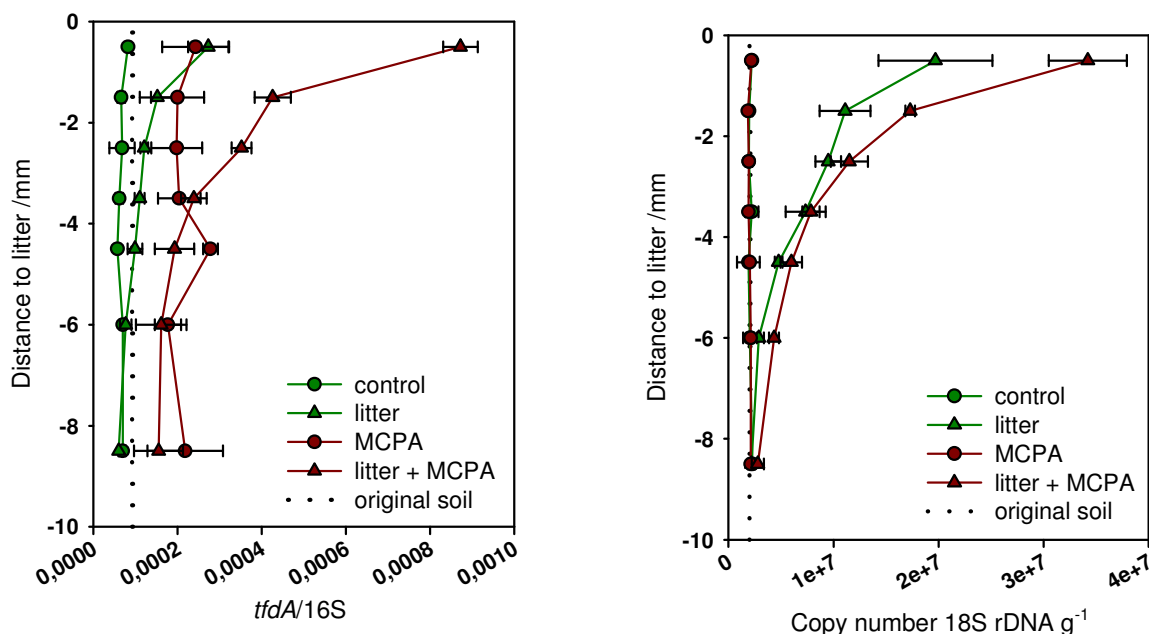


Figure 2. Specific richness of *tfdA* functional community towards total bacterial community (ratio *tfdA*/16S rRNA) and abundance of fungal community (18S rRNA) (data modified from Poll *et al.*, 2009, in prep.).

Our microcosm study showed that the detritosphere provides a favourable environment for MCPA degradation: Isotopic measurements revealed that litter induced an additional release of $^{14}\text{CO}_2$ evolved from ^{14}C -labeled MCPA, thereby enhancing the soil purifying capability (data not shown). Analyses of 16S rRNA and 18S rRNA sequence abundances in different layers of the detritosphere showed that the higher availability of DOC in the 0-4 mm zone stimulated both bacterial and fungal abundances (Figure 2, right side). In addition, *tfdA* sequence abundance in this zone significantly increased in specific richness of MCPA degraders (Figure 2, left side). Whereas the bacterial community increased in soil with MCPA even in the absence of litter, the fungal community increased only if MCPA as well as litter were added to soil cores (Figure 2, right side). Therefore, bacterial and fungal communities' regulation in response to MCPA exposure seems to be different in this environment. Further studies are required to show whether MCPA at the soil-litter interface is degraded by adapted bacterial and/or fungal populations that only partly use the carbon of the MCPA as a nutrient source for their growth.

Isotopic and molecular data are used to set up a computer model to simulate the dynamics of the total bacterial and fungal communities, and specific MCPA degrading microbial community as well as the fate of MCPA in the detritosphere. The model is formulated as a set of fully coupled (partial and ordinary) differential equations that are solved with a fully implicit finite difference scheme. The model describes sorption, transport and degradation of MCPA, transport and degradation of DOC through soil, and changes in bacterial and fungal communities and the MCPA degrading community, respectively. In accordance with the experimental set-up, modeling of the water regime is simplified by assuming steady state conditions. Transport of microorganisms is neglected. Model development is based on the detritosphere model by Ingwersen *et al.* (2008) which is an extended and modified version of the NICA model (Blagodatsky and Richter, 1998).

Conclusion

Our study at a biogeochemical interface (in the detritosphere) offered the opportunity to better understand the biological mechanisms of degradation of xenobiotic compounds of varying complexity. Using MCPA as a model substance, we found that low molecular weight organic compounds in the first 4 mm of the detritosphere stimulated the development of bacterial and fungal communities as well as the development of the MCPA-degrading community. The efficient usage of carbon resources by a complex microbial community in the detritosphere could explain priming effects that are often described in soils. We will get an even closer mechanistic understanding by coupling taxonomical and physiological approaches. We will be able to find out, for example, whether fungal growth under MCPA and litter treatment is caused by changing competition within the soil microbiota, by cross-feeding or by direct fungal use of carbon from MCPA.

References

- Baelum J, Henriksen T, Hansen HCB, Jacobsen CS (2006) Degradation of 4-chloro-2-methylphenoxyacetic acid in top- and subsoil is quantitatively linked to the class III *tfdA* gene. *Applied Environmental Microbiology* **72**, 1476-1486.
- Beadle CA, Smith ARW (1982) The purification and properties of 2,4-dichlorophenol hydroxylase from a strain of *Acinetobacter* species. *European Journal of Biochemistry* **123**, 323-332.
- Bell GR (1957) Some morphological and biochemical characteristics of a soil bacterium which decomposes 2,4-dichlorophenoxyacetic acid. *Canadian Journal of Microbiology* **3**, 821-840.
- Blagodatsky SA, Richter O (1998) Microbial growth in soil and nitrogen turnover: A theoretical model considering the activity state of microorganisms. *Soil Biology and Biochemistry* **30**, 1743-1755.
- Evans WC, Smith BS., Fernley HN, Davies JI (1971) Bacterial metabolism of 2, 4-dichlorophenoxyacetate. *Biochemistry Journal* **122**, 543-551.
- Ingwersen J, Poll C, Streck T, Kandeler E (2008) Micro-scale modelling of carbon turnover driven by microbial succession at a biogeochemical interface. *Soil Biology and Biochemistry* **40**, 872-886.
- Leander M, Vallaeyts T, Fulthorpe RR (1998) Amplification of putative chlorocatechol dioxygenase gene fragments from beta and alpha proteobacteria. *Canadian Journal of Microbiology* **44**, 482-486.
- Ledger T, Pieper DH, Gonzalez B (2006) Chlorophenol hydroxylases encoded by plasmid pJP4 differentially contribute to chlorophenoxy acetic acid degradation. *Applied Environmental Microbiology* **72**, 2783-2792.
- Martin-Laurent F, Piutti S, Hallet S, Wagschal I, Philippot L, Catroux G, Soulas G (2003) Monitoring of atrazine treatment on soil bacterial, fungal and atrazine-degrading communities by quantitative competitive PCR. *Pest Management Science* **59**, 259-268.
- Shailubhai K, Sahasrabudhe S, Vora A, Modi VV (1983) Degradation of chlorinated derivatives of phenoxyacetic acid by *Aspergillus niger*. *FEMS Microbiology Letters* **1**, 279-282.
- Vallaeyts T, Soulas G (1992) Gene *tfd* from the degrading bacterium *Alcaligenes paradoxus* TV1 could be used as probe for the research of soil micro-organisms able to degrade this herbicide. Proceedings of the International Symposium on Environmental Aspects of Pesticide Microbiology, Sigtuna, pp. 177-183.
- Vieubl e Gonod L, Chenu C, Soulas G (2003) Spatial variability of 2,4-dichlorophenoxyacetic acid (2,4-D) mineralisation potential at a millimeter scale in soil. *Soil Biology and Biochemistry* **35**, 373-382.
- Vieubl e Gonod L, Chadoeuf J, Chenu, C (2006) Spatial distribution of microbial 2, 4-dichlorophenoxy acetic mineralization from field to microhabitat scale. *Soil Science Society of America Journal* **70**, 64-71.
- Vieubl e Gonod L, Martin-Laurent F, Chenu C (2006) 2,4-D impact on bacterial communities, and the activity and genetic potential of 2,4-D degrading communities in soil. *FEMS Microbiology Ecology* **58**, 529-537.

Geochemistry and mineralogy of volcanic soils from Ocean Fogo island (Cape Verde)

Rosa Marques^{A, C}, M. Isabel Prudêncio^{A, C}, Fernando Rocha^{B, C}, Eduardo Ferreira da Silva^{B, C}

^AInstituto Tecnológico e Nuclear, EN 10, 2686-953 Sacavém, Portugal, Email rmarques@itn.pt

^BDepartamento de Geociências – Universidade de Aveiro, Campus Universitário de Santiago, 3810 – 193 Aveiro, Portugal, Email frocha@geo.ua.pt

^CGeoBioTec – GeoBiociências, GeoTecnologias e GeoEngenharias (Foundation for Science and Technology), Email frocha@geo.ua.pt

Abstract

The chemical and mineralogical study of topsoils (< 2mm) from the ocean volcanic island of Fogo was performed aiming the establishment of geochemical patterns of soils, especially the trace element distribution. The morphology of this semi-arid island corresponds to a conic volcano edifice, with three main stratigraphic units: (I) a carbonatite unit, (II) a major volcanic sequence (nephelinites and associated lavas, scoria and tuffs), and (III) a post caldera sequence including several historic eruptions. The chemical and mineralogical analyses were done using neutron activation analysis and X-ray diffraction. The topsoil developed on carbonatites is clearly distinguished by high contents of K, Rb, Cs, W, Th and rare earth elements (REE). The soils from unit II have a similar chemical composition, except one sample that presents higher REE, Fe, As, Cs, Ba, Zr, Hf, Ta and Th contents. The main mineral compounds identified in Fogo topsoils are pyroxenes, feldspathsoids, magnetite-maghemite, titanomagnetite, zeolites and phyllosilicates. The soil developed in carbonatites shows a distinct mineralogical association, with calcite, mica, phyllosilicates, and feldspars. Quartz and mica are in general found in the studied soils of this volcanic island, derived most probably from particulate deposition from the atmosphere transported by wind from North Africa (Sahara).

Key Words

Soil, Fogo island, trace elements, REE, mineralogy, atmospheric deposition

Introduction

The island of Fogo (15.0N, 24.5W) is located in the south-western part of Cape Verde and is the fourth bigger island (476 km² area) of this archipelago (Figure 1). This is a relatively simple island-volcano, corresponding practically to an active volcano with a maximum altitude of 2829 m. The island is characterized by a semi-arid climate, raining mainly between July and October. The average annual temperature of Fogo island is about 25°C. However, in Chã das Caldeiras (See Figure 1b) in December and January the temperature decreases to 0°C (Mota Gomes, 2006).

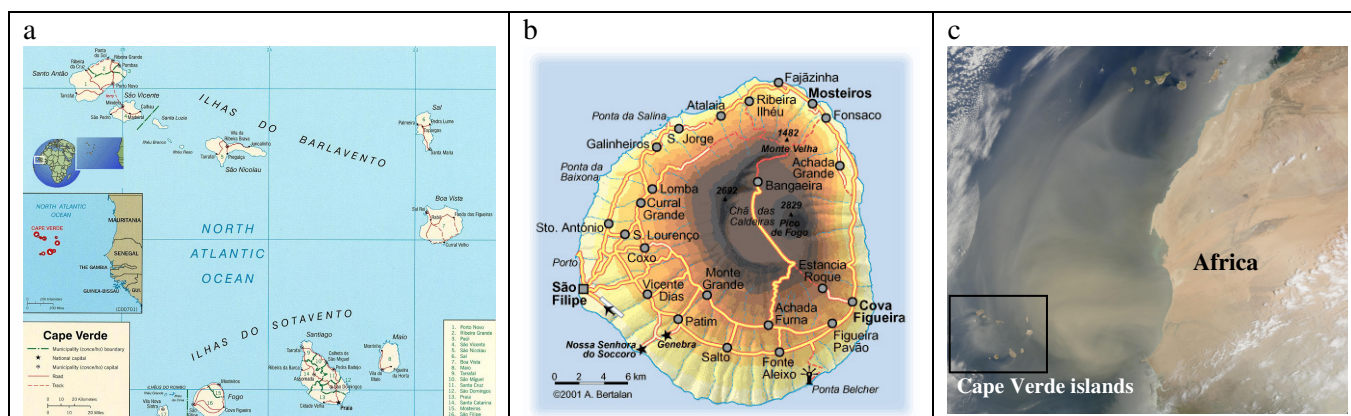


Figure 1. a- Location of Fogo island (www.okcapeverde.com/Cape-Verde-Islands-Map.jpg); b- Fogo island map; and c- NASA image SeaWiFS collected in May 2007 – dust from North Africa often blows across the Atlantic in to Cape Verde islands (http://oceancolor.gsfc.nasa.gov/cgi/image_archive.cgi?c=DUST).

Three main stratigraphic units include the volcanic rocks of Fogo: (I) a carbonatite unit exposed in fluvial valleys near S. Filipe and assumed by most authors as the oldest rocks of the island, (II) a major volcanic

sequence related to the sub-aerial shield-building of the island volcano (nephelinites and associated lavas with layers of scoria or tuffs, previous to the caldera formation), and (III) a post caldera sequence including several historic eruptions (Madeira *et al.*, 2005; Madeira and Brum da Silveira, 2005).

In this work a detailed chemical characterization (28 trace and major elements) of topsoils collected on the west slope of Fogo Island (Figure 2) in the two first units (carbonatite and sub-aerial shield-building), was obtained by neutron activation analysis. A mineralogical study was also done by X-ray diffraction. The main objective of this work is the establishment of geochemical patterns of topsoils derived by weathering of different types of volcanic rocks, particularly trace elements distribution. The correlation of the chemical composition with the mineral phases is also done. The evaluation of atmospheric deposition is also a major goal (Derry and Chadwick, 2007), since a contribution of fine materials transported by Trade Winds from North Africa (Sahara) is expected (see Figure 1c). This work is being done in the framework of a larger project compiling a geochemical atlas of low/medium density of Cape Verde islands.

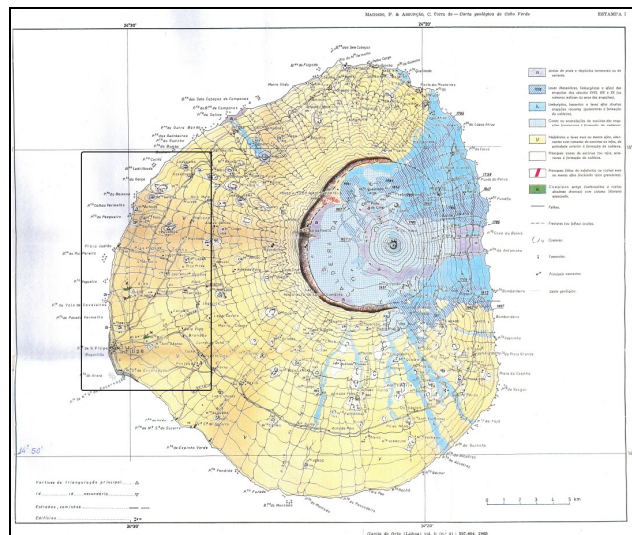


Figure 2. Geological map of Fogo island with the indication of the studied area (black rectangle) (Machado F, Assunção C. Torre de, Carta Geológica de Cabo Verde, 1965)

Methods

Sample collection and analytical methods

A field work was done in the Fogo island in October of 2009 in order to select and collect topsoils (regolith). In depth coring was done to collect surface (0-25 cm) samples. The whole sample (<2mm) was obtained by sieving and then ground in agate mortar.

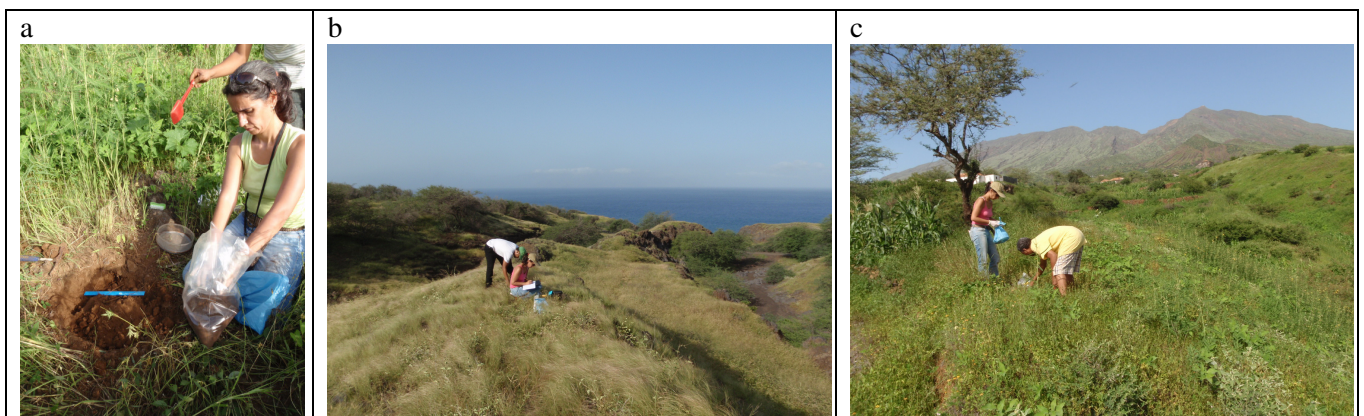


Figure 3. a- Sampling a topsoil of unit II; b and c- sampling locations of inter-fluvial areas of unit II.

The mineralogical composition of whole samples was obtained by X-ray diffraction (non-oriented aggregates). The neutron activation analysis was applied for the determination of chemical contents in the whole sample of

topsoils. Reference samples of soil (GSD9) and sediment (GSS4) from the IGGE from the People's Republic of China were used as standards. The irradiation of the samples and standards were done in the core grid of the Portuguese Research Reactor. The chemical contents of Na, K, Fe, Sc, Cr, Co, Zn, Ga, As, Br, Rb, Zr, Sb, Cs, Ba, La, Ce, Nd, Sm, Eu, Tb, Yb, Lu, Hf, Ta, W, Th e U were obtained with a good precision and accuracy (in general <5%) (Gouveia and Prudêncio, 2000).

Results

The chemical results obtained so far show that the soil developed on carbonatites (unit I sample) is easily distinguished by higher contents of rare earth elements (REE), particularly the light and middle ones, K (2.17% K₂O), Rb (222 µg/g), Cs (1.65 µg/g), W (4.56 µg/g), and Th (9.17 µg/g) and lower contents of Sc (12 µg/g) and Cr (41.1 µg/g). Also a significant negative Ce anomaly was found in the carbonatite soil (Figure 4).

Among the soils developed in unit II (volcanic sequence related to the sub-aerial shield-building of the island volcano), most of the samples already analysed present a similar geochemical pattern (called unit II-a in the present work), except for one sample collected in the north-western part of the studied area (unit II-b sample). Concerning the REE, unit II-b presents higher contents of REE, especially light and middle REE (see Figure 4a), and higher contents of Fe (19.1 % Fe₂O₃T), As (3.56 µg/g), Cs (1.45 µg/g), Ba (913 µg/g), Zr (573 µg/g), Hf (10.1 µg/g), Ta (9.12 µg/g) and Th (8.87 µg/g).

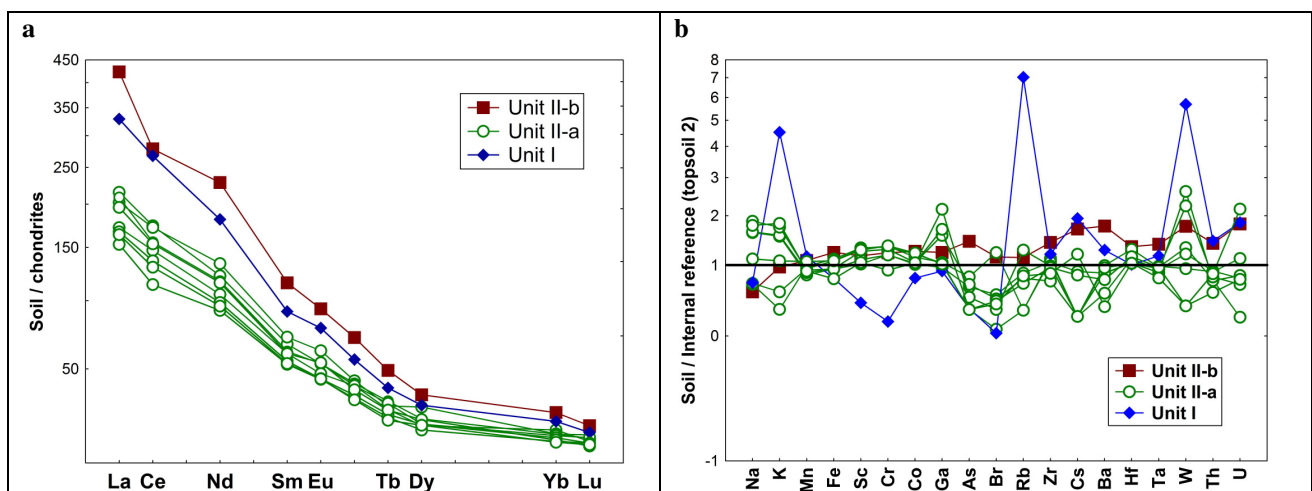


Figure 4. a- Chondrites-normalized patterns of REE of the whole sample (<2mm) of topsoils from Fogo island (chondrites values of Anders and Grevesse (1989) times 1.36, obtained by Korotev (1996)); b- chemical contents in topsoils from Fogo island relative to an internal reference sample (topsoil 2 belonging to the unit II).

In the topsoils of unit II-a, the higher chemical contents variations were found for Na, K, Ga, Br, W and U (Figure 4b). The REE fractionation observed is mainly due to a higher variation of the light REE contents (see Figure 4a). High contents of Br are found (up to 193 µg/g), which has been already found in other Atlantic islands of Azores (Vieira *et al.*, 2004).

The mineralogical study by XRD point to the existence of a significant vitreous component, since low crystallinity was revealed by the diffractograms obtained, as could be expected for these volcanic soils. Among the mineral compounds identified by XRD in Fogo topsoils of unit II, pyroxenes, feldspathoids, magnetite-maghemite, titanomagnetite, and zeolites were found. The soil derived by weathering of carbonatites is mainly composed of calcite, mica, phyllosilicates, and feldspars; traces of zircon and apatite were also detected. It should be noted that different proportions of quartz and mica were also detected in these soils, which can be derived from atmospheric deposition of grains transported by wind from North Africa (see Figure 1 iii), as already found in the Canary archipelago (Mizota and Matsuhisa, 1995).

Conclusion

The results obtained so far show that topsoils of the ocean Fogo island present significant chemical variations mainly in the concentrations of REE (particularly the light and middle REE), K, Sc, Cr, Fe, As, Br, Rb, Zr, Cs, Ba, Hf, Ta, W, Th and U. The differences found are related with the parent rock, topography and the geographic

location. Bromine may have been added to the soils by wet deposition (ocean origin), explaining the high contents of this volatile element found in some soils.

Despite the reduced number of samples already analysed, the chemical and mineralogical composition appears to contribute for the characterization and differentiation of topsoils of the Fogo island (among and within the same geological unit). Quartz and mica found in the topsoils of this ocean volcanic island may be transported from North Africa (Sahara) deserts by Trade Winds. Chemical and mineralogical characterization of a larger number of samples of different lithology and geographic locations of the island is being undertaken.

References

- Anders E, Grevesse N (1989) Abundances of the elements: Meteoritic and solar. *Geochimica and Cosmochimica Acta* **53**, 197-214.
- Derry LA, Chadwick A (2007) Contributions from earth's atmosphere to soil. *Elements* **3**, 333-338.
- Gouveia MA, Prudêncio MI (2000) New data on sixteen reference materials obtained by INAA. *Journal of Radioanalytical and Nuclear Chemistry* **245**(1), 105-108.
- Korotev RL (1996) On the relationship between the Apollo 16 ancient regolith breccias and feldspathic fragmental breccias, and the composition of the prebasin crust in the Central Highlands of the Moon. *Meteoritics & Planetary Science Journal of the Meteoritical Society* **31**, 403-412.
- Machado F, Assunção C Torre de (1965) Carta Geológica de Cabo Verde.
- Madeira J, Munhá J, Tassinari CGC, Mata J, Brum da Silveira A, Martins S (2005) K/Ar Ages of carbonatites from the island of Fogo (Cape Verde). Actas da XIV Semana da geoquímica e VII Congresso de geoquímica dos países de língua Portuguesa. 475-478.
- Madeira J, Brum da Silveira A (2005) Geomorphic and structural analysis of the Fogo island volcano (Cape Verde). Abstract volume of SAL2005 International Workshop on ocean island volcanism, Sal, Cape Verde.
- Mizota C, Matsuhisa Y (1995) Isotopic evidence for the eolian origin of quartz and mica developed on volcanic materials in the Canary Archipelago. *Geoderma* **66**, 313-320.
- Mota Gomes A (2006) A problemática da Geologia e dos Recursos Hídricos na Ilha do Fogo. Relatório inédito, Praia, Cabo Verde.
- Vieira BJH, Soares PM, Prudêncio MI, Freitas MC, Rodrigues AF (2004) Caracterização química (terras raras e outros elementos) de solos das Ilhas de Santa Maria e Terceira (Açores, Portugal). *Geociências* **16**(1/2), 5-12.

Geochemistry, mineralogy and micropaleontology of a pedogenic calcrete profile (Slimene, NE Tunisia)

Maria Isabel Prudêncio^{A,C}, Francisco Ruiz^B, Maria Isabel Dias^{A,C}, Rosa Marques^{A,C}, João Carlos Waerenborgh^A, Maria José Trindade^{A,C}, Manuel Abad^B, Dulce Franco^A

^AInstituto Tecnológico e Nuclear, EN 10, 2686-953 Sacavém, Portugal, Email iprudenc@itn.pt

^BDep. Geodinámica y Paleontología, Univ. Huelva, 21071 Huelva, Spain, Email ruizmu@uhu.es

^CGeoBioTec – GeoBiociências, GeoTecnologias e GeoEngenharias (Foundation for Science and Technology)

Abstract

A calcrete profile developed on the top of a calcareous consolidated dune in a coastal area of NE Tunisia (semi-arid climate) was studied focussing on: (i) geochemistry of rare earth elements (REE) and other trace and major elements during the processes associated with calcrete formation, and (ii) mineralogy of the different horizons of the profile. The profile shows a vertical sequence: surface horizon, sub-surface horizon, lithoclast-rich horizon, laminar-structured level, and the old dune. Chemical and mineralogical analyses were performed by neutron activation analysis and X-ray diffraction (whole samples and clay fraction).

The calcrete is mainly composed of quartz, calcite and K-feldspar. Phyllosilicates were also found in the other levels. Hematite was only detected in surface levels. The clay minerals present are kaolinite, illite and chlorite. Smectite also occurs in the matrix of the nodular horizon. The microfauna identified is the one commonly found in dunes close to the sea (terrestrial environment). Co, U, Br and heavy REE enrichment occur in the evaporite carbonate rich levels, while the light REE, Hf, Zr, Cr, Th, Cs, Ta, Ga, Rb, and K appear to be retained in the upper levels.

Key Words

Soil, calcrete, semi-arid environment, geochemistry, mineralogy, microfauna

Introduction

Calcretes occur in the semi-arid and arid regions, and are accumulations of fine-grained low magnesium calcite having formed within the meteoric vadose zone, facilitated by loss of H₂O and CO₂, by pedogenic alteration and replacement of the host material. Biological influences are commonly found.

Detailed chemical and mineralogical studies of soils and sediments of the semi-arid area of the El Melah coastal lagoon (NE Tunisia) with a closing evolution dynamic have been done. Among the different mineral phases found, carbonates appear to play an important role on the trace elements distribution in the surface environments under a semi-arid climate (Ruiz, 2006; Prudêncio *et al.*, 2007; 2010). In this work a mineralogical, chemical and micropaleontological study of a calcrete profile developed on the top of a calcareous consolidated dune located near Slimene, in the central area of the El Melah lagoon, is done. The evaluation of the redistribution of chemical elements during the weathering processes associated with calcrete formation, particularly the dissolution of carbonates and precipitation in the vadose zone, is a major goal.

Methods

Sample collection

The sampling location, the profile and the sampled levels are shown in Figure 1, where a vertical sequence, with clear zonations from the surface downwards can be seen: (1) a reddish modern soil at the land surface, appr. 50 cm thick, (2) a lithoclast-rich horizon (1m thick). The clasts are subrounded to stellate in shape due to dissolution, in a terrigenous yellowish matrix, (3) a laminar structured calcrete up to 30 cm thick, and (4) the consolidated dune. The samples reference and description are given in Table 1.

Samples were sieved into <2mm and grounded. Nodules and laminar calcrete were finely ground. The <2µm fraction was obtained by wet sieving and sedimentation according to Stokes law.

Analytical Methods

Chemical and mineralogical analyses of samples from all levels were performed by neutron activation analysis and X-ray diffraction (bulk samples and clay fraction). Chemical contents of Na, K, Mn, Fe, Sc, Cr, Co, Zn, Ga, As, Br, Rb, Zr, Sb, Cs, Ba, La, Ce, Nd, Sm, Eu, Tb, Dy, Yb, Lu, Hf, Ta, Th, and U were obtained. Relative precision and accuracy are, in general, to within 5% (Gouveia and Prudêncio, 2000). Iron detailed studies were done by Mössbauer spectroscopy. A micropaleontological study of all levels, with the taxonomical determination of ostracode species was performed. For this purpose, a fixed quantity (15 g dry weight) was

sieved through a 63µm mesh. If possible, 500 individuals were picked from each sample, with an extrapolation to the whole sample. This number exceeds clearly the number of individuals (300) required for the statistical analysis of the ostracode assemblages (e.g., Ruiz *et al.*, 1997).

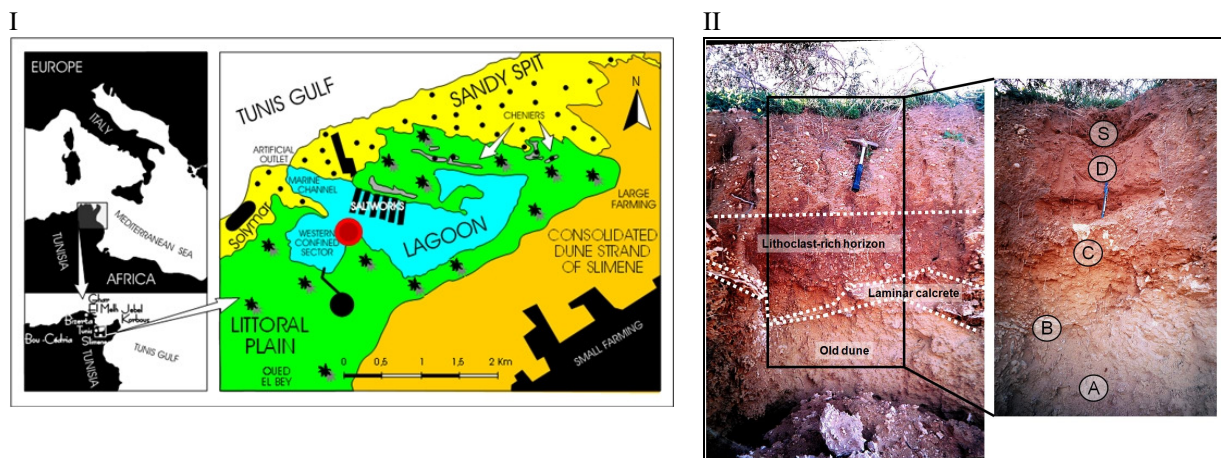


Figure 1. I) El Melah lagoon area: location of the calcrete profile (red circle); II) The pedogenic calcrete profile before (left) and after (right) cleaning and sampling with the identification of the sampled levels. A- old dune; B- laminar-structured level; C- lithoclast-rich horizon; D - sub-surface horizon (25-50 cm depth); and S – surface horizon (0-25cm depth).

Results

Quartz, calcite and feldspars are present in the whole samples of all levels (Table 1). The calcrete is mainly composed of quartz, calcite and K-feldspar. Phyllosilicates and plagioclase also occur in the other levels. Hematite is present in the surface, sub-surface and in the terrigenous matrix of level C, explaining the reddish colour of these levels (see Figure 1). The clay minerals present are kaolinite, illite and chlorite. Smectite also occurs in the terrigenous matrix of the lithoclasts-rich horizon (C) above the laminar structure. Goethite is the dominant iron oxide in the clay fraction of the surface and sub-surface levels (S and D).

Table 1. Sample reference, description, and mineral composition (whole sample and <2µm fraction). Qz-quartz, Ca-calcite, Phyl-phyllsilicates, KFs-K-feldspar, Plg-plagioclase, Hem-hematite; K-kaolinite, I-illite, C-chlorite, Sm-smectite; G-goethite; Gy-gypsum. (*) after decarbonation

Sample	Description	Whole sample	Clay fraction
S	Surface (0-25cm)	Qz, Ca, Plg, Phyl, Hem	K, I, C, Ca, Qz, Gy
D	Sub-surface (25-50 cm)	Qz, Ca, Phyl, KFs, Plg, Hem	K, I, C, Ca, Qz, Gy
C	Terrigenous matrix of level C	Qz, Ca, Phyl, KFs, Plg, Hem	K, I, C, Sm, Qz
CN	Nodules of level C (45% carbonates)	Qz, Ca, KFs	I, K, C, Qz, G (*)
B	Laminar calcrete (50% carbonates)	Qz, Ca, KFs	I, K, C, Qz, G (*)
A	Old dune (parent rock)	Qz, Ca, KFs, Plg, Phyl	

Microfauna commonly found in dunes close to the sea was observed in the studied profile: (i) surface levels (S and D) - gastropods (terrestrial environment); (ii) carbonated nodules (CN of level C) - microfauna is almost absent, with the presence of very rare specimens of marine foraminifers (*Ammonia beccarii*); (iii) laminar-structure (level B) - microfauna is covered by a coarse calcareous sheet that impedes the taxonomical determination of numerous specimens. Nevertheless, all individuals belong to marine species of foraminifers (*Ammonia beccarii*, *Elphidium crispum*, *Quinqueloculina spp.*), ostracods (*Bairdia mediterranea*, *Cytheretta adriatica*), spines of echinoderms and undifferentiated fragments of bivalves; and (iv) old dune (level A - eolian deposits close to the sea) - dune sands partially composed of marine provenance where fragments of marine species of very scarce ostracods (*Pontocythere elongata*), foraminifers (*Ammonia beccarii*, *Ammonia tepida*, *Quinqueloculina spp.*), and rounded fragments of spines of echinoderms, bryozoos remains and undifferentiated fragments of bivalves were found.

The in depth chemical variation, normalized to Sc (conservative element) correlations are shown in the tree-clustering (Figure 2). Among the elements studied, Br, Co, U heavy REE, Na, and Sb are the most enriched in

the calcrete (B, CN). Concerning Co, U and Br the in depth variations (Figure 3) may be explained as follows: calcite precipitation requires high pH values (often >9), favouring the uptake of Co^{2+} in calcite; in carbonated groundwater U is transported as extremely soluble uranyl dicarbonate and tricarbonate complex ions. Removal of CO_2 , while making CaCO_3 less soluble, increases pH. Evaporite or common-ion precipitation of carbonate results in eventual precipitation of carnotite along with carbonate; Br/Sc distribution suggests a biological role in carbonate precipitation. In the surface horizons an enrichment of the following elements is observed: light REE, Hf, Zr, Cr, Th, Cs, Ga, Rb, Ta, and K.

The investigation of the iron crystalchemistry in levels S, D and C by Mössbauer spectroscopy showed that: (a) Fe is more reduced in the upper level (9%) than in levels D and C (4%); (b) Fe^{3+} occurs in iron oxides - goethite and hematite, and clay minerals. The ratio goethite/hematite appears to increase downwards along the profile; and (c) Fe^{2+} is mainly present in clay minerals.

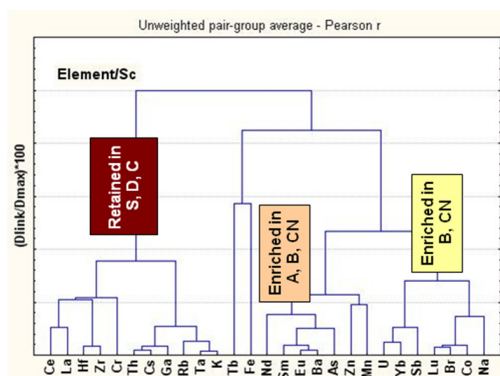


Figure 2. Tree-clustering showing the correlation among variables (element/Sc).

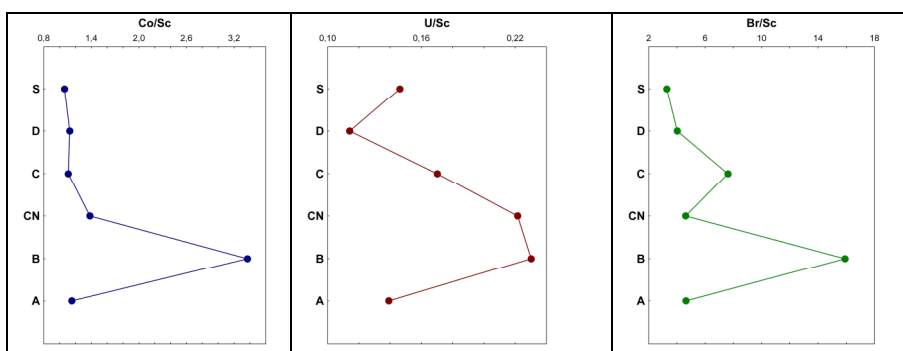


Figure 3. In depth profiles of Co/Sc, U/Sc, and Br/Sc ratios.

The clay fraction is in general enriched relative to the whole sample in the elements studied, but Hf and Zr (Figure 4). Surface levels (S and D) present similar geochemical patterns. The old dune (A) presents a different pattern compared to the terrigenous matrix of level C. REE are concentrated in the clay fraction, increasing upwards; a positive Ce anomaly was found in the old dune and in superficial level relative to the whole sample (see Figure 5III).

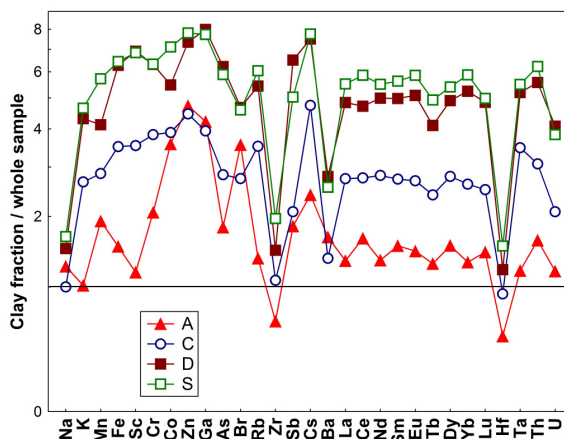


Figure 4. Chemical contents of the clay fraction relative to the respective whole sample.

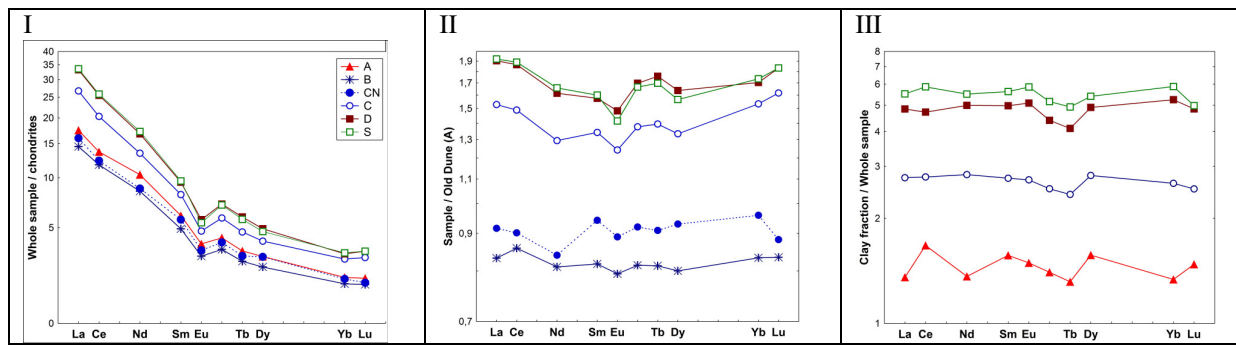


Figure 5. REE patterns: I- whole sample relative to chondrites; II- whole sample relative to sample A (parent rock); and III- clay fraction relative to the respective whole sample.

The enrichment of REE in the upper levels relative to the old dune (Figure 5II) may correspond to (i) sorption into clay minerals and iron oxides in the case of the LREE, and (ii) precipitation of pedogenic calcite in the case of the HREE as already found by Compton *et al.*, 2003 in soil profiles and evaporate salt pan sediments from a small granite catchment in a semi-arid climate (South Africa). The MREE are enriched in the old dune, and in the nodular and laminar calcrete. A lower negative Eu anomaly occurs in the carbonates rich levels pointing to its uptake by calcite and evaporite carbonates after the breakdown of feldspars.

Conclusion

The results obtained by studying a calcrete profile, where a reddish soil was derived by weathering of a calcareous consolidated dune under a semi-arid environment point to: (i) similar mineralogical association down to the laminar-structure level, except for the presence of smectite in the terrigenous matrix of the nodular level above the laminar structure, indicating restricted drainage conditions. The presence of hematite in the upper levels indicates more oxidizing conditions; (ii) among the chemical elements studied an enrichment of Br in the calcrete was found, suggesting an important biological role in the carbonates precipitation. Co and U uptake and an enrichment of the heavy REE relative to the light REE are also observed in the calcrete; (iii) a higher fractionation of the REE in the superficial levels was found, which may be explained by the incorporation of the light REE in clay minerals and iron oxides, as well as the migration downwards of the heavy REE due to carbonates dissolution.

References

- Cheng LK, Sturchio NC, Bedzyk MJ (2000) Local structure of Co^{2+} incorporated at the calcite surface: an X-ray standing wave and SEXAFS study. *Physical Review B* **61**, 4877-4883.
- Compton JS, White RA, Smith M (2003) Rare earth element behavior in soils and salt pan sediments of a semi-arid granitic terrain in the Western Cape, South Africa. *Chemical Geology* **201**, 239-255.
- Gouveia MA, Prudêncio MI (2000) New data on sixteen reference materials obtained by INAA. *Journal of Radioanalytical and Nuclear Chemistry* **245**(1), 105-108.
- Kelly SD, Newville MG, Cheng L, Kemner KM, Sutton SR, Fenter P, Sturchio NC, Spötl (2003) Uranyl incorporation in natural calcite. *Environmental Science & Technology* **37**, 1284-1287.
- Prudêncio MI, Dias MI, Ruiz F, Waerenborgh JC, Duplay J, Marques R, Franco D, Ben Ahmed R, Gouveia MA, Abad M (2010) Soils in the semi-arid area of the El Melah Lagoon (NE Tunisia) - Variability associated with a closing evolution. *Catena* **80**, 9-22.
- Ruiz F, Abad M, Galán E, Gonzales I, Aguilá I, Olías M, Gómez Ariza JL, Cantano M (2006) The present environmental scenario of El Melah Lagoon (NE Tunisia) and its evolution to a future sabkha. *Journal of African Earth Sciences* **44**, 289-302.
- Ruiz F, González-Regalado ML, Muñoz JM (1997) Multivariate Analysis applied to Total and Living Fauna: seasonal Ecology of Recent Benthic Ostracoda off the North Cádiz Gulf (SW Spain). *Marine Micropaleontology* **31**, 183-203.
- Prudêncio MI, Gonzales MI, Dias MI, Galán E, Ruiz F (2007) Geochemistry of sediments from El Melah lagoon (NE Tunisia): A contribution for the evaluation of anthropogenic inputs. *Journal of Arid Environments* **69**, 285-298.

Influence of temperature on solute release from organic horizons in Siberian permafrost terrain

Masayuki Kawahigashi^A Anatoly Prokushkin^B Akira Noguchi^A, Isao Hasegawa^A, Hiroaki Sumida^A

^ACollege of Bioresource Sciences, Nihon University, Fujisawa, Kanagawa, 2528510, Japan, Email khigashi@brs.nihon-u.ac.jp

^BSukachev Institute of Forestry, Siberian Division, Russian Academy of Science, Akademgorodok, Krasnoyarsk, 660036, Russia, Email prokushkin@ksc.krasn.ru

Abstract

Solutes released from organic horizons in Siberian permafrost affected soils have a significant role for organic carbon sequestration by sorption onto mineral soils and for plant nutrition. Since ground temperature influences the solutes released through degradation of organic matter, organic carbon and major plant nutrients in water extracts of organic horizons under various temperature conditions ranging from -20 to 550°C were determined. Solute release of the frozen sample was greater than those from the incubated samples at 25°C. The solution pH of the frozen sample was also lower due to dissociation of released organic acids. Destruction of plant tissue and microbial cell death and lysis by freezing probably increases solute concentrations. Heating the organic horizon samples up to 180°C drastically increased solute release concurrent with low pH values. Thermal denaturation of organic materials can promote organic C solubilisation and cation and anion productions. Temperatures over 250°C made organic materials insoluble, resulting in less release of solutes and neutral pH values. Carbonization of organic materials in the temperature range between 250 and 550°C increases char products and hydrophobicity, resulting in less solute release. Seasonal freeze-thaw cycles and heating by forest fires strongly control dynamics of biogenic elements in the Siberian permafrost terrain.

Key Words

Permafrost, dissolved organic matter (dom), forest fire, Siberia, biodegradation

Introduction

Thick organic horizons are not only great carbon sinks (Prokushkin *et al.*, 2006) but also sources of biogenic elements through their biodegradation. High concentration of dissolved organic carbons (DOC) released from organic horizons can be retained by mineral soils by sorption processes (Kawahigashi *et al.*, 2006), enabling the soils in this region to be the greatest terrestrial carbon sink. Release of bases, N and P from the organic horizons probably contribute to net primary production in the taiga forest, and is also responsible for river water chemistry especially in the spring melt season (Pokrovsky *et al.*, 2005). The greatest concentrations of solutes were probably produced through a freeze-thaw process in the organic horizon during winter to spring. Central Siberia has little rain fall and relatively high air temperature in summer, resulting in dry soil. The drying process of the organic horizons can also increase solute release after rewetting (Kawahigashi *et al.*, 2008).

A high temperature ignition frequently attacks the organic horizons in central Siberia when forest fires have occurred. Usually ground fires with a low intensity of burning run on the forest floor, resulting in partial combustion of organic horizons. The heating conditions drastically change physical and chemical properties of organic horizons, affecting solutes released and composition.

The aim of this study is evaluation of solutes release using organic horizon samples prepared at a wide range of temperatures from frozen to igniting temperatures.

Methods

Sampling site

The study site was a mature Larch forest in the Kochechum River watershed (central Evenkia, Russia, 64° N, 100° E). The forest was 105 years old after the previous forest fire. Permafrost was found at 40 cm depth from the mineral soil surface. The permafrost table in the region prevents soil water percolation and drainage, keeping the soil moist, despite low precipitation of around 350mm in a year. The soil was classified as Oxyaquic Cryosol (WRB system) derived from the Siberian Basalt. The organic horizon consisting of Oi, Oe and Oa horizons had a 15 cm thickness due to the slow microbial decomposition under low soil temperature. Forest fires have often happened in this area. The forest fire in this region is a ground fire due to the low density of trees in the forest, affecting thickness and properties of organic horizons by burning (Ito 2005). Organic horizon samples were collected from the mature forest and the burned forest stands two months after the latest forest fire.

Sample preparation

Cubic samples composed of a 10 cm square bottom with a depth of the horizon were cut out from an organic horizon using a knife carefully taking care of contamination of minerals. Living mosses or lichens covering the organic horizons were removed from the samples for following experiments. After bringing back samples kept in an insulating bag, subsamples were kept in a deep freezer (-20°C). A subsample from the deep freezer was left in an incubator at 25°C keeping the field moisture for two weeks. Frozen subsamples after melting at the ambient temperature were kept in an oven set at 65°C for 4 days to completely desiccate the field moisture. The dried subsamples were kept at 105°C in an oven for 24 hours and the other dried samples were kept in a muffle furnace for 15 minutes at 180, 250, 350, 430, 550°C, respectively. These nine subsamples prepared at different temperature were used for further experiments.

Water extraction and chemical analyses

Solutes from the organic horizons samples were extracted with ten fold amounts of water (W/V), taking into account the field soil moisture, at 25 °C for 24 hours without shaking. The same extraction was conducted for the frozen sample (-20°C) after defrost. After the extraction, pH values were measured immediately using a glass electrode. Extracts were obtained by filtration using 0.2 μ m cellulose acetate membranes (Millipore Co Ltd, Tokyo). Filtrates were diluted with ultra-pure water to suitable concentration range taking into account analytical detection limits. Nitrate, chloride, fluoride, sulfuric and phosphoric anions were determined by injection of the diluted solutions into an ion chromatograph (Compact IC-761; Methrom, Herisau, Switzerland). Base cations were determined by atomic absorption spectrometry (Z-5000; Hitachi, Hi-Tech, Tokyo, Japan). Total and inorganic carbon in the soil solutions were determined using a Shimadzu TOC-5000 analyzer (Shimadzu, Kyoto, Japan). Dissolved organic carbon (DOC) was calculated by subtracting inorganic carbon from total carbon.

Results and Discussion

Weight losses of the samples were not significant below 25 °C. Water vapour loss and organic matter combustion decreased the sample weight significantly at 65°C and 250°C respectively. Almost 60% of bulk samples were finally lost by an oxidative combustion at 550°C. Figure 1 A indicated the change in pH of the extract from each temperature sample. pH values were low around 4 at -20, 65, 105 and 180 °C. The solution pH was high at 25°C incubation. With increasing the heating temperature between 180 and 350°C, pH increased drastically, reaching pH 7. pH at the burned site was 5.17, indicating relatively higher pH compared to those of unburned samples incubated below 25 °C. An increasing trend of pH along with heating temperature has been confirmed by Prokushkin *et al.* (2007) using same Siberian organic horizons.

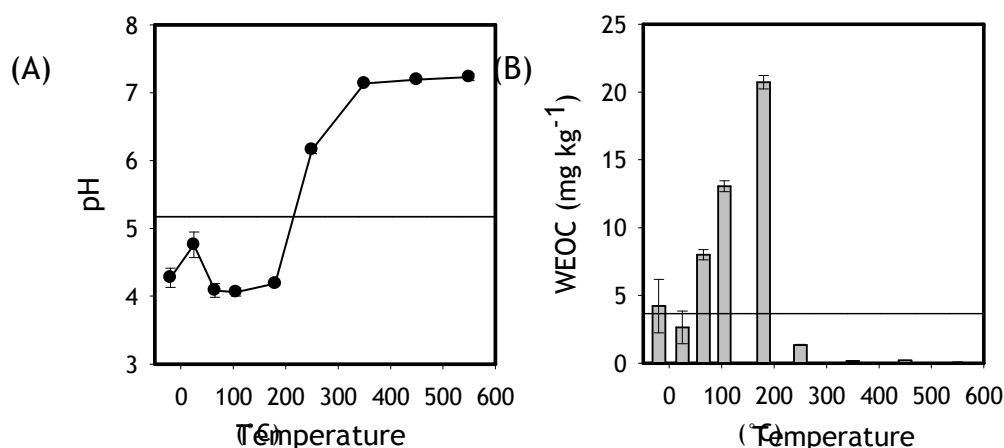


Figure 1. Changes in solution pH (A) and water extractable organic carbons (WEOC) (B) after incubation or oxidative combustion. The line in both figures indicates the values for an organic horizon sample obtained from the burned site 2 months after the latest forest fire which occurred in 2005.

Figure 1B showed WEOC (mg kg⁻¹) content of organic horizons. The temperature dependent of WEOC seems to be reciprocal to pH changes. Released protons from dissociated organic acids can decrease pH of the solution. Frozen samples release greater amount of WEOC compared to the incubated samples at 25°C. Biodegradation of WEOC at 25 °C probably decreased WEOC extracted. On the other hand, freezing promoted WEOC release probably due to plant tissue destruction, microbial death and cell lysis. Heating from 65 to 180°C increased

WEOC almost twice to five times as compared to that at the 25°C incubation. Organic substances composed of plant tissues released through organic matter decomposition during the range of heating. Drying below 105 °C could also chemically denature organic horizons and contribute to the WEOC production. Water soluble organic C comprised a very small amount for samples heated over 250 °C that showed high water repellence. Organic horizons under the latest burned forest site released WEOC equivalent to the frozen unburned sample, indicating that physical-chemical properties of the burned organic materials had probably biologically changed after the forest fire.

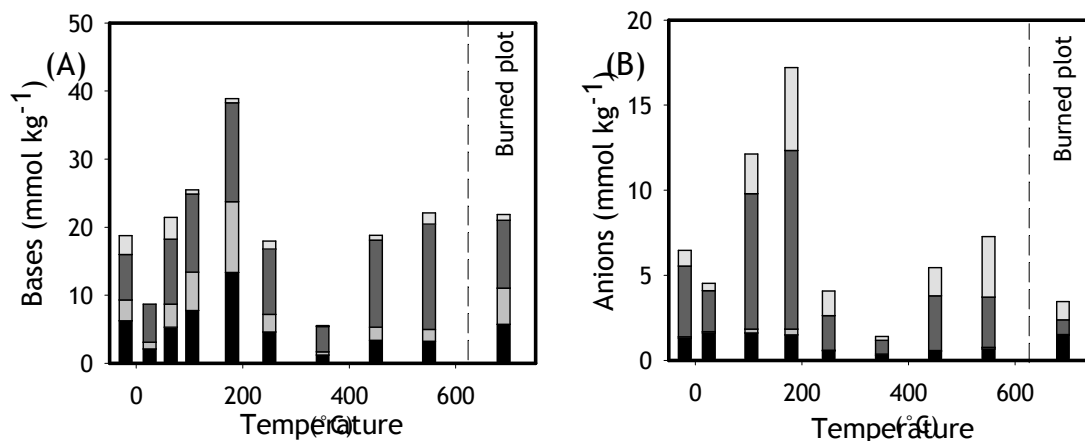


Figure 2. Changes in base cation content (A) and anion contents (B) in water extracts from organic horizons after incubation or oxidative combustions. Colour density of each bar indicate Ca, Mg, K and Na for bases and Cl⁻, NO₃⁻, PO₄³⁻, SO₄²⁻ for anions from bottom to top. Bar of the right side is cation and anion contents from the burned site 2 months after the latest forest fire that occurred in 2005.

Sum of released base cations and anions are shown in Figure 2. Both temperature dependencies were similar. Frozen samples released greater amount of cations and anions as compared to the sample incubated at 25 °C. The higher the temperature up to 180°C is, the soluble ions. The lowest contents of released ions were observed at 350°C the same as for WEOC. The higher heating temperatures of 450 and 550 °C made more water soluble K and SO₄ than at 350°C. Potassium was the dominant soluble cation in all samples followed by Ca. In the anion compositions phosphate was dominant. Anions were always deficient to total charge of cations, indicating compensation by organic anions for the deficit (Nambu and Yonebayashi, 1999). The compositions of cations and anions in the solute from the 2005 burned site were different from laboratory burned samples (up to 250°C heating). Other field factors such as microbial activity, solar radiation, moisture and so on can chemically change burned organic materials in the field after the forest fire.

Conclusion

The organic horizons changed their solute release potential depending on temperature. Freezing promoted solute release probably due to destruction of plant tissues and microbial cell lysis. Despite drastic increase in solute production by the drying process up to 105 °C, the compositions of cations and anions were not largely different from those of frozen and 25 °C incubated samples. Incomplete combustion of organic materials at 180 °C enabled the greatest release of solutes. However, the high concentration of solutes can be easily flushed out by ground surface water flow, especially in early spring, because the composition and soluble organic C at the burned site was almost equivalent to the samples without heating. The ion composition and organic C release changed with heating over 250°C. Charcoal was formed under high temperature heating, making the carbon solubility of burned organic materials lower. On the other hand, potassium and sulphuric ions increased at the higher heating temperature. Potassium being abundant in larch leaves was easily released by the decomposition of litter under high temperature combustion. Ambient temperature of the organic horizons in the Siberian forest influences the physical and chemical properties of organic horizons, controlling the dynamics of biogenic elements in the Siberian permafrost ecosystems.

Acknowledgement

This study was supported by a Grant-in-Aid for Scientific Research (C) (No. 19580070) of Japanese Society for the Promotion of Science (JSPS) and by a core to core program (No. 17001) of JSPS.

References

- Kawahigashi M, Kaiser K, Rodionov A, Guggenberger, G (2006) Sorption of dissolved organic matter by mineral soils of the Siberian forest tundra. *Global Change Biology* 12, 1868-1877.
- Kawahigashi M, Do NM, Nguyen BV, Sumida H (2008) Effects of drying on solutes release from acid sulfate soils distribute in Mekong Delta, Vietnam., *Soil Sci. Plant Nutr.* 54, 495-506.
- Ito A (2005) Modelling of carbon cycle and fire regime in an east Siberian larch forest. *Ecol.Modelling*, 187, 121-139.
- Nambu K, Yonebayashi, K. (1999) Acidic properties of dissolved organic matter leached from organic layers in temperate forests. *Soil Sci. Plant Nutr.* 45, 65-77.
- Prokushkin AS, Tokareva IV (2007) The influence of heating on organic matter of forest litters and soils under experimental conditions. *Eurasian Soil Sci.* 40, 628-635.
- Prokushkin AS, Knorre AA, Kirdeyanov AV, Schulze ED (2006) Productivity of mosses and organic matter accumulation in the litter of Sphagnum larch forest in the permafrost zone. *Rus. J. Ecol.* 37, 252-260.
- Pokrovsky OS, Schott J, Kudryavtzev DI, Dupre B (2005) Basalt weathering in Central Siberia permafrost conditions. *Geochimica Cosmochimica Acta* 69, 5659-5680.

Influences of applying biosolids on the characteristics of five alkaline soil series and biomass of switchgrass

Hung-Yu Lai^A, Liang-Ying Lin^B, Cheng-Tai Fu^C, Kai-Wei Juang^D and Bo-Ching Chen^E

^ADepartment of Post-Modern Agriculture, MingDao University, Changhua, Taiwan, Email soil.lai@mdu.edu.tw

^BDepartment of Soil and Environmental Science, National Chung Hsing University, Taichung, Taiwan, Email grobanlin@yahoo.com.tw

^CDepartment of Horticulture, National Chung Hsing University, Taichung, Taiwan, Email a035774827@yahoo.com.tw

^DDepartment of Agronomy, National Chia-Yi University, Chia-Yi, Taiwan, Email kwjuang@mail.ncyu.edu.tw

^EDepartment of Post-Modern Agriculture, MingDao University, Changhua, Taiwan, Email bcchen@mdu.edu.tw

Abstract

Biosolid (BS) contains abundant in organic matter and nutrients. In order to investigate its positive and negative effects after land application, a pot experiment was conducted using five alkaline soil series amended with different proportions of BS. Amendments of BS efficiently improved the pH value to the neutral levels and significantly increased the contents of organic carbon (OC) and available nutrients in soils, the dry weight (DW) of switchgrass (*Panicum virgatum* L.) also increased. BS significantly increased the electrical conductivity (EC) and concentrations of copper (Cu) and zinc (Zn) in soils.

Key Words

Biosolid, copper (Cu), switchgrass, zinc (Zn)

Introduction

Land-filled and incineration are the two major methods of treating BS produced by wastewater treatment plants. However, because of the limitation of land uses in Taiwan and the enrichment of nutrients and OC in BS, land application of BS seems to be a feasible method in the future. Results of previous studies show that the application of BS increased the yield of barley (Vlamiš *et al.*, 1985; Gardiner *et al.*, 1995) because of the high content of nutrients in BS. Switchgrass, the test crop used in this study, is primary distributed in central and eastern America and it can be further used to produce biomass energy. The objective of this study is to assess the effect of BS on the soil characteristics and the biomass of switchgrass when BS was applied to five alkaline soils.

Methods and Materials

Sampling and Analysis of soil and BS

Five major soil series from cropped lands in Changhua county and Kaohsiung county were used in this study: Chunliao series (Cl), Lukang Series (Lu), Taikang series (Tk), Tapais series (Tp), and Wanho series (Wa). The collected soil samples were air-dried, ground, and passed through a 10-mesh sieve. The basic characteristics analyzed were pH value (water: soil = 2: 1; Thomas 1996), available Ca, Mg, K, and Na (Mehlich, 1984), OC (Nelson and Sommers, 1996), EC (Rhoades, 1996), and the total concentration of Cu and Zn (EPA/Taiwan 2002). The BS was collected from a wastewater treatment plant located in central Taiwan. After pretreatment and except for pH value (water: soil = 5: 1), the same characteristics as for soils were measured.

Incubation

The four treatments of this study included (a) control (BS-CK): without applying BS, (b) BS-2%: applying 20 g of BS per kilogram of mixture of soil and BS, (c) BS-5%: applying 50 g of BS per kilogram of mixture of soil and BS, (d) BS-10%: applying 100 g of BS per kilogram of mixture of soil and BS. One kilogram of each mixture was added into a rectangle (length 22 cm x width 15 cm x height 5 cm) and then placed in a thermostatic chamber at 20 °C. After incubation for three months, the soil samples were air-dried, ground, passed through 10-mesh sieves, and analyzed as described in section 2.1.

Pot experiment

A pot experiment was carried out in the phytotron, the air temperature was controlled (day/night = 30/25°C). A uniform mixture of 30 g of incubated soil sample and 70 g of quartzose sand was added into each pot (10 cm in diameter and 6.5 cm in height) with three replicates. The quartzose sands were passed through 20 mesh sieves and desalted with diluted HCl and deionized water to remove contaminants. One hundred seedlings of switchgrass, one week after germination, were planted in each pot and added deionized water two times per day. Plants were harvested after growing for 30 days, rinsed with tap water to remove adhered soils, and then washed

with deionized water to avoid interference. The DW were determined after oven drying at 70°C for 48 hours. Plant tissues were ground, digested using H₂SO₄/H₂O₂ method (Harmon and Lajtha, 1999), and then Cu and Zn concentrations in the digestant determined with an atomic absorption spectrometer (Perkin Elmer, AAnalyst 200).

Results and Discussion

Basic characteristics of soil and biosolid

Except for sandy clay loam Tk, the texture of Cl, Lu, Tp, and Wa was the same (sandy loam). They were all alkaline soils (pH ranged from 7.20 to 7.91) with low EC (0.1-0.8 dS m⁻¹) and moderate OC (0.2-3.4%). The initial concentration of Cu and Zn was less than 40 mg kg⁻¹. The used BS has abundant available P (962 mg kg⁻¹), available K (202 mg kg⁻¹), and OC (29.4%). Its pH value was 4.90 and EC (11.9 dS m⁻¹) was more than the threshold (4 dS m⁻¹) for an alkaline soil. The total concentration of Cu and Zn in BS was 241 and 1,460 mg kg⁻¹, respectively.

Effect on the soil characteristics and DW of Switchgrass

Among the five soils, the highest content of OC (3.32%) was in Lu and Cl was the lowest (0.28%). Relative to CK, the content of OC for Tp and Cl was significantly increased when the BS application rate was more than 2% ($p < 0.05$). BS also increased the OC in Wa, Tk, and Lu, but its effect was only statistically significant compared with CK when the applying rate was more than 5% or 10% (Figure 1a). Because of the higher content of available P in the BS (962 mg kg⁻¹), the available P in the five soils significantly increased even when the application rate was 2%. The five tested soils were all alkaline soils and their pH values were in the range of 7.20-7.91. Because the BS used in this study exhibited strong acidity (pH 4.90), the application of even 2% of BS significantly decreased pH to neutral levels (Figure 1b). The pH values after amending with BS were more suitable for the growth of most plants compared with BS-CK. Higher EC and higher concentrations of Cu and Zn were found in the BS especially for Zn. The application of BS significantly increased the EC and total concentration of Cu and Zn in the soils ($p < 0.05$). The EC values of the five soils were all less than 0.75 dS m⁻¹ without amending with BS, however, they significantly increased to the levels of 0.50-2.5 after amending with BS ($p < 0.05$) (Figure 1c). The highest EC value was obtained in Lu treated with 10% of BS. The initial concentrations of Cu and Zn of the tested soils were all less than 50 mg kg⁻¹ which can be regarded as non-polluted soils according to the monitoring standards (200 mg Cu kg⁻¹ and 600 mg Zn kg⁻¹) of EPA Taiwan. Significant increases were found after treatment with BS, the final concentrations of Cu and Zn were however all less than 80 and 40 mg kg⁻¹, respectively.

Effect of BS on the DW of Switchgrass

The pH value of Tp and Cl was 7.91 and 7.63, respectively. Seedlings of switchgrass grown in Tp treated with BS-CK and BS-2% and Cl treated with BS-CK died possibly as a result of the unsuitable pH values. The application of BS increased the DW of switchgrass grown in five alkaline soils (Figure 1d). According to the experimental results in section 3.2, the pH value change to the neutral levels and the contents of OC and available nutrients significantly increased after amending with BS. The DW of switchgrass consequently increased.

Conclusion

The application of BS enhanced the contents of OC and nutrients in soil and, the growth and yield of switchgrass grown in five alkaline soils. However, the amount of BS applied should be controlled because of its quite high EC and contents of Cu and Zn.

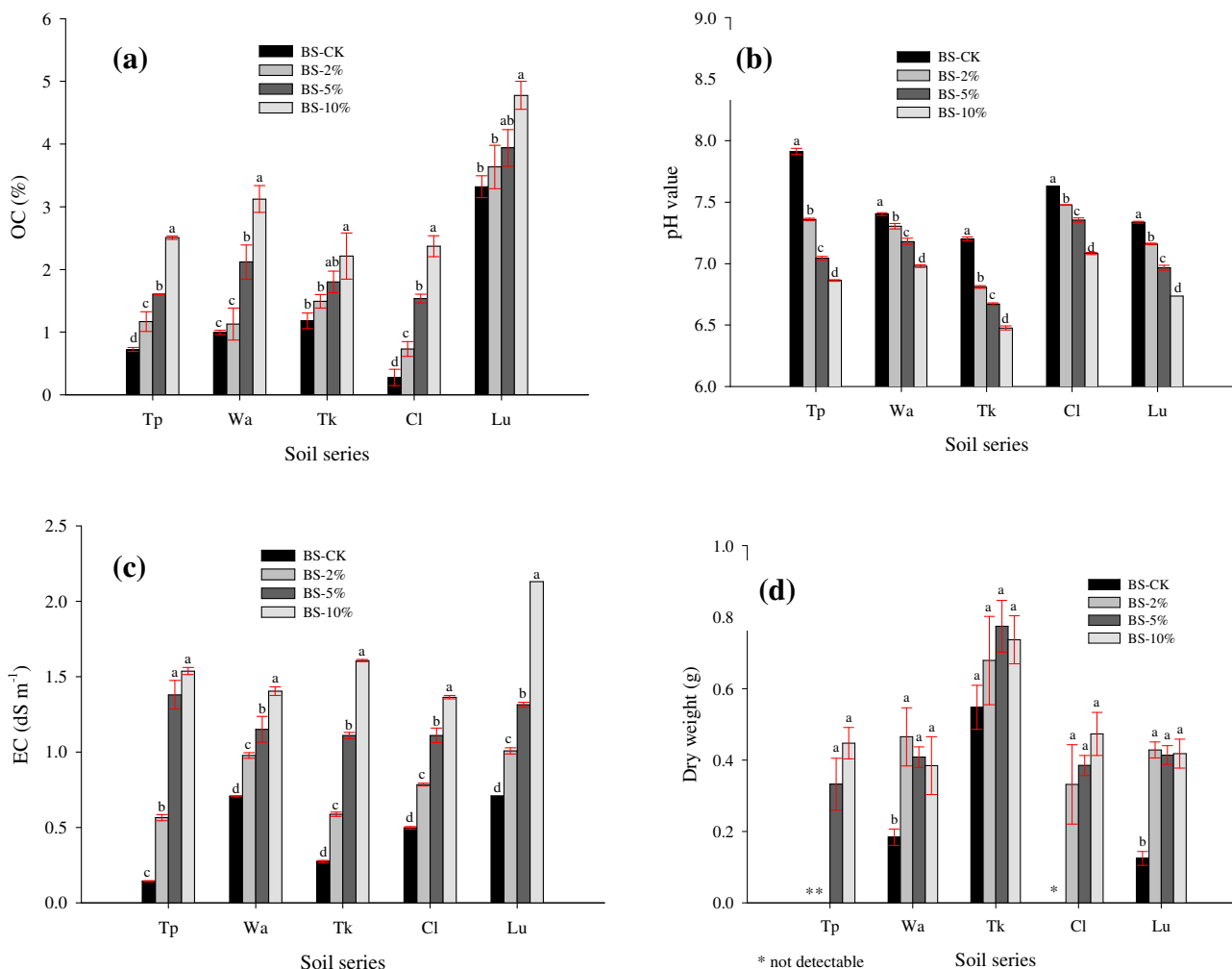


Figure 1. The effects of applying different proportions of biosolid on the (a) organic carbon content, (b) pH values, and (c) electrical conductivity of five alkaline soils and on the (d) dry weight of switchgrass.

References

- EPA/Taiwan (2002) The digestion methods of heavy metal in soils by aqua regia, Method code No: NIEA S321.62C. (Environmental Protection Administration of Taiwan ROC: Taipei, Taiwan).
- Gardiner DT, Miller RW, Badamchian B, Azzari AS, Sisson DR (1995) Effect of repeated sewage sludge application on plant accumulation of heavy metal. *Agriculture Ecosystem and Environment* **55**, 1-6.
- Harmon ME, Lajtha K (1999) Analysis of detritus and organic horizon for mineral and organic constituents. In 'Standard Soil Methods for Long-term Ecological Research'. (Eds. Robertson GP, Coleman DC, Bledsoe CS, Sollins P.), pp. 143-165. (Oxford University Press, Inc.: NY, USA).
- Mehlich A (1984) Mehlich 3 soil test extractant: A modification of Mehlich 2 extractant. *Communications in Soil Science and Plant Analysis* **15**, 1409-1416.
- Nelson DW, Sommers LE (1996) Total carbon, organic carbon, and organic matter. In 'Methods of Soil Analysis, Part 3—Chemical Methods'. (Eds. Sparks DL, Page AL, Helmke PA, Loeppert RH, Soltanpour PN, Tabatabai MA, Johnston CT, Sumner ME), pp. 961-1010. (ASA and SSSA: Madison, WI, USA).
- Rhoades JD (1996) Salinity: Electrical conductivity and total dissolved solids. In 'Methods of Soil Analysis, Part 3—Chemical Methods'. (Eds. Sparks DL, Page AL, Helmke PA, Loeppert RH, Soltanpour PN, Tabatabai MA, Johnston CT, Sumner ME), pp. 417-435. (ASA and SSSA: Madison, WI, USA).
- Thomas GW (1996) Soil pH and soil acidity. In 'Methods of Soil Analysis, Part 3—Chemical Methods'. (Eds. Sparks DL, Page AL, Helmke PA, Loeppert RH, Soltanpour PN, Tabatabai MA, Johnston CT, Sumner ME), pp. 475-490. (ASA and SSSA: Madison, WI, USA)
- Vlamiš J, Williams DE, Corey JE, Page AL, Ganje TJ (1985) Zinc and cadmium uptake by barley in field plots fertilized seven years with urban and suburban sludge. *Soil Science* **139**, 81-87.

Interactions of organic pollutants with soil components investigated by means of molecular modelling

Martin H. Gerzabek^A, Daniel Tunega^A, Adelia J. A. Aquino^A, Hasan Pasalic^B, Georg Haberhauer^C, Hans Lischka^{B,D}

^AInstitute of Soil Research, Dep. Forest and Soil Sciences, University of Natural Resources and Applied Life Sciences Vienna (BOKU), Peter-Jordan-Straße 82, A-1190 Vienna, Austria, Email martin.gerzabek@boku.ac.at

^BInstitute for Theoretical Chemistry, University of Vienna, Währingerstrasse 17, A-1090 Vienna, Austria

^CAustrian Institute of Technology, A-2444 Seibersdorf, Austria

^DInstitute of Organic Chemistry and Biochemistry, Academy of Sciences of the Czech Republic, Flemingovo nam.2, CZ-16610 Prague 6, Czech Republic

Abstract

The major objective of our work is to develop new tools based on theoretical methods for a quick first assessment of the potential behaviour of new compounds in soil interfaces based on a hypothesis that the behaviour of organic compounds on micro scale is driven by interactions of these compounds on the nano scale. Methods of computational chemistry can contribute to elucidate basic processes involved. These methods cover a large range of techniques (especially quantum chemical methods (DFT, DFTB), force-field methods, molecular dynamics (MD), and Monte Carlo(MC)). In this work an intensive study was conducted concerning sorption of polycyclic aromatic hydrocarbons (PAHs) on soil mineral goethite. Here, relatively large sorption energies were calculated. We found a relation between the surface structure/shape of the PAHs molecules and sorption energies. Linear PAHs, especially anthracene, showed the strongest sorption. The origin of adsorption is mostly in dispersion/polarization interactions between surface OH groups and π -electrons of PAHs. Studies of interactions of humic moieties under different chemical environment showed a clear impact of the hydrophobicity of the environment on the observed Gibbs free energies. Owing to the structural complexity and flexibility of humic substances (HS) various “nano” pores and holes can be formed in their structure. These spaces can be filled by various small molecules, e.g. water. Water molecules can form in these spaces a stable network of hydrogen bonds, thus creating “wet spots” in HS.

Key Words

goethite, humic substances, MCPA, molecular modelling, PAHs

Introduction

The progress in a computational power and performance allows an increasing use of various methods developed in theoretical chemistry also for more complex systems like soil. During last ten years, a wide range of model systems was investigated. This includes e.g. the complexation of aluminium cation in the soil solution (Tunega *et al.*, 2000), molecular models of functional groups in humic acids and their interactions (Aquino *et al.*, 2008), interactions of organic chemicals with active sites on surfaces of aluminosilicates and iron oxide-hydroxides (Aquino *et al.*, 2003, 2007), benzene and polycyclic aromatic hydrocarbons (PAHs) in the adsorbed state on iron oxide-hydroxides (Tunega *et al.*, 2009), the interaction of herbicides (phenoxyacetic acid derivatives) with clay surfaces (Tunega *et al.*, 2004) and organic moieties (Aquino *et al.*, 2007). In the present paper we show examples of our most recent research work, elucidating specific mechanisms of interactions on the molecular level. Number of organic compounds on the market possibly released to the environment is increasing year by year and as is the necessity of an early screening of the environmental behaviour of such compounds. The general aim is to develop a toolbox of theoretical methods and models as a basis for an early evaluation of the possible mobility of organic compounds in the soil matrix.

Methods

Goethite

Goethite is a common soil mineral. Its sorption affinity is directly related to surface structure and shape of particles. The size of particles, can vary from 10 to 1000 nm. Goethite specific surface area is relatively high (50–200 m²/g) (Schwertmann and Cornell 1991). One of the most populated goethite surfaces is parallel to the (110) crystallographic plane. This surface is formed from three types of hydroxyl groups: i) OH bound to one iron atom referred as hydroxo sites, ii) hydroxyl groups connected to two iron atoms referred as μ -OH sites, and iii) sites, where oxygen atom is bound to three iron atoms (μ 3-O_IH, μ 3-O_{II}H, and μ 3-O_{III}), referred as μ 3-hydroxo sites. In this work, density functional theory (DFT) calculations were performed to study the interaction

of the (110) goethite surface structure with a set of mono- and polyaromatic compounds, respectively. For this aim the periodic slab model of the (110) surface was constructed on the basis of the experimental bulk structure. The vacuum space of ~ 20 Å was added in a direction to separate individual slabs. The final computational super cell was orthorhombic with lattice vectors $a = 30$ Å, $b = 10.97$ Å, and $c = 18.23$ Å. The electronic structure calculations were performed with the Vienna ab initio simulation package (VASP) using a spin-polarized DFT (SP-DFT) formalism. The local density approximation (LDA) and the generalized gradient approximation (GGA) were used for the description of the electron exchange-correlation interaction.

Solvent effects

The thermodynamic cycle was used to compute formation Gibbs free energies of three hydrogen-bonded complexes (acetic acid dimer, acetic acid-acetamide, acetic acid-methanol) in three solvents with a different polar strength: water, chloroform, and n-heptane. Only the most stable complexes in gas phase with two cyclic hydrogen bonds were considered. Gibbs free energies of solvation were calculated by means of the explicit and implicit solvation models. Within the explicit solvation model, force-field based MD and MC statistical mechanical simulations in a canonical (NVT) ensemble with a free energy perturbation technique (FEP) were performed on models where studied species were placed in a certain number of solvent molecules in a periodic box. In gas phase, full geometry optimisations of the investigated hydrogen-bonded complexes and their individual constituents were performed quantum-chemically at the DFT level of theory using the hybrid B3LYP functional and the TZVPP basis set. Implicit solvation model (solvent is represented by dielectric continuum with a specific dielectric constant) was studied by means of the COSMO (COnductor like Screening Model) and PCM (Polarizable Continuum Model) approaches as implemented in quantum chemical programs Turbomole and Gaussian using the B3LYP/TZVPP level of theory. For all examined complexes and their respective monomers in solution, full geometry optimisations were performed.

Humic acid nano pores

The modeled configuration involves a stable hydrogen-bonded complex of two polyacrylic acid trimers (TC), formed as each carboxyl group of one trimer is bound via two hydrogen bonds to the opposite carboxyl group of the second trimer. An increasing number of water molecules are added to this aggregate, which is used to study their above-mentioned capacity of holding the two chains together even though their distance is too far for direct hydrogen bonding between the carboxyl groups. Consecutive hydration of TC was studied at different distances between the trimer chains by adding 1-10 water molecules to the TC structure. The geometry optimisations were carried out using two quantum chemical approaches, DFT and DFTB. DFT calculations were performed with the PBE functional and the SVP basis set in order to obtain benchmark results. In addition to the geometry optimisations, molecular dynamics (MD) simulations were performed using the DFTB method.

Results

Goethite – PAHs interactions

A systematic DFT study of interactions between a set of mono- and polyaromatic hydrocarbons (PAHs) and the (110) goethite surface was performed in this work (Figure 1). It was found that PAHs form relatively weak surface complexes having their molecular plane practically parallel to the surface plane. The origin of the interactions is in the polarization of the π -system by polar OH groups and in the formation of weak hydrogen bonds where the π -system acts as a proton acceptor. The computed averaged perpendicular distances of the molecular plane of PAHs to the hydrogen atoms of the surface OH groups range from 2.3 to 2.7 Å. Computed interaction energies regularly increase for the linearly shaped molecules from benzene to anthracene. Two other PAHs with a non-linear shape, phenanthrene and pyrene, are less strongly bound to the surface although they have a similar (phenanthrene) or even larger size (pyrene) than anthracene. These differences were explained by the specific configuration of the surface hydroxyl groups of goethite. The three types of OH groups, μ -OH, μ 3-O_{II}H, and -OH, form a valley, the width of it fits very well the molecular shape of the linear PAHs. It was found that with anthracene as example the linear PAHs can easily slide along the valley of OH groups with practically no barrier. In summary it is concluded from our results that the (110) goethite surface will withhold linear PAHs significantly better than non-linear ones.

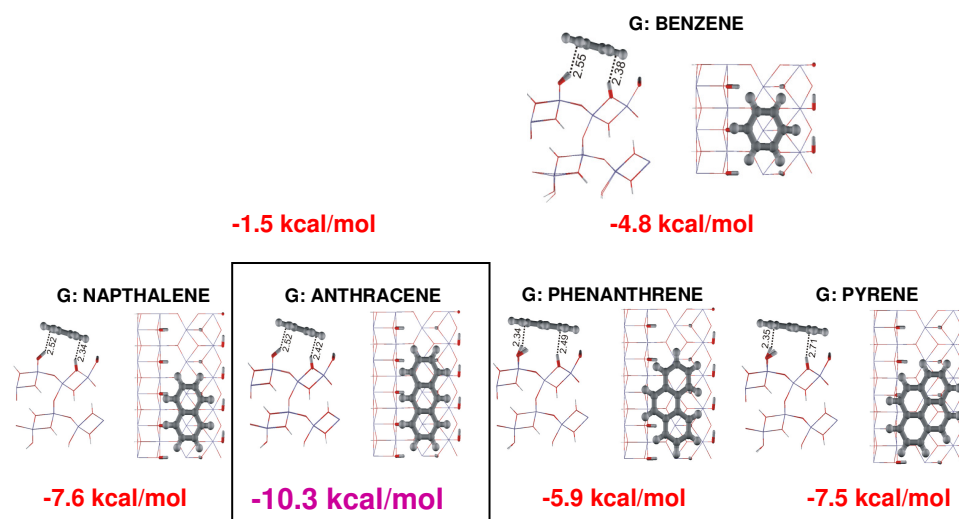


Figure 1. Two views on the optimized surface complexes of the (110) goethite surface with benzene, naphthalene, anthracene, phenanthrene, and pyrene. Dotted lines and numbers represent the averaged perpendicular distances between the molecular plane of the PAHs and the hydrogen atoms of the surface OH groups μ -OH (left) and μ_3 -OH (right), respectively. Black circles represent the surface OH groups with the shortest distance to PAHs (Tunega *et al.*, 2009)

Solvent effects

Solvent effects are of crucial importance to approach more realistic model systems. The thermodynamic stability of selected set of benchmark hydrogen-bonded systems was studied with the goal of obtaining detailed information on solvent effects using water, chloroform and n-heptane as representatives for a wide range in the dielectric constant. It was found that owing to the large perturbing effect of water, the cyclic acetic acid dimer is not stable in aqueous solution. In less polar solvents the double hydrogen bond structure of the acetic acid dimer remains stable. This finding is in agreement with previous theoretical and experimental results. A similar trend as for the acetic acid dimer is also observed for the acetamide complex. For the methanol complex it was found that it is thermodynamically neither stable in gas phase nor in any of the three solvents. Table 1 collects calculated complex formation Gibbs free energies for three complex models in three solvents.

Table 1. Gibbs free energies (ΔG^{sol}) at $T = 298\text{K}$ for the complexation reactions in water (H_2O), chloroform (CHCl_3) and n-heptane (C_7H_{16}) determined from different free energy estimates. All values are given in kcal/mol. (Psalic *et al.*, 2009)

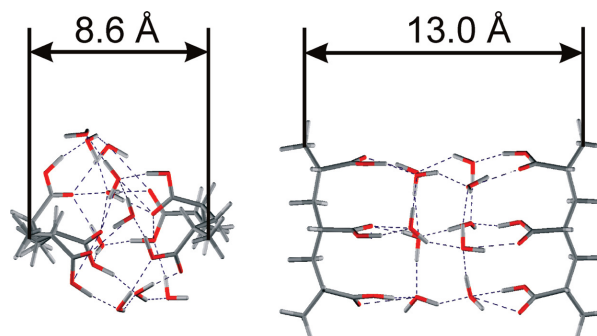
	solvent	MD-FEP	MC-FEP	PCM	COSMO
$\text{AcOH} + \text{AcOH} \rightarrow \text{AcOH} \cdots \text{AcOH}$	H_2O	7.5	7.1	6.5	4.5
	CHCl_3	-3.5	-3.8	-1.5	0.7
	C_7H_{16}	-5.6	-8.0	-3.1	-2.9
$\text{AcOH} + \text{AcNH}_2 \rightarrow \text{AcOH} \cdots \text{AcNH}_2$	H_2O	8.0	7.5	7.5	7.3
	CHCl_3	-1.8	-2.1	0.9	3.2
	C_7H_{16}	-3.3	-5.6	-0.6	-0.6
$\text{AcOH} + \text{MeOH} \rightarrow \text{AcOH} \cdots \text{MeOH}$	H_2O	9.6	9.8	9.4	7.7
	CHCl_3	1.1	2.3	3.7	4.9
	C_7H_{16}	0.5	1.0	2.5	2.3

Humic substances – pore filling mechanism

Displaced polyacrylic acid trimer structures were constructed by horizontal motion of the chains relative to each other in order to study the capacity of the water cluster to hold the two chains together even though their distance is too far for direct hydrogen bonding between the carboxyl groups. DFT/DFTB geometry optimisations and DFTB molecular dynamics simulations were used to investigate the hydrogen-bonded

structures formed and to compute their relative energetic stabilities. At shorter distances between the two oligomer chains an outer solvation is only possible. However, with increasing distance between trimers the water molecules are able to penetrate into the inside of the created free space, keeping the two chains together by means of a formed hydrogen-bonded network. Significant stabilization effect in comparison with outer hydration of 10-20 kcal/mol was observed by this intrusion of water molecules at the distance of ~13 Å (Figure 2). The present model, therefore, strongly supports the hypothesized bridging and stabilization function of water molecules in humic substances provided a local distribution of appropriate functional groups available in the HS matrix (Aquino *et al.*, 2009).

Figure 2. RI-PBE/SVP-optimised poly acrylic acid trimer complex hydrated with 10 water molecules with 4C



fixation at two selected distances (according to Aquino *et al.*, 2009).

Conclusion

It was shown that tools of computational chemistry have a high potential to contribute to the elucidation of basic processes of interactions of soil constituents and organic compounds on soil interfaces on the molecular level.

Acknowledgement

We are grateful for financial support from the Austrian Sciences Fund (project P20893-N19) and the German Research Foundation, within the priority program SPP1315 project GE 1676/1-1.

References

- Aquino AJA, Tunega D, Haberhauer G, Gerzabek MH, Lischka H (2007) Interaction of the 2,4-dichlorophenoxyacetic acid herbicide with soil organic matter moieties: a theoretical study. *European Journal of Soil Science* **58**, 889-899.
- Aquino AJA, Tunega D, Pasalic H, Haberhauer G, Gerzabek MH, Lischka H (2008) The thermodynamic stability of hydrogen bonded and cation bridged complexes of humic acid models - A theoretical study. *Chemical Physics* **349**, 69-76.
- Aquino AJA, Tunega D, Schaumann GE, Haberhauer G, Gerzabek MH, Lischka H (2009) Stabilizing capacity of water bridges in nanopore segments of humic substances: A theoretical investigation. *J. Physical Chemistry C* **113**, 16468-16475.
- Pašalić H, Aquino AJA, Tunega D, Haberhauer G, Gerzabek MH, Lischka H, de Castro Georg H, Coutinho K, Canuto S (2009) Thermodynamic stability of hydrogen-bonded systems in polar and unpolar environments. *Journal of Computational Chemistry*, online published, DOI 10.1002/jcc
- Schwertmann U, Cornell RM (1991) *Iron Oxides in the Laboratory*, VCH, Weinheim
- Tunega D, Haberhauer G, Gerzabek MH, Lischka H (2000) Interaction of acetate anion with hydrated Al³⁺ cation: A theoretical study. *Journal of Physical Chemistry A* **104**, 6824-6833.
- Tunega D, Haberhauer G, Gerzabek MH, Lischka H (2004) Sorption of phenoxyacetic acid herbicides on the kaolinite mineral surface – an ab initio molecular dynamics simulation. *Soil Science* **169**, 44-45.
- Tunega D, Gerzabek MH, Haberhauer G, Lischka H (2009) Model study on sorption of polycyclic aromatic hydrocarbons to goethite. *Journal of Colloid and Interface Science* **330**, 244-249.

Investigating phosphate sorption reactions in acid soils through solution, NMR, and L- and K-edge XANES analyses.

Cassandra Schefe^A, Peter Kappen^B, Lucia Zuin^C, Paul Pigram^B, John Gehman^D, Simone Rochfort^A, Simon Ovenden^E

^AFuture Farming Research Division, Department of Primary Industries, VIC, Australia, Email Cassandra.schefe@dpi.vic.gov.au

^BCentre for Materials and Surface Science and Department of Physics, La Trobe University, Melbourne, VIC, Australia

^CCanadian Light Source, Saskatoon, Canada

^DBio 21 Institute, The University of Melbourne, VIC, Australia

^EDefence Science and Technology Organisation, VIC, Australia

Abstract

The plant availability of phosphorus (P) is decreased in acid soils through increased P sorption onto solid-phase binding sites. This is a significant problem in Victoria, Australia. This research utilised a suite of complementary techniques, including classical solution analysis, nuclear magnetic resonance (NMR) and synchrotron-based X-ray technologies (X-ray Absorption Near Edge Structure, XANES; micro X-ray fluorescence spectroscopy, μ -XRF) to investigate the forms of sorbed P in acid soils. The addition of carboxylic acids modified sorption of applied P, with oxalic acid being most effective in competing with P for binding sites. Solid state ³¹P NMR showed that inorganic P, as PO₄ was the dominant species present in the bulk soil, while XANES provided information on reactions occurring at (P L-edge XANES) or near (P K-edge XANES) the soil surface. For example, the addition of oxalic acid resulted in dissolution of surface-bound Al, exposing previously occluded P.

Key Words

Synchrotron techniques, carboxylic acids, acid soil.

Introduction

Phosphorus (P) is a key nutrient required for plant growth, with inorganic phosphate fertiliser extensively used in the production of food crops in Australia. However, the availability of this P fertiliser for plants is severely reduced in acid soils due to phosphate sorption onto aluminium (Al) hydroxides and other mineral binding sites. This is a significant problem in some areas of Victoria, Australia.

The degree to which applied P is bound onto soil surfaces in acid soils is influenced by many factors, including the type of fertiliser applied, and the presence of competing anions, such as carboxylic acids. However, most of the evidence supporting the interactions between fertiliser type and/or carboxylic acids and solid phase P binding sites has been established through measuring changes in the chemistry of soil solution, and utilising speciation modelling programs. A limitation of this approach is that these solution-based techniques can only determine gross changes in forms of soil P, without improving our understanding of solid phase processes. Therefore, in order to directly investigate P sorption reactions on soil particles, techniques such as solid-state ³¹P nuclear magnetic resonance (NMR) and X-ray absorption near edge structure (XANES), may add value.

The application of synchrotron-based techniques in soil science is relatively new, with P K-edge XANES being the technique of choice in determining 'averaged' P speciation throughout a soil sample (Hesterberg *et al.* 1999), while recently, the P L-edge XANES technique has been used to determine P speciation on soil surfaces (Ajiboye *et al.* 2007a).

The aims of this research were therefore to determine the effect of carboxylic acid addition on P sorption reactions in acid soil, utilising a range of techniques, and (ii), evaluate the sensitivity of the P L-edge XANES technique in determining P speciation on soil surfaces upon the addition of different inorganic phosphate fertilisers.

Methods

Soil collection

The selected soil was a Bleached, Eutrophic, Yellow Dermosol (Isbell, 2002) sourced from the Department of Primary Industries – Rutherglen Centre, Victoria, Australia. A single soil sample was collected from the 0-0.10

m depth, air-dried, and passed through a 2-mm sieve before use. (Soil $\text{pH}_{\text{CaCl}_2}$ 4.6).

Effect of carboxylic acid addition on P reactions in acid soil

Samples were prepared by weighing out 2.5 g samples of soil in triplicate for each treatment. Solutions of 1 mM carboxylic acids (oxalic, p-hydroxybenzoic and coumaric acids) and/or 100 mM P (as KH_2PO_4) were added to the soil in a 1:10 w/w soil:solution ratio and shaken for 17 h. After shaking, solution pH was measured, samples were centrifuged for 12 min and the centrifuged supernatant of all samples filtered through a 0.22 μm filter. The solution was then analysed for total solution P and Al by inductively coupled plasma-atomic emission spectrometry (ICPAES), carboxylic acid concentrations by high pressure liquid chromatography (HPLC), and solution P speciation by ^{31}P NMR. The remaining solid phase was further centrifuged to remove trace amounts of solution and dried in desiccators for 10 d. The dried samples were then finely ground using an agate mortar and pestle and stored in sealed vials prior to total soil P, solid-state ^{31}P MAS NMR and XANES analysis.

The XANES experiments at the P L-edge were performed at the Canadian Light Source, Saskatoon, Canada, using the VLS-PGM beamline. Samples were presented to the beamline on double-sided carbon tape. Micro-X-ray fluorescence (μ -XRF) and micro-XANES (μ -XANES) experiments at the P K-edge were performed at the LUCIA beamline of the Swiss Light Source, Paul Scherrer Institute, Villigen, Switzerland, with samples prepared on thin-sectioned epoxy resin.

Use of P L-edge XANES to determine P speciation on soil surfaces upon addition of different fertilisers

The same soil was used as that detailed above. Solutions of potassium dihydrogen phosphate (KH_2PO_4), triple superphosphate ($\text{Ca}(\text{H}_2\text{PO}_4)_2 \cdot \text{H}_2\text{O}$; TSP) and di-ammonium phosphate ($(\text{NH}_4)_2\text{HPO}_4$; DAP) were added to the soil at a range of concentrations (0, 0.5, 1, 25, 50, 100 mM) in a 1:10 w/w soil:solution ratio. Samples were shaken for 17 h. After shaking, solution pH was measured and samples were centrifuged for 12 min. The supernatant was filtered through a 0.22 μm filter and analysed for total solution P and Al by ICPAES. The remaining solid phase was further centrifuged to remove trace amounts of solution and dried in desiccators for 10 d. The dried samples were then finely ground using an agate mortar and pestle and stored in sealed vials prior to total soil P and P L-edge XANES analysis. The XANES experiments were performed on the VLS-PGM beamline at the Canadian Light Source. Beamline set-up and sample presentation was the same as that used above.

Results

Effect of carboxylic acid addition on P reactions in acid soil

Addition of the various carboxylic acids had different effects on the chemistry of P and Al in soil (Table 1). When no P was added, oxalic acid (OX) addition significantly increased the concentration of endogenous P in solution ($P < 0.005$) compared to the other treatments. Solution Al concentrations were also increased in the OX treatment compared to the untreated soil (OP) ($P < 0.001$), while solution Al was reduced in the hydroxybenzoic acid (HB) and coumaric acid (COU) treatments ($P < 0.001$). The addition of P resulted in sorption of about 5.5 mM of added P (1.7 g kg^{-1}) (Table 1), with no significant differences in sorption between the various treatments (100P, OX+P, HB+P, COU+P). Increased concentrations of Al in solution, compared to the untreated soil ($p < 0.001$; Table 1), suggest that the high concentrations of P applied may also have had an extraction effect, resulting in the solubilisation of endogenous soil Al and P (Rajan 1975).

Strong treatment effects were observed in the P L-edge XANES spectra (Figure 1). The endogenous concentration of P on the solid phase was below the detection limit, as were the coumaric and hydroxybenzoic treatments. However, a strong P signal was observed in the oxalic acid treatment, which could only have come from endogenous P (as no P added). Therefore, it is proposed that oxalic acid-mediated dissolution of Al species from the soil surface resulted in the exposure of previously occluded phosphorus.

Micro-beam techniques (μ -XRF/ μ -XANES) were used to determine the P distribution and speciation in the nil-P treatments, due to the low concentrations of endogenous soil P present ($165\text{--}176 \text{ mg P kg}^{-1}$). In the OP treatment, a slight pre-edge shoulder in the μ -XANES spectrum (Figure 2) suggests that the P may be present as phosphosiderite (Ajiboye *et al.* 2007b). The poorly-defined post-edge structure in the μ -XANES spectrum for OX (Figure 2) indicates that this P may not have been bound to an aluminosilicate mineral. The P present in the HB treatment was either adsorbed onto an Al hydroxide (Toor *et al.* 2006), or present as variscite (Ajiboye *et al.* 2007b). Low P concentrations meant little information could be gained from the COU spectra (Figure 2).

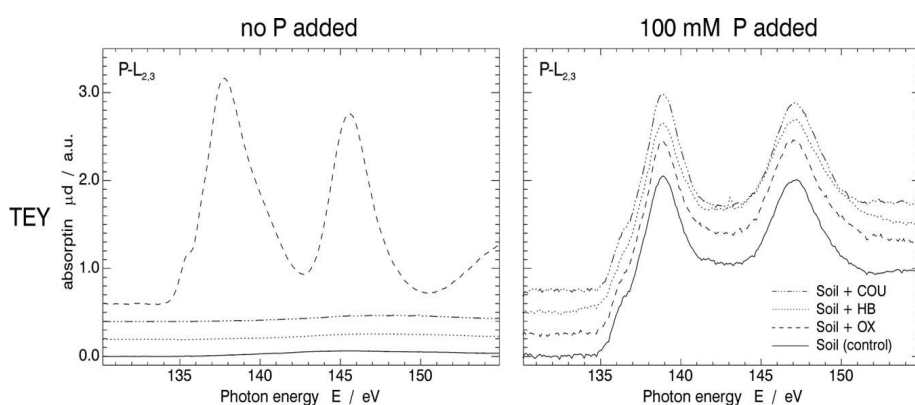


Table 1. Solution chemistry results

Sample	Solution P (mM)	Solution Al (mg/L)
0P	0.006	7.92
OX	0.011	15.64
HB	0.003	0.68
COU	0.004	1.06
100P	94.46	15.82
OX+P	94.53	24.95
HB+P	94.45	36.69
COU+P	94.67	5.17

Figure 1. P L-edge XANES spectra of no P and added P soil treatments, as measured by total electron yield (TEY).

Micro-XANES analysis of 100P was analysed at two discrete locations. The first (100P I) was located on the edge of an Al structure, with the P adsorbed to an Al mineral, likely gibbsite (Toor *et al.* 2006). The second P location (100P II) was co-located with both Al and Mg, although the μ -XANES results are somewhat inconclusive due to noise (Figure 2). A unique pre-edge shoulder and post-edge widening at the base of the white-line of the OX+P μ -XANES is proposed to be due to the P being present as an ammonium phosphate compound (Ajiboye *et al.* 2008), or P adsorption onto a Mg compound, of composition not yet defined (Figure 2). The μ -XANES spectra of HB+P and COU+P indicate that the phosphate in both samples is adsorbed onto an Al mineral, likely gibbsite (Figure 2) (Hesterberg *et al.* 1999).

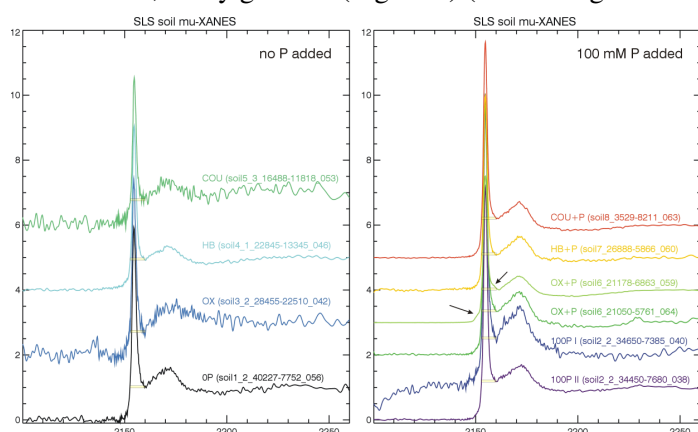


Figure 2. P K-edge μ -XANES spectra of P hotspots

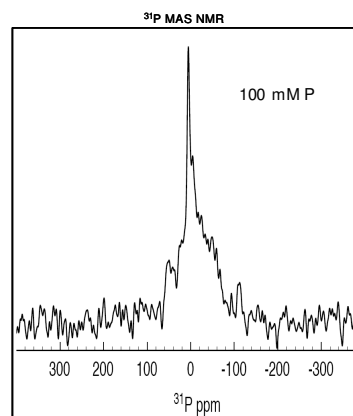


Figure 3. ^{31}P MAS NMR for the 100P treatment

The amount of P present in the 0P treatments was below the detection limit for ^{31}P MAS NMR. Phosphorus was detected in the added P treatments, with PO_4 being the dominant species (Figure 3, only 100P treatment displayed).

This research has shown that the addition of oxalic acid to an acid soil enhanced Al dissolution and exposed 'hotspots' of previously occluded P. Hydroxybenzoic and coumeric acids could not compete with P for solid phase binding sites. The amount of P sorbed did not change in the presence of carboxylic acids. This is likely due to the disparity in the P and carboxylic concentrations used (100 mM and 1 mM respectively), which were designed to reflect the likely concentrations around a dissolving fertiliser granule.

Use of P L-edge XANES to determine P speciation on soil surfaces upon addition of different fertilisers

Solid-phase P was detectable on soil surfaces by P L-edge XANES when 25 mM P was added as TSP and DAP, which equated to *ca.* 920 mg P kg^{-1} (Figure 4). The poor detection with 25 mM KH_2PO_4 addition indicates that 860 mg P kg^{-1} is on the detection limit. According to the XANES spectra, the speciation of surface-bound P does not appear to vary significantly according to P source (Figure 4). As all P sources were in the form of PO_4 , this was not unexpected. However, the quality of the spectra varied significantly between P sources at each of the rates of P addition, with DAP addition consistently producing spectra of the highest quality and intensity.

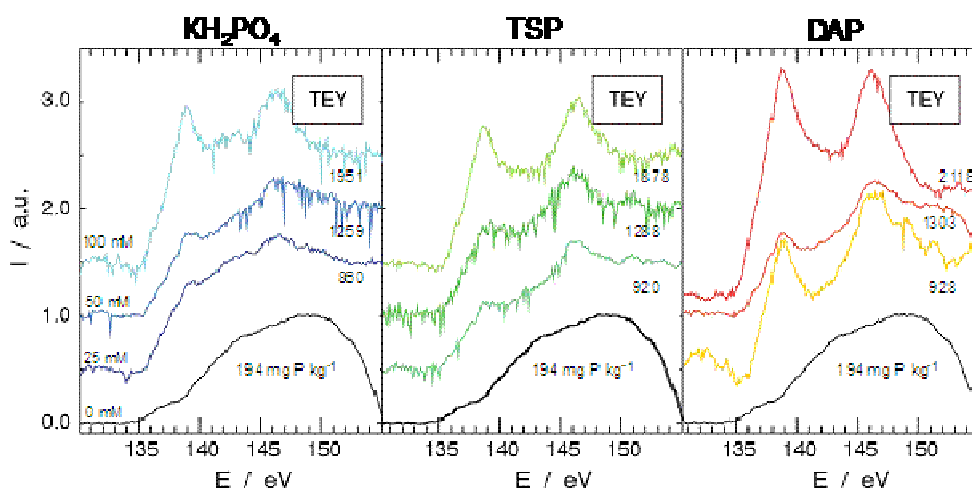


Figure 4. P L-edge XANES spectra (TEY mode) for each P source at each rate of P addition. Only 25, 50 and 100 mM P additions are shown due to lack of detection at lower levels. The values against each spectra are the soil P concentrations (mg P kg^{-1}) for each sample. Spectral ‘noise’ is due to sample charging, an effect often observed when data is collected in TEY mode.

This experiment has definitively demonstrated that the detection limit of soil P for the P L-edge XANES technique is significantly less than that required for P K-edge XANES (920 vs $1800 \text{ mg P kg}^{-1}$). Ongoing data acquisition will determine if this detection limit varies with different soil types, and further spectral interpretation will identify the dominant P species present in each treatment.

Conclusion

Synchrotron-based techniques can add value to soil P investigations as solid-state analysis can be conducted to detection limits beyond that possible using established techniques such as solid-state ^{31}P NMR. In particular, the P L-edge XANES is of benefit in determining changes in soil P chemistry on soil surfaces, as the penetration depth has been estimated to be less than 30 nm, based on Al_2O_3 data. This research has demonstrated the ability of P L-edge XANES to identify changes in the soil surface P chemistry due to the addition of carboxylic acids and/or phosphate. Due to the higher detection limit of P K-edge XANES, a micro-probe is useful in locating areas of high P concentrations, from which to gather spectra. However, a downside of using P K-edge μ -XANES is that as areas of high P concentration are preferentially measured, it is thus difficult to ascertain any treatment effects across the soil sample.

This work highlights the potential for organic C compounds to modify soil P reactions. A greater understanding of these ‘functional components’ of soil organic matter may contribute to more efficient organic matter management, resulting in enhanced P efficiency in acid agricultural soils.

References

- Ajiboye B, Akinremi OO, Hu Y (2007a) P $L_{2,3}$ - Edge XANES: A potential soil P speciation technique. In 'CLS Activity Report 2005 - 2006'. (Ed. M Dalzell) pp. 75-76.
- Ajiboye B, Akinremi OO, Hu Y, Flaten DN (2007b) Phosphorus speciation of sequential extracts of organic amendments using nuclear magnetic resonance and X-ray absorption near-edge structure spectroscopies. *Journal of Environmental Quality* **36**, 1563-1576.
- Ajiboye B, Akinremi OO, Hu Y, Jurgensen A (2008) XANES speciation of phosphorus in organically amended and fertilised Vertisol and Mollisol. *Soil Science Society of America Journal* **72**, 1256-1262.
- Hesterberg D, Zhou W, Hutchison KJ, Beauchemin S, Sayers DE (1999) XAFS study of adsorbed and mineral forms of phosphate. *Journal of Synchrotron Radiation* **6**, 636-638.
- Isbell, R (2002) The Australian Soil Classification, Revised Edition. CSIRO Publishing.
- Rajan SSS (1975) Phosphate adsorption and the displacement of structural silicon in an allophane clay. *Journal of Soil Science* **26**, 250-256.
- Toor GS, Hunger S, Peak JD, Sims JT, Sparks DL (2006) Advances in the characterization of phosphorus in organic wastes: Environmental and agronomic applications. *Advances in Agronomy* **89**, 1-72.

Iodine sorption and its chemical form in the soil–soil solution system in Japanese agricultural fields

Nao K. Ishikawa^A, Shigeo Uchida^A and Keiko Tagami^A

^ANational Institute of Radiological Sciences, Anagawa 4-9-1, Inage-ku, Chiba, Japan, Email nao@nirs.go.jp

Abstract

Iodide (Γ) or iodate (IO_3^-) sorption in two types of Japanese agricultural soil samples was investigated in consideration of microbial effects. A batch sorption test was carried out to observe sorption kinetics under 4 different experimental conditions characterized by temperature or microbial activity. The sorption kinetics results indicated that microbial activity promoted an increase of the soil–soil solution distribution coefficient. In addition, it was observed that the sorption kinetics of IO_3^- was similar to that of Γ for one sample. The results could be attributed to the fact that IO_3^- was transformed to Γ in the soil solution. Therefore, in order to discuss the difference in sorption kinetics between Γ and IO_3^- , it is important to check chemical forms of I in soil solution when IO_3^- is added to the sample.

Key Words

Iodide, iodate, sorption, microbial activity, agricultural soil.

Introduction

Long-lived iodine-129 (^{129}I ; half-life, 1.57×10^7 y) has been released into the environment during operation of nuclear facilities such as spent fuel reprocessing plants (Buraglio *et al.* 2001). ^{129}I is also one of the dominant radionuclides in transuranium waste repository assessment (JAEA and FEPC 2007). Therefore, investigating its behaviour in the environment is important. Researchers have reported on I behaviour in the soil environment, including the volatilization of I from soil to the air (Whitehead 1981; Whitehead 1984; Bostock *et al.* 2003), the effects of bacteria on I in soil (Amachi *et al.* 2003), and I sorption in soils (Yoshida *et al.* 1992). However, there have been only a few reports on the mechanistic and quantitative effects of microbial activity on I behaviour in soil (e.g., Bostock *et al.* 2003). The major chemical forms of I in the soil environment are iodide (Γ) and iodate (IO_3^-) (Gu and Schulz 1991), and I behaviour in agricultural fields such as I sorption in soil (Yoshida *et al.* 1992) and plant uptake of I (Muramatsu *et al.* 1983) have been reported to depend on the chemical forms. However, knowledge about the effect of chemical form of I on I sorption in soil is still limited. In this study, we observed sorption kinetics of Γ and IO_3^- under 4 types of experimental conditions characterized by temperature or microbial activity. Then, we observed chemical forms of I in the soil solution to check the change of chemical forms of I before and after addition of Γ or IO_3^- to soil samples.

Methods

A batch sorption test was carried out to observe sorption kinetics under 4 different experimental conditions designated ST, CO, AN, and GL (Table 1). Two soil samples were used (Table 2). Methods to determine these properties were based on our previous papers (Tagami *et al.* 2006; Ishikawa *et al.* 2008). Each soil sample and deionized water (solid/liquid ratio: 1g/10 mL) were mixed in a plastic bottle and initially shaken for 24 h. The standard condition ST, in which temperature was 23 °C, was the basic condition for determination of soil–soil solution distribution coefficient (K_d) (JAEA 2002). The condition CO, in which temperature was 4 °C, was used to determine the effect of microbial activity at low temperature on I sorption. The other 2 conditions, AN and GL, were used to observe the effects of microbial activity at normal temperature. For AN, 3 types of antibiotics were added to each sample suspension prior to shaking for 24 h to inhibit microbial activity. The initial concentration of each antibiotic was adjusted to 500 mg/L. The condition GL, in which the concentration of glucose was adjusted to 50 g/L after shaking for 24 h, was done to stimulate microbial activity. After all of the sample suspensions were shaken for 24 h, about 10 kBq of ^{125}I ($T_{1/2} = 59.4$ d) as iodide (Γ) or iodate (IO_3^-) were added to each sample bottle. IO_3^- stock solution was prepared using bromine (Muramatsu and Ohmomo 1988).

In order to obtain sorption kinetics under each experimental condition, suspension samples were destructively taken at 3 h, 1, 2, 5, 7, 9, 14, and 21 days after the addition of ^{125}I to the sample suspension. Each sample suspension was centrifuged at 3000 rpm for 10 min (Hitachi, HIMAC CT5L) and then the supernatant was filtered through a 0.45- μm membrane filter. The radioactivities of ^{125}I in the filtrate and the soil sample were measured with a NaI scintillation counter (Aloka, ARC-380). K_d is generally determined by radionuclide

concentration in liquid phase (JAEA 2002) because the added radionuclide should exist in the solid phase or liquid phase. However, it was reported that I could be released from soil to the air (Whitehead, 1981). Therefore, in this study K_d (L/kg) was calculated by the following equation:

$$K_d = (C_s/C_L) \quad (1)$$

where C_L (Bq/L) and C_s (Bq/kg-dry) are the radionuclide concentrations in the liquid phase and solid phase, respectively. Measurements by the isotope exchange method (Muramatsu and Ohmomo 1988) showed that the ^{125}I in the filtrate samples at day 7 of contact time for CO and ST conditions was distributed as 3 chemical forms: elemental iodine and organic iodide; I^- ; and IO_3^- .

Table 1. Experimental conditions.

Experimental condition	Temperature (°C)	Solution
ST	23	Deionized water
CO	4	Deionized water
AN	23	500 mg/L of streptomycin, tetracycline, and cycloheximide
GL	23	50 g/L of glucose

Table 2. Properties of soil samples.

Properties		Sample No.	
		EP-8	EF-38
Clay	(%)	22	22
EC (H ₂ O)	($\mu\text{S}/\text{cm}$)	72	117
pH	(H ₂ O)	6.0	7.2
CEC	(meq/100g)	11	12
C in soil	(g/kg)	21.2	24.1
I in soil	(mg/kg)	0.6	5.1

Results and discussion

Chemical forms of I in soil solution

Figure 1 shows the percentage of each chemical form of I in the soil solution to the initially added I in each sample at day 7 after contact with I under conditions CO and ST. I in soil solution was mainly present as I^- when I^- was added to the sample bottle, while some IO_3^- became I^- in soil solution when IO_3^- was added to the samples. The chemical form of IO_3^- did not change in the control sample which contained deionized water and IO_3^- , therefore, the soil may affect the chemical form change from IO_3^- to I^- in the soil solution.

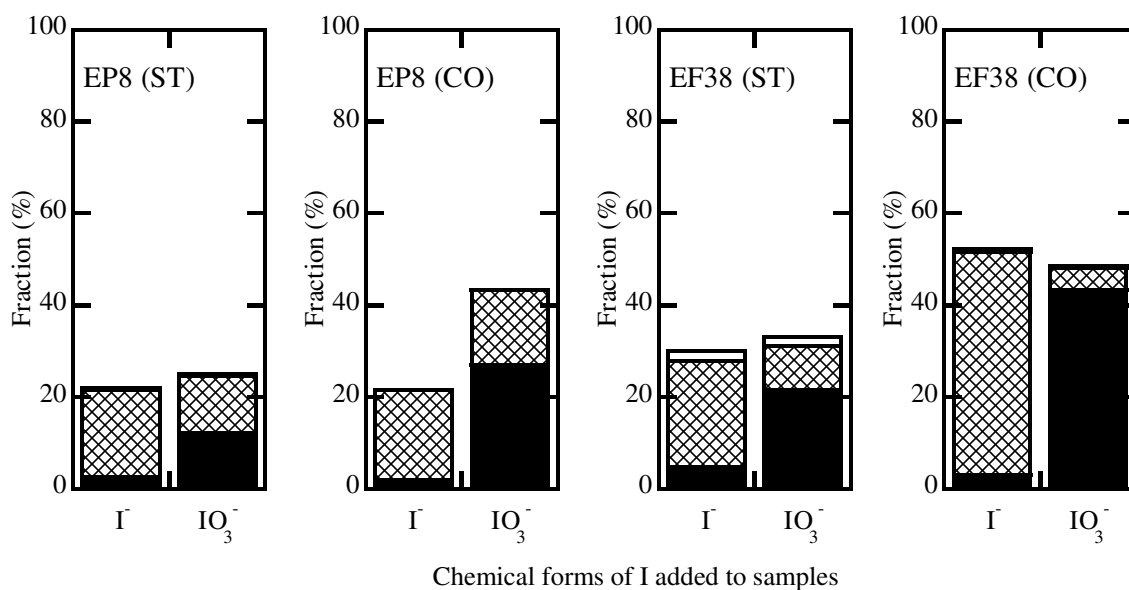


Figure 1. Percentage of elemental iodine and organic iodide (white), I^- (mesh), and IO_3^- (black) in the soil solution to the initially added I at day 7 after contact with I.

Sorption kinetics

The time variation of K_d for each chemical form of I under 4 experimental conditions is shown in Figure 2. For Γ and IO_3^- , the K_d values increased in the order: $\text{GL} > \text{ST} > \text{AN} \approx \text{CO}$, which is the same order as expected for their microbial activity. This result indicated that microbial activity promoted I uptake by the solid phase.

Comparing the sorption kinetics for Γ and IO_3^- , almost the same results were observed for EP8. For EF38, however, the sorption kinetics for Γ had higher values than for IO_3^- . Indeed, K_d under the ST condition for Γ (24 L/kg) was 3 times higher than that for IO_3^- (8 L/kg). The different results between EP8 and EF38 could be attributed to the chemical forms of I in the soil solution. As shown in Figure 1, for EP8 the amount of Γ in the soil solution when Γ was added to the sample was about the same as the amount of Γ in the soil solution when IO_3^- was added to the sample, which could confirm the similar result of Γ and IO_3^- additions. On the other hand, for EF38, which had different results for Γ and IO_3^- , the amount of Γ in the soil solution when IO_3^- was added to the sample was much lower than the amount of Γ in the soil solution when Γ was added to the sample under the ST condition. Previous studies reported K_d for IO_3^- was lower than that for Γ (IAEA 1994; Yoshida *et al.* 1992). Therefore, it appeared that the difference of sorption kinetics between Γ and IO_3^- was possibly dependent on whether IO_3^- forms Γ in the soil solution; it is recognized that IO_3^- could change its chemical form to Γ in the soil solution. The present results could not identify the major factor contributing to the change of chemical form from IO_3^- to Γ in soil solution; therefore, further studies are needed to identify the mechanisms of change of I chemical forms in soil solution.

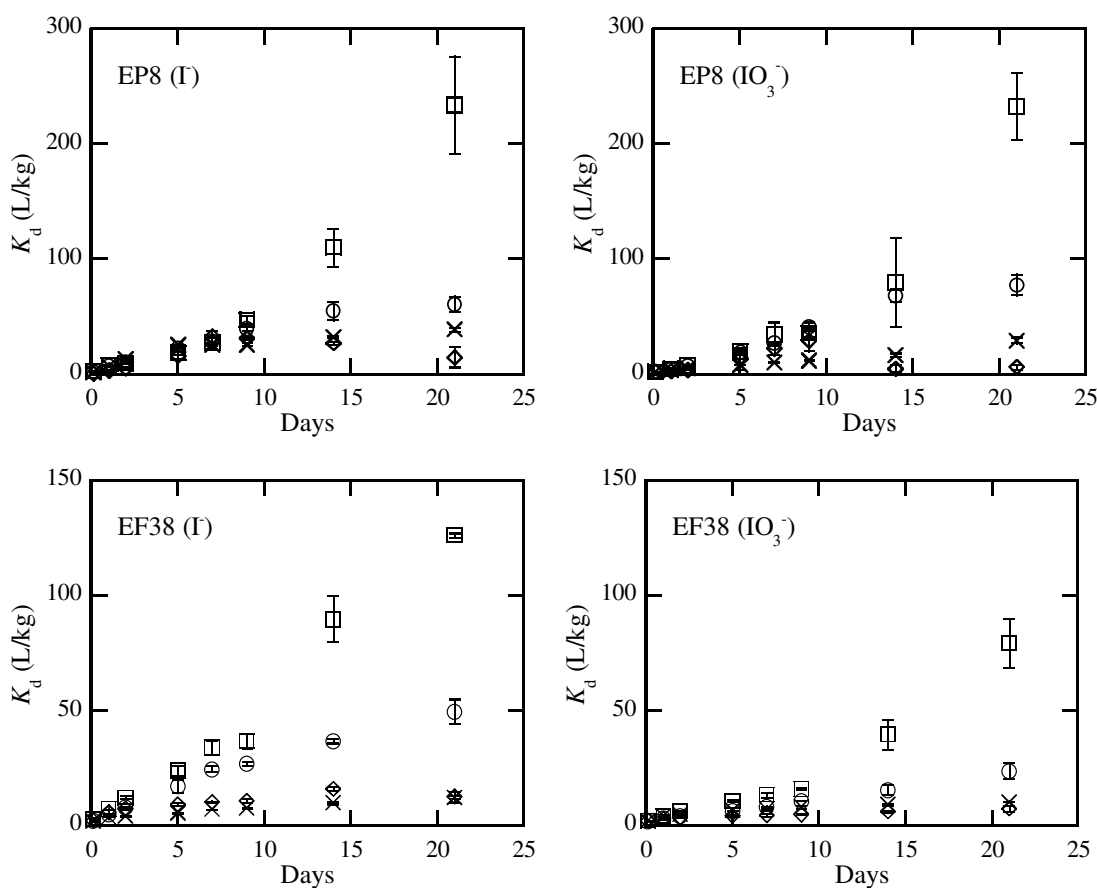


Figure 2. Time variation of the K_d values at 4 different experimental conditions: ST (○), CO (×), AN (◇), and GL (□). Error bars show standard deviation (1σ) of 3 replicates.

Conclusion

We observed the sorption kinetics of I in soil and the chemical forms of I in soil solution when Γ or IO_3^- were added to the soil–soil solution system. For Γ addition, chemical forms of I in soil solution was unchanged, while some IO_3^- in the soil solution became Γ . Our results suggested that the difference in sorption kinetics of IO_3^- possibly depended on whether IO_3^- forms Γ in the soil solution.

Acknowledgements

This work has been partially supported by the Agency for Natural Resources and Energy, the Ministry of Economy, Trade and Industry (METI), Japan. We thank Dr. N. Ishii of National Institute of Radiological Sciences for his advice about this work. In addition, Mr. T. Takamura (Tokyo Nuclear Services Co., Ltd.) is gratefully acknowledged for his technical support.

References

- Amachi S, Kasahara M, Hanada S, Kamagata Y, Shinoyama H, Fujii T, Muramatsu Y (2003) Microbial participation in iodine volatilization from soils. *Environmental Science and Technology* **37**, 3885-3890.
- Bostock AC, Shaw G, Bell JNB (2003) The volatilisation and sorption of ^{129}I in coniferous forest, grassland and frozen soils. *Journal of Environmental Radioactivity* **70**, 29-42.
- Buraglio N, Aldahan A, Possnert G, Vintersved I (2001) ^{129}I from the nuclear reprocessing facilities traced in precipitation and runoff in northern Europe. *Environmental Science and Technology* **35**, 1579-1586.
- Gu B, Schulz RK (1991) 'Anion retention in soil: possible application to reduce migration of buried technetium and iodine, NUREG/CR-5464'. (U.S. Nuclear Regulatory Commission: Washington, DC).
- IAEA (1994) 'Handbook of parameter values for the prediction of radionuclide transfer in temperate environments'. Technical Reports Series vol. 364. (International Atomic Energy Agency: Vienna)
- Ishikawa NK, Uchida S, Tagami K (2008) Soil-soil solution distribution coefficients for Se, Sr, Sn, Sb, and Cs in Japanese agricultural soils. In 'Proceedings of Waste Management '08, Phoenix, AZ'. 34-8093 pp. 1-7.
- JAEA (2002) 'Measurement method of sorption distribution coefficient – basic procedure of batch method for barrier material of near face disposal'. (Atomic Energy Society of Japan: Tokyo).
- JAEA FEPC (2007) 'Second progress report on research and development for TRU waste disposal in Japan'. (Japan Atomic Energy Agency and the Federation of Electric Power Companies of Japan: Tokai).
- Muramatsu Y, Christoffers D, Ohmomo Y (1983) Influence of chemical forms on iodine uptake by plant. *Journal of Radiation Research* **24**, 326-338.
- Muramatsu Y, Ohmomo Y (1988) Tracer experiments for the determination of chemical forms of radioiodine in water samples. *Journal of Radioanalytical and Nuclear Chemistry* **124**, 123-134.
- Tagami K, Uchida S, Hirai I, Tsukada H, Takeda H (2006) Determination of chlorine, bromine and iodine in plant samples by inductively coupled plasma-mass spectrometry after leaching with tetramethyl ammonium hydroxide under a mild temperature condition. *Analytica Chimica Acta* **570**, 88-92.
- Whitehead DC (1981) The volatilisation, from soils and mixtures of soil components, of iodine as potassium iodide. *Journal of Soil Science* **32**, 97-102.
- Whitehead DC (1984) The distribution and transformations of iodine in the environment. *Environment International* **10**, 321-339.
- Yoshida S, Muramatsu Y, Uchida S (1992) Studies on the sorption of I^- (iodide) and IO_3^- (iodate) onto Andosols. *Water Air and Soil Pollution* **63**, 321-329.

Isotopic exchange kinetics of soil P under *Pinus radiata* and Lucerne Understorey

John Scott^A and Leo Condron^B

^ALandcare Research, Hamilton, New Zealand, Email ScottJ@LandcareResearch.co.nz

^BFaculty of Agriculture and Life Sciences, Lincoln University, Lincoln, New Zealand, Email Leo.Condron@lincoln.ac.nz

Abstract

Soil inorganic (Pi) dynamics under radiata pine, radiata pine plus lucerne and lucerne alone grown in soil with high and low soil carbon (C) and phosphorus (P) concentrations was investigated. Isotopic exchange kinetics (IEK) analysis revealed that trees and lucerne combined produced a greater decline in recalcitrant forms of Pi ($E_{>3m}$ pool) than when they were grown alone, except in the high P, low C soil. In the high P, low C soil, the effect of trees and lucerne combined on $E_{>3m}$ was intermediate between the effect determined for trees and lucerne alone. There was strong evidence of significant redistribution of P from less exchangeable to more readily exchangeable IEK pools. When P and C were very low, trees and lucerne were able to actively deplete all pools and when lucerne was combined with the trees such depletion was enhanced further in the $E_{>1yr}$ pool. The redistributed P in the low P soils appeared to be taken up by plants, whereas in the high P soils the trees, trees with lucerne and lucerne alone increased the available E_{24h-3m} Pi pool. This study confirmed that changes in soil Pi forms are strongly influenced by interactions between plant species and soil P and C status.

Key Words

Exchangeable inorganic P pools, soil carbon, inorganic P, organic P, nitrogen, mineralisation

Introduction

Silvopastoral systems are a combination of forestry and agriculture with widely spaced trees that enable livestock grazing. It is practiced to achieve production objectives that would not be possible with only one of the contributing species. In New Zealand silvopastoral systems the main tree grown is radiata pine (*Pinus radiata*), with an understorey of perennial ryegrass (*Lolium perenne*) and white clover (*Trifolium repens*). Pasture production is phosphorus (P) limited in many hill country areas of New Zealand and it is generally uneconomic to apply sufficient fertiliser to remove this P limitation. It is important to elucidate the effect of land use on soil properties with the aim to increase production within fertility constraints.

Condron and Goh (1989) showed that concentrations of organic P (Po) in topsoil increased following the establishment of improved pasture. While, further New Zealand studies have shown that concentrations of organic C and P were significantly lower in mineral soil under plantation forest compared with adjacent grassland (Chen *et al.*, 2000). Increased availability of nitrogen (N) can enhance P availability (Zou *et al.*, 1995). Furthermore, a clear dependence of soil organic P forms on organic C exists (Tiessen *et al.*, 1984). Thus, the effect on P availability in a soil with varying C content and the presence of a N fixing understorey may affect P availability. We (Scott and Condron 2004) reported on Po mineralisation in soils with a range in organic C and total P (TP) concentrations under radiata pine and selected understorey forage species.

We found that the specific mineralization rate (SMR - net mineralisation rate i.e. gross mineralisation less microbial and geochemical uptake) and water soluble organic C (WSOC - is an indicator of root exudation and provides, by inference, the contribution of phosphatase enzymes, organic acids and other C compounds that might be available for microbial activity and Po mineralization) were correlated with plant P uptake. We also found radiata pine alone had the highest SMR, with radiata pine grown with lucerne (*Medicago sativa*) having a similar SMR and lucerne and ryegrass the lowest SMR. However, radiata pine plus lucerne produced the greatest biomass and along with trees alone had the greatest P uptake. P uptake under radiata pine plus lucerne was consistently high across all four soils regardless of Pi and Po availability. Consequently, an independent inorganic P dynamic was contributing to this high and consistent P uptake across all soils.

The plant availability of soil P can be characterised by considering the amount of soil solid phase P which could be taken up by a crop (quantity factor), the concentration of phosphate ions in the soil solution (intensity factor), and the ability of a soil to maintain soil solution P concentration (capacity factor) (Frossard and Sinaj 1997). Isotopically exchangeable Pi is the main source of P for most agricultural plants. Isotopic exchange kinetics (IEK) provides a method that incorporates parameters that describe the capacity and intensity factors enabling the effect of time on Pi exchange to be described. Fardeau (1985) developed an IEK model that enables the

quantity of soil exchangeable Pi over specified time periods to be determined. Consequently, we determined the IEK of three treatments, radiata pine, radiata pine grown with lucerne, and lucerne alone.

We earlier (Scott and Condron, 2004) hypothesized that the effect of conifers and understorey forage species on soil P form and availability is influenced by soil conditions (organic C, and Pi and Po concentration), which, in turn, are determined by land use history. Here we extend our earlier reported work on short term effects of radiata pine and selected pasture species on soil organic phosphorus mineralisation by reporting on the transformation of isotopically exchangeable Pi pools under radiata pine and lucerne grown in 4 combinations of high and low C and P.

Methods

Scott and Condron (2004) explained experimental details and analyses methods other than IEK. Nevertheless, briefly, radiata pine and lucerne seedlings were grown individually and in combination in 4 examples of a Templeton silt loam soil (Immature Pallic Soils (Hewitt, 1998), USDA Udic Haplustepts) containing the 4 combinations of high and low C and P for 36 weeks. The chemical, physical, and P status of the four soils are shown in Table 1. For comparison between soils, L_PL_C will be referred to as the low P low C soil, L_PH_C low P high C, H_PH_C high P high C and H_PL_C as high P low C. An equal amount of soil for each treatment (100 g) was placed in containers. Four replicates of 3 treatments imposed on each soil are reported here. Radiata pine trees only (T), trees and lucerne grown together (T+L), lucerne grown alone (L). After planting, the pots were placed on a capillary mat in a glasshouse in a split plot randomised block design. During the experiment, lucerne was sequentially harvested at growth stages suitable for grazing.

Isotopically exchangeable P

Isotopic exchange kinetic parameters and Pi pools were determined for tree and lucerne combinations following the method described by Fardeau *et al.* (1985) and Frossard and Sinaj (1997).

After the addition of carrier-free ³³P to a soil-water suspension at steady state, the radioactivity decreases with time (Fardeau *et al.*, 1985; Frossard and Sinaj, 1997) such that:

$$r_{(t)}/R = \{r_{(1)}/R\} * \{t + [r_{(1)}/R]^{1/n}\}^{-n} + r_{(\infty)}/R \quad (1)$$

Where R is the total introduced radioactivity (MBq); r₍₁₎ and r_(∞) are respectively the radioactivity remaining in the solution after 1 minute and infinity, and n is a parameter representing the disappearance rate of the tracer from the solution after one minute. The parameter, n, is the slope of the linear regression between log [r_(t)/R] and log(t). The maximum dilution of ³³P, r_(∞)/R, is estimated by the water soluble P (C_p) to total soil inorganic P (P_T) ratio :

$$r_{(\infty)}/R = 10 * C_p/P_T \quad (2)$$

An isotope exchange experimental procedure involves a 1:10 soil:solution ratio therefore 10*C_p is equivalent to the water soluble P in the soil.

Isotopically exchangeable P at time t (E_(t)) can be calculated assuming:

- (i) ³¹PO₄ and ³³PO₄ ions have the same fate in the system and
- (ii) whatever the time, t, the specific activity of the phosphate ions in the soil solution is equivalent to the isotopically exchanged ions in the whole system.

R/r₁ is the ratio of total introduced radioactivity to radioactivity remaining in solution after 1 minute. It is considered an estimate of the P sorbing capacity of the soil (Frossard and Sinaj 1997).

Three factors can be used to characterise Pi availability in soil. Firstly, the intensity factor represented by P concentration in the soil solution (C_p), Secondly, the quantity factor can be explained by the P content of the pool of free ions (E_{1min}) and the quantity of isotopically exchangeable P (E_(t)). Thirdly, the capacity factor which represents the soils fixation capacity can be described by R/r₁ and n.

The quantities of P calculated in the pools of Fardeau *et al.* (1993) multicompartamental model are:

- (i) *The pool of free ions (E_{1min})*

The phosphate in this pool is immediately available for plant uptake. The P ions are in the soil solution or if adsorbed, have the same kinetic properties as those in solution. Exchange between other pools is possible.

(ii) *P* exchangeable between 1 minute and 24 hours ($E_{1\text{min-}24\text{h}}$)

This pool represents P which can be exchanged during the time of active P uptake by a single root or root hair.

(iii) *P* exchangeable between 24 hours and 3 months ($E_{24\text{h-}3\text{m}}$)

This pool represents P which can be exchanged during the time of active P uptake by the entire root system of an annual crop.

(iv) *P* exchangeable between 3 months and a year ($E_{3\text{m-}1\text{yr}}$)

This pool represents the P which can be exchanged after the main period of active P uptake of an annual crop until the end of the agricultural year.

(v) *P* which cannot be exchanged within a year ($E_{>1\text{yr}}$)

This pool is determined as the difference between total inorganic P and the sum of the other exchangeable pools described above. The total inorganic P used was determined by the difference between total P determined by digestion and organic P.

Statistical analysis

A split plot analysis of variance was performed using Genstat 5th edition release 4.2 for Windows™ (VSN International Ltd, Oxford, UK) and an unrestricted least significant difference (LSD, $P = 0.05$) was determined to compare treatment means.

Results

Table 1. Chemical and physical properties determined for the soils prior to planting.

Soil	depth (cm)	pH	C %	N %	C/N	TP $\mu\text{g g}^{-1}$	Clay	Silt	Sand
							<2 μm ----- % volume	2-63 μm	>63 μm -----
L _p L _C	15-20	5.3	2.5	0.21	12	320	18	54	28
L _p H _C	1-5	5.2	5.1	0.40	13	524	12	47	40
H _p H _C	1-5	6.0	4.0	0.34	12	768	18	66	16
H _p L _C	0-5	6.2	2.4	0.20	12	721	13	50	36

Table 2. Isotopic exchange kinetic parameters and Pi pools determined for the soils prior to planting.

Soil	C _p (mg L^{-1})	R/r ₁	n	E _{1min}	E _{1min-24h}	E _{24h-3m}	E _{3m-1yr}	E _{>1yr}	Inorganic P	Organic P
L _p L _C	0.05	1.95	0.41	1.0	18.1	49.4	17.5	49.2	135	185
L _p H _C	0.29	1.41	0.32	4.0	30.9	61.2	23.4	92.3	212	312
H _p H _C	0.26	2.07	0.33	5.3	44.7	93.5	36.2	137.9	318	450
H _p L _C	0.16	2.15	0.32	3.5	29.7	75.1	36.4	206.0	351	370

Table 3. Effects of plant treatments and soils on differences in IEK parameters C_p, R/r₁ and n and Pi pools ($\mu\text{g P g}^{-1} - E_{1\text{min}}, E_{1\text{min-}24\text{h}}, E_{24\text{h-}3\text{m}}, E_{3\text{m-}1\text{yr}}, E_{>1\text{yr}}$) calculated between the original soils and soils after 36 weeks growth.

Soil	C _p (mg L^{-1})			R/r ₁			n		
	T	T+L	L	T	T+L	L	T	T+L	L
L _p L _C	0.003	-0.019	-0.007	0.61	0.76	-0.07	0.028	0.055	0.025
L _p H _C	-0.152	-0.155	-0.119	0.31	0.16	0.07	0.062	0.082	0.050
H _p H _C	-0.128	-0.109	-0.099	0.26	-0.07	-0.03	0.065	0.092	0.057
H _p L _C	-0.026	-0.072	-0.083	0.33	-0.18	0.21	0.018	0.089	0.101
LSD	0.033			0.37			0.062		
cf=soil	0.034			0.33			0.052		

Soil	E _{1min}			E _{1min-24h}			E _{24h-3m}			E _{3m-1yr}			E _{>1yr}		
	T	T+L	L	T	T+L	L	T	T+L	L	T	T+L	L	T	T+L	L
L _p L _C	0.2	-0.1	-0.2	7.1	5.6	-0.4	-10.3	-2.9	-9.7	-8.5	-6.2	-5.9	-18.9	-27.4	-22.1
L _p H _C	-1.7	-2.0	-1.5	-1.8	-0.9	-2.4	-9.8	-7.8	-7.7	-8.2	-8.5	-5.6	-44.8	-49.4	-22.8
H _p H _C	-2.2	-2.3	-1.9	-0.6	5.7	-1.9	11.0	20.7	1.3	-0.4	-2.3	-4.8	-43.0	-67.2	-53.7
H _p L _C	-0.1	-1.7	-1.6	3.6	2.0	5.2	7.6	18.0	24.3	-0.6	-0.8	0.02	-43.6	-87.8	-109.8
LSD	0.6			8.2			19.3			6.8			40.1		
cf≡soil	0.6			9.0			16.5			6.1			37.8		

cf≡soil indicates the LSD (P=0.05) for comparing treatment means for the same soil.

A significant redistribution of P from less exchangeable to more exchangeable fractions and IEK pools occurred.

Conclusion

IEK analysis revealed that trees and lucerne combined produced a greater decline in recalcitrant forms of Pi (E_{>3m} pool) pool than when they were grown alone (except in the high P, low C soil (H_pL_C)). In the high P, low C soil (H_pL_C), the effect of trees and lucerne combined on E_{>3m} was intermediate between the effect determined for trees and lucerne alone. The enhanced depletion of recalcitrant Pi under trees and lucerne may be related to increased N availability.

There was strong evidence of significant redistribution of P from less exchangeable to more readily exchangeable IEK pools. When P and C were very low (L_pL_C), trees and lucerne were able to actively deplete all pools and when lucerne was combined with the trees such depletion was enhanced further in the E_{>1yr} pool. The redistributed P in the low P soils (L_pL_C, L_pH_C) appeared to be taken up by plants, whereas in the high P soils (H_pH_C, H_pL_C) the trees, trees with lucerne and lucerne alone increased the available E_{24h-3m} Pi pool.

In conjunction with the work by Scott and Condrón (2004) it appeared that radiata pine was better able to utilize all forms of P when soil P and C status were low, but not in the low P, high C soil. Because the low C soils showed greater SMR and lower resin Po than the high C soils this suggests a degree of protection afforded Po by the high C, well structured soils and the possible influence of different C forms. The findings of this study confirm that changes in soil P forms are strongly influenced by interactions between plant species and soil P and C status.

References

- Chen CR, Condrón LM, Davis MR, Sherlock RR (2000) Effects of afforestation on phosphorus dynamics and biological properties in a New Zealand grassland soil. *Plant Soil* **220**, 151-163.
- Condrón L M and Goh K M 1989 Effects of long-term phosphatic fertilizer applications on amounts and forms of phosphorus in soils under irrigated pasture in New Zealand. *J. Soil Sci.* **40**, 383-395.
- Fardeau JC, Morel C, Jappé J (1985) Cinétique d'échange des ions phosphate dans les systèmes sol: solution. Vérification expérimentale de l'équation théorique. Paris: C.R. Seances Academy Sciences. T. 300, III 8, 371-376.
- Fardeau JC, Morel C, Oberson A (1993) Phosphore, matière organiques et eutrophisation des écosystèmes. In Decroux J. and Ignazi J.C. Eds., *Matières Organiques et Agricultures*. BLOIS, France: NDT.
- Frossard E, Sinaj S (1997) The isotopic exchange technique: A method to describe the availability of inorganic nutrients. Applications to K, PO₄, SO₄ and Zn. *Isotopes in Environmental and Health Studies* **33**, 61-77.
- Scott JT, Condrón LM (2004) Short term effects of radiata pine and selected pasture species on soil organic phosphorus mineralisation. *Plant and Soil* **266**, 153-163.
- Tiessen H, Stewart J W B and Cole C V 1984 Pathways of phosphorus transformations in soils of differing pedogenesis. *Soil Science* **48**, 853-858.
- Zou X, Binkley D, Caldwell BA (1995) Effects of dinitrogen-fixing trees on phosphorus biogeochemical cycling in contrasting forests. *Soil Science* **59**, 1452-1458.

Liming and acidification kinetics of some acid, neutral and alkaline soils

Arturo Aguirre Gómez^{A,B}, Frida Ma. León R.^B, Armando Aguilar M.^B

^ADepartamento de Química, Facultad de Estudios Superiores Cuautitlán-UNAM, Mexico. Email: aag@unam.mx

^BDepartamento de Matemáticas, Facultad de Estudios Superiores Cuautitlán-UNAM, Mexico

Introduction

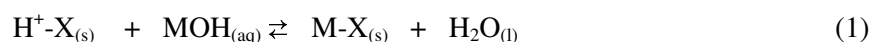
Liming (and acidification) of soils is a common agricultural practice to correct pH. The dose determination is based on traditional rapid methods (titratable acidity-alkalinity; single and double buffer methods, Exchangeable-Al (Thomas and Hargrove 1984; McLean 1982), which frequently under or overestimate the lime/acid requirements. The limitation can be amended if a correct quantitative understanding of the relationship between kinetics and the capacity-intensity acid-base chemistry.

Key Words

Lime requirement; acidification dose; neutralization kinetics

Kinetic-Buffering Theory

The equation governing the kinetic behavior of the neutralization reactions of soils are of the same nature of those found in other areas of chemistry (Frost and Pearson, 1961), soil (Sparks 1989) and environmental sciences (Stumm and Morgan 1996). Thus, as neutralization of a given soil proceeds via the direct reaction of OH⁻ ions with reactive species of the soil solids, here represented as X_(s), a general liming process can be visualized as follows:



where H⁺-X_(s) stands for the acid group to be neutralized, and M is the metal accompanying the liming material (e.g., Ca, Na, etc.). A similar equation can be generated for alkaline soils.

The reaction rate for the OH⁻ consumption due to the neutralization can be expressed by

$$v = -d[\text{OH}^-]/dt = k [\text{OH}^-]^n = k \gamma^n (\text{OH}^-)^n = k' (\text{OH}^-)^n \quad (2)$$

where $-d[\text{OH}^-]/dt$ is the consumption rate of OH⁻ ions with respect to time as the neutralization reaction proceeds; v (moles/L), is the reaction speed; k (L¹⁻ⁿ molⁿ⁻¹ s⁻¹) is the rate constant of the process and n is the reaction order, whereas $[\text{OH}^-]$, (OH^-) , γ stand for the molar concentration, the activity and the activity coefficient of OH⁻ ion, respectively. The log linearization of (2) results in:

$$\log v = \log \{-d[\text{OH}^-]/dt\} = \log k' + n \log(\text{OH}^-) \quad (3)$$

equation that can be plotted substituting $\Delta[\text{OH}^-]$ by $d[\text{OH}^-]$ and Δt by dt , for a series of diverse and several activity-values of OH⁻ ions in solutions to which the pH-value has been measured as a function of time. Thus, a $\log v$ vs. $\log(\text{OH}^-)$ plot should allow the evaluation of k' and n , from the ordinate and abscissa axes, respectively.

Materials and methods

Soil-water suspensions (10g:30dm³) of 5 substrates: humus-compost, MO, Vertisol VR (clay soil), Lixisol, LX (tropical oxidic soil), Luvisol, LV (temperate neutral-oxidic soil) and Sand, AR (inert neutral Arenosol), were acidified/alkalinized monitoring pH with time. Kinetic {pH-t and log r-log (OH⁻)} and Neutralization (Intensity-Capacity: pH-mmol H⁺/OH⁻ and Buffer intensity pH-β (=Δ[OH⁻]/ΔpH) curves were generated.

Results

Overall neutralization pH-time kinetic curves followed the order MO>SA>VR>LV>LX>AR) for pH-buffer. The pH-β [mol dm⁻³] curves resulted in maximum β-values (Figure 2). The significant log-linearized correlations obtained from the kinetic equations, $r = -d[\text{OH}^-]/dt = k'(\text{OH}^-)^n$ for liming and, $r = -d[\text{H}^+]/dt = k'(\text{H}^+)^n$ for acidification resulted in the rate constants, k' , and reaction orders, n , shown in Table 1. The (OH⁻) or (H⁺)-dependent reaction rates showed pseudo-first order kinetics for the mineral acid and neutral soils, and of second order for OM and SA. Rate constants were in the expected order of magnitude with regard to similar and different soil, environmental and chemical processes, as reported in the literature (Table 2). Figure 3 shows the increasing time depending liming requirement caused by slow reactions.

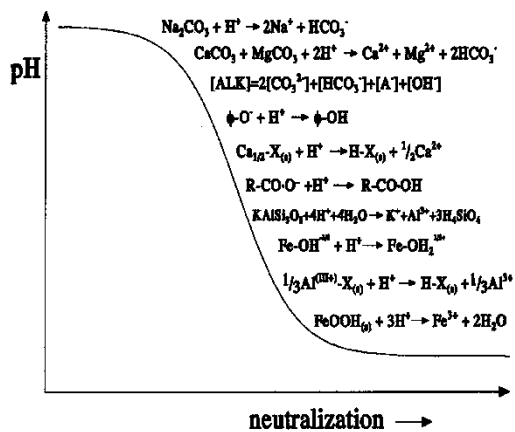


Figure 1. Schematic intensity-capacity neutralization curve of the main acidic-basic functional groups of soil materials

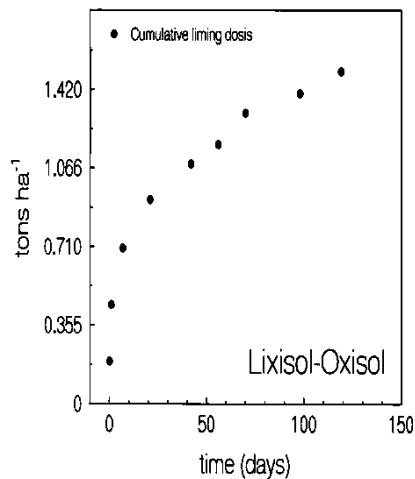


Figure 3. Increasing time dependence of the liming requirement caused by the slow neutralization reactions of functional groups, for $\Delta pH=1$

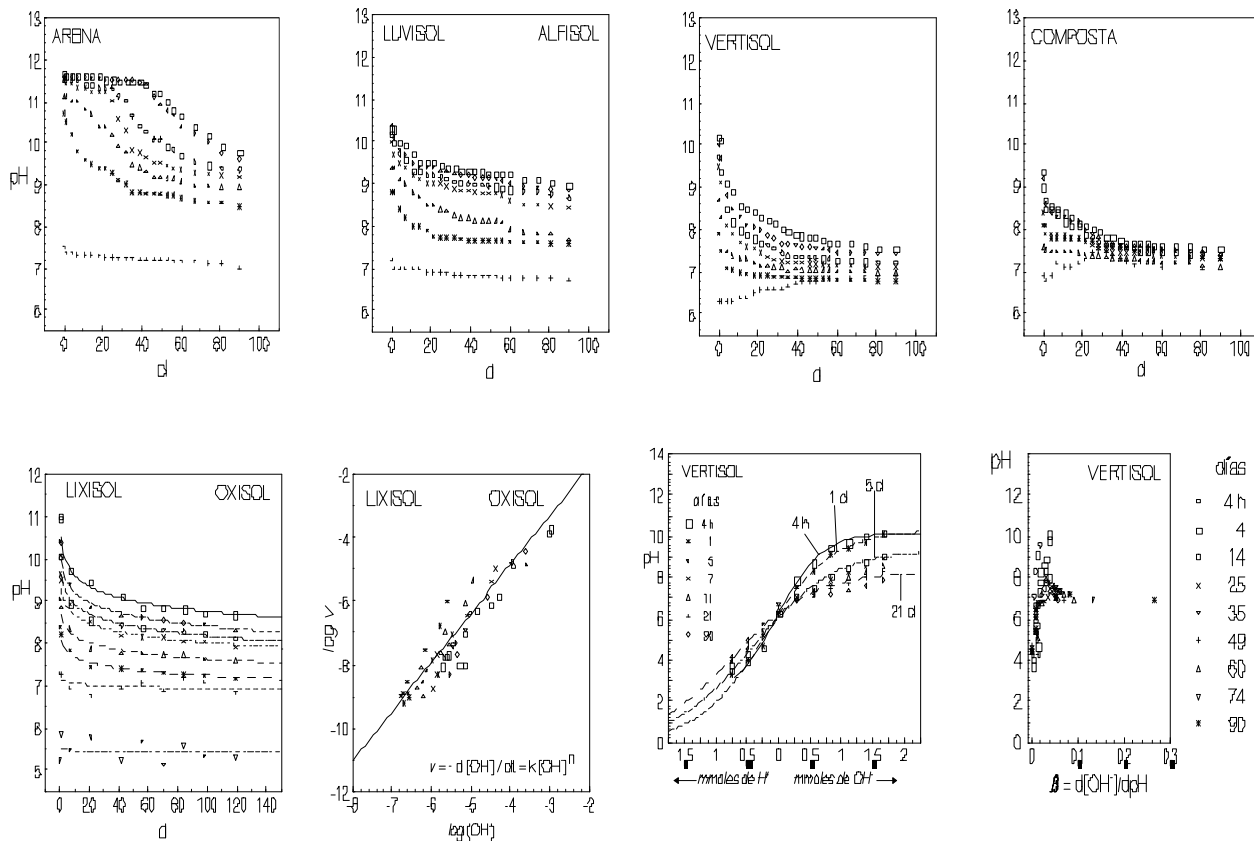


Figure 2. Schematic intensity-capacity neutralization curve of the main acidic-basic functional groups of soil materials

Table 1. Buffer intensity, pH of maximum buffering and kinetic parameters.

Soil	β_{\max}	pH_{β}	n reaction order	$k(\text{s}^{-1})$ rate constant	$\log k(\text{s}^{-1})$	k_s/k_{AR}	$r = \frac{-d[\text{OH}^-]/dt}{\text{mmolOH}^- \text{d}^{-1}}$ for $\Delta\text{pH}=1$
MO	1.87	7.54	2.10	2.9	0.46	6.3E5	0.30
VR	0.27	6.88	1.75	2E-2	-1.7	4.3E3	0.26
LX	0.06	8.72	1.55	2.6E-4	-3.6	56	2.5E-2
LV	0.08	9.34	1.32	1.6E-5	-4.8	3.5	4.2E-3
AR	0.08	9.70	1.21	4.6E-6	-5.3	1	9.4E-4
SA	0.83	8.50	2.03	26.5	1.4	5.8E6	0.36*

Table 2. Rate constants of different chemical processes occurring in nature and laboratory experiments.

REACTIONS	$\log k (\text{s}^{-1})$ $\log (\text{rate constant})$
Dissolution of silicates ^a	-13.4 (Quartz), -12.6 (Kaolinite), -10.6 (Augite), -9.5 (Olivine)
Adsorption and ion exchange ^{a,b}	2-4
Gaseous reaction in the atmosphere ^c : $\text{O} + \text{O}_3 \rightleftharpoons 2\text{O}_2$	6
Oxidation ^a of Fe^{2+} and Mn^{2+} in solution with O_2	10
Neutralization in aqueous media ^d $\text{H}^+ + \text{OH}^- \rightleftharpoons \text{H}_2\text{O}$	11
Complexation of metals ^e	-8 a 1 ($\text{Cr}^{\text{III}+}$, $\text{Co}^{\text{III}+}$)
	1-4 ($\text{Al}^{\text{III}+}$, $\text{Fe}^{\text{III}+}$)
	4-8 (Mg^{2+} , Mn^{2+} , Fe^{2+} , Ni^{2+})
	8-9 (Na^+ , K^+ , Ca^{2+} , Cu^{2+})
Neutralization of soils (this paper)	-5.3 (AR); -4.8 (LV); -3.6(LX); -1.7 (VR); 0.5 (MO); 1.5 (SA)

Conclusions

Whereas rapid methods recommended for evaluating liming or acidification requirements usually underestimate the neutralization dose, especially for soils of slow buffering reaction, the kinetic studies presented here show that the time dependence of the neutralization reaction of the acidic and basic functional groups of soils must be considered if a suitable correction of pH is to be attained. Neutralization kinetics and buffering reaction of soils are the key factors to be considered.

References

- Frost AA, Pearson RG (1961) Kinetics and Mechanism. 405pp. (Wiley & Sons, N.Y. USA.)
- Thomas GW, Hargrove WL (1984) The chemistry of soil acidity. In. Soil Acidity and liming, 2nd edn. (Ed F Adams) Agronomy Series, No 12. (ASA, CSSA and SSSA, Madison, Wisconsin, USA).
- McLean EO (1982) Soil pH and lime requirement. In 'Methods of soil analysis. Part 2'. (Eds AL Page, RH Miller, DR Keeney) No. 9. (SSSA, Madison WI, USA).
- Stumm WY, Morgan JJ (1996) Aquatic Chemistry; An introduction emphasizing chemical equilibria in natural waters. Chapter 3 (Wiley-Interscience).
- Crutzen PJ (1995) Ozone in the troposphere. In 'Composition, Chemistry and Climate of the Atmosphere'. (Ed HB Singh) pp.349-393. (Van Nostrand Reinhold, N.Y., USA).
- Snoeyink VL, Jenkins D (1980) Water Chemistry, Wiley & Sons, N.Y. USA
- Morel FMM, Hering JG (1993) Principles and Applications of Aquatic. Chemistry.
- Sparks DL (1989) Kinetics of Soil Chemical Processes. pp.210. (Academic Press, San Diego, USA.)

Linkage and structure elucidation of non-extractable NP and MCPA residues in organo-clay complexes

Patrick Riefer^A, Timm Klausmeyer^B, Alina Adams^C, Burkhard Schmidt^B, Jan Schwarzbauer^A, Andreas Schäffer^B

^A Institute for Geology and Geochemistry of Petroleum and Coal (LEK), RWTH Aachen University, Aachen, Germany, Email Riefer@lek.rwth-aachen.de

^B Institute for Environmental Biology and Chemodynamics (UBC), RWTH Aachen University, Aachen, Germany, Email Timm.Klausmeyer@bio5.rwth-aachen.de

^C Institute for Technical and Macromolecular Chemistry (ITMC), RWTH Aachen University, Aachen, Germany, Email Alina.Adams@itmc.rwth-aachen.de

Abstract

Organo-clay complexes represent an important biogeochemical interface and thus, play a major role in the immobilisation, bioavailability and persistence of xenobiotics. The ability of soil to incorporate xenobiotics varies from adsorption and sequestration phenomena to chemical reactions resulting in strong covalent linkages. In this study we want to investigate both, the characteristics of the linkages responsible for bound residues as well as the detailed structure of the non-extractable compounds. Therefore, soil samples were incubated with NP (4-(3,5-dimethylhept-3-yl)phenol) and MCPA ((4-chloro-2-methylphenoxy)acetic acid) over an incubation period of 180 and 120 days, respectively. After particle size separation humic fractions (fulvic acid, humic acid, humin) were sequentially chemical degraded to release non-extractable residues. First results showed that on incubation day one 100 % of incorporated nonylphenol derived radioactivity in FA and HA could be extracted after alkaline hydrolysis. Regarding the overall amount of applied radioactivity, on incubation day one 4 % and on day 180 7 % of applied ¹⁴C was incorporated into the humic substances via ester bonds whereas ether bonds played only a minor role in the immobilization process of nonylphenol. Measuring solid-state NMR with humic acid fractions the aromatic moiety of nonylphenol was still intact after 180 days of incubation.

Key Words

Nonylphenol, MCPA, Bound residue, Sequential chemical degradation, Ester bonds, Ether bonds.

Introduction

Regarding the incorporation behavior of anthropogenic substances the organo-clay complexes represent an important biogeochemical interface and thus, play a major role in the immobilization, bioavailability and persistence of such compounds. Klausmeyer *et al.* (not published) have shown that clay-humic complexes are a major sink for xenobiotics like 4(3',5'-dimethyl-3'-heptyl)-phenol (NP) and (4-chloro-2-methylphenoxy)acetic acid (MCPA). To assess the fate and behavior of such substances, one must distinguish between extractable and non-extractable (bound) residues. Bound anthropogenic residues are, basically, those that are not extractable by methods which do not alter their chemical structure (Khan 1982; Roberts 1984). The ability of soil to incorporate xenobiotics varies from adsorption and sequestration phenomena to chemical reactions resulting in strong covalent linkages. The amount of non-extractable residues in soil depends on time and microbial activity (Gaveo 2005). Most of the former studies dealing with bound residues used ¹⁴C-labeled compounds for investigating the amount and distribution in soil. For instance, Barriuso *et al.* (Barriuso 1991) demonstrated that bound radioactivity was located in soil size fractions as well as humic sub-fractions (humic acid, fulvic acid and humin).

The radioactive labeling on the one hand enables the quantification and distribution of compounds but on the other hand gives no information about the molecular structure and binding of incorporated substances. In this study we want to investigate both, the characteristics of the linkages responsible for bound residues as well as the detailed structure of the non-extractable compounds. Therefore, soil samples were incubated with NP and MCPA over an incubation period of 180 and 120 days, respectively. After particle size separation the clay fraction was fractionated into humic acid, fulvic acid and humin. Thereafter the humic fractions were sequentially chemical degraded to distinguish between types of linkages (e.g. ester, ether, C-C bonding) and to release non-extractable residues. The extracts here from received were measured via GC-MS. Additionally, in case of NP the humic acid fraction was measured via ¹³C-CP-MAS-NMR.

Methods

Chemicals

¹³C- and ¹⁴C-labeled 4-(3,5-dimethylhept-3-yl)phenol (NP, 304.14 MBq/mmol) was synthesized via Friedel–Crafts alkylation according to Russ *et al.* (2005). The [ring-U-¹⁴C] (4-chloro-2-methylphenoxy)acetic acid (MCPA, 59.94 MBq/mmol) was provided by Prof. M. H. Gerzabek (University of Vienna) as a mixture of 92 % MCPA methylester and 8 % of the free acid.

Spiking experiments

Aliquots of 559 µg (0.167 MBq) of ¹⁴C-MCPA dissolved in 0.5 mL methanol were applied to approx. 100 g of air-dried, homogenized, and sieved (≤ 2 mm) soil samples from Fuhrberg, Germany. In a second experiment 121 µg (0.167 MBq) of ¹⁴C-NP dissolved in 0.5 mL petrolether was similarly applied to a soil sample from the same location. Additionally 50 g of soil samples were spiked with 50 mg ¹³C-NP dissolved in petrolether. The solvent was evaporated and the flasks were shaken for 15 min in an overhead shaker. The water content of the samples was adjusted to 60% of maximum water holding capacity. The flasks were closed with an absorption device for ¹⁴CO₂ containing soda lime. The samples were incubated over a period of 180 days (NP) and 120 days (MCPA) at 20 °C in the dark.

Particle size and humic substances fractionation

Sand, silt and clay fractions were obtained by an initial manual wet sieving for separation the sand from silt and clay. Silt and clay were separated by centrifugation according to Stemmer *et al.* (Stemmer *et al.* 1998). Further on, the clay fraction containing dominantly organo-clay complexes was extracted by means of Soxhlet extraction with methanol as well as dichloromethane. The Soxhlet extracted clay was shaken with 0.5 M NaOH for 24 h and centrifuged for separating the insoluble humin fraction (HU) from humic acid fraction (HA) and fulvic acid fraction (FA). The supernatant containing HA and FA were acidified with HCl to pH 1. The precipitated HA was separated from FA by centrifugation. All fractions were dried before chemical treatment.

Sequential chemical degradation and analytical methods

FA, HA and HU fractions were separately subjected to the following degradation steps:

Step 1: Ester/amide cleavage (Alkaline hydrolysis)

Separated humic fraction was added to a mixture of methanol, water and potassium hydroxide (2 M) in a glass vessel and closed hermetically. The mixture was heated for 24 hours at 105 °C. After cooling, the solution was acidified to pH-value between 2-3 and extracted three times with diethyl ether. The combined organic layers were dried and concentrated before fractionation on silica gel columns with hexan/dichloromethane (40:60), dichloromethane and methanol.

Step 2: Ether cleavage (BBr₃)

Boron tribromide solution in dichloromethane was added to the dried sample residues from step one. The suspension was ultrasonically treated for 2 hours, then stirred at room temperature for 24 hours and finally ultrasonically treated again. The mixture was extracted three times with diethyl ether. Further work up was the same as in step 1.

Step 3: Oxidation (RuO₄)

To sample residues from step 2, NaIO₄, RuO₄, CCl₄, acetonitrile and water were added. The mixture was stirred for 4 hours at room temperature. After the reaction has been quenched with methanol and concentrated sulphuric acid, the mixture was decanted and the residues three times washed with CCl₄. After addition of water the, the CCl₄-phase was separated and the remaining aqueous solution washed three times with diethyl ether and the washing solution was combined with the CCl₄-phase. The combined organic layers were concentrated and iodine was removed by addition of sodium thiosulfate. The aqueous layer was carefully removed by pipettation and the remaining solution was dried, concentrated and fractionated with dichloromethane and methanol.

Step4: Thermochemolysis (TMAH)

The pre-extracted samples were transferred into digestion bombs and tetramethylammonium hydroxide (TMAH) in methanol (25 %) was added. After ultrasonification, methanol and oxygen were removed by a gentle stream of nitrogen. After closing, the bombs were heated for 2 h at 270 °C, and thereafter, cooled to -18 °C. The bombs content was extracted with diethyl ether, DCM and n-hexane two times. The combined organic layers were dried, concentrated and fractionated with a mixture of pentane, dichloromethane and methanol. The achieved radioactive extracts were measured by liquid scintillation counting for quantification. The extracts containing ¹³C-residues will be measured by GC-FID and GC-MS for structure elucidation. Additionally ¹³C-CP-MAS-NMR was measured with ¹³C-containing humic acid fractions to investigate the structure of the incorporated compounds.

Results

Chemical Degradation

Figure 1 presents the first results of the ^{14}C -labeled nonylphenol degradation experiments. The amount of released radioactivity is referred to the percentage of radioactivity in the specific humic fraction before chemical treatment. The percentage of released ^{14}C is the highest after cleavage of ester/amide bonds. We investigated that on incubation day one 100 % of incorporated radioactivity in FA and HA could be extracted after alkaline hydrolysis which was in detail $0.6 \mu\text{g } ^{14}\text{C}$ in FA and $2.3 \mu\text{g } ^{14}\text{C}$ in HA. However, after two weeks of incubation the percentage of released ^{14}C decreased which points to an alteration of the binding character of incorporated residues and the humic matrix, respectively. Regarding the overall amount of applied radioactivity, at day one 4 % and at day 180 7 % of applied ^{14}C was incorporated into the humic substances via ester/amide bonds. In contrary to the alkaline hydrolysis the amount of radioactivity released after further degradation steps remained approx. steady during the entire incubation period. Reaction with BBr_3 leads to a cleavage of ether and ester linkages. The low amount released indicating that the cleavage of ester bonds via alkaline hydrolysis was nearly complete.

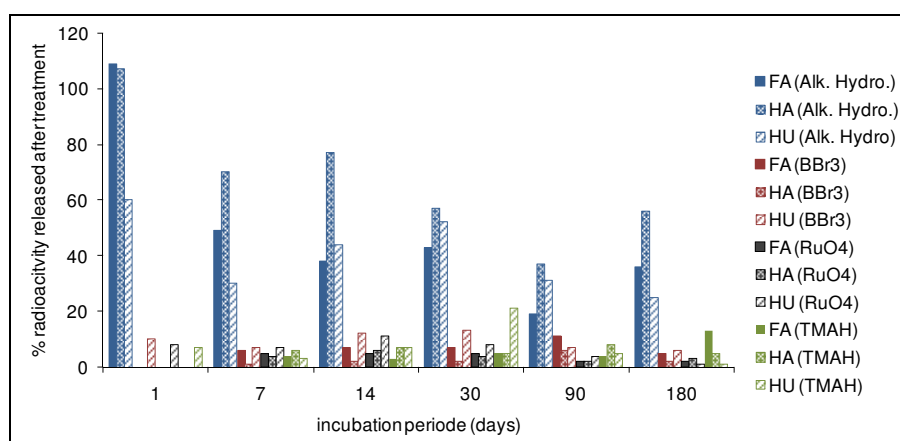


Figure 1. Percentage of released radioactivity after sequential chemical degradation. Ester/amide linkages are predominatly responsible for the formation of non-extractable NP-residues.

^{13}C -CP-MAS-NMR

Solid-state NMR provides information about the constitution of soil and sub-fractions with respect to specific functional groups. In our measurements we used humic acid fractions isolated from organo-clay complexes after different incubation days. In addition a control sample, without NP application, was also measured. The spectra show that the HA is dominated by alkyl C (45-10 ppm) followed by O-alkyl C (110-45 ppm). An overlay of all spectra shows a rise of the aromatic peak (154 ppm) over the incubation time.

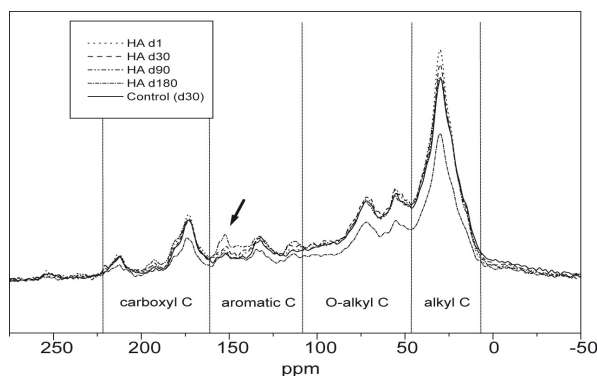


Figure 2. Overlaid solid-state NMR spectra of humic acid fraction separated after different incubation days. The marked peak at 154 ppm indicates an accumulation of the aromatic moiety during the incubation time.

To get information about an increase of the relative amount of the aromatic carbon the area ratio of the signals at 154 ppm compared with the area of the entire spectra was calculated. With increasing incubation time the ratio of the aromatic carbon peak increases. That indicates an incorporation of nonylphenol derived residues into the humic acid fraction with the aromatic moiety still intact after 180 days of incubation.

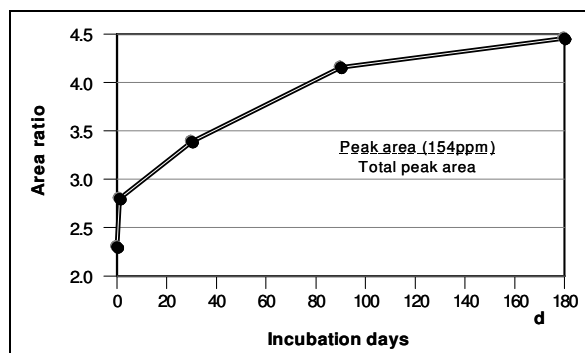


Figure 3. Enrichment of aromatic carbon in the humic acid fraction during the incubation time as shown by an increase of the area ratio of peak area (154 ppm) normalized to the peak area of the total spectra. Incubation day 0 indicates the background signal measured with the control sample.

Conclusion

Within soil sub-fractions organo-clay complexes play a major role in the immobilisation, bioavailability and persistence of anthropogenic compounds. Looking beyond radioactive balancing, sequential chemical degradation, gas chromatography coupled with mass spectrometry and solid-state NMR provide tools investigating the binding and structure characteristics of extractable and non-extractable residues in soil. For the first time we could show that nonylphenol was mainly incorporated into the humic fractions via ester/amide bonds. Moreover, the ^{13}C -CP-MAS-NMR leads to the result that the aromatic moiety of our applied nonylphenol is still intact and the amount increases over 180 days of incubation. Further investigations are still in progress to get more information about the chemical structure of bound and non-bound residues. Similar methodology will be employed with a second anthropogenic compound (MCPA).

References

- Barriuso E, Schiavon M, Andreux F, Protal LM (1991) Localization of atrazine non-extractable (bound) residues in soil size fractions. *Chemosphere* **22**, 1131-1140.
- Gevao B, Jones KC, Semple KT (2005), Formation and release of non-extractable ^{14}C -Dicamba residues in soil under sterile and non-sterile regimes. *Environmental Pollution* **133**, 17-24.
- Khan SA (1982) Distribution and characteristics of bound residues of prometryn in an organic soil. *Journal of Agricultural Food and Chemistry* **30**, 175-179.
- Roberts TR (1984) Non-extractable pesticide residues in soils and plants. *Pure and Applied Chemistry* **56**, 45-956.
- Russ AS, Vinken R, Schuphan I, Schmidt B (2005) Synthesis of branched para-nonylphenol isomers: Occurrence and quantification in two commercial mixtures. *Chemosphere* **60**, 1624-1635.
- Stemmer M, Gerzabek MH, Kandeler E (1998) Organic matter and enzyme activity in particle-size fractions of soils obtained after low-energy sonication. *Soil Biology and Biochemistry* **30**, 9-17.

Litter effects on N dynamics and potential leaching in acid grassland soils

Muhammad Riaz, Ishaq A. Mian, Malcolm S. Cresser

Environment Department, The University of York, Heslington, York, UK. YO105DD. Emails mr548@york.ac.uk,

Abstract

A reconstituted microcosm study, from N-impacted acid grassland soils, was conducted to investigate the role of litter in N dynamics in winter. The study showed that, at UK winter temperatures, litter mineralization and retention of mineral-N from precipitation were the key sources of mineral-N in the mineral soil beneath the litter layer. NH_4^+ -N produced in the litter layer was potentially mobile and resulted in significantly higher NH_4^+ -N accumulation in the upper 5 cm of mineral soils from the surface litter treatment. Mixing of litter to 15 cm depth resulted in significant NH_4^+ -N accumulation in sub-soils. NH_4^+ -N retained in the soil profiles was strongly associated with dissolved organic carbon (DOC). The low nitrification corresponded to low temperature and acidic nature of the soils, however, mixing of litter with a high C:N ratio substantially retarded NO_3^- -N production and favoured NO_3^- -N immobilization. The latter was evident from markedly lower NO_3^- -N concentrations in the drainage water.

Key Words

Nitrogen cycle; leaching; depth; retention; C: N ratio

Introduction

Litter decomposition rates and processes are generally considered key factors in cycling of N, P, S and other nutrients, and hence controls the sustainability of fertility and primary productivity of ecosystems (Henry *et al.* 2008). Dissolved organic carbon (DOC) is an immediate product of litter decomposition, entering the mineral layer (Kalbitz *et al.* 2000), and potentially retains and/or transports metals and organic compounds (Tipping *et al.* 2002). The N liberated from organic matter decomposition, if in excess of microbial and plant needs, would leach primarily as NO_3^- -N, especially for ecosystems that have attained an N-saturation state (Aber *et al.* 1998). Soil organic matter is recognized as a potential sink for NH_4^+ -N via retention on cation exchange sites so mobility of NH_4^+ is generally thought to be non-significant (Mian *et al.* 2009). Duckworth and Cresser (1991) described how the fate of ammonium and nitrate would be controlled by kinetics of their supply, availability of nitrogen and carbon, and the microbial populations associated with these transformations, together with inputs of competing cations. Riaz *et al.* (2008) showed that nitrification and immobilization of ammonium interacted to control the leaching of ammonium down the soil profile in freely draining acid grassland soils. Cresser *et al.* (2004) postulated that in heavily N-polluted upland areas of the UK, especially those with peaty and high organic matter content soils, nitrification and immobilization of ammonium are slow enough for NH_4^+ -N to be in equilibrium with cation exchange sites. When this happens, NH_4^+ -N concentrations in drainage water are similar to effective concentrations in precipitation, with only modification from mobile anion concentrations. In the same context, they also found low rates of nitrate transformations that facilitated leaching to adjacent streams. The present study, therefore, aimed to investigate in N-saturated acid grassland soils, the effects of litter on mineral-N production, mobility and retention in winter when biological uptake is low.

Methods

Site selection, soil sampling and microcosm construction

Soils were sampled from Hob Moor, an unfertilized permanent acid grassland near York, UK (53°57'30"N & 1°4'48"W). The site has been receiving ca. 25 kg N/ha/year from atmospheric deposition (Riaz *et al.* 2009). The grassland soils at Hob Moor range between slowly permeable clay loams and more freely draining (and more acidic) very fine sandy loams and loamy sands. In November, 2008, 10 soil profiles from the study area were selected at random and sampled to 25 cm depth in five 5-cm depth increments. Dried litter was cut into smaller pieces to pass through a 2.0 mm sieve. The microcosms were reconstituted using PVC pipes (length = 29.0 cm, inner diameter = 6.4 cm) with soils sampled from 5 depths. The experimental design used 3 treatments including: control (without addition of litter); surface litter application (20 g litter equivalent to 2 cm deep litter layer); mixed litter (20 g litter was divided into 3 equal portions and a portion added to each of 0-5, 5-10 and 10-15 cm depths). Each microcosm was sealed at the bottom using a perforated plastic cap fitted with 140 μm nylon mesh under a layer of acid-washed quartz sand. The microcosms were then wetted and drained to bring them to field capacity. The experiment consisted of 3 replicates for each treatment and cores were set up under

outdoor ambient winter conditions in York in early December under an open-sided roof structure. The cores were irrigated with 45 ml simulated rain (ca. 14 mm rain fall), twice a week and leachate was collected weekly. The formula for simulated precipitation was based upon mean composition of rainwater collected for previous 4 months over winter period.

Soil and litter initial analysis

Soil and litter pH was measured at a 1:5 m:v (soil:solution) ratio in 0.5M KCl with a pre-calibrated Thermo Orion 420 pH meter. Moisture contents were determined gravimetrically by oven drying soils overnight at 105°C. The same oven dried soil samples were ball milled to form a fine powder and used for measuring C, N and C/N ratio using an Elementar Vario Macro automated C and N Analyser.

Soil and litter analysis after 5 weeks

After 5 weeks, the soil cores were returned to the laboratory and were carefully removed from the PVC pipes. After removing the litter layer from the surface litter treatment, the soil cores then were cut into 5 equal depth sections corresponding to individual soil layers. pH and moisture content were measured using above described protocols. Soils and litter samples were extracted for mineral-N (NH_4^+ -N and NO_3^- -N) determination using both 0.5M KCl and water, both at 1:5 m:v (soil:solution). The extracts were analysed for NH_4^+ -N and NO_3^- -N using a standard Bran & Luebbe Autoanalyser-3 protocol. The difference between KCl-extractable NH_4^+ -N concentrations and water-soluble NH_4^+ -N is viewed as NH_4^+ -N retention index (ΔNH_4^+ -N) in this study. The soil and litter water extractable-dissolved organic carbon (DOC) was determined by extracting 7-g field moist sub-samples with 35 ml deionised water. The filtered supernatants were analysed for DOC with an Elementar Liquitoc TOC analyser.

Leachate collection and analysis

Leachate (i.e. drainage water) pH and EC were measured on the day of sampling every week, and then leachates were analysed for mineral-N (NO_3^- -N and NH_4^+ -N) using a standard Bran & Luebbe Autoanalyser-3 manifold.

Results and discussion

Initial soil and litter physico-chemical characteristics

The soil pH (KCl) varied from 3.29 to 3.61 and soils remained substantially acidic even at 25 cm depth (Table 1). The surface soil layer (0-5 cm) had significantly higher moisture content, but moisture contents of soils from 5-25 cm depths showed no significant differences from each other. Organic carbon content consistently declined over depth, but differences were not always significant between adjacent sampling depths. The decrease in C/N ratio was significant and quite sharp over 0-20 cm depth. The KCl-extractable NH_4^+ -N concentration in the litter horizon was more than 8-fold greater than that in the underlying soil, and this NH_4^+ -N was highly soluble in water (data not shown).

Table 1. Initial characteristics of the soils used for the study.

Soil Layer/depth (cm)	pH (H ₂ O)	pH (KCl)	Moisture content (%)	C (%)	N (%)	C/N ratio
0-5	4.32 ^c	3.29 ^e	33.05 ^a	7.97 ^a	0.50 ^a	16.08 ^a
5-10	4.33 ^c	3.36 ^d	23.45 ^b	3.82 ^b	0.27 ^b	14.17 ^b
10-15	4.35 ^b	3.48 ^c	22.40 ^b	3.07 ^{bc}	0.23 ^{bc}	13.46 ^c
15-20	4.37 ^b	3.57 ^b	21.79 ^b	2.47 ^c	0.19 ^c	12.79 ^d
20-25	4.40 ^a	3.61 ^a	20.36 ^b	2.61 ^c	0.19 ^c	13.44 ^{cd}

All values are means of 4 analytical replicates. Values sharing different letters differ significantly from each other in each column excluding litter layer at $p < 0.05$ (One-way ANOVA, Tukey's HSD post hoc test).

Litter controls on mineral-N production

The presence of added litter layer at the surface contributed significantly higher KCl-extractable mineral-N concentrations compared with the control and mixed litter treatments only at 0-5 cm depth (Figure 1). Mixing of litter, however, resulted in significantly higher mineral-N concentrations than the control at 5-10 cm depth, and higher than the surface litter application and control at 10-15 cm depth. Differences among treatments at 15-25 cm depths were non-significant. The mineral-N concentrations were dominated by NH_4^+ -N in either of the litter treatments in 0-15 cm soil increments. NO_3^- -N concentrations remained consistently lowered especially in the mixed litter treatment. However, soils from the control treatment showed enhanced NO_3^- -N concentrations in

the sub-soils. The significantly higher NH_4^+ -N concentrations in the surface litter treatment could partially be the result of potentially mobile NH_4^+ -N produced in the litter layer (Adamson *et al.* 1993). ΔNH_4^+ -N showed strong association with DOC (Figure 2), indicating its potential in NH_4^+ -N dynamics either as mobile anionic role or sorption to soil particles (Fernando *et al.* 2005). Burge and Broadbent (1961) also found a positive relationship between soil C and NH_4^+ -N fixed in soils. Apart from the low pH and acidic nature of the soils, non-availability of such bound NH_4^+ -N could explain limited nitrification in the mixed litter soils (Kudeyarov 1981). The consistent lower NO_3^- -N production in the mixed litter treatment could also be the consequence of mixing high C:N ratio litter and associated N immobilization (Khalil *et al.* 2005).

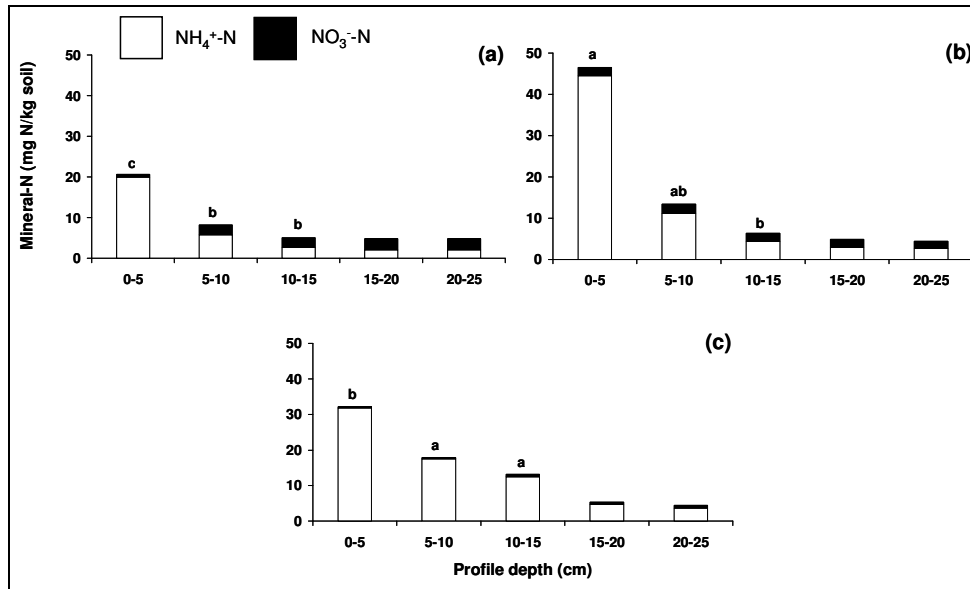


Figure 1. KCl-extractable mineral-N concentrations (mg N/kg soil) a) control, b) surface litter and c) mixed litter treatment. All values are means of 3 replicates. Bars sharing a different letter at specified depth for each treatment differ significantly from each other at $p < 0.05$.

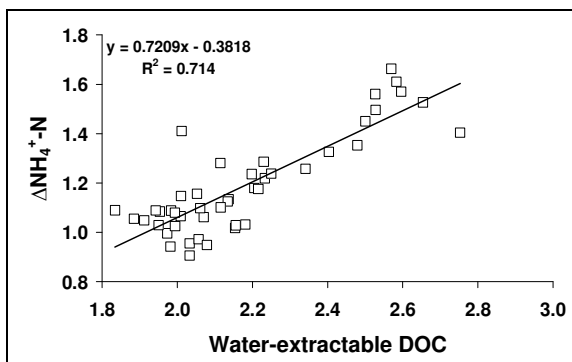


Figure 2. Linear relationship between water-extractable DOC and ΔNH_4^+ -N. Regression analysis was performed on log transformed data ($n=45$). The R^2 value was significant at $p < 0.001$.

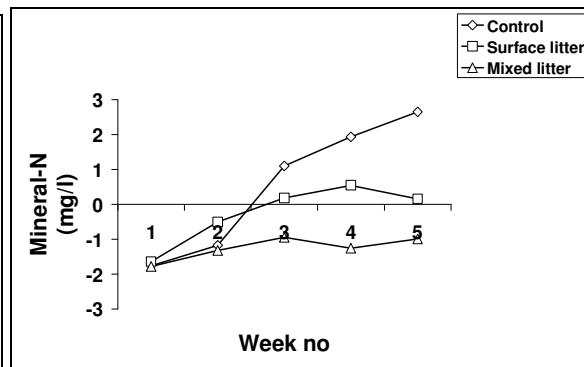


Figure 3. Changes in net mineral-N concentrations in the drainage water for each treatment over 5-week duration in winter. All values are means of 3 replicates.

Mineral-N concentrations in leachate

The net mineral-N (output-input) concentrations in leachate also clearly demonstrated remarkable N retention associated with litter additions (Figure 3). The control soils showed consistent increase in net mineral-N in leachate which indicates that mineral-N was relatively mobile in the absence of organic matter (litter) addition. However, the mixed litter treatment favoured N retention and reduced N concentrations in the leachate. This could be the result of incorporation of high C:N ratio residue which potentially immobilize N, thus reduced N leaching (Homyak *et al.* 2008).

Conclusions

A reconstructed microcosm study from acid grassland soils has shown that litter plays crucial role in mineral-N dynamics in winter. The presence of litter significantly enhanced mineral-N production in 0-15 cm soils. NH_4^+ -N produced in litter layers was potentially mobile and its retention in the soil profiles was strongly associated

with DOC. The mixing of litter effectively and consistently reduced mineral-N concentrations in leachate over winter, when N leaching could potentially occur to degrade water quality.

References

- Aber J, McDowell W, Nadelhoffer K, Alison M, Berntson G, Kamakea M, McNulty S, Currie W, Rustad L, Fernandez I (1998) Nitrogen saturation in temperate forest ecosystems. *BioScience* **48**, 921-934.
- Adamson JA, Hornung M, Kennedy VH, Norris DA, Paterson IS, Stevens PA (1993) Soil solution chemistry and throughfall under adjacent stands of Japanese larch and Sitka spruce at three contrasting sites in Britain. *Forestry* **66**, 51-68.
- Cresser MS, Smart RP, Clark M, Crowe A, Holden D, Chapman PJ, Edwards AC (2004) Controls on leaching of N species in upland moorland catchments. *Water, Air, & Soil Pollution: Focus* **4**, 85-95.
- Duckworth CMS, Cresser MS (1991) Factors influencing nitrogen retention in forest soils. *Environmental Pollution* **72**, 1-21.
- Fernando WARN, Xia K, Rice CW (2005) Sorption and desorption of ammonium from liquid swine waste in soils. *Soil Science Society of America Journal* **69**, 1057-1065.
- Henry H, Brizgys K, Field C (2008) Litter decomposition in a California annual grassland: interactions between photodegradation and litter layer thickness. *Ecosystems* **11**, 545-554.
- Homyak PM, Yanai RD, Burns DA, Briggs RD, Germain RH (2008) Nitrogen immobilization by wood-chip application: Protecting water quality in a northern hardwood forest. *Forest Ecology and Management* **225**, 2598- 2601.
- Kalbitz K, Solinger S, Park J-H, Michalzik B, Matzner E (2000) Controls on the dynamics of dissolved organic matter in soils: a review. *Soil Science* **165**, 277-304.
- Khalil MI, Hossain MB, Schmidhalter U (2005) Carbon and nitrogen mineralization in different upland soils of the subtropics treated with organic materials. *Soil Biology and Biochemistry* **37**, 1507-1518.
- Kudeyarov VN (1981). In 'Terrestrial nitrogen cycles, Ecological Bulletin (Stockholm)'. (Eds. FE Clark, T Rosswall) Vol. 33, pp. 281-290.
- Mian IA, Riaz M, Cresser MS (2009) The importance of ammonium mobility in nitrogen-impacted unfertilized grasslands: A critical reassessment. *Environmental Pollution* **157**, 1287-1293.
- Riaz M, Mian IA, Cresser MS (2008) Extent and causes of 3D spatial variations in potential N mineralization and the risk of ammonium and nitrate leaching from an N-impacted permanent grassland near York, UK. *Environmental Pollution* **156**, 1075-1082.
- Tipping E (2002) Cation Binding by Humic Substances. In 'Cambridge Environmental Chemistry Series' Vol. 12 (Cambridge University Press).

Mechanisms controlling dynamics at the soil-water interface

Dörte Diehl and Gabriele E. Schaumann

Department of Environmental and Soil Chemistry, Institute for Environmental Sciences, University Koblenz-Landau, Landau, Germany, Email diehl@uni-landau.de

Abstract

Since the characteristics of the soil-water interface are not static but continuously changing, the relevant processes and mechanisms have a high impact on habitat, filter, buffer, storage and transformation functions. Linking the individual results and conclusions of recent studies regarding the dynamics of wetting characteristics under changing environmental conditions as water content (WC), pH and drying and wetting temperature of two contrasting anthropogenic sites in Berlin (Germany), lead to two hypothetical models explaining differences in the nature of repellency between the sites and between wettable and repellent samples within each site. The chemical nature of repellency found at the one site can be best explained by hydrolysis-condensation reactions. The physicochemical nature of repellency on the other site seems to be controlled by the arrangement of amphiphilic molecules as micelles or reverse micelles during the drying process. The surface characteristics of the so formed layers on the soil particle surfaces depend on number and size of amphiphilic molecules, pH and ionic strength in the soil solution. Probably, specific local soil characteristics determine which mechanism dominates and controls the nature of repellency. Thus, critical conditions which may favour SWR may be identified. A challenge for the further research is the development of methods which may verify the suggested mechanisms with model substances as well as with complex natural soil samples and to verify the relevance of the suggested mechanisms for soils of differing soil-type, climate, and land-use.

Key Words

Soil water repellency, pH, wetting, drying, activation energy, amphiphile

Introduction

Surface characteristics of soils are one of the main factors controlling processes at the soil-water interface like wetting, sorption or dissolution processes and, thereby, have a high impact on natural soil functions like habitat, filter, buffer, storage and transformation functions. Since surface characteristics are not static soil properties but continuously changing, the relevant processes and mechanisms are in the focus of the presented study. These mechanisms help to gain further insight into the behaviour of soil and its dynamics under changing environmental conditions. In recent studies, the wetting and surface characteristics of soils from two contrasting anthropogenic sites, the former sewage disposal field Berlin-Buch and the inner-city park Berlin-Tiergarten were investigated with regard to their dependence on environmental parameters such as water content (WC), pH and drying and wetting temperature of wettable and repellent soils (Hurraß and Schaumann 2006; Bayer and Schaumann 2007; Diehl and Schaumann 2007; Diehl *et al.* 2009; Diehl *et al.* submitted). The aim of the present discussion is to link the individual results and conclusions of these studies with each other and to find a more general explanation for dynamics at the soil-water interface.

Results

The overview of main results obtained at the two sites Buch and Tiergarten (Table 1) not only shows a correlation of repellency with environmental conditions but also highlights principal differences in responses of repellency to changes in environmental conditions between the respective sites:

In Buch samples, drying resulted in an approach of SWR of initially wettable and repellent samples. Higher drying temperatures lead to an increased degree of surface hydrophobicity. Since wetting, the reverse process, requires high activation energy, the surface hydrophobization is probably controlled by chemical processes which are strongly linked with changes in water content. The effect of pH on repellency is only observable when moisture status of samples remained unchanged during artificial pH alteration. In Tiergarten samples, repellency differences between initially wettable and repellent samples remain following drying under various conditions as well as following artificially induced pH changes via gas phase. These differences disappear only after addition of liquid NaOH. In contrast to Buch samples, repellent Tiergarten samples have a lower pH and a higher EC in its aqueous extracts than wettable samples and the wetting process requires activation energy in the range of physicochemical processes.

Discussion

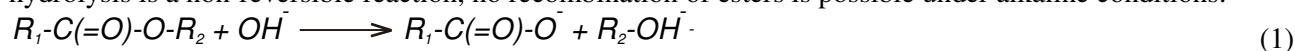
Chemical nature of repellency in Buch samples

To our current knowledge, hydrolysis-condensation reactions can be best explaining the nature of repellency of Buch samples (Table 1). Ester hydrolysis has already been suggested as a possible chemical reaction in the course of wetting of water repellent samples (Todoruk *et al.* 2003). Bound by ester groups, aliphatic dicarboxylic acids may act as bridges between alkyl chains and fatty acids, alcohols and aromatic acids and may be disrupted by base catalysed hydrolysis (Grasset and Amblès 1998) leading to an increasing number of carboxylate groups, i.e., an increasing number of charged sites at the SOM surface and thus an increased wettability.

Table 6. Overview of the main observations of differences in soil characteristics and in responses on changes in environmental conditions between wettable and repellent samples from Buch and Tiergarten.

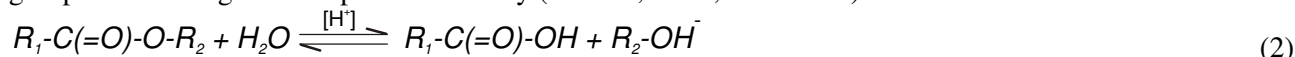
	Buch	Tiergarten
Drying (Diehl <i>et al.</i> 2009)	Increases repellency; differences between wettable and repellent samples decrease.	Increases repellency; differences between wettable and repellent samples remain.
High drying temperature (Diehl <i>et al.</i> 2009)	Increases surface hydrophobicity (DRIFT-CH _N).	Does not significantly affect surface hydrophobicity (DRIFT-CH _N).
Activation energy of wetting (Diehl and Schaumann, 2007)	65-94 kJ/mol	8-42 kJ/mol
pH alteration via gas phase: - exposition to NH ₃ or gaseous HCl enriched atmosphere (Diehl <i>et al.</i> submitted)	SWR Wettable = repellent samples.	SWR Wettable < repellent samples.
pH alteration via liquid phase: - addition of liquid NaOH or HNO ₃ solution (Bayer and Schaumann, 2007)	SWR Wettable = repellent samples.	SWR Wettable = repellent samples.
Field pH (Hurraß and Schaumann, 2006)	No significant relation with SWR.	Repellency only with pH < 4.6.
Electrical conductivity (Hurraß and Schaumann, 2006)	No significant relation with SWR.	Higher conductivity for repellent samples.
Surface tension of aqueous extracts (Hurraß and Schaumann, 2006)	Lower surface tension for repellent samples.	Lower surface tension for repellent samples.

The base catalysed hydrolysis (Equation 1) is an irreversible process (Schmeer *et al.* 1990) and follows two competing reaction pathways in its second step. The one is characterised by a direct proton transfer, and the other by a water-assisted proton transfer through which the energy barrier for the decomposition is significantly lower than through the direct proton transfer (Zhan *et al.* 2000). Thus, under dry conditions, these reactions are slow and accelerated only by increasing OH⁻ concentration, i.e. with increasing pH. This may explain why the dry Buch samples develop increasing wettability with increasing pH after treatment with gaseous NH₃ (Table 1, Buch, red curve). The presence of water accelerates alkaline hydrolysis reactions (Zhan *et al.* 2000). This could explain why Buch samples are completely wettable after addition of liquid NaOH and subsequent incubation for 1 week at 20°C in closed containers (Bayer and Schaumann 2007); (Table 1, Buch, blue curve). Since alkaline hydrolysis is a non-reversible reaction, no recombination of esters is possible under alkaline conditions:



In contrast, long-term drying and drying at elevated temperatures under the original acidic pH conditions led to enhanced esterification and to an establishment of cross-linking, e.g. between carboxylic and hydroxyl functional groups. This has been observed in solid state reactions between carboxylic acids and hydroxyl-groups of cellulosic material (Pantze *et al.* 2008) and could explain why samples from Buch which reveal significant differences in wettability in field moist state reached a comparable degree of repellency after long-term drying or after drying at elevated temperatures.

A reduction in pH favours acidic catalysed hydrolysis (Equation 2) which is a reversible process driven by excess or deficiency of water. The ester concentration at the equilibrium point is independent from the pH but highly depends on the amount of available water. The pH solely determines the rate at which the equilibrium is reached. This can explain why the repellency of dry Buch samples remains constant with decreasing pH (Table 1, Buch, red curve). Only the addition of liquid acid solution (Bayer and Schaumann 2007) provides the excess of water necessary for shifting the equilibrium towards a significantly higher number of hydroxyl and carboxyl groups and leading to a complete wettability (Table 1, Buch, blue curve).



The suggested mechanism is not restricted to esterification but generally includes hydrolysis-condensation reactions which in SOM can occur between a variety of substances, e.g., carbohydrates, proteins, lipids etc.

Physicochemical nature of repellency in Tiergarten

The physicochemical nature of repellency in Tiergarten linked with differences in pH, electrical conductivity (EC) and surface tension in aqueous extracts between wettable and repellent samples may be best explained by changes in the spatial orientation of amphiphilic molecules on the soil particle surface during wetting and subsequent drying:

At high ionic strength, repulsion forces between charged functional groups are effectively shielded by the counter ions (Fleer *et al.* 1993). This allows charged groups to stay closer to each other and leads to more compact structures at the water-air interface. Upon drying, water evaporates slowly from the outside to the inside of the hydrated SOM surface layer. Hydrophilic groups orientate towards the inwards receding water front whereas hydrophobic chains orientate towards the air (Swift 1999; Horne and McIntosh 2000). Smaller, water-soluble amphiphilic molecules may form a hydrophobic layer by micelle-like intermolecular aggregations at the surface (Terashima *et al.* 2004); (Figure 1, top).

At low ionic strength, a smaller amount of amphiphilic molecules may enrich at the water-air interface resulting in a higher concentration in the solution. This leads to the formation of micelles when critical micelle concentration is reached. Upon drying, hydrophilic groups tend to stay as long as possible in contact with water avoiding approaching each other, and form an outward directed hydrophilic layer (Figure 1, bottom).

These mechanisms may also explain how the addition of liquid NaOH solution may transform wettable into repellent samples. Thereby not only pH but also ionic strength increases and may therefore induce a change in conformational arrangement of amphiphilic molecules at the SOM surface. Despite increasing pH and an increasing number of negatively charged groups, repellency persists within a certain pH range because the ionic strength also increases. At a higher pH, deprotonation overbalances the effects of ionic strength. Thus, in a pH range above 7, repulsion forces cannot be effectively weakened leading to an aggregation of hydrophobic groups and surface exposition of hydrophilic groups (Table 1, Tiergarten, blue curve).

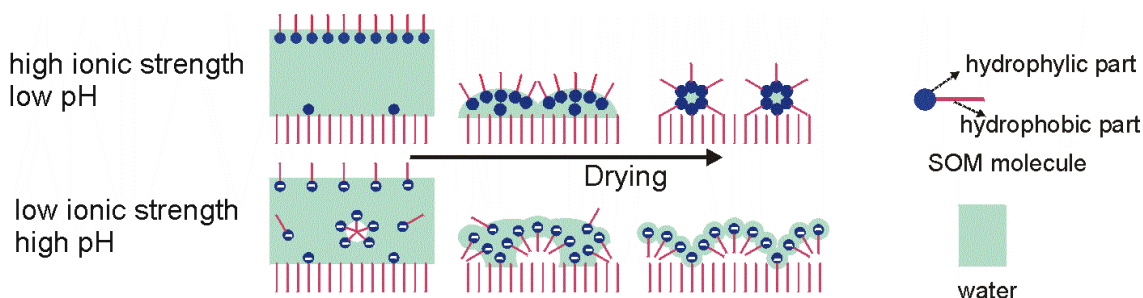


Figure 8. Suggested model of orientation of amphiphilic organic molecules at the SOM surface during drying in dependence of pH and ionic strength of the soil solution.

Conclusion

The differences in the nature of repellency between the sites and between wettable and repellent samples within each site help to draw some conclusions on the appearance of SWR and on the factors which determine the degree and nature of SWR. The two suggested mechanisms of chemical and physicochemical control of repellency are probably not restricted to one of the two sites but occur in some degree on both sites. Furthermore, it cannot be excluded that additional mechanisms play an important role for repellency at other sites. Specific local soil characteristics determine which mechanism dominates and controls the nature of

repellency. However, the two suggested mechanisms together with the previous history of the sites allow identifying critical conditions which may favour SWR: Long hot and dry periods may enhance soil water repellency especially in soils with low pH and high organic accumulation. In these soils chemically bonded water can be released from organic matter by condensation reactions. Rewetting requires high activation energy, i.e. it is slow at ambient temperatures but can be accelerated by elevated temperature as long as the water does not evaporate. Special care is also needed in soils with a relatively high salt concentration, a low pH, and a SOM containing a relatively high amount of water soluble amphiphilic molecules. The combination of high ionic strength and low pH in the soil solution can favour the appearance of SWR after drying. In order to verify the suggested mechanisms, further investigations are needed. On the one hand, smaller-scaled methods are required to investigate the respective processes in molecular range, starting with model substances and extending these methods to complex natural soil samples. On the other hand, the relevance of the identified processes for a wide ranges of climates, soil types and land-use has to be tested and, eventually, additional relevant processes to be identified.

References

- Bayer JV, Schaumann GE (2007) Development of soil water repellency in the course of isothermal drying and upon pH changes in two urban soils. *Hydrological Processes* **21**, 2266 - 2275.
- Diehl D, Bayer JV, Woche SK, Bryant R, Doerr SH, Schaumann GE (submitted) Reaction of soil water repellency on artificially induced changes in soil pH. *Geoderma*
- Diehl D, Ellerbrock RH, Schaumann GE (2009) DRIFT-Spectroscopy of untreated and dried soil samples of different wettability. *European Journal of Soil Science* **60**, 557-566.
- Diehl D, Schaumann GE (2007) Wetting mechanism assessed from time dependent sessile drop shape. *Hydrological Processes* **21**, 2255 - 2265.
- Fleer GJ, Stuart MAC, Scheutjens MHM, Cosgrove T, Vincent B (1993) 'Polymers at Interfaces'. (Chapman and Hall: London).
- Grasset L, Amblès A (1998) Structure of humin and humic acid from an acid soil as revealed by phase transfer catalyzed hydrolysis. *Organic Geochemistry* **29**, 881-891.
- Horne DJ, McIntosh JC (2000) Hydrophobic compounds in sands in New Zealand-extraction, characterisation and proposed mechanisms for repellency expression. *Journal of Hydrology* **231-232**, 35-46.
- Hurraß J, Schaumann GE (2006) Properties of soil organic matter and aqueous extracts of actually water repellent and wettable soil samples. *Geoderma* **132**, 222-239.
- Pantze A, Karlsson O, Westermark U (2008) Esterification of carboxylic acids on cellulosic material: Solidstate reactions. *Holzforschung* **62**, 136-141.
- Schmeer G, Riembauer S, Barthel J (1990) The influence of hydrophobic solvation on the alkaline hydrolysis of ethyl esters of polar substituted 2-methylpropionic acids in water. *Journal of Solution Chemistry* **19**, 1175-1189.
- Swift RS (1999) Macromolecular properties of soil humic substances: fact, fiction, and opinion. *Soil Science* **164**, 790-802.
- Terashima M, Fukushima M, Tanaka S (2004) Influence of pH on the surface activity of humic acid. Micelle-like aggregate formation and interfacial adsorption. *Colloids and Surfaces, A: Physicochemical and Engineering Aspects* **247**, 77-83.
- Todoruk TR, Litvina M, Kantzas A, Langford CH (2003) Low-Field NMR Relaxometry: A Study of Interactions of Water with Water-Repellant Soils. *Environmental Science and Technology* **37**, 2878-2882.
- Zhan CG, Landry DW, Ornstein RL (2000) Reaction Pathways and Energy Barriers for Alkaline Hydrolysis of Carboxylic Acid Esters in Water Studied by a Hybrid Supermolecule-Polarizable Continuum Approach. *Journal of American Chemical Society* **122**, 2621-2627.

Method for water extractable phosphorous in saline-sodic soils

Jessica Drake^A, Lorna Fitzsimons^A, Ben Macdonald^A, John Field^A, Emlyn Williams^B and Richard Greene^A

^AThe Fenner School for Environment and Society, ANU, Acton ACT 2601, Email Jessica.Drake@anu.edu.au

^BStatistical Consulting Unit, ANU, Action ACT 2601

Abstract

Soil phosphorous dynamics in saline-sodic soils is not well understood and lack of applicable methods for saline-sodic soils is a major problem. One method used for soluble-P measurements in saline-sodic soils includes using anion exchange resins. Water addition to dry saline-sodic soils may cause reactions and fluxes in the pH which can result in inaccurate measures of soluble-P. A low-molar salt solution can be used to stabilise the pH for extraction. Six mixes of a saline-sodic soil were extracted with a low-molar salt solution and compared with the standard deionised water extraction using the anion exchange resin method. Two further extracts were undertaken on all the soils, following the Hedley procedure. The first fraction of P was shown to be significantly less ($p > 0.005$) with a salt extraction, compared to water extraction. Subsequent P was not recovered in the second and third extraction. Further research is being undertaken on the recovery rates of soluble-P with low-molar salt extractants; through recovery rates, full-fractionation of different saline-sodic soils; and determining correction factors.

Key Words

Phosphorous; saline; sodic; nutrients; methods

Introduction

Water soluble-P and P dynamics in saline-sodic soils has undergone limited research. Curtin and Naidu (1998) suggest that this is largely due to the lack of methods suitable for saline-sodic soils. Exchangeable sodium and pH influence solubility of P in soils (Curtin and Naidu 1998; Gupta and Abrol 1990; Naidu and Rengasamy 1995). Thus, sodic soils have inherently high rates of available P. Saline-sodic soils with high pH (>8.0) may also contain Ca-P complexes. Common P-extraction techniques, such as Colwell (1963) and Olsen *et al.* (1954), use extractants which may extract Ca-P complexes or contain Na which may overestimate soluble-P (Curtin and Naidu 1998). Colwell and Olsen methods are not advisable for P analysis when considering plant available sources due to over or under estimation of different P-fractions (Curtin and Naidu 1998). Suggested methods to deal with these problems include ion-exchange membranes (Curtin and Naidu 1998), ammonium fluoride (Bray and Kurtz 1945; Hazelton and Murphy 2007) and NH_4HCO_3 with DTPA (diethylenetriamine penta-acetic acid) (Chun *et al.* 2007). These methods use water or other non-cation extractants. This limits chemical interference with Ca-P complexes or changes in solubility of P. Subsequent fractionation of P using the Hedley method (Hedley and Stewart 1982) can be undertaken to determine levels of P in other forms. An appropriate fertiliser or organic amendment regime can then be determined.

Water extraction of P in saline-sodic soils also has limitations. The addition of water to a saline-sodic soil after drying can cause a chain of reactions due to the high surface potential of the soil (Curtin and Naidu 1998; Thomas 1996). Depending on the amount of exchangeable Na, Ca, other cations and the presence of carbonates, the pH of the solution can increase or decrease with water addition (Curtin and Naidu 1998; Thomas 1996). Therefore, the fractions of P may be altered from the time it was sampled. A low-molar salt solution has been used in some P-extraction techniques (Lajtha *et al.* 1999) to limit variability of changing salt concentrations (Thomas 1996). Low molar salt solutions have not previously been used in the anion exchange resin method as a method of stabilising the pH over the 18 hours of extraction. This paper will demonstrate the efficacy of the extraction of water soluble-P in dried saline-sodic soils using a low-molarity salt solution compared to deionised water. It will examine whether there is a loss of P as a result of water extraction by undertaking two subsequent extractions using the Hedley fractionation method (Hedley and Stewart 1982; Lajtha *et al.* 1999). The potential for a low-molarity salt solution to buffer pH change in the extraction of water soluble-P in saline-sodic soils is included.

Methods

Saline-sodic regolith from the Cowal Gold Mine, characterised as a mix of lake-bed sediments and cracking clays, with some oxide and waste materials were used. The pH (1:5 H_2O) ranged between 7.55 and 8.84; EC

ranged between 1.3-1.6 dS/m and the ESP was 28. The soils had been previously ameliorated for 12 weeks under a 2 x 3 factorial experiment (with or without gypsum, no compost / compost or fresh woodmulch). Soils were divided into 6 mixes, depending on treatments they had received (Table 1). Approximately 0.25g of each soil mix was measured out 8 times for each of the two exchange methods. Four reps from each sample were then used as replicates for each of the extractants. In half of the soils, 30mL of deionised water was added, the other half received 30mL of 0.05M KCl solution. Anion exchange membranes were added to each tube and left on rotation for 18hrs. Membranes were extracted at 18hrs and placed into a weighed volume of approximately 25mL of 0.5M HCl. P was extracted from the membranes by rotation for another two hours. Soil was kept for two more extractions using NaHCO₃ and NaOH in the Hedley method (Hedley and Stewart 1982; Lajtha *et al.* 1999). The malachite green procedure was then used to analyse P in each of the extracts (Lajtha *et al.* 1999), using a Varian Cary 50 at 630nm absorbancy.

Table 1: Soil Classes and treatments undertaken over a 12 week period

Soil Mix	Contents
1	Soil
2	Soil + Compost
3	Soil + Woodmulch
4	Soil + Gypsum
5	Soil + Gypsum + Compost
6	Soil + Gypsum + Woodmulch

Results

P extracted using KCl was lower compared to water extraction, with an average difference of between 0.52 and 37.86ppm. In soils with compost added (mix 2 and 5), the difference between the two extracts was highest, with averages of 25.11 and 37.86ppm lower with KCl extract (Figure 1). The average standard deviation between the replicates for water or KCl was 2.31 and 1.24 respectively. The correlation coefficient of the two data sets is 0.4034, and data sets were significantly different $p > 0.005$. The difference between the DI water and KCl on second (NaHCO₃) and third (NaOH) extracts was reverse, with KCl averaging between 0.12 and 9.40ppm more P present (Table 2). An exception for NaOH extracts occurred in soils 5 and 6, which had less P in the KCl extracted soils. The average recovery of P in the later fractions was only 8.2-74.2% of the difference between the first extracts. The total of all three extracts have an average difference between 1.2 and 24.5ppm for the soils originally extracted with KCl. Total recovery of P in soils extracted with KCl was between 79.2 and 95.7% of total P in soils extracted with DI water, with the two lowest averages being the soils treated with compost (2 and 5). Correlation of the extract-totals is strong, with a factor > 1.0 .

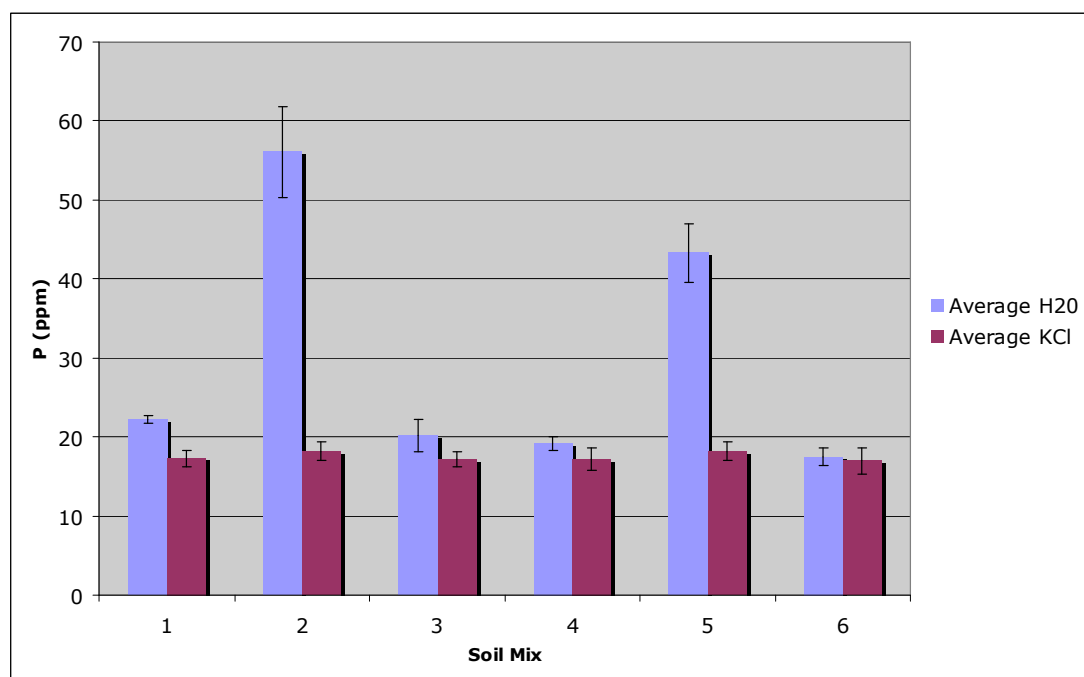


Figure 1. Average P-extracted (ppm) for DI Water and KCl extracts with error bars (standard deviation).

Table 2. Average soil P from replicates of the three extracts

Soil Mix	First Extract		2 nd Extract		3 rd Extract		Total of 3 Extracts	
	Water (ppm)	KCL (ppm)	Water (ppm)	KCL (ppm)	Water (ppm)	KCL (ppm)	Water – KCl (ppm)	KCl as % of Water
1	22.27	17.27	7.09	7.42	5.39	5.51	4.54	86.94
2	56.06	18.20	66.98	76.38	20.73	24.65	24.54	82.93
3	20.24	17.12	6.35	7.01	5.07	6.02	5.12	83.82
4	19.18	17.16	6.73	7.30	4.58	4.76	1.28	95.79
5	43.30	18.19	50.48	53.70	17.03	15.88	23.05	79.20
6	17.51	16.98	6.35	7.03	4.61	4.30	3.22	89.79

Discussion

There was a reduced amount of extracted soluble-P with a low-molar salt solution compared to DI water. Subsequent extractions from soil extracted with salt-solution had increased levels of P, but not sufficient to be equal to the different amount in the initial extraction. It is possible the salt-solution caused a decrease in pH (Thomas 1996). This would have locked the P into other fractions that were not recovered in the scope of this experiment. Furthermore, DI water may have made P more available in the first extract compared to later fractions due to an increase in pH (Thomas 1996). Full fractionation of total P using the Hedley procedure is required to understand the dynamics of P with KCl and water extracts. The pH should also be measured hourly to understand any reactions occurring in the solutions that may affect pH and consequent P solubility and dynamics. The KCl may have also had interference with the ion-exchange membrane. Chloride may have taken up some of the positions on the membranes, making them less available to P ions. This problem may be reduced by using more membranes. A different salt solution may also be used in place of KCl. A lower molar salt-solution (0.01 or less) should also be tested to determine if it recovers a greater level of soil P. Correction factors are used to deal with change in partial pressure when measuring pH in 0.01M CaCl₂ (Thomas 1996). Therefore, a correction factor may be necessary when extracting with a salt solution. Compost added to a soil was shown to have the strongest rate of non-recovery compared to the other soil treatments. Additions to soil should be thoroughly analysed for full P-fractionation, eH, pH and EC to determine any interactions that may have occurred in the soil system, including those of P dynamics. Further investigation of the recovery of P with low-molar salt solutions is being undertaken. Both recovery of P and other saline-sodic and non-saline-sodic soils are being investigated. It is anticipated that full fractionation and P-sorption capacity will highlight any changes in P fractions with low-molar or water extractions.

Conclusion

Phosphorous dynamics in saline-sodic soils is not well understood. Current methods utilise soil fractionation, and water extractable P as the first fraction. Water extracts can cause changes in soil chemistry, which may influence the recovery of P in different fractions. Salt-solutions in place of water may limit changes in P fractions. A low-molar salt solution was compared with water as a first fraction extractant. The recovery of P was lower in salt-solution compared to water, and was not recovered after a further two extracts. This may have been due to changes in pH caused by the salt-solution, water, interference on anion exchange membranes, molarity of salt solutions, need for correction factors and lack of understanding regarding P fractionation. Further research is being undertaken to determine the recovery rate of soluble-P with low-molar salt solutions, including a wide range of saline-sodic, sodic and other soils. Full fractionation and sorption capacity of the soils is expected to demonstrate whether salt-solutions or water change soil P fractions. A correction factor will be formulated if required. Data will also be used to further understand soil P dynamics in saline-sodic soils.

References

Bray R, Kurtz L (1945) Determination of total, organic and available forms of phosphorous in soils. *Soil Science* **59**, 39-45.

- Chun S, Rai H, Nishiyama M, Matsumodo S (2007) Using Organic Matter with Chemical Amendments to Improve Calcareous Sodic Soil. *Communications in Soil Science and Plant Analysis* **38**, 205-216.
- Colwell J (1963) The estimation of the phosphorus fertilizer requirements of wheat in southern New South Wales by soil analysis. *Australian Journal of Experimental Agriculture and Animal Husbandry* **3**, 190-198.
- Curtin Da, Naidu R (1998) Fertility Constraints to Plant Production. *In Sodic Soils: Distribution, Properties, Management and Environmental Consequences* Eds. M Sumner and R Naidu. Oxford University Press.
- Gupta R, Abrol I (1990) Salt-Affected Soils: Their reclamation and management for crop production. *Advances in Soil Science* **11**, 223-288.
- Hazelton P, Murphy B (2007) Interpreting soil test results: What do all the numbers mean? . CSIRO Publishing, Collingwood.
- Hedley M, Stewart J (1982) Method to measure microbial phosphate in soils. *Soil Biology and Biochemistry* **14**, 377-385.
- Lajtha K, Driscoll C, Jarrell W, Elliott E (1999) Soil Phosphorous: Characterisation and Total Element Analysis. *In Standard Soil Methods for Long-Term Ecological Research* Eds. G Roberston, D. Coleman, C. Bledsoe and P. Sollins. Oxford University Press.
- Naidu R, Rengasamy P (1995) Ion Interactions And Constraints to Plant Nutrition in Australian Sodic Soils. *In Australian Sodic Soils: Distribution, Properties and Management* Eds. R. Naidu, M. Sumner and P. Rengasamy. CSIRO Publishing.
- Olsen S, Cole C, Watanabe F, Dean L (1954) Estimation of Available Phosphorous in Soils by Extraction with Sodium Bicarbonate. USDA Circular. 939
- Thomas G (1996) Soil pH and Soil Acidity. *In Methods of Soil Analysis: Part 3 - Chemical Methods* Ed. D. Sparks. SSSA Inc.

Microbial dynamics in soils under long-term glyphosate tolerant cropping systems

Richard Dick, Nicola Lorenz, Michal Wojno and Matt Lane

School of Environment and Natural Resources, Ohio State University, Columbus OH 43210 USA.

Corresponding author Email Richard.Dick@snr.osu.edu

Abstract

Glyphosate is a non-selective, broad-spectrum herbicide now widely used. Early research on short-term effects on soil microbiology was inconclusive, but now long-term applications of glyphosate to tolerant cropping (GTC) systems may be shifting microbial communities and causing plant nutrition deficiencies and diseases. A field survey of 10 pairs of fields (K sufficient and deficient) under >10 yrs GTC showed significant negative correlations between microbial biomass K and K crop uptake suggesting glyphosate applications caused microbial immobilization of K. A 28 day experiment with a single glyphosate application and another experiment with repeated glyphosate application was done on soils from >10 yrs GTC or soils that had never received glyphosate. The soils that had been under GTC showed no shift in fatty acid profiling of microbial communities (suggesting they had adapted) compared to the non-GTC soils where unique fatty acids were stimulated by the addition of glyphosate. For example, gram positive bacteria responded to glyphosate in non-GTC soils but not GTC soils. This suggested that adding glyphosate does cause a shift in a sub population of the soil. DNA-DGGE analysis of GTC fields identified *Fusarium* species that are known to be pathogenic. The results suggest there is sub-population shift that is occurring with long-term GTC.

Introduction

Non Target Effects of Glyphosate

There is a growing body of anecdotal information and preliminary research that suggests long term and repeated use of glyphosate in both glyphosate tolerant cropping systems and in other agricultural applications is changing the soil microbial community, worldwide. This is manifesting various undesirable effects on crops that have included stimulation of diseases and nutrient deficiencies (International Conference Symposium: *Mineral nutrition and disease problems in modern agriculture: Threats to sustainability*, Informações Agrônomicas 119, 2007). There is evidence that glyphosate causes nutrient deficiency on Fe, Ca, Mg (Carmak 2007), Ni (Wood 2007), and Mn (Huber 2007). Glyphosate kills plants by making it susceptible to fungal diseases caused by *Fusarium* and *Pythium* (Johal and Rahe 1990). A four year study in Canada showed that glyphosate-treated wheat had higher levels of *Fusarium* head blight (a toxic fungal disease) than wheat fields where no glyphosate had been applied (Fernandez *et al.* 2007). Furthermore, this study was the first to report the possibility of residual effects from RR wheat causing disease in barley. Although relatively few trials have been conducted in the US, the majority typically has shown yield decrease of 5 to 10% by RR soybeans compared to non-RR varieties (consistently in the northern US corn belt) (Gaska and Boerboom, UW, Madison, person comm. 2009). Exceptions to this were a study in Iowa that showed no significant yield differences between RR and non-RR soybeans and a study in Illinois RR varieties yielded 1 bu/ac more than conventional non-RR varieties. (Gaska and Boerboom, UW, Madison, person comm. 2009)

In very controlled studies under hydroponic conditions Kremer *et al.* (2005) showed that treated RR soybeans transported glyphosate to the roots where it was released and stimulated *Fusarium* in the plant roots, to such a degree that he considers the elevation of *Fusarium* levels to be glyphosate's "secondary mode of action." Although they did not investigate the pathogenesis of *Fusarium* colonies, this outcome raises the question of whether *Fusarium* is stimulated in soils of RR systems that could cause disease epidemics. In Australia recent concerns have been expressed that 90 percent of Australia's cotton belt could be inundated by the soil borne pathogen *Fusarium* wilt within the next decade because of the widespread use of RR cotton. *Fusarium* can be a serious disease such as Fusarium Head Blight (FHB) which for wheat and barley in Saskatchewan has been responsible for serious crop losses (Fernandez *et al.* 2007). About a fifth of the wheat crop in Europe every year is lost to FHB and in Michigan during 2002 there were 30 to 40% yield losses. There is a growing incidence of potassium deficiency on corn across the Midwest, which appears to be related to the widespread adoption of RR soybean systems that are in rotation with corn (Norton *et al.* 2005). This K deficiency is exacerbated by no-tillage, where it causes yield reduction over conventional tillage (Norton *et al.* 2005; Vyn *et al.* 2002). Fast growing, high yielding corn hybrids are more susceptible to K deficiency, but K deficiency has occurred with

other cultivars as well. It is largely unknown why glyphosate based cropping systems might affect K availability. Preliminary research (Kremer *et al.* 2005), limited evidence from the literature, and our understanding of K cycling suggest that glyphosate causes an interaction of soil biology that may be inducing K deficiency in plants. Glyphosate has been shown to stimulate fungi (Arauj *et al.* 2003), and the roots of glyphosate tolerant crops leak glyphosate and elevated levels of C exudates into soils (Kremer *et al.* 2005). Weed *et al.* (1969) showed that fungi can rapidly take up K and there is evidence that microbial biomass K increases after K fertilization (Perrott *et al.* 1990) or fluctuates seasonally (Roberts 1968). We hypothesize that glyphosate systems cause a microbial shift towards fungal dominance or specific fungal genera such as *Fusarium* (Kremer *et al.* 2005), which rapidly take up K and transfer it to non-exchangeable/plant, unavailable forms.

Glyphosate Effects on Soil Microbial Communities

Glyphosate application on agricultural fields has been shown to penetrate the upper 2 mm of the soil (Haney *et al.* 2000) at recommended field application rates. Single application or short term studies in the field and lab have shown that microbial biomass is unaffected or stimulated (Hart and Brookes 1996; Liphardzi *et al.* 2005; Haney *et al.* 2000). In similar, short term applications, glyphosate even at rates significantly above recommended rates generally show minimal or transitory effects on soil biology (Savin *et al.* 2007; Zaboly *et al.* 2008; Ratcliff *et al.* 2008). However, detailed studies in the soil rhizosphere have shown that glyphosate leaks out of the roots within hours after application (Carmak 2007; Kremer *et al.* 2005). Root exudation of glyphosate tolerant soybeans under hydroponic growth releases greater amounts of glyphosate than a non-tolerant cultivar after foliar application of glyphosate (Kremer *et al.* 2005). The glyphosate tolerant soybean exudates, besides glyphosate, had high levels of carbohydrate and amino acid content. Exposing this exudate to isolated fungi and bacteria stimulated several fungi (Kremer *et al.* 2005). Other studies that directly exposed microbes to glyphosate have found: 1) stimulation of mycorrhizal fungi (Laatikainen and Hinonen-Tanski 2002); 2) that fungi are the main glyphosate degraders (Krzysko-Lupicka *et al.* 1997); and 3) that bacteria are the main incorporators of glyphosate (Charney *et al.* 2004). Thus, short term or single applications may not have permanent changes of the soil community that are measurable in the bulk soil, but there still may be microsites in the rhizospheres of crops that could negatively affect crop production (Norton *et al.* 2005). One of the few studies on long-term glyphosate applications (6 yrs) did cause a shift in microbial communities (Araujo *et al.* 2003). Indeed, the reports on RR cotton, RR wheat, and anecdotal information indicates it takes a number of years of RR cropping before detrimental impacts are measurable.

Procedures

A field survey on GTC fields and lab incubation were done to investigate how long-term GTC may be impacting soil microbial communities. The objective of this study was to determine the effect of long-term GTC on: (1) soil K dynamics; (2) soil microbial structure (ester linked fatty acid methyl ester, EL-FAME profiling); (3) biomass K (K_{mic}); and (4) *Fusarium* diversity.

Objective 1: Determine microbial community and microbial biomass K shifts in soils from fields deficient or sufficient in plant available K under long-term glyphosate tolerant cropping.

Based on information from farmers experiencing unexplained K deficiency under GTC and recent reports we hypothesized that long-term GTC is stimulating K immobilization and possibly *Fusarium* species. Hence the latter could further contribute to reduced K uptake in crops by damaging roots or otherwise impeding crop growth. The use of glyphosate could stimulate a specific fungal genus or cause a general shift in the microbial community towards fungal dominance.

Procedure 1

Ten paired sites (deficient vs. sufficient in plant available K) across the mid-west corn belt of the US sites under no-tillage were selected that had been under GTC for > 10 years. In April, June and July 2007 as well as in March, June and August 2008 sites were sampled. In the summers of 2007 and 2008, bulk soil samples were taken in the vicinity of the corn and soybean plants and another set of soil samples was strictly taken in the rhizosphere. All soils were passed through a 2 mm sieve and stored at 4°C until further analysis. Soils for DNA extraction were stored at -80°C. In July 2007 and August 2008 plant leaf tissue was collected. At each sampling spot, three plants were selected and leaf tissue from the V5 to V7 growth stage was collected. Microbial fatty acids were extracted using the EL-FAME protocol described in Schutter and Dick (2000). Methyl nonadecanoate served as an internal standard, which allowed calculation of FAME concentrations (Zelles 1996). Soil microbial biomass potassium (K_{mic}) was extracted after chloroform fumigation extraction (Lorenz *et al.*

2009). Soil DNA was extracted using a MoBIO® Power soil DNA extraction kit. Subsequently, extracted DNA was stored at -80°C until further processing. For PCR, an aliquot of the ultra-frozen DNA was diluted (1:10) and stored at -20°C. Subsequently, PCR was performed using a PTC-200 Thermal Cycler (MJ Research®). Fusarium-specific PCR was performed targeting a partial region of the translation elongation factor-1 alpha gene (Yergeau *et al.* 2005, Wakelin *et al.* 2008). PCR products were verified on an Agarose gel and cleaned with a QIAquick PCR product cleaning kit (QIAGEN®). Subsequently, PCR products were applied on a denaturing gradient gel and separated electrophoretically at 90V overnight using a Dcode system (Bio-Rad®). Denaturing gradient gels were stained using SYBR green immediately after electrophoresis and pictures were taken using a Digital Gel Logic 4 camera (Kodak®). Cloning was done with a TOPO TA cloning kit with DH5 α -T1 chemically competent E.coli (Invitrogen®). Plasmids were isolated from E.coli clones with a PureLink quick plasmid miniprep kit (Invitrogen®) and a QIAprep spin miniprep kit (QIAGEN®). Sequencing of the Plasmids was performed by the Plant-Microbe Genomics Facility at the Ohio State University, Biological Sciences Department, Columbus, Ohio.

Objective 2: Evaluate the effect of repeated applications of glyphosate on soil microbial communities in a long term soil incubation study

Roundup Ready (RR) systems, with up to 2 or 3 applications per year of glyphosate on RR soybeans in rotation with corn, are widespread in the Midwest. With the increasing use of RR corn, soils will be receiving double the glyphosate of the past 10 years. Analyzing the soils today from such fields does not reveal the historical shift in microbial communities that may have occurred. The goal of this experiment is to replicate 5 years of RR applications in a microcosm study. The approach was to manipulate soils that had no or varying degrees of long-term glyphosate applications in a short-term incubation with repeated applications on a 21 day basis (equivalent to the cumulative amount of a.i. of glyphosate equal to that of 5 years of RR systems in the field). Then we will monitor the shift in microbial communities over months rather than the years required for a field study.

Procedure 2

Two experiments were done. The first was a 28 day incubation of soil that was sampled at 2, 7 14 and 28 d after applying glyphosate to either GTC (>10 yrs) or non-GTC soils. The second experiment was a 3 x 2 factorial design with: three soils from farmers' fields (organic farm that has never had glyphosate applied; non-GMO soybean-corn farm that has had occasional applications of glyphosate in pre-growing season burn downs; or a farm with >10 years of repeated applications of glyphosate using RR soybeans) and two levels of repeated glyphosate applications (control or recommended a.i. glyphosate/application). The sites were chosen because the texture and total C (soil organic matter) are virtually identical and all are of the same classification. The glyphosate treatment was applied every 21 days for 8 months (simulating 5 yrs of field applications). This application interval is based on a preliminary study where we found that 21 days after the glyphosate application, respiration returned to base line levels - suggesting the community had reached an equilibrium and exhausted the available glyphosate. At 0.5, 1, 2, 4, 6, and 8 months soil samples were collected and analyzed for ester linked fatty acid methyl esters (EL-FAME) as described above.

Results and Discussion

Experiment 1

All the deficient and sufficient K fields had > 100 ppm exchangeable K, that by classic interpretations would indicate there was no K deficiency. However, results showed that 5 out of the 10 sites where farmers had experienced K deficiency in the past, there was deficiency based on tissue analysis of K in corn plants. For these fields we found a negative correlation between K_{mic} and K uptake – suggesting there was microbial immobilization of K. Analysis of FAME profiles showed that the long-term effect of glyphosate on microbial communities was not a 'broad band' change in microbial community diversity or structure but rather a shift in certain subgroups. DGGE profiling followed by sequencing revealed certain pathogenic species were present in GTC fields and K deficient soils.

Experiment 2

In the 28 day incubation where soils from long-term glyphosate or no glyphosate were amended with glyphosate, EL-FAME profiling showed certain groups of soil bacteria responded to the glyphosate addition only when the soil had never received glyphosate before (e.g. Gr+ were suppressed over Gr- bacteria with 19 unique FAs changing with the addition of glyphosate). Conversely, the long-term GTC soils showed no shift in the microbial community due to glyphosate and had elevated levels of respiration, suggesting that the

community had adapted to glyphosate applications. In the second experiment with repeated applications after 60 days unique fatty acids were stimulated only in the organically managed soils. This is shown in Table 1.

Additional Studies

Greenhouse manipulative studies will be presented which evaluates responses to GRC soybeans and corn treated with glyphosate growing in soil that have had long-term GTC or non-GTC (organic and non-GMO fields) management. We will report on *Fusarium* species' responses and the results of a novel stable carbon isotope technique (^{13}C) which is allowed us to track glyphosate- ^{13}C into rhizosphere microbial groups to determine which microbes are feeding on glyphosate leaked by glyphosate tolerant roots.

Table 1. Unique fatty acid biomarkers that were stimulated in organically managed soils after glyphosate application that were unaffected in the long-term glyphosate treated soil.

FAME Biomarker		Organism
13.0 ISO	**	
16.1 ω 9c	**	
16.1 ω 5c	**	Arbuscular Mycorrhizal Fungi
16.0 10 ME	***	Actinomycetes
19.0 Cyclo ω 8c	**	Gram- Bacteria
20:4 ω 6,9,12,15c	ns	Protozoa

Multivariate evaluation by microbiological indicators of winter-summer crop rotation and no-tillage system in Oxisol (Brazil)

Clovis Daniel Borges José Eduardo Corá and Ely Nahas

Faculdade de Ciências Agropecuária e Veterinárias, Universidade Estadual Paulista Júlio de Mesquita Filho UNESP, SP, Brazil, Email clovis.borges@posgrad.fcav.unesp.br, cora@fcav.unesp.br, enahas@fcav.unesp.br.

Abstract

Crop rotations have agronomic advantage. Type of crop rotations in combination with no-tillage system has not been evaluated systematically in Brazil. The objective of this work was to evaluate the effect of the crop rotation on the soil microbiological properties (MP) and the effect of winter crops on summer crops in no-tillage systems in a tropical region. This ecosystem management has been carried out annually since 2002. The summer crops are continuous soybean, continuous corn and soybean/corn rotation (SM). The winter crops are: corn, sunflower, radish, millet, pigeon pea, sorghum and sunn hemp. Samples were collected in April 2008 at 0-0,15m depth after summer crops were harvested. Microbial respiratory activity, the activity of the enzymes dehydrogenase, urease and phosphatase, the biomass C, N and P, *q*MIC, organic matter and organic carbon contents were determined. Data was analyzed by principal components analysis (PCA). Soybean/corn sequence influenced the MP more than continuous corn and continuous soybean. For soybean/corn sequence soil, the main variables selected by PCA were biomass C, N and P, respiratory and phosphatase activities, and *q*MIC. Pigeon pea, sorghum and sunn hemp strongly affected the soil properties when compared with the other winter crops.

Key Words

Crop sequences, dehydrogenase, urease, phosphatase, bio-indicators

Introduction

Crop rotation improves soil structure and fertility due to growth of dissimilar types of crops in sequential seasons (Balota *et al.* 2003; Govaerts *et al.* 2008). Alternate crops also diminish the incidence of pathogens and pests. The positive effects attributed to the use of no-tillage systems on soil quality have been due to the crop residue that was retained on the soil (Govaerts *et al.* 2008), to soil aggregation (Balota *et al.* 2003), carbon sequestration (Lal 2004), and increased development of microbial biomass (Angers *et al.* 1993; Mercante *et al.* 2008). Principal component analysis is an important tool to discriminate managements, being useful to evaluate the quality of the soil being able to classify the most sensitive indicators of changes in the soil (Benintende *et al.* 2008). The objective of this study was to evaluate the effect of no-tillage associated with crop rotation on soil microbiological attributes.

Methods

The study was conducted in April 2008, after summer crops, at Jaboticabal (Brazil) (21° 25'S, 48° 18'W), with monthly average temperatures ranging from 18 to 32 °C and with a dry winter and rainy summer. The soil is an Oxisol (Rhodic Eutrudox), according to the USDA Soil Taxonomy system. The experimental design consisted of a randomized complete block with three replications. The experiment was conducted since 2002 (six growing season). The treatment consisted of three summer (October to February) crop sequences (continuous soybean, continuous corn, and soybean/corn rotation) combined with seven winter (March to September) crops: corn (*Zea mays L.*), sunflower (*Helianthus annuus L.*), radish (*Raphanus sativus L.*), millet (*Pennisetum americanum (L.) Leeke*), pigeon pea (*Cajanus cajan (L.) Millsp.*), sorghum (*Sorghum bicolor (L.) Moench*) and sunn hemp (*Crotalaria juncea L.*). Basal respiration was determined according to Rezende *et al.* (2004). Microbial biomass C, N and P (respectively, MBC, MBN and MBP) were evaluated by the fumigation-extraction methods proposed by Vance *et al.* (1987), Brookes *et al.* (1985) and Brookes *et al.* (1982), respectively. Metabolic quotient (*q*CO₂) was obtained by the relation between basal respiration and microbial biomass C (Anderson and Domsch 1990) and *q*MIC by the relation between microbial biomass C and total organic carbon. Dehydrogenase, urease and phosphatase activities were assayed using the methods of Casida (1977), McGarity and Myers (1967), and Tabatabai and Bremner (1969), respectively. Organic carbon (OC) was determined by dichromate oxidation (Sims and Haby 1971). Soil moisture was obtained after drying the soil samples for 24 h at 105°C, and organic matter (OM) after incineration the soil at 550 °C for 24 h. The data set was submitted to principal components analysis (PCA) using StatSoft software.

Results

Analysis of the principal components for summer crop system showed that the first and second components explained 100% of the total variance (Figure 1) 51% of the variability comes from the X-axis and 49% of additional original variability from the Y-axis. The PCA biplot showed three clusters: soybean/corn rotation, continuous soybean and continuous corn. The main variables selected by PCA for continuous soybean summer sequence were MBC, MBN, MBP, phosphatase activity, $qMIC$, and basal respiration. Continuous soybean influenced urease activity, organic matter, and soil moisture contents, while continuous corn influenced dehydrogenase activity, qCO_2 , and organic carbon (Figure 1).

The biplot of the PCA for all attributes influenced by winter crops showed that the first and second components explained 78% of the total variance (Figure 2), being 51% of the variability comes from the X-axis and 27% of additional original variability from the Y-axis. The PCA biplot showed two clusters. One cluster included pigeon pea, sorghum, and sunn hemp which was influenced strongly by qCO_2 , C-CO₂, soil moisture, OC, OM, MBP, phosphatase, urease and dehydrogenase activities (Figure 2). The other including radish and millet was affected strongly by MBC, MBN, and $qMIC$. Sunflower and corn winter crops have a low influence soil microbiological attributes (Figure 2).

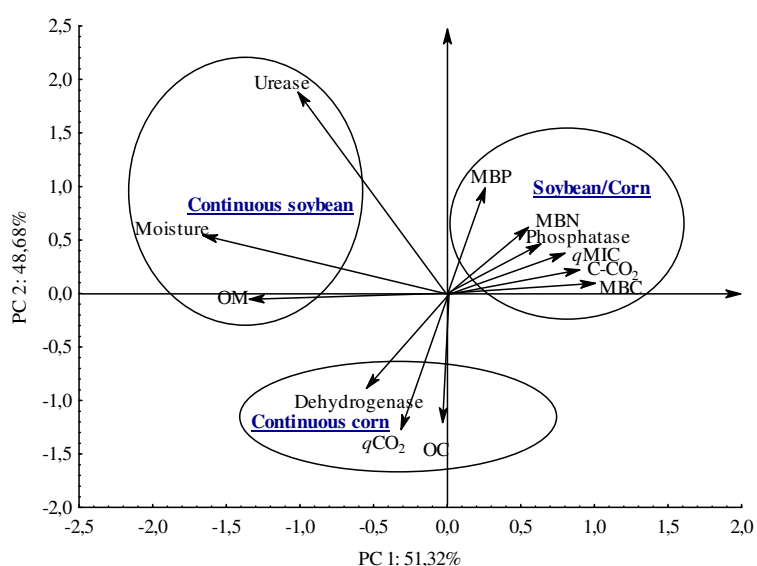


Figure 1. Bi-plot of principal components of the crop summer sequence. Microbial biomass carbon (MBC) ($\mu\text{g C/g dry soil}$), nitrogen (MBN) ($\mu\text{g N/g dry soil}$), and phosphorous (MBP) ($\mu\text{g P/g dry soil}$), microbial quotient ($qMIC$) (%), metabolic quotient (qCO_2) ($\mu\text{g C-CO}_2/\mu\text{g C-MBC/h}$), respiratory microbial activity (C-CO₂) ($\mu\text{g C-CO}_2/100\text{ g dry soil}$), dehydrogenase activity ($\mu\text{g TFF/g dry soil/ 24 h}$), urease activity ($\mu\text{g NH}_4\text{-N/g dry soil/ 3 h}$), phosphatase activity ($\mu\text{g pNP/g}^1\text{ dry soil/h}$), organic carbon (OC) (mg C/g dry soil), and organic matter (OM) (%).

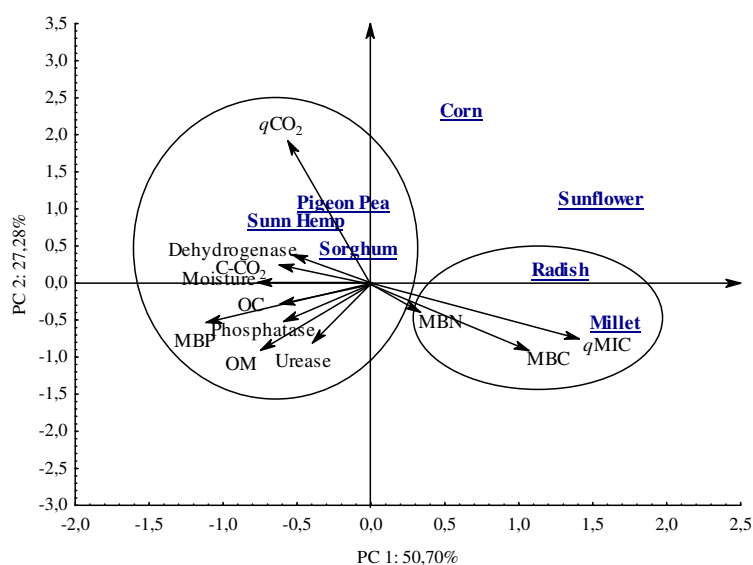


Figure 2. Bi-plot of principal components for winter crops. Abbreviations see Figure 1.

Conclusion

Microbiological attributes were influenced differently by the summer crop sequence and winter crops. The soybean/corn sequence increased soil quality compared to continuous corn and continuous soybean, probably due to greater stimulus of microbial activities. The winter crops pigeon pea, sorghum, and sunn hemp had positive effects on microbial attributes compared to the other winter crops. These effects can be attributed to the crop residue remaining on the soil surface in the no-tillage system and due to the crop rotation ecosystems which probably influenced microbial activity.

Acknowledgments

This work was supported by FAPESP grant.

References

- Anderson TH, Domsch KH (1990) Application of eco-physiological quotients ($q\text{CO}_2$ and $q\text{D}$) on microbial biomasses from soils of different cropping histories. *Soil Biology and Biochemistry* **22**, 251–255.
- Angers DA, Bissonnette N, Légère A, Samson N (1993) Microbial and biochemical changes induced by rotation and tillage in a soil under barley production. *Canadian Journal of Soil Science* **73**, 39-50.
- Balota EL, Colozzi-Filho A, Andrade DS, Dick RP (2003) Microbial biomass in soils under different tillage in crop rotation systems. *Biology and Fertility Soils* **38**, 15-20.
- Benintende SM, Benintende MC, Sterren MA, De Battista JJ (2008) Soil microbiological indicators of soil quality in four rice rotations systems. *Ecological Indicators* **8**, 704-708.
- Brookes PC, Powlson DS, Jenkinson DS (1982) Measurement of microbial biomass phosphorus in soil. *Soil Biology and Biochemistry* **14**, 319-329.
- Brookes PC, Landman A, Pruden G, Jenkinson DS (1985) Chloroform fumigation and the release of soil nitrogen: a rapid extraction method to measure microbial biomass nitrogen in Soil. *Soil Biology and Biochemistry* **17**, 837-842.
- Casida Jr LE (1977) Microbial metabolic activity in soil as measured by dehydrogenase determinations. *Applied and Environmental Microbiology* **34**, 630-636.
- Govaerts B, Mezzalama M, Sayre KD, Crossa J, Lichter K, Troch V, Vanherck K, De Corte P, Deckers J (2008) Long-term consequences of tillage, residue management, and crop rotation on selected soil microflora groups in the subtropical highlands. *Applied Soil Ecology* **38**, 197-210.
- Lal R (2004) Climate change and food security soil carbon sequestration impacts on global. *Science* **304**, 1623-1627.
- McGarity JW, Myers MG. (1967) A survey of urease activity in soils of Northern New South Wales. *Plant and Soil* **27**, 217-238.
- Mercante FM, Silva RF, Francelino CSF, Cavalheiro JCT, Otsubo AA (2008) Biomassa microbiana em um Argissolo Vermelho, em diferentes coberturas vegetais, em área cultivada com mandioca. *Acta Scientia Agronomica* **34**, 479-485.
- Rezende LA, Assis LC, Nahas E (2004) Carbon, nitrogen and phosphorus mineralization in two soils amended with distillery yeast. *Bioresource Technology* **94**, 159-167.
- Sims JR, Haby VA (1971) Simplified colorimetric determination of soil organic matter. *Soil Science* **112**, 137-141.
- Tabatabai MA, Remner JM (1969) Use of p-nitrophenyl phosphate for assay of soil phosphatase activity. *Soil Biology and Biochemistry* **1**, 301-307.
- Vance ED, Brookes PC, Jenkinson DS (1987) An extraction method for measuring soil microbial biomass C. *Soil Biology and Biochemistry* **19**, 703-707.

Nickel Speciation in Serpentine Soils using Synchrotron Radiation Techniques

Matthew Siebecker and Donald L Sparks

152 Townsend Hall, Department of Plant and Soil Sciences and Delaware Environmental Institute, Newark, DE, USA, mgs@udel.edu

Abstract

We examined nickel in serpentine soils from Southwest Oregon to determine metal speciation and co-localization. Serpentine soils naturally contain elevated concentrations of nickel, manganese, chromium, and cobalt and are the media on which many Ni hyperaccumulating plants evolved. Hyperaccumulators are effective at removing extraordinary amounts of nickel from serpentine soils and are considered excellent candidates for phytoremediation of Ni contaminated soils. Nickel contaminated soil results from nickel refining and steel production. Nickel has been identified in over 800 hazardous waste sites in the US and is a common soil contaminant near nickel refineries in Canada and Russia. Our results will help to elucidate metal uptake mechanisms used by hyperaccumulating plants by identifying soil Ni species. X-Ray Absorption Spectroscopy (XAS) yields a more accurate picture of metal speciation in mineralized or contaminated soils than traditional, sequential chemical extractions. We employed synchrotron-based X-Ray Fluorescence (SXRF) mapping, bulk- and micro- Extended X-Ray Absorption Fine Structure Spectroscopy (EXAFS), and micro-X-Ray Diffraction (μ -XRD). From these techniques, we determined that Ni co-localizes with iron and manganese in serpentine soils, and the major species contributing to the Ni EXAFS spectra include Ni-containing Fe and Mn minerals and Layered Double Hydroxide (LDH) phase minerals.

Key Words

Nickel speciation, serpentine soil, X-ray absorption spectroscopy, phytoremediation

Introduction

The fate of trace metals (e.g., Ni) in soil systems is a significant issue in environmental science and health. Metal enriched soils are prevalent in nature, originating from both anthropogenic and geogenic sources. Anthropogenic inputs include waste from municipal incineration, stainless steel production, coal combustion, and nickel refinery emissions. Geogenic sources of Ni include magmatic sulfide ores and lateritic silicates found in serpentine soils. Anthropogenic Ni in soil poses significant health risks to communities neighboring nickel emission sources. A Ni refinery in Port Colborne, Ontario, Canada enriched 345 km² of land with Ni, and farms in the immediate vicinity of the refinery demonstrated reduced vegetable crop yields (McNear *et al.*, 2007). Ni refinery emissions have been underestimated in parts of northwestern and central Russia (Boyd *et al.*, 2009). Soil contaminated from smelter emissions on the Kola Peninsula, Russia, contained 9000 ppm Ni, which is 450 times higher than background concentrations. Native plants like berries and mushrooms growing 3000 km² around the smelter complex contain elevated nickel concentration, making the food unsuitable for human consumption (Barcan *et al.*, 1998). Complete Ni leaching from the Ao layer of the soil was calculated to be 160–270 years (Barcan, 2002). One may be exposed to nickel by air, skin contact with soil, or metals containing nickel; however, the major source of exposure to nickel is food. Nickel refinery dust is carcinogenic to humans (ATSDR, 2005). Although Ni is an essential micronutrient for plant growth, elevated Ni concentrations in soils are toxic to crops.

While serpentine soils have been studied extensively, to our knowledge no study has appeared on the direct speciation of nickel naturally present in serpentine soils using synchrotron-based XAS. Traditionally, sequential chemical extractions were used to ascertain soil metal speciation and involved repeated extractions with increasingly aggressive reagents. These techniques were effective in determining that nickel accumulates partly in magnesium silicates but mostly with manganese and iron oxides (Alexander *et al.*, 2007). However, these techniques are limited by the possibility of sample alteration. XAS is capable of determining *in-situ* metal speciation with minimal chemical sample treatment.

Methods

Basic soil characterization was performed. Soil pH was determined by mixing the soil with distilled water in a 1:1 ratio and measuring the pH. Percent organic matter was determined by the loss-on-ignition method. Elemental compositions were determined via microwave digestion with nitric acid followed by ICP-OES. For synchrotron studies, soil samples were ground to a powder and dusted on kapton tape, removing excess dust. Sufficient incident energy to simultaneously excite fluorescence from Ni, Co, Fe, and Mn for mapping was used

to enable determination of local metal associations and co-occurrence. Multi-element fluorescence data were collected with a Ge multi-element detector positioned 90° to the incident beam (45° to the sample). Because of the well-defined energy resolution of the multi-element detector, special attention was paid to selecting the fluorescence of the Ni K-alpha peak so that the resulting spectra did not include fluorescence from the Fe K-beta peak. Course XRF maps (1-3 mm² using an X-ray beam spot of ~60µm²) were used to observe distinct metal correlations and to identify regions of interest (i.e., “hotspots”) for µ-EXAFS and µ-XRD analysis. Fine XRF maps (200µm²) were generated using shorter dwell times. With the monochromator calibrated for nickel, µ-EXAFS spectra were collected from approximately 50eV below the absorption edge energy to k values of 10 Å⁻¹ in the EXAFS region, and µ-XRD data were collected with a CCD detector. Multiple scans were collected until satisfactory signal to noise ratios were achieved. For each sample, depending on the number of hotspots and concentration, XRF mapping required a total of 2 to 4 hours and EXAFS scans required 4 to 6 hours. Micro-XRD spectra were collected for 60 seconds per scan. EXAFS spectra collected from heterogeneous systems were analyzed by principle component analysis, target transformation, and linear least squares fitting to extract structural information for the coordination shells and the most dominant Ni species contributing to the spectra.

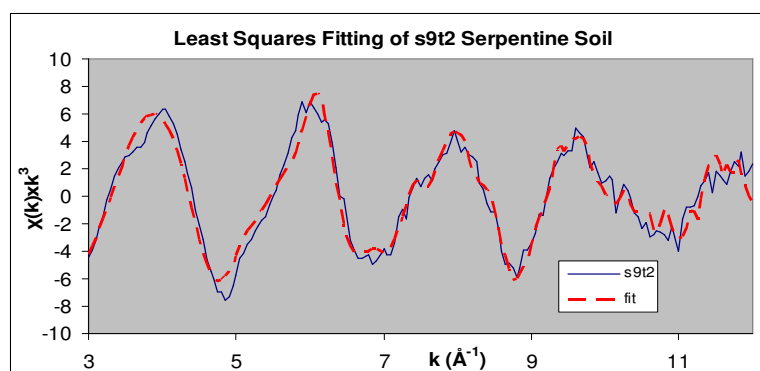
Results and Discussion

Table 1 presents the basic soil characterization data. For serpentine soils, the pH is considered slightly low. Elevated Ni concentrations are evident. Samples also contained elevated amounts of Cr and Mn.

pH	Texture	OM (%)	Co	Cr	Mn	Fe	Ni
5.9-6.9	loamy sand to clay loam	2.7 -6.5	63 - 310	500 - 3080	350 - 3300	32000 - 190000	560 - 7500

Table 1. Soil characterization data, elemental concentrations given in parts per million (ppm)

Figure 1 presents the results of least squares fitting (LSF) of the Ni EXAFS spectra from serpentine soil (s9t2) from Oregon. LSF shows some of the major contributing Ni species. Figure 1 was deduced from a suite of over 25 Ni EXAFS standard spectra. This spectrum was collected at beamline 11-2 at the Stanford Synchrotron Radiation Laboratory. Multiple sweeps were calibrated using a Ni internal reference foil, averaged, and background subtracted using SixPack software. From the spectra, it is evident that manganese and iron minerals, as well as Ni/Al-LDH phases, play a large role in Ni speciation in the serpentine soil. From the fitted data, Ni hydroxides, oxides, and pure phyllosilicate phases do not appear to be important components in this serpentine soil.



Component	%
Ni/Al-LDH	34.1
Gaspetite (Ni,Mg,Fe)CO ₃	25.9
Ni-Mn-Oxide	60.3

Figure 1. Least Squares Fitting of a Ni EXAFS spectrum for serpentine soil s9t2.

Figure 2 presents the XRF maps of nickel, iron, and manganese for the s18t2 serpentine soil sample. These maps were generated at beam-line X26A at the National Synchrotron Light Source at Brookhaven National Laboratory. Incident X-Ray energy was 11000eV. Each map describes the same 1x1mm area of sample. Ni fluorescence coordinates highly with the fluorescence of iron, indicating that these two elements are highly coordinated within the sample. It is important to distinguish from the scale bars that the sample contains much more Fe than Ni, which denotes that Ni is partitioned into iron-containing minerals. This specific soil contains approximately 20% iron. Although to a lesser degree, Ni is also associated with Mn, indicated by the white circles. From this 1x1mm sample area, two µ-EXAFS spectra were obtained to assess the heterogeneity of Ni-

speciation on the micron-scale.

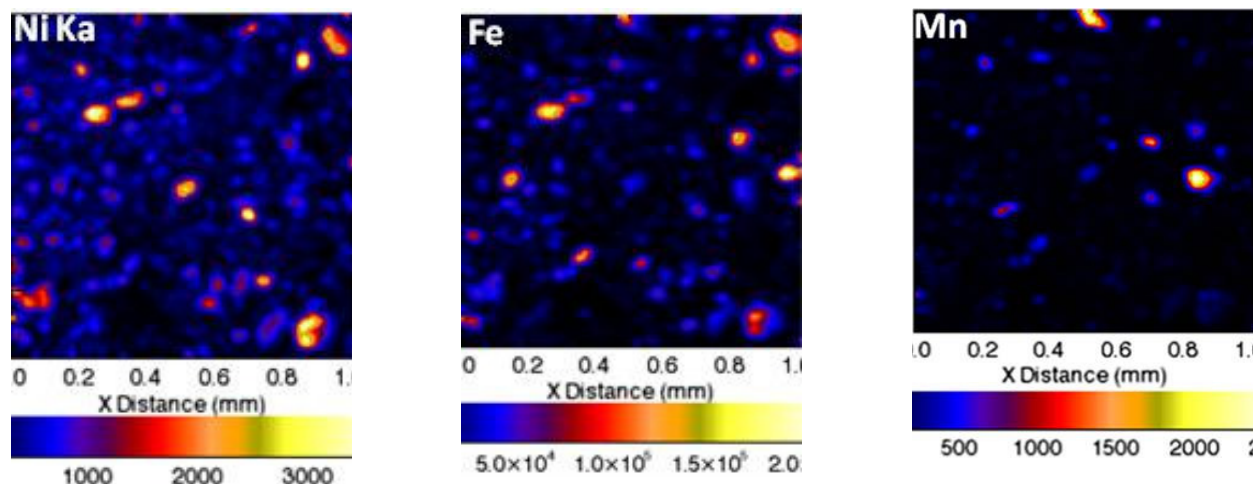


Figure 2. Multi-element fluorescence mapping from the s18t2 serpentine soil sample. Map intensities are independent of each other. The scale bar for each element is specific for its map, and its unit is in number of fluorescence photons counted per second by the multi-element detector.

Conclusion

We have provided spectroscopic evidence and confirmation that Ni accumulates largely with iron and manganese in serpentine soils from southwest Oregon. These data provide the first spectroscopic evidence confirming Ni association with Fe and Mn. The LSF of sample s9t2 provides convincing evidence that Ni is associated with both Fe and Mn because Ni-Fe and Ni-Mn reference spectra contribute significantly to the Ni EXAFS serpentine soil spectrum. Additionally, LDH phases are known to develop with Ni at higher pH. Because serpentine soils generally have slightly alkaline pH it is reasonable to conclude that their formation is possible. Because hyperaccumulator plants are native to this type of soil, they must employ a mechanism that can either remove Ni from Fe/Mn compounds or dissolve those compounds to effectively liberate nickel into the soil solution where it can be taken up into the above ground biomass.

References

- Agency for Toxic Substances and Disease Registry – ATSDR (2005) Toxicological Profile for Nickel. U.S. Dept. of Health and Human Services Public Health Service
- Alexander EB, Coleman RG, Keeler-Wolfe T, Harrison SP (2007) ‘Serpentine Geocology of Western North America: Geology, Soils, and Vegetation.’ (Oxford University Press: New York)
- Barcan V, Kovnatsky E, Smetannikova M (1998) Absorption of heavy metals in wild berries and edible mushrooms in an area affected by smelter emissions. *Water, Air, and Soil Pollution* 103, 173– 95.
- Barcan V (2002) Leaching of nickel and copper from soil contaminated by metallurgical dust. *Environment International* 28, 63-68.
- Boyd R, Barnes S-J, De Caritat P, Chekushin VA, Melezhik VA, Reimann C, Zientek ML (2009) Emissions from the copper–nickel industry on the Kola Peninsula and at Noril’sk, Russia. *Atmospheric Environment* 43, 1474-1480.
- Chaney RL, Angle JS, Broadhurst CL, Peters CA, Tappero RV, Sparks DL (2007) Improved understanding of hyperaccumulation yields commercial phytoextraction and phytomining technologies. *Journal of Environmental Quality* 36, 1429-1443.
- McNear Jr DH, Chaney RL, Sparks DL (2007) The effects of soil type and chemical treatment on nickel speciation in refinery enriched soils: A multi-technique investigation. *Geochimica et Cosmochimica Acta* 71(9), 2190-2208.

Nitrate reduction in the interactive reaction system of L17 and soil minerals

Tong-xu Liu^A, Xiao-min Li^A and Fang-bai Li^A

^AGuangdong Key Laboratory of Agricultural Environment Pollution Integrated Control, Guangdong Institute of Eco-Environmental and Soil Sciences, Guangzhou 510650, PR China, Email txliu@soil.gd.cn, cefbli@soil.gd.cn

Abstract

In this study, the potential for microbially catalyzed NO_3^- reduction with iron oxide was examined using *Klebsiella pneumoniae* strain L17 and four types of iron oxides under anaerobic conditions. The results showed that L17 had the capacity of nitrate reduction, and iron oxides can accelerate the reduction rate significantly. The biogenic Fe(II) contributed to the acceleration slightly, which was not enough to reduce so much nitrogen. To investigate the role of iron oxide for the nitrate reduction, a series of minerals but iron oxides with L17 were combined for nitrate reduction, and the results showed all the oxides can accelerate the reduction rate, indicating that the electron might transfer to nitrate through the oxides but not experiencing iron oxide's reduction. Hence, besides the well-known mechanism: direct microbial reduction and reduction by the biogenic Fe(II), a new mechanism was proposed whereby soil minerals can mediate electron transfer to accelerate the microbial nitrate reduction. This study could be helpful in understanding the relationship between the redox cycles of Fe and N in subsurface sedimentary environments.

Key Words

Nitrogen cycle, iron cycle, electron transfer, denitrification, dissimilatory iron reduction.

Introduction

Nitrogen is an essential element for living organisms, and the availability of a suitable nitrogen source often limits primary productivity in both natural environments and agriculture (Cabello *et al.* 2004). It is well known that the natural nitrate reduction is mainly attributed to the biotic process of direct enzyme catalysis by nitrate reduction bacteria (Gonzalez *et al.* 2006), while various abiotic and biotic-abiotic combined processes have also been reported to be responsible for the natural reduction of nitrate in anoxic environment (Jørgensen *et al.* 2009). Firstly, the biotic processes involve (i) the anaerobic reduction of NO_3^- to N_2O and N_2 (denitrification), (ii) the conversion of NO_3^- into ammonia (dissimilatory ammonification), and (iii) the conversion of nitrate to ammonia, which is used by the cell to incorporate nitrogen into biomolecules (assimilation) (Gonzalez *et al.* 2006). Secondly, it is suggested that ferrous iron as electron donors is capable of reducing nitrate in anaerobic, sedimentary environments (Jørgensen *et al.* 2009). Reduction of nitrate to ammonia can proceed at appreciable rates in abiotic systems in the presence of green rust compounds at circumstance pH (Ottley *et al.* 1997). The presence of crystalline iron oxide (lepidocrocite and goethite) surfaces accelerates low-temperature reduction of NO_3^- coupled to Fe(II) oxidation at pH values greater than 8.0 (Hansen *et al.* 2009). Thirdly, microbially catalyzed nitrate reduction coupled to Fe(II) oxidation under anaerobic environment has also been reported (Straub *et al.* 1996; Weber *et al.* 2001), and the role of biogenic Fe(II) was taken into consideration for nitrogen cycling.

The occurrence of biological Fe(II)-dependent nitrate reduction in a variety of natural systems suggests that this reaction may play a significant role in coupling the redox cycles of Fe and N in sedimentary environments. However, it is also observed that the molar ratios of NO_3^- consumed to Fe(II) oxidized exceeded the theoretical stoichiometry (Straub *et al.* 1996; Weber *et al.* 2001; Nielsen *et al.* 1998). The reason for this disagreement is unclear in these previous studies. Hence, the study was aim at explaining the reason of above disagreement in the simulated system of bacteria/soil mineral/nitrate, and the mechanism will be further discussed.

Methods

Materials

NaNO_3 ($\geq 99.0\%$) were purchased from Sigma-Aldrich without further purification. Other chemicals being of analytical grade were purchased from Guangzhou Chemical Reagent Factory, China. *Klebsiella pneumoniae* strain L17 was a dissimilatory iron reducing bacterium (DIRB), isolated subterranean forest sediment in Zhaoqing, China (Li *et al.* 2009). Goethite ($\alpha\text{-FeOOH}$), Lepidocrocite ($\gamma\text{-FeOOH}$), hematite ($\alpha\text{-Fe}_2\text{O}_3$), and Maghemite ($\gamma\text{-Fe}_2\text{O}_3$) were synthesized according to procedures as previously described (Li *et al.* 2009), while Bismuth oxide (Bi_2O_3), Aluminium oxide (Al_2O_3), Neodymium oxide (Nd_2O_3), Zirconium dioxide (ZrO_2), and

Titanium dioxide (TiO₂) were purchased from Sigma-Aldrich without further purification.

Experimental procedure

To avoid the interference of other inorganic anions in detection, the anaerobic NaHCO₃-buffered (30 mM, pH 6.8, N₂:CO₂ (80:20) atmosphere) medium only contained 7.5 mM NaNO₃ or NaNO₂ as electron acceptor and 5 mM glucose as electron donor, and harvested cells of *K. pneumoniae* L17 were added with final concentration of ca. 10⁷ cells/ml. Cells were grown in nutrient broth under aerobic conditions on a rotary shaker at 180 rev/min at 30°C, and harvested by centrifugation at 6,900 × *g* for 10 min at 4 °C when it approached the exponential phase. The pellets were washed three times and resuspended in sterile fresh basal medium to an optical density of 0.7 to 1.1 (λ = 600 nm). The density of 1.1 corresponded to approximately 1.4 × 10⁸ cells/ml, based on preliminary experiments that correlated culture optical density with viable cell counts determined by serial dilution and plating. Several batch experiments for NO₃⁻/NO₂⁻ reduction including controls were conducted in this study: (1) Fe²⁺ (0.3 mM); (2) α-FeOOH (25 mM); (3) α-FeOOH (25 mM) + Fe²⁺ (0.3 mM); (4) L17; (5) L17 + α-FeOOH, γ-FeOOH, α-Fe₂O₃, γ-Fe₂O₃, Bi₂O₃, Al₂O₃, Nd₂O₃, ZrO₂, or TiO₂ (4.5 g/L). Standard anaerobic techniques were used throughout all experiments as previously described (Li *et al.* 2009). Inoculation and sampling were conducted by using sterile syringes and needles. All vials were conducted in duplicate and incubated in a BACTRON Anaerobic/Environmental Chamber II (SHELLAB, Sheldon Manufacturing Inc.) at 30°C in dark.

Analytical methods.

To remove the cells and oxide, samples for determination of NO₃⁻/NO₂⁻ must be filtrated using a 0.22-μm syringe filter after centrifugation at 8,500 × *g* for 20 min. The concentration of NO₃⁻/NO₂⁻ was determined by ion chromatography (Dionex ICS-90) with an ion column (IonPac AS14A 4 × 250 mm). A mobile phase consisting of Na₂CO₃ (8.0 mM) and NaHCO₃ (1.0 mM) solutions was operated at a flow rate of 1.0 mL/min. The total concentration of Fe(II), including dissolved and sorbed Fe(II), was determined by extracting Fe(II) from the samples using 0.5 mol/L HCl for 1.5 h and assaying the extract using 1,10-phenanthroline colorimetric assay. Dissolved Fe(II) was determined by removing the mineral and adsorbed Fe(II) from the aqueous phase using a 0.22-μm syringe filter and then assaying the filtrate by 1,10-phenanthroline. Adsorbed Fe(II) was calculated as the difference between the total and dissolved Fe(II).

Results

NO₃⁻ reduction

Figure 1a showed that L17 can reduce nitrate efficiently from 7.5 mM to 0 mM in 4 days, while the NO₃⁻ reduction rate was obviously accelerated by the addition of iron oxides, and the total NO₃⁻ (7.5 mM) disappeared completely just in 2 days. The first-order-rate constants (*k*) in Figure 1c suggested that the *k* values of L17/α-FeOOH, L17/γ-FeOOH, L17/α-Fe₂O₃, and L17/γ-Fe₂O₃ were 2.1732/d, 2.3132/d, 2.6806/d, and 2.8828/d, much higher than that of L17 alone (0.6503/d). To illustrate the role of biogenic Fe(II) from dissimilatory iron reduction, the controls of Fe²⁺, α-FeOOH, and Fe²⁺/α-FeOOH were simultaneously conducted, and the results showed that no significant reduction of NO₃⁻ was observed with Fe²⁺ or α-FeOOH alone, while 10% of NO₃⁻ was reduced in the Fe²⁺/α-FeOOH system after 4 days reaction, indicating that the biogenic Fe(II) just had minor contribution to the nitrate reduction in the L17/IOs system. Hence, the acceleration of nitrate reduction might be due to not only the biogenic Fe(II) but also some other unexpected factors. Herein we proposed a hypothesis that the IOs, as an semiconductor oxides, can transfer electron from L17, to confirm this hypothesis, a series of minerals but not iron oxides (non-IOs) were used in this reaction system, such as Bi₂O₃, Al₂O₃, Nd₂O₃, ZrO₂, and TiO₂. As shown in Figure 1b, in comparison with L17 alone, the NO₃⁻ reduction rate was accelerated by the addition of non-IOs, and The first-order-rate constants (*k*) in Figure 1c suggested that the *k* values of L17/Bi₂O₃, L17/Al₂O₃, L17/Nd₂O₃, L17/ZrO₂, and L17/TiO₂ were 0.766/d, 1.1243/d, 1.2695/d, 1.4583/d and 1.6038/d, higher than that of L17 alone (0.6503/d). The above important finding suggested that the acceleration of nitrate reduction might be attributed to the possible mechanism that the electron from L17 can be transferred through the semiconductor, which can lead an increase of electron transfer.

Proposed mechanisms and reduction pathways

Based on the above discussion, the electron transfer from cell to nitrate/nitrite may have three ways (Figure 2), (i) the direct reduction via the metabolism of the bacterium, (ii) the reduction by biogenic adsorbed Fe(II) of dissimilatory iron reduction, besides these two ways, a new way was proposed as (iii) the semiconductor-

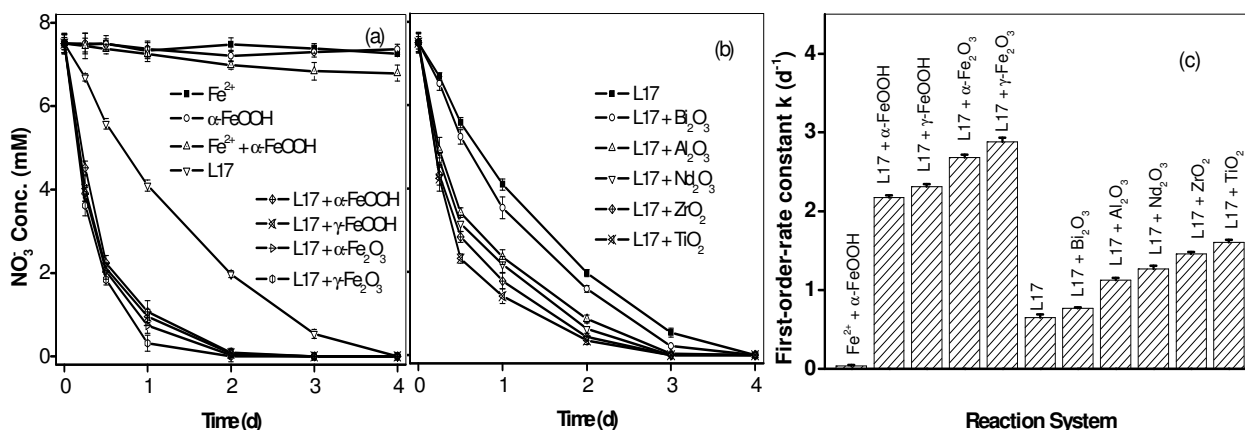


Figure 1. NO₃⁻ reduction in the reaction system of (a) L17 + iron oxides (L17/IOs), (b) L17 + minerals but not iron oxides (L17/non-IOs), and (c) the first-order-rate constants of various reaction systems (k₁/d).

mediated electron transfer process. It must be clear that the electron transfer for the reduction of nitrate and Fe(III) oxide is originally driven by the microbe L17. And the biogenic adsorbed Fe(II) can also contribute to the denitrification slightly, while a large fraction of electron from L17 was directly transferred to nitrogen through the iron oxide, which lead a significant enhancement of nitrate/nitrite reduction. Regarding to semiconductor-mediated electron transfer process, an important question was raised how the electron from the L17 transfer through the semiconductor. Herein we proposed another hypothesis, which was described as: the electron from cells can be injected to the conduction band of semiconductors, and then transferred to the surface, finally, it can be accepted by the surface reducible species, including nitrate, Fe(III) and so on. Next work will be focused on proving this hypothesis.

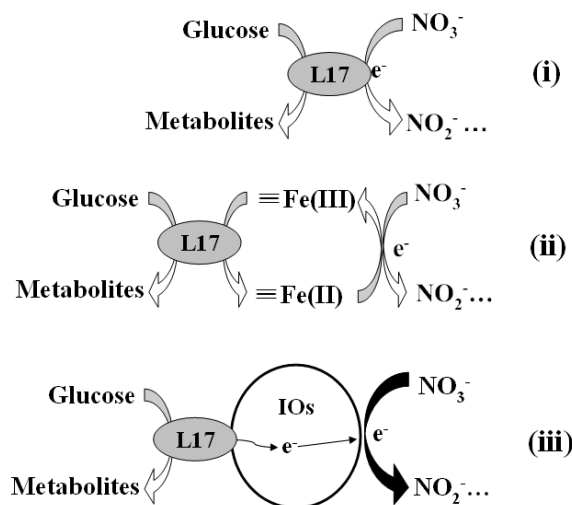


Figure 2. The proposed mechanism of NO₃⁻ reduction in the system of L17 and soil minerals: (i) direct microbial reduction, (ii) reduction by the biogenic Fe(II), (iii) reduction by mineral-mediated electron transfer.

Conclusion

The study showed that L17 had the capacity of nitrate reduction, and iron oxides can accelerate the reduction rate significantly. But the biogenic Fe(II) contributed to the acceleration slightly, which was not enough to reduce so much nitrogen. A series of non iron oxides with L17 were combined for nitrate reduction, and the results showed all the oxides can accelerate the reduction rate, indicating that the electron might transfer to nitrate through the oxides but not experiencing iron oxide's reduction. Hence, besides the well-known mechanism: direct microbial reduction and reduction by the biogenic Fe(II), a new mechanism was confirmed as soil mineral can mediate electron transfer to accelerate the microbial nitrate reduction.

References

Cabello P, Roldan MD, Moreno-Vivian C (2004) Nitrate reduction and the nitrogen cycle in archaea. *Microbiology* **150**, 3527–3546.

- Gonzalez PJ, Correia C, Moura I, Brondino CD, Moura JGG (2006) Bacterial nitrate reductases: Molecular and biological aspects of nitrate reduction. *Journal of Inorganic Biochemistry* **100**, 1015–1023.
- Hansen HCB, Koch CB, Nancke-Krogh H, Borggaard OK, Sørensen J (1996) Abiotic nitrate reduction to ammonium: Key role of green rust. *Environmental Science and Technology* **30**, 2053–2056.
- Jørgensen CJ, Jacobsen OS, Elberling B, Aamand J (2009) Microbial oxidation of pyrite coupled to nitrate reduction in anoxic groundwater sediment. *Environmental Science & Technology* **43**, 4851–4857.
- Li XM, Zhou SG, Li FB, Wu CY, Zhuang L, Xu W, Liu L (2009) Fe(III) oxide reduction and carbon tetrachloride dechlorination by a newly isolated *Klebsiella pneumoniae* strain L17. *Journal of Applied Microbiology* **106**, 130–139.
- Liu L, Li FB, Feng CH, Li XZ (2009) Microbial fuel cell with an azo-dye-feeding cathode. *Applied Microbiology and Biotechnology* **85**, 175–183.
- Nielsen JL, Nielsen PH (1998) Microbial nitrate-dependent oxidation of ferrous iron in activated sludge. *Environmental Science and Technology* **32**, 3556–3561.
- Ottley CJ, Davison W, Edmunds WM (1997) Chemical catalysis of nitrate reduction by iron(II). *Geochim. Cosmochim. Acta* **61**, 1819–1828.
- Straub KL, Benz M, Schink B, Widdel F (1996) Anaerobic, nitrate-dependent microbial oxidation of ferrous iron. *Appl. Environ. Microbiol.* **62**, 1458–1460.
- Weber KA, Picardal FW, Roden EE (2001) Microbially catalyzed nitrate-dependent oxidation of biogenic solid-phase Fe(II) compounds. *Environmental Science and Technology* **35**, 1644–1650.

Phenolic compounds in NaOH extracts of UK soils and their contribution to antioxidant capacity

David L. Rimmer and Geoffrey D. Abbott

School of Civil Engineering and Geosciences, Newcastle University, Newcastle upon Tyne NE1 7RU, UK, E-mail david.rimmer@ncl.ac.uk

Abstract

Antioxidants are released during the extraction of soils with NaOH, which also releases phenolic compounds from plant and soil material. This raises the possibility that phenolics are important contributors to the antioxidant capacity (AOC) of soils. Both the AOCs and the concentrations of 12 phenolic compounds were measured in NaOH extracts of a range of UK soils. Samples of surface and subsurface horizons were taken from 24 sites representing the major soil types (brown soils, gleys, podzols, peats and lithomorphous soils). The internal standards method was used to quantify the phenolics, which were detected by gas chromatography. The AOC of the extracts was measured using the ABTS free radical method. There were differences in the phenolic distributions extracted from soils with different land uses/plant inputs, as well as differences between surface and subsurface samples. A linear relationship was found between the AOCs of the extracts and the sum of the phenolic compounds. The AOCs of the individual phenolic compounds were also measured. The calculated contribution of the individual phenolics to the AOC of the extracts was small and less than 10% of the total AOC in all cases. Thus the measured phenolic compounds were not important contributors to the AOCs, and other unidentified antioxidant compounds were probably present.

Key Words

Soil organic matter mineralization

Introduction

Phenolic compounds in soils have been studied for at least 50 years and much of the work related to podzolization processes (Bloomfield, 1952; Vance *et al.*, 1986). The relationship between phenolics in crop residues and soil processes, such as residue decomposition, nutrient release, and aggregate formation, was investigated by Martens (2002a, b), who established that phenolics were metabolized in soil at a much slower rate than the carbohydrates and amino acids.

Many naturally occurring antioxidants are phenolics, for example vitamin E. Antioxidant molecules terminate the chain reaction of damaging free radical formation by being transformed into unreactive, stable free radicals and thereby control oxidation processes (Halliwell and Gutteridge, 2007). The degradation of food involves oxidation by free radicals and is retarded by antioxidants (Gaman and Sherrington, 1990). Therefore, it was hypothesised that antioxidants are present in soil and that they are involved in the protection of soil organic matter from oxidation (Rimmer, 2006). Subsequently we showed that antioxidants can be extracted from soils with NaOH, in proportion to their organic carbon contents (Rimmer and Smith 2009).

Because many phenolic compounds have antioxidant properties, and because previous studies have demonstrated the presence, and importance, of phenols in soils (e.g. Martens, 2002a, b), the objectives of the present study were to: measure the antioxidant capacity (AOC) and the concentration of a group of phenolic compounds in NaOH extracts of soils, and to calculate the contribution of the measured phenolics to the AOC. By using samples of surface and subsurface horizons from a wide range of UK soil types from sites with a range of land uses, we aimed to identify any differences in both the phenolic compounds and the AOC resulting from differences in horizon, soil type, and land use.

Materials and methods

Soils

Samples from 24 sites, representing the major soil groups in the UK, were collected. By separately sampling the different soil horizons at each site, we obtained samples from 48 horizons for the study. The sites were selected to cover the soil groups: brown soils, gleys, podzols, peats, and lithomorphous soils (Avery, 1990).

Measurement of antioxidant capacity

The method chosen was the Trolox equivalent antioxidant capacity (Re *et al.*, 1999). This uses a stable coloured free radical in aqueous solution, with the measurement of antioxidant capacity being the decrease in absorbance of the solution in a UV-VIS spectrophotometer following addition of the antioxidant. The radical used is 2,2'-azinobis(3-ethylbenzothiazoline-6-sulphonate) (ABTS). Calibration with a standard antioxidant, Trolox (an analogue of vitamin E), allowed the absorbance decrease results to be expressed as Trolox equivalent concentrations (μM).

Extraction method

Two extraction methods were used in the study of phenolic acids by Martens (2002a), namely 1 M NaOH at room temperature and 4 M NaOH autoclaved at 120°C. Previously we used 1 M NaOH to bring antioxidants into solution (Rimmer and Smith, 2009). Here we compared 1 M and 4 M NaOH methods and found that 4 M NaOH was significantly more effective in bringing antioxidants into solution, and was adopted.

Analysis of phenolic compounds

The 12 phenolics quantified were: *p*-hydroxy-benzaldehyde, vanillin, *p*-hydroxy-acetophenone, acetovanillone, *p*-hydroxy-benzoic acid, vanillic acid, syringaldehyde, *p*-coumaric acid, acetosyringone, syringic acid, ferulic acid, and sinapic acid. These are the same as those quantified by Martens (2002a), and are the most abundant ones in the extracts, although it is likely that many others, such as guaiacol, syringol and their derivatives will also be present. The isolation and analysis of these compounds was based on the procedures described by Martens (2002a). The samples were analysed on a gas chromatograph and compounds were identified by comparison of retention time with those of standards. Compounds were quantified by using the internal standards method.

Antioxidant capacity of phenolic compounds

The antioxidant capacity of each of the 12 phenolic compounds was measured by dissolving 10 g of the compound in ethanol and diluting with deionised water. Aliquots of these solutions were assayed for antioxidant capacity using ABTS with calibration against Trolox, as described above (Re *et al.*, 1999).

Results and discussion

Phenolic compounds

The concentrations of the extracted phenolic compounds are shown in Figure 1. The overall pattern (Figure 1a) shows that the three compounds with the greatest concentrations were: *p*-hydroxybenzoic acid, vanillic acid, and ferulic acid. These compounds were also dominant for the subset of surface samples, which had a similar pattern of distribution (data not shown). By contrast for the subsurface samples, vanillin had the greatest median concentration, followed by vanillic acid and *p*-hydroxybenzoic acid. Martens (2002b) in his study of soil amended with plant residues found that there was only an increase in the concentration of *p*-hydroxybenzoic acid over the 84-day incubation. This increase was attributed to its production by microbial synthesis (Moorman *et al.*, 1992), which may explain why overall it had the greatest concentration in the soils of this study, and particularly for surface samples.

The effect of land use on the concentrations of phenolic compounds extracted from surface soils is also shown in Figure 1. Pasture was the dominant land use and the pattern seen (Figure 1b) was similar to that for all samples (Figure 1a). In arable soils (Figure 1c) there was a completely different pattern with acetosyringone having the greatest concentration, while vanillic acid was most important in both semi-natural and woodland soils (data not shown).

Martens (2002a) presented data on phenolic compounds from surface soils of a single soil type but under different management/cropping. The methods of extraction, purification and quantification were the same as in the present study. The concentrations obtained were of a similar magnitude, and the dominant compounds were similar to those above. In the prairie soil these were: *p*-coumaric acid, ferulic acid, and *p*-hydroxybenzoic acid. For the cropped soils, acetosyringone replaced ferulic acid in the list, as it did in the arable soils of the present study. We conclude therefore that the vegetation, and particularly vegetation residues, play an important role in determining the phenolic compounds extracted.

The concentrations of the phenolic compounds measured in the extracts were summed. The median value of the summed amounts of the phenolic compounds for surface soils was approximately 10 times greater than that for subsurface horizons, and reflected differences in the organic matter content of the samples. This is in agreement

with Martens (2002b), who reported that the total phenolic content of a single soil incubated with various plant residues increased as organic C increased.

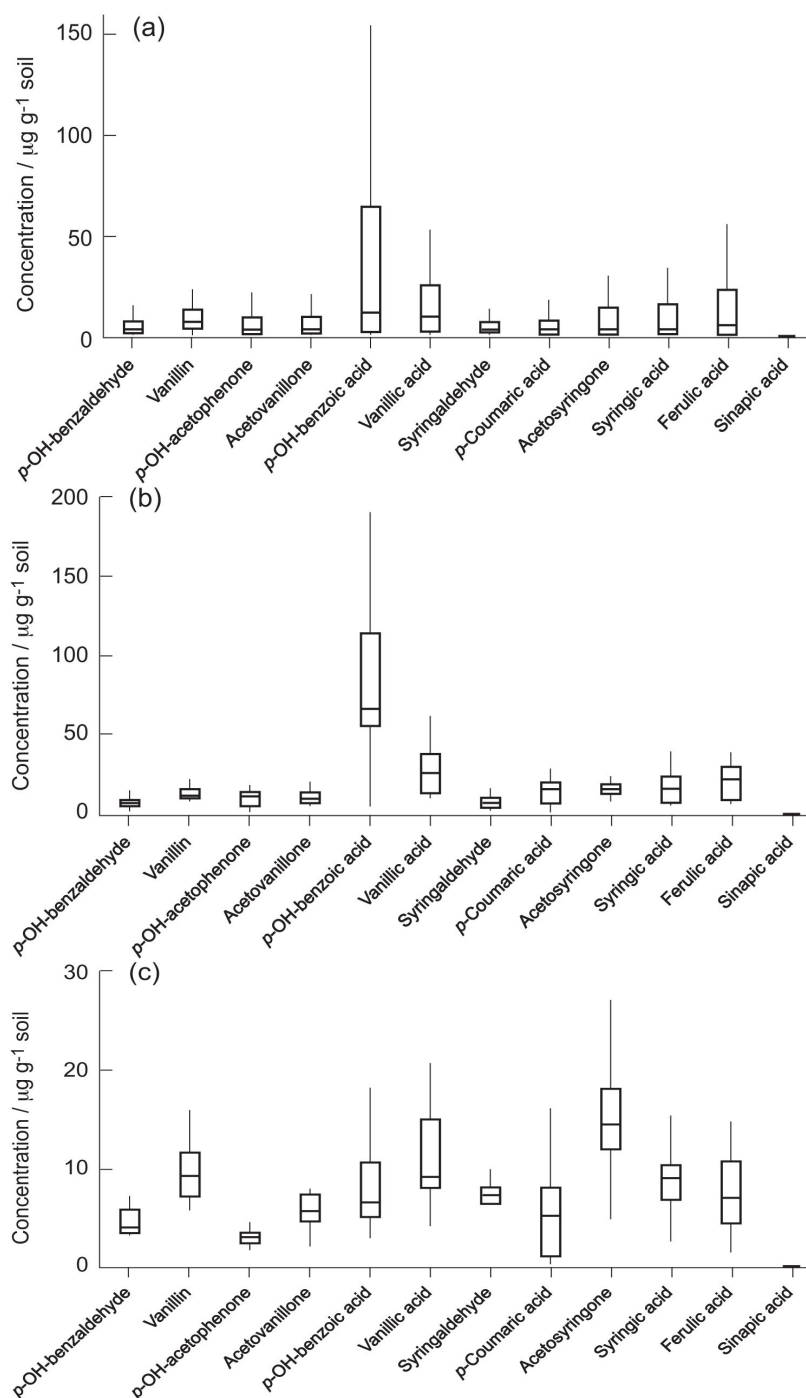


Figure 1. Box plots showing the concentration of the 12 phenolic compounds extracted from (a) all samples, and from surface samples of (b) pasture and (c) arable soils. The line within the box marks the median concentration and the boundaries of the box indicate the 25th and 75th percentiles. Whiskers indicate the minimum and maximum concentrations, excluding outliers.

Antioxidant capacity

The median values of antioxidant capacity ranged from 1.32 to 102 $\mu\text{mol Trolox equivalent g}^{-1}$ soil, and there was a positive correlation between AOC and C content ($r_s^2 = 0.814$, $P < 0.001$). Surface horizons had greater antioxidant capacities than subsurface horizons and the difference was significant ($P < 0.001$). This increase in antioxidant capacity with C content agrees with earlier findings (Rimmer and Smith, 2009).

There were significant differences between soil types with brown soils and gleys, which had small carbon contents, having the smallest antioxidant capacities and peats the largest, with the other soil types being intermediate. There were clear differences with land use; the order of increasing antioxidant capacities was arable < woodland < pasture < semi-natural vegetation, which again reflected increasing carbon contents.

The contribution of individual antioxidant compounds to the measured antioxidant capacities

The sum of phenolic compounds was positively correlated with the antioxidant capacities ($r_s^2 = 0.767$, $P < 0.001$). Six of the compounds had measurable antioxidant capacities (vanillin, vanillic acid, *p*-coumaric acid, syringic acid, ferulic acid, and sinapic acid). The sum of those six phenolics was also positively correlated with the antioxidant capacities ($r_s^2 = 0.817$, $P < 0.001$). This suggested that these antioxidant compounds could be important contributors to the overall antioxidant capacity.

This was tested by using the measured antioxidant capacities of the six antioxidants and their concentrations to calculate their contribution to the total antioxidant capacities of the extracts. The results showed that the contributions were very small. In surface samples it was generally greater (median value: 3.07%) than in subsurface samples (median value: 1.31%). A possible explanation for this is that the overall antioxidant capacity of the six compounds acting together is greater than the sum of their individual capacities or, more likely, that there are other unidentified antioxidant compounds present in the extracts.

Conclusions

Increasing concentrations of phenolic compounds were extracted from different soils with increasing organic matter content. Large differences were found between the amounts of individual phenolic compounds extracted from different soils which were dependent on the land use. This effect will be the result of different plant residues with different phenolic compositions being incorporated in the soil. Antioxidant capacities were also proportional to the SOM content, and this explained differences between soil types and land uses.

We hypothesised that phenolic compounds would be important contributors to the antioxidant capacity of soil extracts. We found that the sum of the phenolic compounds measured was positively correlated with the antioxidant capacities (AOC), which agreed with the hypothesis. However, not all of the phenolic compounds that we quantified had antioxidant capacity, and those that had were only minor contributors (< 10%) to the overall AOC of the extracts. This suggests that other unidentified antioxidant molecules were probably present in the extracts.

References

- Avery BW (1990) 'Soils of the British Isles'. (CAB International: Wallingford, UK).
- Bloomfield C (1952) Translocation of iron in podzol formation. *Nature* **170**, 540.
- Gaman PM, Sherrington KB (1990) 'The Science of Food' (3rd edn). (Pergamon: Oxford).
- Halliwell B, Gutteridge JMC (2007) 'Free Radicals in Biology and Medicine' (4th edn). (Oxford University Press: Oxford).
- Martens DA (2002a) Identification of phenolic acid composition of alkali-extracted plants and soils. *Soil Science Society of America Journal* **66**, 1240-1248.
- Martens DA (2002b) Relationship between plant phenolic acids released during soil mineralization and aggregate stabilization. *Soil Science Society of America Journal* **66**, 1857-1867.
- Moorman TB, Becerril JM, Lydon J, Duke SO (1992) Production of hydroxybenzoic acids by *Bradyrhizobium japonicum* strains after treatment with glyphosphate. *Journal of Agricultural and Food Chemistry* **40**, 289-293.
- Re R, Pellegrini N, Proteggente A, Pannala A, Yang M, Rice-Evans C (1999) Antioxidant activity applying an improved ABTS radical cation decolorization assay. *Free Radical Biology and Medicine* **26**, 1231-1237.
- Rimmer DL (2006) Free radicals, antioxidants, and soil organic matter recalcitrance. *European Journal of Soil Science* **57**, 91-94.
- Rimmer DL, Smith AM (2009) Antioxidants in soil organic matter and in associated plant materials. *European Journal of Soil Science* **60**, 170-175.
- Vance GF, Mokma DL, Boyd SA (1986) Phenolic compounds in soils of hydrosquences and developmental sequences of Spodosols. *Soil Science Society of America Journal* **50**, 992-996.

Phosphate Dissolution Caused by Bioreduction of Poorly Crystalline Al(III)/Fe(III) Hydroxide Coprecipitated Minerals

Yu-Ting Liu and Dean Hesterberg

North Carolina State University, Department of Soil Science, Raleigh, NC 27560, yliu21@ncsu.edu; dean_hesterberg@ncsu.edu

Abstract

Under reducing conditions, phosphate dissolution has been attributed to the release of that associated with Fe(III)-oxide minerals, whereas, for Al(III)-oxide minerals, the dissolution of associated phosphate has been considered to be less susceptible. The objective of this research was to determine bioreduction of Fe(III) and dissolution of phosphate as affected by the proportion of Al(III) in Fe(III)/Al(III)-hydroxide coprecipitates (Al-FH). Aqueous suspensions of phosphated Al-FHs with 0 to 100% Al/(Al+Fe) molar ratios were microbially reduced using *Shewanella putrefaciens* CN32. During 4 d-reduction, 33 % of initial Fe(III) was reduced from pure Fe(III) hydroxide; however, the Fe(II) production from Al-FH with 50% Al coprecipitation was 64 % of initial Fe(III). The presence of Al did enhance the reducibility of Fe(III) in Al-FH systems by altering surface chemistry of Al-FH. Accompanying Fe bioreduction, phosphate dissolution occurred and varied with different Al contents in Al-FHs, indicating that redox-inactive Al(III) play an distinct role in controlling phosphate cycles by affecting reduction of poorly crystalline Fe(III) hydroxide.

Key Words

Phosphate, dissolution, Fe hydroxide, bioreduction, Al hydroxide, coprecipitation

Introduction

Phosphate is a major nutrient in soils and a pollutant in aquatic environments; its fate in soils and associated environments has been of interest to scientists concerned with plant nutrition and environmental protection (Sharpley *et al.* 2002). Soil with lower redox potentials may show enhanced phosphate dissolution, which has been implied to be related to the reductive dissolution of Fe-oxides (Patrick and Khalid 1974; Holford and Patrick 1981; Phillips 1998). The biogeochemical cycling of Fe in aquatic and terrestrial environments is often driven by and coupled with microbial processes. Poorly crystalline and crystalline Fe(III) (hydr)oxides can be utilized as electron acceptors by dissimilatory Fe-reducing bacteria (DIRB) (Lovley and Phillips 1986). In soils, most Fe (hydr)oxide are Al-substituted (Schwertmann and Taylor 1989) due to the ubiquity and abundance of Al in rocks and soils. Therefore, coprecipitated systems between Al and Fe (hydr)oxides are properly considered as a potential media affecting phosphate agrogeochemical cycles. The objective of this study was to determine the bioreducibility of Fe(III) hydroxide as affected by proportion of Al(III) in Fe(III)/Al(III)-hydroxide coprecipitates (Al-FH) and the following phosphate dissolution.

Material and Methods

Materials of Al-FH were synthesized by mixing solutions of $\text{Fe}(\text{NO}_3)_3 \cdot 9\text{H}_2\text{O}$ and $\text{Al}(\text{NO}_3)_3 \cdot 9\text{H}_2\text{O}$ and hydrolyzing with 1.0 M KOH with Al/(Al+Fe) molar ratios of 0, 0.1, 0.2, 0.5, 0.75, and 1.0 (hereafter referred as 0-, 10-, 20-, 50-, 75-, and 100-Al-FH). Bioreduction of Al-FH with pre-sorbed PO_4 was conducted by inoculating dissimilatory Fe(III)-reducing bacteria, *Shewanella putrefaciens* CN 32. Concentrations of Al+Fe and pre-sorbed P were 50 mM and 1000 mmol/kg, respectively. Local structure transformation of bioreduced Al-FH was examined using X-ray absorption spectroscopy (XAS) at the National Synchrotron Light Source, Brookhaven National Laboratory in Upton, NY. The initial pH was 6.8, but drifted to between 8.6~8.8 during 4 d of incubation.

Results and Discussion

Fe(III) bioreduction.

No significant Fe(II) dissolution was observed during Al-FH bioreduction. Total Fe(II) production (0.5 M HCl extractable) during 4 d-incubation of various Al-FH is shown in Figure 1a. In general, Fe(III) reduction increased over time (except 100-Al-FH). With regard to various Al coprecipitations, the Fe(II) production decreased as Al proportion increased at the first day of incubation. At the end of incubation, however, Al-FH with 10% Al coprecipitation produced greatest Fe(III) reduction, and the Fe(II) concentration dropped as Al proportion increased from 10 to 75%. In order to evidence the effect of Al coprecipitation on Fe(III) reduction, Fe(II) production is converted to the percentage of initial Fe(III) addition and shown in Figure 1b. The

proportion of Fe(III) reduced tended to increase as Al coprecipitation increased from 0% to 50% at the first day. This trend was more pronounced after 4 d-incubation, wherein the proportion of Fe(III) reduced from 50-Al-FH (65 %) approximately doubled that from pure Fe hydroxide (33 %), suggesting that the coprecipitation of Al hydroxide may promote the long-term reducibility of Al-FHs. Al-FHs with 12 d-bioreduction were examined by extended X-ray absorption fine structure(EXAFS) spectroscopy to determine the related mechanisms. The second shell of all samples was ascribed to Fe-Fe paths with interatomic distance of 3.04 and 3.47 Å (Figure 2). The rising second-shell intensity of 0-Al-FH implied the increasing crystallinity of 0-Al-FH structure during bioreduction, whereas 75-Al-FH behaved in an opposite way. Inhibiting the crystallization of Fe (III) hydroxide by Al coprecipitates could enhance the reducibility of Al-FH in that it renders surfaces of Fe(III) hydroxides more accessible for electron transfers.

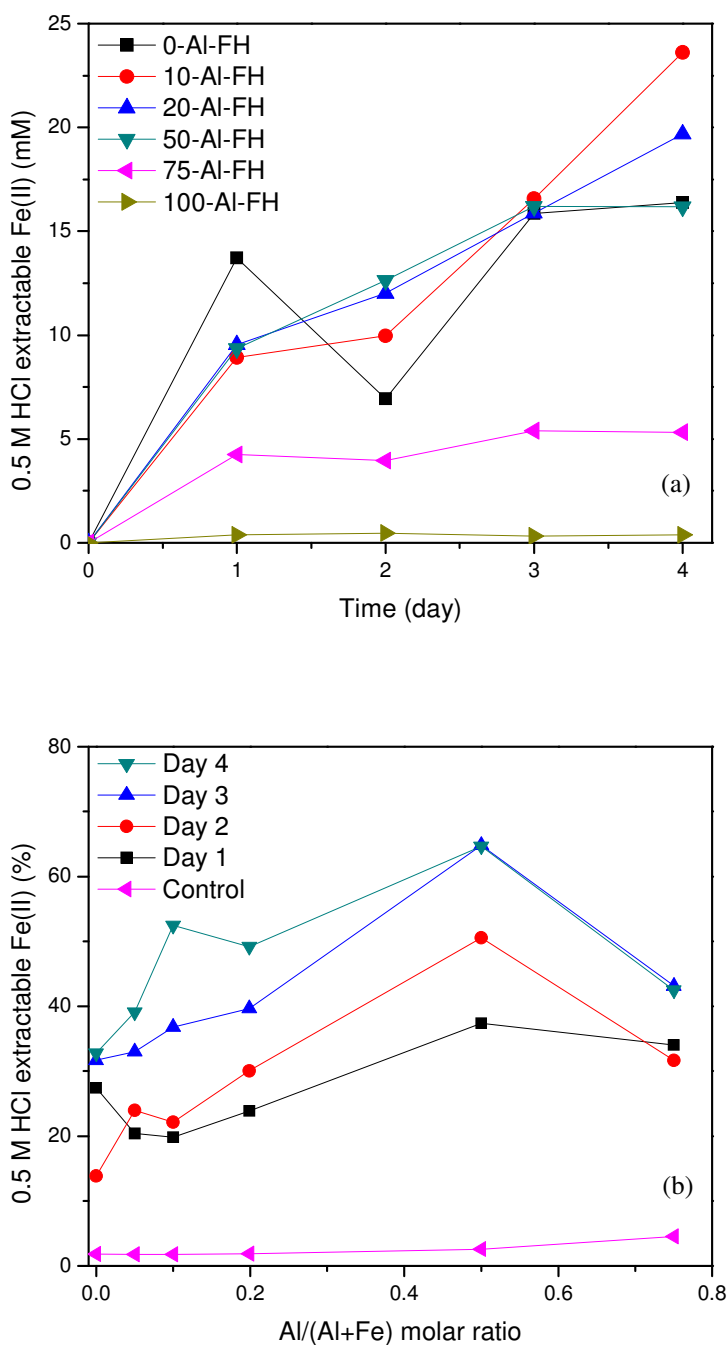


Figure 1. HCl-extractable Fe(II) produced during bioreduction of various Al-FHs represented as (a) concentration and (b) percentage of initial Fe(III) addition. Fe(II) production of uninoculated controls were collected at the fourth day.

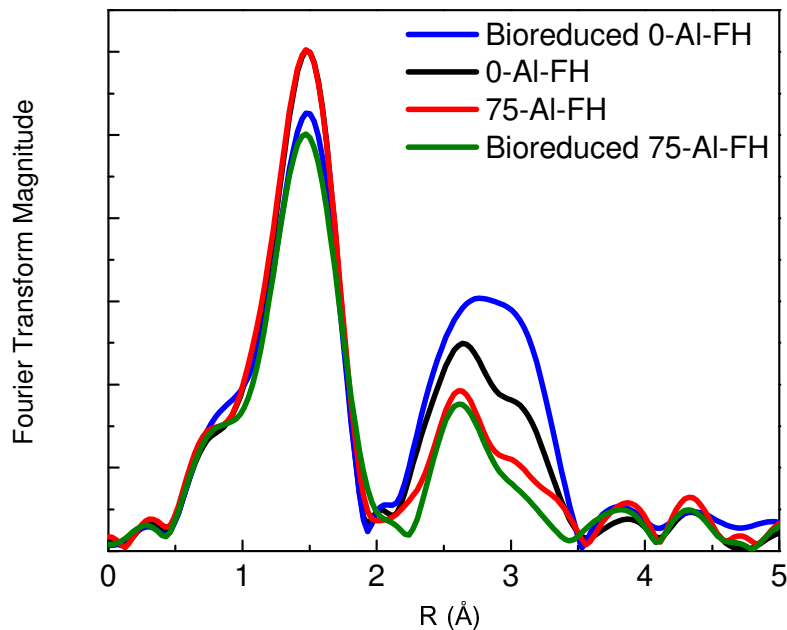


Figure 2. Fourier transformed Fe K-edge EXAFS spectra of 0-Al-FH and 75-Al-FH and that with 12 d-bioreduction (without phase correction).

Phosphate dissolution

Phosphate dissolution accompanied Fe(III) bioreduction of various Al-FHs is shown in Figure 3. In the absence of Al coprecipitation, dissolved phosphate increased by up to 5-fold over time, reaching 12.6 $\mu\text{mol/L}$ after 4 d-incubation. Two possibilities could account for phosphate dissolution: (1) reductive dissolution of phosphated Fe(III) sites, and/or (2) the increasing pH happened during Fe(III) reduction process (Figure 4).

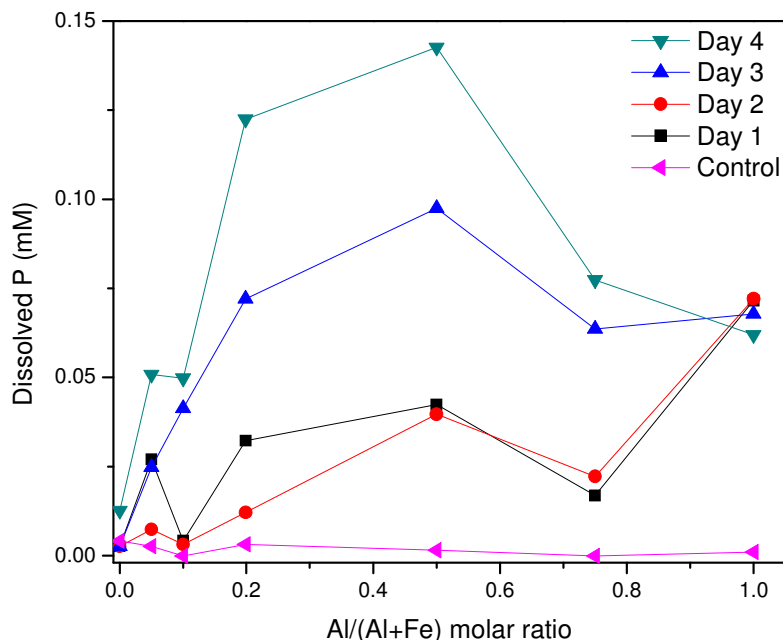


Figure 3. Dissolved phosphate occurred during bioreduction of various Al-FHs. Dissolved phosphate of uninoculated controls were collected at the fourth day.

Phosphate dissolution from various Al-FHs also increased over time generally, except that from pure Al hydroxide. In the suspension of 50-Al-FH, dissolved phosphate reached the greatest concentration during 4 d-incubation than that from other Al-FHs. Wherein, phosphate concentration stayed constant initially but increased

essentially at the last 2d-incubation, which rose from 97.5 $\mu\text{mol/L}$ at day 3 to 142.6 $\mu\text{mol/L}$ at day 4. Although phosphate concentration increased almost 50% in 24h, the pH values of these two samples were similar. Therefore, phosphate dissolution caused by the increasing pH might be considered as a minor effect. At the end of incubation, dissolved phosphate increased substantially as the proportion of Al in the coprecipitates increased from 0 to 50%, and then decreased as Al proportion was further increased to 75%. The behavior of phosphate dissolution mimicked the tendency of Fe(II) production represented as proportion of initial Fe(III) addition (Figure 1b), indicating surface chemistry of Al-FH may have decisive effects in reductive phosphate dissolution.

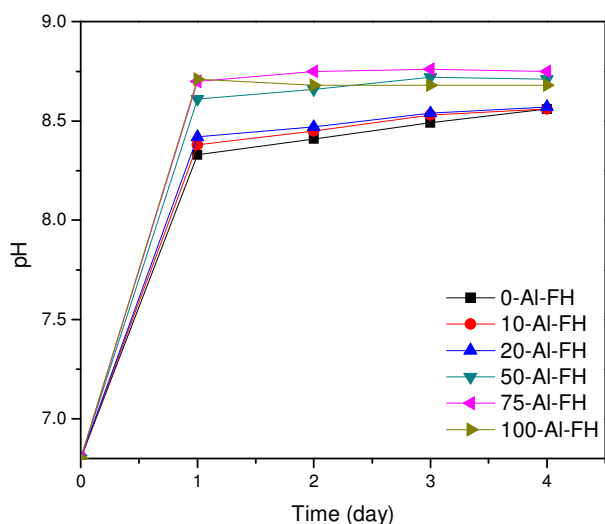


Figure 4. The pH values during four day-bioreduction of various Al-FHs. The pH values for uninoculated controls were collected at the fourth day and ranged from 6.91~6.99 among all Al-FHs (data not shown).

Conclusion

This research demonstrated that phosphate dissolution could be induced by microbial reduction of poorly crystalline Fe(III) hydroxide, and this Fe(III) bioreduction was enhanced with increasing Al(III) hydroxide coprecipitation. Bacterially mediated redox processes strongly influence Fe(III) reducibility, which may be controlled by surface chemical properties of Fe-bearing minerals. Studies in local structure transformation during bioreduction process are necessary. The ubiquity of Al(III) in soils has generated interest in determining its impact on biogeochemical destinies of iron and phosphate. Regardless of the redox-inactive nature, Al(III) could potentially affects Fe(III) reduction and phosphate dissolution in reductive aquatic and terrestrial environments.

Reference

- Holford ICR, Patrick WH (1981) Effects of duration of anaerobiosis and reoxidation on phosphate sorption characteristics of an acid soil. *Australian Journal of Soil Research* **19**, 69–78.
- Lovley DR, Phillips EJP (1986) Availability of ferric iron for microbial reduction in bottom sediments of the freshwater tidal Potomac River. *Applied and Environmental Microbiology* **52**, 751-757.
- Patrick WH, Khalid RA (1974) Phosphate release and sorption by soils and sediments: Effect of aerobic and anaerobic conditions. *Science* **186**, 53–55.
- Phillips IR (1998) Phosphorus availability and sorption under alternating waterlogged and drying conditions. *Communications in Soil Science and Plant Analysis* **29**, 3045–3059.
- Schwertmann U, Taylor RM (1989) Iron oxides. In 'Minerals in soil environment'. (Eds JB Dixon, SB Weed) pp. 379-438. (Soil Science Society America: Madison, WI)
- Sharpley AN, Kleinman PJA, McDowell RW, Gitau M, Bryant RB (2002) Modeling phosphorus transport in agricultural watersheds: Processes and possibilities. *Journal of Soil and Water Conservation* **57**, 425-439.

Restructuring of biogeochemical interfaces: Role of cations and heat treatment

Gabriele E. Schaumann^A, Dörte Diehl^A, Jette Schwarz^A, Julia V. Bayer^A, Jörg Bachmann^B, Susanne K. Woche^B, Marc-Oliver Göbel^B, Bernd Marschner^C, Anastasia Shchegolikina^C, Friederike Lang^D, Jaane Krüger^D, Sören Thiele-Bruhn^E, Tatjana Schneckenburger^E

^ADepartment of Environmental and Soil Chemistry, Institute for Environmental Sciences, University Koblenz-Landau, Landau, Germany. Email schaumann@uni-landau.de

^BFaculty of Natural Sciences, Institute of Soil Science, Leibniz University Hannover, , Germany. Email bachmann@ifbk.uni-hannover.de

^CDepartment of Soil Science and Soil Ecology, Geographical Institute, Ruhr-University Bochum, Bochum, Germany. Email:

bernd.marschner@rub.de

^DDepartment of Soil Science, Institute of Ecology, Berlin University of Technology, Berlin, Germany, Email fritzi.lang@tu-berlin.de

^ESoil Science, Department of Geography/Geosciences, University of Trier, Trier, Germany. E-mail: thiele@uni-trier.de

Abstract

The main objective of this study is to evaluate the impact of temperature and cation sorption on important physical and structural parameters of soil organic matter of a mineral soil and a peat. Sieved soil samples (< 2 mm) were stored under constant conditions (rel. humidity 31%, T = 20 °C) for at least 6 weeks. Matrix characteristics, surface properties and sorption characteristics are subjected to slow and continuous changes lasting for weeks and months. Dynamics in the field are expected to induce comparable processes affecting interfacial and bulk properties, which are, however, up to now unknown. Unravelling these processes will help to develop a mechanistic understanding of functioning of soil organic matter as biogeochemical interface with respect to wettability, sorption and biodegradation of organic chemicals.

Key words

soil organic matter, cations, aging, wettability, temperature treatment, sorption, soil pollutants, kinetics

Introduction

Interfacial and matrix properties of soil samples are subjected to slow and continuous changes lasting for weeks and months (Schaumann 2006). They are further affected by temperature, storage conditions and cation content. Dynamics of these factors in the field are expected to induce comparable processes, which are, however, up to now unknown. Unravelling these processes would help to develop a mechanistic understanding of functioning of soil organic matter as biogeochemical interface with respect to wettability, sorption and biodegradation of organic chemicals. Temperature treatment is expected to (i) accelerate the processes in soil and (ii) induce irreversible changes in the samples. Therefore, samples treated with different temperatures are expected to be different even after long storage times. The specific objective of this joint study is to understand the interplay between SOM-cation interactions, physicochemical aging and sorption of organic chemicals. We expect to observe cross-linking effects of cations (Schaumann, Lang *et al.* 2006) and aging effects (Schaumann 2006) resulting in increased matrix rigidity, contact angle and sorption capacity. Temperature treatment is expected to (i) accelerate the aging and restructuring processes in soil and (ii) induce irreversible changes in the samples

Material & methods

Sample preparation and cation and temperature treatment. The samples were taken from 2 sites, Totes Moor (sapric peat, "SP") and Lakwiese (Glyinc Podzol, "LW") and air-dried. The peat samples were ground after drying. All samples were sieved to < 2 mm and stored for at least 6 weeks at 31% RH and 20°C prior to cation treatment. For cation treatment, the samples were shaken for 3 hours with the ratio by weight of 1/10 for LW and 1/25 for SP. The following solutions were used: **control**: H₂O dest., **"H⁺"**: H₂O dest. + 30 g Amberlite®IR hydrogen form in gaze bags (PP-149/34), **"Na"**: 0.01 M NaCl, **"Ca"**: 0.01 M CaCl₂, **"Al"**: 0.01 M AlCl₃. Samples were shaken for 3 hours in a rotary shaker, filtered with a Büchner funnel and dried at 25 °C for 4 days and gently homogenized to destroy aggregates and crusts developed during drying. Subsamples were subjected to temperature treatment as follows: **"25"**: No further treatment, **"40"**: 2*12h in sealed bottles at 40°C, **"60"**: 2*12h in sealed bottles at 60°C, **"105"**: 0.5 h at 105°C in sealed bottles.

Then, the samples were stored isothermally at 20°C and 31% relative humidity for 1,2,4, 6 and 8 weeks. Samples were investigated for matrix properties, surface properties and sorption characteristics directly before

and after the temperature treatment and after each point of time during aging. For the contact angle measurements, were heated after cation treatment described above to 40, 60, and 105 degrees in a drying oven for 24 hours and also fractionated into fraction < 63 μm . Samples were stored in PE containers and contact angle measurements were conducted within 2 days after storage. Repeated contact angle measurements were made after 8 and 12 weeks, respectively.

Matrix characteristics

Matrix rigidity was assessed by Differential Scanning Calorimetry (DSC) in terms of the glass transition-like step transition temperature (T^*) as described by Hurrass & Schaumann (2005). The proton NMR relaxation time indicates the mobility of proton containing molecules. The shorter the relaxation time, the stronger water is bound or the smaller the pores are in which the water is confined. We determined transverse relaxation time T_2 at 7.5 MHz with a Bruker minispec mq 7.5 employing the Hahn Spin Echo method. Longitudinal relaxation times were determined at 20 MHz using a fast field cycling relaxometer as described by Conte *et al.* (2009). Thermal decomposition profiles were analyzed with DSC in a ramp of -50°C to 550°C with 10 K min^{-1} heating and synthetic air as purge gas (50 mL min^{-1}). DSC measured the energy transformation in the samples occurring during heating. In this experiment, the combustion process was monitored. This analysis gives insight into organic matter quality under the influence of the respective sample treatment with respect to thermal stability.

Contact angle

Contact angle was determined by Wilhelmy plate method (WPM) and by sessile drop method (SDM). For contact angle measurement via WPM (CA_{WPM}), samples were fixed on a rectangular glass slide completely covered by double sided adhesive tape and suspended from the balance of a Dynamic Contact Angle Meter and Tensiometer (DCAT 21, DataPhysics, Filderstadt, Germany), and contact angle was determined as described by Bachmann *et al.* (2000). For contact angle measurement via SDM (CA_{SDM}), a thin layer of the soil sample was attached to one side of a glass microscope slide using double sided adhesive tape (Bachmann, Ellies *et al.* 2000). CA_{SDM} was calculated from the tangent to the three-phase contact point associated with the ellipse that best fitted the drop shape (Bachmann, Ellies *et al.* 2000; Diehl and Schaumann 2007).

Sorption characteristics

Batch trials according to the OECD Guideline 106 were conducted in 0.01M CaCl_2 -solution at soil-to-solution ratios of 1:10 (LW) and 1:20 (FS). The model xenobiotics, Naphthalene and Naphthalene-2,7-diol, were added at $10\mu\text{mol/L}$ and sorption kinetics were recorded at time steps of 0.5, 1.0, 2.0, 4.0, 8.0, and 24 h. Kinetics in each of the two soils were tested with and without cation treatment using NaCl, and after additional heat treatment at 40°C and 60°C , respectively, and aging for 0, 2, and 4 weeks.(= 24 soil variants). In another experiment, the radiolabel xenoestrogen compound Nonylphenol was used to determine sorption properties of treated and aged soils. Directly after the temperature treatment (40°C , 60°C or 100°C) and after 2 and 4 weeks of storage 2 g of controls and sodium chlorite treated samples were used for sorption experiment in Teflon chambers. The soil was separated in one half-chamber by membrane with MWCO 1 kDa of the Nonylphenol water solution (soil:liquid 1:5) using NaN_3 to prevent microbial activity. After 22 h of shaking on over-head shaker the aliquot of pure radioactive solution was mixed with scintillation cocktail (Ultima Gold LSC-cocktail, Packard Bioscience, USA) and analyzed for ^{14}C activity by liquid scintillation counting (Beckmann LS 6000 TA). Based on the measurements the carbon normalised partition coefficient (K_{oc}) was calculated.

Zeta potential of dispersible colloids.

Colloids were extracted with doubly deionised water (soil/solution ratio 1:10). After shaking for 16 h the samples were centrifuged (cut off $1\mu\text{m}$ for particles with the density of 2 g cm^{-3}) and the zeta potential and the size distribution of the colloids was determined with a Zetasizer 2000 (Malvern Instruments) and photon correlation spectrometer (Malvern).

Results & discussion

The temperature treatment has strong effects on matrix rigidity, contact angle and sorption characteristics, and cation treatment shows significant differences in OM thermal decomposition profiles.

Figures 1 A and B show that the same sample can significantly increase its contact angle by the simultaneous impact of temperature and Al^{3+} . The coarse fraction 2000-63 μm is more hydrophobic than the total soil and less affected by the described impact factors. We also observed an effect of aging, since all samples showed larger contact angles after 2 months, especially after treatment with higher valent cations Ca^{2+} and Al^{3+} (data not shown). These changes obviously also affect the sorption characteristics (Figures 1E and 1F), since with increasing time the corresponding K_{oc} value increased for the investigated samples LW and SP, respectively. Comparably, we observed strong effect of the temperature treatment on matrix rigidity expressed by the step transition temperature (Figure 1C), while the cation effect was significantly less expressed.

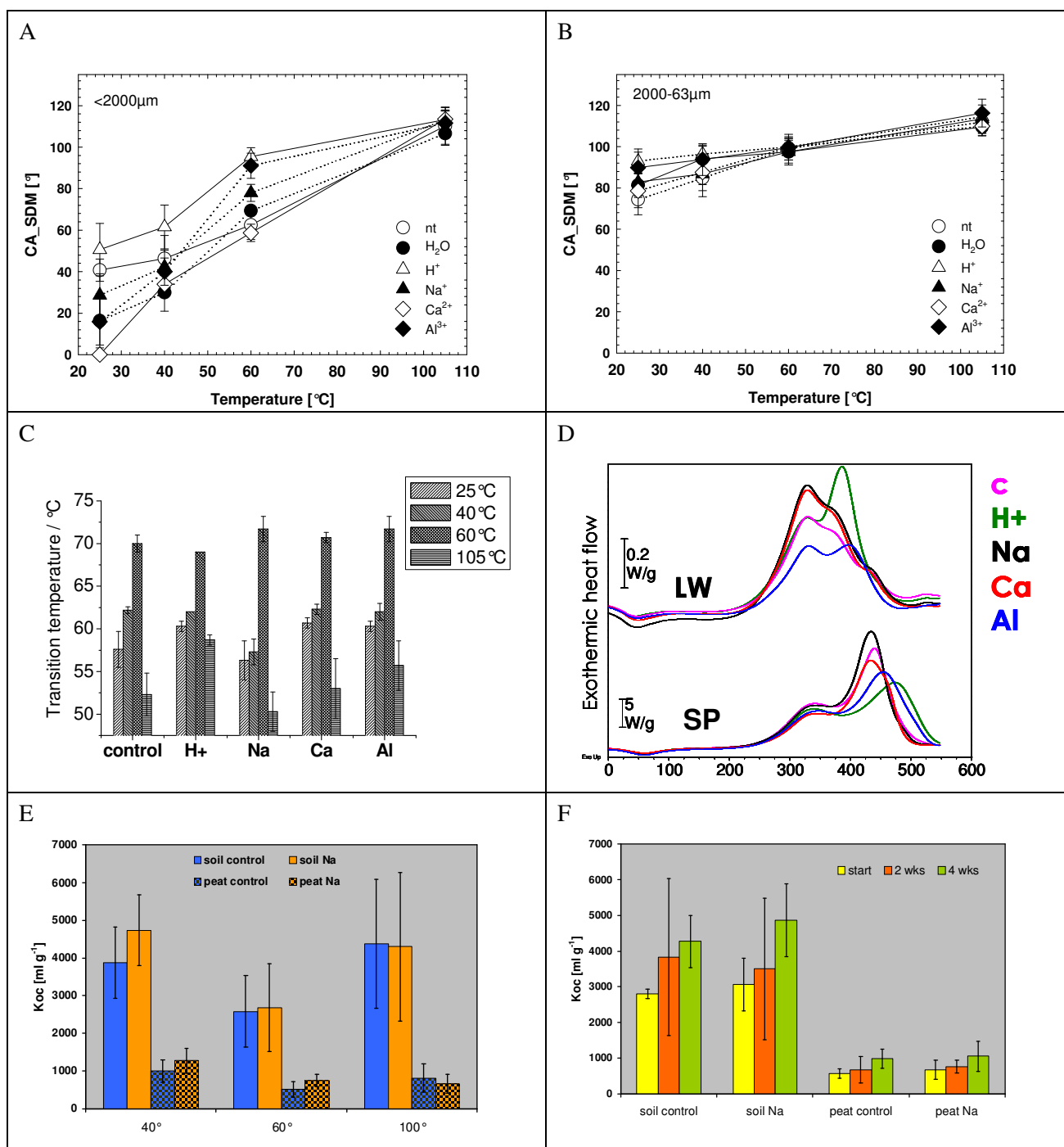


Figure 9: Contact angles of the sieved (<63 μm ; A) and coarse (2000-63 μm ; B) fraction, DSC step transition temperature of the treated SP sample (C), thermal decomposition profiles of treated LW and SP samples (C). E, F: Nonylphenol sorption characteristics of the treated samples.

Sorption of Naphthalene and Naphthalene-2,7-diol to a different soil was enhanced in aged samples and correlated with SOM matrix rigidity and coefficients of fast soil sorption (data not shown). Therefore, we also presume clearly enhanced sorption to the aged and heated soil samples, respectively, in this experiment, since both treatments increase matrix rigidity.

The results thus indicate significant effects of temperature pre-treatment, aging and cation treatment on numerous properties which are relevant for biogeochemical interfaces. However, the cation effects on sorption characteristics and contact angle are less pronounced but not negligible. Aging effects can be observed at least for matrix rigidity, NMR relaxation times (data not shown) and for sorption characteristics as well as for contact angles. The differences are significant, and interpretation and requires further discussion. Cation treatment changes organic matter stability. But surprisingly, it appears to have lower effects on matrix rigidity and contact angle than the temperature pre-treatment. Cation effects may even disappear almost completely upon temperature treatment at 105°C. Temperature pre-treatment above 40°C was shown to have sustainable effects on contact angle, matrix rigidity, but effects were also observable in the 40°C treatment.

These partly unexpected results need to be discussed in more detail after complete evaluation. Under the impact of temperature, the sample may change its behaviour from good wettable to strongly hydrophobic, which is in line with frequent observations after wildfires.

First conclusions

Our results proof the dependence of the supramolecular properties of soil organic matter from environmental conditions and the conditions of sample storage. These properties determine the functioning of biogeochemical interfaces. To fully understand the functioning of biogeochemical interfaces the processes of aging of labile structures in organic matter have to be identified by further investigations.

Further emphasis will be laid on comparison of the findings with designed model soil compounds in all groups in order to verify hypotheses deduced from the results of this joint experiment. It should also be the focus of further investigations, if the observed effects are reversible, i.e. can be reproduced after rewetting and drying like in natural soil. Combining various properties relevant for biogeochemical interface functioning in samples prepared after exactly the same protocol in various groups, this joint research will help to provide a mechanistic understanding of the relevance of labile structures in organic matter for functioning of biogeochemical interfaces. However, at the present state it might be concluded, that time, temperature as well as higher-charged cations like Al^{3+} modified the structure of the entire organic matter towards more hydrophobicity. This effect is not restricted to the surface or the interphase, since structural properties like glass transition temperature or the DSC signal of the bulk samples are also affected by the described impact factors. We conclude further that some important properties of soil samples are strongly affected by storage temperature and time.

References

- Bachmann J, Ellies A, Hartge KH (2000) Development and application of a new sessile drop contact angle method to assess soil water repellency. *Journal of Hydrology* **231-232**, 66-75.
- Conte P, Maccotta A, De Pasquale C, Bubici S, Alonzo G (2009) Dissolution Mechanism of Crystalline Cellulose in H_3PO_4 As Assessed by High-Field NMR Spectroscopy and Fast Field Cycling NMR Relaxometry. *Journal of Agricultural and Food Chemistry* **57**, 8748-8752.
- Diehl D, Schaumann GE (2007) Wetting mechanism assessed from time dependent sessile drop shape. *Hydrological Processes* **21**, 2255 - 2265.
- Hurraß J, Schaumann GE (2005) Is glassiness a common characteristic of soil organic matter? *Environmental Science and Technology* **39**, 9534-9540.
- Schaumann GE (2006) Soil organic matter beyond molecular structure. 2. Amorphous nature and physical aging. *Journal of Plant Nutrition and Soil Science* **169**, 157-167.
- Schaumann GE, Lang F, Frank J (2006) Do multivalent cations induce cross-links in DOM precipitates? In 'Humic Substances - Linking Structure to Functions. Proceedings of the 13th Meeting of the International Humic Substances Society in Karlsruhe'. (Eds FH Frimmel and G Abbt-Braun) pp. 941-944. (Universität Karlsruhe: Karlsruhe)

Retention of Na⁺ Cations in Nanopores and Its Implications to Sodic Soils

C.P. Schulthess and D.R. Ferreira

Department of Plant Science and Landscape Architecture, University of Connecticut, Storrs, CT 06269-4067 USA,
c.schulthess@uconn.edu, daniel.ferreira@uconn.edu

Abstract

The management of sodic soils often involves the addition of Ca²⁺ cations because it is believed that these divalent cations will easily desorb the Na⁺ cations from the soil solid phase. However, the adsorption of cations in the interstitial region of minerals is counterintuitive, particularly if the diameter of the interstitial region is less than 1 nanometer. These very small dimensions are common in many soil minerals. Using zeolites, the ideal cation for treating sodic soils may be another monovalent cation, such as K⁺, rather than Ca²⁺. The reasons for this reversal of selectivity in nanopore regions of minerals may be due to a NISE (nanopore inner-sphere enhancement) effect. An enhanced liquid-phase stability of the Na⁺ ion in the presence of K⁺ ions may also be involved.

Key Words

Cation adsorption, nanopores, zeolite, ion hydration, sodium retention

Introduction

In the US, saline soils are found primarily in the arid Midwest and along the coastal states in the eastern and southern parts of the country. The greatest concentration of saline soils are in North Dakota, South Dakota, Michigan, and Colorado. The Natural Resources Conservation Service (NRCS) estimates that there are 500,000 to 725,000 hectares of saline soils in North Dakota's Red River Valley alone. These predominantly affect prime farmland and result in a loss of \$50-\$90 million in production each year to the state (NRCS 2007).

Saline soils are also problematic in East Asia. China alone is estimated to have 99.1 million hectares of saline soil (Matsumoto *et al.* 1998). Australia currently has 975,000 hectares of saline soils and another 4.5 million hectares are in danger of becoming saline (McFarlane *et al.* 2004). Saline soils can be an even more serious issue for low lying island countries such as Myanmar. The damage from the tsunami that struck Myanmar in May of 2008 was measured in terms of the number of fatalities and destroyed homes. But the salt intrusion onto agricultural lands due to the inundation by the ocean water was also damaging. Sodic soils are a subset of saline soils, where the salt present is high in sodium (Na⁺). Sodium is, for the most part, considered an indifferent electrolyte and adsorbs weakly in typical soils. It is usually desorbed quite easily by competing ions. The current view on how sodic soils are formed is that a constant source of sodium, such as a sodium rich bedrock, releases Na⁺ ions into the soil or groundwater. Only because of the constant release of sodium, according to this theory, does sodium build up in sodic soils. The most common method of remediating sodic soils is either through the management of the irrigation water (namely, by leaching the Na⁺ out of the soil profile) or through ion exchange of sodium with calcium through the use of gypsum (CaSO₄·2H₂O) (Oster 1982). Lime (CaCO₃) can also be added, but this is less common since sodic soils are typically already alkaline. Calcium, being divalent, is expected to be able to easily desorb Na⁺ from the exchange sites on the mineral surfaces. Also, gypsum and lime are plentiful, cheap, and easily obtained in most parts of the world. The retention of Na⁺ by soil minerals is known to be weak in most cases. However, recent studies by Schulthess *et al.* (2010) have found that the retention strength of ions in the nanopore interstitial region of soil minerals is much stronger than on their external surface sites. In some cases, for example, Na⁺ adsorption is much stronger than the adsorption of divalent cations, such as Ca²⁺ and Ni²⁺. Curiously, other monovalent cations are also held very strongly in the interstitial regions, such as K⁺ which is held even more strongly than the Na⁺ ions. The proposed explanation for this phenomenon is tentative at the present time, but it appears to be closely related to the ionic diameter of the adsorbing species, the pore diameter of the interstitial spaces in the mineral, and the amount of space remaining for the hydrating water molecules in the interstitial spaces.

Our understanding of the Na⁺ adsorption processes and that of other ions are closely tied to our management of sodic soils. The objectives of this study were to compare the retention of several cations on zeolite minerals with interstitial cavities of different sizes, and to find a cation that can effectively desorb sodium cations better than calcium cations. The basic premise of this research is based on the theories presented by Schulthess *et al.*

(2010), which we coin the nanopore inner-sphere enhancement (NISE) effect. Basically, small pores have the potential of reversing the adsorption selectivity observed on macropores or on external surface sites.

Materials and Methods

Two zeolite materials were used for this study: ZSM-5 and zeolite-Y. The ZSM-5 zeolite has interconnected pores with dimensions of 0.55×0.51 nm and 0.56×0.53 nm. The zeolite-Y has interconnected pores that are 0.74 nm in diameter. Slurries of these zeolites were prepared in a closed reactor and purged with N₂ gas to remove any adsorbed inorganic-C present. These zeolites do contain a large amount of adsorbed inorganic-C and the purging of this contaminant takes several days to complete. Batch adsorption experiments were performed with these zeolites as a function of pH. Mixtures were prepared in 50-mL nominal centrifuge tubes consisting of zeolite slurry, NaOH, HCl, and other salt solutions as needed. The amount of Na⁺ cations present in each reaction container was kept constant by adding a fixed quantity of NaOH solution to each sample and adjusting the pH with variable quantities of a HCl solution. The added salt solutions included KCl, MgCl₂, CaCl₂, and BaCl₂. The samples were then centrifuged and the supernatant solutions were analyzed for pH and remaining cations present using inductively coupled plasma optical emission spectroscopy (ICP-OES). The amount of cations adsorbed by the zeolites are based on the amount added minus the amount remaining in solution.

Results

The adsorption of sodium (Na⁺) cations on zeolite minerals is surprisingly strong. However, there are marked differences in adsorption strength observed among different zeolites. Figure 1 shows a strong retention of Na⁺ ions on ZSM-5 zeolite. The presence of equimolar concentrations of K⁺ ions has a very strong desorption effect on Na⁺, whereas an equimolar concentration of Ca²⁺ has a very weak effect (Figure 1). Figure 2 shows that the retention of K⁺ on ZSM-5 is very strong, but the retention of Ca²⁺ is very weak. The fact that Ca²⁺ ions have a minor impact on Na⁺ retention, but K⁺ ions have a large impact, is counterintuitive and very significant to our understanding of how these ions are stabilized in the interstitial region of minerals.

Adsorption on zeolite-Y was much weaker, but still noteworthy (Figure 3). The impact of equimolar concentrations of Ca²⁺ and K⁺ on Na⁺ adsorption was similar to the effects observed in Figure 1. Figures 3 and 4 show that the retention of Na⁺, K⁺, and Ca²⁺ are all relatively weak on zeolite-Y, but all are nearly the same strength. Once again, the fact that Ca²⁺ ions have a minor impact on Na⁺ retention, but K⁺ ions have a large impact, is counterintuitive and very significant to our understanding of how these ions are stabilized in the interstitial region of minerals.

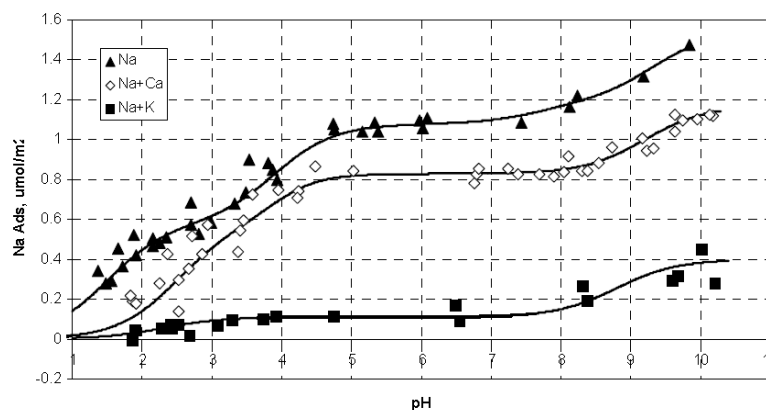


Figure 1. Adsorption ($\mu\text{mol}/\text{m}^2$) of Na⁺ cations on ZSM-5 (medium nanopores present) as a function of pH in the presence and absence of Ca²⁺ and K⁺ cations.

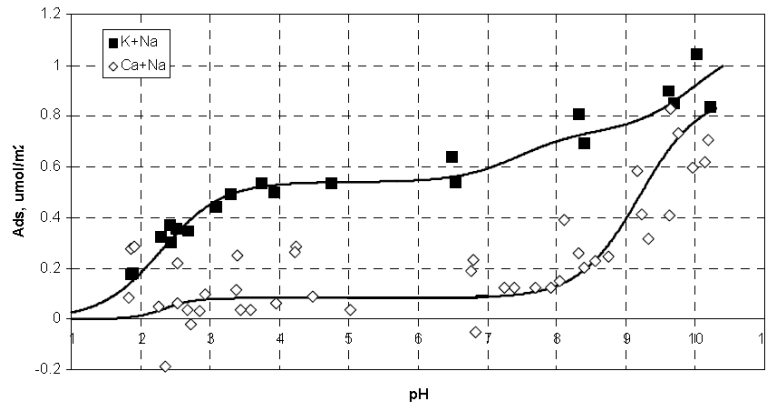


Figure 2. Adsorption ($\mu\text{mol}/\text{m}^2$) of Ca^{2+} and K^+ cations on ZSM-5 (medium nanopores present) as a function of pH in the presence of Na^+ .

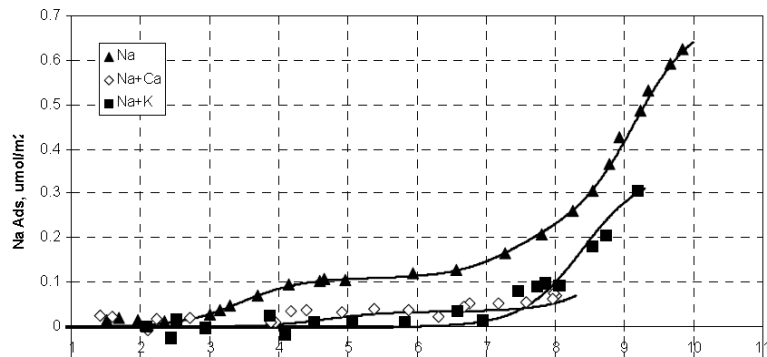


Figure 3. Adsorption ($\mu\text{mol}/\text{m}^2$) of Na^+ cations on zeolite Y (large nanopores present) as a function of pH in the presence and absence of Ca^{2+} and K^+ cations.

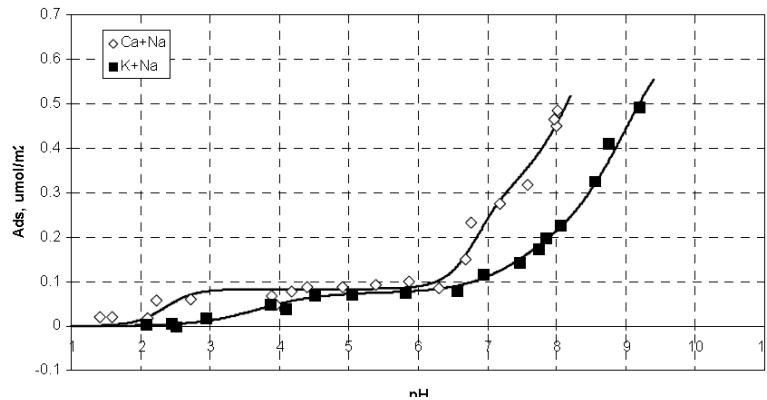


Figure 4. Adsorption ($\mu\text{mol}/\text{m}^2$) of Ca^{2+} and K^+ cations on zeolite Y (large nanopores present) as a function of pH in the presence of Na^+ .

Conclusions

The retention of Na^+ cations by porous minerals, specifically those with interstitial spacing in the subnanometer diameter range, is much stronger than previously anticipated. The desorption of this cation by other cations is possible, but it is wrong to assume that divalent cations are more effective than monovalent cations. The stability of the ion in the liquid phase versus in the nanopore regions of the mineral should be evaluated carefully if a full understanding of the processes involved are to be understood. This can have significant implications on how sodic soils are managed in the field.

References

- McFarlane D, George RJ, Cacetta PA (2004). The extent and potential area of salt-affected land in Western Australia estimated using remote sensing and digital terrain models. In '1st National Salinity Engineering Conference, 9-12 November, 2004'. (Eds S Dogramaci, A Waterhouse) p. 55-60. (Institution of Engineers, Perth, Australia).
- Matsumoto S, Zhao Q, Yang J, Zhu S, Li L (1998) Soil salinization and its environmental hazard on sustainable agriculture in east Asia and neighboring regions. *Global Environ. Res.* **1**, 75-81.
- Natural Resources Conservation Service (2007) Saline soils in the Red River Valley. http://a-cs.confex.com/recording/crops/2007am/pdf/free/4db77adf5df9ff0d3caf5cafe28f496/paper34519_1.pdf
- Oster JD (1982) Gypsum usage in irrigated agriculture: A review. *Nutrient Cycling in Agroecosystems* **3**, 73-89.
- Schulthess CP, Taylor RW, Ferreira DR (2010) The nanopore inner-sphere enhancement (NISE) effect on adsorption processes: Na⁺ and Ni²⁺ cations. *Soil Sci. Soc. Am. J.* submitted.

Sensitive analysis of poly-carboxylic acids in soil solution by capillary electrophoresis after excimer-forming fluorescence derivatization

Naoki Moritsuka^{AD}, A. Deri Tomos^A, Davey L. Jones^B and Guy Kirk^C

^A School of Biological Sciences, Bangor University, UK, E-mail: a.d.tomos@bangor.ac.uk

^B School of Environment, Natural Resources & Geography, Bangor University, UK, E-mail: d.jones@bangor.ac.uk

^C School of Applied Sciences, Cranfield University, UK, E-mail: g.kirk@cranfield.ac.uk

^D Present address: Graduate School of Agriculture, Kyoto University, Japan, E-mail: morituka@kais.kyoto-u.ac.jp

Abstract

A sensitive method for the determination of citrate and malate in sub-microliter samples of soil solution is described. The organic acids were derivatized with a pyrene reagent (1-pyrenebutanoic acid hydrazide) and analysed by micellar electrokinetic chromatography separation. The citrate and malate derivatives were detected within 10 min by using a fluorescence detector with a broad excitation wavelength of 240-400 nm and an emission wavelength of 400 nm. The detection limits (noise x 3) were about 0.24 μM for citrate and 0.72 μM for malate. By using internal standardization, this method was applicable to the determination of citrate and malate in soil solution. Furthermore, application of siphon injection with a commercial micropipette enabled the injection of a sub-microliter sample into the analytical system with acceptable reproducibility. When combined with a microsampling method, the method presented here will be useful for the sensitive and selective analysis of citrate and malate in soil solution with high spatial resolution.

Key Words

Organic acids, Soil solution, Capillary electrophoresis, Excimer-forming fluorescence derivatization

Introduction

Low-molecular-weight organic acids are involved in many processes of soil located in the vicinity of living or dead organisms, i.e. rhizosphere and detritusphere. These include nutrient acquisition, metal detoxification and mineral weathering. Since most of these roles rely to a large extent on the ability of the organic acids to complex metal cations, it is mainly the poly-carboxylic acids such as citrate, malate and oxalate that have been hypothesized to perform these processes (Jones *et al.* 2003). Analysis of organic acids in soil solution has often been made by high performance liquid chromatography (HPLC) and capillary electrophoresis (CE). The HPLC methods include reverse-phase chromatography and ion chromatography in ion-exchange and ion-exclusion modes (Tani *et al.* 2001), whereas the CE methods usually apply the indirect ultraviolet (UV) detection due to the low absorbing ability of organic acids in the UV and visible ranges (Dahlén *et al.* 2000). The smaller sample volume attained by on-capillary detection with a smaller path length is a suitable feature of CE for the analysis of soil solution with high spatial resolution. However, this feature also causes the lower detection ability than HPLC. Nohta *et al.* (2003) recently developed a very sensitive fluorescence assay for poly-carboxylic acids, which relies on intramolecular excimer-forming fluorescence derivatization with a pyrene reagent. They used an HPLC separation system. This fluorescent derivatization provides a promising sensitive and selective analysis of poly-carboxylic acids by CE. This is especially true of soil solutions whose concentrations of poly-carboxylic acids are sometimes too low to be detected by CE with the conventional indirect UV detection.

In this paper, we describe the application of this fluorescence derivatization method to CE with a special interest in the analysis of soil solution. In addition, we propose a novel and practical method for introducing sub-microliter samples into a CE capillary, which is useful for the analysis of soil solution at high spatial resolution.

Methods

Reagents and chemicals

1-pyrenebutanoic acid hydrazide (PBH) was purchased from Invitrogen. *N*-(3-Dimethylaminopropyl)-*N'*-ethylcarbodiimide hydrochloride (EDC-HCl) was purchased from Sigma-Aldrich. Other chemicals used were analytical grade. The solutions of PBH (5 mM in dimethylsulfoxide (DMSO)), EDC-HCl (0.2 M in water) and pyridine (40% v/v in DMSO) were prepared before use. The pyridine solution was mixed with the EDC-HCl solution at 1:1 (v/v), and this solution was further mixed with the PBH solution at 1:1 (v/v). This reagent mixture (RM) was prepared immediately after preparation of each solution. The RM was stable for 2 days after preparation when it was stored in the dark at room temperature.

Derivatization procedure for standard solutions

Standard solutions of citrate and malate with a volume ranging from 500 nL to 100 μ L were placed in a 0.5 mL microcentrifuge tube and the same volume of the RM was added to each. For manipulation of a 500 nL solution, a micropipette (Pipetman P2, Gilson) was used with care. Then the tube was sealed, heated at 40°C for 60 min in a block heater and cooled in ice for about 10 min (Nohta *et al.* 2003). The resulting solution was applied to the CE instrument without further dilution.

Capillary electrophoresis

Analysis was carried out in a custom-built capillary electrophoresis system (Bazzanella *et al.* 1998) equipped with a fluorescence detector (Argos 250 B, Flux Instruments, Basel, Switzerland) and a high-voltage power supply (HCN 6 M-30000, FuG Elektronik GmbH, Rosenheim, Germany). A fused-silica capillary of 75- μ m I.D. and 363- μ m O.D. (TSP075375, Polymicro Technologies, Arizona, USA) was used. The total length of the capillary was 80 cm, and the length from the inlet to the detector was 57 cm. On the injection side, about 2 mm of the polyimide coating was removed to reduce the outer diameter and facilitate the introduction of the sample using a micropipette as described below. Unlike the commercial system in which the inlet point of the capillary is sealed and inaccessible, the capillary in our system is flexible and accessible. Owing to this modification, it was possible to siphon sub-microliter solutions into the capillary by lifting the capillary and dipping it into a sample solution located in a micropipette tip (e.g., Diamond DL10, Gilson) as depicted in Figure 1. The difference in height between the inlet and the outlet electrode buffer (5 cm) was sufficient to set up a siphon. For sample introduction, this was run for 50 seconds. For sub-microliter samples, a volume of 500 nL was usually held in the pipette tip. The volume could be reduced to be about 200 nL by careful manipulation of a micropipette. For bigger samples (> 10 μ L), injection was carried out by lifting the capillary and dipping it in a sample located in a horizontally inclined microcentrifuge tube rather than a pipette tip. For the separation of derivatized compounds, micellar electrokinetic chromatography was used. The buffer was composed of 50 mM sodium dodecyl sulfate (SDS), 20 mM sodium tetraborate and 5% (v/v) acetonitrile. It was used without adjustment of the pH (9.2). Separation was carried out at a constant voltage of 30 kV (negative at the detection side) with a current of between 80 and 100 μ A. The instrument did not include temperature control of the capillary, which was run at ambient temperature. For detection, the fluorescence detector was operated at a broad excitation wavelength (240-400 nm) and an emission wavelength of 400 nm.

To compare the sensitivity of fluorescence detection with that of the conventional method, citrate and malate in water were also analysed by the indirect UV method according to Bazzanella *et al.* (1998).

Derivatization and analysis for soil solution samples

Two Cambisols were collected from a subsurface horizon (about 20-40 cm) at Henfaes Agricultural Research Station of Bangor University in Abergwyngregyn. One was located on a flat grassland used as a pasture (Cambisol-1), and the other was located on a hill slope predominated by bracken (Cambisol-2). Two Andosols were also collected from a surface 0-15 cm at experimental farms of National Institute of Agro-Environmental Sciences in Tsukuba (Andosol-1) and of Shimane University in Ohta (Andosol-2). Soil solution samples were collected from these four soils by adding deionized water at 50% (v/w) and vacuum suctioning the water out using a hollow fibre sampler after a few hours (Yanai *et al.* 1993). The pH and the concentrations of Ca and Mg in the soil solutions are given in Table 1. In order to evaluate the influence of solutes in soil solution on the derivatization reaction, the samples spiked with standards at the rate of 1:1 (v/v) were subjected to the above derivatization procedures. The influence of pure metal cations on derivatization was also evaluated.

Results

Performance of micropipette injection method

The sample volume introduced into the CE system is usually up to 10 nL, although this depends on the injection method. For commercial CE system, however, the volume required for analysis is usually more than 5 μ L. This means that more than 99% of the sample prepared for injection is wasted. The micropipette injection method described here could decrease the required sample volume to a few hundred nanoliters. The reproducibility of our method was evaluated by introducing 500 nL of 1 μ M Fluorescein sodium salt by siphon under controlled conditions (50 sec, 5 cm height) and detecting it under the same conditions as those used for the analysis of poly-carboxylic acids. The relative standard deviations for retention time and the peak area were 2.99% and 8.02%, respectively, for 10 successive runs. These values indicate that this injection method can be influenced by some artefacts but still provides a simple and reliable way for treating sub-microliter samples with simple equipment. The reproducibility might be improved by the temperature control of the capillary.

Separation and detection of poly-carboxylic acid standards

An electropherogram obtained from a mixture of citrate and malate at 40 μM before derivatization is shown in Figure 2. Citrate and malate derivatives were separated from each other. The sensitivity was better for citrate than the first malate peak. When oxalate is present, the peak of the oxalate derivative overlapped with the second malate peak. This separation is therefore effective for citrate and malate but not for oxalate. A peak for derivatives of acetate and shikimate, which are mono-carboxylic acids, also appeared at the same retention time as the second malate peak only when they were present at mM concentrations. This shows that the detection is relatively specific to poly-carboxylic acids as described by Nohta *et al.* (2003). As for the retention time, citrate and malate peaks were found within 10 min. This was much shorter than the original HPLC method (50 min) (Nohta *et al.* 2003).

Limits of detection and quantification

From the data of Figure 2, the signal to noise ratios for citrate and malate were calculated to be 506 and 166, respectively. The detection limits (noise \times 3) were about 0.24 and 0.72 μM for citrate and malate before derivatization. Using the indirect UV method with the same injection system, the signal to noise ratios for citrate and malate at 40 μM were calculated to be 6 and 8, respectively (data not shown). Compared with the indirect UV method, therefore, the sensitivity for citrate and malate was improved greatly, despite the additional dilution of the samples during derivatization. Calibration curves for citrate and malate standards showed a linear relationship between the signal and sample concentrations up to 20 μM (40 μM before derivatization) (data not shown). A signal of citrate at 0.5 μM (1 μM before derivatization) could be quantified.

Analysis of soil solution

Analysis of soil solution introduced additional problem, as both the pH of samples and cations present affect the derivatization of organic acids. As shown in Figure 3, peak areas of the citrate and malate derivatives were affected by soil solution matrices to various degrees. Thus, addition of target compounds to a sample prior to derivatization (internal standardization) is needed for the quantitative analysis of citrate or malate in soil solution. The cause for the reduced sensitivity for citrate may be due to cation interference, because polyvalent cations especially Fe^{2+} and Al^{3+} significantly inhibited the derivatization of citrate (Table 2). At the same time, using a phosphate buffer, it was found that the sensitivity for citrate decreased with an increase of the pH from 6 to 8 (data not shown). In terms of the sensitivity, it seems that this method can be applied to samples from a wide range of upland agricultural soils but that it may not be suitable for samples from submerged soils containing abundant Fe^{2+} or samples from extremely alkaline soils.

Conclusions

Excimer-forming fluorescence derivatization of poly-carboxylic organic acids followed by the analysis by CE provided rapid, specific and sensitive determination of citrate and malate in water and soil solutions. Furthermore, application of siphon injection with a commercial micropipette enabled to inject a sub-microliter sample into the analytical system with acceptable reproducibility.

Table 1. The pH and the concentrations of Ca and Mg in the soil solutions used in the experiment.

	pH	Ca (mM)	Mg (mM)
Cambisol 1	7.13	0.30	0.04
Cambisol 2	5.63	n.d.	n.d.
Andosol 1	6.25	0.62	0.42
Andosol 2	6.64	0.46	0.14

The pH was measured by a glass electrode.

Ca and Mg concentrations were measured by CE with the indirect UV detection (Bazzanella *et al.* 1998).

Table 2. (lower left). Influence of cations on peak area of citrate derivative. 20 μM citrate mixed with cation solutions (or deionized water as a control) at 1:1 (v/v) was subjected to derivatization. Values indicate the percentages of peak area relative to a control treatment (means \pm S.D., n=3).

	Relative peak area (%)
1 mM Ca^{2+}	32.0 \pm 2.7
10 mM Ca^{2+}	27.7 \pm 2.2
1 mM Mg^{2+}	14.0 \pm 1.1
10 mM Mg^{2+}	12.8 \pm 1.3
100 μM Fe^{2+}	9.1 \pm 4.1
1 mM Fe^{2+}	Undetectable
100 μM Al^{3+}	8.3 \pm 4.6
1 mM Al^{3+}	Undetectable

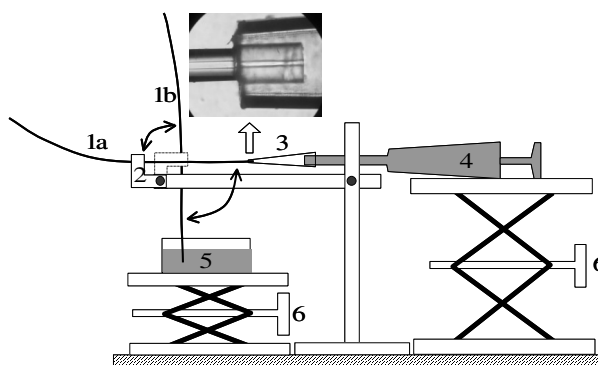


Figure 1 (upper right). Set up for micropipette injection system. 1, capillary at the positions for injection (a) and separation (b); 2, flexible arm; 3, pipette tip; 4, micropipette (Pipetman P2); 5, inlet buffer with an electrode; 6, lift.

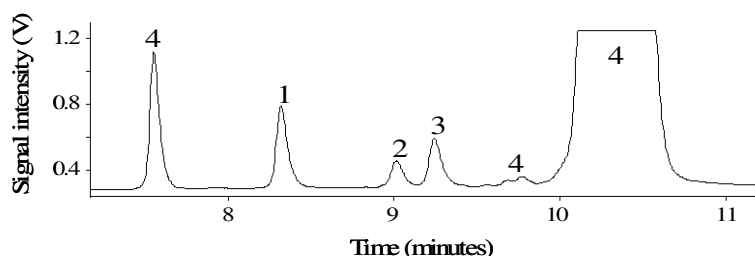


Figure 2. An electropherogram of fluorescent derivatives of citrate and malate, each of which was 40 μM before derivatization. Peaks: 1, citrate; 2, malate; 3, malate (oxalate, acetate or shikimate if present); 4, reagent peaks.

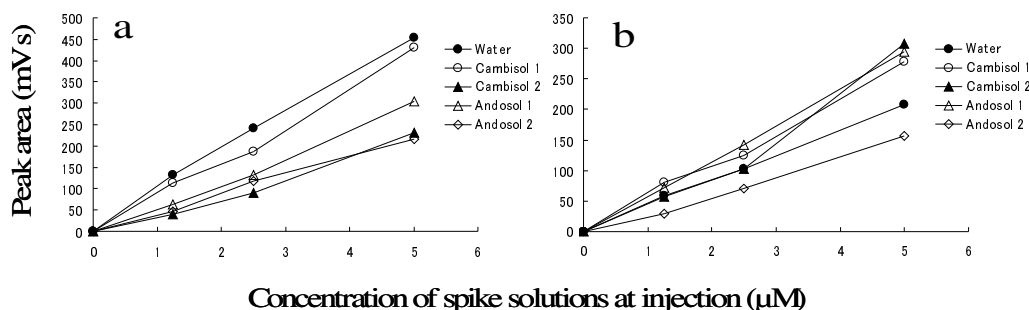


Figure 3. Influence of different soil solution matrices on peak areas of derivatives of citrate (a) and malate (b).

References

- Bazzanella A, Lochmann H, Tomos AD, Bächmann K (1998) Determination of inorganic cations and anions in single plant cells by capillary zone electrophoresis. *J. Chromatogr. A.* **809**, 231-239.
- Dahlén J, Hagberg J, Karlsson S (2000) Analysis of low molecular weight organic acids in water with capillary zone electrophoresis employing indirect photometric detection. *Fresenius J. Anal. Chem.* **366**, 488-493.
- Jones DL, Dennis PG, Owen AG, van Hees PAW (2003) Organic acid behavior in soils – misconceptions and knowledge gaps. *Plant Soil* **248**, 31-41.
- Nohta H, Sonoda J, Yoshida H, Satozono H, Ishida J, Yamaguchi M (2003) Liquid chromatographic determination of dicarboxylic acids based on intramolecular excimer-forming fluorescence derivatization. *J. Chromatogr. A.* **1010**, 37-44.
- Tani M, Shida KS, Tsutsuki K, Kondo R (2001) Determination of water-soluble low-molecular-weight organic acids in soils by ion chromatography. *Soil Sci. Plant Nutr.* **47**, 387-397.
- Yanai J, Araki S, Kyuma K (1993) Use of a looped hollow fiber sampler as a device for non-destructive soil solution sampling from the heterogeneous root zone. *Soil Sci. Plant Nutr.* **39**, 737-743.

Soil microbial ecology of laurel-leaved and *Cryptomeria japonica* forests assessed by dilution plate count and direct microscopic count methods

Ayuko Itsuki^A, Sachiyo Aburatani^B and Shinjiro Kanazawa^C

^ADepartment of Chemical Engineering, Nara National College of Technology, Yamatokoriyama, Nara, Japan, Email itsuki@chem.nara-k.ac.jp

^BComputational Biology Research Center, National Institute of Advanced Industrial Science and Technology, Koto, Tokyo, Japan, Email s.aburatani@aist.go.jp ^CGraduate School of Agriculture, Kyushu University, Higashi, Fukuoka, Japan, Email kana-s@agr.kyushu-u.ac.jp

Abstract

The soil ecology of the organic and mineral soil layers of laurel-leaved and *Cryptomeria japonica* forest in the Kasuga-yama Hill Primeval Forest (Nara, Japan) was assessed. The number of bacteria obtained by the dilution plate count method was less than 0.05% of those counted by the direct microscopic count. We therefore found that forest soil contains large numbers of non-culturable bacteria compared with agricultural soil. The numbers of bacteria and fungi obtained by both the dilution plate count and the direct microscopic count were larger in the deeper horizons (F and H) of the organic layer than in the mineral soil layer. This suggests that active microbial metabolism takes place in the organic layer. The numbers of bacteria and the length of fungal hyphae obtained by the direct count method were greater in the H horizon than in the F horizon. The direct microscopic count revealed numerous non-culturable bacteria and fungi in the soil. The ratio of fungal to bacterial biomass was lower in the laurel-leaved forest soil. The fungal biomass was therefore relatively low in the laurel-leaved forest soil due to differences in forest vegetation.

Key Words

Bacterial number, dilution plate count, direct microscopic count, forest soil, length of fungal hyphae, microbial biomass

Introduction

The world heritage Kasuga-yama Hill Primeval Forest in Nara, Japan, is a lowland laurel-leaved forest, in which natural conditions have been conserved for more than 1160 years (Suganuma 1982). Numerous unique species of plants, animals and insects have been found in the forest, attracting much research attention (Suganuma 1982). However, the microbial ecology of the soil supporting the primeval forest has not been elucidated to date. Therefore, we have started a series of studies to clarify the forest microbial ecology.

In forest ecology, research is often focused on the microbial decomposition processes occurring in the soil organic matter, which is influenced by differences in vegetation, climate, and soil type (Tanabe and Suzuki 1973). Most studies use the dilution plate count method to determine soil bacterial content. However, this method only measures about 1% of the total number of bacteria present in the soil (Someya 1997). Fungal counts are also limited by methods that only count spores suited to specific culture media (Tanabe and Suzuki 1972). In the present study, the organic and mineral soil layer of the soil from the laurel-leaved forest and the *Cryptomeria japonica* forest were examined for the numbers and biomass of bacteria and fungi using both the dilution plate count and the direct microscopic count methods.

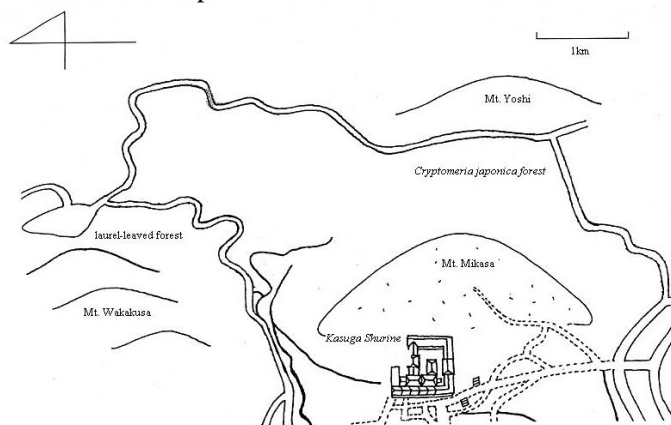


Figure 1. Kasuga-yama Hill Primeval Forest in Nara, Japan. Soil samples were obtained from the laurel-leaved and *C. japonica* forests, as indicated.

Materials and methods

Soil samples

Figure 1 shows the outline of the Kasuga-yama Hill Primeval forest in Nara, Japan. Soil samples were collected from the laurel-leaved forest (B_{B-1}) and the *Cryptomeria japonica* forest (B_{B-2}) in April 2001. The B_{B-1} and B_{B-2} samples were dry brown forest soils. The vegetation of laurel-leaved forest was *Machilus thunbergii* and *Neolitsea aciculata*, while that of *C. japonica* forest was *C. japonica*. The soil was divided into 5 layers, including organic (L, F and H horizons) and mineral soil (A and B horizons) layers (Figure 2).

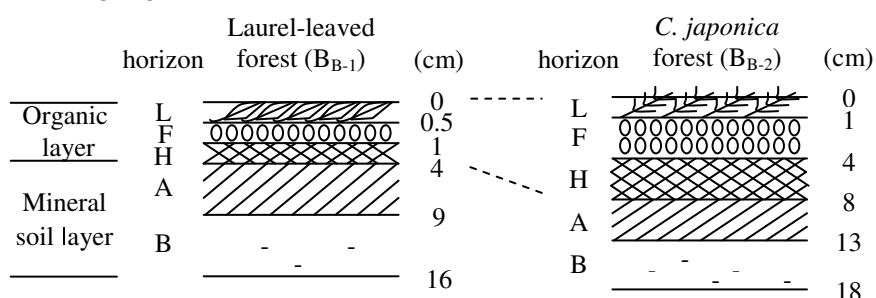


Figure 2. Soil profile of laurel-leaved and *C. japonica* forests.

Soil samples were analyzed for moisture content, pH, and carbon (C) and nitrogen (N) content (Table 1). For microbial analyses, soil samples from each horizon had particle sizes adjusted to <2 mm with scissors. Size-adjusted soil samples (5 g) were suspended in 45 mL of the sterile water and homogenized for 3 min at 12,000 rpm with a Homo blender (500C, Sakuma) (Kanazawa *et al.* 1986).

Measurements of soil microorganisms

The numbers of bacteria and fungi were measured using two methods: the dilution plate count method and the direct microscopic count method. Albumin or Rose Bengal-Streptomycin agar was used for the dilution count method to culture the bacteria or fungi contained in the sample solution at 25°C for 4 or 6 d (Tanabe and Suzuki 1972). The direct microscopic count method for bacteria was performed according to Someya's method (Someya 1995). The sample solution was dispersed for 20 min with an ultrasonic device (US-3, Kenis), diluted ten times, and then 100 µL was filtered through a 0.2 µm filter. Ethidium bromide solution (50 µL of the 100 µg/mL) was placed onto the filter for 3 min then filtered. The filter was dried, placed onto a glass slide and covered with immersion oil. Bacteria were counted under a fluorescence microscope (FX-35A, Nikon). Fungal hyphae length was measured according to the Jones-Mollison method (Jones and Mollison 1948). After 1 mL of the sample solution was added to 9 mL of 1.5% agar solution, an agar membrane was placed on a Haemocytometer. The membrane was stained with phenol-aniline blue solution for 1 h then de-stained. The length of fungal hyphae on the haemocytometer was measured under a light microscope (TK, Kagaku Kyoeisha).

The soil bacterial biomass (B_m) and fungal biomass (F_m) were calculated using the following formulae (Hasebe *et al.* 1984):

$$B_m \text{ (mg/g)} = n \times v_{\text{ave}} \times \rho \times r \quad (1)$$

$$F_m \text{ (mg/g)} = v \times \rho \times r \quad (2)$$

where n = numbers of bacteria (cell/g); v_{ave} = Average bacterial volume (= 0.19 µm³); ρ = Specific gravity of microorganism (= 1.1 g/cm³); r = Rate of dry matter (= 20%); v = Fungal volume (cm³/g)

Table 1. Soil properties from laurel-leaved and *C. japonica* forests.

Vegetation	Soil type	Horizon	Moisture content (%)	pH (H ₂ O)	Total C (g/kg)	Total N (g/kg)	C/N ratio	Volume weight (g/cm ³)
Laurel-leaved forest (B _{B-1})	dry brown forest soil	L	13.7	4.52	467.3	12.6	37.1	0.048
		F	43.8	4.34	402.2	16.9	23.8	0.180
		H	56.5	4.51	318.9	16.9	18.9	0.297
		A	42.5	3.88	189.1	10.5	18.0	0.685
		B	25.0	3.64	38.2	2.0	19.1	0.823
<i>C. japonica</i> forest (B _{B-2})	dry brown forest soil	L	13.7	5.04	498.7	5.8	89.1	0.032
		F	62.0	4.37	361.2	11.9	30.4	0.066
		H	53.4	3.87	201.4	9.5	21.2	0.155
		A	42.0	3.81	106.0	5.8	18.3	0.493
		B	28.4	3.95	30.7	2.0	15.4	0.628

Results

Dilution plate counts of soil bacteria and fungi

The numbers of bacteria and fungi obtained by the dilution plate count method (Figure 3) were larger in the F and H horizons of the organic layer than in the mineral soil layer. When each horizon of the organic layer was compared, the numbers of bacteria and fungi were lowest in the L horizon. Bacterial and fungal counts in the laurel-leaved organic layers were higher than those in the *C. japonica* organic layers.

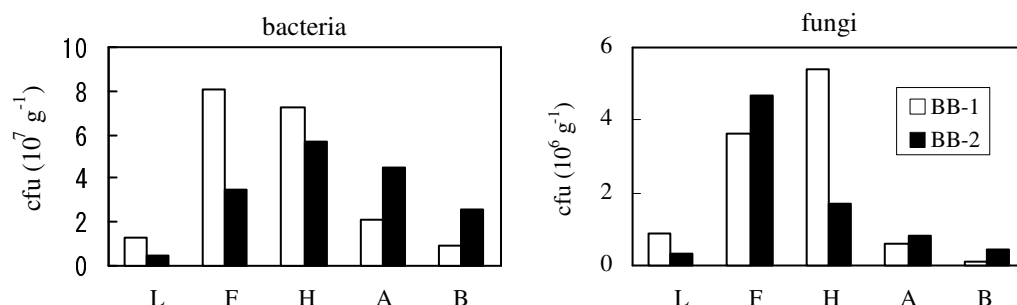


Figure 3. The numbers of bacteria and fungi obtained by the dilution plate count method.

Direct microscopic counts of soil bacteria

A larger number of bacteria was detected using the direct microscopic count method (Figure 4) than using the dilution plate method, which only measures culturable soil bacteria. The numbers of bacteria obtained by the direct microscopic count method showed similar trends to the dilution plate counts: more bacteria were present in the F and H horizons of the organic layer, and the bacterial count was greater in the laurel-leaved compared with the *C. japonica* soils. However the layer distribution of bacteria assessed using the direct plate count method did not necessarily correspond to the results from the dilution plate count method. The difference in the layer distribution of soil microorganisms was clearly reflected in the differences of bacterial biomass. The uppermost L horizon, which contains large amounts of fresh plant residue contained low levels of microorganisms. In the F horizon, there was increased nourishment due to more advanced state of decomposition in this layer. In the H horizon, the organic matter was completely decayed and the amount of bacteria that is able to be grown in nutrient-poor conditions increased, relative to the culturable bacteria.

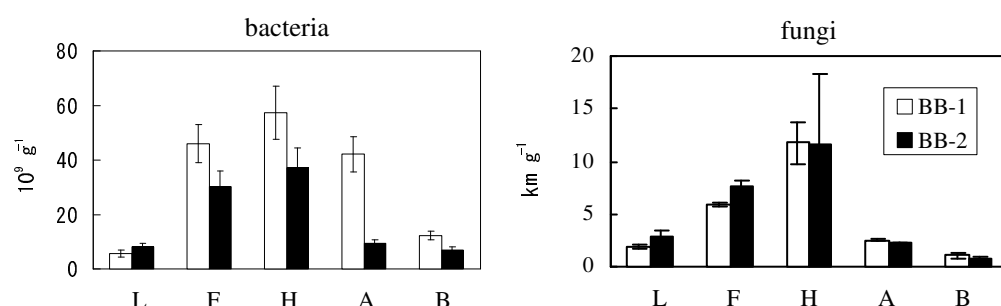


Figure 4. The bacterial number and fungal hyphae length obtained by the direct microscopic count method.

Table 2 shows the ratio of the bacterial count values obtained using the dilution plate count method (P) and the direct microscopic count method (D). The P/D of the A horizon forest soil, which is most comparable to agricultural soils, was only 0.05-0.48%. However, this is much lower than the reported P/D value for agricultural soils of 0.73-3.1% (Marumoto 1994). We found that Kasuga-yama Hill Primeval Forest soil contains large numbers of non-culturable bacteria, compared with agricultural soils. Such information is necessary to understand the metabolism of the forest soil, and will lead to further research on the identity and functions of these bacteria in forest soils.

Table 2. Ratio of the number of bacteria obtained by the dilution plate count method (P) and that obtained by the direct microscopic count method (D).

Horizon	Laurel-leaved forest (B _{B-1})	<i>C. japonica</i> forest (B _{B-2})
L	0.24	0.06
F	0.17	0.12
H	0.13	0.15
A	0.05	0.48
B	0.08	0.37

Fungal hyphae length obtained using the direct microscopic count method

The fungal hyphae (Figure 4) were longer in the organic soil layer than in the mineral soil layer. When each horizon was compared, fungal hyphae were found to be longest in the H horizon.

Bacterial and fungal biomass

Table 3 shows the amount of bacterial (B_m) and fungal (F_m) biomass. The total soil biomass ($B_m + F_m$) in the organic layer was greater than that in the mineral soil layer. The total soil biomass in the organic layer increased with soil depth, and was greatest in the H horizon. In contrast, the total soil biomass in the mineral soil layer decreased with increasing depth. The laurel-leaved forest soil had greater total biomass ($B_m + F_m$) than the *C. japonica* soil. This difference is clearly due to differences in forest vegetation, with higher microbial biomass in the laurel-leaved forest indicating a higher metabolic activity than the *C. japonica* soil. The total soil biomass of the forest soil A horizons was similar to those previously reported for agricultural soils (1.6-3.0 mg/g) (Marumoto 1994). However, the forest organic layers overall were far richer in microorganisms than agricultural soils. Forest soil is a natural ecosystem that is continuously supplied with plant matter, and differs from agricultural soil, in which the organic matter is disturbed by cultivation and readily consumed by nutrient-starved crops.

The ratio of bacterial to fungal biomass (F_m/B_m) was the highest in the H horizon of the organic layer for both forest types. In addition, the F_m/B_m in the laurel-leaved soil was less than that in the *C. japonica* soil, due to vegetation effects. The F_m/B_m of agricultural soil is typically 0.98-3.75 (Sakamoto and Oba 1995), which is similar to the F_m/B_m of A horizons in the forest soils. It has been assumed that the mineral soil layer of forest soils has a greater proportion of fungal biomass than agricultural soil. However, our results show that the forest mineral soil layers are similar to agricultural soils in fungal content. The H horizons of the organic layers in the forest soil had much greater F_m/B_m compared with agricultural soils.

Table 3. Bacterial (B_m) and fungal (F_m) biomass in laurel-leaved and *C. japonica* forest soils.

Horizon	Laurel-leaved forest (B _{B-1})				<i>C. japonica</i> forest (B _{B-2})			
	B_m (mg/g)	F_m (mg/g)	$B_m + F_m$ (mg/g)	F_m/B_m	B_m (mg/g)	F_m (mg/g)	$B_m + F_m$ (mg/g)	F_m/B_m
L	0.23	0.75	0.98	3.21	0.35	1.35	1.7	3.87
F	1.93	5.96	7.89	3.09	1.27	4.32	5.58	3.41
H	2.4	18.51	20.91	7.71	1.55	17.04	18.6	10.96
A	1.76	1.97	3.73	1.12	0.39	1.25	1.64	3.2
B	0.51	1.46	1.97	2.84	0.29	0.32	0.61	1.13

Conclusion

The microbial ecology of the organic and mineral soil layers of laurel-leaved and *Cryptomeria japonica* forest in the Kasuga-yama Hill Primeval Forest (Nara, Japan) was assessed. The direct microscopic count revealed numerous non-culturable bacteria and fungi in the forest soil compared with agricultural soil.

References

- Hasebe A, Kanazawa S, Takai Y (1984) Microbial biomass calculated from directed using fluorescence microscope. *Soil Science and Plant Nutrition* **30**, 175-187.
- Jones PCT, Mollison JE (1948) A technique for the quantitative estimation of soil microorganisms. *Journal of General Microbiology* **2**, 54-69.
- Kanazawa S, Takeshima S, Ohta K (1986) Effect of waring blender treatment on the counts of soil microorganisms. *Soil Science and Plant Nutrition* **32**, 81-89.
- Marumoto T (1994) 'Soil biochemistry'. (Asakura Publishing: Tokyo).
- Sakamoto K, Oba Y (1995) Effect of Various Organic Amendments on Microbial Biomass Flora in Arable Soil. *Soil Science and Plant Nutrition* **66**, 418-421.
- Someya T (1995) Three-dimensional observation of soil bacteria in organic debris with a confocal laser scanning microscope. *Soil Microorganisms* **46**, 61-69.
- Someya T (1997) Ecology of soil microorganisms and new methods. *Japanese Journal of Ecology* **47**, 59-62.
- Suganuma T (1982) 'History of Nara Park (Nature)'. (Daiichihouki Publishing: Nara).
- Tanabe I, Suzuki T (1972) Analysis method of microorganism. *Soil Science and Plant Nutrition* **37**, 34-45.
- Tanabe I, Suzuki T (1973) 'Ecology of soil microorganism'. (Kyoritsu Publishing: Tokyo).

Spectroscopic studies of ternary interactions in an öocyst-surfactant-hematite system

Xiaodong Gao and Jon Chorover

Department of Soil, Water and Environmental Science, University of Arizona, Tucson, USA, Email xdgao@email.arizona.edu

Abstract

Prior studies have indicated that the subsurface transport of *Cryptosporidium parvum* is diminished in sediments containing iron oxides, but the molecular mechanisms are poorly known, as are the impacts thereon of natural organic matter (NOM). Using in-situ attenuated total reflectance (ATR)-FTIR spectroscopy, we examined the molecular mechanisms of viable *Cryptosporidium parvum* öocyst adhesion at the hematite (α -Fe₂O₃)-water interface over a wide range in solution chemistry. The anionic surfactant sodium dodecylsulfate (SDS) was used as a surrogate for NOM to examine the impacts of surfactant-type components on öocyst adhesion mechanisms. Results indicate that, in the absence of SDS, öocyst surface carboxylate groups form inner-sphere complexes with hematite Fe metal centres at low pH and outer-sphere complexes at high pH. Such direct chemical bonding is likely one mechanism whereby Fe oxides diminish öocyst transport. The presence of SDS significantly diminishes Fe-carboxylate complexation in the öocyst-SDS-hematite ternary system. Results suggest that the sulfate groups (OSO₃⁻) of SDS compete effectively for α -Fe₂O₃ surface sites, and this is likely the primary mechanism for decreasing Fe-carboxylate complexation. Sorptive competition with NOM may, therefore, increase the mobility of *C. parvum* öocysts in soils.

Key Words

ATR-FTIR spectroscopy, öocyst adhesion, hematite, SDS, Fe-carboxylate complexes

Introduction

Cryptosporidium parvum is a water-borne protozoan pathogen that is responsible for the gastrointestinal disease Cryptosporidiosis, which is potentially lethal for immuno-compromised individuals (Casemore *et al.* 1997). Öocysts, the encysted, environmental form of the obligate pathogen, exhibit a complex mixture of surface biomacromolecules consisting primarily of amide, carboxylate, phosphate, and polysaccharide functionalities (Gao and Chorover 2009). Ionizable functional groups, such as carboxylate and phosphate groups, may serve as reactive sites for direct bonding to mineral surfaces. In a previous spectroscopic study, we found that formation of inner-sphere versus outer-sphere complexes between öocyst surface carboxyls and hematite surface hydroxyls was dependent on solution chemistry (Gao *et al.* 2009). Such molecular-scale chemical bonding is likely to retard öocyst transport in Fe-rich tropical soils.

Ionic surfactants are ubiquitous in the environment and may play important roles in mediating the fate and transport of pathogenic cells in the subsurface. For example, anionic surfactants can decrease or even reverse the positive surface charge on metal oxides by forming monolayer or bilayer surface patches (Fuerstenau and Colic 1999; Bai *et al.* 2004). This could diminish öocyst adhesion due to an increase in electrostatic repulsive force. However, it is also possible that surfactant coatings could enhance öocyst adhesion to mineral surfaces because of an increase in sorbent hydrophobicity. Furthermore, ionic surfactant compounds can form surface complexes at mineral surfaces (Bai *et al.* 2004; Gao and Chorover 2010), competing for the reactive surface sites with öocyst surface biomolecules. Despite the prevalence of naturally produced and synthetic surfactants in waters contaminated with *C. parvum* öocysts, their influence on öocyst fate and transport remains poorly understood. The main objective of this study was to use SDS as a model compound to examine the effect of surfactant-type NOM components on öocyst adhesion mechanisms using in-situ ATR-FTIR spectroscopy, and to explore the potential effect of anionic surfactant on pathogen transport in the subsurface. Specifically, we compared the ATR-FTIR spectra of öocysts at the aqueous solution – hematite interface in the presence and absence of SDS. By close examination of spectral changes, the molecular interaction mechanisms were determined.

ATR-FTIR spectra of Öocysts suspension

ATR-FTIR spectrum of viable öocyst suspension on the ZnSe internal reflection element (IRE) exhibits IR bands corresponding to amides (1635, 1542, and 1337-1313/cm for amide I, amide II, and amide III, respectively), carboxylate (COO⁻ at 1400/cm), phosphate (1237/cm), and polysaccharide functional groups (C-O-C, C-C, 1150-950/cm) (Figure 1a). The spectrum on the same IRE coated with nano-particulate α -Fe₂O₃ (Figure 1b) is distinctly different from the spectrum for the uncoated IRE. It exhibits much stronger asymmetric and symmetric COO⁻ stretching bands, suggesting the formation of Fe-carboxylate complexes during öocyst

adhesion. In addition, the separation in wavenumber ($\Delta\nu$) of ν_{as} and ν_a COO^- stretching bands (e.g., $\Delta\nu > 200/\text{cm}$ for monodentate, 180 - 150/ cm for binuclear bidentate, and $< 100/\text{cm}$ for mononuclear bidentate) (Deacon and Phillips 1980) allows the complexation mode (inner- versus outer-sphere) to be assigned (Gao *et al.* 2009).

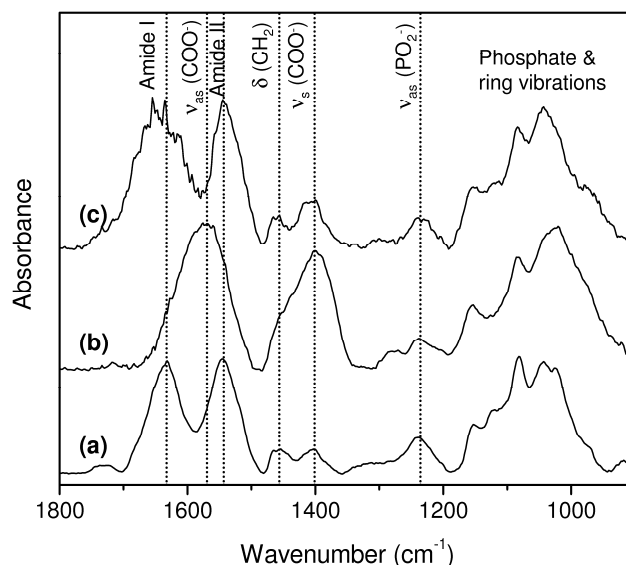


Figure 1. ATR-FTIR spectra of viable oocyst suspension in 10 mM NaCl solution at pH 6 on (a) ZnSe IRE alone, (b) $\alpha\text{-Fe}_2\text{O}_3$ surface in the absence of SDS, and (c) $\alpha\text{-Fe}_2\text{O}_3$ surface in the presence of 0.01 mM SDS.

When SDS is introduced to the ternary system (Figure 1c), the intensity of the asymmetric stretching of COO^- is significantly reduced to the extent that it is masked by the amide group vibrations. The intensity of the symmetric stretching band is substantially reduced as well. Such intensity decreases in carboxylate stretching modes clearly suggests that the presence of SDS significantly diminishes Fe-carboxylate complexation at the hematite surface.

Kinetics of Oocyst-SDS-Hematite ternary interaction

Figure 2 presents the result of experiments of oocyst adhesion to hematite in the absence (Figure 2a-e) and presence (Figure 2f-j) of SDS as a function of interaction time (proceeding from bottom to top) and pH (left to right) in 10 mM NaCl solution. We focus on the spectral region of $\nu_s(\text{COO}^-)$ (1500 - 1200/ cm) because it is subject to minimum influence from the bending vibrations of H_2O and exhibits most distinct changes responding to reaction time. As discussed above, when SDS is absent, the symmetric stretching band increases progressively with interaction time for all pH values due to the formation of the Fe-carboxylate complexes (Figure 2 a-e). Two symmetric stretching bands were observed at low pH (3 and 4.5) at 1370 and 1400/ cm , respectively, whereas only one stretching band at 1400/ cm was observed at higher pH. On the basis of $\Delta\nu$ of ν_{as} and ν_a COO^- , oocysts are bound to hematite via monodentate (Figure 3a) and binuclear bidentate (Figure 3b) complexes. The former predominates at low pH, whereas the latter becomes increasingly prevalent with increasing pH.

In contrast, we observe the opposite trend when SDS is introduced to the ternary system. As shown in Figure 2f-j, the symmetric stretching band decreases with interaction time for all pH values, suggesting that the extent of Fe-carboxylate complexation is diminished gradually in the ternary system. In addition, similar to the spectra in the absence of SDS, the symmetric stretching also contains two bands at 1418 and 1400/ cm in the pH range of 3 - 7.5, indicating the presence of two inner-sphere complexes. However, one of the bands shifted from $\sim 1370/\text{cm}$ in the absence of SDS to 1418/ cm in the presence of 0.01 mM SDS, suggesting that SDS also changed the complexation mode between hematite and oocyst surface carboxylate groups.

The peak position of the asymmetric COO^- stretching was determined at 1577/ cm by peak deconvolution. Thus, based on the $\Delta\nu$ between ν_{as} and ν_s of COO^- , both peaks at 1418/ cm ($\Delta\nu = 159/\text{cm}$) and 1400/ cm ($\Delta\nu = 177/\text{cm}$) could be potentially attributed to binuclear bidentate complexes. In addition, at pH 3, the band at 1400/ cm decreases more quickly relative to the band at 1418/ cm , indicating the complexation mode at

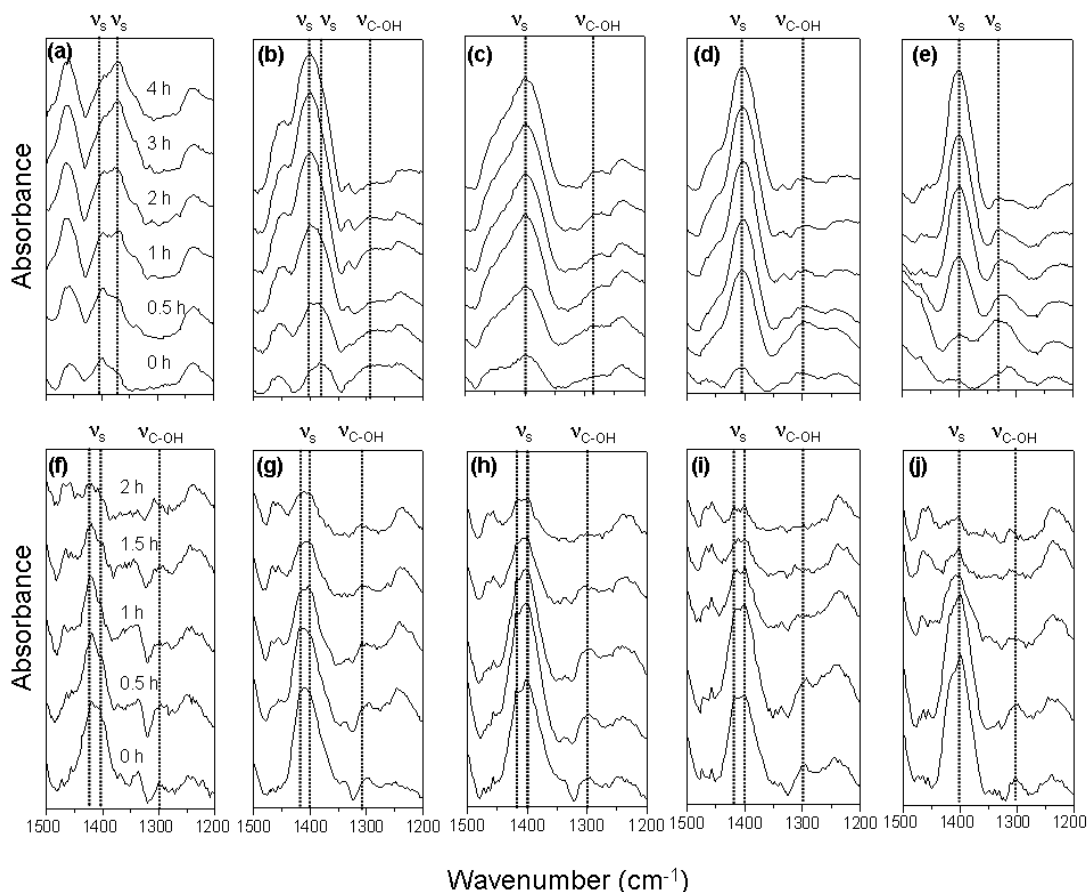


Figure 2. ATR-FTIR spectra of viable oocyst suspension on α -Fe₂O₃ surface in the absence of SDS in 10 mM NaCl solution as a function of reaction time in the region of $\nu_s(\text{COO}^-)$ (1500 - 1200/cm) at (a) pH 3, (b) pH 4.5, (c) pH 6, (d) pH 7.5, (e) pH 9, and in the presence of 0.01 mM SDS at (f) pH 3, (g) pH 4.5, (h) pH 6, (i) pH 7.5, (j) pH 9.

1418/cm is relatively more stable at this pH (Figure 2f). Because the band at 1400/cm occurs in both systems (absence or presence of SDS), we propose that the presence of SDS has shifted the other band (at 1370/cm in the absence of SDS) to 1418/cm in the oocyst-SDS-hematite ternary system, which could be interpreted as a change from monodentate to binuclear bidentate coordination. However, since this assignment derives from symmetry considerations, the band at 1418/cm is also possibly due to carboxylate binding to one Fe(III) (monodentate) and H-bond formation with a hydroxyl group, which possesses similar symmetry to binuclear bidentate coordination. The hydroxyl groups in the ternary system may derive from both the hematite surface and sulfate groups of SDS. The absence of this band in the binary oocysts-hematite system, however, suggests that hematite surface hydroxyls do not form H-bonds with the cell surface carboxylate groups. Hence, we attribute the observed shift to the formation of H-bonds between the sulfate groups of SDS and the carboxylate groups of the monodentate complex, forming a ternary, carboxylate-SDS-mineral complex (Figure 3c). This interpretation is consistent with the change of the dominant monodentate complex in the absence of SDS at pH 3 to the dominant carboxylate-SDS-hematite ternary complex in the ternary system after the introduction of SDS.

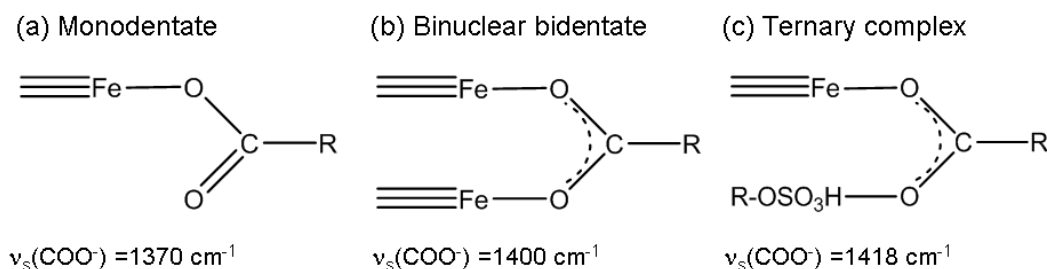


Figure 3. Schematic illustration of the surface complexation structures formed between oocyst surface carboxylate groups and hematite based on the $\Delta\nu$ of ν_{as} and $\nu_s \text{COO}^-$. The peak position associated with each complex was labelled in the figure.

With increasing pH, the spectra exhibit a similar trend with the symmetric COO^- stretching decreasing with reaction time (Figure 2g-j). In the pH range of 4.5 - 7.5, the spectra still contain two bands at 1418 and 1400/cm, corresponding to the carboxylate-SDS-hematite ternary complex and binuclear bidentate complex, respectively. However, the contribution from each complexation mode is noticeably changed. The binuclear bidentate complex represented by the band at 1400/cm becomes relatively stronger with increasing pH. There are two possible explanations for this observation. First, we found that high pH favors the binuclear bidentate complex in NaCl background electrolyte (no SDS) (Gao *et al.* 2009). Another possibility is that gradual deprotonation of sulfate and carboxylate groups with increasing pH hinders the formation of H-bond between them, and thereby reduces the contribution from the ternary complex. When pH increases to 9, the band at 1400/cm becomes the only dominant band.

Molecular mechanism of SDS effect on *Öocyst* adhesion

We speculate that the competition between the OSO_3^- group of SDS and the carboxylate groups in the microbe-mineral interfaces is a primary mechanism for the decrease of the asymmetric and symmetric COO^- stretching in the spectra of the ternary system. If the substitution of the sulfonate groups for the carboxylate groups occurs in the ternary system, the spectra should exhibit an increase of $\nu_{\text{as}}(\text{OSO}_3^-)$ with reaction time associated with the decrease of $\nu_{\text{s}}(\text{COO}^-)$ due to the formation of Fe-sulfate complexation, which was confirmed by the ATR-FTIR data (data now shown).

Conclusions

A molecular understanding of the effect of SDS on *öocyst* adhesion mechanism to hematite was achieved using in-situ ATR-FTIR spectroscopy. Our results suggest that small concentration of surfactants can have profound effect on mechanisms of *öocyst* adhesion and, potentially, transport in the environment. The results indicate that the Fe-carboxylate surface complexation formed between *öocyst* surface biomolecules and hematite was significantly diminished in the *öocysts*-SDS-hematite ternary system. The primary mechanism causing decreased Fe-carboxylate complexation in the presence of SDS is likely due to sulfate substitution by forming Fe-sulfate complexes at hematite surface. In addition, such substitution is favored at higher pH, implying that weakly bounded *öocysts* by outer-sphere complexation can be easily displaced by ionic surfactants. Biosurfactants produced by soil microorganisms are structurally comparable to SDS, and thereby may have similar effect on *öocyst* transport. The results of this study provide critical information of the molecular bonding mechanisms for predicting the fate and transport of pathogenic cells in the subsurface prevalent with surfactant-type compounds.

References

- Bai B, Hankins NP, Hey MJ, Kingman SW (2004) In situ mechanistic study of SDS adsorption on hematite for optimized flotation. *Industrial & Engineering Chemistry Research* **43**, 5326-5338.
- Casemore DP, Wright SE, Coop RL (1997) Cryptosporidiosis-human and animal epidemiology. In 'Cryptosporidium and Cryptosporidiosis'. (Ed R Fayer) pp. 65-92. (CRC Press: Boca Raton, FL).
- Deacon GB, Phillips R (1980) Relationships between the carbon-oxygen stretching frequencies of carboxylate complexes and the type of carboxylate coordination. *Coordination Chemistry Reviews* **33**, 227-250.
- Fuerstenau DW, Colic M (1999) Self-association and reverse hemimicelle formation at solid-water interfaces in dilute surfactant solutions. *Colloids and Surfaces A: Physicochemical and Engineering Aspects* **146**, 33-47.
- Gao X, Chorover J (2009) In-situ monitoring of *Cryptosporidium parvum* *öocyst* surface adhesion using ATR-FTIR spectroscopy. *Colloids and Surfaces B: Biointerfaces* **71**, 169-176.
- Gao X, Chorover J (2010) Adsorption of sodium dodecylsulfate (SDS) at ZnSe and $\alpha\text{-Fe}_2\text{O}_3$ surfaces: Combining infrared spectroscopy and batch uptake studies. *Journal of Colloid and Interface Science*, doi:10.1016/j.jcis.2010.04.011
- Gao X, Metge DW, Ray C, Harvey RW, Chorover J (2009) Surface complexation of carboxylate adheres *Cryptosporidium parvum* *öocysts* to the hematite-water interface. *Environmental Science & Technology* **43**, 7423-7429.

The biogeochemistry of *Sphagnum* mosses - the effects of substrate source on their phenolic composition

Geoffrey D. Abbott^{A,D}, Aminu Muhammad^A, Lisa Belyea^B, Chris Laing^B and Greg L. Cowie^C

^ASchool of Civil Engineering and Geosciences, Newcastle University, Newcastle upon Tyne NE1 7RU, UK.

^BDepartment of Geography, Queen Mary University of London, Mile End Road, London, E1 4NS, UK.

^CMarine Geosciences Group, School of Geosciences, Edinburgh University, Edinburgh, EH9 3JW, UK.

^DCorresponding author. Email geoff.abbott@ncl.ac.uk

Abstract

Several species of peat moss and vascular plants were collected from field incubation litterbag experiments set up in a peatland located in the boreonemoral zone of central Sweden. These were then analysed using THM in the presence of TMAH which revealed the distributions of both lignin- and *Sphagnum*-derived phenols within specific species. THM of seven species of *Sphagnum* indicated the presence of four *Sphagnum*-specific biomarkers; methylated 4-isopropenylphenol, methylated *cis* and *trans* 3-(4'-hydroxyphen-1-yl)-but-2-enoic acid, and methylated 3-(4'-hydroxyphen-1-yl)-but-3-enoic acid.

Key Words

Thermochemolysis, tetramethylammonium hydroxide.

Introduction

Northern peatlands cover an area of around 350×10^6 ha, and store around one-third of global soil carbon (C) (Gorham 1991), however the effect that increasing temperatures and elevated CO₂ levels will have on these systems is of great uncertainty (Davidson and Janssens 2006). *Sphagnum* moss litter is the dominant input of C_{org} into ombrotrophic bogs. It contains phenolics that act both as structural support components and as inhibitors of microbial decomposition of the organic matter (Verhoeven and Liefveld 1997; Freeman *et al.* 2001). There are also vascular plants associated with peatlands which will contribute lignin and other polyphenols. *Sphagnum* does not contain lignin (Mauseth, 1998) and instead biosynthesizes other phenylpropanoids including *trans*-*Sphagnum* acid (Rasmussen *et al.* 1995). Thermally assisted hydrolysis and methylation (THM) in the presence of tetramethylammonium hydroxide (TMAH), otherwise known as TMAH thermochemolysis, can be used to identify lignin phenols (e.g. Mason *et al.* 2009). Thermochemolysis was first introduced as an analytical pyrolysis technique with *in situ* derivatisation using TMAH (Challinor 1989; Kaal and Janssen 2008). The aim of this presentation is to characterize and compare the phenolics of both *Sphagnum* and *Polytrichum* moss species as well as some vascular plant species which contribute to the peat litter of a bog located in central Sweden.

Materials and methods

Site and samples

Samples were collected from Ryggmossen in the boreonemoral zone of central Sweden. In this study, 45 samples were analysed from four distinct sets of samples. A field incubation litterbag experiment of fresh litter had been set up on the site. These litterbags were sampled twice: sampled first in September 2007 giving set 1 (0001-0009), and again in April 2008 resulting in set 2 (0020-0029). These samples consisted of seven species of *Sphagnum* (*S. capillifolium*, *S. fuscum*, *S. majus*, *S. centrale*, *S. balticum*, *S. magellenicum*, *S. angustifolium*), and one species of *Polytrichum* (*P. commune*). The third set of samples (10F-19D), were collected from the field incubation reciprocal transplant experiment in September 2007. Fresh and degraded samples were taken from each habitat; fresh samples from the near surface oxic horizon, and the degraded samples from just below the water table. The final sample sets (0030-0045) are non-*Sphagnum* species sampled from a field monitoring site in April 2008.

TMAH thermochemolysis

On-line thermally assisted hydrolysis and methylation (THM) in the presence of tetramethylammonium hydroxide (TMAH) was performed using a pulsed mode open pyrolysis system, specifically a CDS 1000 pyroprobe unit (Chemical Data Systems, USA) fitted with a platinum coil and a CDS 1500 valved interface. Approximately 1.2 mg of peat sample was weighed into a quartz pyrolysis tube plugged with pre-extracted silica wool. An internal standard, 5 α -androstane was added to the samples to enable accurate quantitative

Table 1. The peatland comprised of four stages.

	Stage	Description
SF	Swamp Forest	seasonally flooded woodland with an understory of shrubs and forest mosses.
FL	Fen Lagg	poorly minerotrophic peatland with a diverse assemblage of sedges, peat mosses, and other plant groups.
BM	Bog Margin	well drained ombrotrophic peatland with low, open tree cover and an understory of dwarf shrubs and peat mosses.
BP	Bog Plateau	ombrotrophic peatland with a distinct microtopography of dry hummocks and wet hollows.

analysis to be carried out on peaks within the chromatogram, and 10 μ l of an aqueous solution of TMAH (25% w/w) was added to the sample immediately prior to THM. The pyroprobe interface was maintained at 340 °C and THM was carried out at 450 °C for 10 s (20 °C/ms temperature ramp) with the products passing into an HP5890 gas chromatograph with an open split (40 mL/min) and a 60 m HP5-MS column (0.25 mm internal diameter, 0.25 μ m film thickness, J&W Scientific, USA). Helium was used as carrier gas at a flow rate of 1 ml/min. The GC oven was programmed to start at 100 °C, held for 2 minutes, then raised to 320 °C at a rate of 3 °C/min, where it was held for 16 min. Product detection was carried out using an HP5000 series mass selective detector in full scan mode (m/z 50 to 700) with compound identification based on the NIST98 mass spectral library, on ion fragmentation patterns and following the conventions described in other studies (Clifford *et al.* 1995; Hatcher *et al.* 1995), together with the comparison of mass spectra and relative retention times with the literature (Mason *et al.* 2009; Vane 2003).

Results and discussion

THM in the presence of TMAH of the peat mosses and herbaceous plants yields methylated phenols including those with guaiacyl, syringyl and *p*-hydroxyphenyl lignin-derived structures as well as the methyl esters of the cinnamyl phenols, ferulic acid and *p*-coumaric acid. However it is important to note that not all of these particular phenolics are necessarily specific only to lignin. For example, 3,4,5-trimethoxy benzoic acid methyl ester can be formed from other biopolymers such as tannins (e.g. Mason *et al.* 2009). There was one compound identified in the TMAH thermochemolysis products of *P. commune* that was absent during the THM of all of the other moss and vascular plant samples, namely 3,4-dimethoxybenzenepropanoic acid methyl ester. This compound is therefore tentatively suggested as being a marker for *P. commune*. Four distinct phenols were found exclusively in all of the different species of *Sphagnum* mosses collected in this study. The mass spectra and relative retention times for these four potential *Sphagnum* biomarkers (Figure 1) were consistent with the following assignments: methylated 4-isopropenylphenol (m/z 133, 148), methylated *cis* and *trans* 3-(4'-hydroxyphen-1-yl)-but-2-enoic acid (m/z 175, 206), and methylated 3-(4'-hydroxyphen-1-yl)-but-3-enoic acid (m/z 133, 148, 206). These compounds were not present in the thermochemolysis products from *Polytrichum commune*. TMAH thermochemolysis of the other mosses and herbaceous plants confirmed that these components are specific to *Sphagnum*. The herbaceous plants and the *P. commune* yielded a full range of lignin-derived phenols as well as 1,3,5-trimethoxybenzene, a significant component of the vascular plant distributions which was absent from the *Sphagnum* thermochemolysis products.

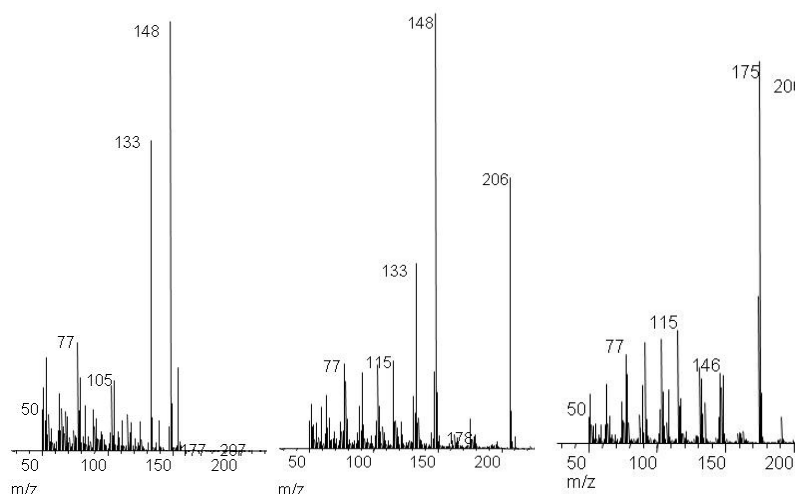


Figure 1. Mass spectra of *Sphagnum* marker 1; 4-isopropenylphenol (m/z 148) and *Sphagnum* marker 3; methylated 3-(4'-hydroxyphen-1-yl)-but-3-enoic acid (m/z 133, 148, 206), and *Sphagnum* markers 2 and 4; *cis* and *trans* 3-(4'-hydroxyphen-1-yl)-but-2-enoic acid (m/z 175, 206).

Conclusions

Lignin is a component of the peat litter and arises from the herbaceous plants present in the litterbag experiments. Biomarkers for a non-lignin source, which is suggested to be *Sphagnum*, have been identified which are the *cis* and *trans* isomers of the methyl esters of 3-(4'-hydroxyphen-1-yl)-but-2-enoic acid as well as 3-(4'-hydroxyphen-1-yl)-but-3-enoic acid methyl ester.

References

- Challinor JM (1989) A pyrolysis-derivatisation-gas chromatography technique for the structural elucidation of some synthetic polymers. *Journal of Analytical and Applied Pyrolysis* **16**, 323-333.
- Clifford DJ, Carson DM, McKinney DE, Bortiatynski JM, Hatcher PG (1995) A new rapid technique for the characterization of lignin in vascular plants: thermochemolysis with tetramethylammonium hydroxide (TMAH). *Organic Geochemistry* **23**, 169-175.
- Davidson EA, Janssens IA (2006) Temperature sensitivity of soil carbon decomposition and feedbacks to climate change. *Nature* **440**, 165-173.
- Gorham E (1991) Northern Peatlands: Role in the Carbon Cycle and Probable Responses to Climatic Warming. *Ecological Applications* **1**, 182-195.
- Hatcher PG, Nanny MA, Minard RD, Dible SD, Carson DM (1995) Comparison of two thermochemolytic methods for the analysis of lignin in decomposing gymnosperm wood: the CuO oxidation method and the method of thermochemolysis with tetramethylammonium hydroxide (TMAH). *Organic Geochemistry* **23**, 881-888.
- Kaal E, Janssen HG (2008) Extending the molecular application range of gas chromatography. *Journal of Chromatography A* **1184**, 43-60.
- Mason SL, Filley TR, Abbott GD (2009) The effect of afforestation on the soil organic carbon (SOC) of a peaty gley soil using on-line thermally assisted hydrolysis and methylation (THM) in the presence of ¹³C-labelled tetramethylammonium hydroxide (TMAH). *Journal of Analytical and Applied Pyrolysis* **85**, 417-425.
- Vane CH (2003) The molecular composition of lignin in spruce decayed by white-rot fungi (*Phanerochaete chrysosporium* and *Trametes versicolor*) using pyrolysis-GC-MS and thermochemolysis with tetramethylammonium hydroxide. *International Biodeterioration and Biodegradation* **51**, 67-75.

The Isolation and Characterization of Humic Substances and Humin from Grey Brown Podzolic and Gley Grassland Soils

Michael H.B. Hayes^A, Roger S. Swift^B, Corinna M. Byrne^A, and Andre J. Simpson^C

^AChemical and Environmental Sciences, University of Limerick, Ireland, Email Michael.H.Hayes@ul.ie; Corinna.Byrne@ul.ie

^BFaculty of Natural Resources, Agriculture and Veterinary Science, University of Queensland, Email r.swift@uq.edu.au

^CDepartment of Chemistry, University of Toronto at Scarborough, Toronto, Canada, Email andre.simpson@utoronto.ca

Abstract

Humic acids (HAs) and fulvic acids (FAs) were isolated by the exhaustive extractions at pH 7, 10.6, and 12.6 of a Grey Brown podzol and of a Gley soil, each in long term grassland. A further exhaustive extraction in base + 6 M urea isolated additional HAs and FAs of significantly different compositions. A subsequent sequential extraction with dimethylsulphoxide (DMSO) + 6 M concentrated H₂SO₄ isolated humin materials. The solvent sequence used is capable of isolating > 90% of the organic matter (OM) in some soils, and at least 70% of the OM in all soils. Solid state CPMAS ¹³C NMR spectroscopy s showed readily observable differences between the compositions of the HAs and FAs isolated at the different pH values, and by the base + urea solvent system. Humin has been considered to be the most intractable component of soil organic matter. However, applications of solid state ¹³C NMR and of liquid state proton NMR have shown that soil humin is composed largely of biological molecules of plant and of microbial origins and with a degree of resistance to biological degradation. That resistance is enhanced by the protection afforded by close associations with the soil mineral colloids.

Key Words

Humic substances, humin, extraction, fractionation, XAD resins, proton and ¹³C NMR.

Introduction

In the classical definitions soil humic substances (HS) are defined as amorphous, polymeric, brown coloured substances that are differentiated on the basis of solubility properties (Hayes and Swift 1978) into humic acids (HAs, precipitated when aqueous alkaline extracts from soil are adjusted to pH 1), fulvic acids (FAs, soluble in aqueous media at all pH values) and humins (insoluble in aqueous media). Humins are considered to be the major components of HS, and to compose 50% and more (Stevenson, 1994) of the transformed or humified components (that bear no morphological resemblances to the structures from which they were derived) of organic materials in soil organic matter (SOM). The procedure used (Swift, 1996) to isolate the Standard soil HAs and FAs of the International Humic Substances Society (IHSS) is widely used. That procedure uses XAD-8 resin to recover the FAs from the FA fraction, or the materials that remain in solution when the pH of the aqueous alkaline extract is adjusted to 1. When XAD-4 resin is placed in tandem with the XAD-8 significant amounts of hydrophilic biological molecules are recovered and these do not satisfy the definition for HS (Hayes *et al.* 2008).

On the basis of the classical definitions, any humified materials that are extracted, following exhaustive extraction in aqueous basic media, in organic solvents, or even in aqueous media containing organic solutes, might be regarded as humins. The present study involves an exhaustive extraction of the classical humic components of SOM, including the isolation of humin residues by novel procedures from a well drained Grey Brown Podzol (GBP) and of the humin materials from a poorly drained Gley soil after the HAs and FAs had been isolated during exhaustive extractions in aqueous sodium hydroxide (NaOH) solutions adjusted to different pH values. ¹³C and ¹H nuclear magnetic resonance (NMR) spectroscopy techniques were employed to show differences in the compositions of the different isolates.

Methods

Soil; extraction and analyses procedures

A well drained GBP soil (45% sand, 20% silt, and 12% clay) and a poorly drained Gley soil (25% sand, 35% silt and 25% clay; were H⁺-exchanged and exhaustively extracted in 0.1 M NaOH adjusted to pH 7, then exhaustively at pH 10.6, and at 12.6. The residual materials were exhaustively extracted in 0.1 M NaOH + 6 M urea. After the urea was washed out the residual soil was dried and exhaustively extracted with dimethylsulphoxide (DMSO) + concentrated H₂SO₄ (6% v/v). The aqueous extracts were diluted to < 50 ppm, the pH was adjusted to 2, and the solution was passed on to XAD-8 and XAD-4 resins in tandem. The HAs and FAs were recovered, as described by Hayes *et al.* (2008), from the materials sorbed on XAD-8. The DMSO/H₂SO₄ mixture was poured into water; the precipitate formed was washed with water and freeze dried

(Song *et al.* 2008).

Instrumental analysis using CPMAS ^{13}C and proton nuclear NMR spectroscopy followed the procedures outlined by Simpson *et al.* (2007) and by Song *et al.* (2008).

Results

Compositions of humic and fulvic acids from the Grey Brown Podzolic soil

Both soils used in the study are in long term grassland and are enriched in SOM (with 6.7×10^4 and 7.2×10^4 kg/ha organic C in the surface layer in the cases of the GBP and the Gley soil, respectively). The CPMAS ^{13}C NMR spectra in Figure 1 clearly show that a fractionation was obtained as the result of applications of aqueous solvents of different pH values. A comparison of the HA isolates in the aqueous media at pH 7, 10.6, and 12.6 shows that the material isolated at the highest pH value, spectrum 3, has clear indications of components of lignin origins, as demonstrated by the characteristic shape of the methoxyl resonance at 56 ppm and the distinct O-aromatic resonance (145-150 ppm). The O-aromatic resonance is distinctive also in the isolates at pH 7 and at pH 10.6, but the shapes of the 50-60 ppm resonance suggest that the structures contain peptide functionalities. There is clear evidence for carbohydrate (70-90 ppm and the anomeric C resonance, 105 ppm) in all three samples, and especially in the cases of spectra 1 and 2, and the resonance around 110 ppm may be indicative of tannins. These spectra show that the HAs contain significant hydrocarbon structures, and the resonances at ca 32 ppm can be indicative of crystalline methylene structures (e.g. those arising from interactions between long chain hydrocarbons in acid and ester functionalities).

Spectrum 4, for the HA isolate in base + urea, is distinctly different from the extracts in the purely aqueous basic media. There is evidence for lignin inputs to the structures (in the O-aromatic resonance, although the 50-60 ppm resonance does not have the characteristic shape for the methoxyl of lignin). The aromaticity resonance is distinct, but it is clear that aromaticity functionality is significantly less in spectrum 4 than in spectra 1, 2, and 3. The contributions of carbohydrate structures to the compositions are significant (70-90, and the 100-105 ppm resonances), and the contours of the 50-60 ppm resonance would suggest the presence of peptide structures. The most distinctive feature of spectrum 4 is, however, the major contribution of hydrocarbon-type structures (10-40 ppm) to the composition. The components in spectrum 4 more closely represent humin structures than those of HAs (*vide infra*).

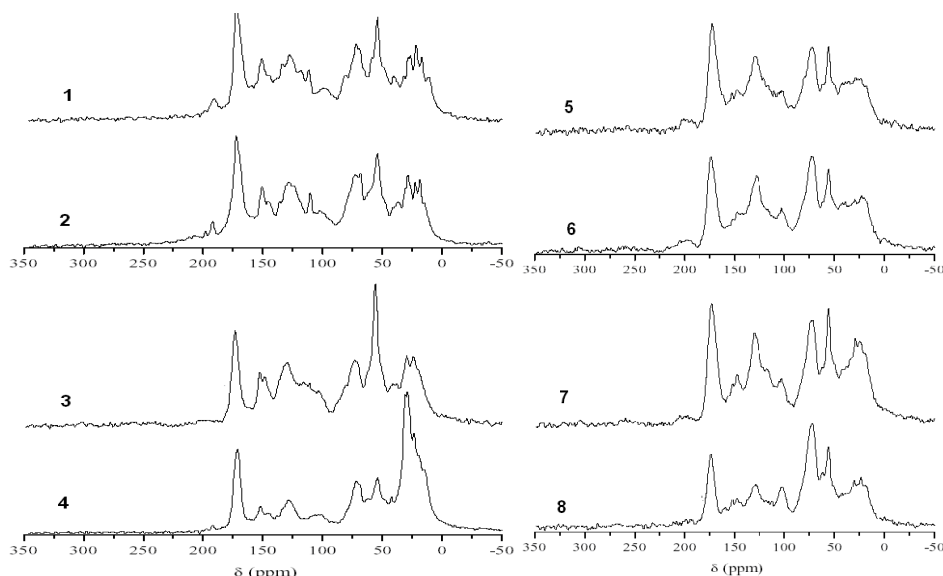


Figure 1. CPMAS ^{13}C NMR spectra of humic (HA) and fulvic (FA) acids isolated from the Grey Brown podzolic soil: 1, HAs isolated at pH 7; 2, HAs isolated at pH 10.6; 3, HAs isolated at pH 12.6; 4, HAs isolated in 0.1 M NaOH + 6 M urea; 5, FAs isolated at pH 7; 6, FAs isolated at pH 10.6; 7, FAs isolated at pH 12.6; 8, FAs isolated in 0.1 M NaOH + 6 M urea.

Spectra 5 to 8 for the FAs also show compositional differences between the isolates at the different pH values and media. Spectra 5 and 6 are relatively similar (as is evident also for the corresponding HAs, spectra 1 and 2), and these spectra provide only weak evidence for residual lignin structures. There is, however, strong evidence for carbohydrate functionality. The resonances at 50-60 ppm are likely to have significant contributions from peptide structures (Hayes *et al.* 2008).

The evidence for contributions from lignin and for carbohydrate is strong in the case of the FA isolate at pH

12.6 (spectrum 7), and the contribution from hydrocarbon structures (which can include lipids, cutin, cutan structures, etc) is greatest for this FA isolate. Again, as was observed for the HAs, the compositions of the FAs in the base + urea isolate are different from those in the aqueous base isolates. Aromaticity is very low in spectrum 8 (compared with that in spectra 5-7), and aliphatic hydrocarbon functionality is also least. There is evidence for material with origins in lignin, and enrichment in carbohydrate is significant.

The significant enrichments of carbohydrate components in all of the FAs is surprising. Polar carbohydrate materials would not be expected to sorb to XAD-8 but to wash through and be retained by the XAD-4 in the resin sequence (Swift 1996; Hayes *et al.* 2008). The abundance of carbohydrate in all of the FAs would suggest that that the carbohydrate components were strongly associated with (perhaps even covalently linked to) the less polar components of the FAs that sorb to XAD-8.

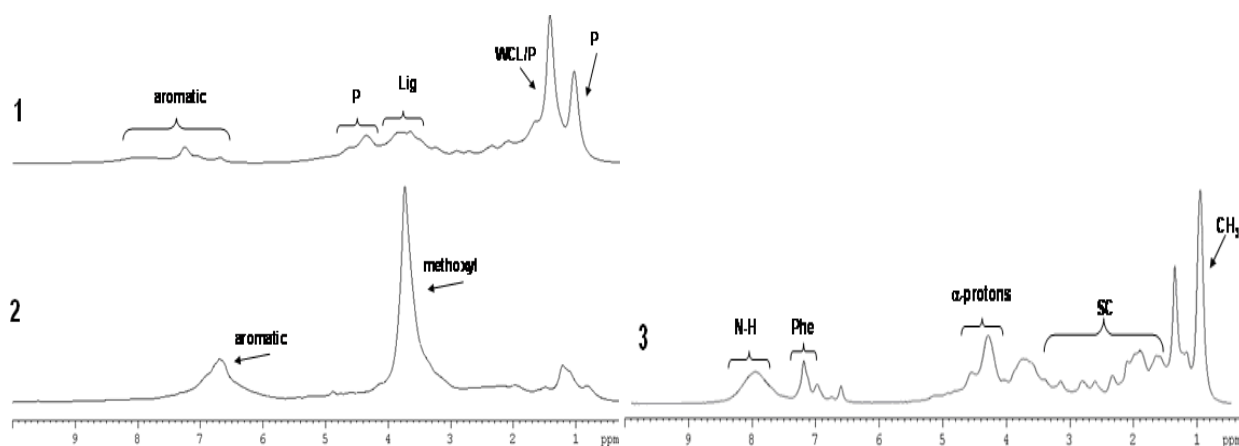


Figure 2. Diffusion edited ^1H NMR spectra in $\text{DMSO}-d_6$ for: 1, humin from the poorly drained Gley soil; 2, Organosolv Lignin; and 3, Cultured soil microbes (Simpson *et al.* 2007). P = protein/peptide; Lig = lignin-derived functionality; W = waxes; L = lipid; Phe = phenylalanine.

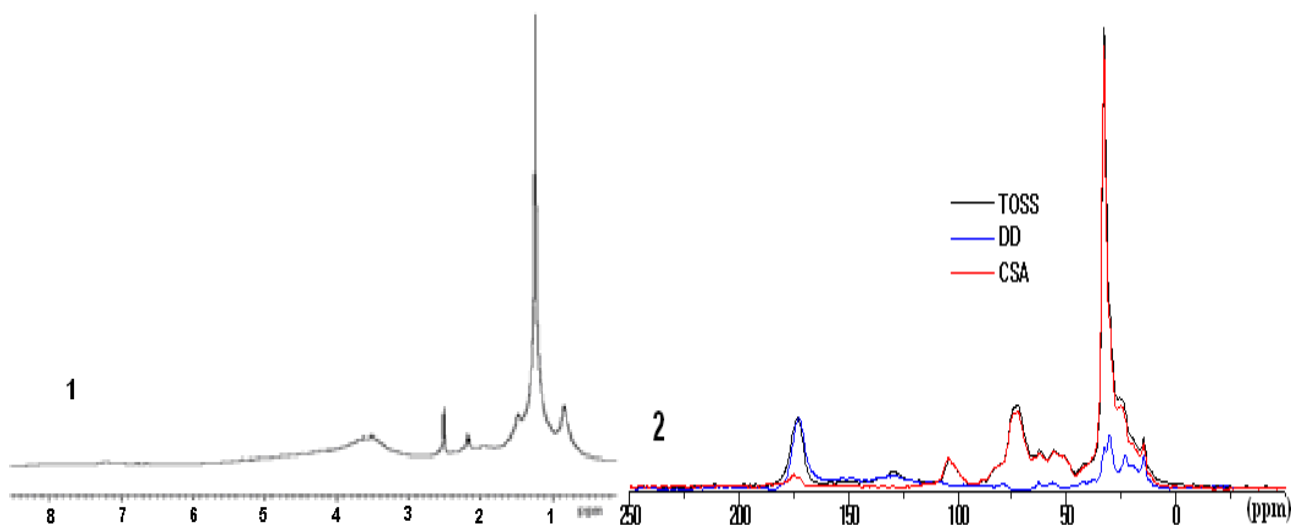


Figure 3. ^1H NMR spectrum in $\text{DMSO}-d_6$ (1) for humin from the Grey Brown Podzolic soil; and the TOSS, Dipolar Dephasing (DD) and Chemical Shift Anisotropy (CSA) ^{13}C NMR solid state spectra (2) for the humin, isolated from the same soil.

Compositions of humin materials

Figure 2(1) shows the diffusion edited proton NMR spectrum for the humin material isolated from the Gley soil. Figures 2(2) and 2(3) are markers for functionalities in organosolv lignin and identified in microbes isolated from soil (Simpson *et al.* 2007), respectively. The major contributors to the structures are aliphatic components composed mainly of lipids, waxes, and various hydrocarbon-type structures. There is evidence also for protein/peptide materials, and there is some evidence for structures with origins in lignin material. Spectrum 3(1), the proton NMR spectrum for the humin isolated from the GBP, is dominated by aliphatic hydrocarbon type structures. It has some of the features of spectrum 2(1), but with less evidence for aromaticity. The solid state spectrum, Figure 2(2), indicates a lack of significant aromaticity, but shows significant carbohydrate, and the resonance at 50-60 ppm can be regarded as protein/peptide functionality. It is clear from

the resonance in the 20-35 ppm region that aliphatic hydrocarbon type structures dominate the composition.

Discussion and Conclusions

It is clear, as was also shown by Hayes *et al.* (2008), that a fractionation of HS is achieved when exhaustive extractions are carried out at increasing pH values. Hayes (2006) has discussed how urea in aqueous base can enhance the isolation of soil humic components, and suggested mechanisms involving the breaking of hydrogen bonds binding the HS to the humin matrix, or allowing conformational changes enabling the liberation of the molecules. Although Song *et al.* (2008) found that HAs and FAs isolated from a Mollisol soil using the urea extraction method were similar to the fractions isolated at pH 12.6 in the sequential extraction, the isolates from the urea-base system in the present study resemble more strongly the humin components in the DMSO/H₂SO₄ than those in the pH 12.6 isolates.

Based on the observation that the DMSO/H₂SO₄ was able to remove substantial amounts of organic matter following exhaustive extractions of HS, Hayes (2006) recognised the potential of the DMSO/H₂SO₄ system for the isolation of humin components. Subsequently Simpson *et al.* (2007) and Song *et al.* (2008) have effectively employed this solvent system for the isolation and studies of the compositions of soil humin materials.

Humin is the major component of SOM, and its composition has baffled soil scientists in the past. The application of modern NMR spectroscopy equipment has indicated that humin is a mixture of materials of plant and of microbial origins, and the structures of the component molecules are likely to be well known. The most abundant components have significant aliphatic hydrocarbon functionalities with major contributions from components, such as waxes, lipids, long chain fatty acids and esters, cutins, cutans, suberins, with significant amounts of carbohydrate and peptide materials and with traces of lignin-derived substances and. Under normal circumstances the carbohydrates and peptides would be readily enzymatically degraded, and their presence as components of the relatively resistant humin fraction is surprising. However, the presence of these, and of lignin-derived components that are major constituents of HAs and of FAs, can be attributed to their associations with and steric protection by the largely non-polar components with a high degree of resistance to microbial degradation. Because these non-polar components have high affinities for the inorganic soil components, and especially for the clays, the protection effect is enhanced and access of enzymes to hydrolysable sites is inhibited. Thus humin should no longer be regarded as the 'mystery component' of SOM, and based on the evidence we now have it is clear that humin does not satisfy the classical definitions for humic substances. It should now be regarded as a mixture of largely identifiable biological molecules derived from plant materials composed predominantly of resistant non-polar moieties in intimate associations with, and protecting some biodegradable biomolecules, all in intimate associations with the soil mineral colloids. On the basis of this evidence it is now appropriate to reconsider the inclusion of humin in the classical definitions of soil humic substances.

References

- Hayes MHB (2006) Solvent systems for the isolation of organic components from soils. *Soil Science Society of America Journal* **70**, 986-994.
- Hayes MHB, Swift RS (1978) The chemistry of soil organic colloids. In 'The Chemistry of Soil Constituents'. (Eds DJ Greenland, MHB Hayes) pp. 179-320. (Wiley: Chichester, England)
- Hayes TM, Hayes MHB, Skjemstad JO, Swift RS (2008). Studies of compositional relationships between organic matter in a grassland soil and its drainage waters. *European Journal of Soil Science* **59**, 603-616.
- Simpson AJ, Song G, Smith E, Lam B, Novotny EH, Hayes MHB (2007) Unraveling the structural components of soil humin using solution state nuclear magnetic resonance spectroscopy. *Environmental Science and Technology* **41**, 876-883.
- Song G, Novotny EH, Simpson AJ, Clapp CE, Hayes MHB (2008) Sequential exhaustive extractions, and characterisations using solid and solution state NMR, of the humic, including humin, components in a Mollisol soil. *European Journal of Soil Science* **59**, 505-516.
- Stevenson FJ (1994) Humus Chemistry: Genesis, Composition, Reactions. 2nd ed (Wiley: New York).
- Swift RS (1996) Organic matter characterization. In 'Methods of Soil Analysis Part 3', SSSA Book Series 5 (Ed DL Sparks) pp. 1011-1069. (SSSA Madison, Wisconsin)

The mobility and persistence of the insecticidal Cry1Aa toxin, Bt (*Bacillus thuringiensis*) in soils

Nordine Helassa^A, Sylvie Noinville^B, Philippe Déjardin^C, Hervé Quiquampoix^A, Siobhán Staunton^A

^AUMR 1222 Eco&Sols, INRA, place Viala, 34060 Montpellier, France Email staunton@montpellier.inra.fr

^BUMR 7075 - LADIR, CNRS, 2 rue Henri Dunant, 94320 Thiais, France

^CUMR 5635 IEM, CNRS, 2 Place Eugène Bataillon, 34095 Montpellier, France

Abstract

The rapid worldwide expansion of genetically modified crops containing the Bt trait gives rise for concern as to the possible impact on non target species. These plants release insecticidal proteins, known as cry into soil during growth and decomposition of crop residues. The fate of the toxin is strongly influenced by its interactions with soil, in particular adsorption which modifies its biological properties, its mobility and its persistence. We describe three series of studies to investigate (i) the adsorption properties (ii) the mobility of the adsorbed protein and (iii) the decline of toxin in soil as a function of time and microbial activity. We conclude that the toxin will be strongly immobilised in soil and that microbial degradation does not determine the observed decline of toxin over periods of weeks and months.

Key Words

Adsorption, protein, genetically modified plants, microbial activity, soil sterilisation

Introduction

Soil dwelling bacteria, *Bacillus thuringiensis* (Bt), synthesize crystalline proteins (Cry) during sporulation that after ingestion by larvae are solubilised and truncated to produce highly target specific, insecticidal proteins. Target specificity results both from the chemical conditions in the insect mid-gut and the presence of receptors in cell membranes allowing pore formation and rapid insect death. Genes for some of these Cry proteins have been inserted into various plants, and since 1996 such genetically modified (GM) plants have been commercialised. These Bt crops often give better yields and improved crop quality in comparison with non Bt crops. There is considerable public concern about the wide-spread cultivation of these crops. Given the very rapid increase in the area of agricultural land world wide used to grow these crops, understanding of potential negative side effects are necessarily limited. Although the bacteria exist spontaneously in soil and various preparations of spores and crystals are widely used for pest control, including in organic farming, there are important differences between bacterially produced toxin and that of GM crops. Firstly, GM plants synthesise directly the toxin, thus bypassing two of the steps that confer target specificity (solubilisation in the alkaline pH of insect mid-gut and enzymatic activation of the protein). Secondly, GM plants synthesize the protein throughout the plant and continuously during plant growth, whereas the activity of commercial preparations of spores and crystals is rapidly lost.

There has been considerable research on the possible impact of Bt crops on non target organisms. To date there has been no strong evidence of direct negative effects. An important factor in determining the exposition of non target organisms to Bt toxin is the interaction of the proteins with soils, and the resulting mobility and persistence of the toxin in the soil environment.

We have investigated the adsorption, the mobility and the persistence of one Cry protein, Cry1Aa, in contact with various soils and soil minerals.

Materials and Methods

The protein was produced by culture of a genetically modified strain of the bacterium (*B. thuringiensis* subsp. *kurstaki* HD-1 provided by CIRAD, Montpellier) cultivated in a fermentor, then purified and activated as previously described (Vié *et al.* 2001). Concentrated solutions of protein were maintained at high salt concentration and high pH to avoid polymerisation. The monomeric state of the protein was verified using dynamic light scattering (Zetasizer HS3000).

Reference clay minerals, montmorillonite and kaolinite, were size fractionated (<2 µm) by sedimentation, made homoionic with sodium and washed until salt free. Mica was freshly cleaved. Glass was acid-washed and, when required, made hydrophobic by silanisation. Four soils with contrasting texture and organic matter content were

selected for incubation experiments. When necessary the protein was labelled with a fluorescent probe (fluorescein isothiocyanate, FITC). Adsorption isotherms as a function of pH were measured in clay suspension with protein analysis by uv-spectroscopy (Helassa *et al.* 2009). Mobility of FITC-labelled protein adsorbed on montmorillonite was measured using FRAP (Fluorescence Recovery After Photobleaching) which has not hitherto been reported for proteins adsorbed on mineral surfaces. Soils were incubated with trace amounts of Cry1Aa under controlled conditions of temperature and moisture content. Various chemical and physical treatments varied the microbiological activity. Soils were sterilised by γ -irradiation, by autoclaving and by addition of HgCl₂, or maintained at 4°C to inhibit microbial activity. Microbial activity was enhanced by addition of trigger solutions of amino acids and/or glucose. Toxin was extracted and analysed using an ELISA test.

Results and Discussion

Adsorption of Cry1Aa on montmorillonite and kaolinite was found to be low affinity and data could be fitted to Langmuir isotherms, as since in Figure 1. Adsorption was measured as a function of pH, but the lowest pH that could be investigated was 6.5, roughly the isoelectric point, since protein oligomerized at acid pH. For both minerals the maximum of adsorption decreased markedly as pH was increased above the isoelectric point. Adsorption was about 40 times greater on montmorillonite than on kaolinite, in line with the difference in their specific surface area. Adsorption capacity with respect to surface area on both minerals followed the same trend as a function of pH, which is surprising given the strong pH dependence of surface charge on kaolinite (Helassa *et al.* 2009). Desorption in water or alkaline buffer was small, thus adsorption was largely irreversible, despite the low affinity isotherms. Desorption was very efficient when non-ionic or zwitterionic detergents were added which is important since current detection techniques of the protein require that it be in solution (Helassa *et al.* 2009).

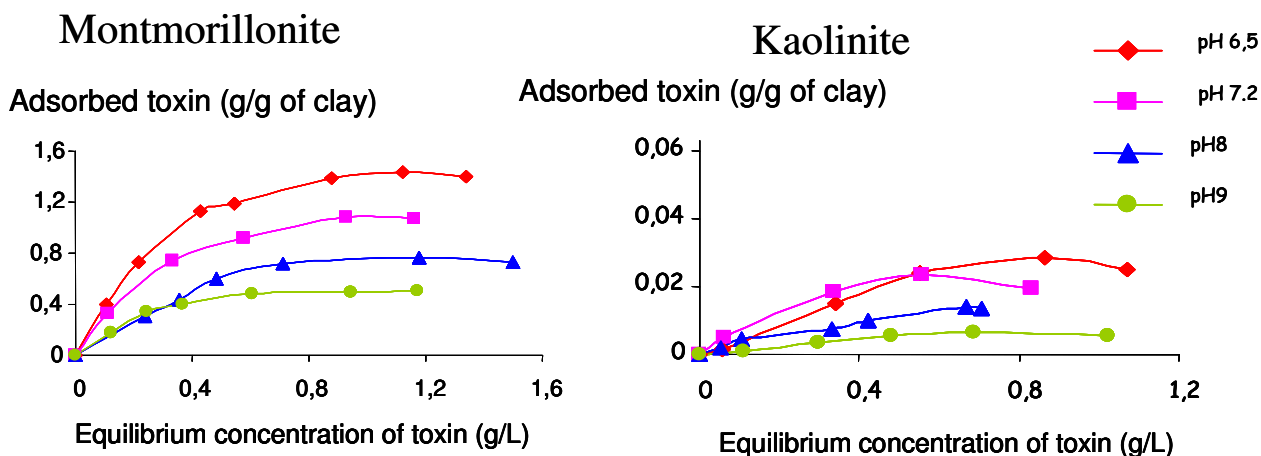


Figure 1. Adsorption isotherms of monomeric Cry1Aa on montmorillonite and kaolinite as a function of pH. The amount of protein adsorbed was calculated by depletion from the initial solutions and proteins quantitatively measured by uv-visible spectroscopy at 280 nm.

It is often assumed that proteins are immobilised by adsorption, however there is little experimental proof of this. The mobility of an adsorbed fluorescent molecule can be deduced by the rate at which fluorescence is recovered after photobleaching. This technique, FRAP, has never previously been applied to environmentally relevant mineral surfaces and proteins. FITC-labelled protein was adsorbed onto montmorillonite in suspension, centrifuged and washed with water to remove excess protein in solution, centrifuged and the pellet smeared onto a glass microscope slide. Protein concentration in remaining solution was negligible. Fluorescence intensity was scanned with a confocal scanning laser microscope and a disc of 12 μ m diameter photobleached with an argon laser and the bleached zone scanned for at least 30 minutes. Figure 2a shows a typical image of the bleached zone, and Figure 2b the repeated scans across a section of the bleached zone. There is some variation in the base line of fluorescence intensity, due to small variations in the intensity of the excitation beam. However the shape of the intensity curve did not vary, and this is considered to be a better indicator of the absence of lateral diffusion. We found no evidence of mobility of the adsorbed protein at any pH value between 6.5 and 9 and no mobility at two levels of protein loading on the clay mineral surface. We thus conclude that the protein is unlikely to diffuse far from its point of introduction in the soil and while this limits dispersion, it could lead to the build-up of hot spots.

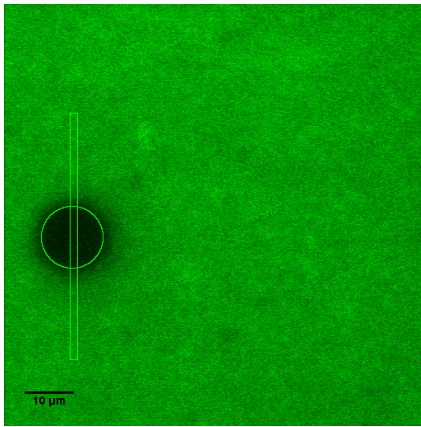


Figure 2a. Typical fluorescence image after photobleaching of a uniform disc of 12 μm of FITC-labelled Cry1Aa adsorbed on montmorillonite.

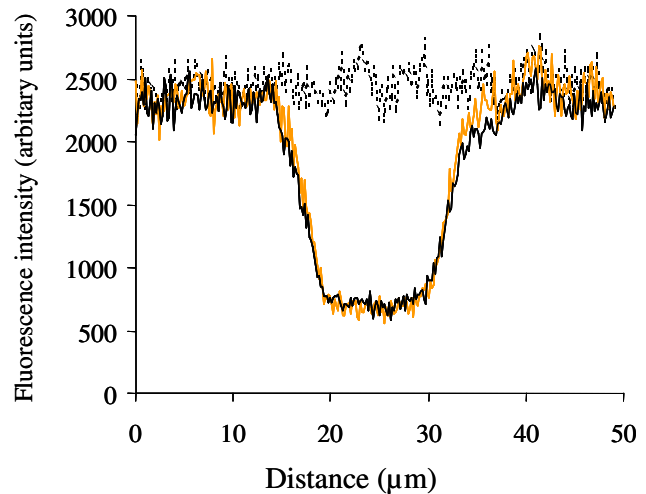


Figure 2b. Fluorescence intensity profiles of FITC-labelled Cry1Aa adsorbed on montmorillonite before (top, flat curve), immediately after and 500 sec after photobleaching.

It is often stated that adsorption of proteins on soil mineral surfaces protects them against microbial breakdown and thus prolongs their persistence in soil. We monitored the detection of Cry1Aa incubated in four contrasting soils and varied the level of microbial activity by sterilising or boosting activity. Two of the soils had clayey texture but differed in their organic matter content, whereas the other two were sandy textured with contrasting organic matter content. After different incubation periods, soils were destructively sampled, the protein extracted in an alkaline solution containing surfactant and another protein (bovine serum albumin). This extractant was found to give similar, high extraction yields for all the soils. The protein extracted was quantified using an Elisa test.

Figure 3 shows the trends in proteins extracted and detected for each of the four soils. There are only small differences in the persistence of the toxin in the contrasting soils. The clayey texture does not appear to provide additional protection against degradation, nor enhance irreversible fixation.

If the decline of detectable Bt toxin with time was due to microbial breakdown, then enhancement of microbial activity would increase the rate of decline and conversely sterilisation or inhibition of microbial activity would maintain a higher level of detectable protein. Figure 4 shows the absence of any effect of sterilisation by either γ -irradiation or autoclaving for one soil. Similar results were obtained for all soils. Concurring results were obtained when microbial activity was boosted with amino acids and/or glucose and when activity was inhibited by HgCl_2 . In marked contrast, at 4°C, when hydrophobic interactions may be favoured, adsorption was smaller and the rate of decline over a 3-week period much slower. We conclude that the decline in extractable, detectable toxin was not determined by microbial activity. However we have not yet been able to distinguish between two possible reasons: firstly that protein becomes more irreversibly bound to soil surfaces with time thus decreasing extractability; secondly that changes in secondary structure of the protein that were maintained after extraction made the protein less well recognised by the Elisa test.

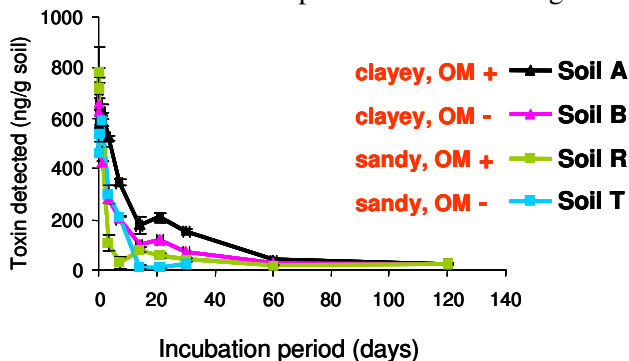


Figure 3. Cry1Aa extracted and detected as a function of incubation period with each soil.

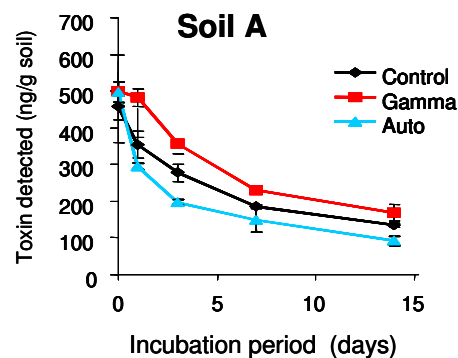


Figure 4. Cry1Aa extracted from Soil A (clayey top soil) and detected as a function of incubation time and sterilisation.

Acknowledgements

This work was financed by the French Agence Nationale de la Recherche (ANR) and the doctoral programmes of the Région Languedoc-Roussillon and the INRA.

References

- Helassa N, Quiquampoix H, Noinville S, Szponarski W, Staunton S (2009) Adsorption and desorption of monomeric Bt (*Bacillus thuringiensis*) Cry1Aa toxin on montmorillonite and kaolinite. *Soil Biology & Biochemistry* **41**, 498-504.
- Icoz I, Stotzky G (2008) Fate and effects of insect-resistant Bt crops in soil ecosystems. *Soil Biology and Biochemistry* **40**, 559-586.
- James C (2007) Global Status of Commercialized Biotech/GM Crops: 2007. (ISAAA) Brief No 37, Ithaca, NY.
- Vié V, Van Mau N, Pomarède P, Dance C, Schwartz JL, Laprade R, Frutos R, Rang C, Masson L, Heitz F, Le Grimellec C (2001) Lipid-induced pore formation of the *Bacillus thuringiensis* Cry1Aa insecticidal toxin. *Journal of Membrane Biology* **180**, 195-203.

Topography and surface properties of clay minerals analyzed by atomic force microscopy

Felix Macht^A, Kai Uwe Totsche^A, Karin Eusterhues^A and Geertje Pronk^B

^ALehrstuhl für Hydrogeologie, Institut für Geowissenschaften, Friedrich-Schiller-Universität Jena, Germany,
Email felix.macht@uni-jena.de

^BLehrstuhl für Bodenkunde, Technische Universität München, Germany.

Abstract

The specific surface area (SSA) of natural particles is an important parameter to quantify surface processes such as dissolution and adsorption. In this study, the SSA of illite and montmorillonite particles was determined by N₂ gas adsorption (BET), the EGME method and atomic force microscopy (AFM). By AFM it was possible to analyze additionally the specific basal surface area (BSA) and the specific edge surface area (ESA). For the calculation of the surface area from the AFM data we used three different approaches, which yielded similar values. Furthermore, there was a strong correlation between the specific surface area and the particles' height. For illite BET estimated a SSA of 46 m²/g, while 54 AFM images resulted in a mean SSA of 64 m²/g. For montmorillonite we found a SSA of 79 m²/g by BET and of 246 m²/g by AFM (n=42). We assume that the commonly used preparation method for AFM samples causes delamination of clay minerals, leading to particles with a thickness of only 4 to 10 unit layers.

Key Words

Montmorillonite, illite, specific surface area, specific edge surface area, AFM

Introduction

The specific surface area is an essential parameter to quantify processes at the solid/liquid interface. The gas adsorption method BET (Brunauer *et al.* 1938) is a routine method for specific surface area determination, which uses non-polar gases such as N₂ or Ar to determine the outer surface of solid materials. Unfortunately, the BET method fails to determine the complete surface area of materials featuring outer as well as inner surfaces, e.g., sheet silicates. A more successful alternative is the adsorption method introduced by Carter *et al.* (1965) using liquid ethylene glycol monomethyl ether (EGME) that penetrates into the interlayer space due to its polarity. Both the BET and the EGME method determine bulk values and do not allow quantifying distinct crystal faces. The latter is especially desirable for clay minerals, which are extremely anisotropic: Their basal (001) plane is covered by saturated surface groups, which are chemically less reactive than those on edge surfaces, which are built up of surface groups with broken bonds. Atomic force microscopy (AFM) allows creating three-dimensional height images of single clay particles and determining the edge surface and basal surface area separately. As single particles are measured, the result is not a bulk value, but a distribution of measured surface areas, which reveals information about the heterogeneity of the sample.

In some publications, the specific surface area (SSA), the specific basal surface area (BSA), and the specific edge surface area (ESA) were determined with AFM, and these data were in good agreement with BET-determined SSA data (Bickmore *et al.* 2002, Tournassat *et al.* 2003, Jodin *et al.* 2004, Metz *et al.* 2004, Hassan *et al.* 2006). However, since Metz *et al.* (2004) estimated completely different SSA values with BET and AFM (BET: 34 +/- 2 m²/g versus AFM external SSA: 136 +/- 20 m²/g), it is questionable, as to whether BET and AFM really determine the identical surface area. Metz *et al.* (2004) suggested that the common AFM preparation, using highly diluted suspensions (few tens of mg sample per litre) to separate the individual clay particles, leads to the delamination of the clay minerals.

Here, we present data for the specific surface area (SSA), the specific basal surface area (BSA) and the specific edge surface area (ESA) as determined by AFM for montmorillonite and illite particles. Then, we compare the AFM-SSA with SSA measurements from N₂-BET and EGME and discuss the observed differences.

Methods

Atomic force microscopy

AFM: A suspension of 0.05 g clay mineral per litre 10 M NaOH was dispersed for 2 min in an ultrasonic bath. Three droplets of this suspension were placed on a freshly cleaved mica surface and dried over night. Images were taken with a Picoforce MultiMode AFM (Veeco Instruments, USA) in contact mode under ambient conditions. Three different approaches were used to calculate the specific surface area (SSA), the specific edge

surface area (ESA) and the specific basal surface area (BSA) from AFM-height images:

1) We used the average height h , the base area a , the perimeter at the base area of the particle p and the volume V . With the known density ρ , we calculated the BSA, ESA, and SSA according to the following equations:

$$BSA_1 = 2 \cdot a / (\rho \cdot V)$$

$$ESA_1 = h \cdot p / (\rho \cdot V)$$

$$SSA_1 = BSA_1 + ESA_1$$

2) We applied the method by Bickmore *et al.* (2002). To get a more precise ESA, the particles were cut on every morphological terrace into horizontal slices. Then, the particle's ESA was determined by summing up the ESAs of the single slices:

$$BSA_2 = 2 \cdot a / (\rho \cdot V)$$

$$ESA_2 = \sum h_i \cdot p_i / (\rho \cdot V)$$

$$SSA_2 = BSA_2 + ESA_2,$$

where h_i is the height of one sheet, and p_i the perimeter of a single slice.

3) Each clay mineral is built up of a certain number of unit layers (UL). The specific surface area of one UL of a montmorillonite was determined by XRD to be $754 \text{ m}^2/\text{g}$. (McEwan 1961). We also used this value for illite, because the structures of these two minerals are very similar. With the known length of the unit cell's a-axis a_{UC} and b-axis b_{UC} (McEwan 1961) and a UL's height h_{UL} of 1 nm the SSA, BSA and ESA can be calculated:

$$BSA_3 = BSA_{UL} \cdot h_{UL} / h_{particle}$$

$$ESA_3 = ESA_{UL} \cdot p / (a_{UC} \cdot b_{UC})$$

$$SSA_3 = BSA_3 + ESA_3,$$

where BSA_{UL} is the basal surface area of one UL ($754 \text{ m}^2/\text{g}$) and ESA_{UL} the ESA of one UL.

N₂-BET

N_2 adsorption (BET) was performed with an Autosorb1 instrument (Quantachrome, Odelzhausen, Germany). The SSA was calculated according to the BET equation from 11 measurements recorded for each mineral in the relative pressure range of 0.05 to 0.3. Prior to the measurements, the samples were outgassed for at least 24 h at 313 K in a He flow to remove adsorbed water from the surfaces.

EGME method

Two replicate samples of 1 g were dried at room temperature and in vacuum using a dessicator supplied with P_2O_5 until the weight remained constant. Then, the samples were wetted with 1.5 mL ethylene glycol monomethyl ether (EGME). The excess liquid was removed by evacuating the dessicator supplied with anhydrous $CaCl_2$ until the decrease in weight was less than 1 mg/d for 3 days. The SSA was calculated using the mass of the retained EGME and assuming that a monomolecular layer of the liquid remained on the surface. The molecular coverage of $52 \times 10^{-16} \text{ cm}^2/\text{molecule}$ was adopted from Carter *et al.* (1965).

Results and discussion

Approximately 100 illite ($n=54$) and montmorillonite ($n=42$) samples have been imaged by AFM, and their SSA, BSA and ESA was estimated using the 3 presented approaches. This resulted in similar weighted mean SSA, BSA, and ESA values (Figure 1). For illite, we obtained a weighted mean SSA of $64 \text{ m}^2/\text{g}$, and for montmorillonite of $246 \text{ m}^2/\text{g}$. The weighted mean ESA was $4 \text{ m}^2/\text{g}$ for illite, and $7 \text{ m}^2/\text{g}$ for montmorillonite, resulting in an ESA-to-BSA ratio of 0.06 for illite and 0.04 for montmorillonite. A strong correlation between the particle's height and SSA, but weak correlations between the basal area and SSA as well as between the volume and SSA suggest that the SSA of these particles was mainly determined by their thickness (Figure 2). The EGME method yielded a SSA of $112 \text{ m}^2/\text{g}$ for illite and $450 \text{ m}^2/\text{g}$ for montmorillonite, while N_2 -BET measurements estimated a SSA of $46 \text{ m}^2/\text{g}$ for illite and $72 \text{ m}^2/\text{g}$ for montmorillonite. The SSA determined by the EGME method was nearly twice as high as that determined by AFM, because the EGME method includes the interlayer surface in contrast to AFM. That AFM determined for 30% of the measured montmorillonite and 10% of the illite particles a SSA higher than the EGME-SSA, can be explained due to the fact, that the EGME method estimates bulk values, whereas AFM determines distributions of measured surface areas. We assume that the observed discrepancies between BET and AFM can be due to (i) the BET preparation, namely the outgassing temperature, (ii), the destruction of the original clay particles during AFM preparation or (iii) a non-representative selection of analyzed particles by AFM.

To investigate as to whether the outgassing temperature prior to the BET measurement was responsible for the difference in AFM and BET results, we increased the outgassing temperature from $40 \text{ }^\circ\text{C}$ to $250 \text{ }^\circ\text{C}$. For

montmorillonite, the SSA increased with an increasing outgassing temperature from 70 to 77 m²/g, while a decreasing surface area from 40 to 34 m²/g was observed for illite (Table 1). We conclude that the BET SSA varied with the outgassing temperature, but this variation was not large enough to explain the discrepancy between the BET SSA and the AFM SSA.

To investigate as to whether the AFM preparation caused a delamination of the clay particles, we considered the theoretical thickness of illite and montmorillonite particles based on the measured BET and AFM surface areas. For example, to reach the measured BET SSA of 46 m²/g, an illite particle must consist of 21 ULs, while it consists of only half as much (9 ULs) to obtain a SSA of 64 m²/g as determined by AFM. Assuming an UL height of 1 nm this value fits well with the measured particle height of 10 nm. This suggests that the illite particles must have split into halves during the AFM preparation to explain the observed difference in SSA. Likewise, montmorillonites of 9 ULs (BET SSA of 79 m²/g) would have to delaminate to particles with only 4ULs to explain the AFM-SSA (246 m²/g). We therefore conclude that the AFM preparation or a non-representative selection of analyzed particles by AFM is responsible for the observed discrepancies between SSA values determined by AFM and BET.

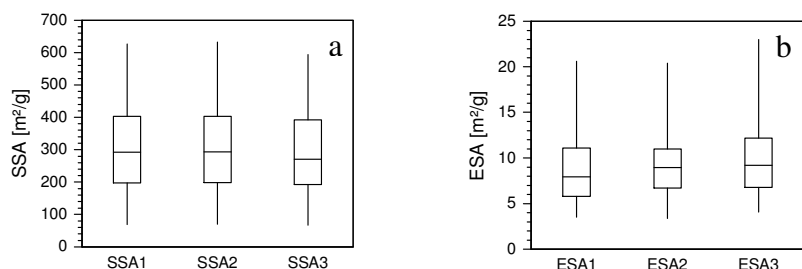


Figure 1. Boxplots of the specific surface area (SSA) a) and the specific edge surface area (ESA) b), comparing the results of the three different approaches used to calculate these values from the AFM images. Data are shown exemplary for the montmorillonite sample (n=42).

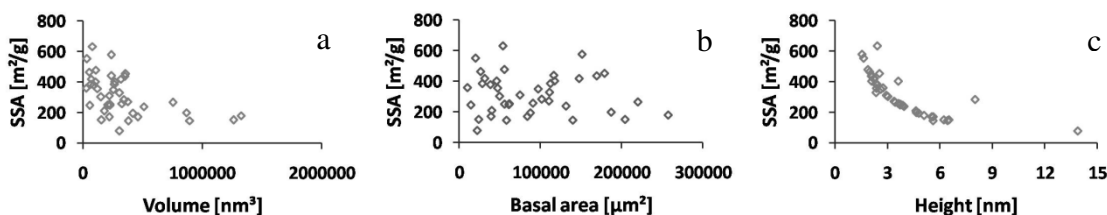


Figure 2. Correlations between the specific surface area (SSA) and the particle volume a), the basal plane b) and the particle height c). Data are shown exemplary for the montmorillonite sample (n=42).

Table 1. Specific surface area values determined by BET using different outgassing temperatures.

Temperature	Illite	Montmorillonite
40 °C	40	70
110 °C	35	73
180 °C	35	76
250 °C	34	77

Conclusion

The specific surface area, the specific basal surface area and the specific edge surface area of two clay mineral samples was determined with AFM. Three different approaches to extract the surface area from the AFM images estimated similar weighted means. It was shown that measuring only the particle height may have led to a reliable SSA calculation for clay minerals. Most AFM values were clearly lower than the EGME values but larger than the N₂-BET values. We explain the first by the fact that EGME values included the interlayer space, but AFM did not. An explanation for the latter may be (i) the different sample preparation, i.e., particle delamination during the AFM preparation or (ii) a non-representative selection of particles for AFM analysis. Currently we are testing both hypotheses: The first by performing particle size analyses (dynamic light scattering) on differently diluted suspensions and the second by taking more AFM images.

References

- Bickmore BR, Bosbach D, Hochella MF Jr., Charlet L, Rufe, E (2001) In situ atomic force microscopy study of hectorite and nontronite dissolution: Implications for phyllosilicate edge surface structures and dissolution mechanisms. *American Mineralogist* **86**, 411-423.
- Bickmore BR, Nagy KL, Sandlin PE, Crater TS (2002) Quantifying surface areas of clays by atomic force microscopy. *American Mineralogist* **87**, 780-783.
- Bosbach D, Charlet L, Bickmore B, Hochella MF Jr (2000) The dissolution of hectorite: In situ, real-time observations using atomic force microscopy. *American Mineralogist* **85**, 1209-2000.
- Brunauer S., Emmett PH, Teller E (1938) Adsorption of gases in multimolecular layers *Journal of American Chemical Society* **60**, 309-319.
- Carter DL, Heilman MD, Gonzalez CL (1965) Ethylene glycol monoethyl ether for determining surface area of silicate minerals, *Soil Science* **100**, 356–360.
- Hassan MS, Villerias F, Gaboriaud F, Razafitianamaharavo A (2006) AFM and low- pressure argon adsorption analysis of geometrical properties of phyllosilicates. *Journal of Colloid and Interface Science* **296**, 614-623.
- Jodin MC, Gaboriaud F, Humbert B (2004) Repercussions of size heterogeneity on the measurement of specific surface areas of colloidal minerals: Combination of macroscopic and microscopic analysis *American Mineralogist* **89**, 1456 – 1462.
- Metz V, Raanan H, Pieper H, Bosbach D, Ganor J (2005) Towards the establishment of a reliable proxy for the reactive surface area of smectite. *Geochemica et Cosmochemica Acta* **69**, No. 10, 2581-2591.
- Nagy KL, Cygan, RT, Hanchar JM, Sturchio NC (1999) Gibbsite growth kinetics on gibbsite, kaolinite, and muscovite substrates: atomic force microscopy evidence for epitaxy and an assessment of reactive surface area. *Geochemica et Cosmochemica Acta* **63**, No. 16, 23337-2351.
- Sutheimer, S. H., Maurice, P. A., Zhou, Q (1999) Dissolution of well and poorly crystallized kaolinites: Al speciation and effects of surface characteristics *American Mineralogist* **84**, 620 – 628.
- Tournassat C, Neaman A, Villiras F, Bosbach D, Charlet L (2003) Nanomorphology of montmorillonite particles: Estimation of the clay edge sorption site density by low- pressure gas adsorption and AFM observation. *American Mineralogist* **88**, 1989- 1995.
- Yoshihiro K (2006) In-situ AFM study of smectite dissolution under alkaline conditions at room temperature. *American Mineralogist* **91**, 1142-1149.

Tracing impact of pedogenic processes on soil solutions with Si and Mg isotopes

Sophie Opfergelt^{A,B}, R. Bastian Georg^A, Kevin W. Burton^A, Rannveig Guicharnaud^C, Sigurdur R. Gislason^D, Alex N. Halliday^A

^ADepartment of Earth Sciences, University of Oxford, Oxford, United Kingdom (Email sophie.opfergelt@earth.ox.ac.uk)

^BSoil Science Unit, Université catholique de Louvain, Louvain-la-Neuve, Belgium (Email sophie.opfergelt@uclouvain.be)

^CAgricultural University of Iceland, Reykjavik, Iceland

^DInstitute of Earth Sciences, University of Iceland, Reykjavik, Iceland

Abstract

During weathering, stable isotopes of Si and Mg are fractionated in soils, directly impacting soil solutions and river signatures. In a monolithological catchment, isotopic variations in rivers would rather be related to pedogenic processes such as mineral dissolution, sequestration in secondary minerals via neoformation or adsorption, and plant uptake. However, separating inorganic from biologically driven isotopic fractionation remains complex. The present study investigates Mg and Si isotope fractionation in soil solutions from four typical Icelandic soils from a basaltic catchment (Borgarfjörður): Histic Andosol, Histosol, Gleyic Andosol, Brown andosol. When compared to the basaltic host rock, soil solutions were found to be enriched in heavy Si isotopes and in light Mg isotopes. This observation supports the current view of preferential sequestration of light Si isotopes and heavy Mg isotopes in secondary minerals leading to a dissolved phase enriched in heavy Si and light Mg. Although our results seem to support the idea of weathering induced fractionation, we need to stress that isotopic variations in surface horizons still need to be investigated in relation to plant uptake. The combination of these two isotope systems will contribute to a better understanding of the influence of inorganic versus biological fractionation in a natural system.

Key Words

Andosol, basaltic catchment, weathering, MC-ICP-MS, Iceland

Introduction

Continental weathering does not only play a pivotal role in long-term climate and CO₂ regulation, it also sustains the biosphere by providing nutrients. Understanding weathering and associated rates is therefore important to understand the rates at which weathering-climate feedback mechanisms operate. Stable isotopes of Si and Mg are fractionated during weathering processes and might help to assess solute-solid interaction rates on small (soils) and large scales (catchments). The riverine isotopic composition of above elements in a monolithological catchment can be related to pedogenic processes, such as mineral dissolution, sequestration in secondary minerals via neoformation or adsorption, and plant uptake (Georg *et al.*, 2007). However, separating inorganic from biologically driven isotopic fractionation remains complex, owing the tight coupling of biology and weathering within the “critical zone”.

Silicon stable isotopes were used in small catchments to relate isotopic variations to soil processes, e.g. neoformation of secondary minerals (Ziegler *et al.*, 2005; Opfergelt *et al.*, 2010), Si adsorption onto oxides (Delstanche *et al.*, 2009; Opfergelt *et al.*, 2009), and Si isotope fractionation during weathering on larger scales (Georg *et al.*, 2007). All these studies have shown the preferential uptake of light Si isotopes into secondary products, such as clays. Similarly, plant uptake was shown to favour light Si isotopes (Ding *et al.* 2005; Opfergelt *et al.*, 2006). Magnesium isotopes are also fractionated by plant uptake favouring heavy Mg isotopes (Black *et al.*, 2008) and during neoformation of secondary minerals, likely favouring heavy Mg (Tipper *et al.*, 2006). However, Icelandic rivers were found to display a large range of Mg isotopic variations both lighter and heavier relative to the parental basalt, and few measured soils were shown to be isotopically lighter than basalt (Pogge von Strandmann *et al.*, 2008), suggesting isotope fractionation pattern similar to those Si.

This present study investigated the Si and Mg isotope fractionation in Icelandic soil solutions from four soil profiles (Borgarfjörður catchment), in order to elucidate the potential impact of soil weathering on riverine Mg and Si isotopic compositions. The combination of these two isotope systems will contribute to a better understanding of weathering derived fluxes to rivers and hence oceans.

Materials and Methods

Study site in Iceland

The Borgarfjörður catchment is located in West Iceland and is dominantly basaltic (Gislason *et al.*, 1996). Four typical Iceland soil types (Arnalds, 2004) were selected and described following FAO guidelines (FAO, 2006): Histic Andosol (HA), Histisol (H), Gleyic Andosol (GA), Brown Andosol (BA) (Figure 1).

Among the four soil profiles, ten soil solutions were collected in September 2009 using macro rhizon soil moisture samplers (length 9cm, diameter 4.5mm, porosity 0.2 μ m) connected with plastic syringes (30ml) in order to cover surface and deeper horizons.

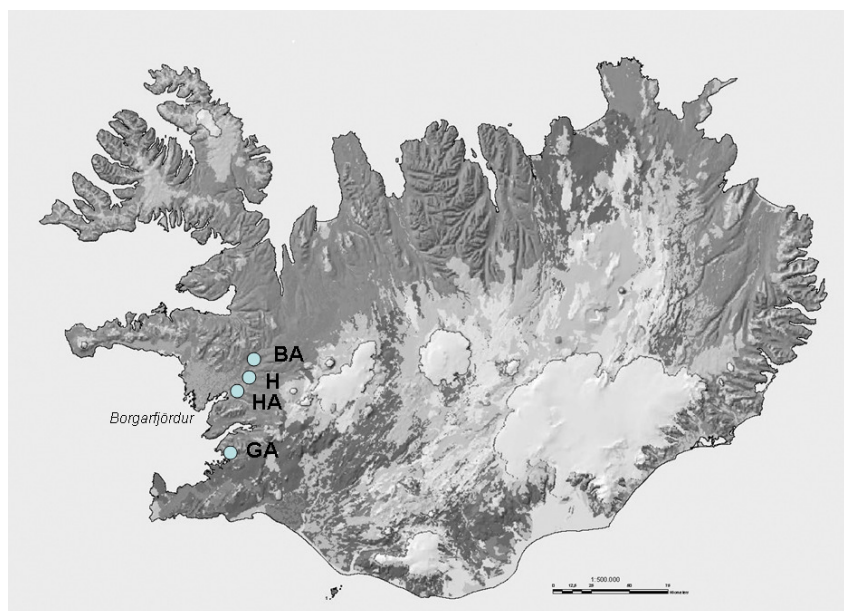


Figure 1. Location of soil sampling sites in Borgarfjörður catchment, West Iceland, 1:500.000 (map modified from Arnalds and Gretarsson 2001). GA = Gleyic andosol, HA = Histic andosol, H = Histisol, BA = Brown andosol.

Soil solutions characterization and isotope analysis

Temperature and pH of soil solutions were measured on the field. Major anion and cation concentrations were analysed at the Department of Earth Sciences in Oxford using the following instrumentation; Anion contents were measured by means of ion-chromatography (861 Advanced Compact IC) using conductivity detection following separation on a Metrohm A-Supp5 (4x50mm) column and a sodium carbonate/bicarbonate solution as mobile phase. Cation concentrations were analysed by quadrupole ICP-MS (Perkin Elmer ELAN 6100 DRC) and Si concentrations by photospectrometry (Hach, DR2800).

Soil solutions were purified for isotopic measurements through cationic exchange resin for Si (Georg *et al.*, 2006) and for Mg (adapted from Wombacher *et al.*, 2009). Silicon and Mg isotope compositions were determined by MC-ICP-MS (NuPlasma HR) and expressed in relative deviations in ‰ from NBS-28 (for Si) and DSM-3 (for Mg) using the common δ -notation. Accuracy was checked on international standards Diatomite ($\delta^{30}\text{Si} = +1.28 \pm 0.23\text{‰}$, n=29) and Cambridge-1 ($\delta^{26}\text{Mg} = -2.61 \pm 0.15\text{‰}$, n=563), and USGS rock standards BHVO-2 ($\delta^{30}\text{Si} = -0.20 \pm 0.16\text{‰}$, n=25; $\delta^{26}\text{Mg} = -0.23 \pm 0.21\text{‰}$, n=18) and BCR-2 ($\delta^{26}\text{Mg} = -0.24 \pm 0.26\text{‰}$, n=23). Recovery for Mg was always better than 98%.

Results and discussion

The pH in soil solutions ranged from 3.6 to 6.2, with temperature varying from 10.9 to 13.1°C. Anion mean concentrations were as follows; F ~0.2ppm ($\pm 5\%$), Cl ~17ppm ($\pm 2\%$), NO₃ ~15ppm ($\pm 2\%$) and SO₄ ~31ppm ($\pm 2\%$). Silicon concentrations ($\pm 2\%$) ranged from 5 to 31ppm with a mean value of 15ppm. Magnesium concentrations were between 1 and ~16ppm with a mean value of 5ppm ($\pm 2\%$). Mean Al and Fe concentrations were 2.6ppm ($\pm 1\%$) and 4ppm ($\pm 3\%$), respectively.

Soil solutions displayed $\delta^{30}\text{Si}$ from -0.2 to +1.26‰ and $\delta^{26}\text{Mg}$ from -0.5 to -1.1‰. When comparing dissolved Si and Mg isotopes with the respective isotope composition of the parental basalt, with $\delta^{30}\text{Si}$ of $-0.33 \pm 0.07\text{‰}$ (mean between measured and Georg *et al.*, 2007) and $\delta^{26}\text{Mg}$ of -0.23‰ (Pogge von Strandmann *et al.*, 2008), our data suggest an enrichment in heavy Si isotopes, but light Mg isotopes in soil solutions relative to the

parental material (see Figure 2 for the Histosol). Surface horizons showed a slight isotope shift, which might be related to plant uptake. This still needs to be investigated in more details.

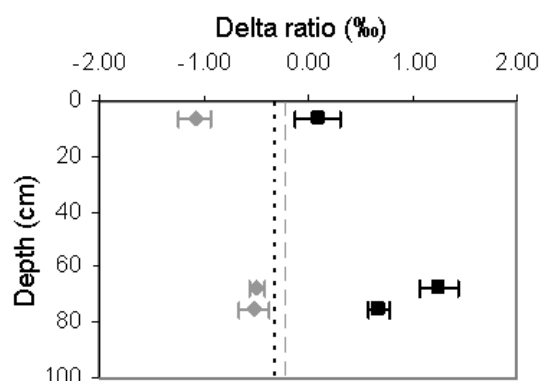


Figure 2. Distribution of $\delta^{30}\text{Si}$ (black square) and $\delta^{26}\text{Mg}$ (grey diamond) in soil solutions with depth within the Histosol ($2\sigma_{\text{SD}}$ error bar). Parental basalt $\delta^{30}\text{Si}$ (black dotted line; measured and Georg *et al.*, 2007) and $\delta^{26}\text{Mg}$ (grey dashed line; Pogge von Strandmann *et al.*, 2008) are given for comparison.

Those preliminary results indicate that soil solutions are enriched in light Mg isotope and heavy Si isotopes relative to the parental basalt. These effects can be related to the preferential sequestration of light Si isotopes in secondary minerals (Ziegler *et al.*, 2005; Opfergelt *et al.*, 2010; Georg *et al.*, 2009), and likely sequestration of heavy Mg isotopes in secondary minerals based on few data available (Tipper *et al.*, 2006).

Conclusion and perspectives

These preliminary results indicate that Mg and Si isotopes are very promising proxies to trace the effect of pedogenic processes on small-scale solute-solid interactions in soils. These data will be complemented by a mineralogical and isotopic characterization of the bulk soil (fraction <2mm) and clay fraction (fraction <2 μm) in order to better constraint the isotope composition of these individual pools and the interaction between them. In the broader picture, our results will contribute to a better understanding of small-scale weathering processes, associated solute-solid interactions and resulting material fluxes in rivers draining basaltic catchments.

References

- Arnalds O, Grétarsson E (2001) Soil map of Iceland, 1:500.000. Second Edition, Agricultural Research Institute (RALA)
- Arnalds O (2004) Volcanic soils of Iceland. *Catena* **56**, 3-20.
- Black JR, Epstein E, Rains WD, Yin Q, and Casey WH (2008) Magnesium-isotope fractionation during plant growth. *Environmental Science & Technology* **42**, 7831-7836.
- Delstanche S, Opfergelt S, Cardinal D, Elsass F, André L, Delvaux B (2009) Silicon isotopic fractionation during adsorption of aqueous monosilicic acid onto iron oxide. *Geochimica Et Cosmochimica Acta* **73**, 923-934.
- Ding TP, Ma GR, Shui MX, Wan DF, Li RH (2005) Silicon isotope study on rice plants from the Zhejiang province, China. *Chemical Geology* **218**, 41-50.
- FAO (2006) Guidelines for soil description. Fourth Edition, Food and Agriculture Organization of the United Nations, Rome, 97p.
- Georg RB, Zhu C, Reynolds BC, Halliday AN (2009) Stable silicon isotopes of groundwater, feldspars, and clay coatings in the Navajo Sandstone aquifer, Black Mesa, Arizona, USA. *Geochimica Et Cosmochimica Acta* **73**, 2229-2241.
- Georg RB, Reynolds BC, West AJ, Burton KW, Halliday AN (2007) Silicon isotope variations accompanying basalt weathering in Iceland. *Earth and Planetary Science Letters* **261**, 476-490.
- Georg RB, Reynolds BC, Frank M, Halliday AN (2006) New sample preparation techniques for the determination of Si isotopic compositions using MC-ICPMS. *Chemical Geology* **235**, 95-104.
- Gislason SR, Arnorsson S, Armannsson H (1996) Chemical weathering of basalt in southwest Iceland: Effects of runoff, age of rocks and vegetative/glacial cover. *American Journal of Science* **296**, 837-907.
- Opfergelt S, Cardinal C, Henriot C, Draye X, André L, Delvaux B (2006) Silicon isotope fractionation by banana (*Musa* spp.) grown in a continuous nutrient flow device. *Plant and Soil* **285**, 333-345.

- Opfergelt S, Cardinal D, André L, Delvigne C, Bremond L, Delvaux B (2010) Variations of $\delta^{30}\text{Si}$ and Ge/Si with weathering and biogenic input in tropical basaltic ash soils under monoculture. *Geochimica Et Cosmochimica Acta* **74**, 225-240.
- Opfergelt S, de Bournonville G, Cardinal D, André L, Delstanche S, Delvaux B (2009) Impact of soil weathering degree on silicon isotopic fractionation during adsorption onto iron oxides in basaltic ash soils, Cameroon. *Geochimica Et Cosmochimica Acta* **73**, 7226-7240.
- Pogge von Strandmann PAE, Burton KW, James RH, van Calsteren P, Gislason SR, and Sigfusson B. (2008) The influence of weathering processes on riverine magnesium isotopes in a basaltic terrain. *Earth and Planetary Science Letters* **276**,187-197.
- Tipper ET, Galy A, Bickle MJ (2006) Riverine evidence for a fractionated reservoir of Ca and Mg on the continents: Implications for the oceanic Ca cycle. *Earth and Planetary Science Letters* **247**, 267-279.
- Wombacher F, Eisenhauer A, Heuser A, Weyer S (2009) Separation of Mg, Ca and Fe from geological reference materials for stable isotope ratio analyses by MC-ICP-MS and double-spike TIMS. *Journal of Analytical Atomic Spectrometry* **24**, 627-636.
- Ziegler K, Chadwick OA, Brzezinski MA, Kelly EF (2005) Natural variations of $\delta^{30}\text{Si}$ ratios during progressive basalt weathering, Hawaiian Islands. *Geochimica Et Cosmochimica Acta* **69**, 4597-4610.

Use of elemental and isotopic ratios to distinguish between lithogenic and biogenic sources of soil mineral nutrients

Art White^A, Marjorie Schulz^A, Thomas Bullen^A, John Fitzpatrick^A, Davison Vivit^A, Rand Evett^B and Edward Tipper^C

^A U.S. Geological Survey, Menlo Park, CA USA afwhite@usgs.gov

^B University of California, Berkeley, CA USA

^C Laboratoire de Géochimie-Cosmochimie, Université de Paris, France

Abstract

Although mineral nutrients such K, Ca, Mg and Si, are vital to plant growth and productivity, their sources and cycling in soils are difficult to characterize due to complex inorganic and biologic interactions. This paper investigates the use of major-trace element ratios Sr/Ca, Rb/K and Ge/Si, as well as the isotopic ratios ⁸⁷Sr/⁸⁶Sr, ⁴⁴Ca/⁴⁰Ca and ²⁴Mg/²²Mg in deciphering temporal and spatial characteristics of mineral nutrients in pore waters, precipitation and vegetation associated with soils on a marine terrace chronosequence near Santa Cruz California. Seasonal plant growth patterns associated with the Mediterranean climate, along with strong soil permeability gradients, instill strong periodicities in elemental and isotopic cycling by the plants which are reflected in both selective extraction and passive litter decomposition.

Key Words

Isotopes, strontium, rubidium, germanium, chronosequence, mineral nutrients

Introduction

The physiological strategies by which plants utilize major mineral nutrients are generally well characterized. (Marschner 1995). However, the sources and fates of these nutrients in the soil environment are less understood due to complex interactions resulting from inputs from precipitation and weathering, as well as dynamic fluxes between pore water and soil organic and inorganic exchange complexes. Recent advances in analytical techniques, principally in mass spectroscopy, have provided access to an array of trace elements and isotopes that serve as important tracers for macronutrient behavior in the soil environment. In this paper, the use of the major-trace element pairs with similar chemical affinities, i. e., Sr/Ca, Rb/K and Ge/Si, in addition to isotopic ratios for ⁸⁷Sr/⁸⁶Sr, ⁴⁴Ca/⁴⁰Ca and ²⁴Mg/²²Mg, are investigated. The soils in this study comprise a chronosequence ranging in age from 65 to 225 kyrs, developed on marine terrace deposits along the coast of northern California. Vegetation consists primarily of annual European grasses whose growth cycle is controlled by a Mediterranean climate consisting of distinct wet and dry seasons. Detailed discussions of site climate, hydrology, geology and chemical weathering are contained in White *et al.* (2009).

Elemental Ratios

Small variations, such as in ionic radii and potentials of otherwise chemically similar elements, produce behavioral differences which are useful in tracing pathways in the soil environment (Tyler, 2004). These differences can be defined by a fractionation factor describing the concentration ratios in the plant and soil pore water

$$K_{\text{trace/major}} = \frac{\left[\frac{C_{\text{trace}}}{C_{\text{major}}} \right]_{\text{plant}}}{\left[\frac{C_{\text{trace}}}{C_{\text{major}}} \right]_{\text{soil}}} \quad (1)$$

Sr/Ca fractionation

Numerous studies have addressed the partitioning of Ca and Sr between soil and vegetation, initially in terms of pathways for radioactive ⁹⁰Sr and more recently, in conjugation with ⁸⁷Sr/⁸⁶Sr, for Ca availability, particularly in forest ecosystems. Results indicate complex interactions in which plants either concentrate or exclude Sr relative to Ca in the soil environment.

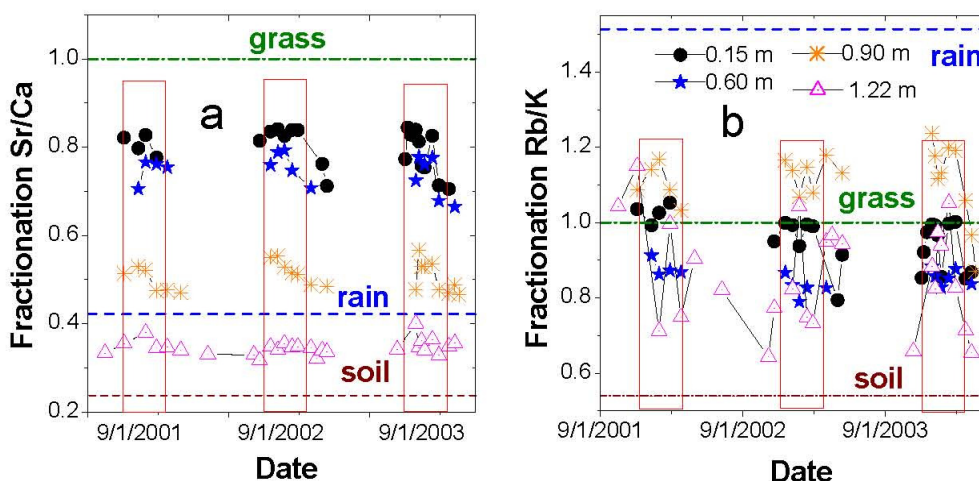


Figure 1. Seasonal variations in apparent fractionation factors (Eqn. 1) for (a) Sr/Ca and (b) Rb/K between plants and pore waters sampled at successively greater depths in the 92 kyr old Santa Cruz terrace. Horizontal lines correspond to zero fractionation of grass relative pore water ($K_{Sr/Ca}$), rain and bulk soil. Rectangular boxes define pore water variations during the growing season.

In the Santa Cruz soils, $K_{Sr/Ca}$ values are always less than unity, indicating the preferential uptake of plant Ca relative Sr (Figure 1a). However these $K_{Sr/Ca}$ values for shallow pore waters remain significantly higher than those for rain and soil weathering, suggesting Ca retention during closed system nutrient cycling. This effect is further elucidated by high, more plant-like $K_{Sr/Ca}$ values at the beginning of the growing season due to inputs to pore water from decaying plant litter. Later in the season, as plant growth intensifies, the $K_{Sr/Ca}$ values decline, indicating the exclusion of Sr relative to Ca in the biomass and consequent enrichment in the pore water. This seasonal cycling is diminished with depth and is nearly absent below the grass rooting depth of about 1 m where $K_{Sr/Ca}$ values approach that expected for plagioclase feldspar weathering (Figure 1a).

Rb/K fractionation

Recently, the partitioning of K and Rb has been investigated in terms of the contribution of biogenic K to watersheds and river systems (Chaudhuri *et al.* 2007). Shallow pore water K/Rb ratios at Santa Cruz are an order of magnitude lower than those of Sr/Ca, reflecting the strong retention of exchangeable Rb relative to K on clays. Although $K_{Rb/K}$ values differ between water samplers (Figure 1b), there is no consistent patterns with depth or seasonality. Average $K_{Rb/K}$ values cluster near unity, indicating that Santa Cruz grasses do not significantly distinguish between K and Rb during nutrient uptake. This conclusion is at odds with the literature consensus that Rb is preferentially excluded in biological material. These previous comparisons were most often made using bulk soils which contain relatively high and more tightly bound Rb compared more readily accessible soil pore water Rb considered in the present study. Unlike for Ca/Sr ratios, fractionation by vegetation is not a *a priori* requirement to explain K/Rb ratios in shallow pore waters which can be simple mixtures between high K/Rb ratios in precipitation and low K/Rb ratios produced by K-feldspar weathering (Figure 1b).

Ge/Si fractionation

Derry *et al.* (2005) suggested that high Ge/Si ratios in rivers reflect the exclusion of Ge and the high proportion of Si cycled by plants, principally in the form of phytoliths (Figure 2a). Such residual Ge increases are supported by low $K_{Ge/Si}$ values (Eqn. 1) for pore waters plotted as functions of depth in the 92 kyrs old Santa Cruz terrace (Figure 2b). The lowest $K_{Ge/Si}$ values occur in shallow pore water at the beginning of the growing season (early January) and increase to near the end of the growth season (April). Ideally, the Ge/Si fractionation factor should remain constant with the apparent seasonal variability in $K_{Ge/Si}$ reflecting the fact that the grass Ge/Si ratios are seasonally integrated values while the pore water ratios reflect changes in seasonal bioaccumulation.

One approach to describing Ge-Si cycling between the pore water and grasses is the Rayleigh relationship commonly used for isotopic fractionation. This can be written for Ge and Si as

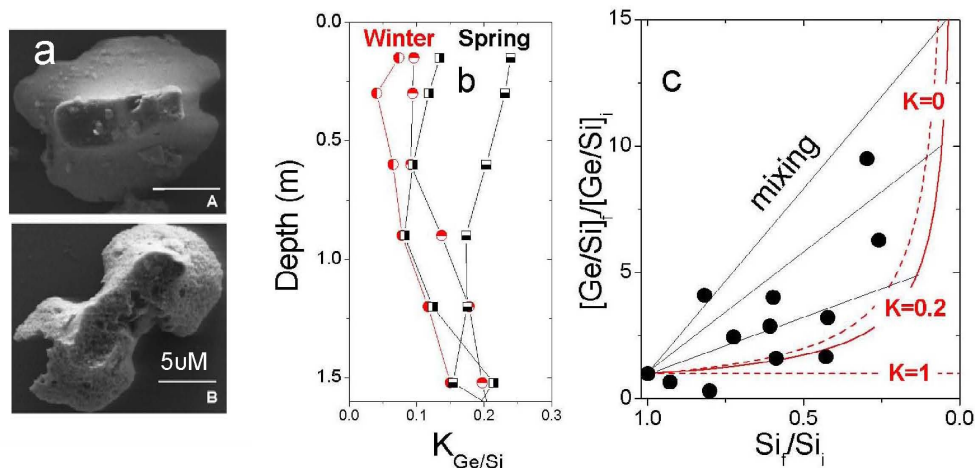


Figure 2. (a) Fresh and partly weathered grass phytoliths isolated from the 92 kyr old Santa Cruz soil. (b) Ge/Si fractionation factors (Eqn. 1) at beginning and conclusion of growing season. (3) Comparison of measured Ge/Si ratios with predicted Rayleigh fractionation curves using different $K_{Ge/Si}$ values (Eqn. 2).

$$\frac{[Ge/Si]_f}{[Ge/Si]_i} = (Si_f/Si_i)^{(K_{Ge/Si}-1)}. \quad (2)$$

where $[Ge/Si]_i$ and $[Ge/Si]_f$ are the initial and final pore water ratios and Si_i and Si_f are the initial and final Si concentrations. The application of this Rayleigh relationship requires two conditions; the system is closed and that irreversible uptake occurs via a reactant, i. e., plant growth. The last condition is presumably met since Ge and Si are incorporated in the grass phytoliths (Figure 2a) and do not re-equilibrate with the pore waters. However the extend to which nutrient uptake occurs under closed system conditions is less well defined.

The model assumes that the initial pore waters at the start of growing season have high Si and low Ge/Si ratios reflecting dissolution of phytoliths in plant litter produced during the previous growing season (Figure 2c). With the onset of new plant grow, Si_f/Si_i decreases and $[Ge/Si]_f/[Ge/Si]_i$ increases. The extents of these changes will be dependent on the fractionation factor. If no fractionation occurs, i. e., $K_{Ge/Si} = 1$, Eqn. 2 results in a straight line in which $[Ge/Si]_f/[Ge/Si]_i = 1$ for all values of Si_f/Si_i . Concurrently, complete exclusion of Ge during Si uptake, i. e., $K_{Ge/Si} = 0$, produces a steep exponential increases in $[Ge/Si]_f/[Ge/Si]_i$. An intermediate exponential line is produced assuming that $K_{Ge/Si}$ is of 0.2, the approximate minimum fractionation shown in Figure 2b. The data points in Figure 2c, corresponding to measured Ge and Si in pore waters from several of the terraces, together exhibit an exponential trend of increasing Ge/Si with Si which is compatible with closed system Rayleigh distillation. However, this data trend suggests a more rapid increase in pore water Ge than expected based the range of possible fractionation factors in Eqn. 2, i. e., $K_{Ge/Si} = 0$ to 1.

The apparent anomaly most likely results from the assumption of sequential processes, i. e., pore water compositions are initially fixed by dissolution of the past seasons' plant litter phytoliths (high Si and low Ge in pore water) followed by the onset of selective extraction during the current seasons' growth (low Si and high Ge in pore water). A more accurate scenario, based on the relatively slow rates of phytolith dissolution, is that of concurrent extraction and leaching. Schematically these processes are shown in Figure 2c by inclusion of linear mixing lines extending backward from biogenically fractionated pore waters toward initial pore water compositions dominated by phytolith dissolution at the initiation of seasonal plant growth. A two step process, involving various degrees of fractionation and mixing, are capable of reproducing the data field shown in Figure 2c

Isotopic Fractionation of Sr, Mg and Ca

The sensitivity of plants to uptake of different isotopes of the same elemental nutrient is dependent, in part, on their respective mass differences, i. e mass fractionation. Due to very small mass differences, plants do not exhibit measureable fractionation of $^{87}Sr/^{86}Sr$. This conclusion is supported by the data for the 95 kyr old soil (Figure 3a) which exhibit consistent trends in pore water and exchange $^{87}Sr/^{86}Sr$ extending between the $^{87}Sr/^{86}Sr$ composition of rain at shallow depths and toward more radiogenic plagioclase at greater depths. Grass $^{87}Sr/^{86}Sr$ falls between shallow pore water and rain implying simple uptake of a mixture of these components with no

fractionation.

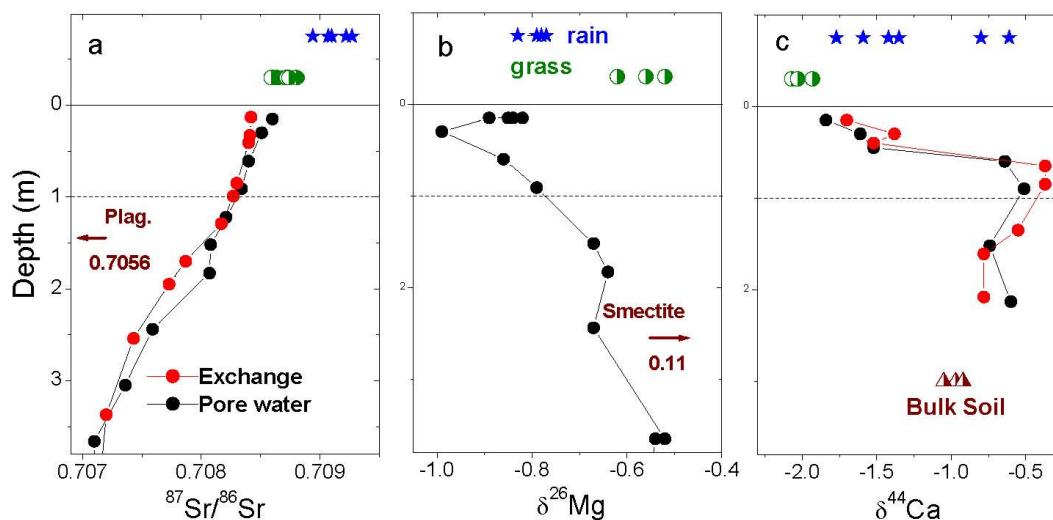


Figure 3. Distributions of selective isotopes of Sr, Mg and Ca in grasses pore waters, exchange sites and precipitation. Dashed line corresponds to maximum grass rotting depth.

Presently little information exists on the distribution of $^{26}\text{Mg}/^{24}\text{Mg}$ in soil environments with the data in Figure 3b representing the first direct comparison with Sr and Ca isotopes. Limited experimental data suggest that plants preferentially take up ^{26}Mg relative to ^{24}Mg , a conclusion supported by the Santa Cruz soils where plants are isotopically heavier than either rain or shallow pore waters (Figure 3b). At depth, $\delta^{26}\text{Mg}$ increases in pore waters due to increasing effects of smectite weathering. $^{44}\text{Ca}/^{40}\text{Ca}$ distributions exhibit the greatest biologic fractionation with $\delta^{44}\text{Ca}$ in grasses and shallow pore waters significantly lower than that of either rain or deeper pore waters reflecting soil weathering (Figure 3c).

Conclusions

The stable isotopes of major elements, in addition to trace-major element pairs of comparable chemical affinity, serve as importance tracers for nutrient cycling between plants and soils. Sr/Ca and Ge/Si fractionation factors are less than unity, indicating consistent discrimination of annual grasses against the heavier trace elements. Rb/K fraction factors are approximately unity, which, contrary to earlier work, indicates a lack of discrimination. A simple closed-system Rayleigh relationship can be used to explain fractionation between plants and pore waters, assuming simultaneous plant extraction and leaching. Isotopic fractionation of Sr, Mg and Ca exhibits a mass dependence, but the actual biologic dependence is determined by plant physiology which selectively enriches grasses with respect to isotopically heavy Mg but discriminate against isotopically heavy Ca.

References

- Chaudhuri S, Clauer N, Semhi K (2007) Plant decay as a major control on river dissolved potassium: A first estimate. *Chemical Geology* **243**, 178-190.
- Derry LA, Kurtz A, Ziegler K, Chadwick O (2005) Biological control of terrestrial silica cycling and export fluxes to watersheds. *Nature* **433**, 728-781
- Marschner H (1995) 'Mineral Nutrition of Higher Plants'. pp 529. (Academic Press, Norfolk).
- Tyler G (2004) Ionic charge, radius and potential control root/shoot concentration ratios of fifty cationic elements. *Science of the Total Environment* **329**, 231-239.
- White AF, Schulz MS, Stonestrom DA, Vivit DV, Fitzpatrick J, Bullen T, Maher K, Blum AE (2009) Chemical Weathering of a Marine Terrace Chronosequence, Santa Cruz, California II: Controls on Solute Fluxes and Comparisons of Long-term and Contemporary Mineral Weathering rates. *Geochimica et Cosmochimica. Acta* **73** 2769-2803.

Spatial Variability of Soil Nutrients and Microbial Biomass of *Moso* Bamboo Forest under Different Management Types

Shunbao Lu^{A,B}, Xiaomin Guo^A, Dekui Niu^A, Dongnan Hu^A, Tianzhen Du^A

^ACollege of Landscape and Art Jiangxi Agricultural University/The Key Laboratory of Genetic Resources and Use of Bamboo in Jiangxi Province, Nanchang China 330045, Email luxunbao8012@126.com

^BCollege of Life Science Jiangxi Normal University, Jiangxi Nanchang China 330022, Email gxmjxau@163.com

Abstract

The spatial variability of soils nutrients and microbial biomass of *Moso* bamboo forest under different management types was investigated in Jiangxi Province, China in this study and results showed soil nutrients decreased gradually from intensive management (IM) to general management (GM) and to extensive management (EM) types. Besides some fluctuations in the concentrations of available K(AK) and total N(TN), soil nutrients in Fengxin country (FXC) turned out to be relatively high in different soil levels, while they were relatively low in Tonggu country (TGC). There were extremely significant differences for available N (AN) in 0-10EM, 10-30EM in TGC and Yongfeng country (YFC), 30-50EM in TGC, 0-10EM and 30-50EM soil layer of available K(AK) in Jing'an country (JAC). There was no spatial effect on TN of 0-10EM in TGC. Interactions were significant among different management types and experimental sites for soil organic matter (SOM) in 0-10EM, AN and AK in 10-30EM soil layer. However, there were very significant interactions for SOM in 0-10EM and 10-30EM, AN and AK in 10-30EM. The available P (AP) and TN concentrations were not sensitive to interactions. Bacteria constituted the largest part of soil microbes, followed by actinomycetes and fungi. The amount of bacteria listed from highest to lowest is FXC, TGC, JAC, YFC in the IM and EM, while the sequence is FXC, JAC, YFC and TGC in the GM. The amount of fungi listed from highest to lowest is FXC, JAC, TGC and YFC. The amount of actinomycetes of JAC was largest, and was least in FXC. A very significant difference exists in the amount of actinomycetes with different management types. SOC and AN are related to amounts of bacteria and fungi, as well as AP to bacteria, AK to fungi. There was little relationship between the five soil nutrients and actinomycetes.

Key Words

Management types, *Moso* bamboo (*Phyllostachys heterocyla* cv. Pubescens), Spatial variability

Introduction

Soil fertility is a comprehensive reflection of various aspects of soil and also an indicator of forest productivity. It will directly influence the growth of bamboo (Huang 2000). Microorganisms are important and active components of soil in forest ecosystems and almost all the biochemical reactions are involved in the soil (Zhou 2007). They play an important role in cycling of materials, energy transformations and maintenance of ecosystem functions (Jin 1991, Xu 1993, Jiao 1997, Nation Biodiversity research 1998). Many important biochemical processes and material cycling of soil can objectively reflect the soil fertility status (Guan 1986, Zhang 1987, Jin 1991, Chen 1993, Zheng 1995). Therefore, it is of great significance that carrying out the research on forest soil nutrients and microorganisms, which will help us use of soil appropriately, make best eco-efficiency of the stands, prevent soil fertility from declining and improve ecological quality of the environment. However, due to the complexity of forest soil conditions, breaking of terrains, spatial variability, spatial and temporal variability of forest soil nutrients is an even more concrete reflection of soil spatial variability. Research on nutrients and microorganisms of soil in *Moso* bamboo forestry will help us understand the geographic variability of it, explore and develop certain theory and techniques in studying accurate fertilization and protecting of *Moso* bamboo forest, and provide a scientific basis to establish *Moso* bamboo forest soil nutrient management systems.

Materials and Methods

Experimental forest overview

Experimental sites are located in northwest Jiangxi Province. It is typical subtropical humid monsoon climate in this region and as well as a main producing region of *Moso* bamboo in Jiangxi province. The investigation point are JAC, FXC, TGC and YFC (114°31' -115°55' E, 25°14' -28°88' N). Experimental plots were set in the central area of bamboo forest. Altitude at the sites is about 200-800 m above sea level. The soil is yellow red, more than 60 cm in depth, 8-16°C in slope, 4.12-5.5 of pH. The climate is mainly humid and mild, with abundant rainfall and sunshine. The average annual temperature is 16.2-19.7°C, with a long frost-free period of 240-307d. Daily

average temperature is stable and activities above 0°C accumulated temperature is 5926-6478°C; ≥10°C accumulated temperature is 5050-5644°C. Extreme maximum temperature could be 41.6°C while extreme minimum temperature could be -5.8°C. Average annual precipitation is 1624.9mm. Average sunshine hours were 1737.1 hours (1986). Water, heat, soil and habitat conditions are very suitable for bamboo growth. The experimental plots are mainly occupied by bamboo and most bamboo appear to be pure forest, while there are still a substantial proportion of some broad-leaved mixed forest with fir, natural defective forest.

Description of the sites, experimental design and soil sampling

Three different management types: IM, GM and EM. Each type was set to repeat three times, namely, three plots. The experimental plots were fertilized with bamboo appropriate fertilizer in the last ten days of February 2009 (375kg·hm⁻²). Soil samples were collected in July 2009. Three points to S-sampling were selected in each plot, and each point was divided into three layers, namely, 0-10 cm, 10-30 cm and 30-50 cm. These soil samples of the same point with the same level were mixed and 1 kg from mixture was taken out and packed with sterile bags, and as soon as possible returned to the laboratory and processed within 2 days. 20 g fresh soil from samples of the 0-10cm soil layer were taken out and placed into sterile bags at 4°C preservation for microbial analysis. The sub-samples of soil were air-dried for several days and processed through a 2-mm sieve for analysing physical and chemical properties.

Analysis of soil nutrients and microbial biomass

A sub-sample from each plot was analysed for chemical properties and microbial biomass. The chemical properties analysis was carried using the methods described by Lu (1998), and soil microbial biomass was carried with methods described by Cheng (2000).

Results

Variability characteristics of soil nutrients in different management type

Soil pH varied from 4.12 to 5.5 in those sites, appearing to be strong acid. Soil nutrients of the same experimental plots under different management types showed different features (Figure 1). Soil nutrients gradually decreased from IM to GM and EM in all depths.

The nutrients were relatively high in different soil layers except soil AK and TN in FXC, while low in TGC. We found that bamboo grew better in TGC than in FXC. The difference was in relation with sites conditions. SOM in 0-10 cm was three times than in 30-50 cm within same experimental plots. There was extremely significant difference among management types and SOC in 0-10 cm soil in TGC, and significant difference 10-30 cm and 30-50 cm in TGC, and SOM in 10-30 cm in YFC. AN in 0-10 cm was higher than 30-50 cm soil layer (Figure 1). The difference was very significant among management types of AN in 0-10 cm and 10-30 cm soil layer in TGC and YFC, and significant in 30-50 cm in TGC.

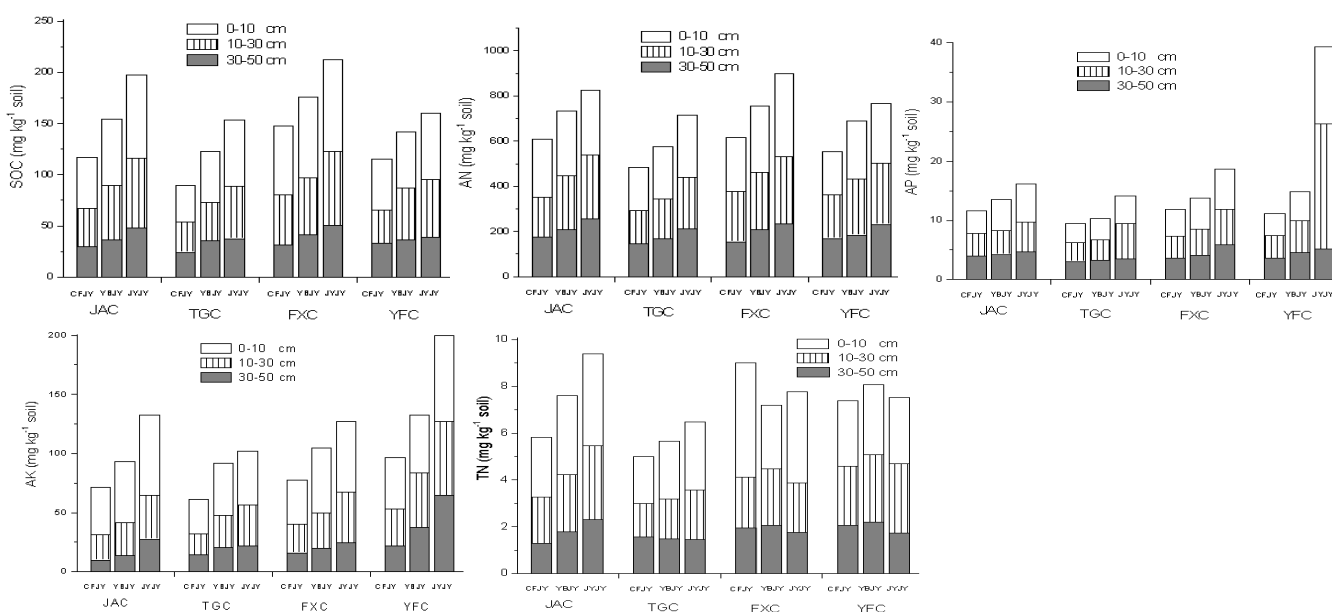


Figure 1. Management type of soil nutrients of bamboo forestry cylindrical scale figure.

Soil AP was low in experimental region, which suggested P fertilizer should be added and soil P content of bamboo supply should be increased. There was extremely significant difference among management types and nutrients in 0-10 cm and 10-30 cm in JAC, AP in 0-10 cm in TGC. Soil AK in TGC was lower than 50mg kg⁻¹ (Figure 1). Part of the forest soil should be replenished with K fertilizer in order to meet the needs of growth of bamboo. Soil AK was more than 70.0mg kg⁻¹ only in YFC. There was significant difference by ANOVA among management types and AK of 0-10 cm and 30-50 cm in JAC. Soil TN in 0-10 cm was 2-3.92g kg⁻¹ in JAC. The difference was not significant among management types to TN except 0-10 cm soil layer in TGC.

The difference was extremely significant among alternation management types and experimental zones of SOM in 0-10 cm, AN and AK in 10-30 cm (Table 1). There was significant difference of SOM and AP in 30-50 cm soil layer, while no effect in experimental zone. There was no effect of interactions to AP in 0-10 cm and 10-30 cm and TN in 30-50 cm soil layer.

Table 1. Two-factor (management and zone) analysis of variance P value of interaction.

	0-10EM		10-30EM		30-50EM	
O.M	PM=0.000**	PZ=0.000**	PM=0.000**	PZ=0.002**	PM=0.003**	PZ=0.092
Available N	PM=0.006**	PZ=0.031*	PM=0.000**	PZ=0.000**	PM=0.000**	PZ=0.015*
Available P	PM=0.079	PZ=0.346	PM=0.179	PZ=0.331	PM=0.024*	PZ=0.053
Available K	PM=0.002**	PZ=0.039*	PM=0.001**	PZ=0.002**	PM=0.053	PZ=0.040*
Total N	PM=0.556	PZ=0.408	PM=0.079	PZ=0.019*	PM=0.768	PZ=0.334

Note: P_M: accompanied probability of management, PZ: accompanied probability of zone, * correlation is significant (P<0.05); ** Correlation is very significant (P<0.01). The same as below.

Difference to the number of soil microbes in different management types of bamboo forestry
There was obvious difference of the quantity of soil microbes in bamboo forestry (Tab.2). Bacteria biomass had the largest amount, followed by actinomycetes and fungi. The proportion of bacteria, fungi and actinomycetes varied with bamboo forestry soil.

Table 2. the same experimental area of different treatments on soil microbial quantity and LSD comparison.

Sample	Manage	Bacteria×107cfu·g ⁻¹	Fungi×105cfu·g ⁻¹	Actinomycetes×106cfu·g ⁻¹	Total Micro.×107cfu·g ⁻¹
JA	JYJY	4.80±0.035Aa	1.67±0.38Aa	6.0±0.59Aa	5.42
	YBJY	3.83±0.035Bb	2.00±0.38Aa	1.5±0.59Bb	4.00
	CFJY	0.70±0.035Cc	0.50±0.38Bb	1.25±0.59Bb	0.83
TG	JYJY	5.43±0.42Aa	1.75±0.30Aa	1.80±0.39Aa	5.63
	YBJY	1.75±0.42Bb	0.3±0.30Bb	1.50±0.39Aa	1.90
	CFJY	1.20±0.42Aa	0.05±0.30Bb	0.10±0.095Bb	1.21
FX	JYJY	10.80±0.54Aa	2.50±0.34Aa	1.10±0.095Aa	10.94
	YBJY	9.65±0.54Aa	1.31±0.34Bb	0.90±0.095Aa	9.87
	CFJY	6.05±0.54Bb	1.01±0.34Bb	0.50±0.095Bb	6.11
YF	JYJY	3.39±0.43Aa	1.88±0.25Aa	1.33±0.13Aa	3.54
	YBJY	2.07±0.43Bb	1.02±0.25Bb	1.29±0.13Aa	2.21
	CFJY	0.41±0.43Cc	0.46±0.25Bb	0.51±0.13Bb	0.47

Note: The data in the table for the various parties mean ± SD; the same experimental area with the columns of different letters that significant differences.

The quantity of bacteria in a decreasing order was as FXC, TGC, JAC and YFC in IM and EM, and FXC, JAC, YFC and TGC in GM (Table 2). The largest amount of bacteria in IM in FXC was 26.3 times than in EM in YFX, indicating that rich microbial resources in FXC. The quantity of bacteria biomass was greater than other plots in FXC. There was extremely significant difference among management types and the quantity of bacteria, which meant that management types had great impact on soil bacteria in bamboo forest soil. The quantity of fungi in a decreasing order was as FXC, JAC, TGC and YFC, the quantity of fungi in FXC was 1.5 times JAC in IM, 500 times than TGC in EM (Table 2). There was extremely significant management type and the quantity of fungi in TGC and YFC, and significant difference in JAC and FXC. The quantity of Actinomycetes was greater in JAC than others, while it was the lowest in FXC and 18.3% times in JAC. There was extremely significant difference among management types and the quantity of soil actinomycetes.

Table 3. Correlation among soil quantity of microorganism and nutrient.

microorganism	SOM		Available N		Available P		Available K		Total N	
	R	P	R	P	R	P	R	P	R	P
Bacteria	0.879**	0.000	0.803**	0.002	0.717**	0.009	0.422	0.172	0.509	0.091
Fungi	0.847**	0.001	0.866**	0.000	0.664*	0.018	0.746**	0.005	0.508	0.091
Actinomces	0.444	0.148	0.327	0.299	0.504	0.094	0.573	0.051	0.288	0.364

Correlation analysis of soil nutrients and microorganisms

The results of correlation among the quantity of soil microorganisms and nutrients showed that there was extremely significant among SOM, AN, AP and bacteria, and no correlation to soil AK and TN, but it had a certain degree of positive correlation (Table 3). The difference was very significant ($P < 0.01$) among SOM, AN and AK and fungal. There was significantly correlation between Fungi and AP, while no difference to TN. No significant difference was among five soil nutrients and actinomycetes, while a positive correlation to some extent. It showed the quantity of actinomycetes was not sensitive to soil nutrients.

Conclusions

(1) Bamboo forestry soil was strongly acidic. The soil nutrients in a decreasing order was as IM, GM and EM. The soil nutrient was high except AK and TN of different soil layer in FXC, while low in TGC. There was extremely significant difference SOM in 0-10 cm and AN and AK in 10-30 cm of interaction of management types and the experimental sites, and significant difference of SOM and AP in 30-50EM soil layer on management types, while no significant difference to experimental sites. There was no effect on interaction on AP in 0-10 cm and TN in 30-50 cm.

(2) The quantity of bacteria was of the largest amount, followed by actinomycetes and fungi at least. The quantity of bacteria in a decreasing order was as FXC, TGC, JAC and YFC in IM and EM conditions, and FXC, JAC, YFC and TGC in GM. The order of the quantity of fungi was FXC, JAC, TGC and YFC, and a great influence of fungi to management types. The quantity of actinomycetes was higher in JAC than others, while was lowest in FXC.

(3) There was extremely significant difference among bacteria with SOM, AN, AP, and no correlation to AK and TN, but positive correlation to a certain degree. There was correlation between fungal and SOM, AN, AK, and a very significant difference and significantly correlated with AP, while little to TN. The difference among five kinds soil nutrients and actinomycetes was not significant, but a positive correlation to some extent. It showed the quantity of actinomycetes was not sensitive to soil nutrients.

Acknowledgements

The work reported here has been funded by IPNI, National Natural Science Foundation of China(30860226), Agricultural Scientific and Technological Production Funds Project of Ministry of Science and Technology(2008C50040562), National Science and Technology Support Project(2008BADA9B0802)), Excellent funded projects for returnee of ministry of personnel(2007-170 watershed ecology), Projects for academic leader of Jiangxi province(030008), Superior Ph.D. thesis in Jiangxi Province incubation program, Teaching Reform of key projects in Jiangxi Province (JXJG-O7-3-44) (graduate students), Jiangxi Provincial Educational Science, *Eleventh Five-Year Plan* Key Project (07ZD038). The authors want to take this opportunity to thank all of the supports.

References

- Biodiversity of China situation report compile team (1998) Nation Biodiversity research[M].Beijing: Environment Press.105-121.
- C Y Huang. Pedology (2000) Beijing :China Agricultural Press.
- D H Zhang, Y Q Chen (1987) Forest soil enzymes and soil fertility. *Forestry Science and Technology Communication*, Vol. 4:1-3.
- H.J. Chen,C.H.Li (1993) Soil enzyme and fertility of fir young forest. *Forest Research*. Vol.6(3):321-326
- J M Jin, L Q Wang (1991) Nature Conservation Conspectus. Beijing: Environmental Science Press,15-46.
- Jiangxi Forest Editorial committee (1986) Jiangxi Forest. Beijing: China Forestry Press.
- L J Cheng, Xue Q H (2000) Microbiology experiment technology. Beijing: The World Publish Company.
- L X Zhou (2007) Microbiological characteristics of soil the instructions of the role of soil health, *Biodiversity Science*,Vol.15 (2):162-171.
- R K Lu (1999) Soil Agricultural Chemical Analysis Method. Beijing: China Agricultural Sci-Tech. Press.

- R Z Jiao, C D Yang, X N Tu, et al. (1997) The change of undergrowth, soil microorganism, enzyme activity and nutrient in different developing stage of the Chinese fir Plantation. *Forest Research*.Vol. 10 (4):373-379.
- S Y Guan (1986) Soil enzyme and its research method. Beijing :Agricultural Press.260-332.
- W J Zheng, L M Wang, P Lin (1995) soils activity in subtropical rain forest Fujian He Xi. *Journal of Ecology*. 14(2):16-20.
- Y B Xu, H Y Chen (1993) P. massoniana and C. fissa Rehd.et Wilsmixed forest soil fertility levels of. H Z Wang, et al. *China Southern mixed forest research*. Beijing: China Forestry Publishing Press.235-241.